



XA9745910

IAEA-TECDOC-978

***Fuel performance and
fission product behaviour
in gas cooled reactors***



INTERNATIONAL ATOMIC ENERGY AGENCY

IAEA

November 1997

29 - 04

The IAEA does not normally maintain stocks of reports in this series.
However, microfiche copies of these reports can be obtained from

INIS Clearinghouse
International Atomic Energy Agency
Wagramerstrasse 5
P.O. Box 100
A-1400 Vienna, Austria

Orders should be accompanied by prepayment of Austrian Schillings 100,—
in the form of a cheque or in the form of IAEA microfiche service coupons
which may be ordered separately from the INIS Clearinghouse.

The originating Section of this publication in the IAEA was:

Nuclear Power Technology Development Section
International Atomic Energy Agency
Wagramerstrasse 5
P.O. Box 100
A-1400 Vienna, Austria

FUEL PERFORMANCE AND FISSION PRODUCT BEHAVIOUR
IN GAS COOLED REACTORS
IAEA, VIENNA, 1997
IAEA-TECDOC-978
ISSN 1011-4289

© IAEA, 1997

Printed by the IAEA in Austria
November 1997

FOREWORD

The Co-ordinated Research Programme (CRP) on Validation of Predictive Methods for Fuel and Fission Product Behaviour was organized within the frame of the International Working Group on Gas Cooled Reactors (IWGGCR). This International Working Group serves as a forum for exchange of information on national programmes, provides advice to the IAEA on international co-operative activities in advanced technologies of gas cooled reactors (GCRs), and supports the conduct of these activities.

Advanced GCR designs currently being developed are predicted to achieve a high degree of safety through reliance on inherent safety features. Such design features should permit the technical demonstration of exceptional public protection with significantly reduced emergency planning requirements. For advanced GCRs, this predicted high degree of safety largely derives from the ability of the ceramic coated fuel particles to retain the fission products under normal and accident conditions, the safe neutron physics behaviour of the core, the chemical stability of the core and the ability of the design to dissipate decay heat by natural heat transport mechanisms without reaching excessive temperatures. Prior to licensing and commercial deployment of advanced GCRs, these features must first be demonstrated under experimental conditions representing realistic reactor conditions, and the methods used to predict the performance of the fuel and reactor must be validated against these experimental data. Within this CRP, the participants addressed the fuel performance and fission product behaviour in GCRs.

The objectives of this CRP were to review and document the status of the experimental data base and of the predictive methods for GCR fuel performance and fission product behaviour; and to verify and validate methodologies for the prediction of fuel performance and fission product transport.

The following Member State national institutions participated in the performance of this CRP:

- Forschungszentrum Jülich (FZJ), Jülich, Germany
- Japan Atomic Energy Research Institute (JAERI), Tokai-mura, Japan
- Oak Ridge National Laboratory (ORNL), Oak Ridge, Tennessee, in co-operation with General Atomics (GA), San Diego, California, USA
- Russian Research Center Kurchatov Institute (RRC-KI), Moscow, Russian Federation
- Centre d'Etudes de Grenoble (CEA-CEG), Grenoble, France
- AEA Technology, Harwell, United Kingdom
- Institute for Nuclear Energy Technology (INET), Tsinghua University, Beijing, China.

This report has been edited by K. Verfondern, FZJ, and documents the CRP activities with respect to the technical areas of fuel performance during normal and accident oxidizing and non-oxidizing conditions, transport of gaseous and metallic fission products during normal and accident conditions, performance of advanced fuels and GCR fuel design and fabrication programmes.

EDITORIAL NOTE

In preparing this publication for press, staff of the IAEA have made up the pages from the original manuscript(s). The views expressed do not necessarily reflect those of the IAEA, the governments of the nominating Member States or the nominating organizations.

Throughout the text names of Member States are retained as they were when the text was compiled.

The use of particular designations of countries or territories does not imply any judgement by the publisher, the IAEA, as to the legal status of such countries or territories, of their authorities and institutions or of the delimitation of their boundaries.

The mention of names of specific companies or products (whether or not indicated as registered) does not imply any intention to infringe proprietary rights, nor should it be construed as an endorsement or recommendation on the part of the IAEA.

CONTENTS

1. INTRODUCTION	1
2. HTGR FUEL DESIGN AND FABRICATION	3
2.1. Coated particle	3
2.2. Fuel element	7
2.3. Fuel quality during manufacture	10
2.3.1. The Chinese program	11
2.3.1.1. Design specifications of the HTR-10 fuel element	11
2.3.1.2. Manufacture technology	11
2.3.1.3. Pre-irradiation characterization and inspection	13
2.3.1.4. Strength and Young's Modulus of pyrolytic SiC coatings	17
2.3.2. The German program	23
2.3.2.1. Manufacturing defects	24
2.3.2.2. Design basis for free uranium	26
2.3.2.3. Uranium contamination	27
2.3.3. The Japanese program	28
2.3.3.1. Design criteria for HTTR first loading fuel	29
2.3.3.2. Manufacturing defects	29
2.3.4. The Russian program	32
2.3.5. The US program	39
2.3.5.1. Design requirements	39
2.3.5.2. Fuel design	39
2.3.5.3. Fuel quality requirements	39
2.3.5.4. Process history	39
2.3.5.5. Fuel fabrication	41
2.3.5.6. Compact fabrication	41
2.4. Summary of Chapter 2	41
References of Chapter 2	42
3. NORMAL OPERATION. TRISO FUEL PERFORMANCE UNDER IRRADIATION ...	45
3.1. Fission product inventories of the active core	45
3.2. Fuel failure mechanisms and models	46
3.2.1. Kernel migration ("amoeba effect")	46
3.2.2. Fission product interaction with silicon carbide	47
3.2.3. Pressure vessel failure	47
3.3. Fission product release models	48
3.3.1. Gas release	48
3.3.2. Metal release	56
3.3.2.1. Calculation models	56
3.3.2.2. Model valuation	61
3.3.2.3. Uptake of fission product metals by silicon carbide	61
3.3.3. Future needs	62
3.4. Fuel irradiation test programs	62
3.4.1. The Chinese program	65
3.4.2. The German program	65
3.4.2.1. In-pile failure and fission gas release	65
3.4.2.2. HTR-MODUL source terms	70
3.4.3. The Japanese program	72
3.4.4. The Russian program	78

3.4.4.1. Weak irradiation method (activation method)	78
3.4.4.2. Methods and results of reactor and post-reactor investigations	87
3.4.5. The US program.....	100
3.4.5.1. Accelerated irradiations.....	101
3.4.5.2. Comparison of coated fuel particle performance in accelerated irradiation testing and in an operating reactor.....	102
3.4.5.3. Irradiation with high- and low-enriched uranium fuel	102
3.4.5.4. Irradiation test of particle design changes	105
3.4.5.5. Further work and closure.....	106
3.5. Reactor operating experience	106
3.5.1. Dragon HTGR	106
3.5.2. Peach Bottom Unit 1	107
3.5.3. Fort St. Vrain nuclear generating station	108
3.5.4. AVR	112
3.5.5. THTR-300.....	115
3.6. Summary of Chapter 3.....	117
References of Chapter 3	118
4. FUEL PERFORMANCE AND FISSION PRODUCT BEHAVIOR UNDER HEATUP, NON-OXIDIZING CONDITIONS.....	125
4.1. Postirradiation heating experiments	125
4.1.1. Postirradiation heating tests in Germany	125
4.1.1.1. Equipment	125
4.1.1.2. Data of fuel samples.....	125
4.1.1.3. Experimental results.....	126
4.1.1.4. Modeling	145
4.1.2. Postirradiation heating tests in Japan	159
4.1.2.1. Equipment	159
4.1.2.2. Data of fuel samples.....	160
4.1.2.3. Results of isothermal heating tests.....	162
4.1.2.4. Results of temperature ramp tests	165
4.1.2.5. Modeling	166
4.1.3. Russian Federation	168
4.1.3.1. Experimental work	168
4.1.3.2. Modeling	168
4.1.4. Heating of irradiated particles in the USA	174
4.1.4.1. The ORNL core conduction cooldown test facility.....	174
4.1.4.2. The US model for transient fission gas release	177
4.1.4.3. The SHELL model	184
4.1.4.4. The UT-KFA model for fission product release from pebble bed fuel.....	184
4.2. Irradiation testing at very high temperatures (1500-2000°C)	188
4.2.1. High temperature irradiation in Japan	188
4.2.1.1. Irradiation capsules	188
4.2.1.2. Data of fuel samples.....	188
4.2.1.3. Results of irradiation tests.....	188
4.2.2. High temperature irradiation in the USA.....	190
4.2.2.1. Experimental details.....	190
4.2.2.2. Heating test results	191
4.2.2.3. Discussion of experimental results.....	192
4.2.2.4. Modeling	194
4.3. Reactivity-initiated accident testing.....	198

4.3.1. Pulse tests in NSRR, Japan	198
4.3.1.1. Pulse irradiation conditions.....	198
4.3.1.2. Data of fuel samples.....	198
4.3.1.3. Results of RIA tests.....	198
4.3.2. Pulse tests in HYDRA and IGR, Russia	199
4.3.2.1. Tests using the HYDRA reactor.....	201
4.3.2.2. Tests using the IGR reactor	201
4.3.2.3. Temperature and stress calculations.....	207
4.4. Summary of Chapter 4	209
References of Chapter 4	210
5. FUEL PERFORMANCE AND FISSION PRODUCT BEHAVIOR UNDER OXIDIZING CONDITIONS	217
5.1. General course of the accidents	217
5.2. Experimental and analytical approach to the accidents	218
5.2.1. Experimental efforts.....	218
5.2.2. Analytical efforts.....	218
5.3. Water ingress accidents	218
5.3.1. Particles with exposed fuel.....	218
5.3.1.1. Water vapor injection during irradiation.....	219
5.3.1.2. Changes in kernels exposed to water vapor during and after irradiation	231
5.3.1.3. German postirradiation water vapor injection.....	234
5.3.4. Air ingress accidents	243
5.4.1. Response of graphite and carbonaceous material.....	244
5.4.2. Response of coated fuel particles	246
5.4.2.1. German postirradiation heating, introduction	246
5.4.2.2. Postirradiation heating results	246
5.5. Summary of Chapter 5	253
References of Chapter 5	255
6. EX-CORE FISSION PRODUCT TRANSPORT DURING NORMAL AND ACCIDENT CONDITIONS	259
6.1. Fission product transport in primary coolant circuit.....	261
6.1.1. Fission product transport and deposition during normal operation	261
6.1.1.1. Plateout models and computer codes	261
6.1.1.2. Aerosol ("dust") effects	265
6.1.1.3. Integral plateout data.....	273
6.1.1.4. Fission product distribution at initiation of the accident.....	321
6.1.2. Fission product transport during accidents (reentrainment)	323
6.1.2.1. Chemical desorption.....	323
6.1.2.2. Mechanical reentrainment ("lift-off")	330
6.1.2.3. Removal by liquid water ("washoff").....	346
6.1.2.4. Steam-induced vaporization ("steamoff")	353
6.2. Decontamination of primary circuit components	361
6.2.1. Introduction	361
6.2.2. Decontamination experience	361
6.2.2.1. Light water reactor decontamination experience	363
6.2.2.2. French gas-cooled and sodium-cooled reactor decontamination experience	364
6.2.2.3. Rapsodie reactor decommissioning	365

6.2.2.4. AVR helium-cooled reactor decontamination experience	366
6.2.2.5. Fort St. Vrain helium circulator decontamination.....	367
6.2.2.6. Peach Bottom HTGR component samples decontamination	368
6.2.2.7. Decontamination of CAGR gas circulator components.....	369
6.2.2.8. Decontamination of gas turbine materials.....	369
6.2.2.9. Dragon reactor decontamination experience.....	370
6.2.2.10. Fission product behavior in OGL-1 and HENDEL loop tests.....	370
6.2.3. Conclusions	371
6.3. Fission product transport in reactor building.....	372
6.3.1. FRG contribution	372
6.3.1.1. Fission product release into the reactor building	372
6.3.1.2. Deposition constants and escape probabilities	373
6.3.1.3. Filter efficiencies.....	377
6.3.2. Japanese contribution	378
6.3.3. US contribution	379
6.4. Summary of Chapter 6.....	380
References of Chapter 6.....	382
 7. ADVANCED FUELS	393
7.1. ZrC-coated fuel particles	393
7.1.1. Fuel particle design	394
7.1.2. Coating processes.....	394
7.1.3. Characterization techniques	396
7.1.4. Fuel performance during normal operation.....	397
7.1.5. Fuel performance during accidents	403
7.1.5.1. Non-oxidizing conditions.....	403
7.1.5.2. Oxidizing conditions	404
7.1.6. Fission product retentiveness	405
7.2. Fuel element	409
7.2.1. Corrosion resistant spherical fuel element	409
7.2.1.1. Process for production of corrosion resistant spherical fuel elements ..	409
7.2.1.2. Properties of corrosion resistant spherical fuel elements	411
7.2.1.3. Corrosion.....	414
7.2.2. Monolithic fuel rod	418
7.2.2.1. Development of monolithic fuel in the UK.....	419
7.2.2.2. Development of monolithic fuel in Germany	420
7.2.2.3. Development of monolithic fuel in Japan	421
7.2.2.3. A plausible order for developing various advanced fuel particles	423
7.3. Summary of Chapter 7	424
References of Chapter 7.....	426
 8. CONCLUSIONS	431
APPENDIX A: MATERIAL PROPERTY DATA	435
APPENDIX B: THE RUSSIAN "ACTIVATION MODEL" OF FISSION PRODUCT RELEASE FROM HTGR FUEL ELEMENTS	501
PARTICIPANTS AND CONTRIBUTORS TO DRAFTING AND REVIEW.....	529

1. INTRODUCTION

Three decades of work on fuel and fission products in the High-Temperature Gas-Cooled Reactor (HTGR) in half a dozen countries around the world have shown remarkable achievements that are documented here.

The key to achieving good fuel performance is the choice of the right materials:

- high density oxidic kernel
- low density buffer layer derived from ethyne
- TRISO coating, i.e., the sequence pyrocarbon, silicon carbide, pyrocarbon
- low-temperature isotropic pyrocarbons derived from propene
- high-quality SiC of near theoretical density derived from methyltrichlorosilane

Also an optimized design needs to be specified so as to make negligible any performance limiting phenomena. Another essential is reproducible manufacturing processes with emphasis on achieving spherical kernels and spherical particles with very low defect fractions. In modern HTGR fuel, the level of defective coated particles is practically zero. It is only during pressing of fuel bodies that particle defects do occur, but on a very low level.

Also reported are studies on the consequences of hypothetical accident scenarios (e.g., air ingress) in terms of fuel failure and fission product release.

A wide range of tools has been developed for predicting fission product transport and release. Their application to operating reactors – AVR, THTR, Fort St. Vrain – has provided an important validation. For licensing applications, a comprehensive set of codes is available for predicting fission product behavior in-core and ex-core including plateout.

Alternative advanced fuel studies are reported showing the potential for even better fission product retention at extreme temperatures by using ZrC coating (instead of SiC) as the use of ZrC provides an inherent corrosion protection against fuel kernel migration.

While commercial deployment of HTGRs appears uncertain in the United States and in Europe, this knowledge gained for HTGRs can appropriately be applied to the construction of reactors in future.

The International Atomic Energy Agency has provided the forum and support for this extensive documentation of methods and data.

NEXT PAGE(S)
left BLANK

2. HTGR FUEL DESIGN AND FABRICATION

2.1. COATED PARTICLE

The fundamental characteristics of ceramic coated particle fuel for HTGRs have been investigated for three decades. Several countries have initiated fuel development and qualification programs with the coated particle as the basic unit.

The objectives of the coated particle development program at UKAEA [1, 2, 3] that has started in 1961, have been to define the essentials of a production route for the manufacture of nuclear fuel kernels and coated particles and to identify the important process parameters that determine the particle properties and hence the irradiation performance. Detailed characterization assessments of the various components of the coated particles have enabled a number of advanced coated particle designs to be optimized. The versatility of the UKAEA powder agglomeration process for the fabrication of highly spherical carbide or oxide kernels is exemplified by its ability to produce virtually monosized kernels in the range from 200 to 1000 μm in diameter, with controlled porosities in the range from 5 to 20 % and the facility with which solid fission product and oxygen getters may be incorporated. The principles of the UKAEA pyrocarbon (PyC) and silicon carbide (SiC) coating processes, together with the experience of coated particles on a large scale (kernel batch sizes up to 25 kg) have been delineated. The understanding of the important parameters controlling deposition processes has led to optimum specifications for coater design and process route such that high sphericity is maintained throughout coating with an acceptable spread in coating properties. More recent detailed investigations of process variables have identified the factors controlling PyC microstructure and the effect that coat defects and substrate shapes have on the ability of SiC to contain the gaseous fission products released by the fuel kernel during in-reactor operation. The proportion of defective particles is reduced to less than 10^{-5} by establishing process specifications to minimize coating-kernel bonding and misshapen kernels. The UKAEA fabrication development has been terminated in 1974.

In the **Federal Republic of Germany (FRG)**, the production process for spherical fuel elements with high-enriched $(\text{Th},\text{U})\text{O}_2$ particles with a BISO coating as fuel for the AVR and THTR reactors was fully established and licensed in the 1970s. In the early 1980s, TRISO coated particles with low-enriched uranium (LEU) were chosen as reference fuel for new HTGR designs. These particles consist of a 10.6 % enriched UO_2 kernel with a diameter of 500 μm surrounded by subsequent layers of buffer (thickness: 95 μm), inner pyrocarbon (inner PyC, 40 μm), silicon carbide (SiC, 35 μm), and finally outer pyrocarbon (outer PyC, 40 μm) as shown in Fig. 2-1. The qualification program for the LEU reference fuel has been addressed to irradiation and accident conditions confirming the "1600 °C concept" (meaning that this acceptable temperature limit will not be exceeded in any conceivable accident scenario) as a new passive safety concept for future German modular HTGRs [4]. In the final step of the qualification program, the so-called proof tests, full size fuel elements have been tested in the Material Test Reactor (MTR) HFR Petten under simulated HTGR operating conditions. Testing limits for modern German HTGR fuel have been chosen to envelope the required normal operating conditions. Values reached so

far in various irradiation experiments are a burnup of 15 %FIMA (design limit: 8-10), a fast neutron fluence of $8 \times 10^{25} \text{ m}^{-2}$, $E > 16 \text{ fJ}$ (design limit: $2-3 \times 10^{25}$), and an irradiation temperature of 1250°C [5]. In 1989, the German manufacturing company HOBEG decided to abandon all production and development activities due to lack of commercial interests [4].

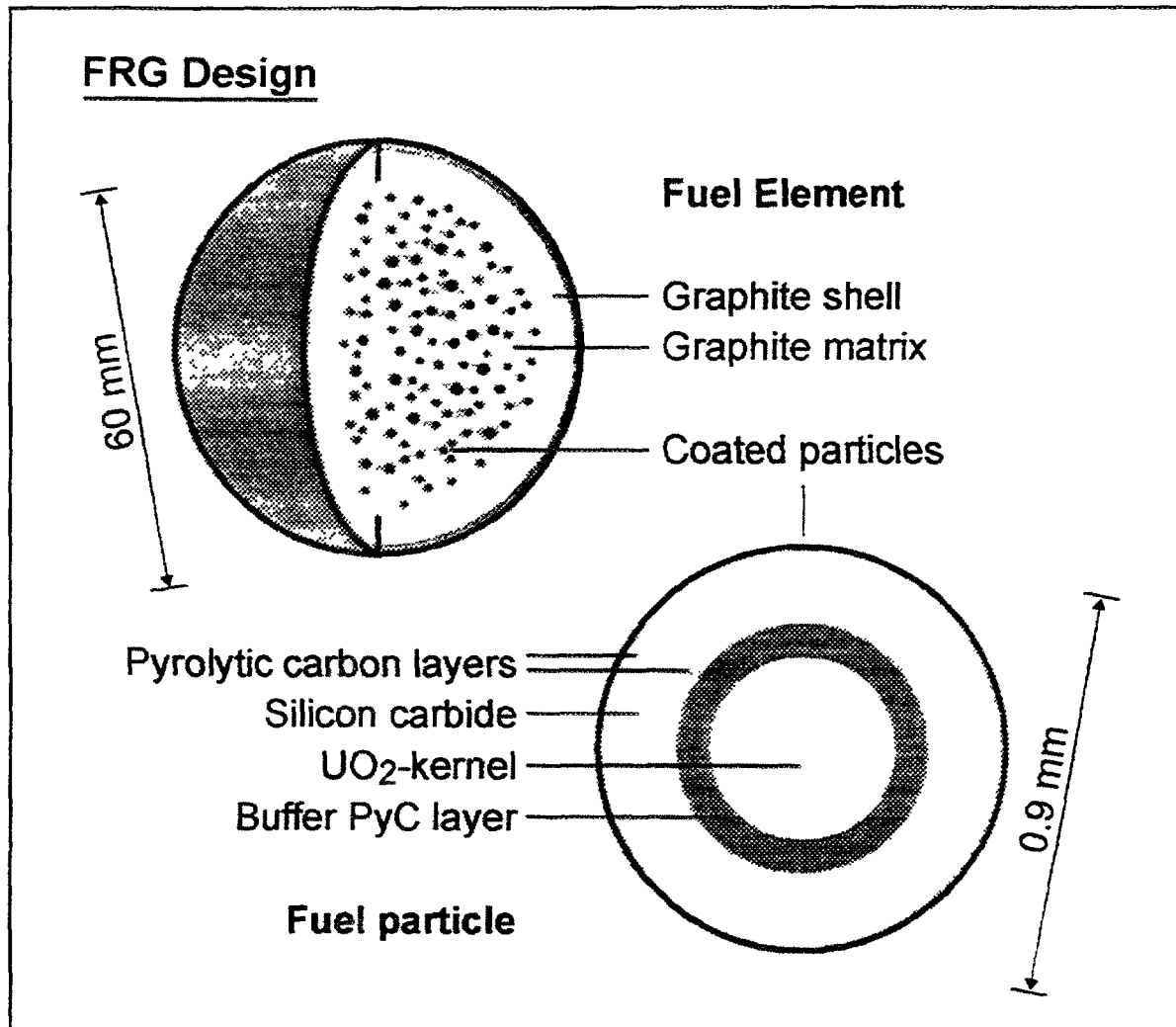


Fig. 2-1: FRG reference design for fuel particles and fuel element

The United States reference fuel design is based on a two-particle concept of fissile and fertile particles. The fissile particle consists of a fuel kernel (diameter 350 μm) containing 19.9 % enriched uranium oxycarbide (UCO) which is surrounded by a 100 μm buffer layer, 35 μm inner PyC layer, 35 μm SiC layer, and 40 μm outer PyC layer. The fertile TRISO particle has a 500 μm diameter U_{nat}CO kernel surrounded by 65 μm buffer, 40 μm inner PyC, 35 μm SiC, and 40 μm outer PyC layers. The conditions required for US fuel are more severe than German fuel. Design limits here are a burnup of 26 %FIMA for the fissile particle and a fast fluence of $4.5 \times 10^{25} \text{ m}^{-2}$, $E > 29 \text{ fJ}$ ¹ [6]. The original USA design employed a thorium oxide fertile kernel, surrounded by BISO coatings. Subsequently, the BISO coatings on the fertile fuel were changed to TRISO

¹ Conversion factor for the unit of the fast neutron fluence from $E>29 \text{ fJ}$ to $E>16 \text{ fJ}$ is 1.1

US Design

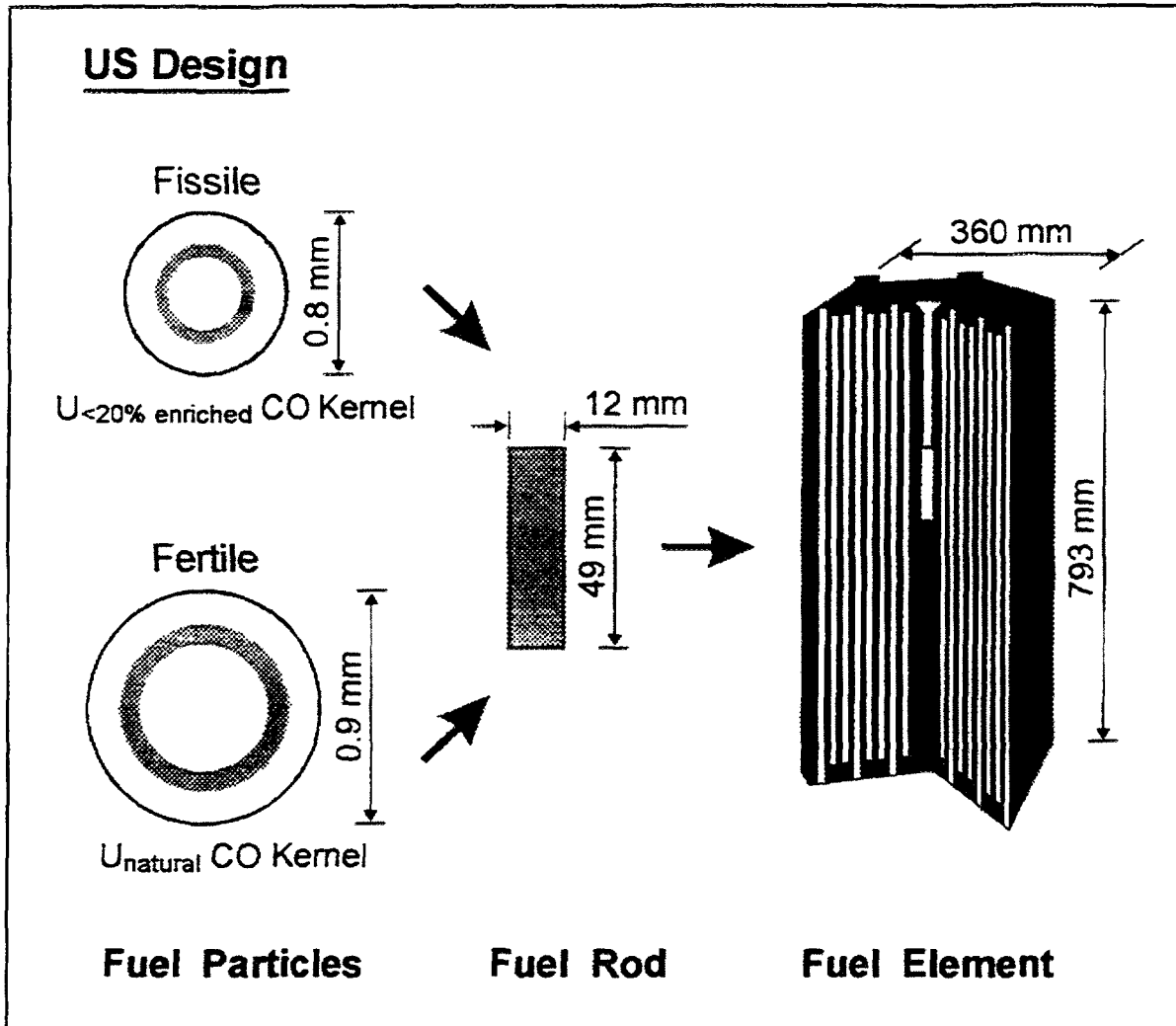


Fig. 2-2: US reference design for fuel particles and fuel element

coatings. Finally, the TRISO coated thorium particles were replaced by natural uranium oxy-carbide kernels, surrounded by TRISO coatings. Fig. 2-2 gives the US reference design for fuel particles and fuel elements [7].

The reference coated particle design in Japan for the first HTTR core has been completed using low enriched (3.3 - 9.9 %, average 6 %) UO₂ fuel (Fig. 2-3). The TRISO particle has a kernel diameter of 600 μm and layer thicknesses of 60 μm for buffer, 30 μm for the inner PyC, 25-35 μm for SiC, and 45 μm for the outer PyC. The main differences compared to the FRG and the US design are a larger particle kernel and a thinner buffer layer. The burnup design limit for the HTTR reference fuel is as low as 3.6 %FIMA. For the HTTR second core, efforts are being put into the development of "advanced fuel" covering the improvement of the fabrication process, the optimization of the particle design, for instance a smaller kernel and thicker buffer and SiC layers to allow for a higher burnup, and the development of a ZrC coating [8].

The reference particle design in the Russian Federation for its version of a 200-250 MW(th) small modular HTGR, called VGM, consists of a TRISO coated particle with a 500 μm LEU UO₂ particle kernel with 8 % (values range between 6.5 and 10.0 %) enriched uranium, a 90 - 100 μm buffer layer, a 70 - 80 μm inner PyC layer, a 60 μm SiC layer

Japanese Design

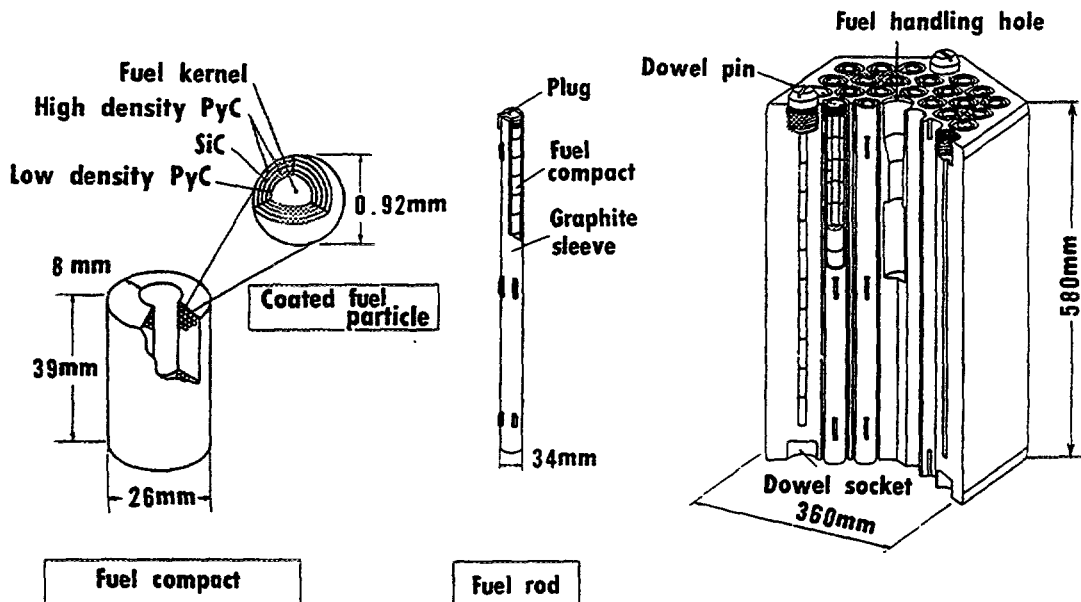


Fig. 2-3: Japanese reference design for fuel particles and fuel element

and a $60 \mu\text{m}$ outer PyC layer. The burnup design limit is 80 GWd/t corresponding to $8.8 \% \text{FIMA}$. There is a broad experience in reactor experiments with Russian fuel even under large reactivity transients. Fuel has been tested so far in the temperature range $800\text{-}1600^\circ\text{C}$ up to 625 effective full power days (efpd) with maximum burnups of $10\text{-}15 \% \text{FIMA}$ and neutron fluences up to $2.3 \times 10^{25} \text{ m}^{-2}$, $E > 29 \text{ fJ}$ [9]. (The very high temperatures, e.g., 1600°C , were carried out in postirradiation heating tests.)

Also in the Institute for Nuclear Energy Technology (INET, Tsinghua University, Beijing) R&D program in China for an HTR fuel element to be inserted in the 10 MW(th) HTR Test Modul, TRISO coated fuel particles have been manufactured with the following nominal geometrical data with only a small difference compared to the design data given in Table 2-1: $501 \mu\text{m}$ kernel diameter, and layer thicknesses of $92 \mu\text{m}$ for buffer, $39 \mu\text{m}$ for the inner PyC, $36 \mu\text{m}$ for SiC and $34 \mu\text{m}$ for the outer PyC [10]. The fuel loading is 5 g uranium per fuel ball with an enrichment of 17% . Preliminary operational design data are a maximum burnup of about $88,000 \text{ MWd/t}$ ($\approx 9.6 \% \text{FIMA}$), a fast neutron fluence up to $1.0 \times 10^{25} \text{ m}^{-2}$ with a maximum fuel temperature of $830\text{-}860^\circ\text{C}$. At present, particles produced on a laboratory scale were irradiated with burnups $< 1 \% \text{FIMA}$ [11].

As can be seen above, **BISO** coated fuel particles are no longer a part of any country's HTGR fuel reference design. BISO fuel was used in the real-time operating German HTGRs AVR and THTR-300 as well as the US Peach Bottom HTGR, all of which have terminated their operation in the meantime. In Japan, BISO coated fuel particles are also used in experimental investigations. For former reactor designs which used BISO fuel

(HTTR-300, AVR), the fraction of free uranium in the active core differ from those of TRISO particles. In contrast to TRISO particles, the manufacturing process of BISO fuel introduces a high heavy metal contamination fraction into the matrix graphite (3×10^{-4}) and into the HTI layer of the BISO coating (9×10^{-4}) due to high deposition temperatures > 2000 °C [12]. On the other hand, there are almost no particle defects due to TRISO fuel manufacture ($< 10^{-4}$), significantly lower than the design limit specification of 6×10^{-4} .

Characteristic data on each country's coated particle reference design are summarized in Table 2-1.

2.2. FUEL ELEMENT

Two main fuel element concepts are presently in use, the spherical fuel element and the block-type fuel element.

The FRG fuel element design (Fig. 2-1) is a graphite sphere with a diameter of 60 mm. The reference fuel sphere contains approximately 11,000 TRISO coated fissile particles. The particles are overcoated with an A3 matrix graphite layer with a thickness of ≈ 200 μm to prevent direct contact of the particles and then embedded in the same A3 matrix graphite material. The outermost 5 mm of the fuel sphere is a shell of matrix graphite only without any particles. The heavy metal loading of the reference fuel element is 0.5 g fissile (U-235) and 6.5 g fertile (U-238) material. The active core of the German 200 MW(th) HTR-Module consists of about 360,000 spherical fuel elements.

The US fuel element design (Fig. 2-2) is a hexagonal graphite block (793 mm in length and 360 mm wide across the flat surface) of the type H-451 containing 102 coolant channels (diameter 15.9 mm) and 210 fuel holes which are filled with fuel compacts (formerly referred to as rods) and sealed. The fuel compacts (diameter 12 mm) are a mixture of TRISO coated fissile and fertile particles and graphite shim particles bonded by a carbonaceous matrix. A small radial gap of 0.13 mm exists between the fuel compact and the fuel hole. The active core of the 350 MW(th) steam-cycle MHTGR consists of 660 graphite fuel elements, and the core of the 600 MW(th) direct-cycle GT-MHR consists of 1020 elements stacked 10 element high columns arranged in an annular core.

Japan's fuel design (Fig. 2-3) consists of block-type fuel, similar to the previous Dragon Project "pin-in-block" design. Each hexagonal graphite block (580 mm in length and 360 mm wide across the flat surface) has 31 or 33 fuel holes, each containing an annular fuel pin (inner diameter 26.25 mm, outer diameter 34 mm) which consists of 14 fuel compacts in a graphite sleeve. Fuel element block and fuel pin sleeve consist of the graphite IG-110. A fuel compact made of graphite matrix powder with the shape of an annular cylinder (39 mm tall, inner diameter 10 mm, outer diameter 26 mm) contains 13,500 TRISO coated fissile particles which are overcoated similar to the German design. The coolant flows through a gap between fuel rod and fuel hole. The HTTR active core is composed of about 70,000 fuel compacts.

The Russian Federation has also chosen spherical fuel elements with 60 mm diameter including a 5 mm fuel-free graphite shell as reference design for the 200 MW(th) HTGR of modular type, called VGM. The main components of the matrix material are the

Table 2-1: HTGR reference TRISO fuel design data

	FRG	US		Japan	USSR	China
Kernel						
Composition	UO ₂	Fissile	Fertile			
Diameter [μm]	500	350	500	600	500	500
Enrichment [%]	10.6	19.9	natural	3.4 - 9.9	8.0 ⁽²⁾	17.0
Heavy metal loading per compact or sphere [g]	7			13.5	7.0 ⁽²⁾	5
Coating thickness [μm]						
Buffer	95	100	65	60	90-100	90
Inner PyC	40	35	35	30	70-80	40
Silicon carbide	35	35	35	25 ⁽¹⁾	60	35
Outer PyC	40	40	40	45	60	40
Protective overcoating	≈ 200	-	-	≈ 200		≈ 200
Fuel element						
Type	Sphere	Block		Block	Sphere	Sphere
Graphite grade	A3-3	H-451		IG-110	30PG MPG-6	Chinese graphite
No. of coated particles per compact or sphere	≈ 11,000	≈ 6,500	≈ 3,700	≈ 13,500	13,000 - 16,000 ⁽²⁾	8,300

Table 2-1: HTGR reference TRISO fuel design data (continued)

	FRG	US		Japan	USSR	China
		Fissile	Fertile			
Volume packing fraction [%]	10		51	30	12 - 15 ⁽²⁾	4
Design limits						
Temperature [°C]	1250		700-1250	1495	1400 ⁽²⁾	1000
Burnup [% FIMA]	8-10	≤ 26	≤ 7	3.6	8.8 ⁽²⁾	11.0
Neutron fluence [10^{25} m^{-2} , E>16 fJ]	2-3		4.5 (E>29 fJ)	1.3 (E>29 fJ)	3.0 ⁽²⁾	1.0

(1) Specification value for 1st HTTR core, actual value is 25-35 μm

(2) Specification value for VGM reactor

artificial graphites on the basis of calcinated (30PG) or uncalcinated (MPG-6) graphite. Its active core is planned to be composed of about 350,000 fuel elements.

The design of the fuel element in **China** is similar to the German one. The reference fuel element for the HTR-10 contains 8,300 TRISO coated particles. Pre-irradiation properties of the fuel element produced on the laboratory scale have reached the design specification. Commissioning of the prototype scale production will be started at the beginning of 1997. Irradiation qualification is scheduled to start about one year later. 27,000 fuel elements will be produced for the first core of the HTR-10 at the end of 1998.

2.3. FUEL QUALITY DURING MANUFACTURE

The as-manufactured quality of HTGR fuel is expressed in terms of the fraction of accessible or free uranium; this includes the uranium present as heavy metal contamination outside particles with intact SiC layers and the uranium in particles whose kernels are exposed, i.e. particles in which all coating layers are fractured or permeable.

The large-scale production experience in the **FRG** has led to a high quality spherical fuel element with a mean defect fraction of 3×10^{-5} (102 detected defects out of 3.3 millions coated particles) [13]. This corresponds - in the average - to only one defective particle every 2 - 3 fuel elements. Almost all free uranium found by the burn-leach technique can be attributed to defective particles, i.e. particles with exposed kernels [14]. Only traces of natural uranium are found as heavy metal contamination of the matrix graphite, close to the detection limit of around 10^{-6} . Thus the free uranium is less than the upper design limit of 6×10^{-5} guaranteed by the former German manufacturing company HOBEG. A fissile uranium fraction of 1×10^{-7} has been assumed in KFA safety analyses calculations for the HTR-Module fuel elements. A design limit for the heavy metal contamination was set at 50 μg per ball [15] corresponding to a fraction of about 7×10^{-7} .

For **Japan**'s fuel, a mass scale production on the order of 200 kg uranium per year started in 1983, and is planned to be doubled in 1992 for HTTR fuel production. The fraction of particles with a defective SiC layer in a fuel element expressing the quality of the fabricated fuel has been measured to be on the order of 5×10^{-4} [16]. Modified fabrication methods could even reduce this fraction to 3.9×10^{-6} [17]. The heavy metal contamination in the fuel compacts was found to be around 3×10^{-5} . It could also be reduced by almost one order of magnitude when using an improved fabrication process. Compared to these values, the regulatory requirement for the total amount of free uranium of $< 2 \times 10^{-3}$ includes a large safety margin. This upper limit has been defined with respect to the maximum allowable radiation exposure of the public. The expected free uranium fraction, however, is 5.5×10^{-4} .

US fuel manufacturing and quality control methods [18] consider manufacturing defects of individual coating layers. A different modeling approach is assumed for particles with excessive heavy metal dispersion, for those with missing inner PyC layers, for those with initially defective SiC layers, for those with missing buffer layers, and for those with missing or initially failed outer PyC layers, with the sum of each fraction giving the total fraction of particles with manufacturing defects. The determination of the fraction of particles with specific defects is strongly dependent on the experimental techniques to measure them. The burn-leach technique is used for measurement of both the heavy metal

contamination and the fraction of particles with failed SiC coating, in total the fraction of "free" uranium. A wet chemical technique is used to measure the uranium content outside particles with an intact outer PyC layer which is treated as heavy metal contamination. US specification limits are 1×10^{-5} for the heavy metal contamination in the fuel compact matrix material and 5×10^{-5} for the fraction of particles with a defective SiC layer [19], which is equal to the HOBEG burn-leach specification of 6×10^{-5} .

Data characterizing the required as-manufactured quality of the **Russian Federation's** modular HTGR fuel are for the VGM: a U-235 contamination of 4×10^{-6} and a fraction of defective coated particles of $< 10^{-4}$ [20]. Besides their "traditional" technology for fuel manufacture, the former USSR has developed a second one using a pyrocarbon binder which is said to provide better mechanical properties. The Russian fuel production is on a laboratory scale so far.

The manufacturing process for spherical fuel elements in **China** is also adopted from the German procedure but uses Chinese natural graphite. The fraction of free uranium is surprisingly low at 4×10^{-6} [10]. Particle and fuel production is still on a laboratory scale.

2.3.1. The Chinese Program

An R&D program of the HTGR fuel element has been set up at INET, Tsinghua University. The main aim of the program is to develop the manufacture and qualification technology of the HTGR fuel element in general and to manufacture fuel elements for the Chinese experimental reactor HTR-10 in particular. In the following, the R&D of HTGR fuel element in China is briefly introduced.

2.3.1.1. Design Specifications of the HTR-10 Fuel Element

The HTR-10 experimental reactor uses spherical fuel elements. The main specifications of the fuel element and the coated fuel particle are given in Tables 2-2 and 2-3, respectively.

2.3.1.2. Manufacture Technology

Manufacture of the HTGR fuel element includes kernel preparation, coating applying and spherical fuel element fabrication. The kernel is prepared by modified external gelation method. On the basis of conventional external gelation technology, a small amount of internal gelation reagent, HMTA², is added into the sol. The gelation process is thus modified and the structure of the gel sphere (finally the quality of the UO₂ micro-spheres) is improved. The gel sphere is aged over night at room temperature, washed with demineral water, calcinated at 500 °C, reduced at 900 °C, and sintered at 1500 °C. The kernel obtained is classified and inspected according to the specification set, then released for coating.

Coating is carried out in a 2 inch fluidized bed (a 6 inch fluidized bed will be used for production). The buffer layer is coated at a temperature of 1100 - 1400 °C, the coating gas is C₂H₂. Ar is used as the carrying and dilute gas. The inner pyrolytic carbon layer is coated at 1370 - 1420 °C, the carbon source is C₃H₆. Dilute and carrying gas is Ar.

² HMTA = Hexamethylenetetramine

Table 2-2: Specifications of the HTR-10 fuel element

Spherical fuel element	Design value	Experimental value
Diameter [mm]	60 – 0.2	60 – 0.2
Uranium load [g/fuel element]	5.0 ± 0.1	-
Density of graphite matrix [g/cm ³]	1.75 ± 0.02	1.73
Chemical composition [ppm]		
Total ash	≤ 300	130 - 190
Lithium	≤ 0.3	0.007 - 0.023
Boron equivalent	≤ 3.0	0.15
Thermal conductivity of matrix [W/(m K) at 1273 K]	≥ 25	≤ 30
Corrosion rate [mg/(cm ² h) at 1273 K, 1 Vol% H ₂ O, He]	≤ 1.3	1.1
Erosion rate [mg/h]	≤ 6	5.7
Crushing strength [kN]	≥ 18	18.8
Drop strength [times, 4 m, pebble bed]	≥ 50	440 - 739
Anisotropy a _⊥ / a	≤ 1.3	1.29
Free uranium	≤ 5.0*10 ⁻⁴	-

SiC layer is coated at a temperature of 1500 - 1570 °C, MTS³ is used as the source for Si and C. Ar and H₂ are used as the dilute and carrying gas, the ratio of Ar / H₂ is 1. The coating parameter for the outer PyC layer is the same as for the inner PyC layer. The coated fuel particles are first classified and inspected before being released for spherical fuel element fabrication.

The spherical fuel element is formed in a rubber mould, i.e. under quasi-isostatical pressing condition. The forming pressure for the fuel zone pre-pressing is 30 MPa. For spherical fuel element final pressing, the forming pressure is 300 MPa. After forming, the spherical fuel element is first carbonized at a temperature of 800 °C, then is heat-treated at 1950 °C to improve the corrosion resistant performance during the service. The detail flow sheet of the manufacture process is shown in Figs. 2-4 to 2-6. The uranium load per element is actually controlled by the coating and overcoating process.

The results of laboratory scale R&D are given in Tables 2-2 and 2-3. Prototype scale is now phasing in. There may be some change in parameters, however, no significant change on the manufacture and qualification technology is foreseen.

³ MTS = Methyltrichlorosilane (CH₃SiCl₃)

Table 2-3: Specifications of the coated fuel particle in the HTR-10 fuel element

Coated fuel particle	Design value	Experimental value
KERNEL		
Material	UO ₂	UO ₂
O / U	< 2.01	
Density [g/cm ³]	> 10.4	10.83
Diameter [μm]	500	501
Standard deviation [μm]	25	10.2
d _{max} / d _{min} > 1.2	$\leq 1.0 \times 10^{-2}$	$\leq 0.75 \times 10^{-2}$
Odd shaped particles	$\leq 1.0 \times 10^{-4}$	$\leq 1.0 \times 10^{-4}$
BUFFER LAYER		
Thickness [μm]	90	90.2
Standard deviation [μm]	18	4.4
Density [g/cm ³]	≤ 1.1	1.02
Standard deviation [g/cm ³]	-	0.03
INNER PYROLYtic LTI CARBON LAYER		
Thickness [μm]	40 ± 10	39.6 ± 2.8
Density [g/cm ³]	1.9 ± 0.1	1.86 ± 0.06
Anisotropic factor (BAF)	≤ 1.1	< 1.02
PYROLYtic SILICON CARBIDE LAYER		
Thickness [μm]	35 ± 4	35 ± 2.6
Density [g/cm ³]	≥ 3.18	3.21 ± 0.02
OUTER PYROLYtic LTI CARBON LAYER		
Thickness [μm]	40 ± 10	42 ± 3.0
Density [g/cm ³]	1.9 ± 0.1	1.87 ± 0.02
Anisotropic factor (BAF)	≤ 1.1	1.01 ± 0.01

2.3.1.3. Pre-Irradiation Characterization and Inspection

A comprehensive **pre-irradiation** characterization program is carried out. Characterization methods for all items specified in the design specification have been developed, often several characterization methods for some important items. The necessary equipment has been installed. The main aim is to determine the properties of the fuel element manufactured to see if the design specification is fulfilled or not. Pre-irradiation characte-

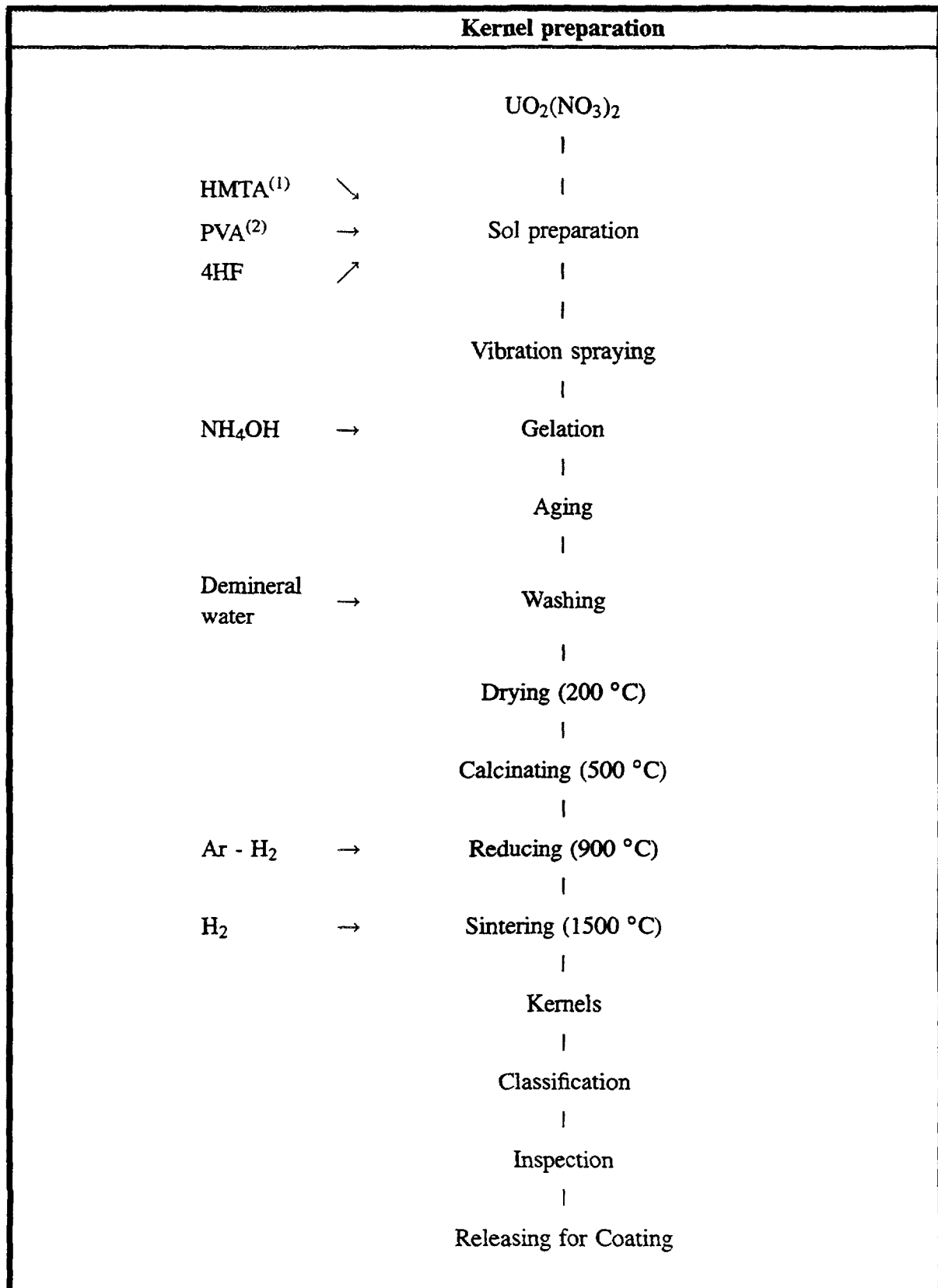


Fig. 2-4: Flow sheet for the process of kernel preparation

(1) HMTA = Hexamethylenetetramine

(2) PVA = Polyvinylalcohol

Coating the kernels

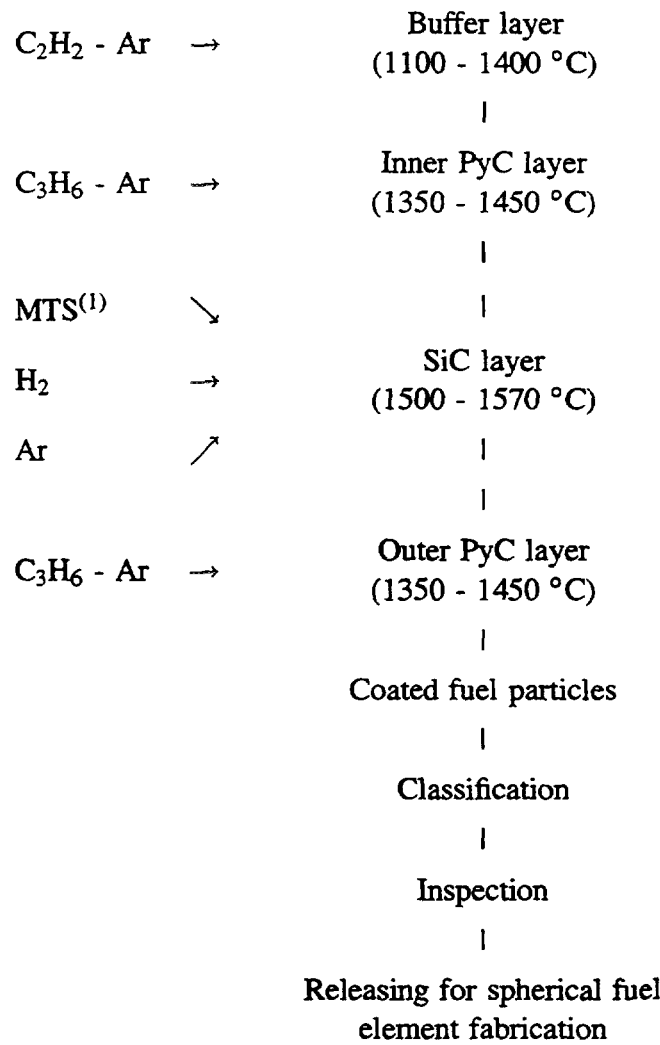


Fig. 2-5: Flow sheet for the process of kernel coating

(1) MTS = Methyltrichlorosilane (CH_3SiCl_3)

rization is not restricted only to the items listed in the design specification, for example, the observation and examination of the microstructure of the coating layers is also carried out routinely.

SiC is the key component of the coatings, the quality of SiC is vital to the performance of TRISO coated fuel particles in service. However, only three parameters, i.e. density, thickness, and standard deviation of thickness, have been specified for this layer. According to the literature, SiC coatings that have the same value for these parameters may behave differently under irradiation. There must be some properties which play an important role and have not been clarified up to now. Under the auspices of the International Atomic Energy Agency, an effort to clarify the problem is being carried out [21]. Samples of

Manufacturing of spherical fuel element

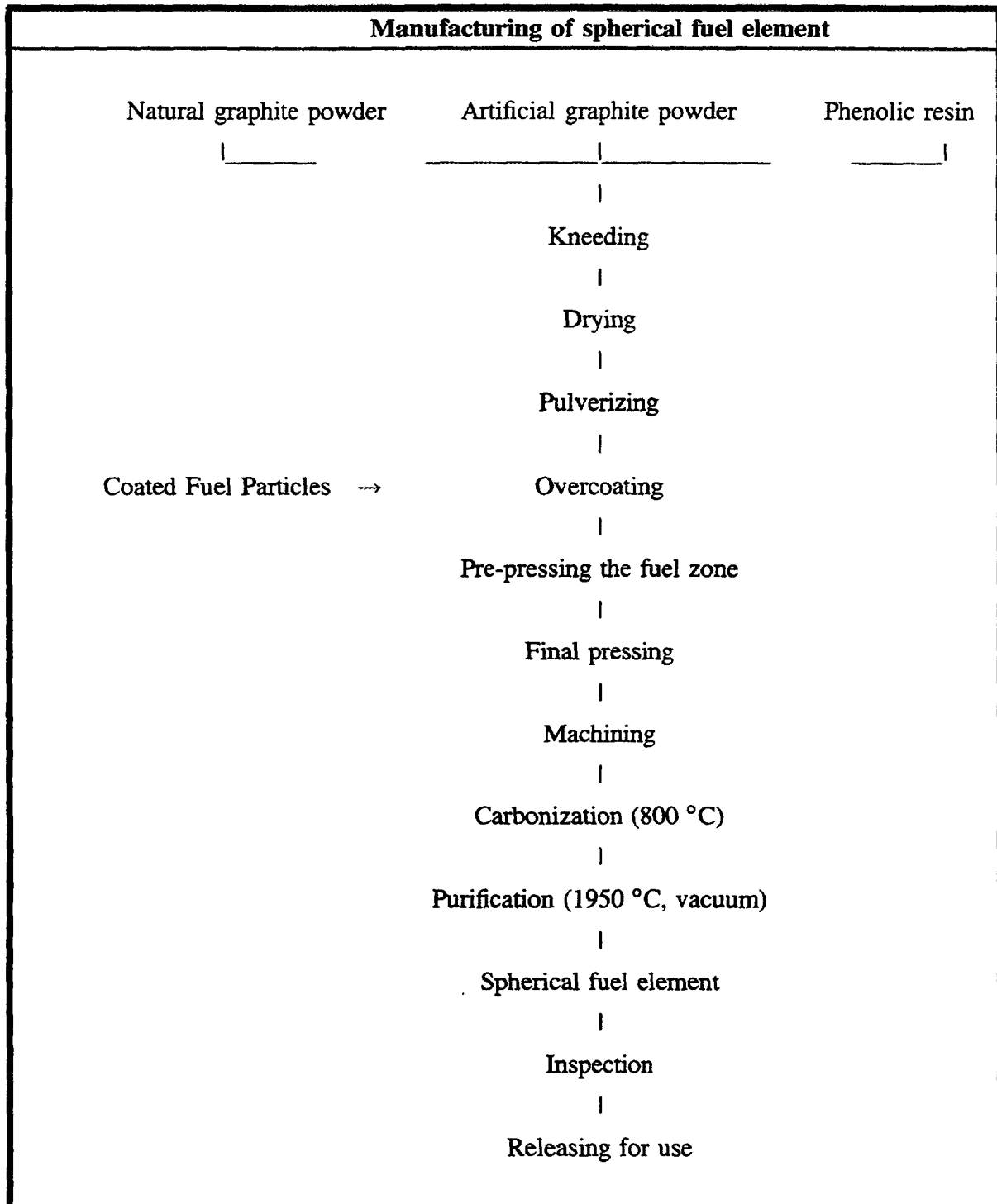


Fig. 2-6: Flow sheet for the process of spherical fuel element manufacturing

SiC have been prepared at temperatures ranged from 1450 to 1650 °C with a step of 50 °C. The contamination of the SiC layer was determined, the microstructure of SiC deposited was observed and the mechanic properties (tensile strength, Weibull parameter and Young's modulus) were measured. The preliminary evaluation shows that the density of SiC measured by sink-float method has to be used carefully, because it may give wrong information if SiC has a porous structure; the SiC may be contaminated under certain

circumstances (see section 2.3.1.4.3.). This may play a role on the uncertainty of the irradiation behavior of TRISO coated particles having the same values determined for the three specified parameters.

2.3.1.4. Strength and Young's Modulus of Pyrolytic SiC Coatings

Not only does nuclear fission release a huge amount of energy, it also produces lots of radioactive fission products. To prevent these radioactive products from being released into the primary circuit and from there into the environment to harm the staff and the public, they should be confined as fully as possible in the place where they are produced. In HTGRs, the basic unit which confines fission products is the coated fuel particle. Soon after the success of R&D of BISO coated particles, it was found that the pyrolytic carbon coating is not so effective in retaining solid fission products, e.g. Cs, Sr, Ba, and Ag as in retaining gaseous fission products, e.g. Kr and Xe. This shortcoming of pyrolytic carbon becomes especially serious when the fuel cycle changes from HEU to LEU; the operation temperature is raised to increase the efficiency of using fission energy, e.g., to utilize HTGRs for high temperature process heat application and direct-cycle helium turbine; and the burnup is increased to improve the efficiency of fuel utilization. Furthermore, under high temperature and high burnup, high density pyrolytic carbon will lose its mechanical stability through irradiation and thermally induced creep. Therefore people search for new coating materials to fortify the pyrolytic carbon coating. SiC is an ideal material because of its low thermal neutron cross section, high retention ability for solid fission products, good irradiation stability, high thermal conductivity, high strength, and no thermal creep up to 1900 °C. Since the first success in producing SiC coating more than 30 years ago [22], it continues to attract scientists and engineers who devote their effort in R&D of HTGR fuel. To overcome the shortcoming of high brittleness of SiC, it is embedded in the high dense pyrolytic carbon coating, and particles of this kind are called TRISO coated particles in distinguishing from BISO particles which are coated with pyrolytic carbon only. Great success of TRISO coated particles in irradiation tests and in reactor service makes it a standard fuel for future HTGRs [23].

TRISO coated particles have been chosen for the fuel element of the Chinese HTR-10 reactor [24, 25] and an R&D program for the HTGR fuel element is being carried out. In this chapter, the investigation of the effect of deposition temperature on strength and Young's modulus of the SiC is reported [26, 27].

2.3.1.4.1. Deposition of SiC Coating

Deposition of SiC coating was carried out in a 2" fluidized bed. A schematical diagram of the coater is shown in Fig. 2-7. The procedure of SiC coating was as follows: the fluidized bed was heated under flowing Ar up to the temperature set for the experiment. Particles which had already been coated with a buffer layer and an inner dense PyC layer were loaded into the fluidized bed. The gas flow rate was adjusted to optimize the fluidization state. MTS was introduced into the fluidized bed which decomposed and formed SiC. The SiC deposited onto the substrate for the time set. After deposition, the fluidized bed was cooled down under flowing Ar to temperatures lower than the threshold of oxidation temperature of graphite. The Ar flow was switched off, the fluidized bed was

cooled further down to room temperature, then the coated particles were unloaded.

The temperature range studied was from 1450 to 1650 °C, the temperature increment was 50 °C. MTS is the source of Si and C for the formation of SiC. It was metered in by heating the MTS container to the temperature set in a thermostat, H₂ combines with the pyrolytically produced chlorine from MTS and it suppresses the formation of free carbon. It was also used to sweep the MTS vapor into the main stream of the coating gas. Fig. 2-8 is a schematic diagram of MTS supply system. The concentration of MTS was adjusted by changing the temperature of the thermostat and/or the flowrate of the sweep gas. The amount of MTS metered in was predicted by MTS vapor pressure at the temperature set and the sweep gas flow rate, and checked by weighing the MTS before and after the coating process. In the present work, the concentration of MTS was kept at about 1 %. Other parameters of deposition were the following:

Particle loading	80 g
Ar / H ₂ ratio	1 : 1
MTS / H ₂ ratio	1 : 50
Total gas flow rate	500 l/h

2.3.1.4.2. Effect of Deposition Temperature on Strength and Young's Modulus of Deposited SiC

Strength and Young's modulus are very important parameters of SiC, especially in TRISO coated particles. The SiC coating is assumed to be the only layer which confines the fission products and fuel [28], therefore the mechanical performance of TRISO particles will be very much dependent on these parameters. They are indispensable input data for coated particle design and also serve as important **characterization parameters** in quality control during production of coated particles. Instruments for determining these parameters have been developed and manufactured [29] according to the principle of the brittle ring test developed at KFA Juelich, Germany [30, 31]. The sample was manually prepared by a metallographic method, the sampling size was equal to or greater than 30 rings for each deposition temperature. The results are given in Table 2-4.

2.3.1.4.3. Discussion and Conclusions

The **density of the SiC** deposited is shown in Fig. 2-9. It can be seen from the table and the figure that the strength of SiC increases with increase of the density, except for the SiC deposited at 1450 °C, which has a high density and a low strength. However, one can see from Fig. 2-9 that the trend of the density curve is abnormal. From SEM observations (Figs. 2-10 and 2-11) and common knowledge, the density of SiC deposited at 1450 °C should be lower than the one deposited at 1500 °C. The density measurement was repeated three times, the result remained the same. The reason for this abnormal phenomenon is not clearly known yet. One explanation is that the density was measured by titration method; the SiC has a porous structure, the pores are interconnected and open

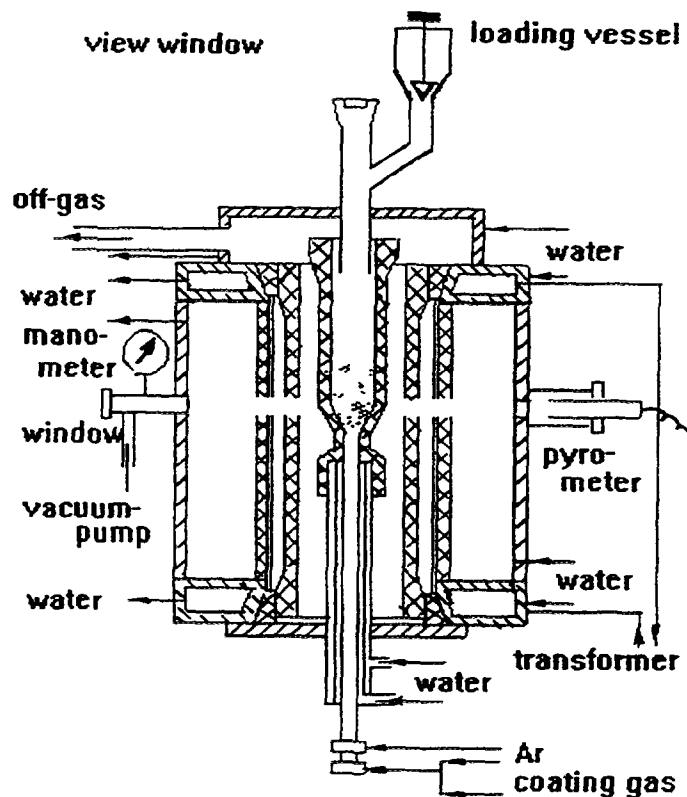


Fig. 2-7: Schematical diagram of the 2" fluidized bed

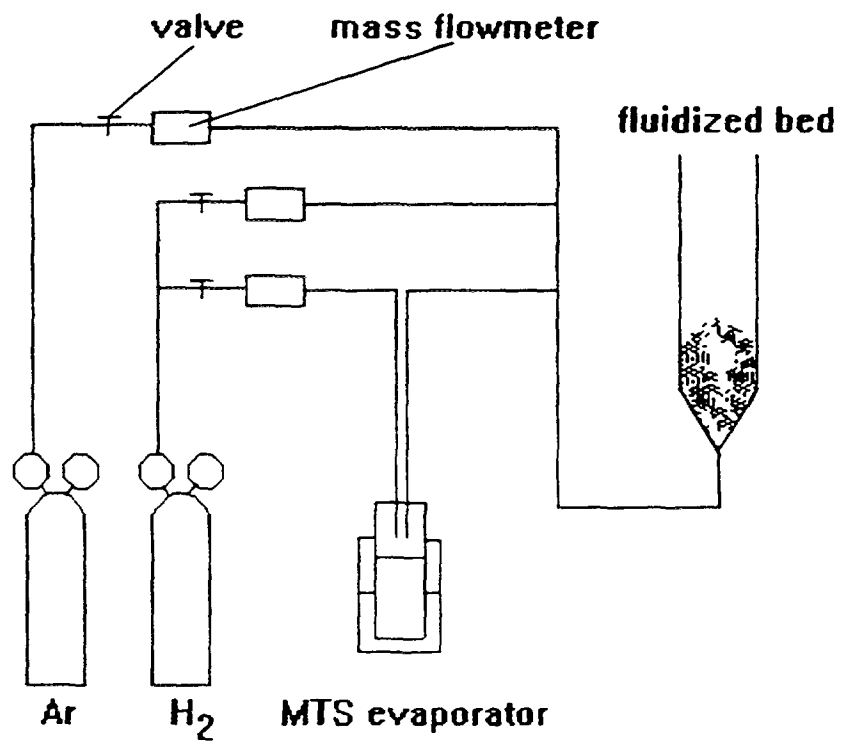


Fig. 2-8: Schematical diagram of MTS supply system

Table 2-4: Results of SiC strength and Young's Modulus measurements

Parameter	Temperature [°C]				
	1450	1500	1550	1600	1650
Strength [MPa]					
Average σ	670	1285	1447	736	693
Standard deviation s	146	223	269	153	214
s / σ [%]	22	17	19	21	31
Weibull parameter m	5.4	6.4	6.6	5.8	4.1
Young's modulus [GPa]					
Average E	392	455	422	330	330
Standard deviation s	188	107	111	172	118
s / E [%]	48	24	26	52	36

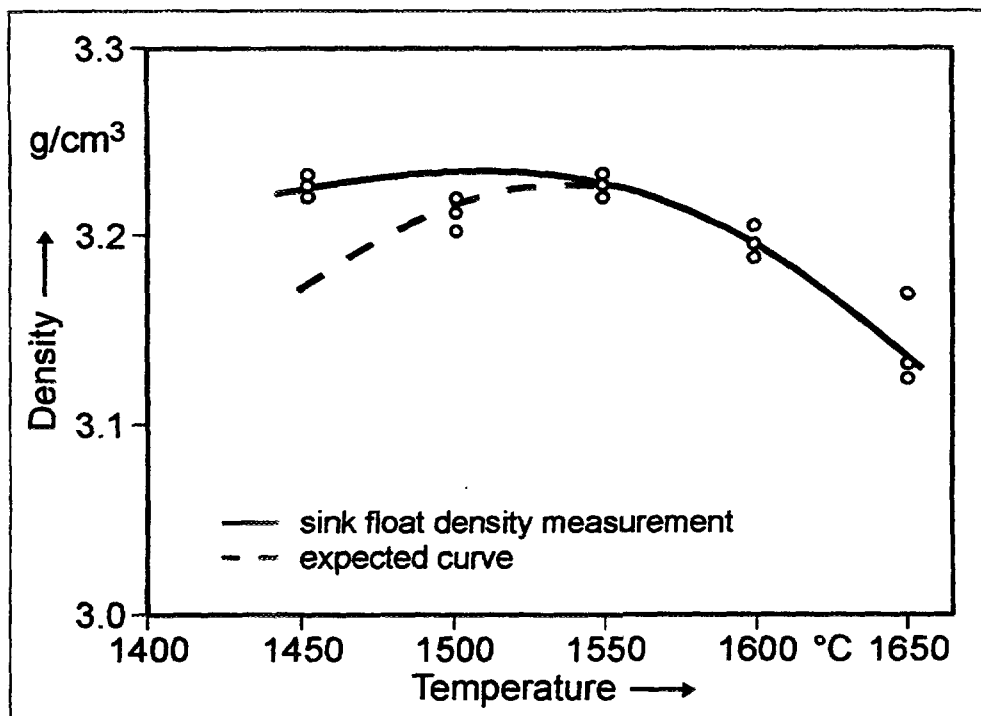


Fig. 2-9: Effect of temperature on the density of deposited SiC

to the outside; the titration liquid penetrates the pores; therefore, instead of the apparent density, the true density is measured, the apparent density of the SiC is actually lower than the one deposited at 1500 °C.

The measured data of **SiC strength** and **Young's modulus** conform quite well with the SEM observations of the SiC structure. The surface morphology and the fracture structure

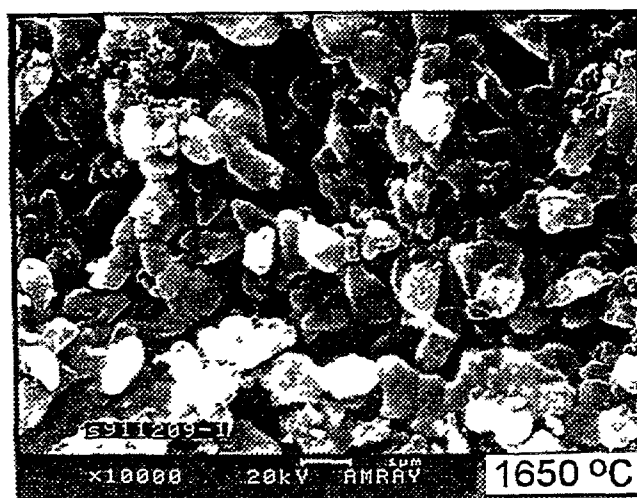
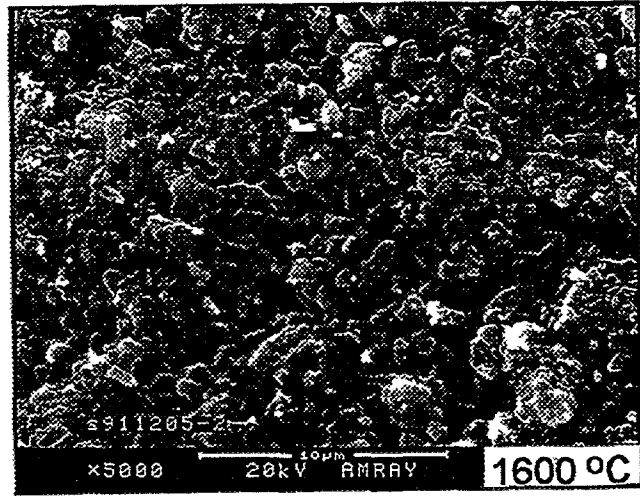
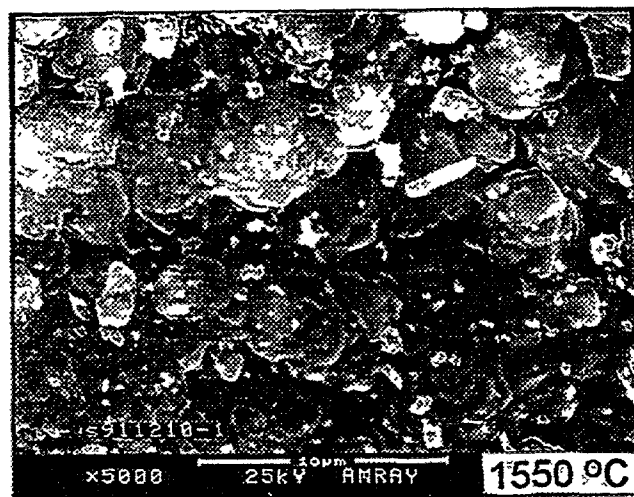
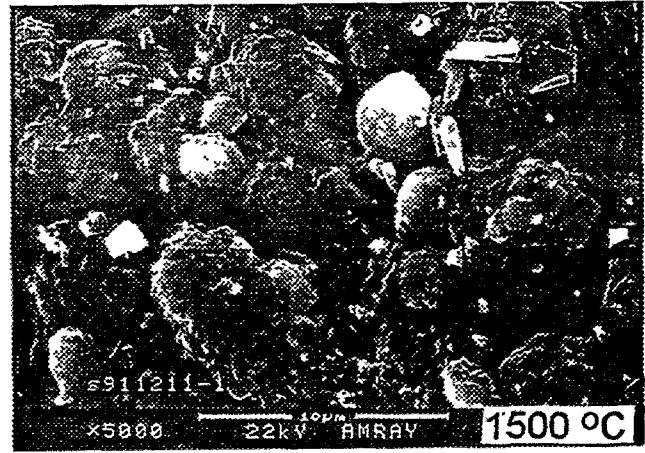
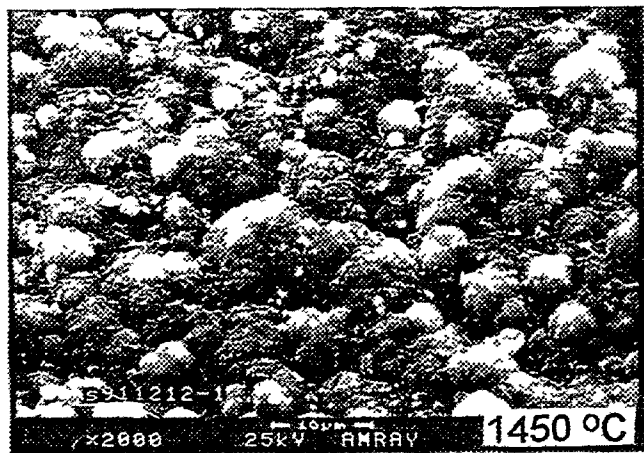


Fig. 2-10: Effect of temperature on the surface morphology of deposited SiC

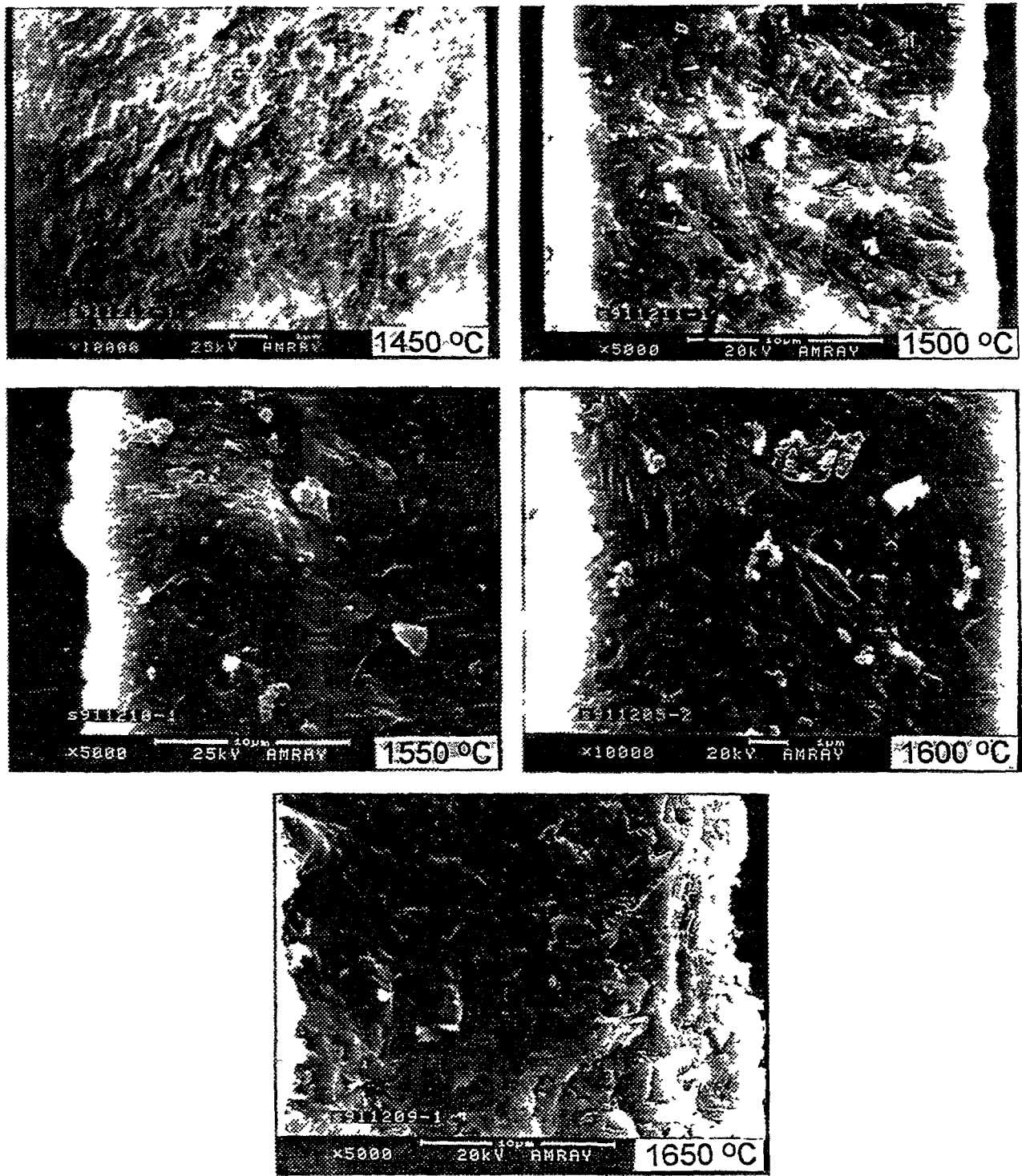


Fig. 2-11: Effect of temperature on the fracture surface structure of deposited SiC

of SiC are shown in Fig. 2-10 and 2-11. It can be seen from the figures that the surface morphology and the fracture structure change remarkably with the change of the deposition temperature. The rougher the surface, the lower the strength and Young's modulus; the more homogeneous the fracture structure, the higher the strength and Young's modulus.

To maximize strength and Young's modulus, the deposition temperature should be kept in the range between 1500 and 1550 °C.

The measured results are comparable with the data published in references [30] and [31].

2.3.2. The German Program

In Germany, the low-enriched (LEU) open fuel cycle with TRISO coated UO₂ fuel particles was adopted as the reference in 1980. The coating design was taken over from the preceding developments for high-enriched (Th,U)O₂ fuel kernels. In contrast to the BISO particles of the THTR type, coated exclusively with pyrolytic carbon, the (much lower) release of fission products from fuel elements with TRISO particles is predominantly determined by defective particles and only to a slight extent by the heavy metal contamination of the matrix material. A comprehensive characterization study on silicon carbide has been conducted at the Research Center Jülich [32].

Defective/failed TRISO coatings may originate during fabrication ("defects"), during normal operation and as a result of accident conditions ("coating failure" if it results from in-pile operation or from accidents). In the present contribution, the **fabrication-related defective particle fractions** in the HTGR reference element will be statistically determined and evaluated on the basis of quality control measurements by the manufacturer. Furthermore, the fissile material contamination of the outer coating and the matrix material is to be estimated to provide a complete data set for the fabrication-related source terms of fission product release.

Figures for failed particle fractions arising during operation as a result of temperature, burnup and neutron fluence in the reactor core are derived from a series of irradiation experiments with representative fuel elements. The essential aim of these investigations is to determine a statistically supported expected and design value for the operationally induced particle defect and failure fraction in the HTGR core.

Manufacture of HTGR fuel elements results in the following three fission product sources:

- particles with defective TRISO coatings,
- uranium contamination of the outer pyrocarbon layer,
- uranium and thorium contamination of the matrix material.

Defective particles may arise during the semi-isostatic cold pressing of spherical fuel elements, when the fragile TRISO particles embedded in the matrix material experience mechanical contact in spite of their protective overcoating. This primarily effects particles with inadequate overcoating or particles with considerable deviations from spherical geometry.

The uranium contamination of the outer PyC layer originates from the coating process in the fluidized bed furnace. During pyrolytic deposition, contamination of the furnace internals and the fluidized bed atmosphere are incorporated into this coating.

The uranium and thorium contamination of the matrix material are largely caused by raw material impurities in the natural graphite used. This involves natural uranium with 0.7 % enrichment. The uranium contamination of the outer pyrocarbon layer also contributes slightly since, during the final high-temperature treatment of the fuel elements at 1950 °C, approximately 30 % of the outer PyC layer contamination enters the matrix.

2.3.2.1. Manufacturing Defects

As part of the specified quality control, fabrication-related composite defects are measured by the **burn-leach test**. In this test, the fuel element matrix – including the accessible pyrocarbon layers – is burned at 850 °C. The residue – including particles without the outer PyC layer – is treated with nitric acid at 95 °C and the uranium content of the acid is determined by fluorimetry. Intact SiC layers are not attacked by this process. This method thus covers the total uranium quantity in the matrix material, the outer PyC layers and the kernels and PyC layers within defective SiC coatings.⁴

Most of the measured free uranium values of representative fuel elements with TRISO particles are below the measuring limit which is about two orders of magnitude smaller than the contribution of a single particle. The few measured values above the measuring limit correspond to one or several times the inventory of a single particle (Fig. 2-12). Accordingly, the results of the burn-leach test can be expressed in terms of an integer number of fabrication-related defective particles for the production of AVR fuel elements with LEU UO₂ TRISO particles and for the test elements of the generic LEU irradiation program with test HFR-K3 and the HTR MODUL reference irradiation experiments HFR-K5 and HFR-K6 (“Proof Tests”).

Table 2-5 shows the results of the major German UO₂ manufacturing campaigns in the 1980s. Measured free uranium fractions are between $8 \cdot 10^{-6}$ and $51 \cdot 10^{-6}$. The values for manufacture from 1985 onwards are about a factor of five lower than the previous results. This improvement in quality was by automating the particle overcoating technology.

The pre-1985 production runs show a mean value of 0.64 defective particles per fuel element, the post-1985 productions a mean value of 0.12 defective particles per fuel element. The production before 1985 is significantly different from that after 1985. On the other hand, the results of AVR 21-2 and HFR-K5/6 (“**proof tests**”) do not differ significantly from each other so that they may be combined. The comparison of particle defects between the older and newer production runs is shown in Fig. 2-13 whereby the prediction for 2, 3, 4, 5 etc. particle defects are more than an order of magnitude lower in the newer fuel due to the automated overcoating.

⁴ The uranium fraction within defective SiC layers and outside all the SiC layers is termed “free uranium” in the German program, termed “contamination” in the US HTGR program, and termed “tramp uranium” in the US LWR industry.

Table 2-5: Defective particles in spherical TRISO fuel elements of the German program

Production → Year →	AVR 19 1981	AVR 21-1 1983	AVR 21-2 1985	Proof Tests 1988
Number of fuel elements manufactured	24,600	20,500	14,000	150
Number of batches ⁽¹⁾	65	54	29	8
Number of particles per fuel element	16,400	9,560	9,560	14,600
Measured free uranium fraction ⁽²⁾	$5.1 \cdot 10^{-5}$	$4.3 \cdot 10^{-5}$	$7.8 \cdot 10^{-6}$	$1.3 \cdot 10^{-5}$
Number of burn-leach tests	70	55	40	10
	Number of fuel element in burn-leach test with x defective particles, determined by comparison to single particle uranium inventory			
x = 0	31	42	38	8
x = 1	26	8	1	1
x = 2	9	2	1	1
x = 3	4	2	0	0
x = 4	0	0	0	0
x = 5	0	0	0	0
x = 6	0	1	0	0
x ≥ 7	0	0	0	0
Measured free uranium fraction derived from counting defect particles	$4.9 \cdot 10^{-5}$	$4.6 \cdot 10^{-5}$	$7.8 \cdot 10^{-6}$	$2.1 \cdot 10^{-5}$
Average number of defect particles per fuel element	0.64		0.12	
Free uranium fraction expected/upper 95% confidence limit for the years ≈ 1980 - 1990	$3.9 \cdot 10^{-5} / 4.7 \cdot 10^{-5}$			
Free uranium fraction expected/upper 95% confidence limit for the years ≈ 1985 - 1990			$1.1 \cdot 10^{-5} / 2.2 \cdot 10^{-5}$	

(1) Coating runs using 5 kg (AVR 19, Proof Tests (HFR-K5/-K6)) and 3 kg (AVR 21) of uranium per coating batch

(2) Average of all free uranium values (measured value = detection limit for values below the detection limit)

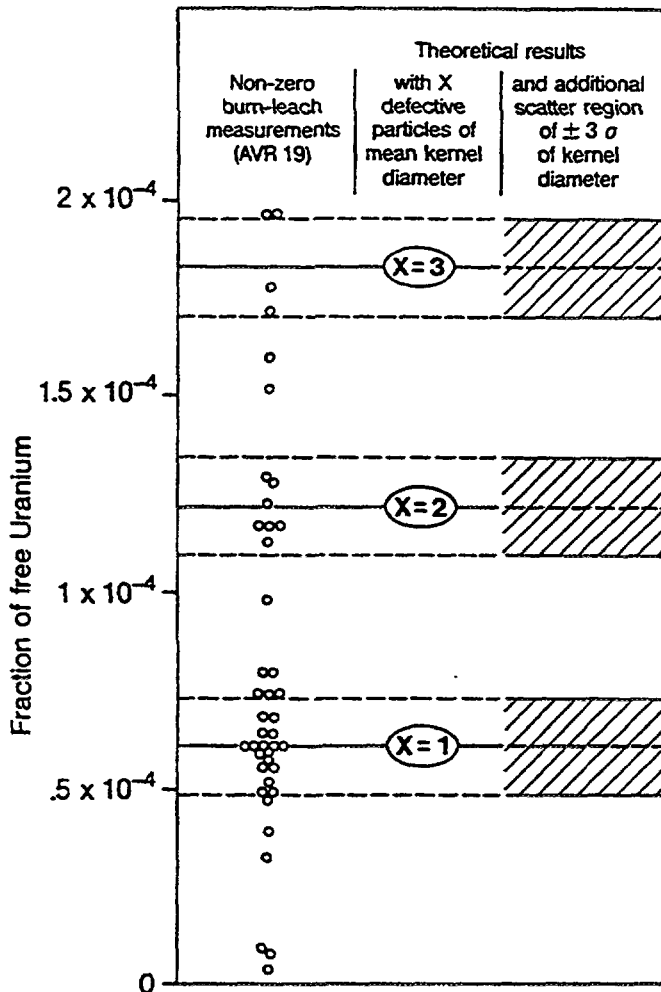


Fig. 2-12: Non-zero free uranium measurements in the seventy burn-leach tests from the quality control of the AVR 19 (GLE 3) production

2.3.2.2. Design Basis for Free Uranium

The expected and the design basis value of the average fabrication-related defective particle fraction in the HTGR core is required for radiological analyses. These values are derived from the statistical analysis of the free uranium values of production from 1985 onwards. After pooling the evaluation of all quality control data from AVR 21-2 and the proof test fuel production, an **expected value** of the average fabrication-related defective particle fraction in the HTGR core of 1.1×10^{-5} results with a **design value** of 2.2×10^{-5} . The latter result has been obtained from BetaInv(C , $n+1$, $N+1-n$) with $C=0.95$ confidence range and $n=6$ defects out of $N=10 \times 14,600 + 40 \times 9,560 = 528,400$ coated particles in the tests (for explanation see section 3.4.2.1.).

The expected value of 1.1×10^{-5} and the one-sided upper 95 % confidence limit (design value) of 2.2×10^{-5} are to be used for radiological analyses. They must not be confused with the **specification limit** for individual fuel element batches, which is 6×10^{-5} . As expected,

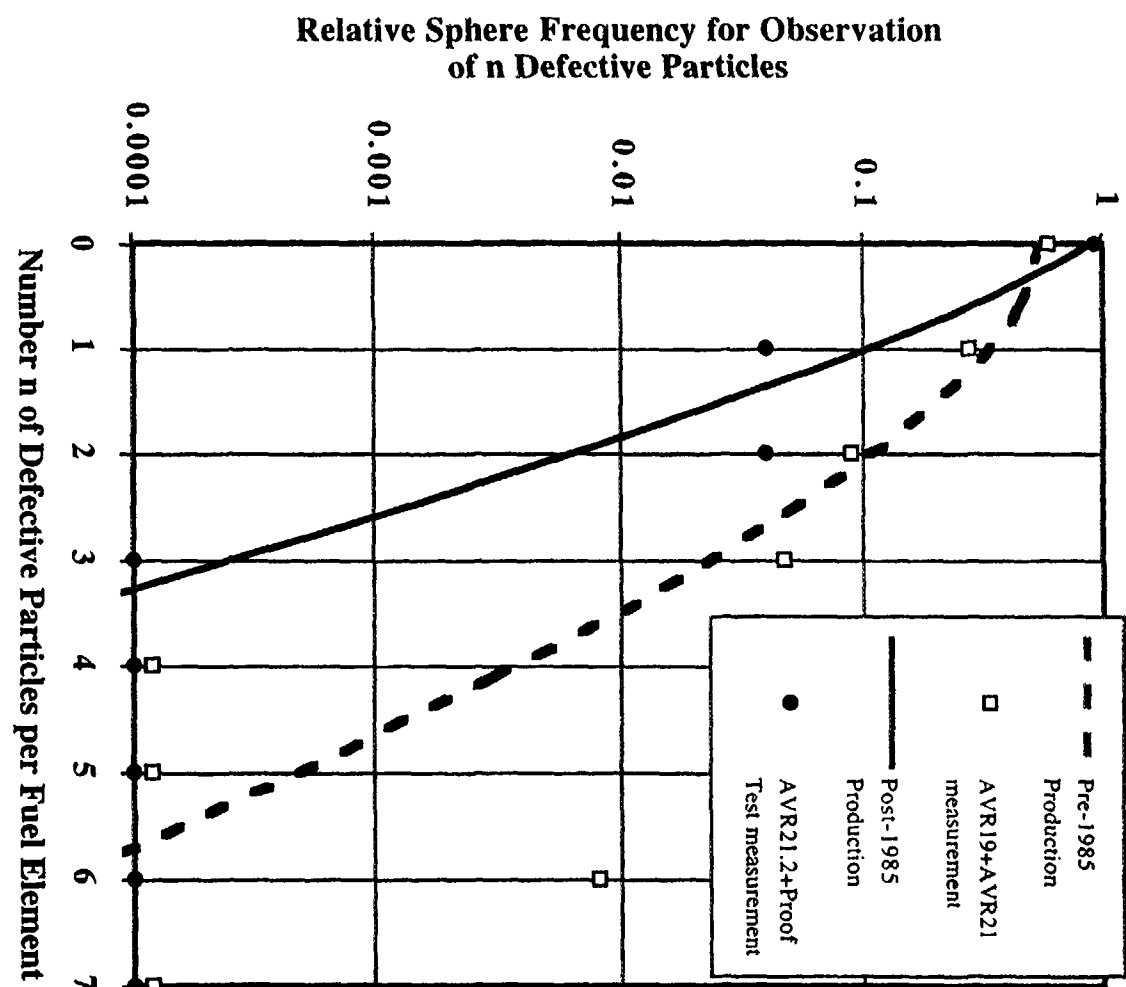


Fig. 2-13: Comparison of relative particle defect distributions prior to 1985 (AVR 19 and AVR 21-1) and after 1985 (AVR 21-2 and Proof Tests) shows the improvements achieved with the automated overcoating. Lines are predictions from a Poisson distribution with $\mu=0.64$ and $\mu=0.12$, respectively.

2.3.2.3. Uranium Contamination

The uranium contamination in the outer pyrocarbon layer is determined by a burn-leach test of loose particles in the individual coating batches. The measured data are usually below the detection limit of 1×10^{-6} . Higher values indicate defective SiC layers. This detection limit is conservatively selected as the design value for the uranium contamination

of the outer PyC coating. Heating experiments for AVR fuel elements with TRISO particles (Kr-85 and Cs-137 release at 1600 °C) indicate uranium contamination of the outer PyC coating of between 1 and 5×10^{-7} . On the basis of this information, the expected and design values of the uranium fraction in the outer LTI-PyC layers of TRISO particles are set at 3×10^{-7} and 1×10^{-6} , respectively.

Apart from detailed studies on release characteristics, a more extensive analysis of these values is unnecessary since they are contained in the free uranium value and thus already covered by the defective particle fraction.

The raw material impurities of representative test elements were measured by neutron-activation analysis at the KFA. Average contamination for uranium of 50 ng per gram carbon and for thorium of 250 ng per gram carbon resulted for the present choice of raw material (Hauzenberg natural graphite). These values were converted into effective uranium contamination for the enrichment of the power reactor.

An effective uranium concentration of 6×10^{-7} results from the natural uranium contamination of 50 ng/gC (0.72 % enrichment) for the fuel element of the **HTR MODUL** (200 gC) with 7 g uranium and 7.7 % U-235 enrichment for 66 % power of the U-235 fissions and 34 % of the Pu-239/Pu-241 fission events. On the basis of THTR data, an effective uranium contamination of 2×10^{-6} was estimated for the thorium impurity of 250 ng/gC. The design value is set twice as high as the expected value. Expected and design values of the effective uranium concentration (7.7 % U-235 enrichment) of the matrix of (rounded) 3×10^{-6} and 5×10^{-6} , respectively, thus result for the uranium used in the fuel elements of the HTR MODUL equilibrium core. These values must be taken into consideration in selecting raw materials for future HTGR fuel elements since their contribution to fission product release – at least in the case of the expected value – is not negligible.

2.3.3. The Japanese Program

In the framework of the former Japanese HTGR program called “VHTR Development Project”, the fuel manufacturing tests commenced at JAERI and NFI in 1969. The test at JAERI has been concentrating on fundamental research of coating processes, whereas the test at NFI has been done on processes of the fuel manufacturing. From the start of the program, the VHTR fuel was designed to be TRISO coated low-enriched fuel particles. By adoption of the low-enriched fuel, the JAERI program in development of the fuel was not affected by the influence of INFCE⁵ at the end of 1970’s which effectively ended the use of high-enriched uranium. In 1987, when the “VHTR Development Project” was changed to the current **HTTR project**, the design of the coated fuel particles remained unchanged, although the designs of the fuel compact and the fuel block were modified.

Efforts to improve fuel quality in manufacture was undertaken in 1987, although the fraction of the defective coated fuel particles⁶ (SiC coating failure) in the fuel compacts

⁵ INFCE = “International Nuclear Fuel Cycle Evaluation”, an agreement from 1977 whose goal it was to conduct a technical valuation of the single stations of the fuel cycle and of conceivable alternatives.

⁶ Definition of the defective coated fuel particles prevailed at JAERI has two different meanings: failure of SiC coating layer which is decided by the burn-acid-leaching method, and failure of through-coating layer by the acid-leaching method after disintegration of the fuel compacts.

during manufacture met the fuel design criteria of 2×10^{-3} . Modification in manufacturing technology resulted in a great improvement in quality of the fuel manufactured thereafter, as mentioned below. Based on the new technology, manufacture of the HTTR first loading fuel has begun at NFI in June 1995, and it will last for two years to complete it.

2.3.3.1. Design Criteria for HTTR First Loading Fuel

In the safety design of HTGR fuels, it is important to retain fission products within the coated fuel particles so that their release to the primary coolant may not exceed an acceptable level. From this point of view, the basic design criteria for the fuel are to minimize the failure fraction of as-manufactured fuel coating layers and to avoid significant additional fuel failures during operation. To meet the latter criteria for the first loading fuel, the fuel temperature is limited below 1495 °C under abnormal transient conditions, and the fuel burnup is limited to 3.6 %FIMA for the HTTR first loading fuel.

Based on the circumstances mentioned above, the **safety design requirements** for the HTTR fuel have been provided as follows:

- (a) The initial failure fraction in the coating layers of the coated fuel particles shall be regulatorily less than 2×10^{-3} in terms of the sum of heavy metal contamination and SiC defectiveness, while the expected one is 10^{-5} . The value of 2×10^{-3} was determined from the view point of limit of off-site exposure during normal operation.
- (b) The coated fuel particles shall not fail systematically under the normal operation conditions, that is, in the safety analysis.
 - (1) The penetration depth of the Pd/SiC interaction shall not exceed the thickness of the SiC layer of 25 μm , because the fully penetrating Pd/SiC interaction is thought to lead to loss of fission product retention in the SiC coating layer.⁷
 - (2) The distance of kernel migration (see section 3.2.1.) shall not exceed the thickness of the buffer layer plus the inner PyC layer of 90 μm to avoid failure of the SiC layer.
- (c) The fuel shall be designed so as to maintain its integrity even in consideration of irradiation-induced damage and chemical attack through the fuel life time, that is, the additional failure fraction in the coating layers of the fuel particles shall be regulatorily less than 2×10^{-3} in the fuel life time.
- (d) The maximum fuel temperature shall not exceed 1600 °C at any anticipated transient to avoid fuel failure, thus in other words from fuel side, the layers of the coated fuel particles shall remain intact below 1600 °C at any anticipated transient.

2.3.3.2. Manufacturing Defects

Ideally, the coating layers should remain intact before and during irradiation. However, a small fraction of the fuel particles with defective coating layers are virtually present in a manufacturing batch. Among several modes of defective coating layers, a **defective SiC coating layer** is the most harmful from the standpoint of fission product retention. The defective SiC coating layer can be detected by the burn-leach method, where the fuel

⁷ The US program assumed SiC failure, when the Pd penetration depth reached the coating half thickness.

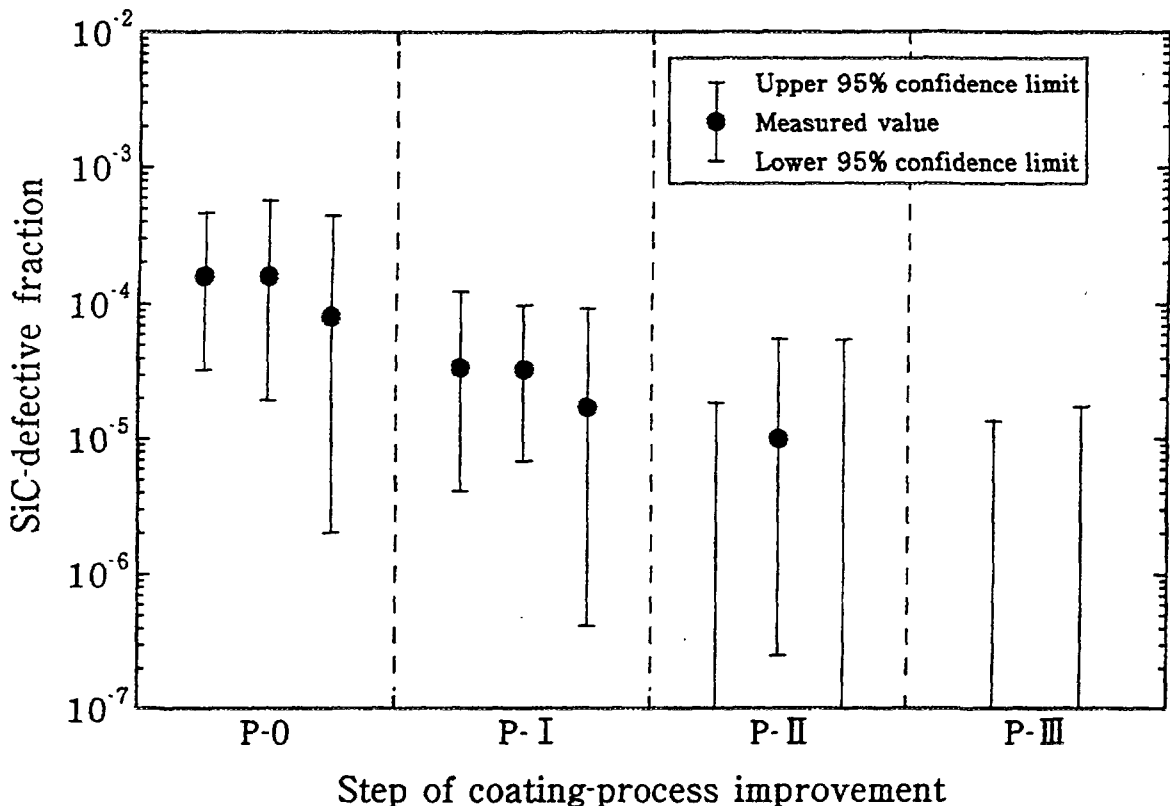


Fig. 2-14: Typical examples of SiC-defective fraction of the as-manufactured TRISO coated particles as a function of the step of coating process improvement. Step P-0 is the conventional process. Step P-I is the improved process in control of the particle fluidization. Steps P-II and P-III are the further improved processes without unloading/loading of the porous PyC- and SiC-coated particles and the porous PyC-, inner PyC- and SiC-coated particles, respectively [37]. (The lines without a data point indicate the 95 % confidence level, while the lower confidence level as well as the measured value is 0.)

compact or the fuel particles are heated at 800 - 900 °C in air to oxidize the matrix graphite and the outer PyC layers, followed by the acid leaching of the exposed uranium. The defective SiC coating layer exposes uranium during burning.

During the last decade, much effort has been made to reduce the fraction of defective SiC coating layers of the as-manufactured fuels and the quality has been improved by the modification of manufacturing conditions and processes [33, 34, 35, 36, 37]. From the observation of several hundred thousand particles, it was understood that the coating failure may occur

- (a) during particle fluidization in the coater by mechanical shocks and by chemical reactions,
- (b) during unloading/loading of particles from/to the coater by mechanical shocks, and
- (c) during compacting process [36, 37].

To reduce the defective particle fraction, the **TRISO coating process** was improved by three steps, as shown in Fig. 2-14 [37]. In the first step (P-I), the particle fluidization

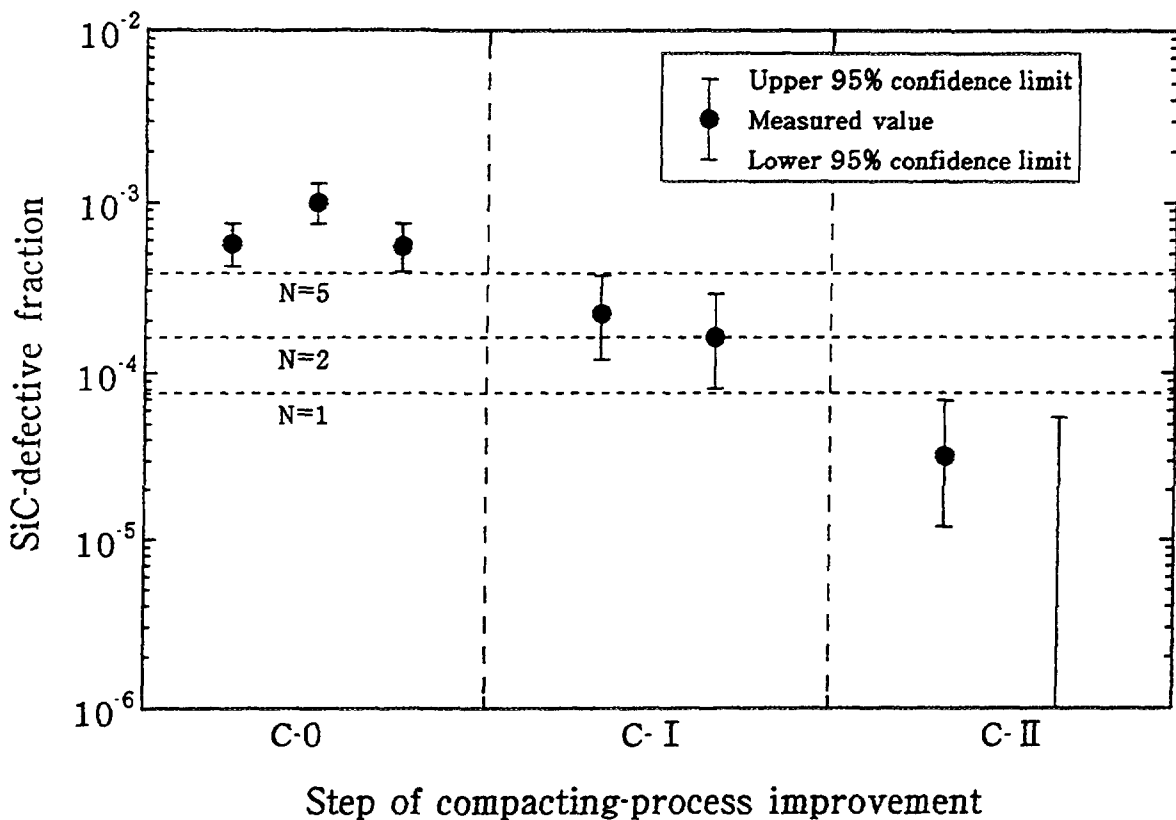


Fig. 2-15: Typical examples of SiC-defective fraction of the as-manufactured fuel compacts as a function of the step of compacting process improvement. Step C-0 is the conventional process. Step C-I is the conventional process with particles of high quality. Step C-II is the improved process in the conditions of pressing speed and temperature of the warm pressing of the fuel compacts [37]. (The lines without a data point indicate the 95 % confidence level, while the lower confidence level as well as the measured value is 0.)

modes in the coater were so controlled that strong mechanical shocks were not given to the particles. Adequate control of the particle fluidization modes could be attained by modifications of the gas flow rates, and the shape and size of the inlet gas nozzle of the coater [35]. The control of the particle fluidization modes was the effective step to reduce the coating failures during particle fluidization. In the second and third step (P-II and P-III), the TRISO coating process without unloading / loading of the porous PyC-, inner PyC- and SiC-coated particles ("once-through" coating) was developed which was used in Germany [38]. This process eliminated the causes of coating failures during unloading / loading of the particles, and was effective to reduce the SiC defective fraction of the particles.

The compacting process was also improved, as shown in Fig. 2-15 [37]. In the conventional process (C-0), more than five SiC-defective particles were contained in a fuel compact. Even when the particles of high quality were used (C-I), two or three particles out of about 13,500 had SiC defects. In the C-II step in Fig. 2-15, the conditions of pressing speed and temperature of the warm pressing of the fuel compacts were optimized to reduce the SiC defective fraction of the particles. The improvement in quality was achieved by the modification and the optimization of the coating and the compacting processes, where less

than one SiC-defective particle was contained in a fuel compact even at 95 % confidence limit [37].

2.3.4. The Russian Program

Three HTGR reactor designs were developed in Russia starting in 1960-70 in successive order VGR-50, VG-400, and VGM with a thermal power of 60, 400, and 250 MW(th), respectively, and an outlet helium temperature of 750 and 950 °C.

Multi-purpose functions of HTGR predetermined the necessity of location of the nuclear system in the vicinity of large technological complexes and settlements. Such locations require the development of a multi-barrier system, providing nuclear power plant (NPP) radiation safety during all regimes of its operation, including emergency regimes. That is why very stringent requirements were imposed on the fuel element as the main barrier for preventing fission product release to provide radiation safety of the population, NPP personnel and technological practice. Among these requirements are the following: tightness with regard to all main radiologically dangerous radionuclides and to accumulation of tritium in the system, as it is well known that tritium can migrate easily inside the technological circuits at high temperatures and this can lead to non-allowed contamination of the technological product (for example fertilizers during their fabrication).

While analyzing the problems of radiation safety, the **requirements of an innovative system** are the following:

- exclude the evacuation of the population during severe (beyond design basis) accidents,
- access should be possible for periodic maintenance of the main equipment of the primary circuit in the process of operation either directly during reactor operation or shortly after its shutdown (\approx 1–2 weeks).

The second condition is more strict than the first one and that is why the requirement for the fuel element tightness were in first place oriented towards the assurance of personnel safety.

In the quantitative aspect, these requirements could be reduced to the following parameters:

- equilibrium activity of the primary circuit coolant with regard to volatile fission products shall not exceed 100 - 200 Ci (Xe, Kr) and 1000 - 2000 Ci (I, Tl), respectively;
- activity with regard to Cs, Sr shall not exceed 10 - 20 Ci at the end of the campaign;
- activity of other radionuclides, Ag-110m in particular was considered to assess radiation impact during the reactor operation, but it was not formulated as a fuel element requirement criterion, as the requirements to the above main radionuclides allowed to ensure the safety of nuclear power system use reliably enough.

The requirements for fission product retention to the fuel element must be fulfilled at provision of a number of other important requirements connected with the peculiarities of HTGR use was imposed for the fuel element, such as, for example, graphite blocks

Table 2-6: Main technical requirements to fuel element for HTGRs designed in CIS

Design parameter	VGR-50	VG-400	VGM	
	SIA "Lutch"	FSC-KhPTI, Kharkov, Ukraine		
Coated particle				
Kernel composition	UO ₂	UO ₂	UO ₂	UO ₂
Kernel diameter [μm]	500	500	500	500
Coating layer sequence	Buffer / PyC / PyC / SiC / PyC	Buffer / PyC / SiC / PyC	Buffer / PyC / SiC / PyC	Buffer / PyC+SiC / SiC / PyC+SiC
CP layer thickness [μm]	70 / 25 / 25 / 55 / 70	90 / 70 / 60 / 60	90 / 70 / 60 / 60	65 / 55 / 65 / 55
Fuel element				
Heavy metal loading [g/FE]	2.4	6.2	7.	7.
U 235 enrichment [%]	21.	6.5	8.0	8.0
Number of CP per FE	4,000 - 5,000	11,000 - 14,000	13,000 - 16,000	13,000 - 16,000
Volume loading of CP [%]	5.3 - 7.0	10.6 - 13.1	12. - 15.	12. - 15.
Matrix graphite	KPD ⁽¹⁾ , GCP ⁽²⁾	KPD ⁽¹⁾ , GCP ⁽²⁾	KPD ⁽¹⁾	GCP ⁽²⁾
Operating requirements				
Mean operating time [d]	225	≈ 1095	960	
Maximum burnup [%FIMA]	11.	8.8	8.8	
Maximum fast fluence [10^{25} m ⁻²]	1.2 [E > 0.7 MeV]	1.7 [E > 0.18 MeV]	3. [E > 0.1 MeV]	

Table 2-6: Main technical requirements to fuel element for HTGRs designed in CIS (continued)

Design parameter	VGR-50	VG-400	VGM	
			SIA "Lutch"	FSC-KhPTI, Kharkov, Ukraine
Maximum fuel temperature [°C]	1450	1400	1400	
Maximum power/FE [kW]	2.1	2.6 [T _{gas} = 950 °C]	1.8	
Relative leak (F)	< 10 ⁻⁴ (Xe 133) < 10 ⁻⁴ (I 131) < 10 ⁻⁴ (Cs, Sr)	< 10 ⁻⁵ (fission gas) < 10 ⁻⁵ (Cs, Sr)	< 10 ⁻⁵ (Xe 133, I 131) < 10 ⁻⁵ (Cs 137, Sr 90)	
Relative leak during accidents (F)	< 10 ⁻³	< 10 ⁻⁴	< 10 ⁻⁴ (Xe, I)	
Fraction damage of particle coating at test end	< 10 ⁻³	< 10 ⁻⁴	< 10 ⁻⁴	
Contamination of FE matrix by U 235 [g/FE]	< 2*10 ⁻⁵	< 2*10 ⁻⁶	< 2*10 ⁻⁶	
Impurity in helium [vpm]		H ₂ O: 0.6 - 10 H ₂ : 50 - 100 CO: 50 - 100 CO ₂ : 2 - 100 CH ₄ : 0.2 - 2 N ₂ : 25 - 50		

(1) KPD = Carbonization under pressure (SIA "Lutch")

(2) GCP = Graphite impregnated with pyrocarbon (FSC-Kharkov Phys. Techn. Inst.)

and fuel elements wear during their multiple circulation along the circuit, for the static > 20 kN and impact strength, corrosion stability (< 3 mg/cm²) and stability in the oxidizing atmosphere. Great attention was paid to the last requirement after the accident at the 4th unit of the Chernobyl NPP. The work on coating of fuel cladding by metal carbides (SiC) with protective layers (considering the experience of the 60s) was started and the results were positive.

Spherical fuel elements which were developed in two directions are assumed to be used. Fuel elements of both options have the form of a ball with the outer diameter 60 mm and consist of a graphite cladding and the core of the fuel element in form of a ball with the diameter 50 mm. The fuel is homogeneously distributed within the matrix graphite volume in the form of coated particles. Uranium dioxide is used as fuel. Main technical requirements to the fuel elements are listed in Table 2-6.

The program for fuel element development and fabrication incorporates the development of the fabrication technology, methods and means of quality control, study of fuel elements serviceability in the reactor core, complex of property studies, etc. Studies of fission product migration are divided into pre-reactor, reactor and post-reactor investigations (Figs. 2-16 – 2-18). Experiments are conducted in the test facilities “OSA”, “PODS-NEZNIK”, “SATURN”, “LAZER” as well as in the channels “PG-100”, “KASHTAN”, “KARAT” and others.

As the fuel elements (as for AVR-type in Germany) were not tested on a mass scale, main attention was drawn to the development of quality control methods and means. In particular, the **method of “weak” irradiation**⁸ of coated particles and fuel elements was developed and widely used, which allowed to assess the influence of different technological processes and testing regimes on the integral quality parameter, fission gas release (Xe-135) and also cesium release.

An undestructive method has been developed to **control the thickness of PyC coatings of coated particles** [39]. The PyC coating control is conducted during the coated particle manufacture beginning with PyC coating of density 1.8 g/cm³. The control method consists of a comparison of the densities of the coated particle and a specially selected heavy liquid during submerging of the particles after the coating of every single layer of different thickness. The density of the liquid is being selected in the range of 2.5 - 6.0 g/cm³. The coating thickness is calculated on a selected fraction of coated particles from the correlation

$$\frac{T}{D} = 0.5 \left[\left(\frac{\gamma_k - \gamma_c}{\gamma_s - \gamma_c} \right)^{1/3} - 1 \right] \quad (2-1)$$

⁸ “Weak” irradiation means short irradiation at room temperature.

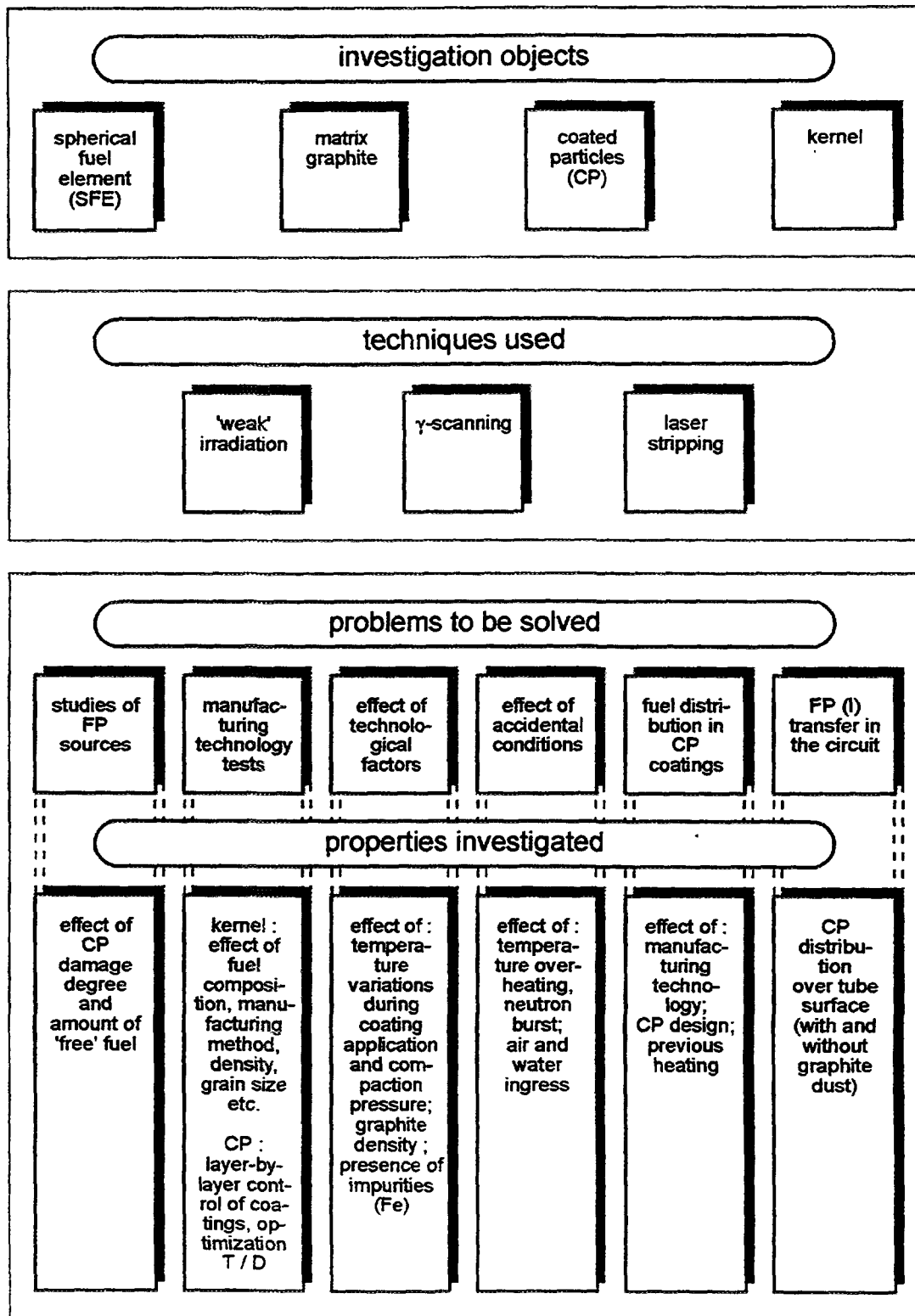


Fig. 2-16: Pre-reactor investigations

PROCEDURE

Measurement of β and γ activity of gaseous fission products released from coated particles and spherical fuel elements in resource (loop) tests

RANGE

β [Bq]	$3.7 \cdot 10^{-1} - 3.7 \cdot 10^{+5}$
γ [Bq]	$3.7 \cdot 10^{+1} - 3.7 \cdot 10^{+10}$
Flow rate [l/min]	0.1 - 0.5
Relative release	$10^{-7} - 10^{-1}$

ERROR

β	40 %
γ	25 %
Flow rate	30 %
Relative release	up to 50 %

Fig. 2-17: Reactor tests

where

T is the coating thickness [mm]

D is the fuel kernel diameter [mm]

γ_i is the density [g/cm^3]

$i = k$: kernel

$i = c$: coating

$i = s$: solution

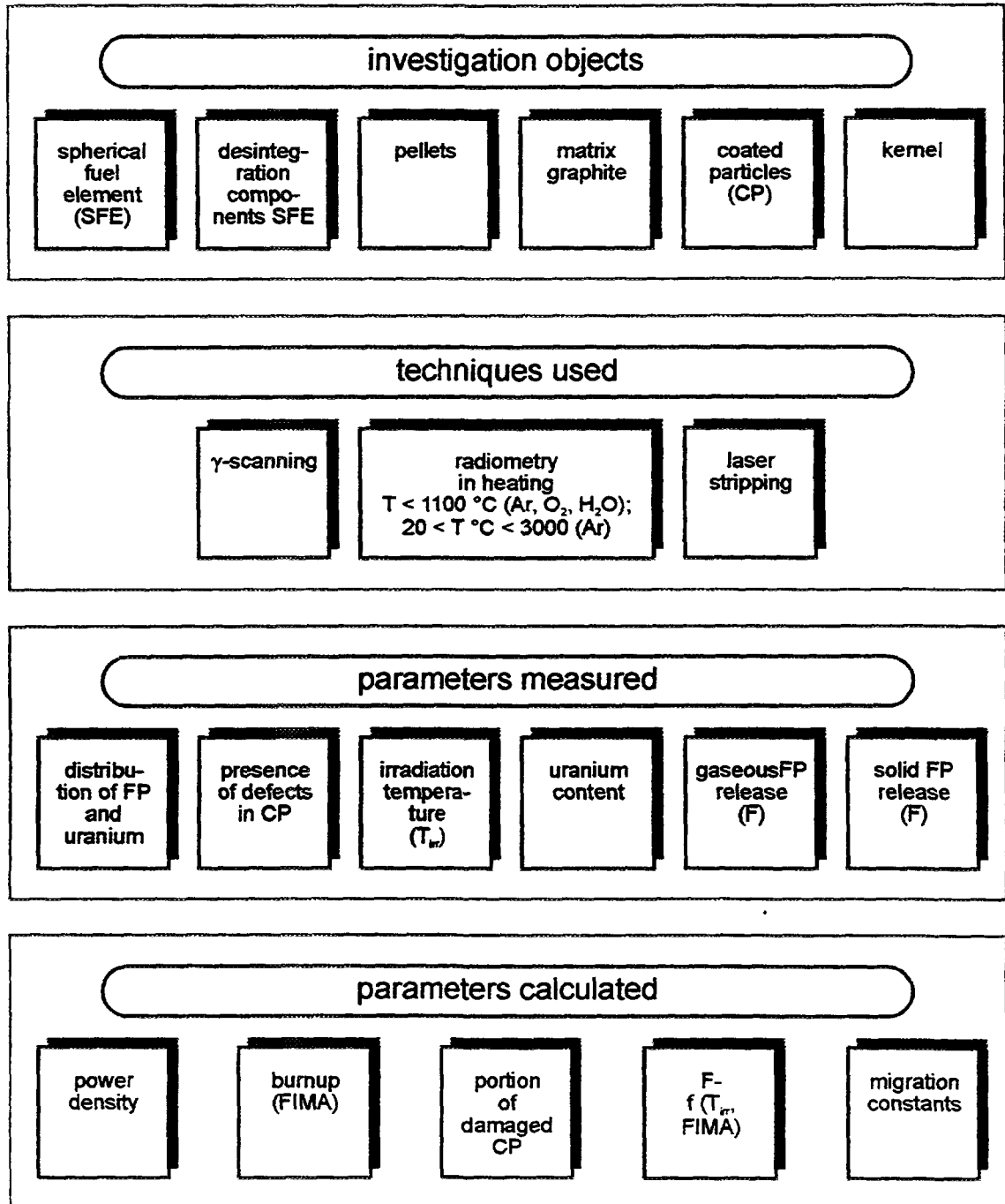


Fig. 2-18: Post-reactor investigations

2.3.5. The US Program

The design requirements, the history of fuel fabrication in the US and the current fabrication process are addressed.

2.3.5.1. Design Requirements

Given the radionuclide control requirements as, for example, at the site boundary, radionuclide releases from the plant and other components can be successively derived with a top-down methodology. For example, fuel and target performance criteria are derived from allowable core release limits and as-manufactured fuel attributes are derived from in-reactor fuel and target performance criteria. With iteration of the top-down methodology, lower level requirements are refined.

2.3.5.2. Fuel Design

The reference fuel kernel is a mixture of UO_2 and UC_2 . The rationale for using this mixture is based on the favorable properties derived as a result of the fission product chemistry. The presence of both the oxide and carbide phases determine the oxygen potential in the kernel up to about 34 %FIMA. During this period, the UC_2 is decreased as it reacts with the oxygen released from UO_2 by fission ($\text{UC}_2 + \text{O}_2 \rightarrow \text{UO}_2 + 2\text{C}$). At 34 %FIMA, the UC_2 phase disappears and the oxygen potential of the system is controlled by the $\text{SrO}-\text{SrC}_2-\text{CO}$ equilibrium up to about 38 %FIMA. Beyond 38 %FIMA, the $\text{ZrO}_2-\text{ZrC}-\text{CO}$ equilibrium is established and controls the oxygen potential up to about 75 %FIMA. The chemical compositions of UCO were derived by thermodynamic calculations and verified in irradiations. By controlling the oxygen potential, a carbon monoxide buildup and overpressurization are avoided, thereby preventing thermal migration and reducing the probability for pressure vessel failure and SiC oxidation.

2.3.5.3. Fuel Quality Requirements

The fuel quality requirements are given in Tables 2-7 and 2-8.

2.3.5.4. Process History

Peach Bottom Unit 1 and Fort St. Vrain (FSV) initial cores and reload fuel were manufactured in the US. For cores 1 and 2 of Peach Bottom Unit 1, about 3500 kg of BISO coated, high-enriched uranium (HEU) $(\text{Th},\text{U})\text{C}_2$ particles were manufactured and assembled into more than 48,000 annular fuel compacts in cylindrical fuel elements. The FSV initial core required about 20,000 kg of HEU $(\text{Th},\text{U})\text{C}_2$ and ThC_2 TRISO coated particles assembled into about 1500 hexagonal prismatic fuel elements. Subsequently, three one-sixth core (250 fuel elements) FSV reload segments were manufactured. In addition, more than 14,000 kg of coated particles have been manufactured for other US nuclear programs.

Table 2-7: As-fabricated quality requirements for NP-MHTGR fuel

Quality requirements	Fraction fissile or fertile	
	Mean	95 % confidence ⁽¹⁾ < 5 % compacts exceed
<i>Fuel particles</i>		
Defective SiC	$\leq 5.0 \times 10^{-5}$	$\leq 1.0 \times 10^{-4}$
Total heavy metal (HM) contamination	$\leq 1.0 \times 10^{-5}$	$\leq 2.0 \times 10^{-5}$
Total fraction HM outside intact SiC	$\leq 6.0 \times 10^{-5}$	$\leq 1.2 \times 10^{-4}$
Missing or defective buffer	$\leq 5.0 \times 10^{-5}$	$\leq 2.0 \times 10^{-5}$
Missing or defective inner PyC	$\leq 4.0 \times 10^{-5}$	$\leq 1.0 \times 10^{-5}$
Missing or defective outer PyC	$\leq 1.0 \times 10^{-4}$	$\leq 1.0 \times 10^{-3}$
<i>Fuel compacts</i>		
Defective SiC	$\leq 5.0 \times 10^{-5}$	$\leq 1.0 \times 10^{-4}$
Uranium contamination	$\leq 1.0 \times 10^{-5}$	$\leq 2.0 \times 10^{-5}$
Total fraction HM outside intact SiC	$\leq 6.0 \times 10^{-5}$	$\leq 1.2 \times 10^{-4}$
Missing or defective inner PyC	$\leq 4.0 \times 10^{-5}$	$\leq 1.0 \times 10^{-4}$

(1) 95 % confidence means that less than 5 % of the compact lots in a segment exceed the limits shown. Compact lots exceeding the limit must contain less than 5 % of the total compacts in that segment.

Table 2-8: NP-MHTGR end-of-life fuel performance requirements

Parameter	NP-MHTGR driver fuel Allowable fraction (core average)	
	> 50 % confidence	> 95 % confidence
Fuel failure during normal operation	$\leq 1.0 \times 10^{-4}$	$\leq 4.0 \times 10^{-4}$
Incremental failure during design basis accident	$\leq 3.0 \times 10^{-4}$	$\leq 1.2 \times 10^{-3}$

2.3.5.5. Fuel Fabrication

The most recently selected methods to be used in the fuel fabrication process for the kernel, and for the buffer, inner pyrocarbon, silicon carbide, outer pyrocarbon, and seal coatings are discussed in reference [40].

The kernel composition, a mixture of UO_2 and UC_2 , is referred to by the acronym UCO. The UCO kernel is to be fabricated using the internal gel precipitation process [41, 42]. This process produces consistently high quality kernels with the correct dimensions and specified characteristics, minimizes the environmental processing of wastes and scrap recycle materials, and meets the specific performance requirements. The gelled spheres are stabilized, the kernels are air dried, calcined and then sintered. Thereafter a high temperature sintering removes excess oxygen. The kernels are then exposed to argon and argon/CO gas mixtures to chemically adjust the ratio of carbon and densify the kernel, resulting in the final kernel form.

2.3.5.6. Compact Fabrication

The fuel particles are embedded in a fuel compact composed of the coated fuel particles, a carbon matrix, and graphite shim. The matrix is originally 47 % petroleum pitch, 38 % filler, 10 % octadecanol, and 5 % polystyrene. The matrix is injected into a mold at 160 °C. Afterwards, cooling to below ambient temperature solidifies the compact. The compact, packed in Al_2O_3 , is then carbonized at 900 °C to decompose organic compounds and to obtain a solid carbon compact. The size of the alumina particles must be controlled to restrain the compact but allow the escape of volatile gases. Thereafter the compacts are heated at 1650 °C briefly to stabilize the compact. The diameter of the resulting compact is between 12.37 and 12.72 mm and an adjustable length, expected to be 49.3 mm in most applications.

2.4. SUMMARY OF CHAPTER 2

The investigation of fundamental characteristics of HTGR coated particle fuel fabrication has taken place since 30 years. For all countries' reference concepts, the fuel is based on TRISO coated fuel particles with low-enriched uranium. Two directions for the fuel element design have been pursued, the block type in Japan and the US, and the spherical fuel element in Germany, Russia, and China.

Particle and fuel element production in China is still on a laboratory scale, but will soon evolve to prototype scale. Experimental data on reference fuel revealed a low level of free uranium at 4×10^{-6} . The qualification program concentrates on characterization and inspection of fuel to be used in the HTR-10 experimental reactor with special focus on the observation of coating microstructure and the investigation of SiC strength and Youngs modulus as important parameters.

In Germany, high quality fuel was achieved in the early 1980s due to large-scale production experience. Measurements of "free uranium" outside an intact SiC layer have shown a reduction of the U_{free} fraction by a factor of 5 compared to fuel production before 1985. An expected value of 1.1×10^{-5} is used in radiological safety analyses. Measurement

data on uranium contamination of the matrix graphite are usually below the detection limit, i.e., $< 10^{-6}$. In 1989, it was decided to terminate the German activities on HTGR fuel production and development.

The Japanese fuel development has also managed to produce high quality fuel by modification of manufacturing conditions of both coating and compacting processes. The result is a 95 % confidence level of less than one defective particle per fuel compact. The expected free uranium fraction is 5×10^{-4} which is well below the regulatory requirement for the U_{free} fraction to be $< 2 \times 10^{-3}$. The fuel production for the HTTR first loading has begun in June 1995 and will last for about two years.

The US reference fuel design is based upon a two-particle concept of fissile and fertile UCO coated particles. The fuel kernel composition, a mixture of UO₂ and UC₂, leads to curtailment of CO formation and pressurization and mitigates thermal migration, pressure vessel failure and SiC oxidation. Operational requirements for burnup and neutron fluence are more demanding compared to other countries' fuel designs. Specification limits are 10^{-5} for the heavy metal contamination and 5×10^{-5} for the fraction of defective SiC coatings.

Russia has gained a broad experience with its fuel in pre-reactor, reactor, and post-reactor experiments where even energetic reactivity transients have been imposed. The fuel design for the 250 MW(th) modular reactor VGM has a fraction of defective particles $< 10^{-4}$ and a U-235 contamination of 4×10^{-6} . The fuel production, however, is on a laboratory scale so far. Therefore focus was directed towards the development of quality control methods. One that is being widely used is the method of "weak" irradiation of the fuel.

REFERENCES OF CHAPTER 2

- [1] HOWARD, R.M., PRICE, M.S.T., SHEPHERD, L.R. (ED.), A Summary and Evaluation of the Achievements of the Dragon Project and its Contribution to the Development of the High Temperature Reactor, Dragon Report DP-1000, O.E.C.D. High Temperature Reactor Project (1978).
- [2] VOICE, E.H., LAMB, D.N., The Deposition and Structure of Pyrolytic Silicon Carbide, Dragon Report DP-667, O.E.C.D. High Temperature Reactor Project (1969).
- [3] ALLEN, P.L., FORD, L.H., SHENNAN, J.V., Nuclear Fuel Coated Particle Development in the Reactor Fuel Element Laboratories of the U.K. Atomic Energy Authority, Nucl. Techn. 35 (1977) 246-253.
- [4] BALTHESEN, E., HTR Fuel Element Development in the Federal Republic of Germany, Behaviour of GCR Fuel under Accident Conditions (Proc. IAEA Specialists' Meeting, Oak Ridge, 1990), IAEA, IWGGCR/25, Vienna (1991) 24-25.
- [5] KÜHNLEIN, W., Fission Product Release under Normal Operating Conditions, Unification of Coated Particle Performance Models and Fission Product Transport Data for the HTR (IAEA Technical Workshop, Jülich, 1991).
- [6] NABIELEK, H., FUKUDA, K., KANIA, M.J., HTR Fuels for Gas-Turbine Applications, Closed-Cycle Gas-Turbine Modular High-Temperature Gas-Cooled Reactor (Proc. GCRA Int. Workshop, Boston, 1991), MIT, Cambridge (1991) 4-8 - 4-14.
- [7] DUNN, T.D., DATTA, K., HOOT, C., Preliminary Safety Assessment of the 450 MWT MHTGR, Behaviour of GCR Fuel under Accident Conditions (Proc. IAEA

- Specialists' Meeting, Oak Ridge, 1990), IAEA, IWGGCR/25, Vienna (1991) 111-116.
- [8] SHIOZAWA, S., Overview of Current Research and Development Programmes for Fuel in Japan, Behaviour of GCR Fuel under Accident Conditions (Proc. IAEA Specialists' Meeting, Oak Ridge, 1990), IAEA, IWGGCR/25, Vienna (1991) 19-21.
 - [9] GREBENNICK, V.N., Review of Current Work on Investigation of HTGR Fuel in the Union of Soviet Socialist Republics, Behaviour of GCR Fuel under Accident Conditions (Proc. IAEA Specialists' Meeting, Oak Ridge, 1990), IAEA, IWGGCR/25, Vienna (1991) 25-27.
 - [10] XU, S., et al., Manufacture of HTR Fuel Element, High Technology Letter **1** (1995) 87-90.
 - [11] XU, S., et al., Fission Product Release Experiment of Coated Fuel Particles, Chinese Journal of Nuclear Science and Technology (1991) 144-151.
 - [12] HEIT, W., Matrixkontamination der THTR-Brennelemente, Private Communication (1987).
 - [13] VERFONDERN, K., SCHENK, W., NABIELEK, H., Passive Safety Characteristics of Fuel for a Modular High-Temperature Reactor and Fuel Performance Modeling under Accident Conditions, Nucl. Techn. **91** (1990) 235-246.
 - [14] RAGOSS, H., Kontamination und Partikelbruch im Modul-Referenz-Brennelement, Technical Note No. 76.00733.1, Interatom (1989).
 - [15] LOHNERT, G.H., NABIELEK, H., SCHENK, W., The Fuel Element of the HTR-Module, a Prerequisite of an Inherently Safe Reactor, Nucl. Eng. Des. **109** (1988) 257-263.
 - [16] BABA, O., Evaluation of the Fuel Failure Fraction in HTTR, Unification of Coated Particle Performance Models and Fission Product Transport Data for the HTR (IAEA Technical Workshop, Jülich, 1991).
 - [17] SAITO, S., et al., Safety Requirements and Research and Development on HTTR Fuel in Japan, Behaviour of GCR Fuel under Accident Conditions (Proc. IAEA Specialists' Meeting, Oak Ridge, 1990), IAEA, IWGGCR/25, Vienna (1991) 31-36.
 - [18] BRESNICK, S., MHTGR Fuel Process and Quality Control Description, Report DOE-HTGR-90257, General Atomics (1991).
 - [19] VERFONDERN, K., DUNN, T.D. BOLIN, J.M., Comparison of US/FRG Accident Condition Models for HTGR Fuel Failure and Radionuclide Release, Report JüL-2458, Research Center Jülich (1991).
 - [20] MOMOT, G.W., KHROULEV, A.A., Limits of Safe Operation in Terms of Fission Product Release from the Fuel Element and its Justification, Fuel and Graphite for HTR (Proc. 1st Soviet/German Seminar, Moscow, 1990), Internal Report KFA-HTA-IB-6/90, Research Center Jülich (1990) 319-335.
 - [21] XU, S., et al., Effect of Deposition Temperature on the Properties of Pyrolytic SiC, J. Nucl. Mater. **224** (1995) 12-16.
 - [22] BICKERDIKE, R.L., et al., Study on Coated Particle Fuel, Dragon Report 139, O.E.C.D. High Temperature Reactor Project (1963).
 - [23] GONTARD, R., NABIELEK, H., Performance Evaluation of Modern HTR TRISO Fuels, Internal Report KFA-HTA-IB-05/90, Research Center Jülich (1990).
 - [24] XU, S., CHENG, B., JIN, L., Design of HTR Fuel Element, Chin. J. Nucl. Sci. Techn. **13** (1993) No. 4 (in Chinese).

- [25] XU, S., et al., Research and Development of HTR Fuel Element, China Nuclear Science and Technology Report CNIC-00573 (1992).
- [26] XU, S., et al., Effect of Deposition Temperature on the Properties of Pyrolytic SiC, *J. Nucl. Mater.* **224** (1995) 12-16.
- [27] XU, S., Strength and Working Stress of SiC Coating Layer of Coated Fuel Particles for High Temperature Gas-Cooled Reactor, *Nucl. Power Eng.* **17** (1996) 62-67 (in Chinese).
- [28] BONGARTZ, K., Status of the Fuel Stress and Failure Rate Calculations at KFA, Report Jü1-1686, Research Center Jülich (1980).
- [29] ZHU, M., LI, E., TANG, C., Development of Apparatus for Determining Static Young's Modulus of Small Size Ring-Shaped Specimen, *Function Materials* **24** (1993) 455-460 (in Chinese).
- [30] BONGARTZ, K., et al., Measurement of Young's Modulus and Fracture Stress on HTR Particle Coatings by Brittle Ring Test, *J. Nucl. Mater.* **45** (1972) 261-264.
- [31] BONGARTZ, K., et al., The Brittle Ring Test: A Method for Measuring Strength and Young's Modulus on Coatings of HTR Fuel Particles, *J. Nucl. Mater.* **62** (1976) 123-127.
- [32] WALLURA, E., et al., Siliziumcarbid-Hüllschichten von Kernbrennstoffteilchen – Eine Charakterisierungsstudie, Report Jü1-1871, Research Center Jülich (1983).
- [33] MINATO, K., et al., Failure Mechanism of Coated Fuel Particles during Fabrication, Report JAERI-M 86-083, Japan Atomic Energy Research Institute (1986).
- [34] FUKUDA, K., et al., Research and Development of HTTR Coated Particle Fuel, *J. Nucl. Sci. Techn. 28* (1991) 570-581.
- [35] MINATO, K., et al., Internal Flaws in the Silicon Carbide Coating of Fuel Particles for High-temperature Gas-Cooled Reactor, *Nucl. Techn. 106* (1994) 342-349.
- [36] MINATO, K., et al., Coating Failure Mechanisms of Fuel Particles for High-Temperature Gas-Cooled Reactors during Coating Processes, *Nucl. Techn. 111* (1995) 260-269.
- [37] KIKUCHI, H., et al., Improvement in Quality of HTTR Fuel, (Proc. Annual Meeting of the Atomic Energy Society, 1995) B55.
- [38] MEHNER, A.-W., et al., Spherical Fuel Elements for Advanced HTR Manufacture and Qualification by Irradiation Testing, *J. Nucl. Mater.* **171** (1990) 9-18.
- [39] KHROULEV, A.A., et al., Method of the Parameters PC Determination, Patent No. 140464, USSR (1979).
- [40] MCCARDELL, R.K., et al., NP-MHTGR Fuel Development Program Plan: Appendix B, Report EGG-NPR-8971, Idaho National Engineering Laboratory (1992).
- [41] SPENSE, R., Sol Gel Spherical Fuel, Conf. on Metallurgical Technology of Uranium and Uranium Alloys, American Society for Metals (1981).
- [42] HUSCHKA, H., VYGEN, P., Coated Fuel Particles: Requirements and Status of Fabrication Technology, *Nucl. Tech.* **35** (1977) 239-246.

3. NORMAL OPERATION TRISO FUEL PERFORMANCE UNDER IRRADIATION

3.1. FISSION PRODUCT INVENTORIES OF THE ACTIVE CORE

The code **ORIGEN** [1] is generally accepted as the standard for calculating the amount of fission product species across the fuel zone. Test calculations have shown that the fission product inventories are being calculated with sufficient accuracy for HTGR safety analyses. Corresponding codes used at General Atomics are **GARGOYLE** and **RADC** [2]. Table 3-1 lists the inventories of radiologically relevant fission products in the equilibrium core of the 200 MW(th) HTR-MODUL. The ORIGEN burnup calculations were based on an equilibrium core, where the spherical fuel elements are reloaded to the core 15 times during a nominal life time of 1025 d [3].

Table 3-1: ORIGEN burnup calculations for fission product inventories in the equilibrium core

Nuclide	Half life	Core inventory [GBq]		
		HTR-MODUL (after 1025 efpd)	HTR-10 (after 1161 efpd)	HTTR (after 660 efpd)
Kr-85m	4.4 h	9.25×10^7	3.4×10^6	1.3×10^6
Xe-133	5.33 d	4.44×10^8	1.9×10^7	6.8×10^7
Xe-135	9.2 h	6.66×10^7	7.6×10^6	6.8×10^7
I-131	8.1 d	2.07×10^8	9.3×10^6	3.2×10^7
I-133	20.8 h	4.44×10^8	2.0×10^7	6.7×10^7
Cs-134	2.1 a	1.44×10^7	3.0×10^5	
Cs-137	30.2 a	1.67×10^7	6.7×10^5	2.6×10^6
Sr-89	50.8 d	2.89×10^8	1.2×10^7	
Sr-90	28.9 a	1.37×10^7	5.2×10^5	
Ag-110m	249.9 d	1.89×10^5	2.0×10^3	

With regard to the modeling of sorption processes on graphite surfaces (see Appendix A.2) and, in particular, co-sorption, all longer-lived plus the stable nuclides of a species plus chemically similar species have to be summarized to an overall inventory value which is for the HTR-MODUL [4]:

cesium (+ rubidium): 6×10^{25} atoms

strontium (+ barium): 8×10^{25} atoms

3.2. FUEL FAILURE MECHANISMS AND MODELS

3.2.1. Kernel Migration (“Amoeba Effect”)

Temperature gradients in coated particles due to extreme operating conditions or due to asymmetrical fuel kernel production lead to carbon transport from the "hot" side to the "cold" side of the inner pyrocarbon layer causing a migration of the fuel kernel toward the "hot" side (amoeba effect).

Kernel migration is not expected to occur in **German HTGR fuel** of a pebble bed reactor because low power densities and the homogeneous fuel distribution do not provide sufficiently strong temperature gradients [5].

Japanese HTTR fuel, however, is assumed to be exposed to severe temperature gradients. Experimental data on kernel migration distances from irradiation tests with high temperature gradients up to 150 K/cm have been gathered. From these measurements, a design equation for the kernel migration rate as function of the irradiation temperature has been derived demonstrating that even under severest HTTR conditions, the migration distance of the kernel calculated to be 55 μm was far below the safety design limit of 90 μm , i.e. the sum of buffer and inner PyC layer thicknesses [6].

In former **US modeling**, kernel migration has been recognized to be important because of the expected large temperature gradients in large-sized HTGRs. The migration of oxide-based particle kernels with a failed coating was examined by heating them in a thermal gradient at temperatures of 1100-1350 °C. In general, kernel migration increases with time and temperature and, in oxide kernels, with CO production. However, in UCO kernels, CO formation is suppressed and no kernel migration occurs [7].

Probabilities of SiC failure as function of the migration distance of the kernel toward the SiC layer are tabulated in a computer routine where the migration distance is dependent on time, temperature gradient, and kernel migration coefficients as function of temperature and kernel material. Data have been derived from experiments with HEU (Th,U)C₂, ThC₂, UC₂, and ThO₂ kernels in TRISO and BISO particles. However, failure by kernel migration is considered negligible for the present MHTGR core design.

A **Russian calculation model** has been developed [8] which describes the kernel migration phenomenon in the temperature range 1000 - 1250 °C and in the burnup range 0.5 - 5 %FIMA. The basis of the model is the heat exchange from the surface of an unsymmetrical particle kernel with an external medium which induces a thermal gradient. The external medium consists of fission gases (Xe, Kr) and reaction products of oxygen (CO, CO₂) which fill the free volume provided by the buffer and the gap between kernel and buffer. The equilibrium partial pressures of CO and CO₂ are dependent on temperature and burnup. A diffusive transport of carbon (oxides) occurs from the hot to the cold side of the inner pyrocarbon layer. A comparison of model calculations with experimental results is not given in [8].

Experimental studies in Russia have also been conducted at higher temperatures 1300-1800 °C and with temperature gradients up to 450-2500 K/cm. Metallographic sections

through coated particles with $\leq 12\%$ FIMA and a temperature gradient of 20 K/cm at 1400°C have revealed migration distances $\leq 8\text{ }\mu\text{m}$ [9].

3.2.2. Fission Product Interaction with Silicon Carbide

The interaction of the fission product species palladium with silicon carbide has been experimentally investigated at JAERI for HTTR reference design fuel by measuring the depth of penetration of the resulting intermetallic compound into the SiC layer [10]. The maximum Pd-SiC interaction depth was found to be dependent on the cubic root of the calculated Pd amount released from the kernel. From these measurements, it could be concluded that with respect to HTTR conditions a maximum penetration depth of $11\text{ }\mu\text{m}$ at end-of-life could be expected which is less than half of the total SiC layer thickness. However, the permissible pressure within the coated particle would be less than that for no Pd penetration.

In the US, reaction kinetics of the SiC attack by palladium have been experimentally investigated with the attack rate of fission products on the SiC layer found to be highly temperature-dependent [11] based on experimental work by Montgomery). Failure of the SiC layer is assumed to take place as soon as more than 50 % of the original SiC thickness has corroded. Although Pd is suspected to be a species of major importance, other metallic fission products are also believed to be involved. In carbide fuel, lanthanide fission products are expected to cause similar corrosion problems.

3.2.3. Pressure Vessel Failure

In Germany, the computer code CONVOL has been developed [12] to calculate the particle failure fraction under isothermal irradiation conditions. It determines the tangential stresses within the SiC layer taking into account the internal fission gas pressure, the tensile stress evoked by kernel swelling, and the tensile stress created by the neutron fluence-induced shrinkage of the pyrocarbon layers. Experimental data, however, could not be used for verification of the model predictions because of the calculational results being many orders of magnitude less than the probability for one particle to fail; at least they did not disagree with an observed zero failure fraction [13].

According to the US modeling approach [11], a pressure vessel model is regarded significant under normal operating conditions only for particles which do not meet the specifications (for instance too large kernels with too thin buffer layers). Standard (intact) particles are not expected to fail from pressure occurring within the coated particles. The failure probability of particles with initially missing or defective buffer is calculated as a function of burnup and temperature while fission product release from particles with missing or defective outer PyC is assumed to be controlled by fission product diffusion through the SiC layer. These models and assumptions for fuel performance during normal operation are incorporated into the calculation code SURVEY [14].

The effects of irradiation temperature, neutron fluence, burnup, particle component geometries and densities on the PyC and SiC layer stresses have been estimated using the computational results with analytical stress models such as PISA [15]. Thermal creep reduces the potential of pressure vessel failure of the outer PyC layer at high temperatures.

For the US-MHTGR normal operation, no significant pressure vessel failure of standard particles is expected to occur [16]. The US pressure vessel model is more significant as a particle design tool rather than a predictive tool for coated particle performance.

In Japan, JAERI developed a failure model to predict the failure fraction of TRISO coated particles under high burnup irradiation conditions [17]. The model considers the failure fraction to be dependent not only on the SiC pressure vessel failure but also on the failure of the PyC layers. The failure probability of each coating layer is described by a Weibull distribution with microscopic surface flaws considered to be critical failure initiation sites. The stresses that act on the coating layers of the fuel particle are assumed to be caused by the pressure of fission gases and CO gas released from the UO₂ kernel and by fast neutron-induced shrinkage of the PyC layers. The maximum stress is evaluated by a rigid SiC model with spherical shell [18].

Based on the model, parametric calculations were carried out for the first-loading-fuel of the HTTR and the high burnup fuel. The results show that the maximum tensile stress on the SiC layer in the intact particle is almost zero, and it is evaluated that no pressure vessel failure is predicted under HTTR operating conditions. The failure probabilities that an intact particle or an as-fabricated SiC-failed particle turn into a through-coatings failed particle were also evaluated. This model predicted that the as-fabricated SiC-failed particle results in a through-coatings failed particle much earlier than the intact particle does. However, the SiC-failed particle can keep its outer PyC integrity for a while and does not fail immediately after irradiation starts.

3.3. FISSION PRODUCT RELEASE MODELS

Fission product release behavior under normal operating conditions is of significant interest in safety analyses. Activity released into the primary circuit provides the major contribution to the accident-induced source terms especially in small-sized HTGRs, since the incremental release from the fuel at elevated temperatures is expected to remain comparably small. Fission product activity is available either as coolant activity or as plateout activity on surfaces of the primary circuit or as dust-borne activity providing potentially significant exposure levels with a severe impact on maintenance procedures. Within the active core, re-adsorption processes of metallic radionuclides from the coolant lead to an increased activity level in the outermost part of the fuel elements as it has been observed in the AVR reactor.

3.3.1. Gas Release

The activity of gaseous fission products in the coolant is a direct indicator of fuel performance. Its main sources are the heavy metal contamination in the fuel graphite and defective/failed coated particles. Standard particles within the specification limits are not expected to contribute to the release of fission products under normal operating conditions.

For the release of long-lived fission gases from the kernel, the classical formulation

for diffusive release from a sphere is applied, with the fractional release given by [19]:

$$F = 1 - \frac{6}{D' t} \sum_{n=1}^{\infty} \frac{1 - e^{-n^2 \pi^2 D' t}}{n^4 \pi^4} \quad (3-1)$$

where

- t is the irradiation time [s]
- D' is the reduced diffusion coefficient [s^{-1}]
 $D' = D / a^2$
- D is the diffusion coefficient [m^2/s]
- a is the kernel radius [m]

For short-lived gaseous fission product species, production in and release from the kernel will quickly reach a steady state. The **Booth model** [20] is most commonly taken to determine the ratio of the release rate to the birth rate, (R/B). (R/B) is a function of the kernel diffusion coefficient, the decay constants of the fission product isotopes and of the surface to volume ratio, ($S/V=3/a$), of a sphere equivalent to the representative grain of fuel with radius a. In practice, the kernel is often regarded as a solid sphere, and the diffusion coefficient derived from experimental data using the kernel radius. The Booth model is applicable only to the diffusive release of fission products from kernels and from matrix graphite grains (which contain the heavy metal contamination) as simulated by equivalent spheres. It can also be used for gaseous precursor nuclides of radiologically relevant long-lived metallic fission products (Xe-137, Kr-89, Kr-90).

$$R / B = \frac{3}{x} (\coth x - \frac{1}{x}) \quad (3-2)$$

where

$$x = \sqrt{\frac{\lambda a^2}{D}} \quad (3-3)$$

and

- λ is the decay constant [s^{-1}]
- a is the kernel radius [m]
- D/a^2 is the reduced diffusion coefficient [s^{-1}]

If $x \gg 1$) then:

$$R / B \approx \frac{3}{x} = 3 \sqrt{\frac{D}{\lambda a^2}} \quad (3-4)$$

showing the characteristic feature of the $1/\sqrt{\lambda}$ dependence for short-lived isotopes (valid for a smooth surface sphere).

When the kernel is surrounded by fuel particle coatings, application of the Booth model is not strictly correct as the following indicates. Recoiled fission product atoms, 2 to 3 % of which are ejected from the fuel kernel, have terminal sites mainly in the buffer coating. Atoms at sites of relatively lower binding energy can readily escape from the buffer by diffusion and thus contribute to the total release from particles with exposed kernels. This course of events is reflected in the power of D/λ , say n , where $n = \partial \ln(R/B)/\partial \ln(D/\lambda)$. In the Booth model $n = 0.5$. Experimentation, however, yields a range of n values having approximate limits of 0.1 and 0.5. Such results confirm the eventual release of recoiled atoms. A detailed quantitative evaluation of this mechanism has yet to be made.

The **HRB model** for fission gas release from defective fuel particles [21] is also based on Booth's R/B equation and its approximation. But this model distinguishes between the different components, grains and pores, of both the particle kernel and the buffer layer. The complete equation is given by:

$$(R/B)(\lambda, T) = F [f_{kk}(R/B)_{kk} + f_{kp} + f_{pk}(R/B)_{pk} + f_{pp}] (R/B)_p \quad (3-5)$$

where

f_{kk} is the ratio of birth rate in particle kernel grains over B

f_{kp} is the ratio of birth rate in particle kernel pores over B

f_{pk} is the ratio of birth rate in buffer grains over B

f_{pp} is the ratio of birth rate in buffer pores over B

$f_i = b_i/B$ and $\sum b_i = B$

F is a factor describing the type of defect of the particle coating
($F = 1$ for the most releasing type: kernel + buffer only)

$(R/B)_p$ is the release-rate-to-birth-rate ratio for the pores

The magnitude of f -values which contain the recoil effect are empirically estimated. $(R/B)_p$ is supposed to show the $T^{3/2}$ dependence of a gas phase diffusion but due to a negligible retention of the pores, it can be approximated by $(R/B)_p \approx 1$. At lower temperatures < 700 °C, the diffusion of gaseous atoms from recoil sites in the buffer is more significant than the diffusive release from the kernel grains.

Values of the parameters required in the model are listed in Appendix A, section A.4.

The **US model** for steady state fission gas release from fuel particles with exposed kernels [19, 22] incorporates the Booth model and, in an empirical manner, the effects of temperature, burnup, the mechanisms of athermal and vacancy migration diffusion [23, 24], both irradiation induced, intrinsic diffusion [23] and a buffer-recoil contribution to release [25]. For radionuclide i:

$$(R/B)_i = \left\{ 3 \sqrt{\frac{D'}{\lambda_i}} f(T) f(Bu) + f(I) \right\} / \{1 + f(I)\} \quad (3-6)$$

where

$$\begin{aligned} f(T) &= A + (1 - A) \exp\{Q/(RT_0) - Q/(RT)\} \\ f(Bu) &= 1 + \sigma(Bu)^m \\ f(I) &= \exp\{\alpha(T - T_s)\} \end{aligned} \quad (3-7)$$

and

- D' is the reduced diffusion coefficient [s^{-1}]
- T is the temperature [K]
- Bu is the burnup [%FIMA]
- Q is the activation energy [J/mol]
- R is the ideal gas constant, $R = 8.3143$ [J/(mol K)]
- $T_0 = 1373$ K

For each gaseous fission product element (Kr, Xe) and each fuel composition, UC_xO_y and UO_2 , ThO_2 , and UC_2 , the values of D', Q, $\exp\{Q/(RT_0)\}$, and the constants A, σ , m, α , and T_s must be specified. For the US model, these values are presented in Appendix A, section A.4.

The **US model for transient fission gas release from fuel particles with exposed kernels** [26] is derived from a model framework [26], from the solution of differential equations for the release and decay of nuclides, including a precursor [26] where appropriate, and an embedded fractional release function [26] corresponding to a solution of the diffusion equation which accounts for transport, trapping and emission of diffusants [26, 27].

The framework is defined by three characteristics: (1) two subpopulations of the fission product atoms one of which is rapidly released and the other slowly, but steadily, released from the fuel, (2) subdivision of the former subpopulation into independent subsystems containing a fixed number of atoms of a specific nuclide, and (3) the temperature behavior of the subsystems.

The fractional release function which enters the model as the time derivative, is

$$f(T) = f_\beta(T) \sqrt{1 - \exp\{-\alpha(T)t\}} + S(T)t \quad (3-8)$$

where f , f_β , α , and S are functions of temperature [26] deduced from isothermal experiments in the range 1430 to 2060 °C. In equation (3-8), the first term on the right-hand side represents the rapidly released fission gases and the second term, the slowly, but steadily released fission gases.

On the basis of the diffusion trapping model [26, 27], the functions of equation (3-8) have the following meanings: f_β is the product of the surface to volume ratio (for the equivalent sphere) and the diffusion trapping length (i.e., the square root of the mean square distance an atom migrates to reach a trap), α is the product of $4/\pi$ and the rate of trapping, and S is the product of f_β and half the rate of emission (escape from traps).

These meanings are significant below a critical temperature, T^* . Above the critical temperature, a different mechanism of release becomes dominant. The mechanism is surmised to involve the transport of collectives of fission gas. Above T^* , the fractional release of krypton and xenon isotopes is a strong function of temperature and rapidly approaches 1 [26]. The contribution of mechanisms dominant below T^* at temperatures above T^* is not greater than 10 %. Unfortunately, no attempt to apply a theoretical model to the region of temperature greater than T^* has been made. Nevertheless, given the temperature dependencies of f , f_β , α , and S , the fractional releases were quite accurately calculated for heating experiments at temperatures below and above T^* . During these experiments, the temperatures were steadily increased from 927 to 2027 °C [26].

Data for the US model of transient fission gas release from fuel particles with exposed kernels [26] has only be obtained for UC_2 and ThO_2 . Data for UC_xO_y ($x+y=2$) and UO_2 would be expected to be intermediate to those for UC_2 and ThO_2 . Note also that T^* is 1690 °C for UC_2 and 1990 °C for ThO_2 .

The **CEGB model** for diffusive release of fission gas from single and polycrystalline UO_2 [23] framed in the simple Booth equation, is

$$R / B \simeq \frac{S}{V} \sqrt{\frac{D}{\lambda}} \quad (3-9)$$

with a composite expression for D given by

$$D = AF + B\sqrt{F} \exp\{-Q_v/(RT)\} + D_o \exp\{-Q_I/(RT)\} \quad (3-10)$$

where

S/V is the surface to volume ratio of UO_2 [mm^{-1}]

D is the diffusion coefficient of fission gases in UO_2 [m^2/s]

λ is the isotope decay constant [s^{-1}]

A is a constant for athermal diffusion in oxide fuels [m^5]

F is the fission rate density [$m^{-3}s^{-1}$]

B is a constant [$m^3 (m/s)^{0.5}$]

Q_v is an activation energy related to vacancy diffusion [J/mol]

D_o is a constant [m^2/s]

Q_I is the activation energy for intrinsic diffusion [J/mol]

R is the gas constant, $R = 8.314$ J/mol/K

T is the temperature [K]

The above description of the composite diffusion coefficient, equation (3-10), has three terms each of which represent one of the three mechanisms important for fission gas

transport in and release from UO₂. The first and second terms on the right-hand side of equation (3-10) represent irradiation-induced transport mechanisms. The first term, D_a, represents an athermal mechanism which depends on the fission rate density and the effect of fission fragments. The athermicity extends from 130 to 1000 °C. The second term, D_v, represents enhanced diffusion based on the non-equilibrium lattice vacancy concentrations resulting from irradiation damage. This mechanism is important in the range between 800 and 1400 °C. The third term, D_I, represents intrinsic diffusion mainly at temperatures above 1400 °C but extending to lower temperatures in low-rated experiments.

For each gaseous fission product element (Kr, Xe) in UO₂, the values of A, B, Q_v, D_o, and Q_I must be specified. For the UK model, these values are presented in Appendix A, section A.4. In addition, appropriate values of λ, F, T, and S/V are needed.

The **JAERI approach** of modeling the release of short-lived noble gases from failed coated particles and matrix contamination [28] is based on an empirical equation which has been generated from previous irradiation experiments with fuel compacts and loose particles. It describes the Kr-88 R/B measurements per failed particle as a function of the irradiation temperature. The release of fission gases other than Kr-88 is then determined by assuming constant ratios of the R/B to that of Kr-88 with the ratios determined using an analytical diffusion model which also considers the effect of precursors:

$$(R/B)_i = K_i \sqrt{\frac{\lambda_{Kr-88}}{\lambda_i}} (R/B)_{Kr-88} \quad (3-11)$$

where K_i is the parameter for nuclide i. Values of K_i for noble gases and iodine are listed in Appendix A, section A.4.

Good agreement except at lower temperatures was found when applying this model to irradiation tests with fuel compacts which contained artificially failed particles. However, R/B measurements from compacts with contaminated matrix were different from the calculated release behavior predicted with this model. The model is taken to estimate the activity circulating in the primary system of the HTTR.

Another **JAERI model** to calculate fission gas release from oxide fuel is based on a modeling approach developed at Chalk River/Canada [29]. It is an extended Booth type model which takes account of a diffusive transport in the oxide fuel, a partial retention of gas in trapping sites which are available as either closed voids or larger irradiation-induced crystal defects, and a possible re-solution of trapped gas with a subsequent diffusive transport. This model is similar to the diffusion-trapping model of transport in graphite.

JAERI is also developing a new model on fission gas release from a fuel compact [30]. When the failure fraction in the fuel compact is high, the conventional model gives relatively good or conservative prediction. Therefore, in the design of the HTTR, in which 1 % of the failure fraction was assumed, the activity of fission gases in the primary coolant was evaluated by the conventional model. On the other hand, the failure fraction has decreased to the order of 10⁻⁶ - 10⁻⁵ according to an improvement of the fuel fabrication technique. It means that the modeling of fission gas release from matrix contamination uranium is becoming important for accurate evaluation. Moreover, since the fuel will be

used up to a higher burnup than the first loading fuel of the HTTR in future, a fission gas release model should be developed which is applicable up to high burnups and high fast neutron irradiation.

Based on this situation, a revision of the fission gas release model was carried out. Key issues of the revision of the fission gas release model are as follows:

1. Fission gas releases from the matrix contamination uranium and from the failed particles are separately modeled.
2. Burnup and fast neutron irradiation effects on diffusion releases from the failed particles and from the fuel compact matrix are taken into account in the model.

In the revised model, fractional release is written as following equation

$$R / B = (f_{kd} + f_{kr}) f_{md} \Phi_k + (f_{md} + f_{mr}) \Phi_c \quad (3-12)$$

where

f_{kd} is the fractional release from the kernel by diffusion

f_{kr} is the recoil release fraction from the kernel

f_{md} is the fractional release from the fuel compact by diffusion

f_{mr} is the recoil release fraction from the fuel compact matrix

Φ_k is the fraction of through-coatings failed particles

Φ_c is the fraction of uranium contamination in the fuel compact matrix

Fractional release from the through-coatings failed particles increases with burnup in general because the irradiation-enhanced diffusion occurs as a result of burnup. A correction factor by fast neutron irradiation in the fuel compact matrix is employed considering the effect of irradiation-retarded diffusion. In general, the release fraction decreases with the fast neutron irradiation by forming trap-sites of fission products. The release fraction by fission recoil of the contaminated uranium in the fuel compact matrix is calculated by the fuel compact geometry, which is assumed to be an infinite hollow cylinder, and recoil distance of the fission product.

An applicability of the revised fission gas release model has been investigated through comparison with experimental data and the following conclusions were obtained. (1) The calculated results by the revised model are smaller than those of the conventional model and show better consistency with the measured data. This improvement is made mainly by revision of the release model in the low fuel temperature region. (2) Calculated (R/B)s with the revised model indicate an increase with irradiation time although the conventional model could not reproduce this behavior. This behavior is considered to be the burnup and the fast neutron irradiation effects on the diffusion release of fission gas.

A numerical determination of the gas release during normal operation is given by the **KFA computer code STADIF-II** [31]. It describes the steady state fission gas and

iodine release from defective particles, recoil effect, and graphite contamination by using an uncoupled two-phase (grain, pore or grain boundary) diffusion model, but considers no sorption effect on graphite surfaces. The code also allows for calculation of the coolant activities taking account of the purification system, for iodine in addition plateout constants. Calculated krypton and xenon release values are in good agreement with AVR experimental results.

The **US code RADC** [2] determines the R/B values of various gaseous fission product isotopes and thus can estimate their inventories in the fuel, in the primary coolant, and on the surfaces exposed to the coolant within the HTGR system. The main input data are the diffusion coefficients derived from experiments with as-manufactured fuel compacts and defective fuel particles, and the removal rates due to plateout and due to the purification system.

The **Russian method** of determining the fission gas and iodine release under normal operating conditions is characterized by a temperature dependent release velocity $R(T)$ - equivalent to a change of the activity per unit time - of the nuclides out of a core volume element ΔV [32]:

$$R = \frac{\sum R(T) \Delta V(T)}{V} \quad (3-13)$$

$\Delta V(T)$ corresponds to the part of fuel elements in the core at temperature T.

The main sources of fission products are identified as defective particles (ϕ) and heavy metal contamination of the particle coatings and the matrix graphite (ω). Regarding - for completeness - also particles with an intact coating (mt), the overall release velocity reads as follows:

$$R = R_\phi + R_\omega + R_{mt} \quad (3-14)$$

According to the so-called two-group activation model [33], the release over birth ratio is given by:

$$F = (R/B)_i = m_i f(\alpha_f, \tau) + (1 - m_i) f(\alpha_s, \tau) \quad (3-15)$$

where

$$f(\alpha_j, \tau) = 1 - \frac{1 - e^{-\alpha_j \tau}}{1 - e^{-\lambda \tau}} \frac{\lambda e^{-\lambda \tau}}{\alpha_j + \lambda} \quad (3-16)$$

and

- α_j is the release constant [s^{-1}]
indices $j=f$ and $j=s$ represent the two groups of fission products considered in the activation model
- λ is the decay constant [s^{-1}]
- τ is the irradiation time [s]
- m_i are the spectral characteristics
derived from experiments with irradiated fuel elements
index $i = \phi$: defective particles
index $i = \omega$: heavy metal contamination
index $i = mt$: intact particles

For most of the volatile nuclides, the approximation $\alpha_f \gg \lambda \gg \alpha_s$ is valid, thus:

$$R(T) = [m_\phi(T) \phi B] \Delta V(T) \\ [m_\omega(T) \omega B] \Delta V(T) \\ [m_{mt}(T) (1 - \phi - \omega) B] \Delta V(T) \quad (3-17)$$

where

- B is the birth rate
- ϕ is the fraction of defective particles
- ω is the fraction of heavy metal contamination
- mt is the fraction of intact particles, $mt = 1 - \phi - \omega$

Integration over the total core volume provides the overall volatile fission product release into the coolant. Release rates from defective particles and from heavy metal contamination have been measured in experiments.

A detailed description of the Russian two-group activation model is given in the Appendix B.

3.3.2. Metal Release

3.3.2.1. Calculation Models

The transient release behavior of (long-lived) metallic fission products can be predicted by using diffusion models. An intact TRISO particle coating represents a highly efficient barrier against fission product release at normal operation temperatures (except for silver). Therefore, the most important input data for coated particle performance during normal operation will be the fractions of defective/failed coated particles and the fraction of heavy metal contamination in the fuel element graphite in combination with the transport data in kernel material and fuel element graphite. In addition to diffusion, other release mechanisms during normal operation are the recoil effect and the knockout effect. Both represent a geometrical problem and are not dependent on temperature making them relatively more significant at lower temperatures.

Gaseous precursor nuclides of metallic fission products must also be considered, in particular the strontium isotope Sr-89. It is not clearly known to what extent the presence of the nuclides Cs-137 and Sr-90 in the coolant is caused by precursors, by formation of contaminated dust due to fuel element abrasion, or by direct release of the radionuclides and/or their compounds. With respect to the Fort St. Vrain HTGR, diffusion tube measurements have indicated that direct release does not occur. Sources of primary circuit contamination are the formation of contaminated dust and gaseous precursors only [34]. In contrast, direct release seems to be dominant in the AVR reactor [35] and is therefore assumed in actual German safety analyses. Sources of this direct release by coated particles with intact or defective coatings and by fuel contamination of graphite are considered separately. Reliable data on fuel in particles with defective coatings and in graphite are obtained by the fuel element qualification program.

The pebble version of the **KFA diffusion model FRESCO** [36] has been widely used to describe the metallic fission product release behavior from a spherical fuel element both under irradiation and elevated temperature conditions. This model includes specific irradiation effects such as recoil and the buildup of fission product inventories dependent on the decay constant. It is based on effective diffusion coefficients for the fission product species in the different fuel materials. Transport data for normal operating conditions are given in Appendix A. By choosing average fuel operating conditions, a FRESCO-II calculation can be taken to describe a representative fuel element during its lifetime even for a fuel sphere to pass several times the active core (multipass loading scheme) as planned for the German small-sized HTGRs. The release results can then be extrapolated for all fuel spheres over the plant's lifetime.

An example of a FRESCO-II prediction showing the release of metallic fission products from a spherical fuel element is given in Fig. 3-1 for the design of a 170 MW(th) modular HTGR for process heat applications [37]. 15 reshuffling periods for the fuel spheres with the operating temperature ranging between 400 and 1200 °C were assumed. The fractional release curves are characterized by the three processes of radioactive decay, buildup of the inventory, and diffusive transport. The low temperature at cycle start causes the release curve to drop due to the small diffusion transport while the inventory – for long-lived fission products – is steadily increasing and the radioactive decay is insignificant. At the end of a cycle when the fuel temperature reaches its maximum, the diffusive release becomes dominant.

The **JAERI computer code FORNAX** [38] is similar to the diffusion code FRESCO-II in describing the metallic fission product release from the particle kernel by diffusion and recoil and the diffusive transport through the coating materials in a fuel element. Three different types of fuel particles are considered in the FORNAX model: standard (intact) particles, failed particles (= exposed kernels) and - at a stage in between - particles with a degraded SiC layer simulated by a larger diffusion coefficient. Calculated results show good agreement with residual cesium and silver activities in the particles and plated-out activities inside the capsules from irradiation tests [38]. The FORNAX model is also applied to accident conditions.

The verification result showed that the calculated fractional release was larger than the measured one on the average [38]. It was guessed that this discrepancy was caused by

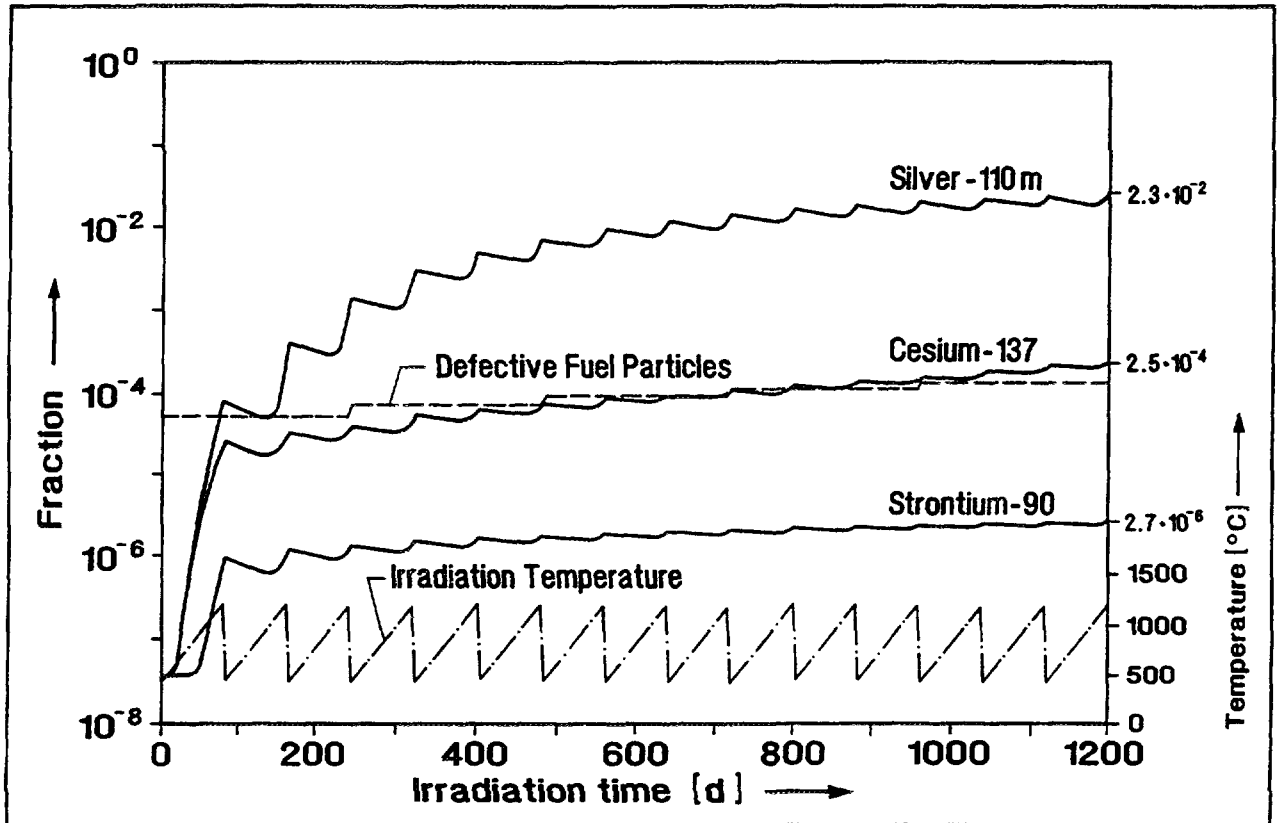


Fig. 3-1: Fractional release of Cs-137, Sr-90, and Ag-110m from a spherical fuel element during its lifetime in a 170 MW(th) process heat modular HTGR (based on design values) [37]. Temperature and particle failure function are input to the FRESCO-II calculation.

simplified modeling of failed particles. The release model of cesium was investigated by comparing measured and calculated fractional releases in the ICF-51H capsule irradiation test, which contained three kinds of coated particles of artificially failed particles simulating through-coatings failed particles, as-manufactured SiC-failed particles and intact particles [39, 40]. Through the investigation, the model was revised to establish an accurate cesium release model.

The ICF-51H capsule included six inner capsules. Each inner capsule contained one type of fuel particle. There were three types of fuel particle, intact, as-fabricated SiC-failed and artificially failed particles. The intact particles had all intact layers and were selected by visual observation and X-ray radiography. The SiC-failed particles were also selected by X-ray radiograph observation and had failed inner PyC and SiC layers but intact outer PyC layer. The artificially failed particles were made by drilling of a hole that reached from the outside of the outer PyC to the surface of the kernel. The diameter of the hole was about $200 \mu\text{m}$. The ratio of fractional releases at the end of irradiation from the failed particles to the intact particles for each inner capsule is shown in Fig. 3-2. The X-axis is measured and the Y-axis is the calculated ratio. The figure shows that (1) the calculated fractional release

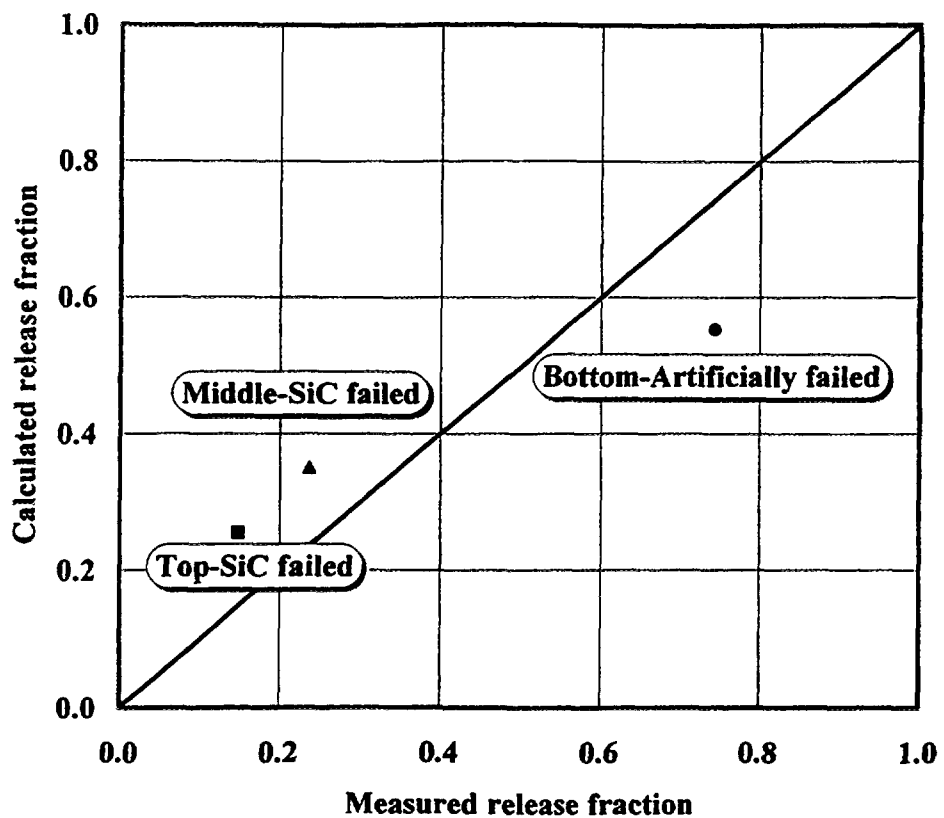


Fig. 3-2: Measured versus calculated ratio of release fraction from failed over that from intact particles in the ICF-51H irradiation test

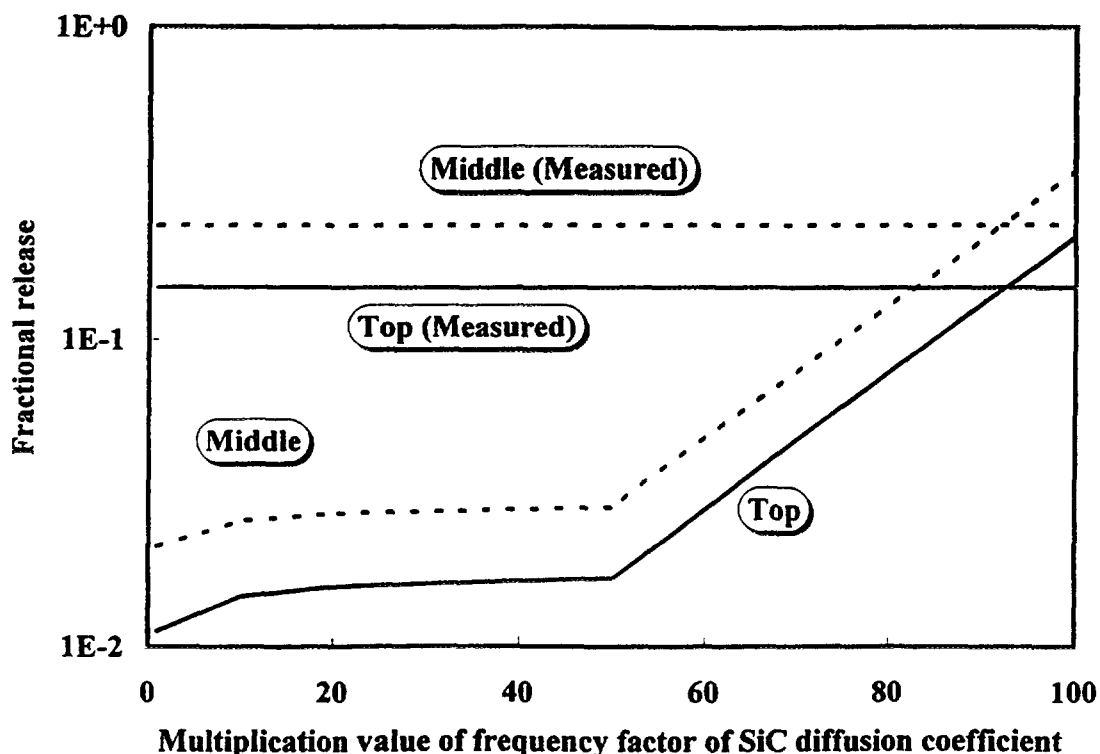


Fig. 3-3: Fractional release versus frequency factor to determine equivalent diffusion coefficients

from the SiC-failed particles is overestimated and (2) the calculated fractional release from through-coatings failed particles is underestimated.

X-ray microradiography of the irradiated artificially failed particles showed that the UO₂ kernels were carburized and some amounts of UO₂ escaped from the particles. Since the diffusion coefficient of cesium in uranium carbide is much larger than that in the UO₂, the calculated fractional release with the UO₂ diffusion coefficient gave a smaller value when compared with the experimental data. The experimental data indicate that the fractional release of cesium from the carburized, through-coatings failed particles was nearly 100 %.

On the other hand, the calculated fractional releases from the SiC-failed particles were overestimated. In the model, the SiC-failed particle was treated as a particle completely missing the SiC layer and the diffusion coefficient in the failed SiC layer was assumed to be the same as the diffusion coefficient in the PyC layer. The result suggests that the failed SiC layer has a higher retention effect than the model predicts, i.e., the equivalent diffusion coefficient in the real failed SiC layer is smaller than that in the PyC layer. Since the SiC layer has the smallest diffusion coefficient in the coating layers, cesium accumulates at the inner surface of the SiC layer. In the SiC-failed particle, cesium will be transported to the break area in the SiC layer according to the gradient of cesium concentration. In order to represent this process, an equivalent diffusion coefficient (EDC) in the failed-SiC layer is assumed. Since the EDC will strongly depend on the break area of the SiC layer, it should be determined with the fractional release from as-fabricated SiC-failed particles. The comparison of the measured and calculated fractional releases for the SiC-failed particles was carried out. In the calculations, the frequency factor of the SiC diffusion coefficient was changed to determine the EDC. The results of the top and the middle inner capsules are shown in Fig. 3-3. The calculated fractional releases agree with measured values when the frequency factor of the equivalent SiC diffusion coefficient is about 90 times higher both for the top and for the middle inner capsules. It means that as-fabricated SiC-failed particles irradiated in the ICF-51H capsule had almost the same configuration of failure from the view point of cesium release.

The KFA diffusion code SPTRAN [41] has been recently modified for use under normal operating conditions [42]. No significant difference in the method of modeling fission product release from the fuel between this code and FRESCO-II can be detected. Validation calculations of irradiation tests or reactor experiments have not yet been presented for SPTRAN.

The GA codes COPAR2 [43] and TRAFIC-FD [44] determine the release of metallic fission products from the HTGR core into the primary coolant circuit. The codes model a one-dimensional Fickian migration through the fuel particle, fuel compact, and structural graphite to the coolant hole surface. COPAR2 calculates release from the kernels through the coatings into the matrix, and TRAFIC-FD calculates transport from the compact through the graphite and into the flowing helium coolant. Sorption on fuel compact matrix material and evaporation from the graphite surfaces into the coolant are taken into account as well as the recoil effect and radioactive decay. A multiple-path, multiple-species code, called TRAMP [45], includes diffusion as a result of thermal gradients, the in-grain and grain surface diffusion as a result of concentration gradients, and the convection of the coolant

through the permeable graphite (pores). The TRAFIC code is specialized for a rapid computation of block-averaged metallic fission product release at many spatial positions in the HTGR core using an irregular space and time dependent temperature history.

3.3.2.2. Model Valuation

The principal disadvantage of existing release models for normal operating conditions is their inability to handle all the important phenomena in the active core of an HTGR at the same time. For example, the normal operation release results calculated using the diffusion model FRESCO-II for a single spherical fuel element must be extrapolated over the whole pebble bed. The feed-back given by gas-borne activity on the release behavior which has been observed in AVR fuel elements to create an increased metallic fission product concentration in the outermost fuel-free graphite shell due to re-adsorption processes in colder core regions, is not considered in the models. Modeling of the coolant inlet effects also requires a connection to plateout processes in the primary circuit. Consideration of this readsorption effect as well as the production of dust by fuel element abrasion and its effect on fission product transport, and of the effect of precursor nuclides, would complete a comprehensive model for the core release behavior under normal operating conditions.

3.3.2.3. Uptake of Fission Product Metals by Silicon Carbide

The fission metal content of SiC following the irradiation of TRISO coated fuel particles in the High Flux Isotope Reactor (HFIR) at ORNL, the R2 Reactor at Studsvik and the Fort St. Vrain (FSV) Reactor at temperatures between 512 and 1200 °C, burnups between 0.9 and 45 %FIMA, fast neutron fluences between 1.9×10^{25} and $7.8 \times 10^{25} \text{ m}^{-2}$ and for 171 to 519 effective full power days (efpd) has been measured [46]. Analysis of these measurements has lead to the conclusion that the quantities of the metallic fission products, cesium, cerium, europium, ruthenium, and antimony, are proportional to the number of neutrons that have passed through the SiC. The linearity of the relation between the quantity of fission products in the SiC and the neutron fluence is improved by accounting for the differences in the ratio of the number of atoms in the SiC and the number of neutrons that have passed through it. This ratio is 3 to 4 times larger for the graphite moderated reactor, FSV, than for the water moderated reactors, HFIR and R2.

No explicit dependence of the fission product content of the SiC was found on time, burnup, temperature, or kernel enrichment. A qualitative model to account for this was conjectured to have the following components:

1. Structural damage in the SiC coating from the slowing down of fast neutrons creates sites at which the fission products bind or paths by which they may enter the coating and
2. the fission product atoms move into the SiC coating to occupy these sites and perhaps along the paths generated by fast neutrons.

According to the first element of the model, the fission product quantities are proportional to the number of sites created during the slowing down of fast neutrons. If the fission product content of the SiC is proportional to the number of damage sites in the irradiated SiC, then an estimate of the probability of neutron damage with respect to fission product

binding can be made. From an alternative viewpoint, the effect of the neutron damage is to increase the solubility of fission products in SiC. The strengths of the binding of fission products to SiC appear to be larger than small multiplies of kT where T is in the temperature range 512 to 1200 °C.

3.3.3. Future Needs

In addition to further experimental studies of fission product release from “quality fuels”, the presently available data needs to be evaluated with the same overall fission product release model. A key item is the identification of the “reference” model(s). Such an effort would give understanding to the relative performance of fuels obtained at the various research centers, and help improve the “reference” model(s).

3.4. FUEL IRRADIATION TEST PROGRAMS

Testing of HTGR fuel during irradiation has been conducted both in real-time operating HTGRs and in various MTRs. Testing limits have been chosen to provide a broad envelope around the required normal operating conditions of HTGR designs.

Within the FRG UO₂ LEU TRISO irradiation program, six tests have been made comprising a total of 260,420 coated particles. The use of different techniques for detection of defective/failed particles (cold gas test, cesium profile, chlorination) leads to slight differences in the results with the cesium profile method tending toward higher numbers. The comparison of the measured Kr-88 R/B-values before (“Beginning-of-Life” BOL) and after (“End-of-Life” EOL) irradiation, however, has shown that no in-pile particle failure occurred. All detected defects could be concluded to originate from the manufacturing process [47]. Using statistical analysis, an upper limit for the irradiation induced failure fraction is represented by 2×10^{-5} at the 95 % confidence level. No additional particle failure is expected for burnups up to approximately 9 %FIMA to assure the design limit chosen at 2×10^{-4} . In the status report [48], the design value was the same, whereas the expected value was previously chosen to be half of the design value.

During normal operation of the US-MHTGR, an additional fuel particle fraction of 5×10^{-5} at 50 % confidence level and 2×10^{-4} at 95 % confidence level, respectively, is assumed to have a failed SiC layer. The fraction of 5×10^{-5} particles with initially missing buffer layers has completely turned into exposed kernels [16]. The US program also uses a fuel performance model for irradiation induced failure of the outer PyC layer. The fraction of particles with a failed outer PyC layer is as large as 3×10^{-2} [16]. A qualification program similar to the German one has recently started, in order to demonstrate the quality goals for modern US fuel.

The performance of Japan’s fuel under normal operating conditions has been investigated in many irradiation experiments to verify the safety design requirements of HTTR fuel; i.e., no additional systematic failure is expected to occur during normal operation with a maximum design fuel temperature of 1495 °C (nominal value ≈ 1300 °C). An upper regulatory defect limit for as-manufactured coated particles was set at 2×10^{-3} at the 95 % confidence level [6]. Due to this high design value, no higher level of failure during normal (and abnormal) transients is expected to occur. However, for purposes of conservatism

Table 3-2: As-manufactured fuel quality and in-reactor performance criteria

	FRG	US	Japan	USSR	China
As-manufactured free uranium					
Heavy metal contamination	$1*10^{-7}$	$1*10^{-5}$	$1*10^{-5}$	$4*10^{-6}$	$4*10^{-6}$
Exposed kernels	$3*10^{-5}$	-	$1*10^{-5}$	$< 5*10^{-5}$	
Defective SiC, intact outer PyC	-	$5*10^{-5}$	$5*10^{-4}$	$< 10^{-4}$	
Total (expected value)	$3*10^{-5}^{(1)}$	$6*10^{-5}$	$5*10^{-4}$		
Total (design value)	$6*10^{-5}^{(1)}$	$1.2*10^{-4}$	$2*10^{-3}$	$< 10^{-4}$	$\leq 3*10^{-4}$
Irradiation-induced failures					
Expected value	$2*10^{-5}^{(1)}$	$5*10^{-5}$	0		
Design value	$2*10^{-4}^{(1)}$	$2*10^{-4}$	$8*10^{-3}$	$< 10^{-4}$	$5*10^{-4}$

(1) Initial target of fuel development

and considering a procedure similar to LWR licensing, a total defect fraction of 1 % is used in HTTR safety evaluation studies. A value of only 5×10^{-4} was experimentally found in compacts irradiated to 1.5 %FIMA and reaching a temperature of 1750 °C. The maximum failure fraction increased by about two orders of magnitude compared to the initial value in irradiation experiments where a burnup of 4 %FIMA at 1720 °C was reached [49].

Two major failure mechanisms during normal operation have been studied in detail in the Japanese program: kernel migration inside the coated particle and interaction of the fission product species palladium with silicon carbide (see chapter 2). Neither one has been experimentally found to cause any further damage to the fuel under HTTR design operating conditions. R/B values of Kr-88 have shown that there was no significant increase of the fuel failure fraction [6].

In the **Russian Federation**'s experimental studies, major observations, besides kernel migration, were a vaporization-condensation effect to happen via radial microcracks in buffer and inner PyC layers, and a fuel creeping effect caused by isolated gas-filled bubbles in the kernel [50].

The goal of the fuel performance qualification program in **China** is to reach the FRG design values. The current plan is to conduct first irradiation tests at 1000 °C up to 10 %FIMA. No specific data for Chinese fuel have been given so far.

Available data on defective/failed TRISO particle fractions and heavy metal contamination from the different countries' fuel qualification program are summarized in Table 3-2.

For fuel particles with **BISO** coating, the end-of-life failure fraction to be used in German safety analysis calculations was derived from experimental data to be as high as 2×10^{-3} . A failure fraction of even 1 % was found under extremely conservative irradiation conditions and has been used as the design value for KFA safety analysis calculations for the THTR-300 [51].

3.4.1. The Chinese Program

Preliminary irradiation experiments have been carried out in the Chinese research reactor in 1989. The burnup is 0.4 and 0.8 %FIMA, fission product release rate is in the range of 10^{-6} to 10^{-7} . Some samples are irradiated in the FRJ2 reactor, KFA Jülich, Germany with a planned burnup of 2.5 %FIMA, the experiment is now underway.

The final **irradiation qualification** of the fuel element for the HTR-10 will be carried out in cooperation with the Kurchatov Institute, Moscow, Russia. The irradiation parameters set are as follows: temperature 1000 °C, burnup 100,000 MWd/tU (\approx 11.0 %FIMA), fast neutron fluence $1.0 \times 10^{25} \text{ m}^{-2}$.

The release of fission products will be continuously monitored, the impurities of the sweeping gas will be periodically measured. To match the time schedule of the construction of HTR-10, the irradiation experiment will be carried out to a burnup of 30,000 MWd/tU (\approx 3.3 %FIMA). At this burnup, a temperature excursion to 1200 °C for 200 h will be done, and an intermediate evaluation report of the irradiation result will be issued. The irradiation will continue to a burnup of 60,000 MWd/tU (\approx 6.6 %FIMA) at 1000 °C, and another temperature excursion to 1200 °C for 200 h will be carried out and the second intermediate report will be issued. The irradiation experiment will be resumed until the goal of 100,000 MWd/tU (\approx 11.0 %FIMA) burnup is reached.

Postirradiation experiments will be carried out after the sample was properly cooled. Spherical fuel elements and coated particles irradiated loosely will be thoroughly examined. The sample will be visually inspected and photographed. Dimension and weight change of the specimens will be measured. Fission product content and distribution in the matrix of the fuel element and various components of the coated particles will be measured after the spherical fuel element is disintegrated. Microstructure of the coated fuel particles both loosely irradiated and separated from the spherical fuel element will be observed. Accident simulation experiments will be carried out on one of the spherical fuel elements irradiated. The fuel element will be heated up to 1600 °C for 200 hours, fission product release rates will be determined, and the change of structure and properties of fuel element and coated particles will be examined. The results will be evaluated and documented.

The status of the R&D of the HTR-10 fuel element is: the laboratory scale is phasing out, the prototype scale is phasing in. Presently it is tried to get the facilities for prototype scale R&D ready. The final irradiation qualification will start at the end of 1997.

3.4.2. The German Program

The in-reactor performance of LEU fuels, together with follow-up postirradiation examinations, fission product release analyses, and postirradiation accident simulation tests, have demonstrated a high level of fuel performance of the reference UO₂ system.

3.4.2.1. In-Pile Failure and Fission Gas Release

The (operation-related) failed fraction is derived from the release of rare gases measured in-pile in five most representative irradiation experiments with German reference

Table 3-3: Parameters and results from irradiation tests with modern, high-quality UO₂ TRISO particles in the German program

Experiment	Specimen per capsule	No. of particles	Irradiation time [efpd]	Temperature surface/center [°C]	Burnup [%FIMA]	Fluence [10 ²⁵ m ⁻² , E>16 fJ]	Release at end of irradiation	
							R/B Kr-85m	Fractional release Cs-137
HFR-P4/1	12 small spheres	19,600	351	915 / 940	11.0 - 14.0	5.5 - 8.0	8*10 ⁻⁸	5*10 ⁻⁶
HFR-P4/2				920 / 945	9.6 - 14.9	5.5 - 8.0	8*10 ⁻⁸	5*10 ⁻⁶
HFR-P4/3				1050 / 1075	9.9 - 14.0	5.5 - 8.0	9*10 ⁻⁸	2*10 ⁻⁵
SL-P1		19,600	330	780 / 800	8.6 - 11.3	5.0 - 6.7	1*10 ⁻⁶	5*10 ⁻⁶
HFR-K3/1	1 fuel element	16,400	359	1020 / 1200	7.5	4.0	2*10 ⁻⁷	9*10 ⁻⁶
HFR-K3/2				700 / 920	10.0	5.8	1*10 ⁻⁷	2*10 ⁻⁵
HFR-K3/3				700 / 920	10.6	5.9	1*10 ⁻⁷	2*10 ⁻⁵
HFR-K3/4				1020 / 1220	9.0	4.9	3*10 ⁻⁷	1*10 ⁻⁵
FRJ2-K13/1	16,400	396	396	985 / 1125	7.5	0.2	2*10 ⁻⁸	2*10 ⁻⁵
FRJ2-K13/2				990 / 1150	8.0	0.2	2*10 ⁻⁹	2*10 ⁻⁵
FRJ2-K13/3				990 / 1150	7.9	0.2	7*10 ⁻⁹	6*10 ⁻⁶
FRJ2-K13/4				980 / 1120	7.6	0.2	7*10 ⁻⁹	6*10 ⁻⁶
FRJ2-K15/1	9,600	533	533	800 / 970	14.1	0.2	1*10 ⁻⁶	1*10 ⁻⁶
FRJ2-K15/2				980 / 1150	15.3	0.2	5*10 ⁻⁹	9*10 ⁻⁷
FRJ2-K15/3				800 / 990	14.8	0.1	3*10 ⁻⁹	4*10 ⁻⁷

Table 3-3: Parameters and results from irradiation tests with modern, high-quality UO₂ TRISO particles in the German program (continued)

Experiment	Specimen per capsule	No. of particles	Irradiation time [efpd]	Temperature surface/center [°C]	Burnup [%FIMA]	Fluence [10 ²⁵ m ⁻² , E>16 fJ]	Release at end of irradiation	
							R/B Kr-85m	Fractional release Cs-137
FRJ2-P27/1	3 compacts	7,340	232	880 / 1080	7.6	1.4	2*10 ⁻⁶	2*10 ⁻⁵
FRJ2-P27/2				1220 / 1320	8.0	1.7	1*10 ⁻⁵	1*10 ⁻⁴
FRJ2-P27/3				1080 / 1130	7.6	1.3	1*10 ⁻⁷	1*10 ⁻⁵
HFR-K5/1	1 fuel element	14,600	359	cycled	6.7	4.0	2*10 ⁻⁷	not yet measured
HFR-K5/2					8.8	5.8	1*10 ⁻⁷	
HFR-K5/3					9.1	5.9	1*10 ⁻⁷	
HFR-K5/4					8.7	4.9	3*10 ⁻⁷	
HFR-K6/1		14,600	359	cycled	7.2	4.0	2*10 ⁻⁷	
HFR-K6/2					9.3	5.8	1*10 ⁻⁷	
HFR-K6/3					9.7	5.9	1*10 ⁻⁷	
HFR-K6/4					9.2	4.9	3*10 ⁻⁷	

fuel elements with LEU TRISO particles. These experiments with a total of 19 fuel elements and 276,680 TRISO particles cover production before and after 1985:

Fuel manufactured before 1985:	HFR-K3	4 fuel elements
	FRJ2-K13	4 fuel elements
	FRJ2-K15	3 fuel elements
Fuel manufactured after 1985:	HFR-K5	4 fuel elements
	HFR-K6	4 fuel elements

The burnups and neutron fluences achieved, as well as the R/B values for Kr-85m at the end of irradiation, are compiled in Table 3-3 together with other high quality TRISO fuels of different geometrical configuration (FRJ2-P27, HFR-P4, and SL-P1) [5].

The analysis of the measured rare gas releases shows that in no single case was a failed particle generated during irradiation. Tests HFR-K3, FRJ2-K13 and -K15 also had no manufacturing defects. HFR-K5/4 had one manufacturing defect, but no additional in-pile failure; all the other spheres were both at zero defects and zero failures.

Gas release from the irradiation experiment FRJ2-K15 in the Jülich DIDO reactor with three fuel elements from the AVR 21-2 production is shown in Fig. 3-4. The results demonstrate that none of the three elements, which were irradiated in individually monitored capsules, contained failed particles. Also the level of uranium contamination is extremely low and can be derived to be around 4 ppb trace contamination.

The results of calculations of irradiation experiments with the FRESCO diffusion model (those for FRJ2-K15 are given by the solid line in Fig. 3-4) indicate [52] that Kr-88 R/B values were not significantly influenced by the fast neutron fluence or by the fuel burnup for the ranges covered. Fuel temperature had an effect through its influence on diffusion coefficients, but the effect was generally small. The greatest influence on R/B values was the presence of significant surface contamination on the coated fuel particles. Relative to graphite matrix contamination, the contamination level in the graphite grains and the effective diameter of the grains had a significant influence on R/B values. In general, the calculated Kr-88 R/B values for the various tests gave good agreement with the measured R/B values if account were taken of reasonable variations in (i) fuel surface contamination, (ii) fuel contamination within the outer PyC layer of the fuel particles, (iii) contamination in the graphite grains, and (iv) effective grain diameter [52].

Due to the measurement of a finite random sample, the one-sided confidence range $C = \text{prob}(0 \leq \zeta \leq x)$ is given for sample size N, number of failures n, and true failure fraction ζ by:

$$C = \frac{\int_0^{\zeta_{\max}} \zeta^n (1 - \zeta)^{N-n} d\zeta}{\int_0^1 \zeta^n (1 - \zeta)^{N-n} d\zeta} = \sum_{j=n+1}^{N+1} \binom{N+1}{j} x^j (1-x)^{N+1-j} \quad (3-18)$$

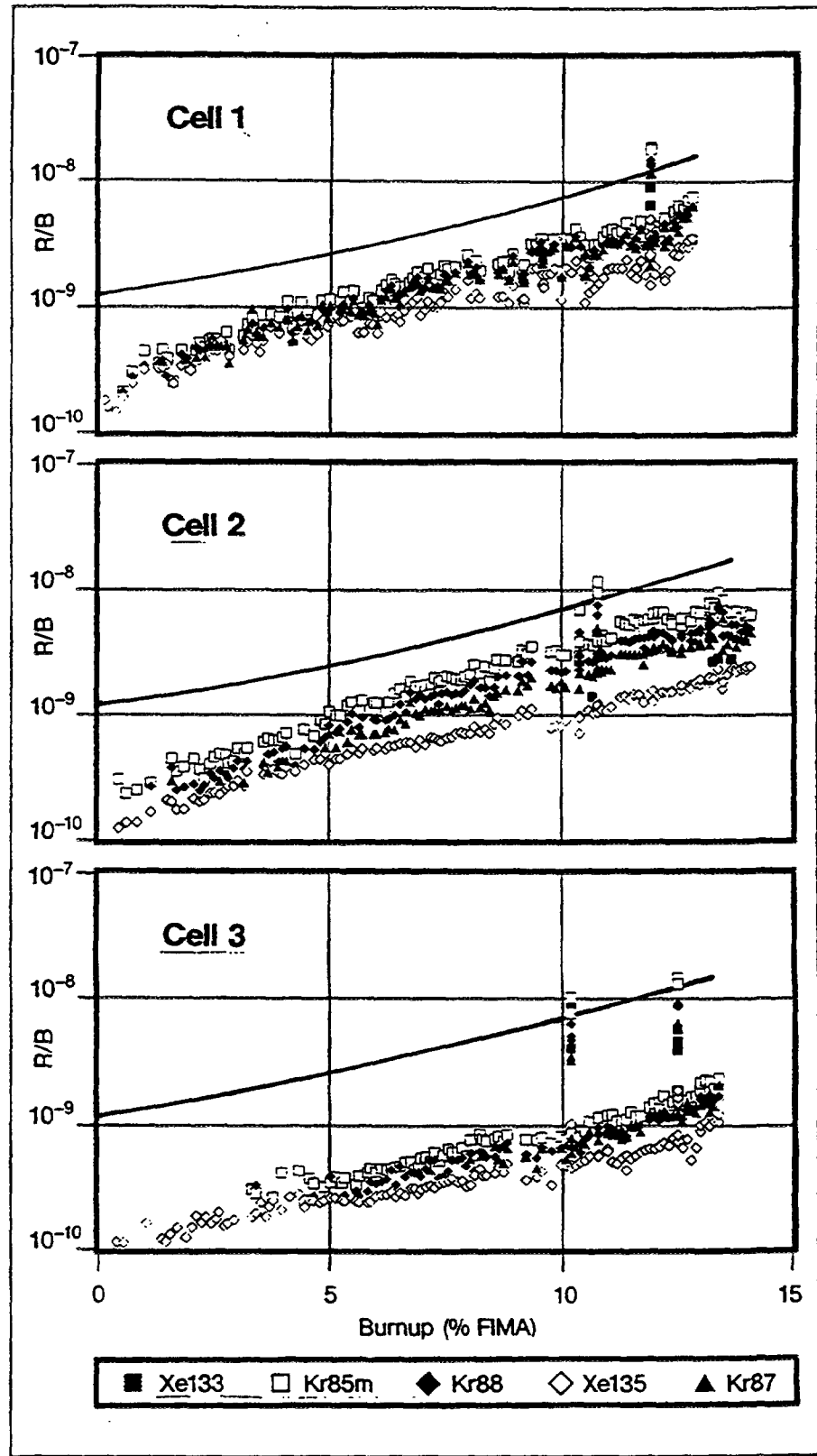


Fig. 3-4: Measured and calculated (Kr-88) fractional steady-state release of short-lived fission gases, R/B , as a function of burnup in the irradiation experiment FRJ2-K15, from [5, 52]. The spikes in R/B were measured during +200 °C temperature transients. The slow increase in R/B is an artefact of the birth rate calculation for 16.7 % enriched uranium, while the actual release is from uranium contamination of natural enrichment.

with the following interpretation: Given that in a random sample of size N, there are n failures observed, C represents the probability that the true failure fraction ζ will be in the range $0 \leq \zeta \leq \zeta_{\max}$. The solution x (upper limit of failure fraction) is found by the inverse of the incomplete beta function: $x = BetaInv(C, n + 1, N + 1 - n)$. For zero observed failures ($n = 0$), the maximum in-pile failure fraction at the 50 % confidence level is given by

$$BetaInv(0.50, 1, N_{Bu} + 1) = 1 - exp[\ln 0.50 / (N_{Bu} + 1)] \quad (3-19)$$

and at the 95 % confidence level by

$$BetaInv(0.95, 1, N_{Bu} + 1) = 1 - exp[\ln 0.05 / (N_{Bu} + 1)] \quad (3-20)$$

where N_{Bu} is the number of particles with burnup $\geq Bu$.

The sample of a given burnup Bu includes the particles of all test elements with burnups $\geq Bu$, since they would also provide the zero result with Bu . The sample for the minimum burnup of 6.7 %FIMA (HFR-K5/1 thus contains 229,600 particles, and for the burnup of 10 %FIMA, there is a zero statistics with 47,200 particles. The seven test elements from the FRJ2 experiments were only weighted with 50 % to take into consideration the low fluence of fast neutrons of these experiments.

The 50 % confidence values for in-reactor failure as a function of burnup Bu in %FIMA can be approximated by (see Fig. 3-5)

$$\Phi_{50\%} = 2.0 * 10^{-6} + 5.7 * 10^{-8} * exp(Bu/2) \quad (3-21)$$

Since the size of the sample decreases with increasing burnup, the 50 % confidence values (“expected” for the reactor core) rise from $3*10^{-6}$ at 5 %FIMA to $11*10^{-6}$ at 10 %FIMA.

The upper limit of the confidence range from 0 to 95 % is given by

$$\Phi_{95\%} = 1.0 * 10^{-5} + 2.4 * 10^{-7} * exp(Bu/2) \quad (3-22)$$

The result is plotted in Fig. 3-2 as the design curve. In the case of 5 %FIMA, the design value of the operation-related defect fraction is $1.3*10^{-5}$ and rises to approximately $4.6*10^{-5}$ at 10 %FIMA.

The release of short-lived nuclides, such as the radiologically dominant I-131 or the rare gases, is determined by the power-weighted average failed particle fraction in the fuel elements of the HTGR core. Taking into consideration the burnup distribution of the fuel elements in the equilibrium core of the HTR-MODUL, $4*10^{-6}$ as the expected value and $2*10^{-5}$ as the design value (95 % confidence) result from the curves of Fig. 3-5 for the power-weighted average operation-related failed particle fraction in the HTR-MODUL core.

3.4.2.2. HTR-MODUL Source Terms

The present statistical derivation of the design value for the fabrication-related defect fraction in the HTGR core assumes a fuel element production with fixed specification

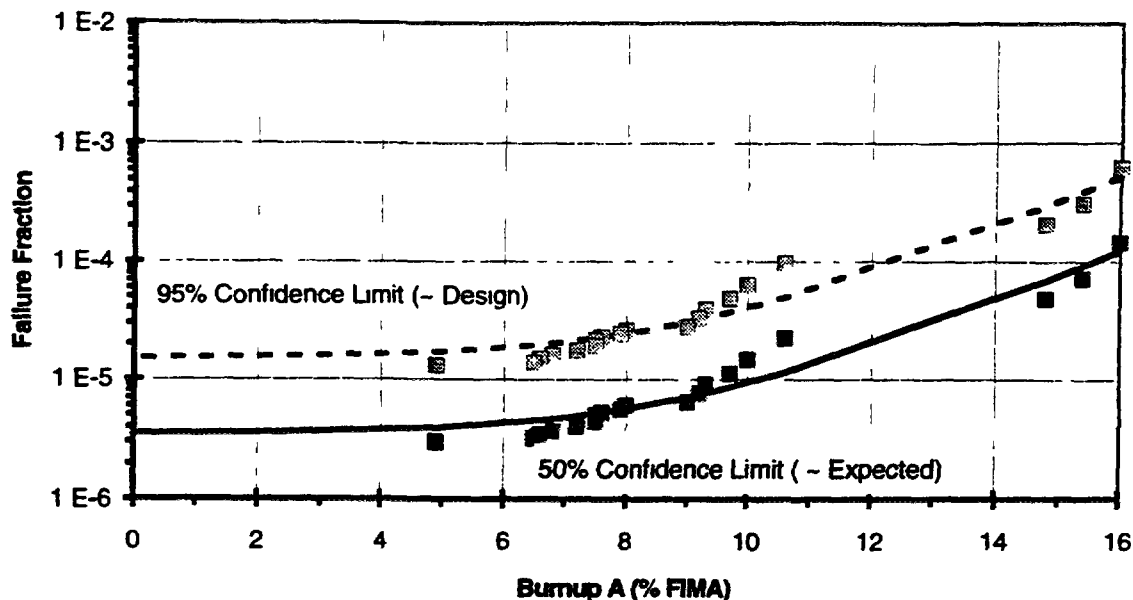


Fig. 3-5: Design value and expected value of the operation-induced failed particle fraction in the core based on the statistical evaluation of zero in-reactor failures in representative fuel element tests

limits relative to the acceptance unit. The design value for the entire core of 3×10^{-5} (95 % confidence) corresponds to the specified average free uranium values of a fuel element batch ($\leq 10,000$ fuel elements) of 6×10^{-5} at most. This acceptance criterion is valid irrespective of the quality of previous production. As a consequence of this statistical procedure which was also used for the THTR fuel elements, the average of the entire core solely determining fuel element behavior in the reactor core and its 95 % confidence limit are considerably lower. This bonus can be used in radiological investigations.

The **contamination values** of the matrix and outer PyC layer are much less effectively authenticated than the fabrication-related defect fraction. This deficiency can in part be accepted since at least the contribution of uranium to this contamination is additively covered by the determination of free uranium (burn-leach). However, since the release characteristics of finely dispersed contamination differ from that of the defective particles, these source terms must be separated.

In Table 3-4, all the newly determined source terms are compared to the planning values (design values) used in 1988 for the licensing procedure of the HTR-MODUL concept. The fabrication- and operation-related defect fractions are lower than the 1988 values by a factor of two. This has been achieved by using and analyzing experimental results obtained in the period 1981 - 1991. However, the effective uranium contamination is much higher, above all since the thorium and U-238 contamination of the matrix material was not taken into consideration in 1988. However, this increase only has a slight effect because the contamination contribution to the overall release is low.

Table 3-4: Source terms of the HTR-MODUL

Release source	Expected value	Design value	Planning value SIEMENS 1988
Effective uranium contamination⁽¹⁾			
Outer LTI-PyC layer	$3 \cdot 10^{-7}$	$1 \cdot 10^{-6}$	
A3 matrix material	$3 \cdot 10^{-6}$	$5 \cdot 10^{-6}$	$3 \cdot 10^{-7}$ ⁽²⁾
Fraction of defective particles			
Fabrication-related	$1 \cdot 10^{-5}$	$2 \cdot 10^{-5}$	$6 \cdot 10^{-5}$
Operation-related ⁽³⁾	$4 \cdot 10^{-6}$	$2 \cdot 10^{-5}$	$1 \cdot 10^{-4}$

(1) U_{nat} and Th contamination relative to 7 g of uranium per fuel element with 7.7 % U-235 enrichment

(2) Corresponding to 50 µg of natural uranium relative to U-235 input, contained in the fabrication-related defect fraction

(3) Power-weighted average for all fuel elements in the core

According to the new design values, the fractions of the individual source terms in I-131 release during normal operation taking into consideration the higher fractional release from matrix contamination ($2 \cdot 10^{-2}$ at 800 °C) are as follows:

PyC contamination (particle):	0.3 %
Matrix contamination (sphere):	15 %
Defective/failed particles	
Fabrication:	32 %
Operation:	53 %

The major contribution originates from the operation-related failed particles. The large distance to the associated expected value shows that this ranking is solely caused by the relatively large statistical uncertainty of the operation-related failed fraction. Correspondingly, the fabrication-related defect fraction dominates for the expected value of I-131 release. In comparison to the 1988 design values, the new values for I-131 release from the fuel elements are reduced by approximately a factor of two.

3.4.3. The Japanese Program

In-pile failure of the coated fuel particles incorporated in the fuel compacts has been tested intensively in the irradiation experiments in an in-pile gas loop, OGL-1, and the gas-swept capsules. The irradiation tests in OGL-1 have been aimed at proving irradiation performance of the fuel elements, and produced many data concerning not only the in-pile failure but also fuel rod behavior, plate-out of the volatile fission products, fission product migration in the fuel elements, and so on.

Table 3-5: In-pile failure of coated fuel particles in fuel compacts irradiated in OGL-1

OGL-1 experiment	Compact name	Number of particles / compact	Irradiation conditions			Failure fraction (Through-coating)		Failure fraction (SiC coating)		EOL R/B (Kr-88)
			Time [efpd]	Temperature [°C]	Burnup [%FIMA]	BOL ⁽¹⁾	EOL	BOL ⁽¹⁾	EOL	
6th	6101	18,000	21.9	980 ⁽²⁾	0.3		$1.5 \cdot 10^{-4}$			$1.5 \cdot 10^{-6}$
	6105			1345	0.4		$3.7 \cdot 10^{-5}$			
	6109			1488	0.4	$(5.1 \cdot 10^{-5})$	$1.1 \cdot 10^{-4}$	$(1.9 \cdot 10^{-3})$	$2.0 \cdot 10^{-3}$	
	6114			1428	0.3		$< 3.0 \cdot 10^{-6}$			
	6120			1093	0.1		$1.8 \cdot 10^{-4}$			
7th	7101	9,000	58.0	984	0.5		$1.1 \cdot 10^{-4}$			$4.0 \cdot 10^{-7}$
	7105			1106	0.7		$1.1 \cdot 10^{-4}$			
	7109			1215	0.8		$1.8 \cdot 10^{-4}$			
	7120			985	0.2		$1.7 \cdot 10^{-4}$			
	7201			1063	0.8		$1.2 \cdot 10^{-7}$			
	7205			1224	1.2	$(2.7 \cdot 10^{-5})$	$7.5 \cdot 10^{-8}$	$(4.4 \cdot 10^{-3})$	$5.6 \cdot 10^{-3}$	
	7209			1376	1.3		$1.5 \cdot 10^{-7}$		$3.4 \cdot 10^{-3}$	
	7220			1068	0.4		$6.9 \cdot 10^{-5}$			

(1) Average fraction measured in several fuel compacts which had been manufactured in the same batch

(2) Maximum temperature in transient tests

Table 3-5: In-pile failure of coated fuel particles in fuel compacts irradiated in OGL-1 (continued)

OGL-1 experiment	Compact name	Number of particles / compact	Irradiation conditions			Failure fraction (Through-coating)		Failure fraction (SiC coating)		EOL R/B (Kr-88)
			Time [efpd]	Temperature [°C]	Burnup [%FIMA]	BOL ⁽¹⁾	EOL	BOL ⁽¹⁾	EOL	
7th	7301	9,000	58.0	1060	0.7		1.7×10^{-7}			-
	7305			1215	1.0		8.0×10^{-5}			
	7309			1358	1.1		1.2×10^{-4}			
	7320			1064	0.3		1.2×10^{-5}			
8th	8101	18,000	53.8	940	0.6		8.7×10^{-5}			1.1×10^{-7}
	8105			1124	0.9		1.1×10^{-4}	(4.7×10^{-4})	1.8×10^{-3}	
	8109			1330	1.0	(5.9×10^{-6})	3.8×10^{-7}			
	8110			1358	1.0		2.9×10^{-4}			
	8114			1370	0.8		1.8×10^{-4}			
	8120			1097	0.3		5.2×10^{-7}			

(1) Average fraction measured in several fuel compacts which had been manufactured in the same batch

Table 3-5: In-pile failure of coated fuel particles in fuel compacts irradiated in OGL-1 (continued)

OGL-1 experiment	Compact name	Number of particles / compact	Irradiation conditions			Failure fraction (Through-coating)		Failure fraction (SiC coating)		EOL R/B (Kr-88)
			Time [efpd]	Temperature [°C]	Burnup [%FIMA]	BOL ⁽¹⁾	EOL	BOL ⁽¹⁾	EOL	
10th	10101	18,000	130.2	879 (979) ⁽²⁾	0.8		5.1×10^{-4}		1.1×10^{-4}	3.2×10^{-6}
	10105			1180 (1380)	2.1		7.7×10^{-4}			
	10109			1331 (1481)	2.8	(2.6×10^{-4})	6.6×10^{-4}	(7.5×10^{-4})	1.2×10^{-3}	
	10114			1270 (1390)	2.6		3.9×10^{-4}			
	10120			1057 (1097)	1.7		1.1×10^{-4}			
12th	12108	13,500	195.0	ND (1300) ⁽³⁾	3.9	(1.0×10^{-4})	7.1×10^{-5}			3.1×10^{-6}
	12113			ND (1300) ⁽³⁾	3.0		4.7×10^{-4}			
13th	13108	13,150	244.0	ND (1340) ⁽³⁾	ND (5.0) ⁽³⁾	4.2×10^{-6}	6.8×10^{-5}	3.9×10^{-6}	ND	6.8×10^{-8}
	13113			ND (1270) ⁽³⁾	ND (3.8) ⁽³⁾	4.2×10^{-6}	1.3×10^{-8}	3.9×10^{-6}	ND	
	13116			ND (1180) ⁽³⁾	ND (2.5) ⁽³⁾	4.2×10^{-6}	9.1×10^{-5}	3.9×10^{-6}	ND	

(1) Average fraction measured in several fuel compacts which had been manufactured in the same batch

(2) Maximum temperature in transient tests

(3) Not analyzed. Numbers in parentheses indicate estimated values.

Table 3-5: In-pile failure of coated fuel particles in fuel compacts irradiated in OGL-1 (continued)

OGL-1 experiment	Compact name	Number of particles / compact	Irradiation conditions			Failure fraction (Through-coating)		Failure fraction (SiC coating)		EOL R/B (Kr-88)
			Time [efpd]	Temperature [°C]	Burnup [%FIMA]	BOL ⁽¹⁾	EOL	BOL ⁽¹⁾	EOL	
14th	14108	13,300	73.0	1345 (1500)	1.5	(4.1*10 ⁻⁵)	3.1*10 ⁻⁴	(6.1*10 ⁻⁵)	-	6.8*10 ⁻⁸
	14111			1295 (1450)	1.4		1.0*10 ⁻⁶			
	14113			1200 (1360)	1.1		3.5*10 ⁻⁶			
15th	15108	12,810	218.0	1344	4.1	(2.7*10 ⁻⁶)	6.0*10 ⁻⁷	(5.1*10 ⁻⁵)	-	3.8*10 ⁻⁷
	15113			1290	3.3		2.4*10 ⁻⁷			
	15116			1180	2.3		3.7*10 ⁻⁸			

(1) Average fraction measured in several fuel compacts which had been manufactured in the same batch

As far as the in-pile failure of the coated fuel particles is concerned, failures of the through-coating layers and SiC layer have been measured in the PIE. Table 3-5 [53] summarizes the irradiation data of the fuel compacts in the OGL-1 fuel elements conducted recently and the defectiveness of the coated fuel particles. The data included in Table 3-5 were obtained from the fuels manufactured before the modification of the coating process as mentioned in section 2.3.3. (step C-0). Temperature transient tests, where the temperature of the fuel was elevated from normal condition to about 1500 °C, were conducted during the 6th and 10th OGL-1 experiment. As can be seen in the table, failure of the SiC coating layer occurred significantly when the fuel was irradiated at higher temperatures than 1450 °C despite low burnup (compact name 6109 at 6th experiment and 10109 at 10th experiment in Table 3-5). It is notable, however, that failure of the through-coating layers in these coated fuel particles was not so remarkable.

With respect to the through-coating failure, a comparison of the fractions of the defective through-coating layers before and after irradiation is illustrated with 95 % confidence limits (Fig. 3-6). Marked increase of the defectiveness in the through-coating layers by irradiation is not observed at any experiment. Although one could find a jump-up of the fractions between the 8th and 9th assembly, it was due to the fact that after the 9th assembly, the manufacturing conditions were changed by constructing the new facilities. Although the fuel had been manufactured by the technology before the modification, through-coating defectiveness before and after the irradiation met the criteria of the HTTR design.

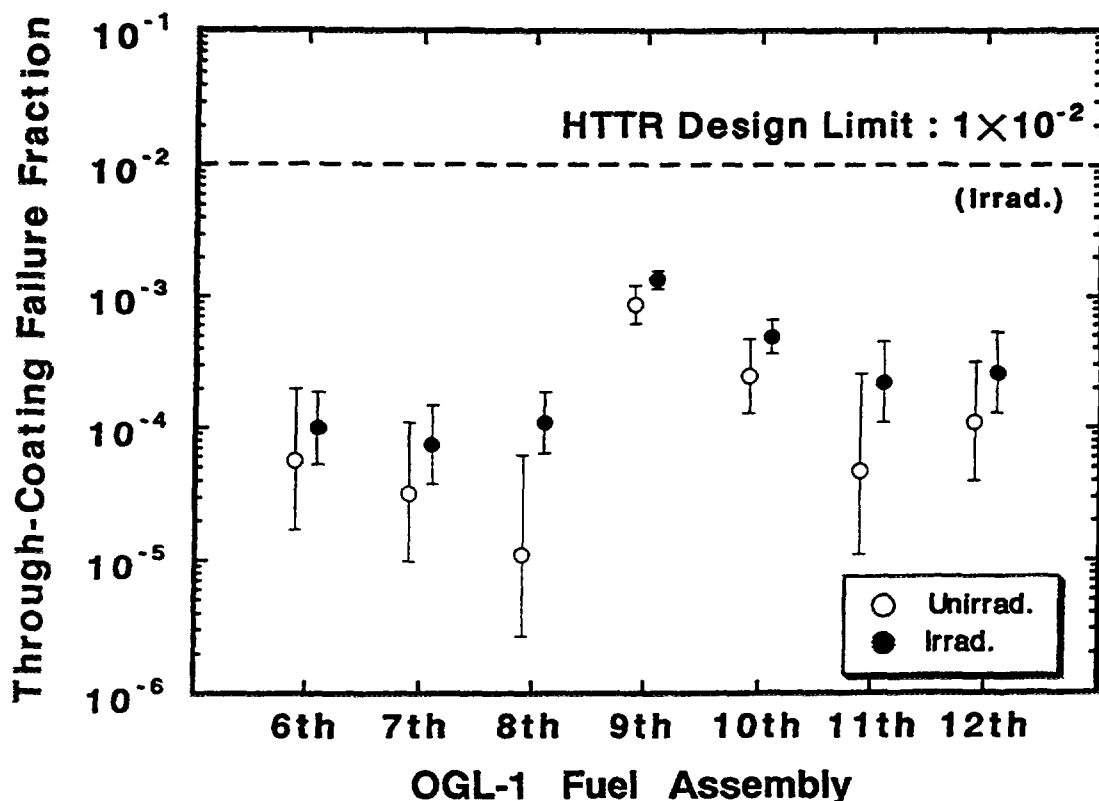


Fig. 3-6: Fractions of defective coated particles (through-coating fraction) loaded in 6th - 12th OGL-1 fuel assemblies

3.4.4. The Russian Program

3.4.4.1. Weak Irradiation Method (Activation Method)

The method of “weak” irradiation uses separate irradiation and annealing of the fuel in the form of coated particles or fuel elements. The irradiation up to a fluence of 1×10^{14} thermal neutrons/cm² was carried out in the stationary reactor F-1 and in the pulse reactor “GIDRA”. The beginning of annealing (time after irradiation for holding the sample) is determined by the choice of the benchmark radionuclide. If the time for holding the sample is in the range of 15 - 40 hours, then 90 % of the fission gas activity is due to Xe-135, and that allows while making measurements in the above time interval, to refer the total activity of the sample to the activity of this radionuclide (when the time for holding the sample is > 60 hours, the activity is determined by Xe-133). In this case, the maximum permissible dose due to irradiation does not require special measures to provide radiation safety. Analysis of the released fission gas is carried out by continuous or periodic gas sampling.

The heating of the samples is carried out within the heating systems of the “OSA” facility in the wide temperature range up to the melting point of uranium dioxide and damage of the particles. The time of the isothermal heating is determined by the time of reaching the constant release rate and can be controlled directly in the process of experiment. Flow ionizing chamber or end-face beta detector, registering the total activity of fission gas release, serve as irradiation detectors. Sensitivity of the radiometric equipment used (with regard to Xe-135) in the flow regime is $\approx 3 \times 10^{-9}$ Ci, during the periodic specimen selection $\approx 2 \times 10^{-9}$ Ci. The error for determination of the relative release value is within the level of 20 % (when fractional release $F > 10^{-5}$).

For the analysis of the release, the **two-group activation model** (see also Appendix B) is used, which presupposes that all fission products in the fuel are within the substance defects, that could be divided into two groups:

1. the first group of defects, containing fission products, is characterized by the activation energy

$$\epsilon < k T_p \quad (3-23)$$

2. the second by

$$\epsilon > k T_p \quad (3-24)$$

where

k is the Boltzmann constant

T_p is the fuel operating temperature

Each group of fission products is characterized by its own release constants α_f or α_s , where $\alpha_s \ll \alpha_f$ (α_f and α_s are the constants of fast and slow release of fission products). The lifetime corresponding to the release constant for each group is equal to

$$\tau_f \sim 1 / \alpha_f \quad (3-25)$$

and

$$\tau_s \sim 1 / \alpha_s \quad (3-26)$$

respectively.

To obtain the values of the main constants, it is necessary to carry out several measurements in consecutive order (A_j). These measurements are to be carried out within the time interval $\Delta\tau_j$. The value of spectrum characteristic "m" which characterizes the fraction of fission products with short lifetime in the heated fuel, is obtained, as a rule, out of the first measurement (if the time for heating is chosen correctly); the α -values are as follows:

$$\begin{aligned} m &\approx F_j(\tau) & \text{for } \frac{1}{\alpha_f} < \tau \ll \frac{1}{\alpha_s} \\ \alpha_f &\approx \frac{\ln(A_{j-1}/A_j)}{\Delta\tau_j} & \text{for } \tau < \frac{1}{\alpha_f} \\ \alpha_s &= \frac{1}{\Delta\tau_j} \ln((1-m)/(1-F_j)) \approx \frac{F_j - F_{j-1}}{\Delta\tau_j} & \text{for } \tau \gg \frac{1}{\alpha_f} \end{aligned} \quad (3-27)$$

where

F_{j-1} , F_j are the relative release values

A_{j-1} , A_j are the activities measured at τ_{j-1} and τ_j

τ_{j-1} , τ_j are the moments of isothermal annealing, $\Delta\tau_j = \tau_j - \tau_{j-1}$

The parameters m , α_f , and α_s generally depend on the properties (density, structure) of fuel, protecting layers, matrix graphite, which can be changed under the influence of irradiation and temperature. That is why usually these parameters are typical for the initial stages of materials and fuel elements.

The following main problems can be solved by the method of "weak" irradiation:

1. Determination of the degree of surface and volume contamination of matrix graphite with uranium using the samples without coated particles
2. Determination of the degree of contamination of the coated particle protective layers with uranium in the process of coating in the fluidized bed systems. The analysis can be carried out quickly enough, and the method is very efficient while verifying the technology.

3. Determination of the amount of coated particles with failure of the complete coating
4. Study of kinetics of fission gas release from different sources (fuel kernels, uranium impurities in graphite, protective layers, fission gas release out of kernels through the “through” defects) depending on time and temperature, during different modes of testing the fuel (coated particles and fuel elements), including accident simulation, which allow to obtain the data base necessary for prediction of the circuit activity and other issues of NPP radiation safety.
5. Selection of specimens before insertion in the irradiation facility. Most of the specimens were undergone a preliminary control on tightness.

For the release prediction in the reactor tests, the correlations

$$\begin{aligned} F(\tau) &\approx m + \frac{\alpha_s}{\lambda + \alpha_s} (1 - m) \left[1 - \frac{\lambda e^{-\lambda\tau}}{\alpha_s} \frac{1 - e^{-\alpha_s\tau}}{1 - e^{-\lambda\tau}} \right] \\ F(\tau) &\approx m \quad \text{for } \lambda \gg \alpha_s \end{aligned} \quad (3-28)$$

are used.

The analyses of the results of experiments for obtaining the release constants are performed quickly enough (< 1 day), therefore the method is effective during the technology development.

Feasibility of the method of “weak” irradiation for obtaining the fission product release constants defining the fission product release under reactor operating conditions and the possibility to estimate fuel contents in the materials of the fuel element design and the amount of defective coated particles were checked by direct comparison with the results of reactor experiments and with the data on contamination obtained by traditional methods, for example, radiation chemistry (Tables 3-6, 3-7, Fig. 3-7, Fig. B-8 in Appendix B). The results of some investigations are given in Figs. 3-8 - 3-14 and in some more figures of Appendix B.

Table 3-6: Determination of U-235 content in powder graphite

Content in prepared sample		Analysis methods [% mass]					
		"Weak" irradiation U-235	2 π radiometry U-235	Mass spectrography		Chemical	
U-235	Natural U			U-235	U-238	U total	(U-235)
4×10^{-4}	-	$(3.9 \pm 0.8) \times 10^{-4}$	2.9×10^{-4}	1.8×10^{-3}	$< 1 \times 10^{-5}$	4.7×10^{-4}	(4.2×10^{-4})
1×10^{-4}	-	$(1.0 \pm 0.2) \times 10^{-4}$	6.2×10^{-5}	1.4×10^{-4}	$< 1 \times 10^{-5}$	$< 5 \times 10^{-5}$	$(< 4.5 \times 10^{-5})$
5×10^{-5}	-	$(4.6 \pm 3.0) \times 10^{-5}$	4.9×10^{-5}	-	-	$< 5 \times 10^{-5}$	$(< 4.5 \times 10^{-5})$
1.25×10^{-5}	-	$(2.0 \pm 0.4) \times 10^{-5}$	1.4×10^{-5}	-	-	$< 5 \times 10^{-5}$	$(< 4.5 \times 10^{-5})$
6.25×10^{-6}	-	$(1.0 \pm 0.3) \times 10^{-5}$	6.6×10^{-6}	-	-	$< 5 \times 10^{-5}$	$(< 4.5 \times 10^{-5})$
1.75×10^{-4}	2.5×10^{-2}	$(1.5 \pm 0.6) \times 10^{-4}$	1.8×10^{-4}	-	-	2.4×10^{-2}	(1.7×10^{-4})
5.25×10^{-5}	7.5×10^{-3}	$(4.6 \pm 1.7) \times 10^{-5}$	5.2×10^{-5}	$< 1 \times 10^{-6}$	8×10^{-3}	6.7×10^{-3}	(4.7×10^{-5})
1.75×10^{-5}	2.5×10^{-3}	$(1.4 \pm 0.7) \times 10^{-5}$	1.8×10^{-5}	$< 5 \times 10^{-6}$	7×10^{-4}	2.5×10^{-3}	(1.75×10^{-5})

Table 3-7: Determination of U-235 content in spherical fuel elements

	Analysis methods [% mass]						Chemical Natural U
	"Weak" irradiation U-235	4 π radiometry U-235 ⁽¹⁾	2 π radiometry U-235	Mass spectrography			
	U-235	U-238		U-235	U-238		
1 (1)	5×10^{-6}	4.5×10^{-5}	2.7×10^{-6}	-	-	-	9×10^{-5}
(2)	-	-	1.0×10^{-6}	-	-	-	4×10^{-4}
(3)	-	-	$< 1 \times 10^{-6}$	-	-	-	2×10^{-4}
2 (1)	$(4.3 \pm 3.3) \times 10^{-6}$	2.7×10^{-5}	$< 1 \times 10^{-6}$	$< 1 \times 10^{-6}$	1.25×10^{-5}	-	8.8×10^{-4}
(2)	-	-	$< 1 \times 10^{-6}$	-	-	-	1.7×10^{-3}
3 (1)	$(7.3 \pm 3.5) \times 10^{-6}$	7.3×10^{-5}	$< 1 \times 10^{-6}$	$< 1 \times 10^{-6}$	3×10^{-6}	-	2.2×10^{-4}
(2)	-	-	$< 1 \times 10^{-6}$	-	-	-	4.8×10^{-4}
4 (1)	$(5.0 \pm 2.0) \times 10^{-5}$	-	-	-	-	-	-
(2)	$(7.0 \pm 4.0) \times 10^{-6}$ (2)	2.4×10^{-5}	$< 1 \times 10^{-6}$	$< 1 \times 10^{-6}$	4×10^{-6}	-	$< 5 \times 10^{-4}$
5	$(2.0 \pm 1.2) \times 10^{-5}$	-	-	-	-	-	-
5 (1)	$(2.8 \pm 2.6) \times 10^{-6}$ (2)	3.3×10^{-3}	1×10^{-5}	6×10^{-6}	3×10^{-5}	-	1×10^{-4}
(2)	-	-	$< 1 \times 10^{-6}$	-	-	-	$< 5 \times 10^{-5}$

(1) Measurement results are given in % of graphite mass in spherical fuel element surface layer ($\approx 1.6 \times 10^{-5}$ m in thickness)

(2) After straping of specimen surface

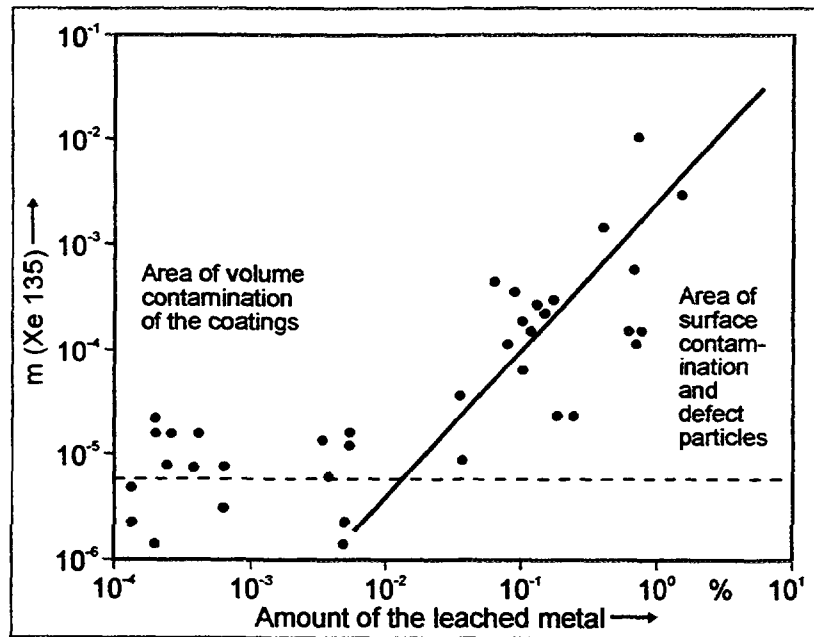


Fig. 3-7: Dependence of the relative release value on the amount of fuel got into the solution during leach

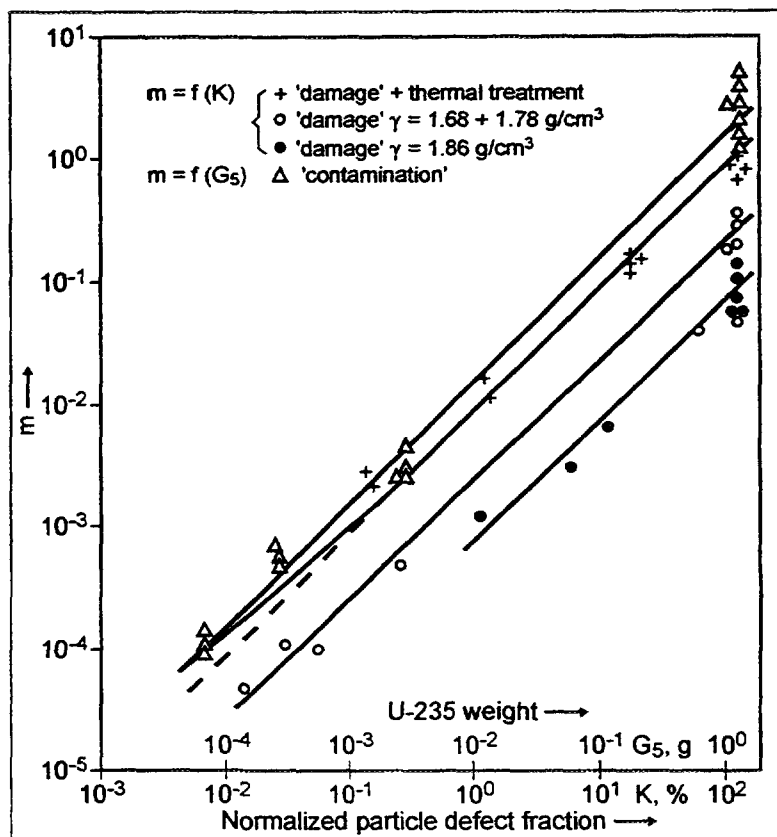


Fig. 3-8: Dependence of the relative release value for Xe-135 on "free" fuel values in the fuel element

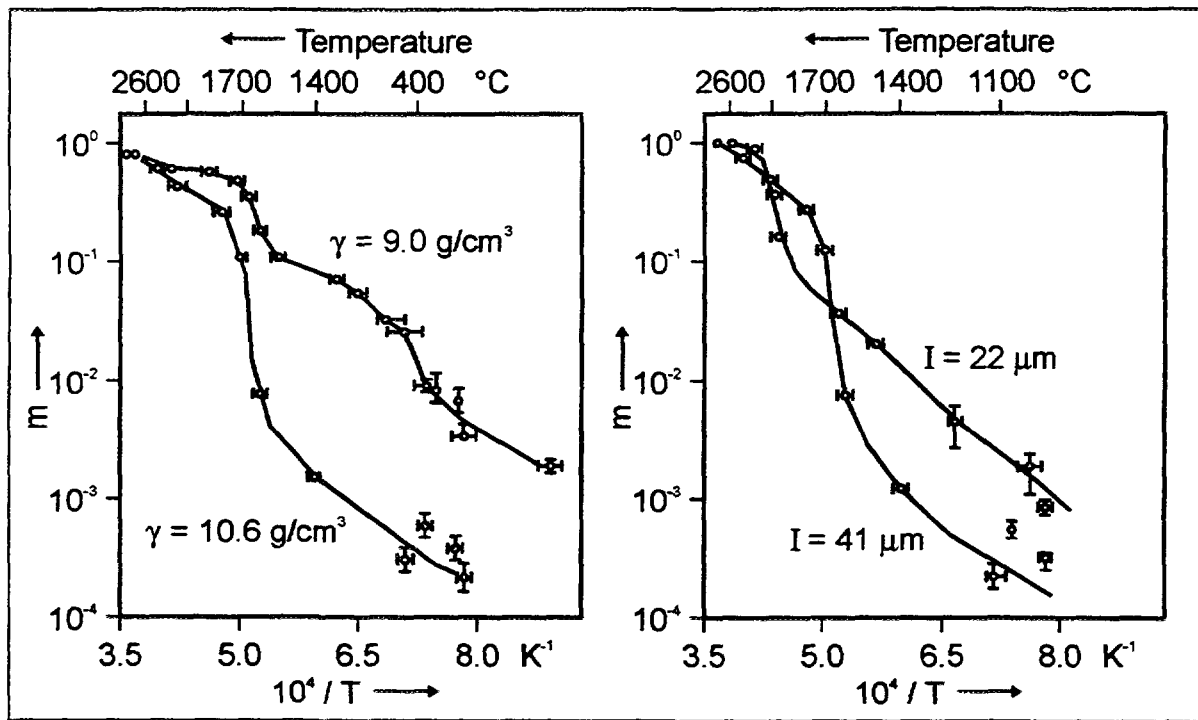


Fig. 3-9: Temperature dependence of the relative release from UO_2 kernels of different density γ (left) and different grain size I (right)

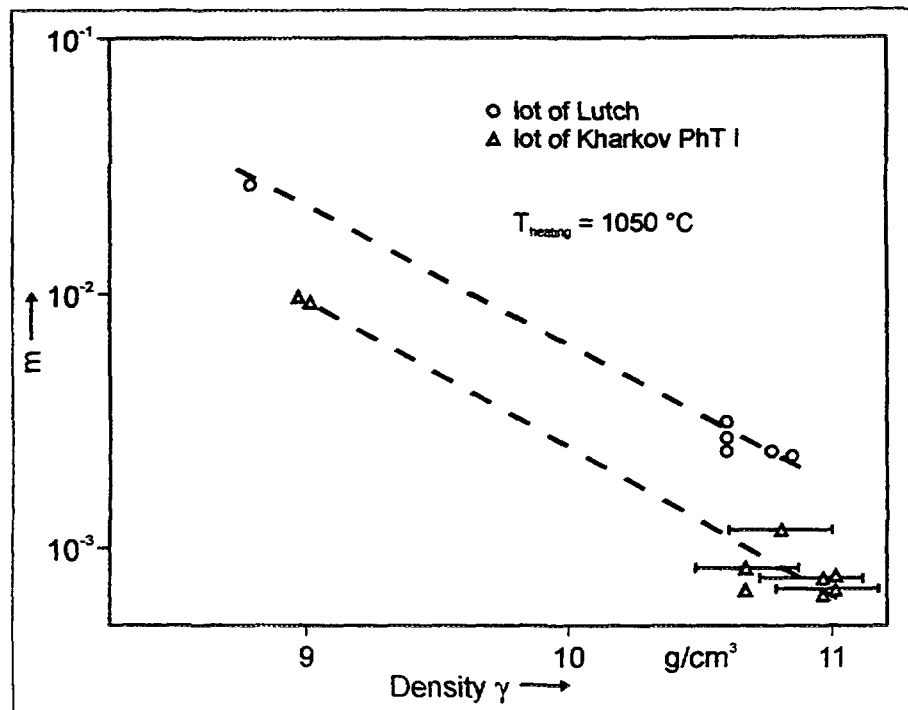


Fig. 3-10: Dependence of the relative release value on kernel density

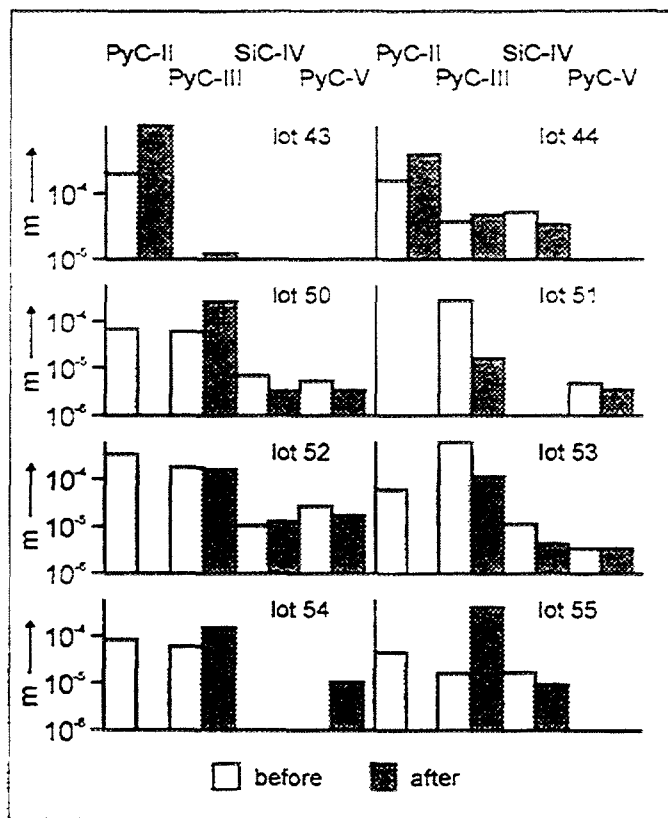


Fig. 3-11: Fission gas relative release values due to uranium contamination with increasing number of layers ("weak" irradiation method)

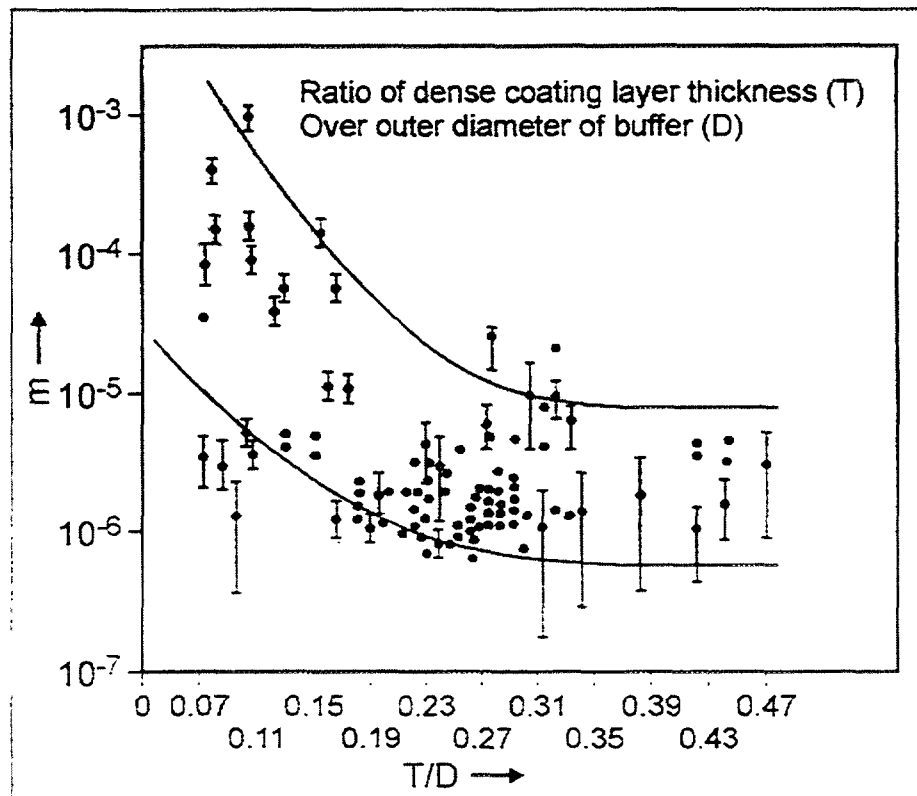


Fig. 3-12: Variation of relative release with normalized thickness of coating

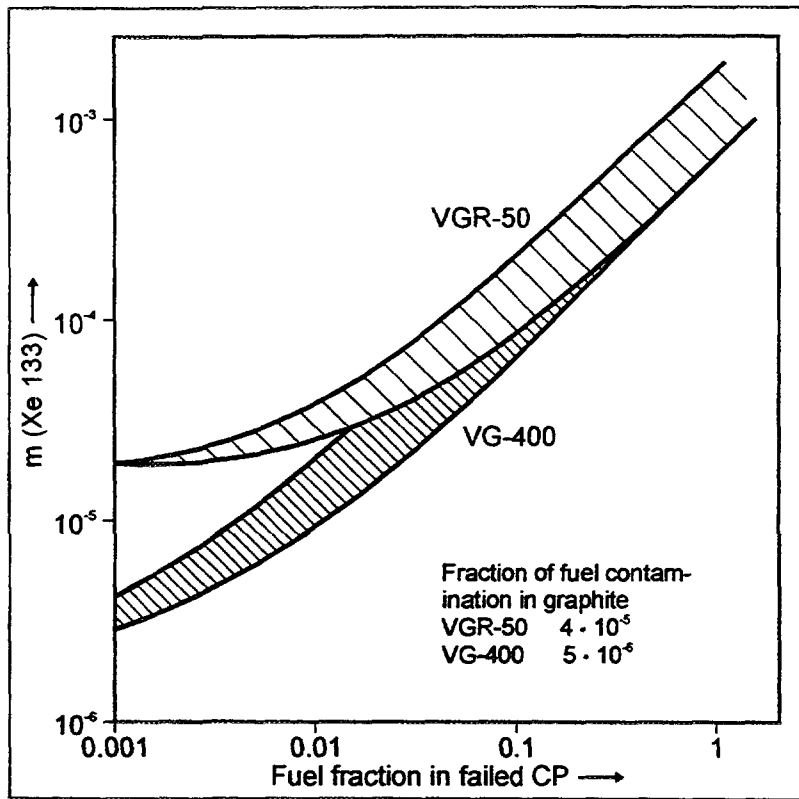


Fig. 3-13: Dependence of Xe-133 release on fuel fraction in failed coated particles

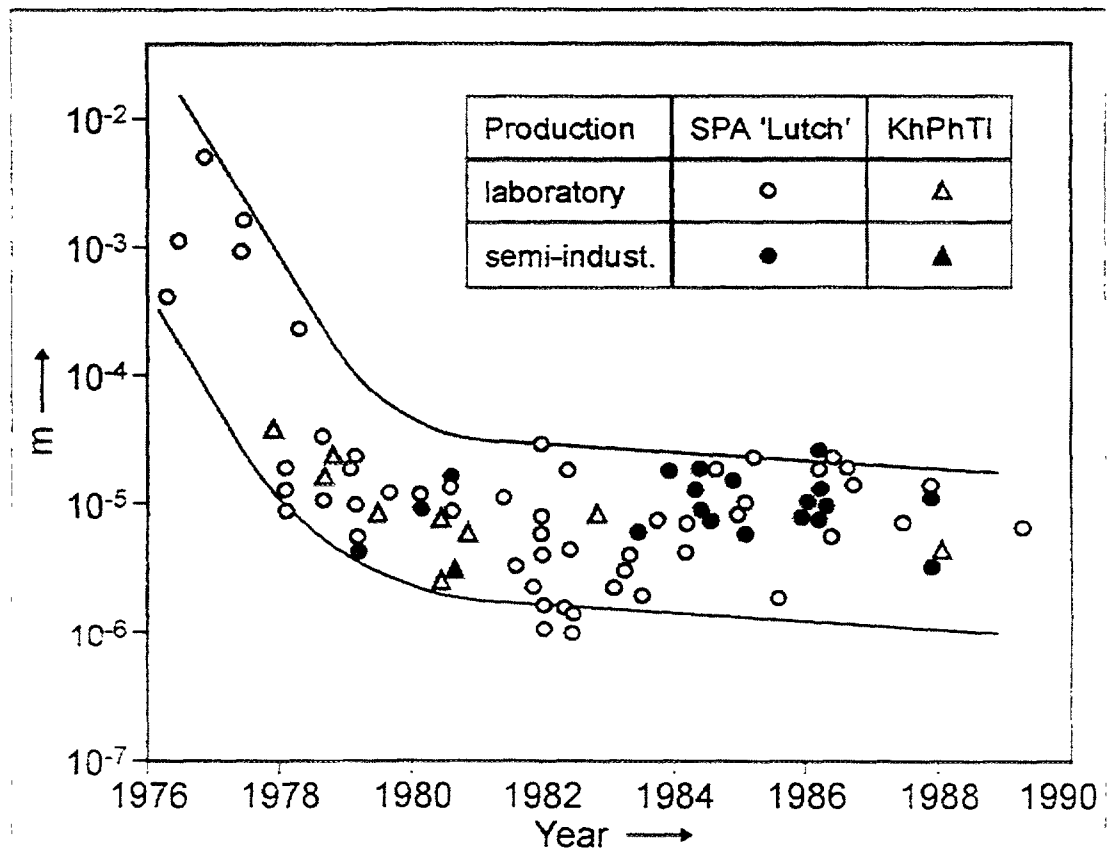


Fig. 3-14: Fuel element quality variation during technology development

3.4.4.2. Methods and Results of Reactor and Post-Reactor Investigations

The main objectives are:

- conduction of comparative tests of coated particles and fuel elements for selection of optimum design and manufacturing technology, substantiation of coated particle and fuel element parameters
- study of processes occurring in the fuel, protective coatings, matrix graphite depending on the irradiation parameters
- conduction of lifetime tests of full-scale fuel elements under conditions characteristic for HTGRs
- investigation of the effects of irradiation and accident conditions.

Four main types of irradiation devices have been used in reactor tests:

- ampoules for tests of coated particles in the form of loose particles, coupons, or pellets with matrix graphite; in some ampoules, gas sampling is possible for the gaseous fission product analysis ("KARAT"),
- ampoules with blow out of gas-carrier for investigation of tablets, kernels, spherical fuel elements with the analysis of the fission product release during irradiation ("KASHTAN", "VOSTOK"),
- helium loop with simultaneous integral analysis of gaseous fission products from all irradiated fuel elements ("PG-100"),
- for simulation of multiple thermal cycling and overheating of spherical fuel elements in the core ("VOSTOK", "UDAR"),
- for simulation of the reactivity accidents (pulse irradiation in reactor "HYDRA", IGR).

Interconnection of various methods of analysis of coated particles, fuel elements, and fission products is illustrated in Fig. 3-15. The investigation results are illustrated by the data in Tables 3-8 - 3-14, and in Figs. 3-16 - 3-20. More results are given in section 4.3.2.1.3.

Table 3-8: Testing conditions of coated particles in channel "KARAT"

Channel, Testing Date	Coated particle lot	Fuel en- richment [%]	Xe-135 release in unirradiation state ("weak" irradiation)	Irradiation conditions			
				Temperature [°C]	Time [efpd]	Max. burnup [%FIMA]	Fluence [10^{25} m $^{-2}$, E>80 fJ]
KARAT-2 1977	72 - 75	36	$3.4 \cdot 10^{-5}$	1200 - 1700	120	14.1	0.75 - 1.0
	71 - 75	36		1400 - 1500		13.2	
KARAT-3 1979	5 - 76	36.4	$1.8 \cdot 10^{-6}$	800 - 1600	≈ 174	13.1	≤ 2.0
	16-UP	21				9.4	
KARAT-4 31.12.80 - 17.02.82	43-UP	36	$(1\text{-}6) \cdot 10^{-6}$	1200 - 1350	≈ 174	9.7	2.0
	44-UP	36	$< 1 \cdot 10^{-6}$	1100 - 1370		8.5	2.2
	65-UP	36	$\leq 4.5 \cdot 10^{-6}$	1130 - 1350		9.7	2.0
	21-V-DP-1-X-78	21	$\approx 3.5 \cdot 10^{-6}$	1130 - 1280		6.7	2.2
	36-07-X-79	36	$< 2.0 \cdot 10^{-6}$	1130 - 1280		14.7	2.2
KARAT-5 14.03.83 - 11.02.84	B95	45	$2 \cdot 10^{-6}$	800 - 1600	≈ 340	18.9	1.5
	107-UP	45	$5.4 \cdot 10^{-6}$			8.8 - 24	1.05 - 1.5
	74-UP	0.7	$5.4 \cdot 10^{-6}$			0.14 - 0.19	1.05 - 1.3
	1 (2)_55	45	$\approx 1.5 \cdot 10^{-6}$			5.7 - 8.8	0.8 - 1.05
KARAT-6 11.12.86 - 17.11.87	21-9-X-84	21	$< 1.4 \cdot 10^{-6}$	850 - 1650	≈ 290	3.1 - 18.5	0.64 - 1.45
	36-7-X-84	36	$< 1.1 \cdot 10^{-6}$				
	36-4-X-82	36	$(2.1 \pm 1.9) \cdot 10^{-6}$				
	45-1-X-82	45	$(3.5 \pm 2.5) \cdot 10^{-6}$				
	2 B 215	45	$< 1.6 \cdot 10^{-6}$				

Table 3-9: Testing conditions of fuel elements in channel "KASHTAN"

Channel	Number of fuel elements Coated particle lot	U-235 content [g/fuel element]	Irradiation conditions				R/B (Xe-135)	
			Time [espd]	Temperature [°C]	Burnup [%FIMA]	Fluence [10^{25} m^{-2} , E>29 fJ]	Initial by "weak" irradiation	Test end
KASHTAN-1	64-75	1.5	393	n. m.	6.8	0.3	n. m.	n. m.
	64-75	1.5		1450	10.6		2.9×10^{-5}	1.5×10^{-3}
	64-75	1.0		1450	14.6		2.8×10^{-5}	5.0×10^{-3}
	64-75	1.0		1500	15.2		1.0×10^{-5}	2.0×10^{-3}
	64-75	1.0		1600 ⁽¹⁾	15.2		3.7×10^{-5}	5.0×10^{-3}
	64-75	1.5		n. m.	12.4		n. m.	n. m.
KASHTAN-2	44/16; 44	1.5	592	1100 - 950	6.8	0.22	1.1×10^{-5}	n. m.
	44/14; 44	1.0		1200 - 820	12.4	0.36	3.9×10^{-5}	$\approx 1 \times 10^{-3}$
	44/6; 44	1.0		1240 - 830	13.6	0.40	1.2×10^{-5}	$10^{-3} - 10^{-2}$
	217; 21-V-OP-X-78	0.5		960 - 760	14.7	0.37	3.0×10^{-6}	$10^{-6} - 10^{-5}$
	210; 21-V-OP-X-78	0.5		1050 - 800	11.6	0.30	3.0×10^{-6}	n. m.
	43/6; 43	1.5		1000 - 1350	10.6	0.35	1.4×10^{-5}	$10^{-3} - 10^{-2}$

(1) Temperature determined by gaseous fission products exit during postirradiation coated particle annealing has been 1700 - 1800 °C

n. m. = not measured

Table 3-9: Testing conditions of fuel elements in channel "KASHTAN" (continued)

Channel	Number of fuel elements Coated particle lot	U-235 content [g/fuel element]	Irradiation conditions				R/B (Xe-135)	
			Time [efpd]	Temperature [°C]	Burnup [%FIMA]	Fluence [10^{25} m $^{-2}$, E>29 fJ]	Initial by "weak" irradiation	Test end
KASHTAN-3	X17-64; 36-1X-80	1.5	1370	1050 - 650	22	0.42	2.4×10^{-5}	1.0×10^{-5}
	X21-43; 36-1X-80	1.5		1200 - 560	28	0.55	7.8×10^{-6}	1.3×10^{-5}
	110/12; 110	1.0		1050 - 470	39	0.54	1.0×10^{-5}	4.3×10^{-5}
	X21-36; 36-2X-80	1.0		1250 - 490	33	0.57	1.9×10^{-5}	6.8×10^{-5}
	110/6; 110	1.0		1150 - 450	41	0.57	6.6×10^{-6}	2.2×10^{-4}
	DOP-13; 55	0.87		1150 - 510	19	0.54	9.0×10^{-6}	6.4×10^{-5}
KASHTAN-4	P-223	1.0	750	1150 - 660	18	0.25	7.3×10^{-5}	2.6×10^{-5}
	X17-49; 36-1-X-80	0.6		1150 - 590	21	0.32	8.3×10^{-5}	2.8×10^{-5}
	P19-4; P8	0.5		1200 - 610	14	0.37	4.2×10^{-6}	7.9×10^{-6}
	P19-6; P8	0.5		1400 - 650	16	0.41	4.0×10^{-6}	7.4×10^{-6}
	H8-4	0.5		1250 - 570	16	0.41	5.4×10^{-5}	4.8×10^{-5}
	H8-6	0.5		1400 - 630	16	0.41	4.3×10^{-5}	3.9×10^{-5}

Table 3-10: Testing conditions of the channels KVG in the PG-100 loop

Channel	Operation time [espd] / No. of thermal cycles	Power of fuel element [kW]	Flow rate helium [g/s]	Temperature helium [°C] input - output	Temperature FE [°C] (1)	Burnup [%FIMA]	Fluence [10^{25} m^{-2} , E>32 fJ]	F (Xe-135)	
								Initial by "weak" irradiation	Test end
KVG-1	637 / 120	0.5 - 2.4	30 - 100	300 - 600	440 - 930	5.5 - 13.	0.8 - 2.3	$\approx 10^{-5}$	$\approx 10^{-5}$
KVG-2	396 / 100	1.3 - 2.6	20 - 60	400 - 800	600 - 1080	6.6 - 18.	0.59 - 1.4	$(1-3)*10^{-6}$	$10^{-5} - 10^{-2}$
KVG-3	56 / 10	0.9 - 5.3	30 - 60	400 - 920	640 - 1350	1.5 - 5.4	0.075 - 0.22	$(3-5)*10^{-5}$	$10^{-5} - 10^{-2}$
KVG-4	469 / 90	0.5 - 1.4	20 - 60	400 - 850	500 - 900	4.2 - 10.	0.69 - 1.74	$(1-2)*10^{-5}$	$3*10^{-5}$
KVG-5	403 / 50	0.5 - 4.8	45 - 65	400 - 900	800 - 1270	5.6 - 14.	0.8 - 1.4	$(4-6)*10^{-6}$	$\approx 5*10^{-5}$

(1) Temperature range is given by the working facility

Table 3-11: Testing parameters of “UDAR” Channels. In all tests, the release was below requirements imposed on the fuel elements.

Parameter	VGR-50	UDAR-2	UDAR-3
Power [kWt/fuel element]	0.53 - 2.16	0.1 - 0.4	0.2 - 0.8
Limits of thermal cycles [°C]	300 - 1000	400 - 800	700 - 1200
Number of thermal cycles	2000	1200	730
Heating speed [°C/s]	1.5	0.7	1.4
Cool down speed [°C/s]	1.5	0.7	1.0
Fuel enrichment [%]	21	36	45
Fuel loading [g U-235/fuel element]	0.5	1.0 - 1.5	2.0 - 3.0

Table 3-12: Characteristics of the coated particles used in the tests [54]

Channel	No. of fuel elements	Coated particle batch	Enrich. [%]	Coating thickness [μm] (Density [g/cm^3])				
				PyC-1	PyC-2	PyC-3	SiC-4	PyC-5
VOSTOK-2	16	2_25 (HTI)	45	85 (1.1)	30 (1.5)	30 (1.8)	40 (3.2)	95 (1.9)
VOSTOK-3	53	B-12 (HTI)	21	80 (0.8)	50 (1.6)	30 (2.1)	55 (3.2)	45 (1.8)
VOSTOK-42	1	2B215 (LTI)	45	100 (1.0)		65 (2.1)	55 (3.2)	85 (1.8)

Table 3-13: Testing of coated particles and fuel elements for HTGR in the IVV-2M reactor in 1982 - 1989

Channel, capsule	Coated particle lot, Number of fuel elements	Irradiation conditions				R/B (Kr-88)	
		Time [efpd]	Nominal temperature [°C]	Burnup [%FIMA]	Fluence $[10^{25} \text{ m}^{-2},$ $E > 32 \text{ fJ}]$	Beginning	End
MT-I, No. 4	106-1, 106-2, 106-3	500	1100 ... 1950	1.4	0.21	n. m.	n. m.
No. 7	1_25, 2_25, 3_25, etc.	1800	(5 levels)	4.9	0.65		
No. 5	(9 lots altogether)	3700		9.0	1.5		
MT-II, No. 10	21B155, 1B215 etc.	1500	1100 ... 1950	4.0	0.6	n. m.	n. m.
No. 11	(10 lots altogether)	4000	(4 levels)	8.5	1.7		
No. 12		8000		14	2.7		
MTI	P8, P28, B295, 2_25, 2B215 etc. (9 lots altogether)	5300	800, 1200, 1400	4 - 12	0.6 - 2.0	-	-
MT-III	2B535	3100	750 - 1400	11 - 17	1.5 - 2.3	-	-
ACY-8-1	1_25, 106-2, 2_25	5400	1100 - 1200	14.3	2	$(1-3)*10^{-7}$	$\approx 10^{-3}$
ACY-8-2	106-3, 3_25, 1_25	2700	1200	5.1	0.7	$10^{-7} - 10^{-6}$	$\approx 10^{-3}$
ACY-8-3	2_55, 21B155, 1B215	5800	1200 - 1300	15.8	2.2	$(1-2)*10^{-7}$	$3*10^{-3} - 10^{-3}$
ACY-8-4	21B155, 2B215, B395	3200	1250 - 1340	15.3	2	$\approx 10^{-3}$	$10^{-3} - 10^{-2}$

Table 3-13: Testing of coated particles and fuel elements for HTGR in the IVV-2M reactor in 1982 - 1989 (continued)

Channel capsule	Coated particle lot Number of fuel elements	Irradiation conditions				R/B (Kr-88)	
		Time [efpd]	Nominal temperature [°C]	Burnup [%FIMA]	Fluence [$10^{25} \text{ m}^{-2}, E > 32 \text{ fJ}$]	Beginning	End
VOSTOK-2, K-1	1_15, No. 15	6800	1190 - 900	15.	1.6	$3 \cdot 10^{-7}$	$1.2 \cdot 10^{-5}$
	2_25, No. 16		1370 - 1130	17.3	1.8	$1 \cdot 10^{-6}$	$1.6 \cdot 10^{-5}$
	2_25, No. 17		1150 - 1070	16.5	1.7	$3 \cdot 10^{-7}$	$4 \cdot 10^{-6}$
	2_25, No. 18		1000 - 1020	14.8	1.3	$1 \cdot 10^{-7}$	$1 \cdot 10^{-7}$
VOSTOK-3, K-1	B12, No. 51	6800	1000 - 950	12.2	1.8	$6 \cdot 10^{-7}$	$2 \cdot 10^{-6}$
	B12, No. 52		1180 - 1050	14.2	2.2	$2 \cdot 10^{-7}$	$4 \cdot 10^{-6}$
	B12, No. 53		1380 - 1230	12.0	1.9	$4 \cdot 10^{-6}$	$6 \cdot 10^{-6}$
	2_55, No. 34		1150 - 1130	17.0	1.4	$1 \cdot 10^{-7}$	$5 \cdot 10^{-5}$
VOSTOK-4, K-1	2B215, No. 61	5260	1100 - 1000	21.2	1.9	$5 \cdot 10^{-7}$	$3.2 \cdot 10^{-5}$
	2B215, No. 63		1200 - 1150	18.7	1.5	$1.6 \cdot 10^{-7}$	$3 \cdot 10^{-5}$
	2B215, No. 1		1400	14.2	1	$1.9 \cdot 10^{-6}$	$5 \cdot 10^{-5}$
	B395, No. 3		900 - 1230	8.8	0.4	$5 \cdot 10^{-7}$	$1.4 \cdot 10^{-5}$
VOSTOK-5, K-1	2B535, No. 5	5000	1000 - 1200	18.5	1.6	$\approx 10^{-6}$	$\approx 10^{-6}$
	2B535, No. 2		1200	21.5	1.9	$5 \cdot 10^{-6}$	$2 \cdot 10^{-5}$
	2B535, No. 8		1400	18.5	1.6	$5 \cdot 10^{-5}$	$\approx 10^{-3}$
	2B535, No. 7		1200 (1500 max)	14.1	1.1	-	$\approx 10^{-7}$

Table 3-14: Values of some coated particle lots and pieces on their basis

No.	Piece form	Coated particle lot	Irradiation Conditions			$F \cdot 10^5$					
			Tem- perature [°C]	Fluence $[10^{25} \text{ m}^{-2}$, $E > 16 \text{ fJ}]$	Burnup [%FIMA]	Burnup < 4 %FIMA			Burnup > 5 %FIMA		
						Kr-85m	Kr-87	Kr-88	Kr-85m	Kr-87	Kr-88
1	PC	21-1-X-80	1200	0.27	6.9	6.7	3.8	4.8	6.7	3.8	4.8
2	PC	36-1-X-80	1200	0.11	3.0	3.4	2.5	3.0	-	-	-
3	PC	21-3-X-81	1200	0.11	3.0	2.8	1.9	2.4	-	-	-
4	PC	21-4-X-82	1200	0.07	1.8	1.1	0.78	1.0	-	-	-
5	PC	21-10-X-87	1250 1500	0.08	0.-2.1 2.1-3.5	0.73 > 10.	0.42 > 10.	0.81 > 10.	-	-	-
6	PC	21-9-X-84	1250	0.22	5.8	0.13	0.09	0.12	0.13	0.09	0.12
7	MFE	21-1-X-80	1250	0.17	13.3	0.35	0.16	0.21	4.0	3.1	-
8	FC	36-1-X-80	1200 1250	0.24	6.5 7.5	- 0.21	- 0.16	0.19 0.20	- 0.83	- 0.80	1.21 0.85
9	FC	21-3-X-81	1250	0.28	8.0	0.25	0.21	0.22	0.53	0.47	0.49
10	MFE	21-3-X-81	1250	0.16	13.5	0.18	0.09	0.14	0.36	0.20	0.30
11	MFE	21-10-X-87	1250	0.42 0.49	0.-8.8 8.8-9.8	0.12 -	0.09 -	0.12 -	0.18 > 10.	0.13 > 10.	0.17 > 10.
12	MFE	21-9-X-84	1250		12.9	0.1	0.07	0.11	0.15	0.10	0.14

Table 3-14: Values of some coated particle lots and pieces on their basis (continued)

No.	Piece form	Coated particle lot	Irradiation Conditions			$F \cdot 10^5$					
			Tem- perature [°C]	Fluence $[10^{25} \text{ m}^{-2}, E > 16 \text{ fJ}]$	Burnup [%FIMA]	Burnup < 4 %FIMA			Burnup > 5 %FIMA		
						Kr-85m	Kr-87	Kr-88	Kr-85m	Kr-87	Kr-88
13	FC	21-4-X-82	1250	0.62	8.0	0.25	0.21	0.21	0.53	0.47	0.47
14	FC	36-6-X-83	1250	0.29	7.5	0.21	0.16	0.20	0.83	0.80	0.85
15	MFE	36-6-X-83	1250	0.31	19.0	0.18	0.15	0.16	0.44	0.26	0.36
16	FC	21-4-X-82 K=1.0-1.05 ⁽¹⁾ K=1.0-1.3 ⁽¹⁾	1250	0.62	8.0	0.18	0.14	0.14	0.34	0.29	0.29
			1250	0.62	8.0	0.25	0.21	0.21	0.53	0.47	0.47

(1) K: non-spherical coefficient

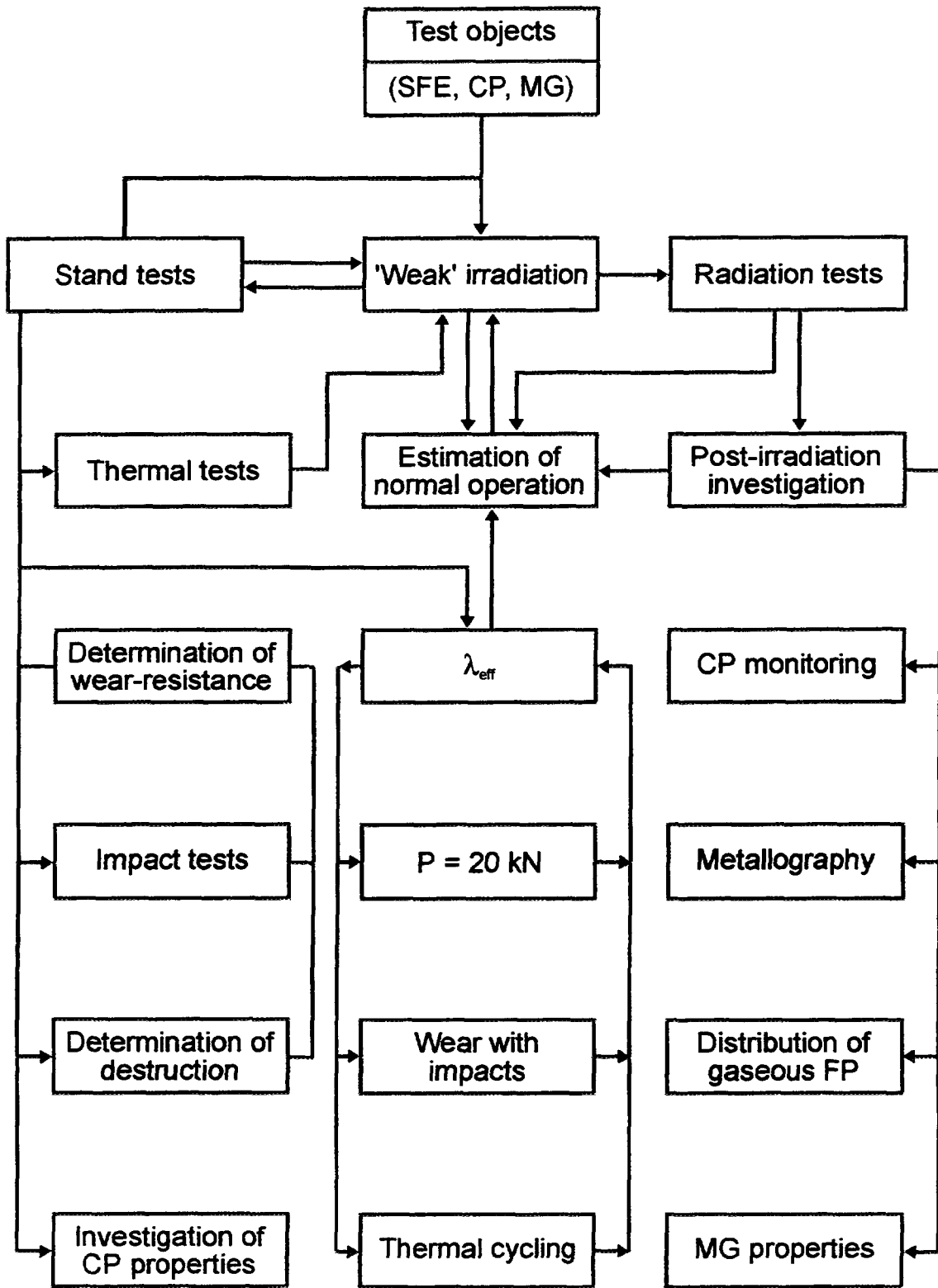


Fig. 3-15: Scheme of experimental treatment of spherical fuel elements

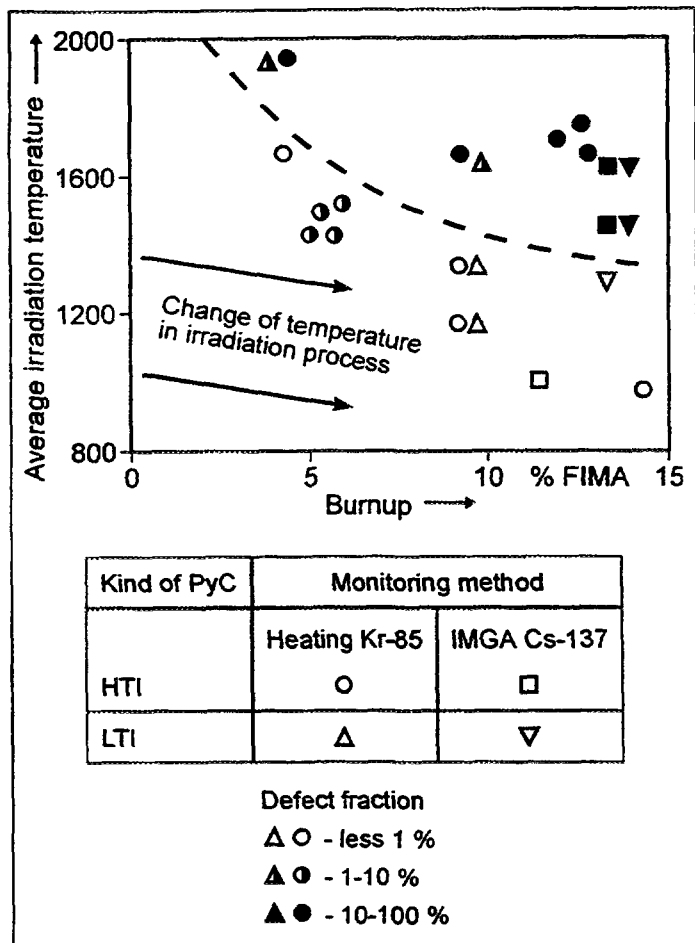


Fig. 3-16: Coated particle performance (part of coupons) during irradiation at high temperatures, maximum flux of thermal neutrons: $1.6 - 2.2 \times 10^{25}/\text{m}^2$ [54]

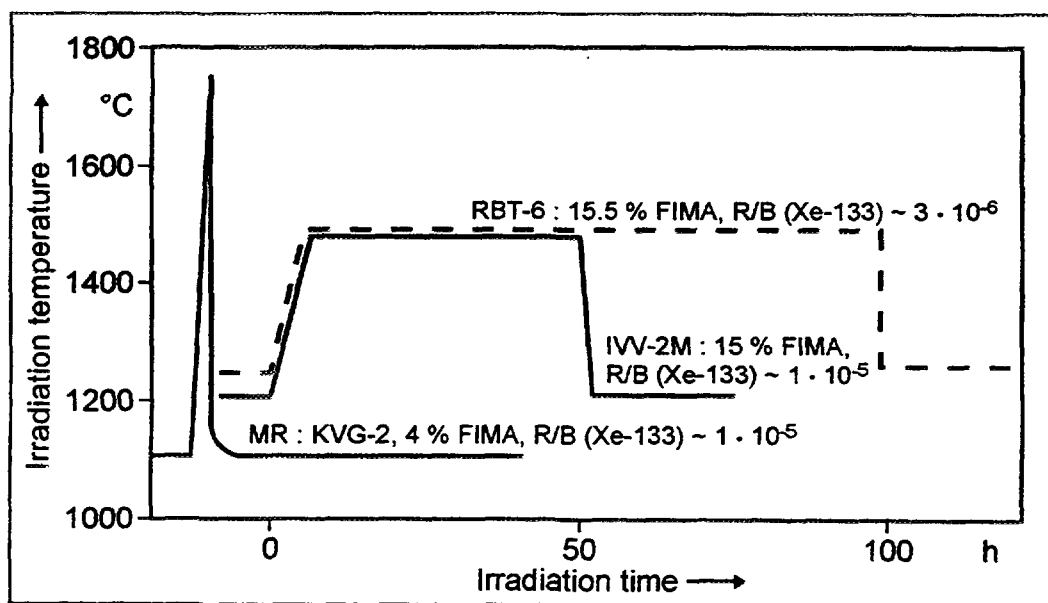


Fig. 3-17: Test conditions of accident fuel element heating during service life irradiation [54]

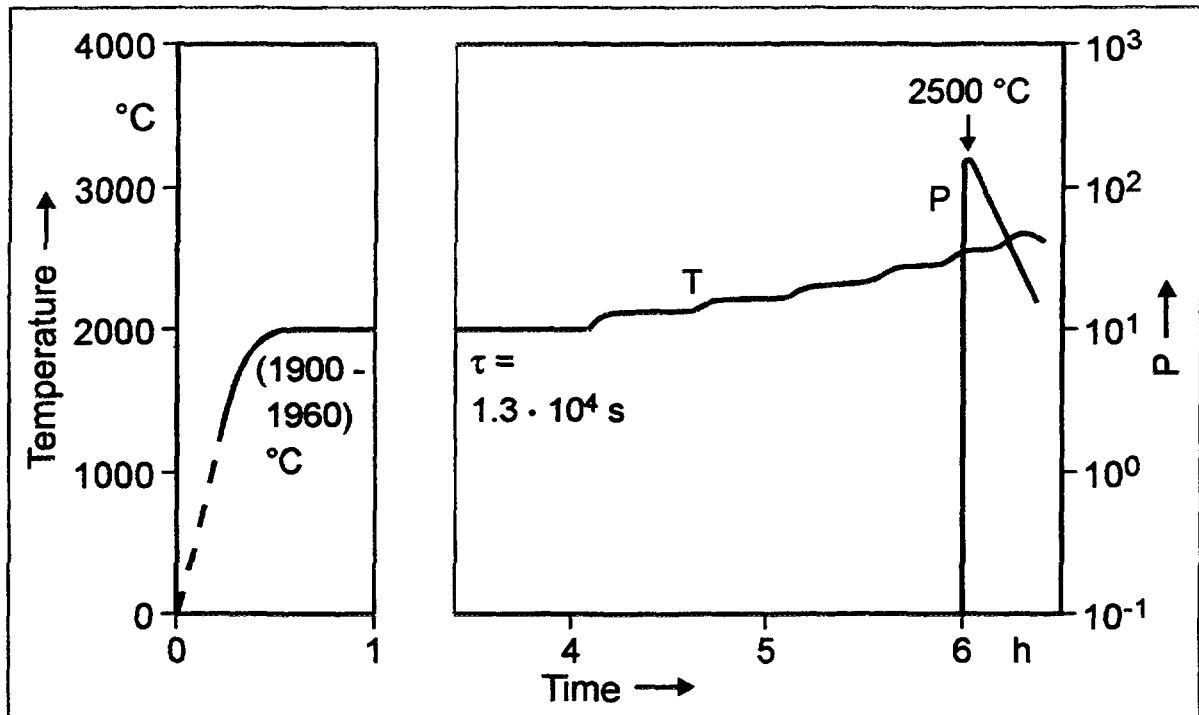


Fig. 3-18: Test results from coated particles irradiated up to 3.8 %FIMA [55]

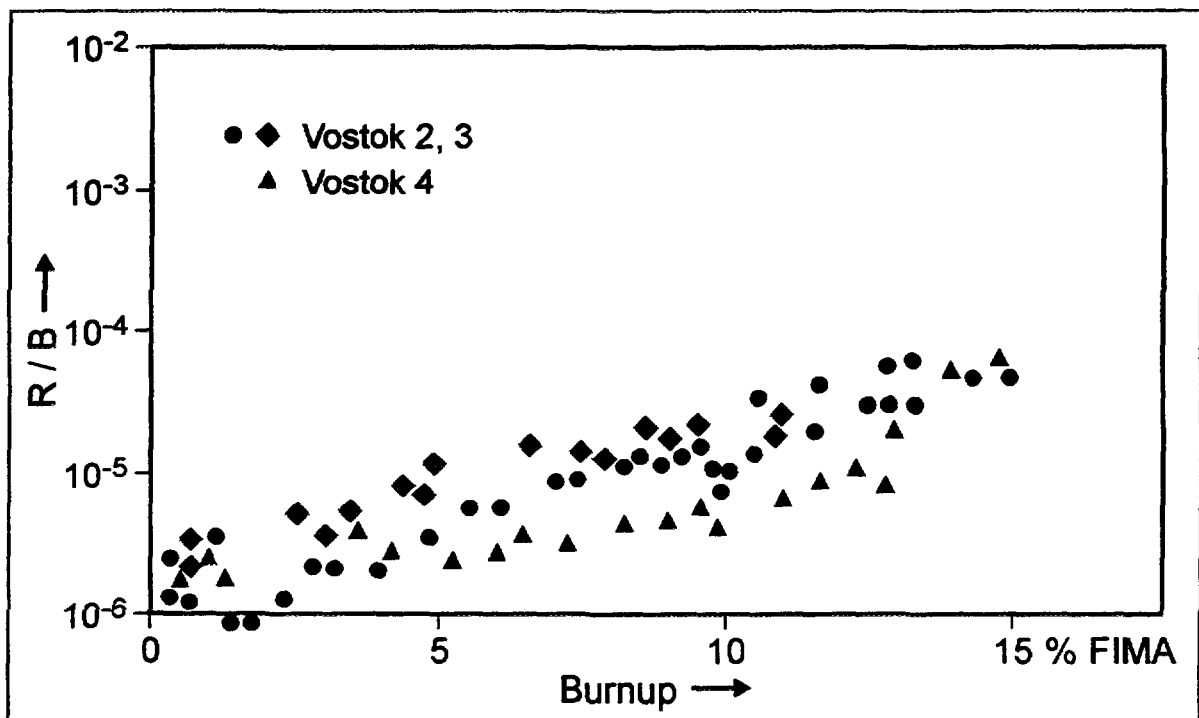


Fig. 3-19: Gaseous fission product release from fuel elements during long-term irradiation [54]

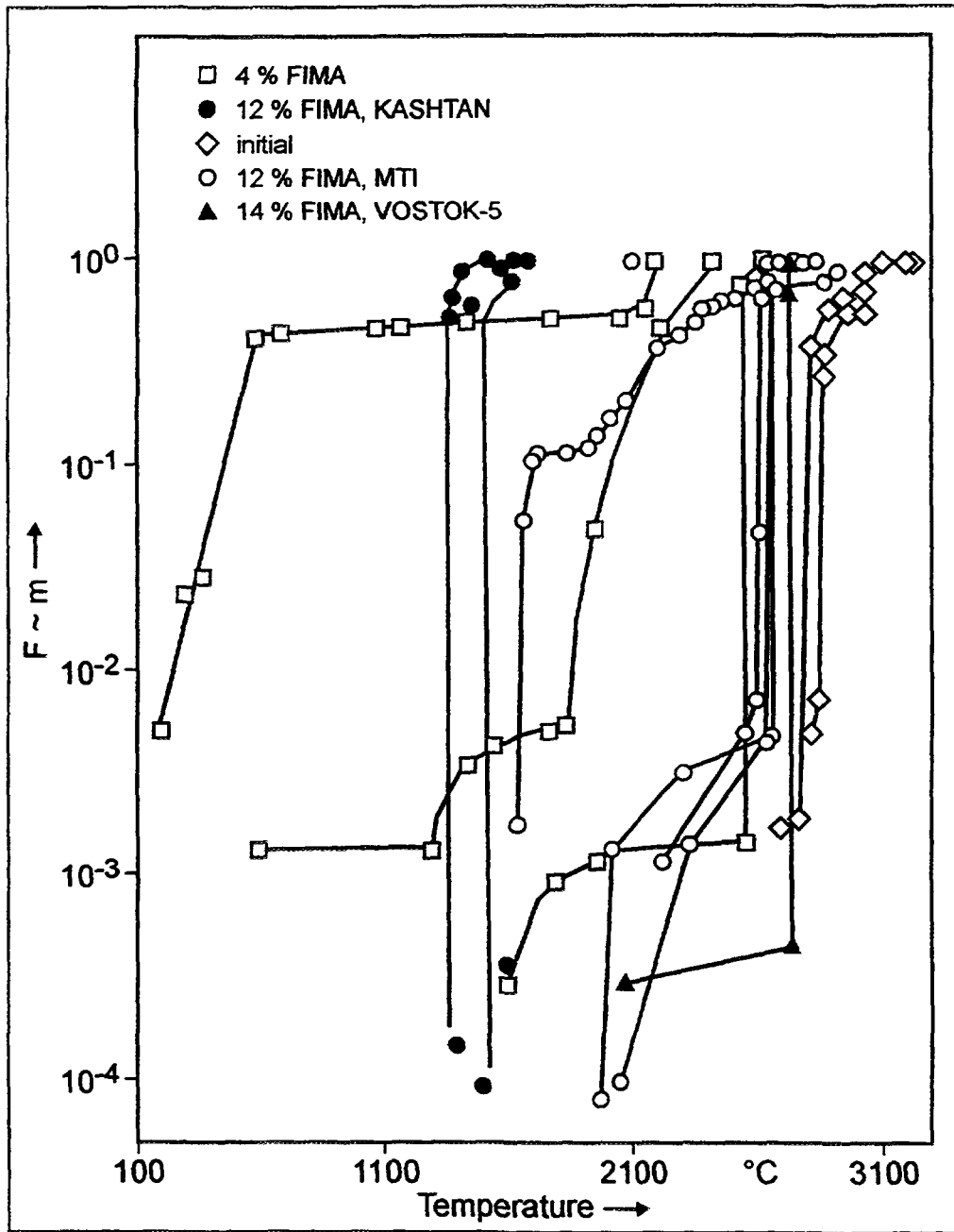


Fig. 3-20: Development of coated particle production technology [55]

3.4.5. The US Program

The functional performance of TRISO coated particle fuel has been demonstrated over the last three decades in test reactors under accelerated, i.e., high neutron flux conditions and in operating gas-cooled reactors. Because of the refractory nature of kernel materials and the fact that the kernel is isolated from the coatings by the buffer layer, the observed coating performance has been largely independent of the composition and enrichment of the kernel, but highly dependent on the properties of the coatings [7, 56]. The entire data base for all particle types, therefore, contributes to the generic data base used in design. Thus for the US, the two primary sources of fuel performance data are accelerated irradiation tests and operating reactors. Data from these sources are discussed in the following paragraphs.

3.4.5.1. Accelerated Irradiations

Testing of coated particle fuel under conditions where the metal burnup and coating irradiation damage is accelerated by a high neutron flux was regarded as essential to gain timely performance information needed to assist in reactor design and safety analysis prior to licensing for operation. Accelerated testing of coated particle fuel has been employed since the onset of development in the late 1950s. This type of testing was to provide data needed to meet a demanding development schedule. Except for the reduced time of exposure, the conditions of accelerated irradiation subjected the fuel particles to a more severe test than would normal HTGR operation. Therefore, when time effects are properly accounted for, performance results from accelerated tests represent a conservative upper limit in the amount of coating degradation than can be expected under normal exposure. Some aspects of the severity of testing under accelerated conditions are discussed below.

The power produced by an individual particle during HTGR operation is about 0.05 W, but under accelerated testing the power may approach 1 W early in the irradiation before the U-235 has been depleted [57]. The increased power associated with accelerated testing is accompanied by a higher temperature differential between the kernel and coatings relative to normal operating conditions. Because the fuel compact temperature in accelerated irradiations is selected to be representative of the temperature under normal operating conditions, the fuel kernel operates at a temperature higher than in a normally operating HTGR. In addition, the larger temperature differential between the kernel and coatings provides a greater thermal driving force than would be present under HTGR operating conditions. Therefore, in regard to thermal effects, the results of accelerated testing of coating performance are viewed as conservative indications of what would be expected under normal operating conditions.

In addition to thermal effects, the coatings are subject to neutron damage during irradiation. The accelerated testing takes place typically in a light water, moderated materials test reactor where the energy spectrum and damage rate in the coatings are different from the HTGR. The effects on fission product behavior and fuel particle performance of the different neutron fluxes and damage rates under normal and accelerated reactor operating conditions have not been adequately addressed. At high irradiation temperatures, carbonaceous materials, such as the inner and outer pyrocarbon coatings in the fuel particles, will densify, i.e., shrink, at relatively high rates. These rates are affected by the graphitizability, anisotropy and porosity of the pyrocarbons. To determine the effects of acceleration, comparative irradiations must be conducted but with pyrocarbons having reproducible properties that are correlated with process variables. The effects of accelerated irradiations may be manifested not only in dimensional changes but also in the failure of any of the coatings and among chemical and transport phenomena.

Accelerated testing has, however, been useful in solving fuel performance problems in operating reactors. For example, the mechanical failure of (78 of 804) fuel element sleeves in Core 1 of the first US HTGR at Peach Bottom, Pennsylvania, was not predicted in advance of the Core 1 startup. However, accelerated irradiation testing conducted in parallel with core fabrication and exposure showed that the failure mechanism was expansion of the highly oriented pyrocarbon coatings. This accelerated testing provided the information

needed to design the improved particles used in the successful second core of the Peach Bottom HTGR.

Because of the large experience base with accelerated testing, acceleration irradiation test data has provided major support for fuel design and performance technology.

3.4.5.2. Comparison of Coated Fuel Particle Performance in Accelerated Irradiation Testing and in an Operating Reactor

In comparing particle performance, only particles with TRISO coatings are considered. In recent times, all groups involved in developing the gas-cooled reactor in their respective countries have adopted the TRISO coating design [58].

In the Peach Bottom Fuel Test Element program, 15 full-sized test elements with HEU TRISO UC₂ and UO₂ were irradiated at time-averaged temperatures as high as 1773 K, fast neutron exposures up to 4×10^{25} n/m² and maximum burnup of 60 %FIMA. Postirradiation examination of the irradiated fuel showed the physical integrity of the coatings to be consistent with results obtained from accelerated fuel tests [59].

Accelerated irradiation testing with the Fort St. Vrain (FSV) proof-test irradiation capsule [60] was used to demonstrate the performance expected in an operating reactor. This test demonstrated that the HTGR requirement for FSV in regard to the fuel production quality and the associated fission product retention was acceptable. The prediction of circulating fission gas reported was consistent with the subsequent operation of the FSV reactor over the reactor operating lifetime [60].

Two destructive examinations were carried out on irradiated FSV fuel elements. There was less fuel compact dimensional change than predicted based on the accelerated irradiation test data. However, the amount of SiC corrosion, although small, appeared to be greater than expected [61, 62, 63, 64].

3.4.5.3. Irradiation with High- and Low-Enriched Uranium Fuel

3.4.5.3.1. HEU Fuel

A large number of irradiation capsule results have been obtained for HEU UC₂, UCO, UO₂, and (Th,U)C₂ TRISO particles [65]. In the US, 52 capsules with HEU fuel were irradiated and an additional 14 were irradiated as part of the German development effort. In 17 of the US capsules the burnup exceeded 70 %FIMA, the temperature was in excess of 1000 °C, and the fast neutron exposure was greater than 5×10^{25} n/m² ($E > 29$ fJ) HTGR. A list of the capsules and exposure conditions of fluence and temperature experienced as well as a graph of the envelopes of these quantities in specific irradiation capsules and reactors have been reported [65].

Two US and four German capsules contained the TRISO coated HEU UCO particles irradiated in isolated piggyback samples in experiments HRB-17 and HRB-18 to 78 %FIMA, 4.2×10^{25} n/m² and 970 K. These samples have been metallographically examined. The kernels and coatings were found to be in excellent condition as shown in Fig. 3-21.

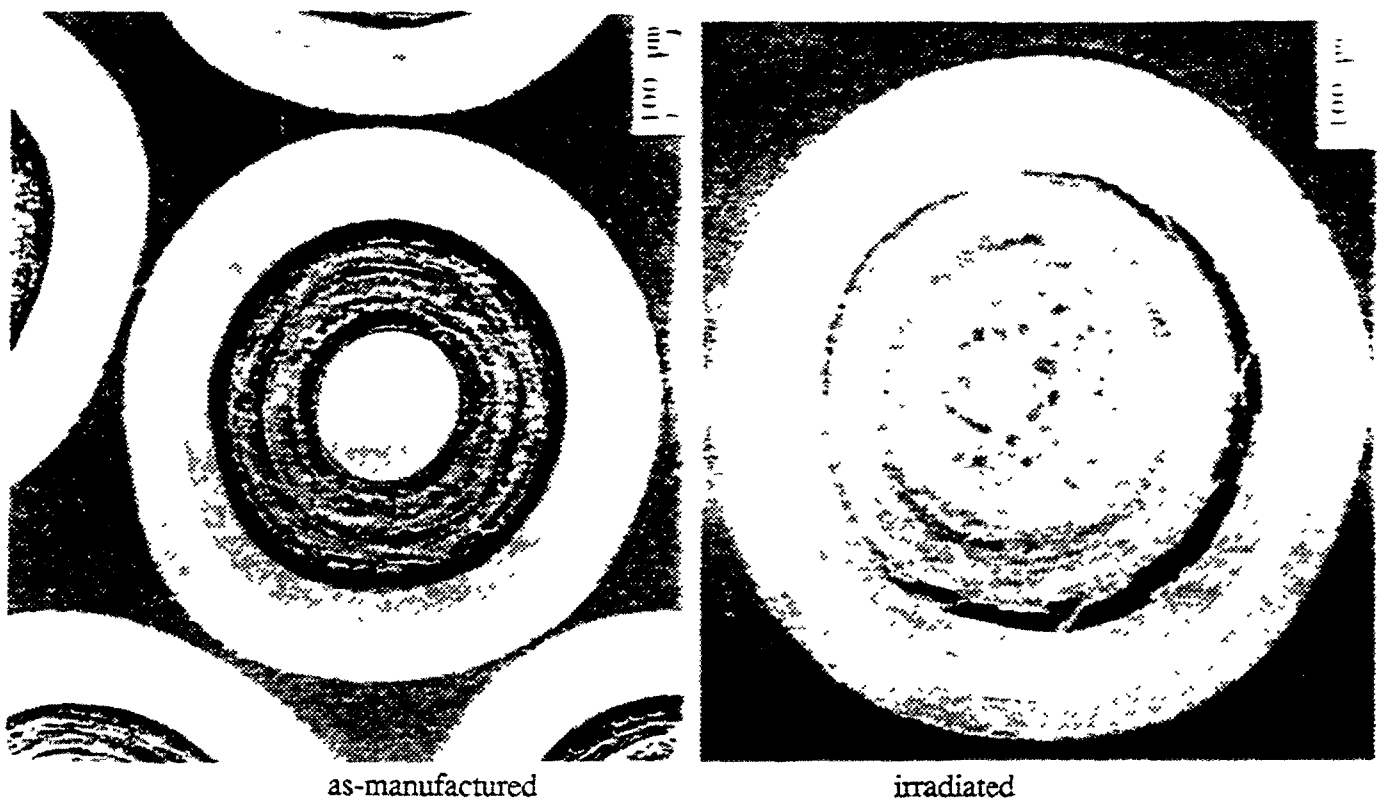


Fig. 3-21: Irradiated HEU $\text{UC}_{0.2}\text{O}_{1.8}$ fuel particles.

Conditions at the end of irradiation: burnup: 78 %FIMA, fast fluence: $4.2 \times 10^{25} \text{ n/m}^2 (\text{E}>29 \text{ fJ})_{\text{HTGR}}$, temperature: 755 °C, configuration: unbonded fuel particles in POCO graphite trays sealed within Incoloy containers.

3.4.5.3.2. LEU Fuel

In the late 1970s, HEU fuel was replaced by LEU fuel (< 20 % U-235) as the reference fuel for the HTGR in accord with the general goal of preventing the proliferation of nuclear weapons. Irradiation performance data, mainly for LEU TRISO UC_2 , UCO, and UO_2 , have been obtained from 8 US and 6 German irradiation capsules [66, 67, 68, 69, 70, 71, 72, 73], as shown in Table 3-15. In addition to the characterization of fissile coated fuel particles, 58 of the irradiation capsule tests, including most of those referenced earlier, contained TRISO ThO_2 particles [57]. As discussed above, the generic nature of the irradiation data permits the coating material performance results from the complete spectrum of fuel types to be used in the design of HTGR fuel.

In the period 1978 to 1981, a US program [74] to test and select suitable LEU fuel materials was conducted. The fissile, two-phase, oxycarbide system of UC_2 and UO_2 , represented commonly by the acronym UCO, and the fertile ThO_2 system were selected. The selection process involved the consideration of heavy metal loadings, circulating and plateout activity, fabrication, irradiation response, performance margins, manufacturing and schedule risks, and transitions from LEU to HEU cycles. The choice of UCO had the desirable results [58] of (1) a lower CO pressure and consequent reduction in kernel migration and of (2) kernel retention of rare earths and the consequent reduction in SiC attack by the rare earths. Note also that in Fig. 3-20 a $\text{UC}_{0.2}\text{O}_{1.8}$ particle irradiated to 78 %FIMA does not show evidence of kernel migration or chemical attack on the SiC.

Table 3-15: Summary of accelerated irradiation capsules containing LEU fuel

Capsule reference	Temperature [K]	Burnup [%FIMA]	Neutron fluence [10^{25} m^{-2} , $E > 29 \text{ fJ}$]	Fissile fuel composition ⁽¹⁾
<i>U.S. capsules</i>				
HRB-14	1233 - 1403	14.5 - 29.5	4.5 - 8.3	UCO, UC ₂ , UO ₂
HRB-15A	1373 - 1573	29	6.5	UCO, UC ₂ , UO ₂ , UO ₂ *
HRB-15B	1088 - 1188	27	6.6	UCO, UC ₂ , UO ₂ *
HRB-16	1323 - 1523	17 - 29	3.1 - 6.3	UCO, UC ₂ , UO ₂ , UO ₂ *
HRB-17	973 - 1273	25	4.3 - 4.6	UCO, UC ₂
HRB-18	973 - 1273	25	4.3 - 4.6	UCO, UC ₂
R2-K13 ⁽²⁾	1273 - 1473	22	7.4 - 7.8	UCO
HFR-B1 ⁽²⁾	1173 - 1523	18.5	5.6	UCO
<i>FRG capsules</i>				
HFR-P4	1273 - 1473	10 - 11.5	6 - 8	UO ₂
HFR-P5	1223 - 1623	5 - 7	3 - 5	UCO, UO ₂
SL-P1	1073	9 - 12	5 - 6	UO ₂
HFR-K3	1173 - 1523	13 - 15	5 - 7	UO ₂
FRJ2-K13	1273	11 - 12	3 - 4	UO ₂
FRJ2-P28	1223 - 1423	11 - 13	1.5 - 2	UO ₂

(1) Note that UO₂* represents either a particle in which ZrC is dispersed in the buffer or a particle in which the kernel has a thin outer layer of pyrocarbon and a layer of ZrC on the pyrocarbon.

(2) US/FRG cooperative irradiation experiments

Major tests of fuel compacts containing UCO (75% UO₂ and 25% UC₂) were conducted in irradiation experiments HRB-15A and R2-K13 in, respectively, the High Flux Isotope Reactor (HFIR) at ORNL and in the R2 Reactor at Studsvik, Sweden. The data from the two experiments were consistent in terms of the in-service failure fraction as a function of the accumulated fluence, ($E > 29 \text{ fJ}$)_{HTGR}, the failed fraction being based on Kr-85m release. A smooth curve through the data contained two linear portions: one with a very small slope at fluences below $4 \times 10^{25} \text{ n/m}^2$ and one with a large slope at fluences above $5.5 \times 10^{25} \text{ n/m}^2$. This consistency, given the higher mean neutron flux in HRB-15A,

a factor of 2.4 larger than in R2-K13, indicates that the absolute fluence and not the rate of accumulation is correlated with or possibly governing the failure.

For these experiments, in retrospect, the peak tolerable fluence appears to be of the order 4×10^{25} n/m². Higher fluences led to an increasing failure fraction as for example, 0.01 and 0.02 at fluences of 6×10^{25} and 7×10^{25} n/m², respectively. The fluence at zero failure fraction obtained by extrapolation of the high-slope, linear portion, may serve as a measure of merit for the irradiation performance in a fuel compact of embedded coated fuel particles of a particular design, and fabricated in a particular batch. In the present case, this fluence is 4.6×10^{25} n/m².

The data from the experiments HRB-15A and R2-K13, however, were not consistent in terms of fission product attack on the SiC coating. The attack was extensive in HRB-15A [67] and essentially absent in R2-K13 [71]. This implies that the accelerated irradiation in HRB-15A was the cause of the attack whereas in R2-K13, under essentially normal conditions, no attack was discernible [71, 75]. Note that the attack was also extensive in other HRB experiments with related batches.

Under HRB irradiation conditions, coated fuel particles experience significantly larger thermal gradients than otherwise. The gradients promote fission product transport to the cool side of the particle, accumulation of Ag, Pd, Ru, and rare earths at the inner SiC surface, penetration of the SiC and reaction of the named fission products with SiC. The latter leads to thinning of the SiC coating and an enhancement of fission product escape from the particle. Judging by the consistency in the failure fraction-fluence data, any release of fission products via reaction with SiC was of lesser importance for fission product release than the consequence of increasing fluence.

3.4.5.4. Irradiation Test of Particle Design Changes

Following the period of work described in Section 3.4.5.3. above, more stringent requirements on fission product release during normal operating and accident conditions were adopted. These demanded lower levels of heavy metal contamination and fewer defective SiC coatings than previously acceptable by factors of 10 and 60, respectively. Reaction of the fuel kernels with the SiC coating gases and coating damage during compaction in the process of fabricating fuel compacts were regarded as the major causes of heavy metal contamination and defective SiC coatings. To avoid the latter, the particle design was changed by increasing the thickness of the inner pyrocarbon layer (35 to 53 μ m) and by adding a crushable, protective pyrocarbon coating on the outer pyrocarbon coating of the normal TRISO coating design. The thicker inner PyC was intended to reduce the extent of reaction between the kernel and coating gas and the crushable protective PyC to reduce compaction damage. The as-manufactured fuel compacts met the new requirements and had R/B values for Kr-85m in the range 10^{-8} to 10^{-7} at the beginning of irradiation in experiment HRB-21.

As the irradiation continued, the correlation of the in-service particle failure with the fast neutron fluence, as observed in experiment HRB-15A and in other HRB experiments, developed but with a measure of merit (see section 3.4.5.3.2., 4th paragraph) lying between 1×10^{25} and 2×10^{25} n/m². This indicated poor performance of the embedded particles in

experiment HRB-21 even with respect to the performance in experiment HRB-15A of the previous particle design.

Study of the data collected during irradiation and postirradiation examinations, and from archival particles and particle stress analyses has led to the following, most probable, contributing causes of particle failure:

Under fast neutron irradiation, shrinkage of the protective PyC and the petroleum pitch component of the compact matrix material, which intruded the protective PyC during compaction, led to cracking which propagated into the outer PyC; the susceptibility to failure of the outer PyC was thus significantly enhanced, particularly by the strong bonding between the protective PyC and the outer PyC.

Strong bonding of the inner PyC to the SiC coating and irradiation induced strains resulted in large stresses and an enhanced susceptibility to inner PyC fracture.

Cracking of the inner PyC created high, local stress concentrations which could lead to failure in the nearby SiC coating. The failure was more likely to occur when bonding between the inner PyC and SiC was strong, and to be more probable with the thicker inner PyC, or when outer PyC coatings were failed.

3.4.5.5. Further Work and Closure

Further work on the fuel compact fabrication has shown that the TRISO fuel particle design can meet HTGR quality requirements. Improvement in the compaction process indicates that the protective PyC is no longer needed. Furthermore, use of an inner PyC of thickness 35 μm can be tolerated by lowering the SiC coating temperature to reduce the extent of reaction of the kernel with the coating gases.

Work was started in the direction of fabricating particles with outer and inner pyrocarbon coatings of a greater isotropy and of a density consistent with the lower SiC deposition temperature, with some SiC impregnation of the inner PyC, and with a smaller SiC grain size and greater strength. These efforts were ended by the cancellation of the HTGR project by the US Department of Energy at the end of fiscal year 1995.

3.5. REACTOR OPERATING EXPERIENCE

3.5.1. Dragon HTGR

The OECD-sponsored, High-Temperature Reactor Project Dragon did an extensive amount of pioneering work in the field of HTGR fuel and fission products. The central achievement of the Dragon Project was the construction and successful operation of the 20 MW(th) Dragon HTGR with a prismatic core at Winfrith in the UK. Their areas of investigation spanned the full scope of this TECDOC and beyond, including: TRISO fuel particle design, fabrication, and irradiation testing, fuel performance modeling, in-reactor radiochemical and coolant chemistry surveillance, fission product release and transport measurement and modeling, and reactor component decontamination.

The Dragon Project began in 1959 and was terminated in 1976 because of unfavorable political circumstances. The Project was a great technical success, but the decision of the UK and others not to continue HTGR development was a major disappointment to the participants. While researchers in many countries have contributed to the early conceptual development of coated particle fuels, the Dragon Project deserves much of the credit for the design and qualification of TRISO coated fuel particles and the development and demonstration of practical fabrication processes for mass producing them.

During the Project, a remarkable variety of coated particle fuels were fabricated and irradiated in materials test reactors and in-pile loops throughout Europe and, especially, in the Dragon HTGR. Their fuel development efforts were organized into four phases: (1) initial survey of a broad spectrum of particle designs with various kernel and coating designs; (2) HEU/Th fuel cycles, including both one- and two-particle systems; (3) LEU fuel cycles, which emphasized the optimization and testing of a TRISO coated UO₂ particle; (4) advanced fuel systems. A number of different TRISO coated PuO_x and PuO_x/C particles were also successfully fabricated and irradiated.

The work was systematically documented in a long series of Dragon Project (DP) reports and was summarized in a final, comprehensive overview report DP-1000 [76], which contains a large number of references to their fuel and fission product research and development. Despite the fact that the research was done two or three decades ago, a number of these Dragon studies remain seminal works to this day: the exhaustive study by Voice [77] of the relationships between coating process parameters and the attendant physical properties of SiC coatings is a classic example. All current and future researchers in the field of HTGR fuel and fission products would benefit greatly from an in-depth study of the Dragon Project work, and DP-1000 is probably the best point of departure.

3.5.2. Peach Bottom Unit 1

The Peach Bottom Atomic Power Station Unit 1 was a 40 MW(e) HTGR demonstration plant. The heart of the Peach Bottom nuclear steam supply system (NSSS) was a helium-cooled, graphite-moderated, 115 MW(th) reactor operating with a 700 °C gas outlet temperature on a thorium-uranium fuel cycle. Peach Bottom operated successfully for seven years until it was shut down for decommissioning in late 1974 because it had completed its demonstration mission. An extensive and highly successful End-of-Life (EOL) R&D Program was conducted with the primary goal of generating real-time integral data to validate HTGR design methods with emphasis on reactor physics, core thermal/fluid dynamics, fission product release and plateout, and materials performance, especially performance of the Incoloy 800 used for the steam-generator superheaters. These EOL data proved particularly useful for validating fission product transport codes; the fission gas release and the cesium release from the core and the cesium plateout in the primary circuit were all predicted within the accuracy goals adopted for the US HTGR program [78].

The reactor core consisted of 804 graphitic fuel elements oriented vertically in a close packed array within the steel reactor vessel. Each fuel element, which was 3.5 inches in diameter and 144 inches long, contained 30 annular fuel compacts comprised of coated fuel particles in a carbonaceous matrix. The fuel kernels were HEU (Th,U)C₂. The Core 1 fuel particles were coated with a single PyC layer solely to prevent hydrolysis of

the carbide kernels during manufacture. However, these so-called "LAMINAR" particles were dimensionally unstable under fast neutron irradiation causing the fuel compacts to swell which in turn caused mechanical interaction between the compacts and outer sleeve resulting in the cracking of up to 10 % of the sleeves. As a consequence, the plant was refueled early, and Core 2 contained BISO coated particles which eliminated the compact swelling problem and provided enhanced fission product retention. Peach Bottom Core 2 performed exceptionally well; but since it contained BISO fuel and the emphasis here is on TRISO fuel, the interested reader is referred to Ref. [78].

More germane to this TECDOC are the 29 full-size fuel test elements (FTEs) irradiated in Peach Bottom which contained at least a fraction of TRISO fuel, especially the 15 test elements in which all of the fissile particles were TRISO coated. A large number of different kernel compositions were tested as TRISO coated particles, including HEU (Th,U) O_2/ThC_2 (the reference FSV fuel), HEU UC₂, UO₂, UC_xO_y, PuO_x and (Th, Pu)O₂. A comprehensive summary report describing the Peach Bottom FTE Program is available [59], and it includes a large number of citations of detailed reports on individual test elements. The Peach Bottom core was an excellent test bed for HTGR fuel development because each fuel element in the core was individually purged so that the R/Bs for test elements could be measured directly without contributions from the rest of the core. In addition, most of the fuel test elements contained additional test samples irradiated as "piggy back" samples in the central graphite spine; these samples included various kinds of loose particles and fission product diffusion samples. Upon discharge from the Peach Bottom core, many of these test elements were subjected to detailed PIEs, typically at ORNL or GA.

The results of the various fuel test element irradiations in Peach Bottom are best understood by reviewing the operational and PIE reports for the individual FTEs. Nevertheless, several common characteristics of these irradiations are noteworthy: (1) large numbers of particles ($> 10^5$) could be irradiated in a single test element; (2) irradiation was in a true HTGR neutron flux spectrum; (3) the irradiations were real time so all of the problems, real and imagined, associated with accelerated tests were avoided (e.g., excessive thermal gradients).

3.5.3. Fort St. Vrain Nuclear Generating Station

The Fort St. Vrain (FSV) reactor was designed to produce 842 MW(th) and 330 MW(e), and had many design features common to prismatic HTGRs, e.g., graphite moderation, helium coolant, and similar designs for fuel particles, fuel elements, and control rods (e.g., [60]). The fuel compacts, which were inserted into machined blind holes in the fuel element, were composed of TRISO coated HEU fuel particles in a carbonaceous matrix derived from petroleum pitch. The reactor core is composed of 247 columns of fuel elements, with six fuel elements stacked in each column.

The primary coolant circuit was wholly contained within a prestressed concrete reactor vessel (PCRV) with the core and reflectors located in the upper part of the cavity, and the steam generators and circulators located in the lower part. The helium coolant flowed downward through the reactor core and was then directed into the reheater, superheater, evaporator, and the economizer sections of the 12 steam generators. From the steam

generators, the helium entered the four circulators and was pumped up, around the outside of the core support floor and the core barrel before entering the plenum above the core to complete the circuit. The superheated and reheated steam was converted to electricity in a conventional steam cycle power conversion turbine-generator system.

Experience with fuel design, development and manufacture for FSV provided the basis for the fuel technology used for the GT-MHR and guided fruitful areas for subsequent fuel quality and performance improvements. For FSV, 2448 hexagonal fuel elements, 7.1 million fuel compacts and 26,600 kg of TRISO coated fuel particles were produced. The fuel was irradiated at temperatures greater than 1300 °C to a maximum burnup in the fissile particles of 16 %FIMA and to a maximum fast neutron fluence of 4.5×10^{25} n/m² ($E > 29$ fJ) with no evidence of significant in-service coating failure.

The FSV kernels were fissile (Th/U)C² and fertile ThC². The grind-screen-melt process used to manufacture FSV kernels produced a wide diameter distribution which were separated by screening into two size ranges, smaller "A" and larger "B" diameters, to a batch of kernels with a narrow enough diameter distribution to coat uniformly. This technique produced particles with a distribution of metal densities needed to the fissile and fertile loadings used to shape the reactor power and simultaneously maintain uniform volume in each compact.

FSV provided invaluable fuel performance, fission product release and plateout data that have been used for validation of GA design methods. The experience gained from the comparison of the FSV measured and predicted fission product release and plateout is directly applicable to the fuel performance assessment of advanced prismatic HTGRs because of the similarities in the core design, particularly the TRISO particle coatings and fuel element designs. The effect of differences in fuel kernel composition can be estimated by using performance models for the particular kernel type, and the effect of differences in the primary circuit components (e.g., gas turbine instead of steam generator, etc.) can be estimated by revising the plateout geometric model for differences in configuration and materials.

Typically, the two dominant source of fission product release from the core are as-manufactured, heavy metal contamination and particles whose coatings fail in service. The models for calculating fuel coating particle failure and fission product release and transport are included in the GA reference fuel performance computer codes SURVEY [14], TRAFIC [44], and PADLOC [79]. These codes have been used to estimate the fuel performance, fission product release, circulating coolant activities and plateout distributions for FSV over the entire operating life of the plant [80], and the measured results were compared to these calculational estimates.

The SURVEY code was used to predict the full-core fuel and graphite temperature distributions, fuel particle coating failure distributions and the full-core gas release rates (R/Bs) as a function of time. Using the calculated fuel temperature histories, burnup and fast fluence histories, and fuel performance models, the fuel particle failures were calculated as a function of time. The gaseous fission product releases were calculated for two key isotopes Kr-85m and Xe-138, and the predictions were compared with measurements taken as part of the FSV radiochemistry surveillance program.

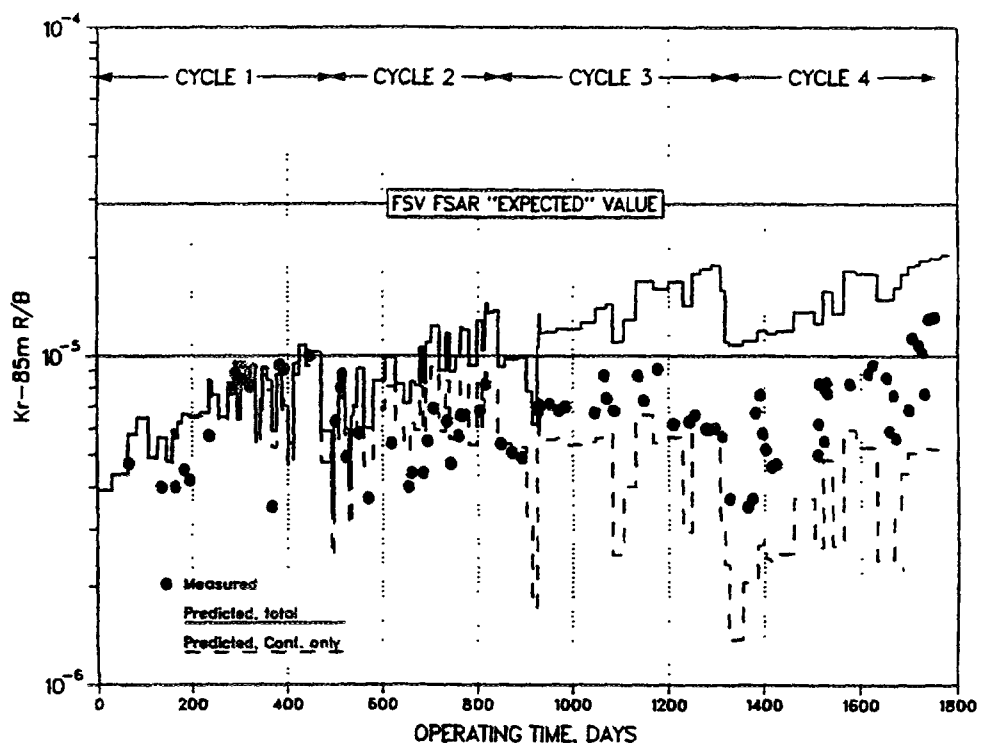


Fig. 3-22: Comparison of Fort St. Vrain predicted and measured Kr-85m release

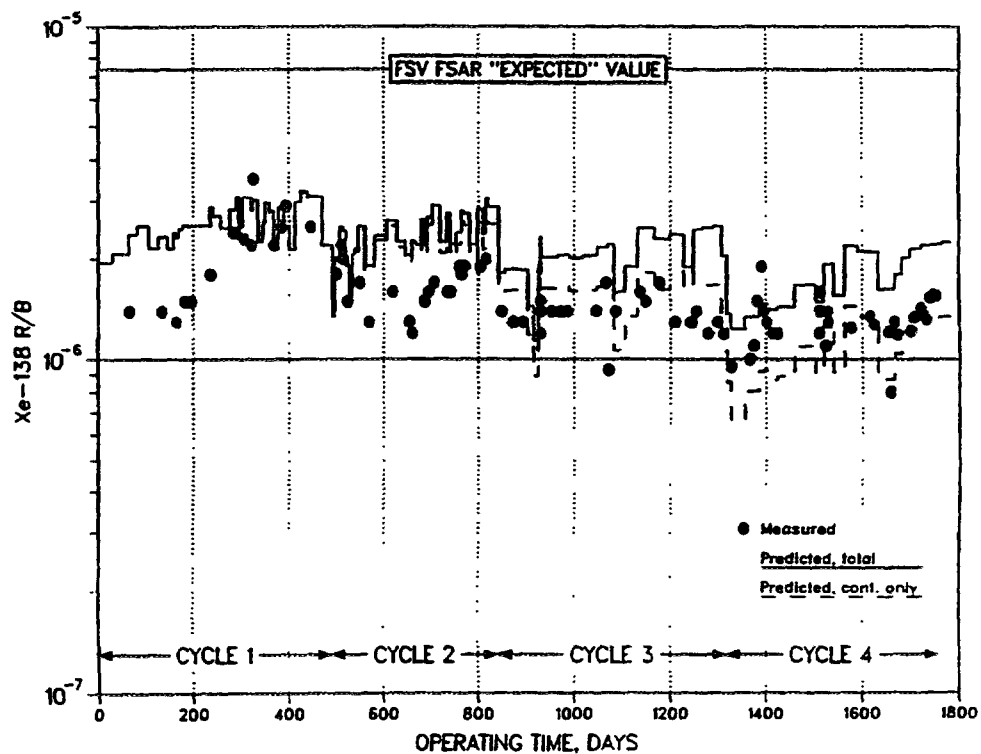


Fig. 3-23: Comparison of Fort St. Vrain predicted and measured Xe-138 release

Table 3-16: Comparison of measured and calculated Fort St. Vrain Plateout at end-of-life

Nuclide	Measured [Ci]	Calculated [Ci]	Calc./Meas.	FSAR: 30 y Expected [Ci]
Sr-90	1.3	1.8	1.4	6.6
Cs-134	1.9	5.7	3.0	-
Cs-137	8.4	13.2	1.6	667

A comparison was made between the predicted and measured fission gas release histories of Kr-85m and Xe-138, as shown in Figures 3-22 and 3-23. This comparison shows that the Kr-85m measured data were overpredicted by a factor between 2 and 4 after cycle 2. The agreement between the predicted and measured Xe-138 release was slightly better than for Kr-85m release. Conservatism in the fission gas release predictions is most likely a result of conservative treatment of coating failure models and, to a lesser degree, to the conservatism in fuel temperature calculations, especially at the fuel element/side reflector interface. This apparent overprediction is particularly important for cesium release predictions. Nevertheless, the agreement between the fission gas predictions and the measured data is well within the factor of 4 margin which is the required predictive accuracy for HTGR fission gas release calculations. Also included in Figures 3-22 and 3-23 are the FSV Final Safety Analysis Report (FSAR) expected (allowable) values which indicate that both the Kr-85m and Xe-138 releases were well below the expected values.

The TRAFIC computer code is used to predict the release of fission product metals from the core during normal operating conditions. The analysis was performed for the key nuclides Sr-90 and Cs-137. The metallic radionuclide release rates from TRAFIC serve as source terms for PADLOC, which is used to calculate plateout distributions of fission metals in the primary coolant circuit.

The FSV plateout data were obtained from the plateout probe measurements and the radiochemical analysis of a circulator removed after reactor operation. Two plateout probes, one in each steam generator loop, were designed to monitor iodines and fission metals released from the core. Plateout probes were removed after cycle 3 and at the end of FSV operations. The activities of metallic fission products (Sr-90, Cs-134 and Cs-137) in the primary circuit were calculated from the probe data. The measured plateout inventories are presented in Table 3-16, along with the inventories calculated by TRAFIC. The FSAR expected plateout inventory levels are also listed. TRAFIC predictions of the metallic fission product inventories for the three isotopes are in reasonable agreement with measurements and consistently conservative.

In general, the FSV fission product release predictions are in good agreement with the measurements. All predictions fall within the design goals of predicting gaseous release within a factor of 4 and metallic release within a factor of 10. Both the fission gas release predictions and measurements are lower than the Expected (allowable) values given in the FSAR. Thus, in spite of the highly irregular operating history of the FSV plant, good fuel

performance has been measured, and this performance is predictable by the reference GA design methods.

3.5.4. AVR

Since the beginning of AVR operations in 1968, which ended in 1989, the 46 MW(th) AVR reactor has been used as test bed for the development of fuel elements (Table 3-17). Initially the AVR had a maximum outlet temperature of 850 °C which was raised to 950 °C in the year 1974. This temperature rise presented no operational problems. A total of 289,789 spherical fuel elements from 26 fuel batches was fed into the core out of which 3000 were taken for general inspection and another 600 had undergone a detailed examination. For modern HTGRs, in particular for process heat applications, interest is concentrated in AVR reloads 15, 19, 21, and 21-2 as high quality TRISO fuels. During the later half of the 1980s, these fuels comprised half of the AVR core.

A large supply of irradiated fuel elements could be drawn from AVR. They were used for extensive characterization tests, for accident simulation tests, and for the demonstration of long-term storage behavior. It was demonstrated that the strength of the fuel elements did not deteriorate. The increase of the corrosion rate in the standard corrosion test at 1000 °C (10 hours in helium with 1 % steam) was found to be a factor of about 2 larger than pre-irradiation values of around 1 mg/(cm² h) [81].

The main parameter to assess the state of irradiation is the measured burnup of fuel elements after withdrawal from the AVR core. For the 10 % enriched GLE-3 fuel elements, the average burnup is 9.6 %FIMA and for the 16.7 % enriched GLE-4 elements 13.1 %FIMA. The accumulated fast neutron fluence and the irradiation temperatures have to be estimated from codes simulating sphere flow, thermohydraulics and nucleonics in the AVR core. LEU fuel elements used in the 1600 - 1800 °C accident simulation tests followed the fluence/burnup dependence of the HTR-MODUL reactor.

Particularly difficult is the assessment of irradiation temperatures in the AVR reactor. This was only made possible with the development of 3D codes to simulate sphere flow, and the distribution of neutrons and temperatures in the core, in conjunction with a sophisticated experiment ("HTA-8"), in which 200 unfueled spheres containing meltable wires were inserted into the AVR core. A variation of alloys span the temperature range from 898 °C (Ag/Cu/Pd) up to 1280 °C (70 % Pd, 30 % Cu). These spheres were detected after one passage through the core and removed. Their radial position in the core could be derived from the exit time, and X-rays made the melted (or not) wires visible giving the maximum temperature during the core passage. Unfortunately, 1280 °C was chosen as the highest melting point. Approx. 20 % of all spheres had all wires melted and had therefore seen surface temperatures > 1280 °C. For an average passage of GLE-3 elements, a maximum surface temperature of 1150 °C has been predicted during 950 °C operation.

Continuous measurements of noble gas activity were conducted in the AVR [82]. Particle failures could then be detected by a considerable increase of the activity (period 1975 - 1977). Also with raising the average gas outlet temperature up to 950 °C, a prompt increase of the noble gas activity by 25 % was observed which is in the expected range of statistical deviation during normal operation [83]. Elevated values found since 1979 may

Table 3-17: AVR fuel reloads in the years 1966 to 1987, from [5]

Reload number	Insertion date	Fuel element type	Number of fuel elements	CP-kernel	Coating	U-235 enrichment [%]
0	7/66	UCC	30,155	(Th,U)C ₂	HTI BISO	93
1	10/68	T	7,510	(Th,U)C ₂	HTI BISO	93
3	4/69	GK	17,770	(Th,U)C ₂	HTI BISO	93
4	7/70	GK	6,210	(Th,U)C ₂	HTI BISO	93
5-1	11/70	GK	25,970	(Th,U)C ₂	HTI BISO	93
5-2	12/71	GO-1	20,825	(Th,U)O ₂	HTI BISO	92
7	1/73	GO-1	7,840	(Th,U)O ₂	HTI BISO	93
6-1	10/73	GO-1	11,000	(Th,U)O ₂	HTI BISO	92
6-2	12/73	GLE-1	2,446	UO ₂	LTI BISO	15 0.7
8-1	5/74	GFB-1	1,440	UO ₂ ThO ₂	LTI BISO	93 -
8-2	5/74	GFB-2	1,610	UO ₂ ThO ₂	LTI TRISO LTI BISO	93 -
9	9/74	THTR-1	5,145	(Th,U)O ₂	HTI BISO	93
10	12/74	THTR-2	10,000	(Th,U)O ₂	HTI BISO	93
11	12/74	THTR-2	5,000	(Th,U)O ₂	HTI BISO	93
12	3/76	GO-1	11,325	(Th,U)O ₂	HTI BISO	93
14	11/76	GO-1	9,930	(Th,U)O ₂	HTI BISO	93
13-1	12/77	GFB-3	6,077	UC ₂ ThO ₂	LTI TRISO LTI BISO	90 -
13-3	12/77	GFB-5	5,354	UCO ThO ₂	LTI TRISO	92 -
13-2	7/80	GFB-4	5,861	UC ₂ ThO ₂	LTI TRISO LTI BISO	90 -
15	2/81	GO-2	6,087	(Th,U)O ₂	LTI TRISO	93
18	7/81	GO-3	11,547	(Th,U)O ₂	HTI BISO	93
19	7/82	GLE-3	24,615	UO ₂	LTI TRISO	10
21	2/84	GLE-4	20,250	UO ₂	LTI TRISO	17
20	10/85	GO-2	11,854	(Th,U)O ₂	LTI TRISO	93
22	9/86	THTR	15,228	(Th,U)O ₂	HTI BISO	93
21-2	10/87	GLE-4	8,740	UO ₂	LTI TRISO	17

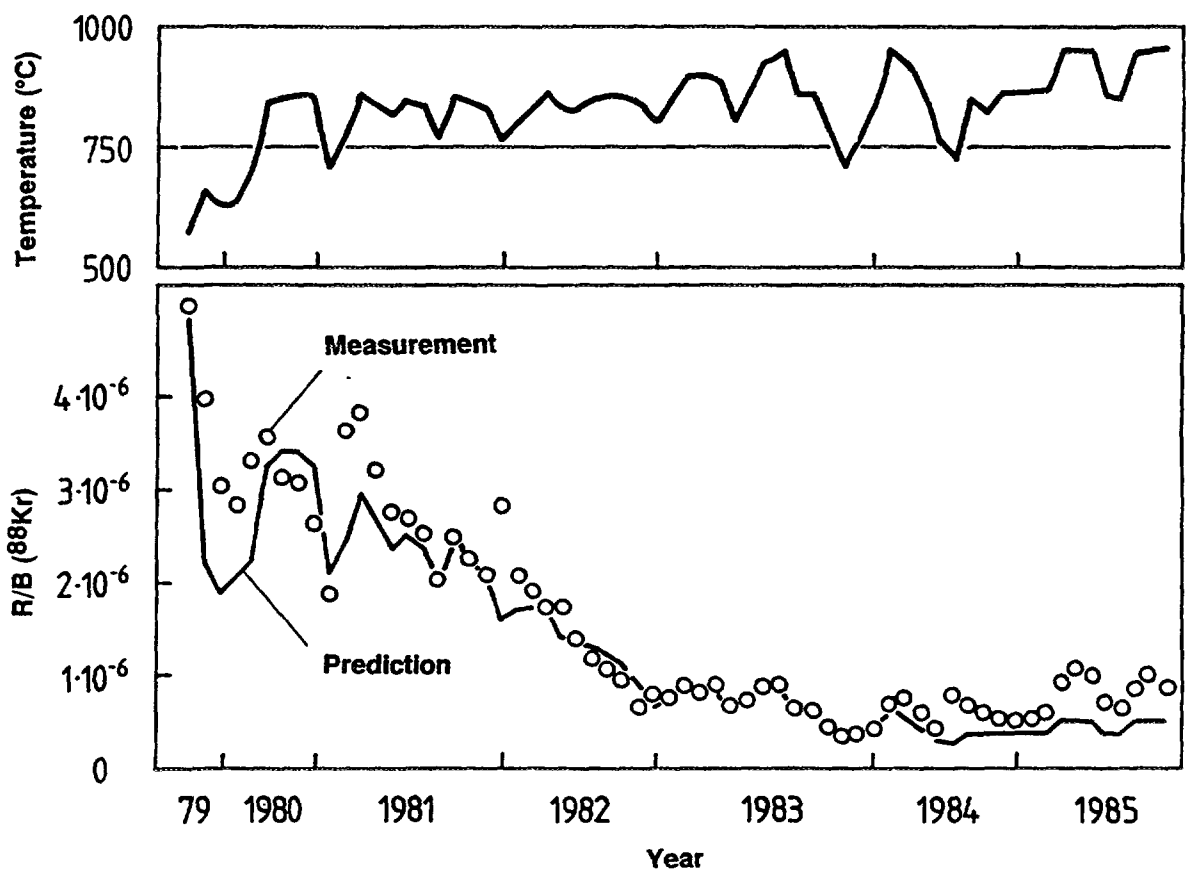


Fig. 3-24: AVR coolant outlet temperature and in-pile fission gas release 1979 - 1985, from [5]

be partly attributed to the water ingress accident in 1978. The relatively low fission gas values since 1983 are due to the increased fraction of clean LEU fuel (Fig. 3-24). Out-of-pile heating tests at 1050 and 1250 °C also indicated the quality of the fuel, in which the R/N (postirradiation heating release rate over fission product inventory) was found to be $< 1 \cdot 10^{-12} \text{ s}^{-1}$ corresponding to a contamination fraction of approx. $1 \cdot 10^{-5}$. A typical distribution of specific activities in the hot coolant as measured in the period 1984 to 1987 at full power and 950 °C gas outlet temperature is presented in Table 3-18.

The activities of solid fission products are several orders of magnitude lower compared to the gaseous species. The measured activity in the coolant mostly originated from the heavy metal contamination in the fuel matrix. Cesium profiles in fuel elements with normal particle performance show an increase of concentration near the surface due to adsorption of cesium from the gaseous phase in cooler parts of the core (cross-contamination). This cesium level in the fuel free zone is much higher compared to profiles in an MTR irradiated fuel element of the same type. It originates from the high levels of fission product metals in the primary circuit with old fuel releasing Cs, Ag, Sr from contamination and particle failure. However, the reduction in this adsorbed activity observed over the years reflects the gradual replacement of BISO by high quality TRISO fuel within the AVR core.

Table 3-18: Specific activities as measured in the primary coolant gas of the AVR, from [84]

Nuclide	Specific Activity [Bq/m ³]
Σ fission noble gases	4.6×10^8
H-3	3.7×10^7
C-14	1.9×10^7
Co-60	1.0×10^1
Sr-90	2.0×10^2
Ag-110m	4.9×10^1
I-131	5.2×10^2
Cs-137	3.0×10^2

A loss-of-coolant accident was simulated with the AVR reactor which was technically related to the concept of a modular HTGR. During the test, most of the heat generated in the core was passively transferred to the steam generator by radiation and convection. The experiment has demonstrated that decay heat can be removed from the core without forced cooling and without causing unacceptably high temperatures in the components (maximum temperature < 900 °C) [85].

In May 1978, a water ingress accident occurred in the AVR. Within 4 days, 25 m³ of water were flowing into the core through a small leak of a few mm² in the steam generator which is installed above the top reflector. During the drying phase, an oxidation was hindered by high hydrogen partial pressure. The permission for a restart was received in April 1980 [86].

In all, the AVR has proved to be a superb instrument in the German fuel element developing program. It enforced industry-scale production and manufacturing capabilities and it provided numerous enough fuel elements for a wide range of investigations.

3.5.5. THTR-300

The 756 MW(th) Thorium-High-Temperature Reactor, THTR-300, was the prototype power plant for a medium-sized pebble bed reactor. Its active core consisted of 600,000 spherical fuel elements each of which contained approx. 38,000 BISO coated fuel particles with a (Th,U)O₂ kernel. Between its first criticality in 1983 and its final shutdown in 1988, the plant has operated more than 16,000 hours amounting to 423 efpd and has generated 2,890 MWh. The operating history is characterized by frequent power changes and several downtimes [87].

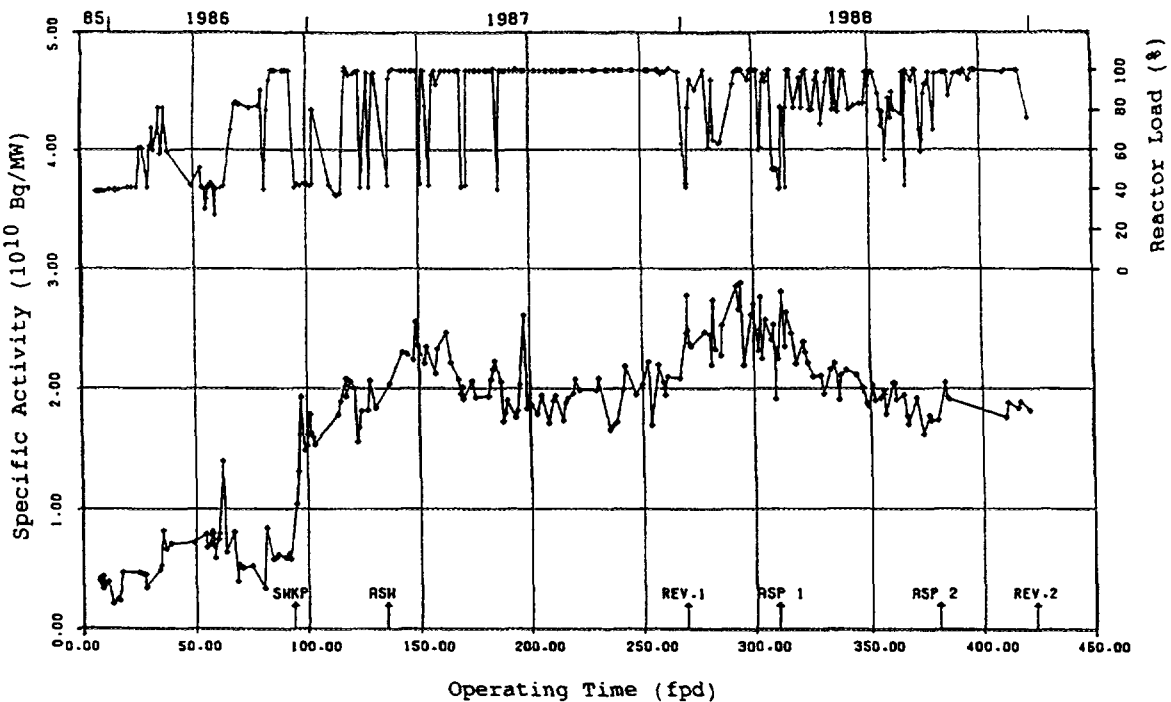


Fig. 3-25: THTR-300 coolant gas activity (sum of 9 noble gas nuclides) as function of effective full power days, from [88]

Fuel performance during operation was tested by quasi-continuous measurements of 4 krypton and 5 xenon isotopes at power levels between 10 and 100 % [88]. The sum of the activities represents about 90 % of the total coolant gas activity. As shown in Fig. 3-25, the activity increased by a factor of 3 in the period between 70 and 150 efpd, and then only small changes occurred. After 300 efpd, the activity decreased continuously. During the rise of the total gas activity, the spectrum of the different noble gases changed significantly: the short-lived nuclides increased to a greater extent than the long-lived isotopes.

Considering the R/B values as a function of the decay constant, it could be concluded that, in accordance with the design model, the dominant source of gaseous activity is the uranium contamination of the matrix graphite from the manufacturing process. Calculations indicated, however, that the observation of the activity increase could not be explained by higher temperatures and/or failed particles in the matrix graphite using the existing models for gas release from heavy metal contamination and from exposed kernels. An additional release source arose from the mechanical damage inflicted during the insertion of the control rods into the pebble bed (a phenomenon that occurs only in medium-sized pebble bed reactors) resulting in an enhanced recoil fraction of primary fission products in the coolant independent of their half-life. A positive correlation was observed between damaged fuel elements and the coolant gas activity. The results with a modified gas release model showed a good agreement with the measurements. An upper limit of the fraction of exposed particle kernels was estimated to be 8×10^{-5} in the core or 5×10^{-3} in the damaged fuel elements, respectively.

Non-radioactive impurities detected in the coolant gas, such as H₂O, CO₂, CO, H₂, CH₄, N₂, and in some rare cases also traces of O₂, have an oxidizing effect on graphite. Approx. 65 kg of carbon were oxidized. This is small compared to the total carbon inventory of 728 tons. The helium purification system was able to cope with all concentrations of impurities without a problem [87].

Inspite of the activity increase, the measured total coolant gas activity in the THTR-300 agreed with the licensed limits for the expected values within a bandwidth of $\pm 20\%$ (at operating times > 100 full power days). The measured activity did not exceed 4 % of the design limit of 3×10^{-4} for heavy metal contamination and 2×10^{-3} for in-service failure fraction thus confirming the experience with coolant gas activity in the AVR [88].

An unexpected event occurred in the fuel element feeding system on May 4, 1986, demonstrating the significance of safety-related man-machine interactions. As a result of operator's errors, 6 out of 41 spherical absorber elements, in the chamber ready to be fed into the core were destroyed and the atmosphere in the chamber ($< 0.5 \text{ Nm}^3$) including long-lived aerosols was inadvertently released through the stack into the environment. Outdoor measurements as well as postcalculations disclosed that the release limits allowed by the authorities were not exceeded and the additional ground contamination of estimated to be 0.1 Bq/m^2 was orders of magnitude lower than the impact given by the Chernobyl radioactive fallout at the same time [89].

3.6. SUMMARY OF CHAPTER 3

The main source of fission products under normal operating conditions is from uranium outside an intact SiC layer which appears as heavy metal contamination in the fuel element graphite or as defective/failed fuel particles. There are several mechanisms for a particle to fail. The important ones are kernel migration, interaction of fission products with the SiC, pressure vessel failure, all off them, however, conceivable only under extreme operating conditions causing large temperature gradients within the particle or for fuel particles outside the specification limits. Modeling of fission product release is primarily based on diffusive transport. The release of short-lived gaseous fission products from a particle kernel (or a graphite grain) can be analytically determined by applying the Booth formula describing the release rate over birth rate ratio R/B as function of diffusivity and decay constant.

The performance of German high-quality fuel production has been tested in irradiation experiments with a total of 19 spherical fuel elements and 276,680 TRISO particles. Gas release analysis has shown that in no single case was a failed particle generated during irradiation. The statistical derivation for the operation-related failed particle fraction in the HTR-MODUL core leads to 4×10^{-6} as expected value and 2×10^{-5} as design value. In Japan, experience with irradiation tests in the in-pile loop OGL-1 has shown that the probability of SiC coating failure increased for irradiation temperatures higher than 1450°C . Both before and after the modification of manufacturing conditions by constructing new facilities, the fuel produced met the criteria of HTTR design. US fuel performance was tested under accelerated irradiation conditions as well as in operating HTGRs involving a whole variety of fuel types. The oxicarbide fuel system was found to yield the desirable results of reduced kernel migration and reduced attack of rare earths on the SiC layer.

Peak fluence of the order 4×10^{25} n/m² are regarded as tolerable. The feasibility of the Russian experimental method of predicting fission product release from fuel elements by using the “weak” irradiation method for obtaining constants necessary for the prediction of fission product release during HTGR operation has been justified. It has been shown that the design fuel elements permit fission product retention at the basic modes of operation including accident conditions, in nominal modes with burnup up to $\approx 12\%$ FIMA.

Operating experience from HTGRs comprised all aspects ranging from fuel fabrication, irradiation testing, and performance modeling to in-reactor chemistry surveillance, fission product release and transport measurement and modeling and reactor component decontamination. The Dragon project from 1959 to 1976 deserves much of the credit for the design and qualification of TRISO coated fuel particles and the development and demonstration of practical fabrication processes for mass producing them. After seven years of operation of the US 40 MW(e) Peach Bottom HTGR, an extensive and highly successful End-of-Life R&D program was conducted with the primary goal to generate real-time integral data to validate design methods. The follow-up plant, the 350 MW(e) Fort St. Vrain, provided invaluable data on fuel performance, fission product release and plateau data that have been used for comparison with the predictive calculations with GA reference computer codes. Measurements of fission gas release as well as of plateau probes were found to be in reasonable agreement with model predictions. The German 15 MW(e) AVR reactor was used as a test bed for a large variety of coated particle designs. The reduction of adsorbed cesium on the fuel element surfaces observed over the last years reflects the gradual replacement of BISO by high quality TRISO fuel within the AVR core. HRB models were applied during the licensing procedure for the 300 MW(e) THTR-300. Measurements of noble gas activities were found to be due to the uranium contamination of the matrix graphite from the manufacturing process in accordance with the design calculations.

REFERENCES OF CHAPTER 3

- [1] BELL, M.J., ORIGEN - The ORNL Isotope Generation and Depletion Code, Report ORNL-4628, Oak Ridge National Laboratory (1973).
- [2] EICHENBERG, T.W., RADC Users Manual, Report CEGA-002814, CEGA Corporation (1993).
- [3] SIEMENS/INTERATOM, Aktivitätsfreisetzung und Strahlenexposition bei der HTR-Modul-Kraftwerksanlage, Teil 2: Störfälle, Technical Note No. 76.00561.4, Siemens/Interatom (1987).
- [4] VERFONDERN, K., MÜLLER, D., Zur Spaltproduktfreisetzung aus dem HTR-Modul (Aktualisierung der Trendanalyse), Technical Note KFA-ISF-AN-3/90-II, Research Center Jülich (1990).
- [5] GONTARD, R., NABIELEK, H., Performance Evaluation of Modern HTR TRISO Fuels, Internal Report KFA-HTA-IB-05/90, Research Center Jülich (1990).
- [6] SAITO, S., et al., Safety Requirements and Research and Development on HTTR Fuel in Japan, Behaviour of GCR Fuel under Accident Conditions (Proc. IAEA Specialists' Meeting, Oak Ridge, 1990), IAEA, IWGGCR/25, Vienna (1991) 31-36.
- [7] HOMAN, F.J., et al., Stoichiometric Effects on Performance of High-Temperature Gas-Cooled Reactor Fuels from the UCO System, Nucl. Techn. 35 (1977) 428-441.

- [8] BALANKIN, S.A., RYBAKOVA, E.A., Mathematical Model of the Behavior of Oxide Microfuel-Elements, Atomnaya Énergiya **58** (1985) 101-104.
- [9] CHERNIKOV, A.S., et al., HTGR Coated Particles, Coating Material Properties and Prereactor Test Results, Fuel Elements and Fuel Composition of HTGR (Proc. JAIF-GKAE Seminar, Tokyo, 1987), JAIF (1987) 3-1 - 3-20.
- [10] MINATO, K., et al., Fission Product Palladium - Silicon Carbide Interaction in HTGR Fuel Particles, J. Nucl. Mater. **172** (1990) 184-196.
- [11] STANSFIELD, O.M., SIMON, W.A., BAXTER, A.M., Fuel Performance Models for High-Temperature Gas-Cooled Reactor Core Design, Report GA-A16982, GA Technologies (1983).
- [12] BONGARTZ, K., NABIELEK, H., A Universal Model for Coated Particle Failure, Structural Mechanics in Reactor Technology (SMIRT) (6th Int. Conf., Paris, 1981), Paper C4/2.
- [13] KFA/HBK, Projektbericht 1982, Internal Report KFA-HBK-IB-1/83, Research Center Jülich (1983).
- [14] HUDRITSCH, W.W., JOVANOVIC, V., GEORGHIOU, D.L., SURVEY, a Computer Code for the Thermal and Fuel Performance Analysis of High-Temperature Gas-Cooled Reactors, User's Manual, Report GA-C17554, GA Technologies (1984).
- [15] PETESSONE, D., PISA: A Coupled, Thermal-Stress Code for Mechanical Analysis of Irradiated Fuel Particles, Report CEGA-002550, Rev. 0, CEGA Corporation (1992).
- [16] VERFONDERN, K., DUNN, T.D. BOLIN, J.M., Comparison of US/FRG Accident Condition Models for HTGR Fuel Failure and Radionuclide Release, Report Jül-2458, Research Center Jülich (1991).
- [17] SAWA, K., SHIOZAWA, S., MINATO, K., FUKUDA, K., Development of a Coated Fuel Particle Failure Model under High Burnup Irradiation, J. Nucl. Sci. Technol. **33** (1996) 712-720.
- [18] BONGARTZ, K., Status of the Fuel Stress and Failure Rate Calculations at KFA, Report Jül-1686, Research Center Jülich (1980).
- [19] NABIELEK, H., MYERS, B.F., Fission Product Retention in HTR Fuel, Gas-Cooled Reactors Today (Proc. BNES Conference, Bristol, 1982), British Nuclear Energy Society, London (1982) 145-152.
- [20] BOOTH, A.H., A Method of Calculating Fission Gas Diffusion from UO₂ Fuel and its Application to the X-2-F Loop Test, Report CRDC-721, Atomic Energy of Canada Limited (1957).
- [21] THIEL, J., Gasfreisetzung aus Defektpartikeln im Experiment FRJ2-P25, Report 232-520-DB1583, HRB Mannheim (1982).
- [22] MYERS, B.F., The Fuel Design Data Manual, Report GA-901866/F, GA Technologies (1987).
- [23] TURNBULL, J.A., et al., The Diffusion Coefficients of Gaseous and Volatile Species During the Irradiation of Uranium Dioxide, J. Nucl. Mat. **107** (1982) 168-184.
- [24] WILLIAMSON, R., AEA Technology, UK, Facsimile message on enhanced vacancy diffusion to B. F. Myers, ORNL, June 6, 1996.
- [25] MYERS, B.F., Fission Gas Release in High Temperature Gas-Cooled Reactors, Archival Viewgraphs, Oak Ridge National Laboratory (1991).
- [26] MYERS, B.F., MORRISSEY, R.E., Licensing Topical Report: The Measurement and Modelling of Time-Dependent Fission Product Release from Failed HTGR Fuel

- Particles under Accident Conditions, Report GA-A15439, General Atomic Company (1978).
- [27] OLANDER, D.R., Fundamental Aspects of Nuclear Reactor Fuel Elements, Report TID-26711-P1, Technical Information Center, Office of Public Affairs, Energy Research and Development Administration (1976).
 - [28] OGAWA, T., et al., Release of Short-Lived Noble Gases from HTGR Fuel with Failed Coated Fuel Particles and Contaminated Matrix, Nucl. Eng. Des. **132** (1991) 31-37.
 - [29] HURST, D.G., Diffusion of Fission Gas, Calculated Diffusion from a Sphere Taking into Account Trapping and Return from Traps, Report AECL-1550, Atomic Energy of Canada Limited (1962).
 - [30] SAWA, K., et al., Development of an Evaluation Method of Fission Product Release Fraction from High Temperature Gas-Cooled Reactor Fuel, Report JAERI-Research 96-063, Japan Atomic Energy Research Institute (1996) (in Japanese).
 - [31] MÜLLER, A., STADIF-II, ein Programm zur Berechnung der stationären Kühlgasaktivität in Kugelhaufen-HTR, Report JüL-1464, Research Center Jülich (1977).
 - [32] MOMOT, G.W., KHRULJEV, A.A., Limits of Safe Operation in Terms of Fission Product Release from the Fuel Element and its Justification, Fuel and Graphite for HTR (Proc. 1st Soviet/German Seminar, Moscow, 1990), Internal Report KFA-HTA-IB-6/90, Research Center Jülich (1990) 319-335.
 - [33] KHROULEV, A.A., et al., State of Works on Fuel Elements and Fission Products Transport for HTGR Radiation Safety Provision, Unification of Coated Particle Performance Models and Fission Product Transport Data for the HTR (IAEA Technical Workshop, Jülich, 1991).
 - [34] BURNETTE, R.D., Analysis of the First Plateout Probe from the Fort St. Vrain HTGR, Trans. Am. Nucl. Soc. **46** (1984) 379-380.
 - [35] WAWRZIK, U., IVENS, G., Operational Monitoring of the Release Behavior of the AVR Core, Fission Product Release and Transport in Gas-cooled Reactors (Proc. IAEA Spec. Meeting, Berkeley, 1985), IAEA IWGGCR/13, Vienna (1986) 15-26.
 - [36] KROHN, H., FINKEN, R., FRESCO-II: Ein Rechenprogramm zur Berechnung der Spaltproduktfreisetzung aus kugelförmigen HTR-Brennelementen in Bestrahlungs- und Ausheizexperimenten, Report JüL-Spez-212, Research Center Jülich (1983).
 - [37] VERFONDERN, K., MOORMANN, R., Fission Product Release from the Core under Normal Operating Conditions, in: WOLTERS, J. (Ed.), Probabilistic Safety Analysis and Assessment on Possible Urban Siting of the Modular HTR for Process Heat Application, Internal Report KFA-ISR-IB-3/90, Research Center Jülich (1990).
 - [38] SAWA, K., et al., Validation of Fission Product Release from Fuel Element of HTTR, J. Nucl. Sci. Tech. **29** (1992) 842-850.
 - [39] TOBITA, T., et al., Metallic Fission Product Release from Failed Coated Fuel Particles (ICF-51H Capsule Irradiation Test), Report JAERI 96-014, Japan Atomic energy Research Institute (1996) (in Japanese).
 - [40] SAWA, K., et al., An Investigation of Cesium Release from Coated Particle Fuel of the High Temperature Gas-cooled Reactor, Nucl. Tech. **116** (1997) 00-00.
 - [41] BERGER-ROSSA, R., Rückhaltung und Umverteilung von Spaltprodukten im Core und im Primärkreislauf von Hochtemperaturreaktoren bei hypothetischen Störfallereignissen, Report JüL-2188, Research Center Jülich (1988).

- [42] MATTKE, U.H., Berechnung der Spaltproduktverteilung in Core und Primärkreislauf eines Hochtemperaturreaktors im Normalbetrieb, Report Jül-2515, Research Center Jülich (1991).
- [43] HUDRITSCH, W.W., COPAR2, A Program to Compute the Release of Fission Products from Coated Particles, GA Document No. 908696, GA Technologies Inc. (1986).
- [44] SMITH, P.D., TRAFIC, A Computer Program for Calculating the Release of Metallic Fission Products from an HTGR Core, Report GA-A14721, General Atomic Company (1978).
- [45] HUDRITSCH, W.W., Fission Product Transport Code TRAMP, Report GA-D15190, General Atomic Company (1981).
- [46] MYERS, B.F., Selective Aspects of Transport in SiC, MHTGR/HTR Fuel Performance under Accident Conditions (Proc. US/FRG Experts' Meeting, Oak Ridge, 1989), Internal Report KFA-HTA-IB-2/90, Research Center Jülich (1990) 199-222.
- [47] KÜHNLEIN, W., Fission Product Release under Normal Operating Conditions, Unification of Coated Particle Performance Models and Fission Product Transport Data for the HTR (IAEA Technical Workshop, Jülich, 1991).
- [48] MOORMANN, R., VERFONDERN, K., Methodik umfassender probabilistischer Sicherheitsanalysen für zukünftige HTR-Anlagenkonzepte - Ein Statusbericht (Stand 1986), Band 3: Spaltproduktfreisetzung, Report Jül-Spez-388/Vol. 3, Research Center Jülich (1987).
- [49] FUKUDA, K., HAYASHI, K., SHIBA, K., Fuel Behavior and Fission Product Release under HTGR Accident Conditions, in: ROGERS, J.T. (Ed.), Fission Product Transport Processes in Reactor Accidents, Hemisphere Publishing Corporation/USA (1990) 197-204.
- [50] DEGALTSEV, I.G., et al., Postirradiation Examination of Particles and Fuel Elements, Fuel and Graphite for HTR (Proc. 1st Soviet/German Seminar, Moscow, 1990), Internal Report KFA-HTA-IB-6/90, Research Center Jülich (1990) 193-221.
- [51] VERFONDERN, K., NABIELEK, H., SCHENK, W., Partikelbruch und Spaltproduktfreisetzung in Brennelementen mit $(\text{Th},\text{U})\text{O}_2$ HTI BISO Partikeln bei Betriebs- und Störfallbedingungen, Internal Report KFA-ISF-IB-4/88, Research Center Jülich (1988).
- [52] KASTEN, P.R., et al., Fuel Performance in Modular High Temperature Gas-Cooled Reactors, Internal Report KFA-ISR-IB-12/94, Research Center Jülich (1994).
- [53] HAYASHI, K., et al., Irradiation Experiments of the 6th - 12th OGL-1 Fuel Assemblies, Report JAERI-Research 94-017, Japan Atomic Energy Research Institute (1994).
- [54] DERYUGIN, A.I., et al., Behaviour of HTGR Coated Particles and Fuel Elements under Normal and Accident Conditions, (Proc. IAEA Specialists' Meeting, Oak Ridge, 1990), IAEA, IWGGCR/25, Vienna (1991) 71-77.
- [55] ZAKRZHEVSKAYA, I.V., et al., Radiation Investigations of HTGR Coated Particles at High Temperatures (up to 3000 °C), Presented at the 1st Research Coordination Meeting on Validation of Predictive method for Fuel and Fission Product Behaviour in Gas-Cooled Reactors, Vienna, Austria (1993).
- [56] HARMON, D.P., SCOTT, C.B., Properties Influencing High-Temperature Gas-Cooled Reactor Coated Fuel Particle Performance, Nucl. Techn. 35 (1977) 343-352.

- [57] GOODIN, D.T., MHTGR Fuel Performance and Supporting Data Base, Report GA-A19877, General Atomics (1989).
- [58] STANSFIELD, O.M., Evolution of HTGR Coated Particle Fuel Design, Energy 16 No. 1/2 (1991) 33-45.
- [59] SAURWEIN, J., et al., Final Report on the Peach Bottom Test Element Program, Report GA-A15999, GA Technologies Inc. (1982).
- [60] BAXTER, A.M., et al., FSV Experience in Support of the GT-MHR Reactor Physics, Fuel Performance and Graphite, Report GA-A21925, General Atomics (1994).
- [61] GA TECHNOLOGIES, Post Irradiation Examination and Evaluation of FSV Fuel Element 1-2415, Report GA-907079, GA Technologies Inc. (1983).
- [62] GA TECHNOLOGIES, Metallographic Examination of Fuel Rods from Segment 2 FSV, Fuel Element 1-2415, Report GA-909968, GA Technologies Inc. (1983).
- [63] MCCORD, F., FTE 2 Post Irradiation Examination, Report GA-908909, GA Technologies Inc. (1986).
- [64] SAURWEIN, J., MILLER, C., YOUNG, C., Post Irradiation Examination of Fuel Element 1-0743, Report GA-A16258, General Atomic Company (1981).
- [65] MCCARDELL, P.K., et al., NP-MHTGR Fuel Development Program Plan, Report EGG-NPR-8971, Rev. C, EG&G, Idaho (1982).
- [66] YOUNG, C., Pre- and Postirradiation Evaluation of Fuel in Capsule HRB-14, Report GA-A15969, General Atomic Company (1980).
- [67] KETTERER, J.W., et al., Capsule HRB-15A Postirradiation Examination Report, Report GA-A16758, GA Technologies Inc. (1984).
- [68] KETTERER, J.W., BULLOCK, R.E., Capsule HRB-15B Postirradiation Examination Report, Report GA-A15940, General Atomic Company (1981).
- [69] KETTERER, J.W., MYERS, B.F., Capsule HRB-16 Postirradiation Examination Report, Report HTGR-85-053, GA Technologies Inc. (1985).
- [70] KETTERER, J.W., MYERS, B.F., Capsules HRB-17/18 Final PIE Report, Report HTGR-86-083, GA Technologies Inc. (1987).
- [71] MYERS, B.F., et al., Capsule R2-K13 Final Report on Cells 2 and 3, Report HTGR-85-068, GA Technologies Inc. (1985).
- [72] BURNETTE, R.D., et al., The Operation of Experiment HFR-B1 in the Petten High Flux Reactor, Report ORNL/TM-12740, Oak Ridge National Laboratory (1994).
- [73] GONTARD, R., HTR-Bestrahlungsexperimente zur Erprobung von Brennelementen mit UO₂ TRISO Partikeln, Internal Report KFA-HBK-IB-5/87, Research Center Jülich (1987).
- [74] TURNER, R.F., et al., Selection of LEU/Th Reference Fuel for the HTGR-SC/C Lead Plant, Report GA-A17123, GA Technologies Inc. (1983).
- [75] MONTGOMERY, F.C., Kinetics of Fission Product - SiC Reactions, Fission Product - SiC Reactions (Workshop, Oak Ridge, 1980).
- [76] HOWARD, R.M., PRICE, M.S.T., SHEPHERD, L.R. (ED.), A Summary and Evaluation of the Achievements of the Dragon Project and its Contribution to the Development of the High Temperature Reactor, Dragon Report DP-1000, O.E.C.D. High Temperature Reactor Project (1978).
- [77] VOICE, E.H., LAMB, D.N., The Deposition and Structure of Pyrolytic Silicon Carbide, Dragon Report DP-667, O.E.C.D. High Temperature Reactor Project (1969).
- [78] STEWARD, K.P., Final Summary Report on the Peach Bottom End-of-Life Program, Report GA-A14404, General Atomic Company (1978).

- [79] HUDRITSCH, W.W., PADLOC, A One-Dimensional Computer Code for Coolant and Plateout Fission Product Concentration, Report GA-A14401, General Atomic Company (1981).
- [80] JOVANOVIC, V., WOOD, D., HOOKS, F., MATTIS, E., FSV Plateout Probe Analysis for Decommissioning Study, Report GA-909658, Rev. B, General Atomics (1992).
- [81] IVENS, G., WIMMERS, M., The AVR as Test Bed for Fuel Elements, in: ASSOCIATION OF GERMAN ENGINEERS (VDI) (Ed.), AVR – Experimental High-Temperature Reactor, 21 Years of Successful Operation for a Future Energy Technology, VDI-Verlag Düsseldorf (1990) 170-185.
- [82] WAWRZIK, U., IVENS, G., Operational Monitoring of the Release Behavior of the AVR Core, Fission Product Release and Transport in Gas-cooled Reactors (Proc. IAEA Spec. Meeting, Berkeley, 1985), IAEA IWGGCR/13, Vienna (1986) 15-26.
- [83] ENGELHARD, J., KRÜGER, K., GOTTAUT, H., Investigation of the Impurities and Fission Products in the AVR Coolant Gas at an Average Hot-Gas Temperature of 950 °C, Nucl. Eng. Des. 34 (1975) 85-92.
- [84] GOTTAUT, H., KRÜGER, K., Results of Experiments at the AVR Reactor, Nucl. Eng. Des. 121 (1990) 143-153.
- [85] KRÜGER, K., et al., Simulation of the Loss-of-Coolant Accident with the AVR Reactor, in: ASSOCIATION OF GERMAN ENGINEERS (VDI) (Ed.), AVR – Experimental High-Temperature Reactor, 21 Years of Successful Operation for a Future Energy Technology, VDI-Verlag Düsseldorf (1990) 245-258.
- [86] KRÖGER, W., Benefit of Safety Assessments, in: ASSOCIATION OF GERMAN ENGINEERS (VDI) (Ed.), AVR – Experimental High-Temperature Reactor, 21 Years of Successful Operation for a Future Energy Technology, VDI-Verlag Düsseldorf (1990) 276-292.
- [87] BÄUMER, R., KALINOWSKI, I., THTR Commissioning and Operating Experience, Energy 16 (1991) 59-70.
- [88] RÖLLIG, K., The THTR Coolant Gas Activity, an Indicator of Fuel Performance, Behaviour of GCR Fuel under Accident Conditions, (Proc. IAEA Specialists' Meeting, Oak Ridge, 1990), IAEA, IWGGCR/25, Vienna (1991) 99-108.
- [89] SCHULTEN, R., WOLTERS, J., Der Zwischenfall am THTR-300, Physik in unserer Zeit, 17 (1986) 156-158.

**NEXT PAGE(S)
left BLANK**

4. FUEL PERFORMANCE AND FISSION PRODUCT BEHAVIOR UNDER HEATUP, NON-OXIDIZING CONDITIONS

4.1. POSTIRRADIATION HEATING EXPERIMENTS

4.1.1. Postirradiation Heating Tests in Germany

Accident simulation tests have been performed since the mid-seventies in Germany, in which KFA Jülich has concentrated on heating complete spherical fuel elements [1, 2, 3]. An early experimental program consisted of heatup ramp tests with $(\text{Th},\text{U})\text{O}_2$ BISO fuel up to 2500 °C [4, 5]. This program was followed by work with fuel elements containing $(\text{Th},\text{U})\text{O}_2$ TRISO and UO_2 TRISO particles [6, 7].

4.1.1.1. Equipment

The equipment for simulation tests (KÜFA) consists of a heating furnace located in a gastight box in the hot cell. The furnace is connected to a helium loop working at a slight overpressure with blowers and filters outside the shielded area (HTGRs have a helium pressure between 1 and 7 MPa during normal operations; the atmospheric pressure in the heating tests is representative of the loss-of-coolant accident). Outside the hot cell box are noble gas traps which contain charcoal cooled by liquid nitrogen. In these, the activity of Kr-85 and Xe-133 is monitored with NaI detectors which generate the release curves during the heating test. To enable measurements of metallic fission products, a water-cooled finger intrudes into the heating furnace which can be removed to exchange the condensation plate without interruption of the heating test. The activity of the plate is measured in a different laboratory with low level background. In the case of larger releases (> 1 % of the sphere inventory), the Cs-137 and Cs-134 loss can also be determined by comparing γ -spectrometric measurements of the sphere before and after the heating test.

4.1.1.2. Data of Fuel Samples

The modern fuel element in the German HTGR concept is the basis of the safety philosophy aimed at retaining fission products at the site of their origin, both during normal operations, during accidents, and during long-term storage. Within the 60 mm diameter spherical fuel element as used in the accident simulation tests, the fuel is discretely dispersed in $\approx 16,000$ coated particles. Their TRISO particles have a 500 μm diameter UO_2 kernel with 10 % U-235 enrichment and a 200 μm thick coating, consisting of a porous buffer layer and two dense layers of pyrocarbon with a silicon carbide layer in between [6]. While all these layers have important mechanical and chemical functions, it is the SiC which guarantees the highest degree of fission product retention [8, 9].

The content of free uranium in fuel elements with TRISO particles is determined by the burn-leach method. This quality control procedure includes all uranium sources not contained by intact silicon carbide coatings. Based on this observation and other experimental evidence, the conclusion can be drawn that virtually all measured free uranium

can be attributed to defective particles. Only a negligible portion of free uranium is due to the natural trace contamination of graphite.

Moreover, accident simulation tests were done with specially designed fuel bodies irradiated to extremely high burnup.

Cylindrical compacts were manufactured from spherical fuel elements with a fuel zone of only 20 mm diameter to be inserted into three HFR-P4 experiments and one Siloe experiment in Grenoble. Only the irradiation experiment HFR-P4/2 used particles with a 51 μm thick silicon carbide layer [10].

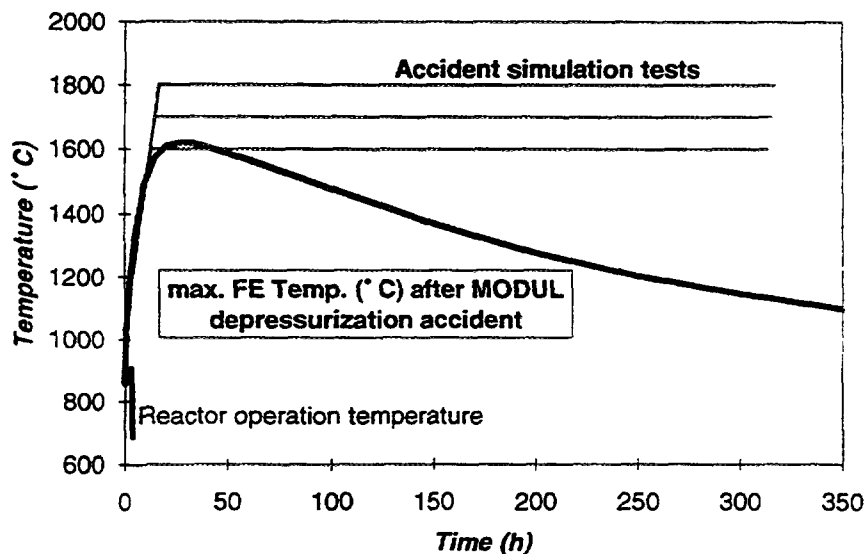


Fig. 4-1: Temperature evolution during a loss-of-coolant accident of a small HTGR and in the heating tests

The measured values for the total free uranium fraction cover a range between 8 and 51×10^{-6} . Conservatively, the defect fraction 30×10^{-6} had been chosen as an expected value for future fuel element production. The more important design value, which radiological calculations of design basis accident are based upon, has been fixed at 60×10^{-6} . The small difference between these two values demonstrates the high confidence that the specification can be met.

4.1.1.3. Experimental Results

4.1.1.3.1. Results Obtained at 1600 - 1800 °C

In the initial generic investigation program, eighteen spherical fuel elements (Table 4-1) and eight fuel compacts (Table 4-2) containing modern TRISO coated fuel have been heated.

The objective of the accident simulation tests is to obtain fission product release data during heating tests both at constant temperature and calculated temperature curves

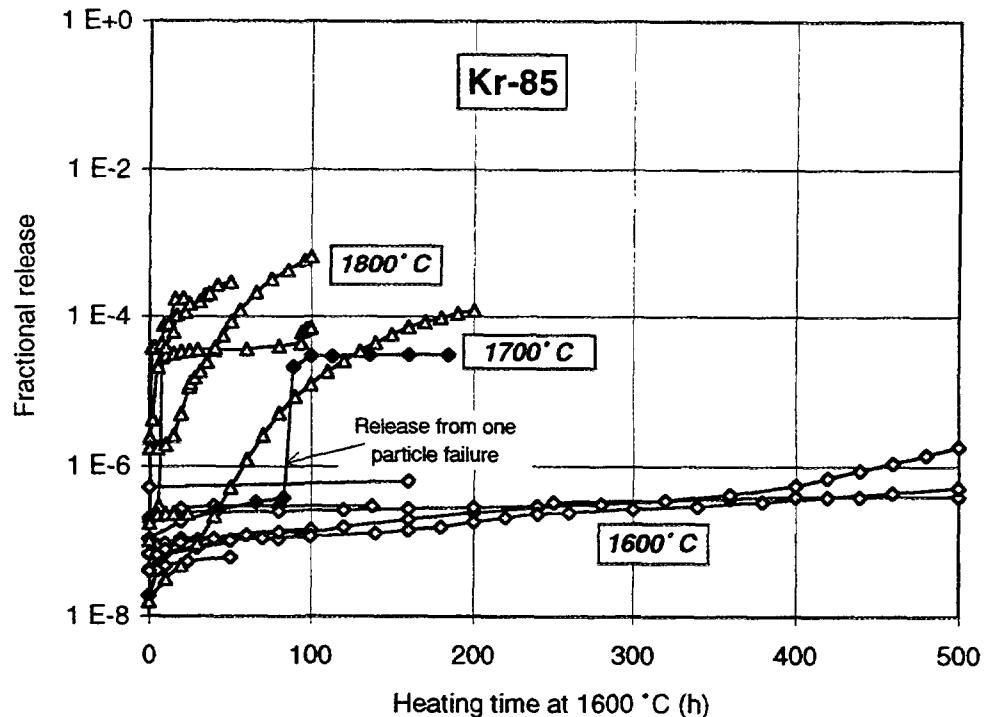


Fig. 4-2: Kr-85 release in isothermal heating tests (KUFA) at 1600 - 1800 °C from fuel elements with UO₂ TRISO particles

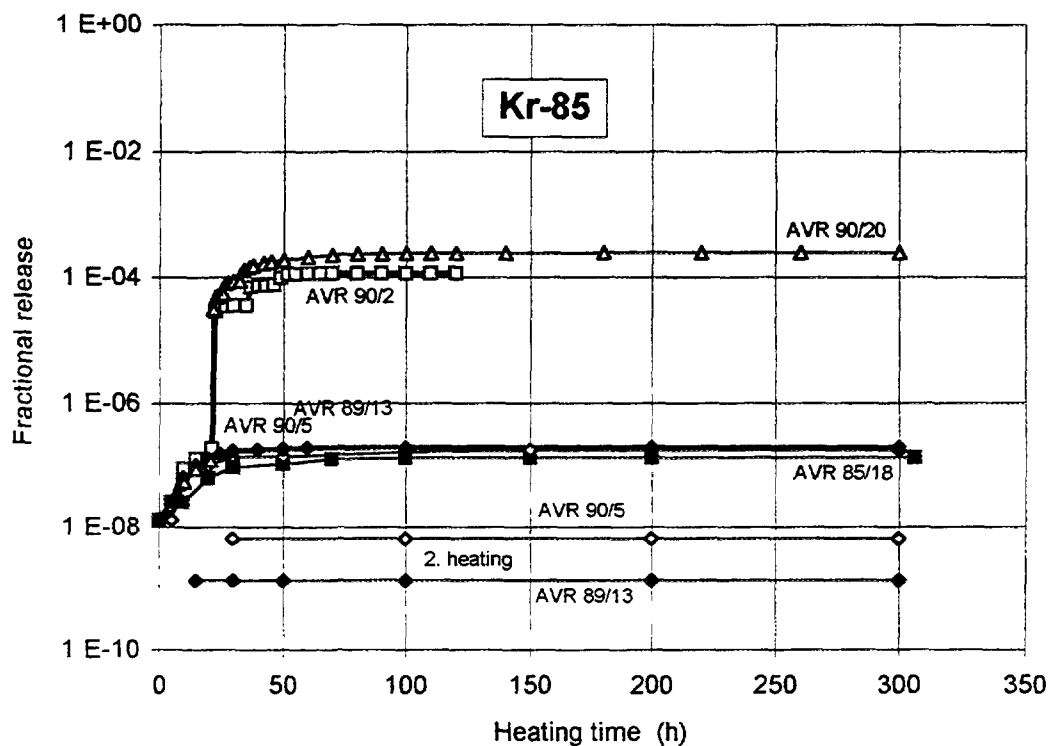


Fig. 4-3: Measured fission product release during simulated HTR-MODUL depressurization accident with loss-of-coolant

Table 4-1: Results of accident simulation tests with irradiated fuel elements

Fuel element UO ₂ TRISO	Burnup [%FIMA]	Fast fluence [10 ²⁵ m ⁻² , E>16 fJ]	Heating test		No. of failed particles ⁽²⁾		Fractional release				
			Temp. [°C]	Time [h]	Manufact.	Heating	Kr-85	Sr-90	Ag- 110m	Cs-134	Cs-137
AVR 71/22	3.5	0.9	1600	500	-	-	4.0*10 ⁻⁷	5.3*10 ⁻⁶	9.0*10 ⁻⁴	6.9*10 ⁻⁵	2.0*10 ⁻⁵
HFR-K3/1	7.7	3.9	1600	500	-	-	1.8*10 ⁻⁶	1.8*10 ⁻⁷	2.7*10 ⁻²	1.3*10 ⁻⁴	1.1*10 ⁻⁴
FRJ2-K13/2	8.0	0.1	1600	138 (160)	-	-	6.4*10 ⁻⁷	3.3*10 ⁻⁷	2.8*10 ⁻³	1.0*10 ⁻⁴	3.9*10 ⁻⁵
AVR 82/20	8.6	2.4	1600	100	-	-	1.5*10 ⁻⁷	3.8*10 ⁻⁶	4.4*10 ⁻³	1.2*10 ⁻⁴	6.2*10 ⁻⁵
AVR 82/9	8.9	2.5	1600	500	-	-	5.3*10 ⁻⁷	8.3*10 ⁻⁵	1.9*10 ⁻²	5.9*10 ⁻⁴	7.6*10 ⁻⁴
AVR 89/13	9.1	2.6	1620 ⁽¹⁾	≈ 10	-	-	2.0*10 ⁻⁷	(3)	8.3*10 ⁻⁴	1.3*10 ⁻⁵	1.1*10 ⁻⁵
			1620 ⁽¹⁾	≈ 10	-	-	1.3E-09	(3)	1.5*10 ⁻²	1.6*10 ⁻⁶	1.4*10 ⁻⁶
AVR 85/18	9.2	2.6	1620 ⁽¹⁾	≈ 10	-	-	1.4*10 ⁻⁷	(3)	6.5*10 ⁻³	1.0*10 ⁻⁵	1.3*10 ⁻⁵
AVR 90/5	9.2	2.7	1620 ⁽¹⁾	≈ 10	-	-	1.9*10 ⁻⁷	(3)	1.1*10 ⁻³	7.7*10 ⁻⁶	9.0*10 ⁻⁶
			1620 ⁽¹⁾	≈ 10	-	-	6.6*10 ⁻⁹	(3)	9.0*10 ⁻⁴	3.5*10 ⁻⁶	3.3*10 ⁻⁶
AVR 90/2	9.3	2.7	1620 ⁽¹⁾	≈ 10	1	2	1.0*10 ⁻⁴	(3)	3.7*10 ⁻²	5.0*10 ⁻⁵	4.6*10 ⁻⁵
AVR 90/20	9.8	2.9	1620 ⁽¹⁾	≈ 10	2	3	2.4*10 ⁻⁴	(3)	7.6*10 ⁻²	5.6*10 ⁻⁶	6.5*10 ⁻⁶

Table 4-1: Results of accident simulation tests with irradiated fuel elements (continued)

Fuel element UO ₂ TRISO	Burnup [%FIMA]	Fast fluence [10 ²⁵ m ⁻² , E>16 fJ]	Heating test		No. of failed particles ⁽²⁾		Fractional release				
			Temp. [°C]	Time [h]	Manufact.	Heating	Kr-85	Sr-90	Ag- 110m	Cs-134	Cs-137
AVR 91/31	9.0	2.6	1700 ⁽¹⁾	≈ 10	2	18	1.2*10 ⁻³	(3)	6.2*10 ⁻¹	3.7*10 ⁻³	2.4*10 ⁻³
AVR 74/11	6.2	1.6	1700	185	1	-	3.0*10 ⁻⁵	7.2*10 ⁻⁶	4.8*10 ⁻²	8.4*10 ⁻⁵	7.6*10 ⁻⁵
FRJ2-K13/4	7.6	0.1	1600	138	-	-	3.0*10 ⁻⁷	2.0*10 ⁻⁸	4.5*10 ⁻⁴	5.7*10 ⁻⁶	2.5*10 ⁻⁶
			1800	100		2	7.2*10 ⁻⁵	1.4*10 ⁻³	5.3*10 ⁻¹	9.7*10 ⁻³	9.9*10 ⁻³
AVR 88/33	8.5	2.3	1600	50	-	-	1.0*10 ⁻⁷	8.4*10 ⁻⁶	1.2*10 ⁻³	1.1*10 ⁻⁴	1.2*10 ⁻⁴
			1800	20		≈ 4	1.8*10 ⁻⁴	2.3*10 ⁻⁴	2.1*10 ⁻¹	4.4*10 ⁻⁴	4.6*10 ⁻⁴
AVR 88/15	8.7	2.4	1600	50		-	6.3*10 ⁻⁸	(3)	9.1*10 ⁻³	8.8*10 ⁻⁶	1.2*10 ⁻⁵
			1800	50		≈ 6	2.9*10 ⁻⁴	1.1*10 ⁻²	8.1*10 ⁻¹	1.3*10 ⁻²	1.4*10 ⁻²
AVR 76/18	7.1	1.9	1800	200	-	≈ 3	1.2*10 ⁻⁴	6.6*10 ⁻²	6.2*10 ⁻¹	5.3*10 ⁻²	4.5*10 ⁻²
AVR 88/41	7.6	2.0	1800	24	-	-	2.4*10 ⁻⁷	1.2*10 ⁻⁴	7.7*10 ⁻²	1.4*10 ⁻⁴	1.5*10 ⁻⁴
HFR-K3/3	10.2	6.0	1800	100	-	≈ 12	6.5*10 ⁻⁴	1.5*10 ⁻³	6.7*10 ⁻¹	6.4*10 ⁻²	5.9*10 ⁻²

(1) Simulating calculated core heatup curve

(2) Out of 16,400 particles

(3) Not measured

Table 4-2: Results of Accident Simulation Tests with Fuel Compacts

Fuel compact	Burnup [%FIMA]	Irradiation temperature [°C]	Heating temperature [°C]	Fractional release			
				Kr-85	Sr-90	Cs-134	Cs-137
SL-P1, 6	10.7	790	1600	7.3×10^{-7}	4.3×10^{-5}	7.5×10^{-4}	3.9×10^{-4}
HFR-P4, 1.12	11.1	900	1600	5.4×10^{-7}	6.0×10^{-6}	3.0×10^{-4}	2.6×10^{-4}
HFR-P4, 1.8	13.8	900	1600	5.4×10^{-5}	1.5×10^{-4}	1.5×10^{-3}	2.0×10^{-3}
HFR-P4, 2.8	13.8	900	1600	8.1×10^{-5}	1.1×10^{-4}	1.5×10^{-3}	1.4×10^{-3}
HFR-P4, 3.7	13.9	1050	1600	9.9×10^{-4}	2.4×10^{-4}	3.5×10^{-3}	3.9×10^{-3}
SL-P1, 10	10.3	790	1700	9.1×10^{-5}	2.1×10^{-2}	9.3×10^{-2}	1.0×10^{-1}
SL-P1, 9	10.7	790	1700	3.7×10^{-5}	5.8×10^{-2}	1.3×10^{-1}	9.8×10^{-2}
HFR-P4, 3.12	9.9	1050	1800	1.0×10^{-3}	(1)	5.2×10^{-1}	5.2×10^{-1}

(1) Not measured

(Fig. 4-1). All gas release data from spheres during heating tests at constant temperatures are shown in Fig. 4-2. The measured isotope Kr-85 has been previously shown to give the same release as Xe-133 and I-131 [11]. As expected, release increases with heating temperature and duration. In the isothermal tests, all 1600 °C release results remain below the level of one particle failure (6×10^{-5} fraction for 16,400 particles) as long as the burnup is below 10 %FIMA.

In addition to the isothermal tests, heating tests with five spherical fuel elements have been performed to follow the temperatures predicted for the transition from normal operations into an accident with unrestricted core heatup in the HTR-MODUL reactor. Conservatively, a 100 °C uncertainty margin has been added to the nominal calculation so that the maximum temperature was 1620 °C occurring 30 hours after accident initiation (“accident scenario tests”). Total test duration was 300 hours. Krypton release results from the accident scenario tests are shown in Fig. 4-3. Two of the tests went through the accident scenario twice in succession to demonstrate the reusability of fuel after an accident.

Results obtained in the accident scenario tests show three cases with zero failure and two cases indicating a small number of manufacturing defects and accident-related failures (Table 4-1): Sphere AVR 90/2 of 9.3 %FIMA with 1 defect and 2 failures, sphere AVR 90/20 of 9.8 %FIMA with 2 defects and 3 failures. From these results, it is concluded that temporarily high irradiation temperatures of 1400 - 1500 °C in the AVR and the burnup range near to 10 %FIMA can lead to the failure of a small number of particles in the 1620 °C accident scenario tests [12].

The differentiation between defects and failures is based on observations in the corrosion furnace KORA tests: During three KORA experiments at 800 °C and intermittent injection of steam, zero release from one fuel element and small Kr-85 release fractions from a single defective particle each on two other spheres have been observed [13]:

- release burst equivalent to 57 % Kr inventory of one particle in AVR 89/30
- release burst equivalent to 16 % Kr inventory of one particle in AVR 92/7

Similar release bursts equivalent to partial release from a single particle can be observed during the early phase of the accident scenario tests and are, therefore, interpreted as release from manufacturing defects. Prior to the heating test, part of the Kr-85 inventory will have been released during irradiation in the AVR. It is somewhat surprising that zero defects (and failures) were observed in the five isothermal heating tests at 1600 °C. From NUKEM burn-leach statistics [8], there should be one defect in 2 or 3 spheres (see Fig. 4-4).

A conservative estimation of accident-related pressure vessel failures in both the 1600 °C isothermal tests and 1620 °C accident scenario tests is given in Table 4-2:

- zero failures with the fuel elements < 9.3 %FIMA burnup
- two failures with the fuel element of 9.3 %FIMA
- three failures with the fuel element of 9.8 %FIMA

The fact that only 48 % of the Kr-85 inventory of one particle has been released during the 1700 °C isothermal heating test with AVR 74/11, leads to the interpretation of a particle defect rather than failure during heating (where near to 100 % release would have

been expected). With the low burnup of 6.2 %FIMA, it took the kernel 83 h at 1700 °C to release its remaining krypton.

Fuel compacts irradiated to burnup/fluence combinations significantly beyond the maximum HTR-MODUL conditions show higher gas release during the postirradiation heating (Fig. 4-5), indicating failure or deterioration of the coating. With 1600 particles per compact, the level of one particle failure is 6×10^{-4} .

The histogram in Fig. 4-6 shows Kr-85 release fractions from compacts with partially extremely high burnups up to 14 %FIMA. In terms of accident-related gas release, extreme temperatures of 1700 - 1800 °C have an effect equivalent to extreme burnup 12 - 14 %FIMA. Limiting accident temperatures to the 1600 °C range and irradiation to 11 %FIMA guarantees complete retention of fission gases and iodine.

The behavior of the Kr-85 release can be explained by two phenomena:

1. Deterioration of the SiC layer results in permeability to fission products, but the remaining intact outer pyrocarbon layer delays the release of krypton. SiC deterioration is caused by fission products like cesium diffusing into the SiC. Higher burnup means higher fission product concentration leading to more SiC deterioration.
2. On rare occasions, a burst of gas release can be observed which is due to pressure-induced complete coating failure.

Several fission product isotopes are shown in Fig. 4-7 indicating the release sequence Ag / Cs / Kr which is observed in all heating tests. Cs-134 and Cs-137 exhibit an identical release behavior, as expected. Sr-90 is always retained [14, 15] in spheres to a higher degree than Cs-137.

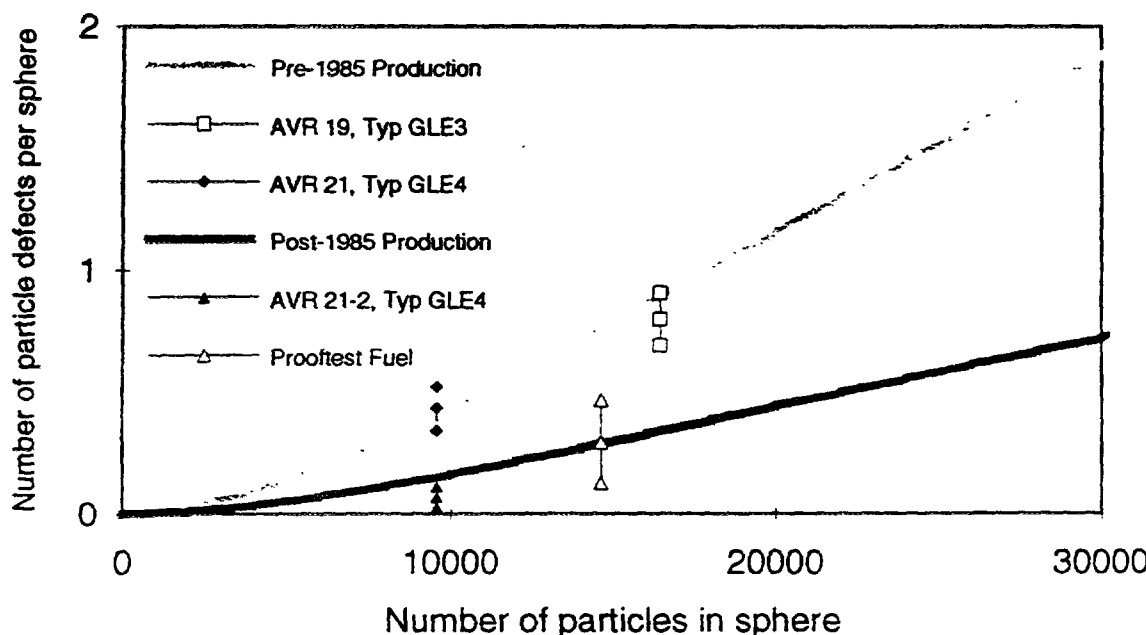


Fig. 4-4: Particle defects in fuel element manufacture (NUKEM)

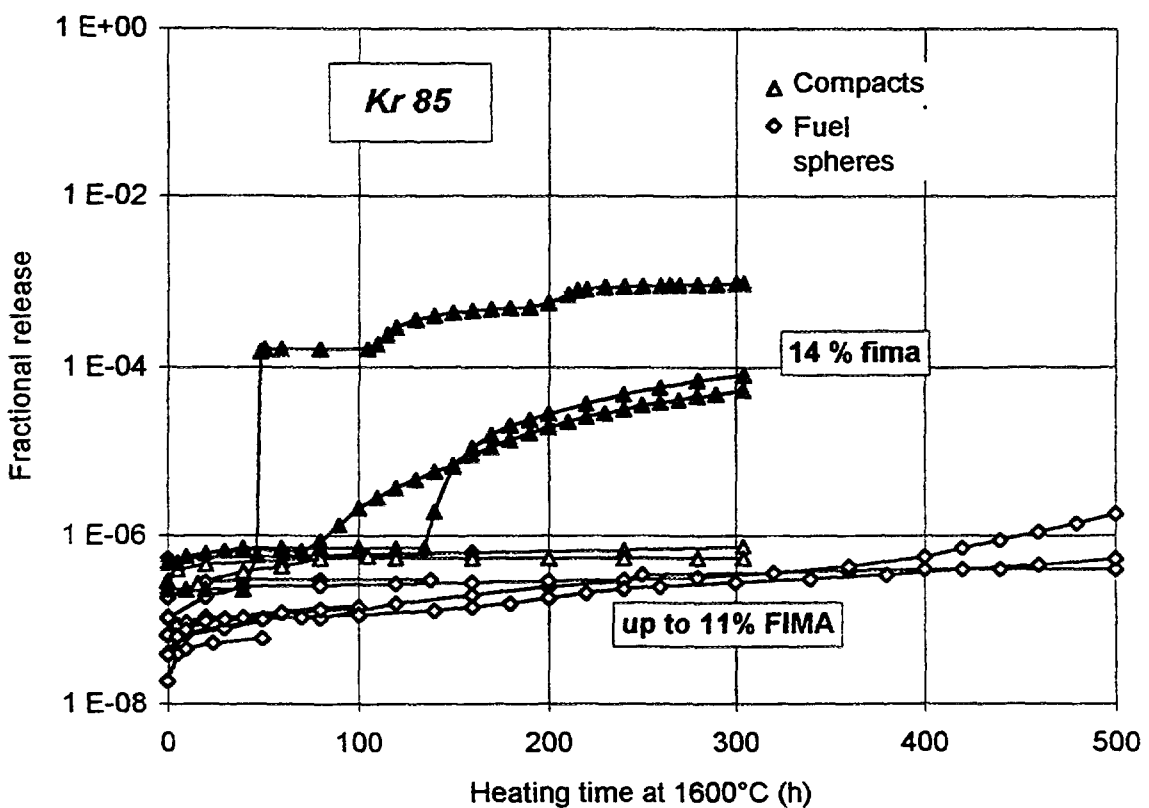


Fig. 4-5: Kr-85 release at 1600 °C from compacts with UO₂ TRISO particles compared with the release from spherical fuel elements

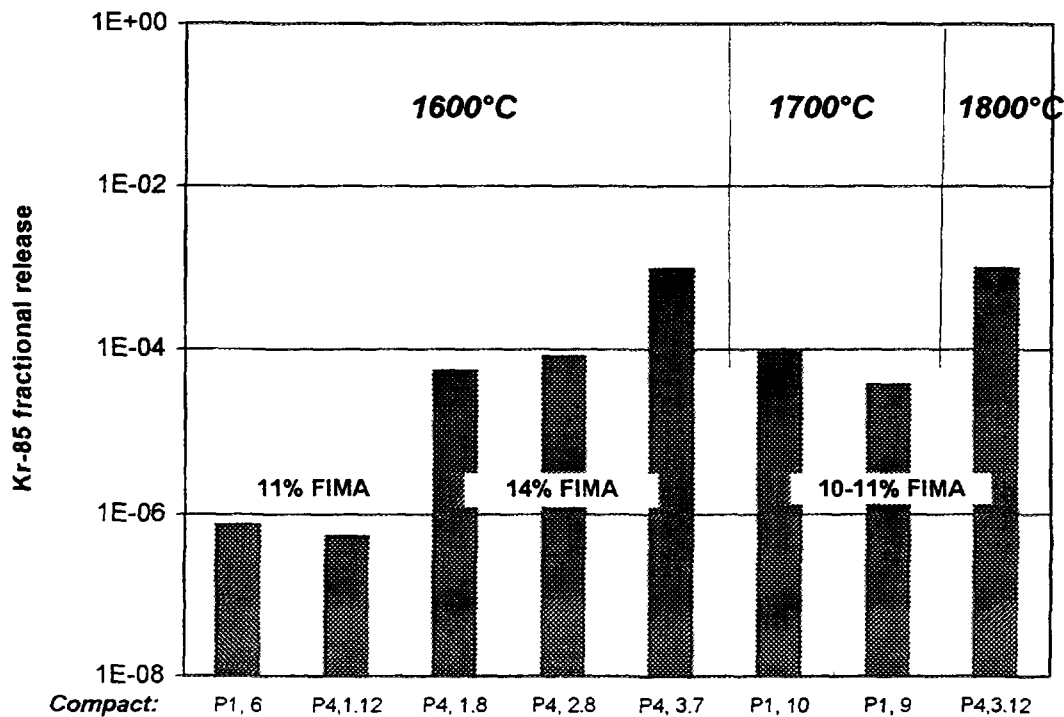


Fig. 4-6: Kr-85 release at 1600 °C from compacts with UO₂ TRISO particles at different temperatures

Table 4-3: Distribution of cesium in the components of fuel elements after isothermal heating tests at 1600 – 1800 °C

Fuel element	Burnup [%FIMA]	Heating test		Fractional Cs-137 content in					Fractional release from fuel element
		Temp. T [°C]	Time at T [h]	Kernel	SiC	Coating (PyC + SiC)	Particle	Matrix	
AVR 71/22	3.5	1600	500	$8.1 \cdot 10^{-1}$	(1)	$1.9 \cdot 10^{-1}$	1.0	$1.8 \cdot 10^{-5}$	$2.0 \cdot 10^{-5}$
HFR-K3/1	7.7	1600	500	$2.9 \cdot 10^{-1}$	$3.3 \cdot 10^{-4}$	$7.1 \cdot 10^{-1}$	1.0	$1.2 \cdot 10^{-3}$	$1.1 \cdot 10^{-4}$
FRJ2-K13/2	8.0	1600	138 (160)	$5.8 \cdot 10^{-1}$	$7.9 \cdot 10^{-4}$	$4.2 \cdot 10^{-1}$	1.0	-	$3.9 \cdot 10^{-5}$
AVR 74/11	6.2	1700	185	$5.8 \cdot 10^{-1}$	(1)	$4.2 \cdot 10^{-1}$	1.0	$2.6 \cdot 10^{-4}$	$7.6 \cdot 10^{-5}$
FRJ2-K13/4	7.6	1800	100	$1.8 \cdot 10^{-1}$	(1)	$5.7 \cdot 10^{-1}$	$7.5 \cdot 10^{-1}$	$2.3 \cdot 10^{-1}$	$9.9 \cdot 10^{-3}$
AVR 76/18	7.1	1800	200	$4.2 \cdot 10^{-1}$	(1)	$4.4 \cdot 10^{-1}$	$8.6 \cdot 10^{-1}$	$1.4 \cdot 10^{-1}$	$4.5 \cdot 10^{-2}$
HFR-K3/3	10.2	1800	100	$1.6 \cdot 10^{-2}$	$1.3 \cdot 10^{-3}$	$5.4 \cdot 10^{-1}$	$5.6 \cdot 10^{-1}$	$8.2 \cdot 10^{-2}$	$5.9 \cdot 10^{-2}$

(1) Not measured

Table 4-4: Cs-137 content in and release from compacts after about 300 h isothermal heating

Fuel element	Heating test temp. T [°C]	Average Cs-137 content in				Fractional release from compact	Total Cs-137
		Kernel ⁽¹⁾	Coating ⁽¹⁾	Particle	Matrix		
SL-P1, 6	1600	9.7×10^{-2}	9.0×10^{-1}	1.0	9.7×10^{-4}	3.9×10^{-4}	1.0
HFR-P4, 1.12	1600	3.3×10^{-2}	9.7×10^{-1}	1.0	5.8×10^{-4}	2.6×10^{-4}	1.0
HFR-P4, 1.8	1600	9.9×10^{-2}	9.0×10^{-1}	1.0	1.3×10^{-3}	2.0×10^{-3}	1.0
HFR-P4, 2.8	1600	8.5×10^{-2}	9.1×10^{-1}	1.0	8.0×10^{-4}	1.4×10^{-3}	1.0
HFR-P4, 3.7	1600	1.5×10^{-1}	8.5×10^{-1}	1.0	1.4×10^{-3}	3.9×10^{-3}	1.0
SL-P1, 10	1700	3.3×10^{-2}	7.6×10^{-1}	8.0×10^{-1}	2.3×10^{-2}	1.0×10^{-1}	9.2×10^{-1}
SL-P1, 9	1700	4.7×10^{-2}	7.5×10^{-1}	8.0×10^{-1}	3.6×10^{-2}	9.8×10^{-2}	9.3×10^{-1}
HFR-P4, 3.12	1800	1.8×10^{-2}	2.8×10^{-1}	3.0×10^{-1}	5.2×10^{-2}	5.2×10^{-1}	8.7×10^{-1}

(1) Fraction in 10 or 9 particles, respectively

Ag-110m is an activated fission product isotope present in very low quantities due to the low fission yield. Therefore, it plays no role in safety considerations. It is, however, the only radionuclide which diffuses through intact silicon carbide already during irradiation at 1200 °C. Silver release from the sphere can reach 1 % of the sphere's inventory. During heating at 1600 - 1800 °C, Ag-110m release values between 2 and 100 % have been observed.

Cesium is the main indicator of SiC deterioration or failure. The sphere release is further delayed by retention in matrix graphite. Strontium follows a similar pattern, but remains in the fuel sphere to a much higher degree than cesium. Krypton is always released later than cesium because of the additional holdup in the pyrocarbon layer. In particles without an outer pyrocarbon layer, krypton is released simultaneously with cesium [8, 16].

Sphere 1 of the irradiation experiment HFR-K3 was irradiated hotter than most other fuels. Therefore, particles had already released some Ag-110m into the matrix graphite during irradiation. In the subsequent heating test at 1600 °C, silver in the matrix graphite is released from the sphere indicating an in-reactor release level of 2 % (Fig. 4-7). Only during the later portion of the 500 h heating test, further increases in release can be observed. Cesium, krypton, and strontium releases remain extremely low during the first 200 h. This demonstrates that this fuel element had no initial coating defects, a low manufacturing contamination level, no in-pile coating failure, and no particle failure during the initial phase of the heating test. Cesium concentration in the fuel free zone of the fuel element before and after heating is shown in the middle of Fig. 4-7. The deconsolidation of the sphere, however, shows that by the end of the 500 h heating, certain amounts of cesium and strontium had been released from the particles, but had been strongly retained in the sphere.

The concentration of fission products in the matrix graphite (i.e. outside particles) of sphere HFR-K3/1 is shown at the right of Fig. 4-7. With Sr-90 being immobile in graphite, its radial profile represents the release from particles. Ag-110m and Cs-137 show radial diffusion profiles through the sphere consistent with their release curves.

The measured Cs-137 distribution in the components of various heated and deconsolidated fuel elements is listed in Table 4-3, those from compacts in Table 4-4.

Fig. 4-8, left-hand side, shows the 1600 - 1800 °C cesium release curves from the fuel compacts irradiated to conditions significantly beyond HTR-MODUL design values in comparison to sphere results at 1600 °C which remain below the level of release of one particle inventory. Release from compacts with moderate irradiation conditions also stays at this low level.

Hereby, cesium release is dominated by heating (= accident) temperature much more than krypton release. On cesium release, the variation of burnup is not very pronounced due to the delay of cesium in matrix graphite.

All cesium release curves from spherical fuel elements are combined in Fig. 4-8, right-hand side, for isothermal heating tests up to 500 h. The early part of the 1600 °C curves is dominated by AVR spheres which release cesium picked up in the AVR core from cross-contamination of old releasing fuel elements. In fuel element AVR 74/11, the cesium inventory from 5 to 10 particles has been released into the matrix graphite during the 1700

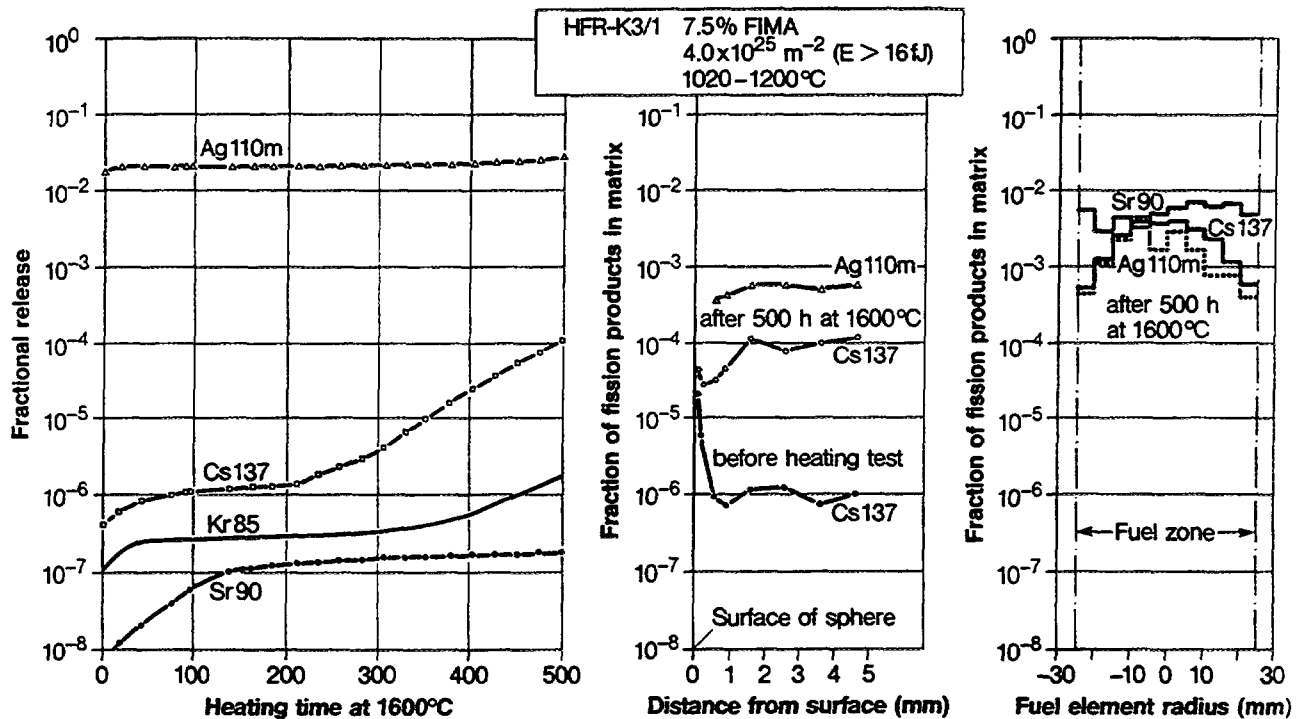


Fig. 4-7: Fission product release and distribution in sphere HFR-K3/1 after irradiation at 1000 - 1200 °C for 359 days and 1600 °C heating

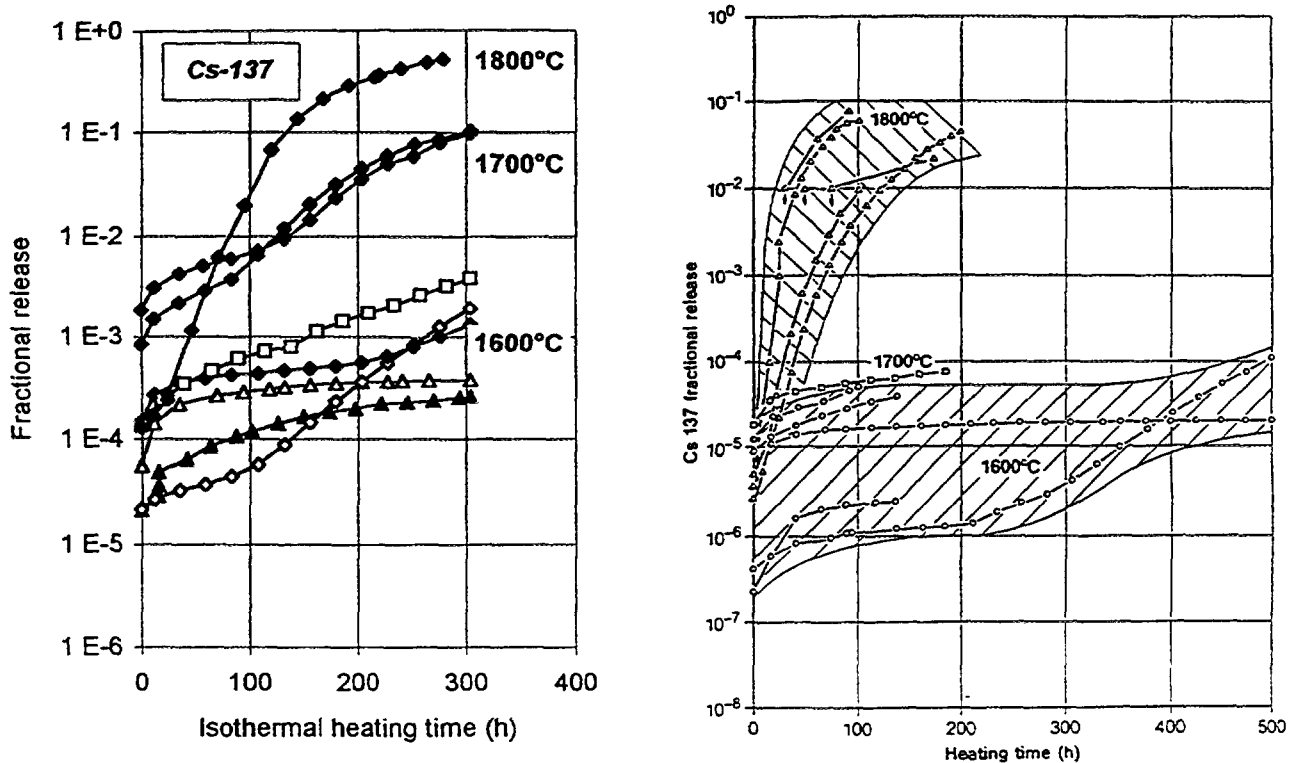


Fig. 4-8: Cs-137 release from fuel compacts (left) and fuel elements (right) with UO₂ TRISO particles

$^{\circ}\text{C}$ heating test to yield a final sphere release fraction of $8*10^{-5}$. Sphere FRJ2-K13/4 had first been heated for 138 h at $1600\text{ }^{\circ}\text{C}$ and subsequently for 100 h at $1800\text{ }^{\circ}\text{C}$. Cesium release results are shown as if these were two independent heating tests.

4.1.1.3.2. Fission Product Release from Heavy Metal Contamination

With the goal to determine both the levels of heavy metal contamination and the iodine / short-lived gas release kinetics from the heavy metal contamination, three fuel elements each had been activated in the Jülich DIDO reactor tests FRJ2-KA1 and FRJ2-KA2. The irradiation was conducted to 0.6 and 2 %FIMA, respectively (Table 4-8) [7, 11].

The fuel was high-quality UO_2 TRISO of 16.7 % enrichment (AVR 21, type GLE-4). The activated fuel elements from FRJ2-KA1 and KA2 have first been heated for 50 h at 1000 , 1200 , or $1400\text{ }^{\circ}\text{C}$ and, finally, at $1600\text{ }^{\circ}\text{C}$. In one case, this was followed by $1800\text{ }^{\circ}\text{C}$ for 50 h; in another case, heating even went to $2000\text{ }^{\circ}\text{C}$ for 2 h.

The measurement of Xe-133 was straightforward. Because the level of heavy metal contamination was, in fact, more than one order of magnitude lower than guaranteed by the fuel manufacturer, I-131 measurements were barely above the detection limit. As shown in Fig. 4-9, there is the expected similarity between the xenon and iodine release curves. A burst-like increase of release is observed during the temperature transition from 1000 to $1600\text{ }^{\circ}\text{C}$ supporting the interpretation of gas release from traps in the matrix graphite. Overall release fractions are extremely low.

All I-131 release results of FRJ2-KA2 are shown in Fig. 4-10. Although the iodine release can be caused only by heavy metal contamination in the matrix graphite, there is another burst from 1600 to $1800\text{ }^{\circ}\text{C}$. This means that there is still a retention for iodine in

Table 4-5: Iodine and xenon release during heating tests of fuel elements irradiated in the Jülich DIDO reactor

Fuel element	Burnup [%FIMA]	Fractional release			
		$1600\text{ }^{\circ}\text{C}, 50\text{ h}$		$1800\text{ }^{\circ}\text{C}, 50\text{ h}$	
		I-131	Xe-133	I-131	Xe-133
FRJ2-KA1/1	0.7	$3.7*10^{-9}$	$5.6*10^{-9}$		
FRJ2-KA1/2	0.9	$5.2*10^{-10}$	$3.7*10^{-9}$		
FRJ2-KA1/3	0.8	$2.3*10^{-9}$	$8.7*10^{-9}$		
FRJ2-KA2/1	1.8	$9.9*10^{-9}$	$1.1*10^{-8}$		
FRJ2-KA2/2	2.0	$9.0*10^{-9}$	$6.9*10^{-9}$		
FRJ2-KA2/3	2.0	$7.1*10^{-9}$	$7.1*10^{-9}$	$5.2*10^{-8}$	$1.7*10^{-8}$
Mean value		$5.4*10^{-9}$	$7.1*10^{-9}$	$5.2*10^{-8}$	$1.7*10^{-8}$

graphite grains even at high temperatures. The 1800 °C test with fuel element FRJ2-KA2/3 leads to the conservative assumption that the total release of iodine from the graphite matrix could be around 1×10^{-7} , equivalent to a contamination of 72 ppb natural uranium. From all FRJ2-KA1 iodine and xenon 1600 °C release values, the average release fraction is 5×10^{-9} , equivalent to 4 ppb trace contamination of uranium; from FRJ2-KA2, it is 8×10^{-9} , equivalent to 6 ppb uranium trace contamination (Table 4-5). The higher FRJ2-KA2 released activities are attributed to the longer in-reactor dwelling time.

I-131 release measurements during 1600 °C from different fuel samples are compared in Fig. 4-11. The measured activities from the six FRJ2-KA1 and -KA2 fuel elements are extremely low.

As is known by comparison to MTR irradiated spheres, the relatively high release of Cs-137 and I-131 from modern, clean AVR elements is caused by cross-contamination from old contaminated AVR spheres. Bare UO₂, as used in most reactor systems, releases all I-131 in the fuel after 15 h at 1600 °C (Fig. 40 in [6]).

4.1.1.3.3. Results Obtained at 1900 - 2500 °C

The controlling factor in the failure of TRISO particles subjected to extreme temperatures is the thermal decomposition of silicon carbide [17, 18]



Krypton release data from irradiated spherical fuel elements during high-temperature heating tests are shown in Fig. 4-12. At temperatures up to 2100 °C, Kr-85 release fractions are low as long as particles do not fail (at medium burnup). Starting at 2200 °C, fission gas release steeply increases during temperature ramp tests. This effect is due to SiC thermal decomposition and subsequent diffusion of fission gases through a still intact outer pyrocarbon (PyC) layer.

With some high-burnup UO₂ fuels, an earlier release of krypton is observed in the curves shown in Fig. 4-12. The increase in gas release at 1700 to 2000°C indicates the operation of a failure mechanism in addition to SiC decomposition. The data suggest that pressure-induced failure of one to ten particles has occurred, followed by continuously increasing particle failures during further heatup. The onset of krypton release occurs earlier, and the level of krypton release is higher as the fuel burnup increases.

As fuel particles are irradiated to high burnup at high irradiation temperatures, the internal gas pressure is increased, exacerbated greatly by the formation of CO in UO₂ fuels under these conditions [19]. All high-burnup spheres were irradiated in the AVR and some 20 % of the fuel elements went through temperatures in excess of 1300 °C. Such high temperatures and long irradiation times are not proposed for future HTGRs. Thus, the combination of high-burnup UO₂ fuel particles and abnormally high irradiation temperatures results in early pressure-induced failures noted in some of the measurements shown in Fig. 4-12, top.

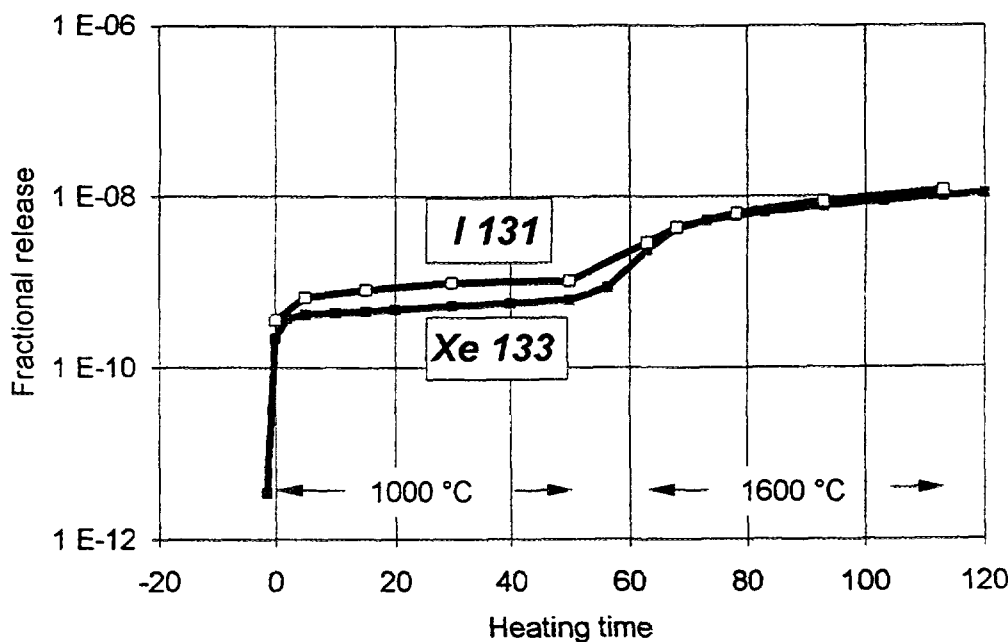


Fig. 4-9: Iodine and xenon release from 17 % enriched UO_2 TRISO fuel element FRJ2-KA2/1 (Type GLE-4) as a function of heating time at 1000 °C and 1600 °C

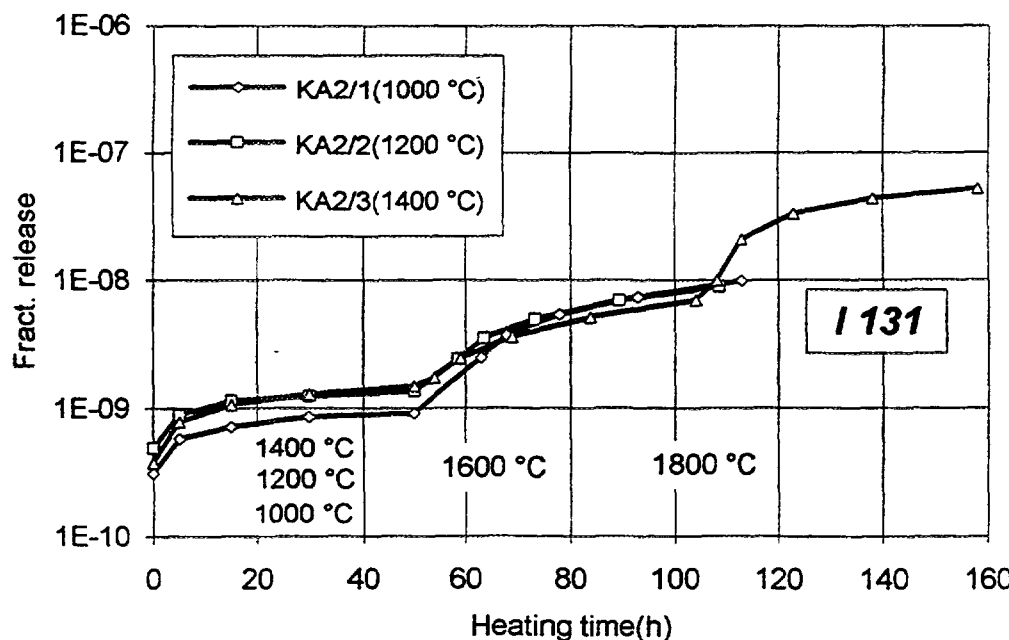


Fig. 4-10: Iodine release from UO_2 TRISO fuel elements (type GLE-4) activated in FRJ2-KA2 to 2 %FIMA as a function of heating time at 1000 / 1200 / 1400 °C, 1600 °C and 1800 °C

In the ramp tests discussed above, the final temperature of 2500 °C is reached after ≈ 30 h. In addition, a series of isothermal tests was conducted at 1900 to 2100 °C. In these cases, the fuel element temperature was increased with the same 50 °C per hour heating rate as in the ramp tests, but the desired temperature was held constant for 30 h. The final release results are listed in Table 4-6. The Kr-85 release profiles are shown in Fig. 4-12, bottom.

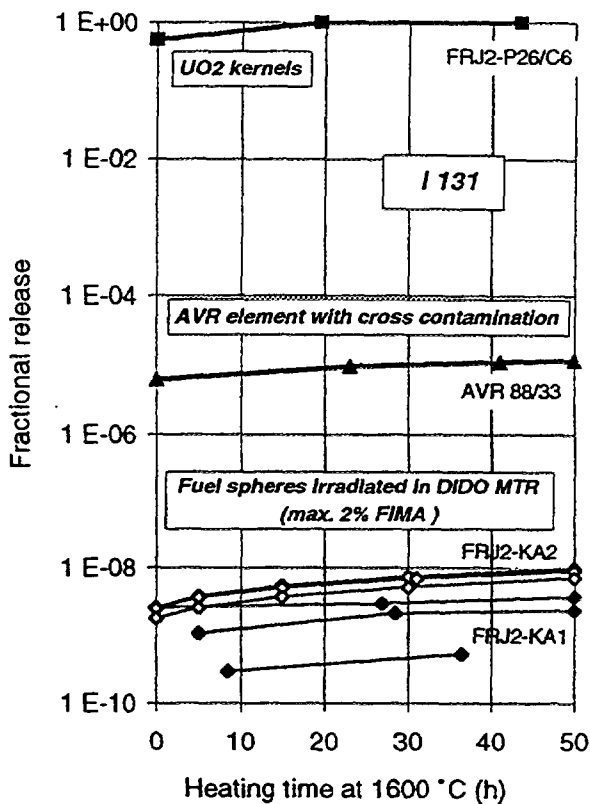
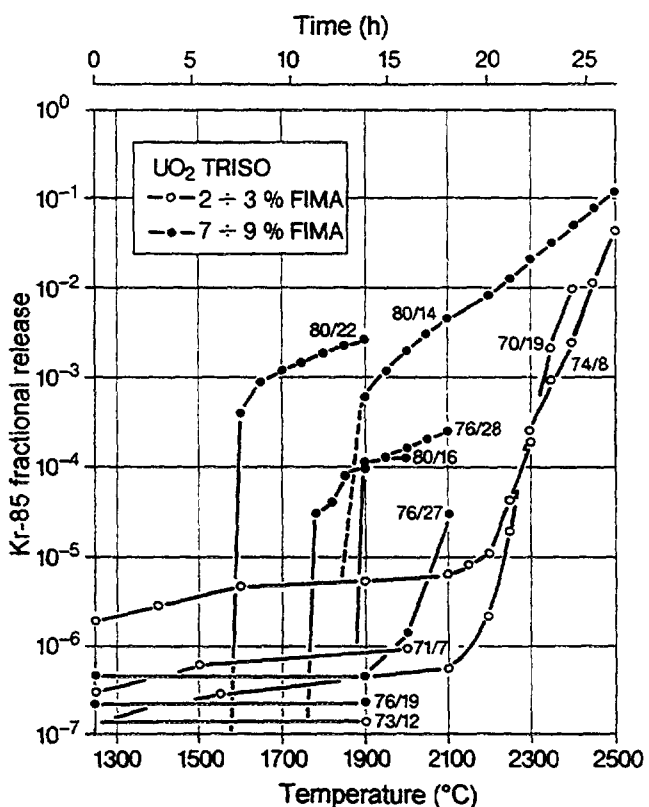


Fig. 4-11: Iodine release from various UO_2 fuels during accident simulation heating tests at $1600\text{ }^\circ\text{C}$

Initial release rates in Fig. 4-12, bottom, are clearly dependent on burnup, but values are converging towards the same level of cumulative fractional release after 30 h of heating. The early part of the gas release profile is dominated by failure of the coating due to high internal gas pressure. After some time at constant temperature, SiC thermal decomposition dominates and becomes the release rate determining mechanism.

Ceramographic sections through irradiated and heated particles show little change to the as-received state at heating temperatures up to $1800\text{ }^\circ\text{C}$ (Fig. 4-13). In this temperature range, fission gas release is still low, but cesium release can reach several percent of the total inventory. Above $2000\text{ }^\circ\text{C}$, thermal decomposition of silicon carbide leads to fission gas release and, ultimately, to the destruction of the particle [6, 7].

(a) linear ramp tests



(b) isothermal heating tests

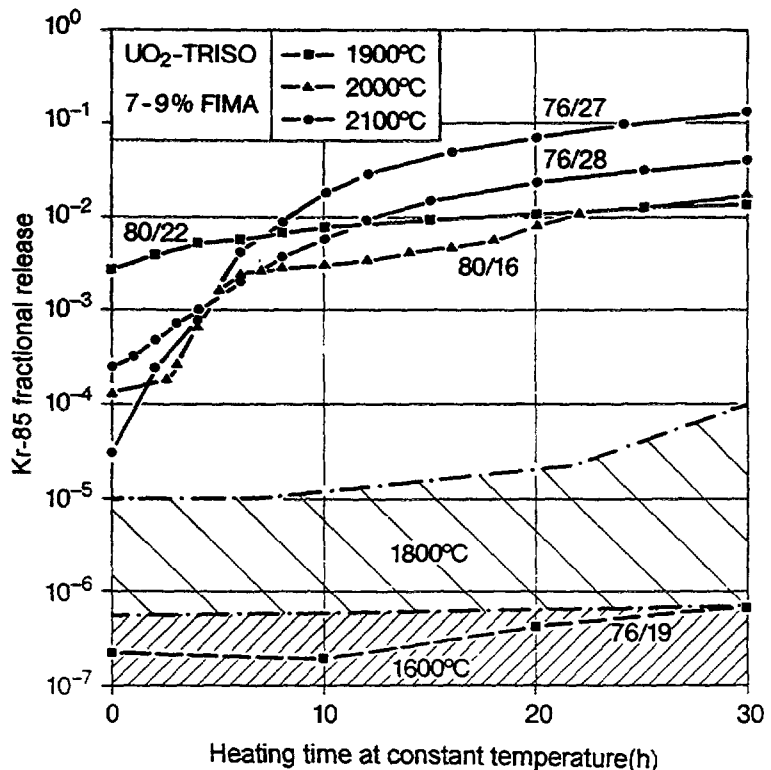


Fig. 4-12: Krypton release from spherical fuel elements containing UO_2 TRISO particles as a function of heating temperature

Table 4-6: Data from irradiated spherical fuel elements with low-burnup and high-burnup UO₂ TRISO particles in 1900 - 2500 °C heating tests

Fuel element	Burnup [%FIMA]	Fast fluence [10 ²⁵ m ⁻² , E>16 fJ]	Time [d]	Heating test		Fractional release	
				Temp. T [°C]	Time at T [h]	Kr-85	Cs-137
Low-burnup fuel							
AVR 73/12	3.1	0.8	430	1900	100	1.4*10 ⁻⁴	1.0*10 ⁻¹
AVR 71/7	1.8	0.5	250	2000	100	8.6*10 ⁻⁵	9.2*10 ⁻²
AVR 70/19	2.2	0.6	300	2400	Ramp	1.0*10 ⁻²	3.0*10 ⁻²
AVR 74/8	2.9	0.7	400	2500	Ramp	4.6*10 ⁻²	2.5*10 ⁻¹
High-burnup fuel							
AVR 76/18	7.3	1.9	1060	1900	30	6.9*10 ⁻⁷	4.6*10 ⁻¹
AVR 80/22	9.1	2.4	1330	1900	30	1.5*10 ⁻²	4.8*10 ⁻²
AVR 80/16	7.8	2	1140	2000	30	1.9*10 ⁻²	2.2*10 ⁻¹
AVR 74/6	5.6	1.4	770	2100	30	2.4*10 ⁻²	4.7*10 ⁻¹
AVR 76/28	6.9	1.8	1010	2100	30	4.8*10 ⁻²	5.5*10 ⁻¹
AVR 76/27	7.4	1.9	1080	2100	30	1.4*10 ⁻¹	6.9*10 ⁻¹
AVR 80/14	8.4	2.2	1220	2500	Ramp	1.4*10 ⁻¹	9.9*10 ⁻¹

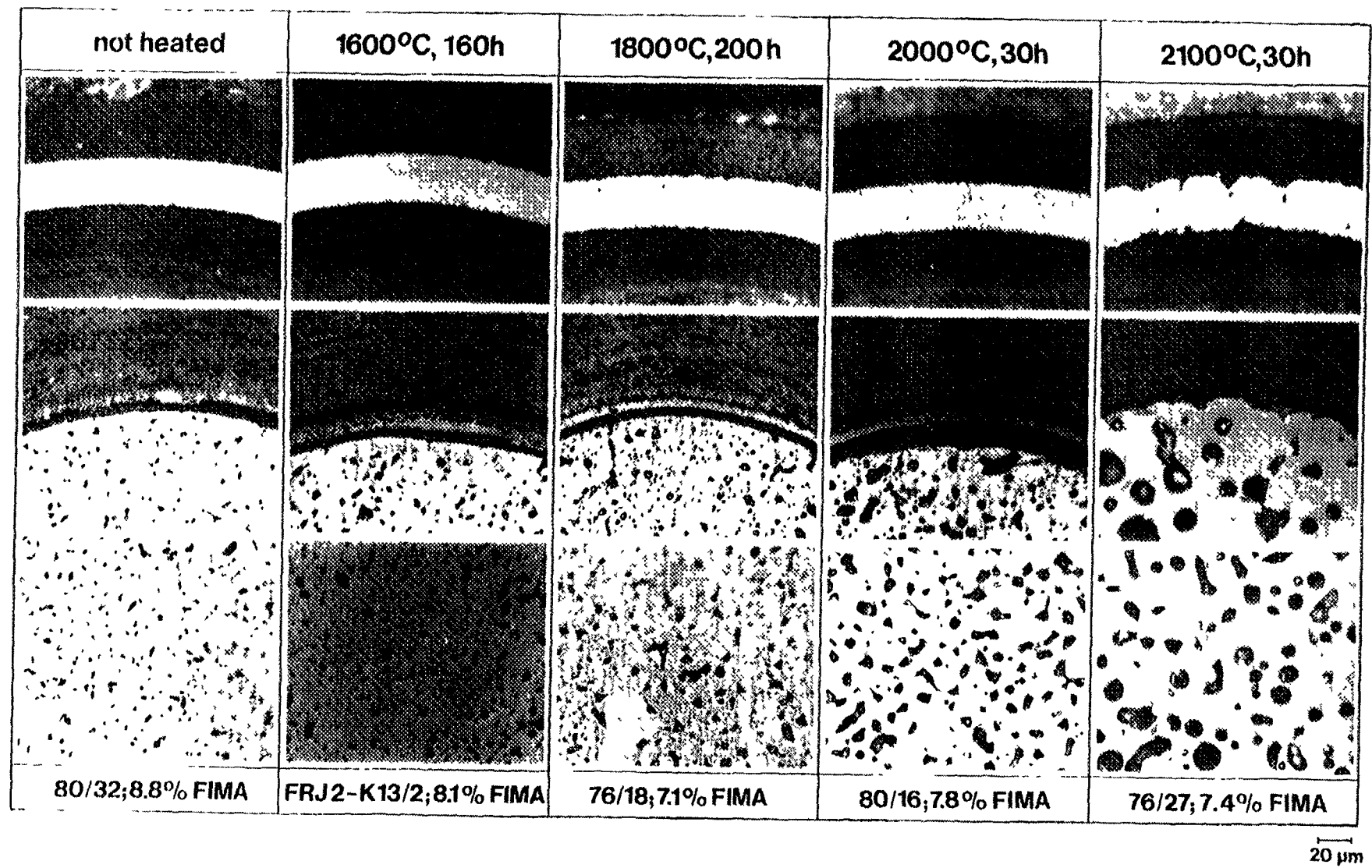


Fig. 4-13: Ceramographic sections through irradiated UO_2 TRISO particles with 35 μm thick silicon carbide layer (top), kernel/buffer interface (middle) and through UO_2 kernel (bottom) after heating tests

4.1.1.4. Modeling

4.1.1.4.1. Particle Failure

Information about the failure of particle coatings under elevated temperature conditions has been gained from series of heating tests. These data have been used to develop corresponding calculational models for both reproducing the experimental data and predicting coated particle performance in future HTGR designs.

Several mechanisms have been found to be responsible for particle failure under core heatup accident conditions:

1. Pressure vessel failure of standard (intact) particles or in particles with defective or missing single coatings
2. Failure of the SiC layer by fission product corrosive attack on silicon carbide
3. Failure of the SiC layer by thermal decomposition of the silicon carbide
4. Enhanced diffusion through the SiC layer at very high temperatures

The **KFA code PANAMA-I** [20] determines the fraction of failed TRISO particles under accident conditions by combining two different failure mechanisms. The first one is a pressure vessel model which is based on the physical description of the spherical SiC layer to act as a pressure vessel. The SiC layer is expected to fail as soon as the stress on the coating caused by the internal gas pressure has exceeded its tensile strength. The gas pressure inside the particle, as derived from the ideal gas law, is strongly dependent on temperature, burnup, fission yield of stable gases, fission gas release from the particle kernel, and oxygen release by fission resulting in CO formation. The stress on the coating is additionally increased by a weakening of the SiC layer due to corrosive attack on the inner surface by fission products. The SiC corrosion is modeled by a thinning rate.¹

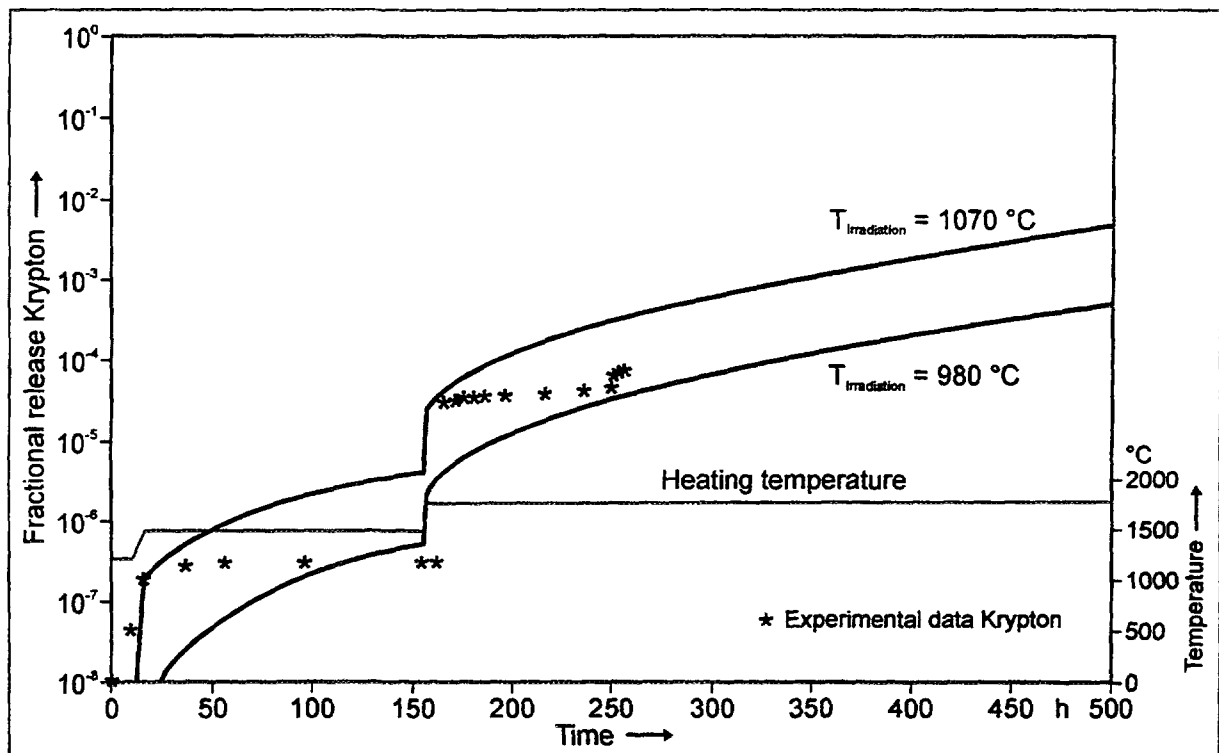
The tensile strength is a material characteristic of the silicon carbide which has been measured in independent SiC ring crack tests [21]. This strength is considered to be reduced by fast neutron fluence. The outer PyC layer which is presumed to contribute to the tensile strength is conservatively neglected in this model.

The second failure mechanism, thermal decomposition of the silicon carbide, becomes dominant at higher temperatures between 1600 and 2000 °C depending on heating time. This has been described by Weibull statistics with pre-exponential factors and Weibull moduli empirically derived for unbonded particles and for particles embedded in a fuel sphere. A thermal decomposition thinning rate has been derived by Benz from SiC weight loss measurements on coated particles without outer PyC after heating [22]. A PANAMA-I calculation is assumed to result in a fraction of particles with a simultaneous failure of all coatings (resulting in exposed kernels) and the fission gas release, respectively, from the failed particles. PANAMA-I uses this as a conservative assumption rather than modeling the failure of individual coatings.

The experience gained with the PANAMA-I model so far has demonstrated in most cases good agreement with measurements from German heating experiments covering both

¹ A uniform thinning of the SiC layer is an assumption in the model; however, it might be not conservative since local thinning has been observed in Japanese experiments.

(a) FRJ2-K13/4



(b) AVR 76/18 (T_{irr} range estimated)

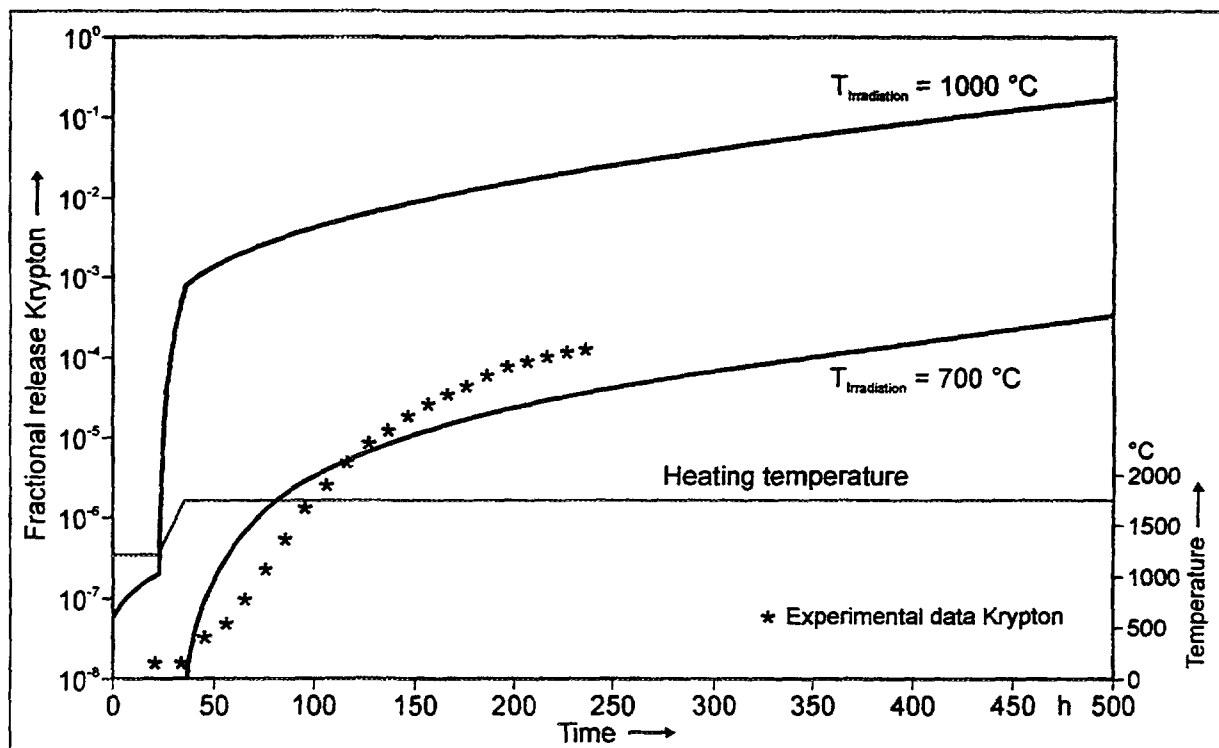


Fig. 4-14: PANAMA-I prediction and experimental data of krypton release during heating tests. Upper and lower release curves refer to maximum and minimum irradiation temperature.

(c) AVR 85/18, AVR 90/2, AVR 90/5 (transient test, T_{irr} range estimated)

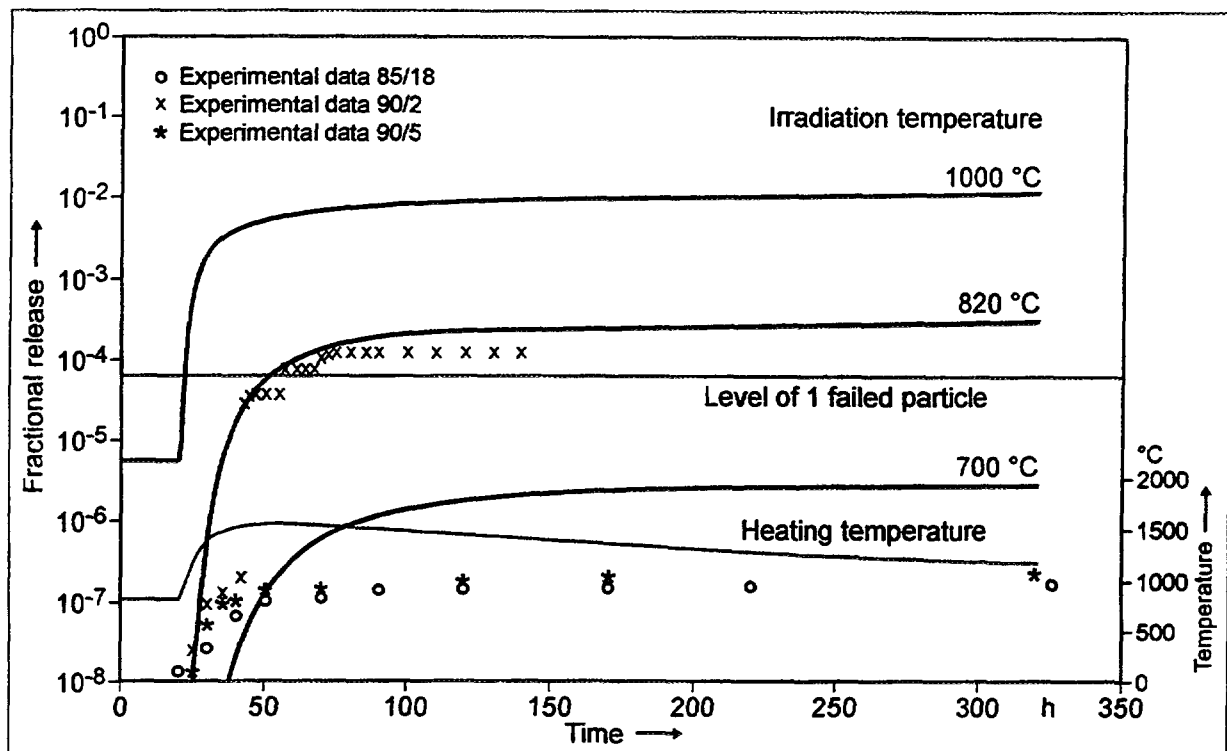


Fig. 4-14: PANAMA-I prediction and experimental data of krypton release during heating tests. Upper and lower release curves refer to maximum and minimum irradiation temperature. (continued)

observed krypton release characteristics of sudden bursts (= complete coating failure) (Fig. 4-14 (a)) and of a gradual increase typical of diffusive transport through the still intact outer PyC layer (Fig. 4-14 (b)) [23]. Fractions of gas release from fuel spheres which were exposed to extreme irradiation conditions in MTRs are in some cases overpredicted by PANAMA-I up to several orders of magnitude.

PANAMA has also been applied to predict the krypton release from AVR GLE-3 fuel spheres which were exposed to a transient heating temperature as predicted for the HTR-MODUL core heatup accident. Maximum temperature in the simulation test was 1620 °C. The calculations shown in Fig. 4-14 (c) have demonstrated that no particle failure would be expected when assuming an average irradiation temperature for the fuel spheres of 700 °C (lower curve). The three particle failures that were observed in heating test AVR 90/2, are in agreement with the calculation if an average temperature of 820 °C is assumed for this sphere (middle curve). The GLE-3 fuel elements are estimated to experience an average irradiation temperature of 725 °C when passing the AVR core close to a buttress and 842 °C when passing the core in the middle between two buttresses. Though it cannot be ascertained which path the heated fuel elements had really used during irradiation, it shows that the assumed average values for T_{irr} which have led to a reproduction of the krypton measurements are in good agreement with the temperature history estimations for the GLE-3 fuel spheres [24].

A joint US/FRG modeling effort resulted in the so-called "Integrated Failure and Release Model for Standard Particles" as a new definition of particle failure. The cesium release is here supposed to indicate a failure of the SiC layer. The diffusion of cesium is assumed to be negligible in this model under the conditions to which the model is applied. The observed delayed krypton release profile can be explained by assuming a diffusive transport through the still intact outer PyC layer whereas there is no holdup for cesium in pyrocarbon at elevated temperatures. This is due to the observation of almost identical release curves for cesium and krypton from particles which did not have an outer PyC layer [25].

In the original version of this model from 1985 [25], both thermal decomposition and corrosion of the SiC layer were taken into account as degradation mechanisms for the SiC layer. Similar to PANAMA-I, the experimental data from Montgomery and Benz, transferred into thinning rates, have been incorporated into a statistical distribution of the SiC degradation process. Its convolution with the distribution of SiC layer thicknesses leads to a complicated formula which is approximated by a Weibull distribution for the probability for a SiC coating to fail. Corresponding Weibull moduli and pre-exponential factors were derived from a small number of German and US heating tests up to 2500 °C (see Appendix A.3.).

The revised version of the "Integrated Failure and Release Model for Standard Particles" from 1988 regards thermal decomposition as the only SiC degradation process [26, 27]. The Weibull modulus and pre-exponential factor were derived from an extended set of German heating test data. An activation energy was derived from these data which was very close to Benz' value for thermal decomposition of the SiC layer, therefore it was concluded that SiC corrosion was insignificant for these heating tests. The pre-exponential factor contains a strong dependence on irradiation temperature and burnup and a weak dependence on fast fluence, which was the result of the fitting procedure rather than any physical interpretation (see Appendix A.3.).² The particle failure fraction in the 1988 version has a minimum value of 6×10^{-6} as cutoff limit to agree with observations from low exposure AVR fuel under heating conditions.

These models were incorporated into the KFA codes PANAMA-II (original version from 1985) and PANAMA-III (revised version from 1988) and into the GA code SORS.³ Both KFA and GA codes produce basically the same results [27]. For one of the basic heating tests, the German R2-K13/1, calculational and experimental data are given in Fig. 4-15. In Fig. 4-16, a comparison is given between the various particle failure models for the hottest location predicted for the US-MHTGR [27].

Due to the larger experimental data base, the application of the revised version provides better agreement with the measurements than the original version of the statistical

² Note that an "activation" energy much different than Benz' value can give as good a correlation with the experimental data, since the coefficient of the Arrhenius expression is an empirical expression so as to give the "right" answer. A more phenomenological satisfying model is to attribute fission product release to diffusion through the SiC, with SiC decomposition affecting the thickness (and possibly density) of the SiC layer. Note that the results in Fig. 4-13 indicate that at very high temperatures (i.e., 2100 °C for 30 h), thermal decomposition reduces the effective thickness of the SiC layer and perhaps reduces its density. At 1800 °C for 200 h, only the SiC density appears affected, and apparently not very much; at 1600 °C for 160 h, the effect appears to be very small. Using the diffusion model, the variation in the diffusion coefficient also varies with the $\log(1/T)$; the effect of SiC thermal decomposition is considered to reduce the thickness of the SiC layer, and perhaps its density, based on experimental measurements [28, 29] (see also section 4.1.4.4.).

³ The actual SORS code is always referenced by its original publication in 1974 [30], though there are later developments in the calculational models now being implemented in this version.

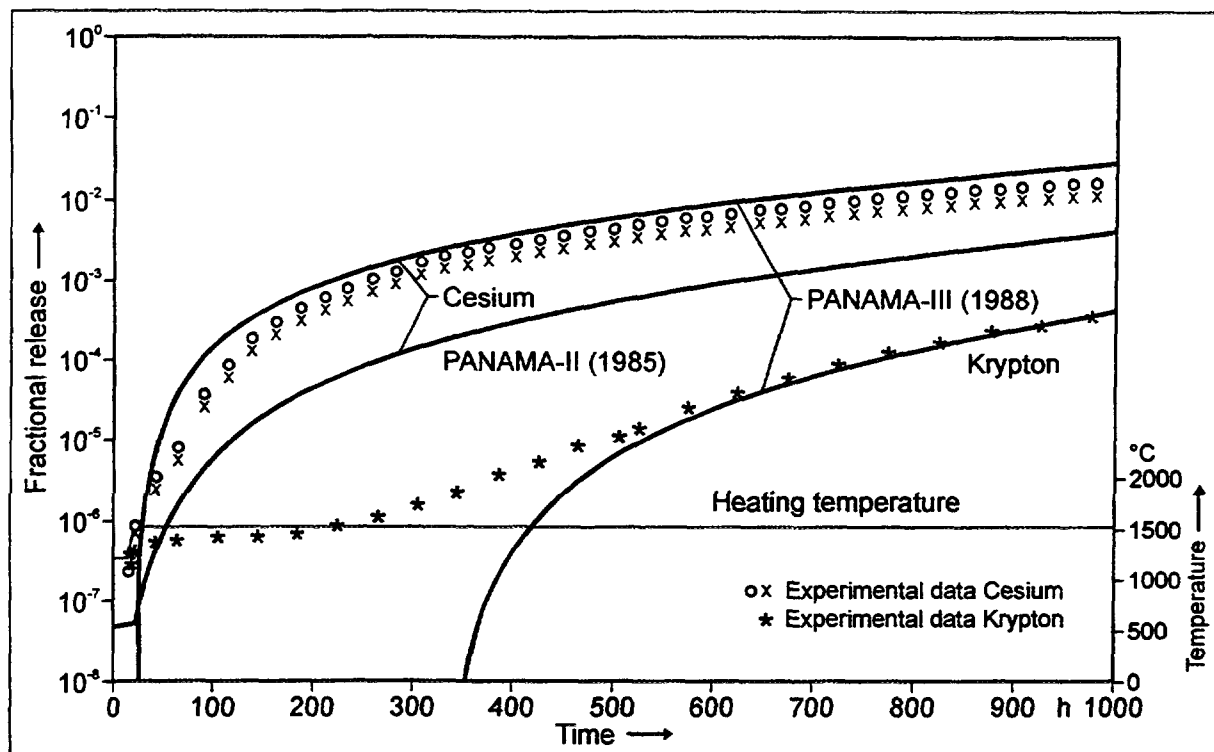


Fig. 4-15: Calculation of cesium and krypton release with the 1985 and 1988 US/FRG statistical models and comparison with measurements for the heating experiment R2-K13/1 [31]

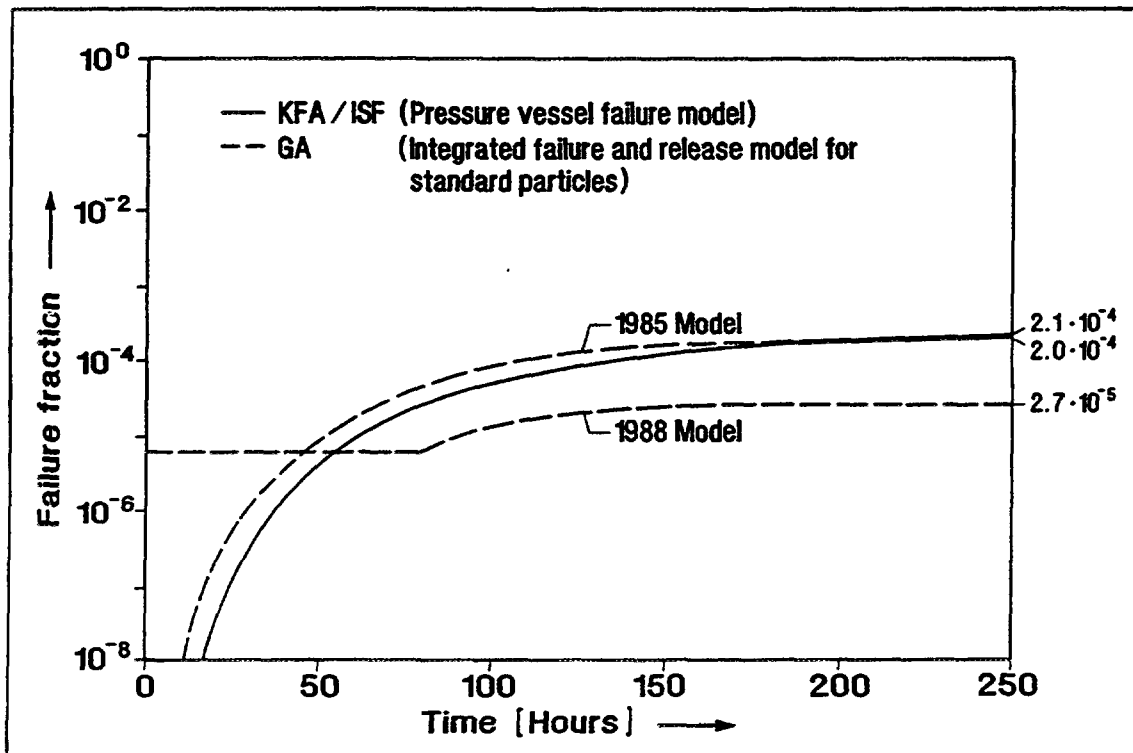


Fig. 4-16: Comparison of fuel particle failure for the maximum temperature history of the US-MHTGR using the 1985 and 1988 US/FRG statistical models and the KFA pressure vessel failure model [27]

model. However, for many heating tests and probably for most of the small-sized HTGR core regions under conduction cooldown conditions, the minimum for the SiC failure rate given in the model equation will not be reached which makes this cutoff limit rate-determining and not the irradiation conditions.

For application of fuel performance models for the lower accident temperature range $\leq 1600^{\circ}\text{C}$, it must be pointed out that the "mathematical" result of a particle failure fraction (which - in PANAMA-I - immediately leads to a gas release fraction) is not necessarily a real failure of a particle. If the calculated value has exceeded a level equivalent to the fraction of one failed particle (which is, for a German spherical fuel element, on the order of 10^{-4}), it could be interpreted as being composed of contributions from several failed particles having released only a fraction of their inventories. The full inventory of a particle is only expected to be released at high temperatures.

The discussion about the different philosophies upon which the calculation models are based, raises the important question of the **definition of a particle failure**. In the classical diffusion codes, a defective particle is modeled like an exposed kernel. In the early statistical model, it is modeled like a non-existing SiC layer. Several models try to handle particles with a degraded SiC layer and seem to approximate best the data in many heating experiments. This is possible only on an empirical basis, since the broad range between the least releasing (intact) coating and the most releasing (non-existing) coating must be covered for instance with a factor representing the type of defect (HRB) or with fitted diffusion data.

Pro and con arguments could be provided by the **IMGA measurements** which describe the distribution of fission product inventories of single coated particles in terms of a particle frequency versus inventory fraction diagram [32]. In theory, a pure diffusion model would create a single line of all particles having retained (or released) the same amount of fission products.⁴ The statistical models also create a single line in the same diagram where a certain fraction of particles has completely released its inventory. Neither model is able to reproduce the existing IMGA results. An example of IMGA measurements is given in Fig. 4-17 for the heating test HFR-K3/3, revealing a variation of the cesium release between 10 and 90 % of the original particle inventory and, furthermore, a bimodal distribution with maxima around 20 and 60 % cesium inventory fractions [32]. The assumption of an additional (or hybrid) release mechanism, diffusion through intact particles combined with a particle failure fraction [33] or degradation of the SiC layer with a subsequent or enhanced diffusive transport through the degraded silicon carbide [34], is one possible explanation. Another is the assumption of an inherent variance of diffusion coefficients to explain the observed variance of remaining cesium fractions in single coated particles [35].

A calculation model based on effective diffusive transport does not claim to be able to explain all aspects of observed fission product release behavior. However, it appears to be easy to logically combine it with additional processes such as particle failure (diffusive release from exposed kernels), SiC degradation (modeled as a thinning of the SiC layer), fast neutron fluence or fission product concentration dependence of diffusivity.

⁴ In reality, some distribution around the average particle inventory would be expected because of: (1) the distribution of the SiC layer thicknesses in particles, and (2) an inherent distribution of diffusion coefficients due to microstructural variations in the layers.

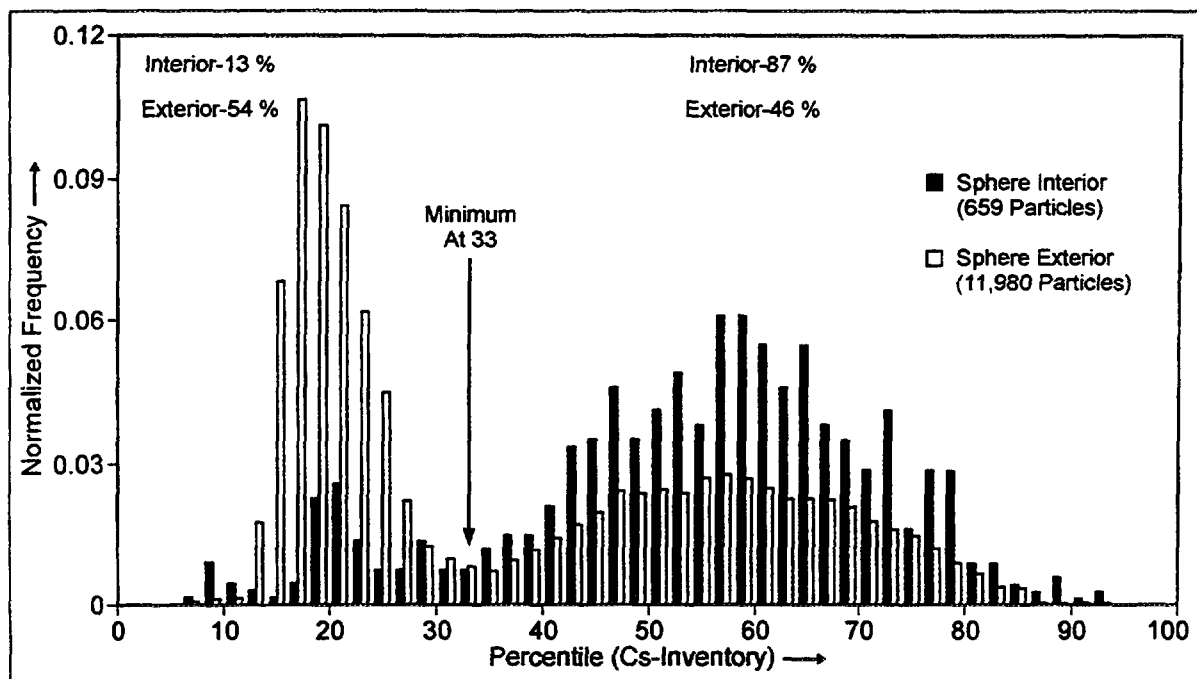


Fig. 4-17: Cesium inventories in individual particles for the heating experiment HFR-K3/3 based on the IMGA measurements of 11,980 particles

The advantage of diffusion codes which include the irradiation (normal operation) phase is their ability to commonly describe the results of heating tests with a single diffusion constant if the irradiation history is adequately considered [36].

4.1.1.4.2. Metallic Fission Product Release

Various kinds of modeling approaches are used to describe the release behavior of metallic fission products from coated fuel particles. The main approach used by many authors is based on a diffusion model, and some later models assume a particle coating failure preceding fission product release. Finally, there are models adopting parts of both modeling approaches.

The calculation model which has been most often used in KFA safety analyses for several types of small and medium-sized HTGRs is the **diffusion model FRESCO**. This model is available in a core version, code FRESCO-I [37], to determine the fission product release from an HTGR core, and in a pebble version, code FRESCO-II [38], which describes the fission product release from a single spherical fuel element under irradiation (normal operation) and heating (core heatup accident) conditions. Simple changes in the input data allow application to various particle types and fission product species to be considered.

Both FRESCO codes use the same numerical method to determine the radionuclide release from the coated particles in discrete steps of time and location. Effective⁵ diffusion coefficients for particle kernel and coating materials are used in the numerical solution of

⁵ "Effective" means that the contributions from all possible transport mechanisms of a fission product species within a material zone are combined into a single diffusion coefficient whose temperature dependence is given by an Arrhenius relation (see Appendix A.1).

the Fickian diffusion equation. The FRESCO code considers the treatment of two different types of particles: standard particles with an intact coating and exposed particle kernels. The non-releasing character of intact coating layers for gaseous fission products (and iodine) is simulated by a "high" value for the diffusion coefficient in question.

A particle failure function in form of a step function is required as input which defines the time points at which a certain fraction of standard particles turn into exposed kernels with the actual fission product inventory in their coatings being immediately released into the fuel element matrix graphite. A particle with a cracked but still existent coating which is observed to better retain (metallic) fission products than an exposed kernel, can be simulated by a lower value for the kernel diffusion coefficient.

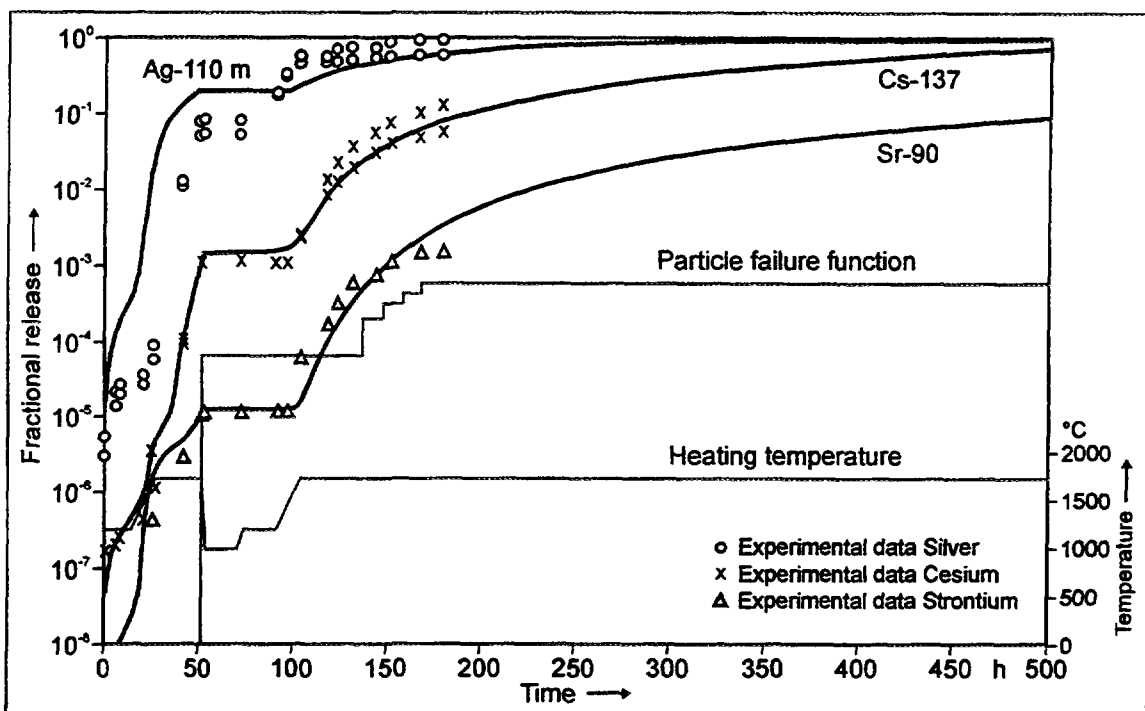
Much experience has been gained so far with the KFA diffusion code FRESCO by predicting and postcalculating heating experiments for validation purposes. The codes have been used for core release predictions under core heatup accident conditions for various HTGR designs. The "pebble" version has also been applied to evaluate and eventually modify the recommended set of diffusion coefficients by fitting the experimental data as shown in Fig. 4-18 for the metallic fission products in the KFA 1800 °C heating test HFR-K3/3. It can be stated that a well assured data set of diffusion coefficients is available to make this model an adequate tool for safety analyses [23].

A further development of the 1985 version of the joint US/FRG statistical model and a companion effort to the on-going revision by Goodin has been made in the **Martin-Goodin-Nabielek (MGN)** model coded in MACINTOSH [39]. This model is based on the same SiC failure formalism as in the revised statistical model (SiC thermal decomposition). But in contrast, the subsequent fission product transport through the failed SiC layer is assumed to proceed as a grain boundary diffusion process within the silicon carbide, with a larger cesium diffusion coefficient required than that recommended in [40]. The retention effect for cesium in matrix graphite was considered to be important as was done in Goodin's revised version of the statistical model, but was modeled differently. MACINTOSH employs a diffusive transport in the graphite rather than the fast fluence dependent retention factor of the 1988 version. The MGN model gave good agreement between measured and calculated shapes of cesium fractional release curves from some KFA heating experiments. However, the calculations underpredicted the concentration profiles and, at the same time, overpredicted the release itself.

The recently developed **KFA code SPTRAN** [41] is in its basic aspects a copy of the FRESCO-I diffusion model. One of the main differences is the method of numerical solution by employing an iteration between fission product concentrations in coated particles and matrix graphite which was later found not to be necessary [42]. Other differences are the handling of defective particles (one time-dependent "representative" defective particle rather than a step function) and the connection of the core cavern with the primary circuit which, however, is not used for predictions in reactor design studies since it introduces a high degree of uncertainty due to plateout processes [42].

Another **KFA code, GRECO**, [43] has been developed a couple of years ago which could be regarded as a refined diffusion model comprising a detailed modeling of transport mechanisms in the microstructure of the particle under accident conditions. An independent

(a) Fractional release vs. heating time in HFR-K3/3



(b) Cesium concentration profiles in the fuel spheres after heating

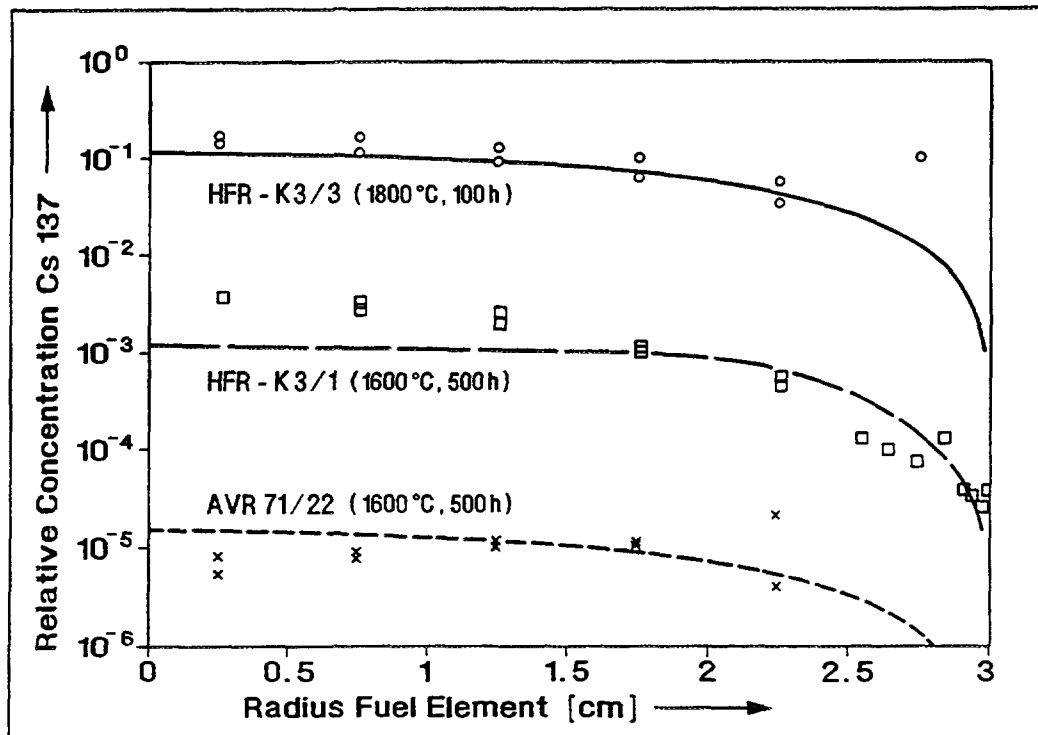


Fig. 4-18: FRESCO-II postcalculations of metallic fission products to derive effective diffusion coefficients in SiC

partial model of GRECO, called GRECO-BREL, calculates fission product release from a spherical fuel element under accident conditions. Compared to simple diffusion codes, these codes need many more input parameters which seem inappropriate to be put into a recommended and validated set of transport data for safety analysis purposes. The GRECO model might be helpful in interpreting postheating examination results.

A collection of actual transport data for various fission product species in HTGR fuel particle materials is given in Appendix A.1.

4.1.1.4.3. Fission Gas and Iodine Release

The release of fission gases and iodine⁶ from coated fuel particles is widely expected to be directly correlated with a defective or failed coating. This idea implies released fission gases (e.g., Kr-85) are the indicator for a broken coating. An intact SiC layer keeps the coated particle gas-tight and an intact outer PyC layer causes a significant delay of the transport of gaseous fission products once they have passed the SiC layer.

Several heating experiments were dedicated to the study of fission gas release from failed particles. The reduced diffusion coefficients determined from these experiments can be used in diffusion models to calculate the gas release.

The **HRB model** of describing the fission gas and iodine release behavior from defective particles during temperature transients is coded in **TRAGAS** [44]. This approach is also based upon the assumption that a simple diffusive transport is not sufficient. Iodine and xenon release data from the German irradiation and heating experiment FRJ2-P28 have been interpreted as a rapid emission from traps in kernel and buffer material, the latter being loaded by recoil from the kernel surface layer. The equation of the fractional release during temperature transients is characterized by two empirical functions, a temperature and time dependent parameter describing the gradual emission from traps and a temperature dependent fraction which escapes the traps in a burst. The burst function due to the recoil release was found to be also dependent on burnup.

The **KFA diffusion codes FRESCO-I and -II** do not contain a trap model for gases in the particle kernel, but instead use a diffusion coefficient for each species consisting of a high temperature and a low temperature branch with different activation energies. This approach conservatively covers the experimental results.

4.1.1.4.4. Fission Product Transport within the Core Cavern

Fission product retention mechanisms in the **fuel element graphite** are very important for the release behavior from an HTGR core.

- Fuel element graphite serves as a release barrier, at least as a further delay for metallic fission products which either result from heavy metal contamination or have already escaped the fuel particles.
- Graphite surfaces in colder regions of the core cavern (active core, reflectors) offer sites to re-adsorb metallic fission products which were previously released into

⁶ It has been standard practice and supported by experimental evidence to assume that fission gases and iodine show a similar release behavior under accident conditions.

- the coolant. Adsorption processes are highly efficient at low coolant velocities in reducing the core release during a core heatup accident in a depressurized reactor.
- There is no significant holdup for fission gases and iodine released from defective coated particles nor an adsorption on graphite surfaces at elevated temperatures. However, gaseous fission products and iodine available from heavy metal contamination in the fuel element graphite are believed to be originally sited within the graphite grains. Thus, a slow transport mechanism is required for them to escape the grain before they are released in a rapid transport via the graphite pores.

There are several models available to describe the radionuclide transport in graphite and its ad-/desorption on graphite surfaces.

The two-dimensional KFA diffusion model FRESCO-I [37] was developed in order to calculate the fission product release behavior in the core cavern of a pebble-bed HTGR. Simple Fickian diffusion is assumed both in the matrix graphite of the fuel element and in the graphitic reflectors. The separate consideration of diffusion in the graphite grains and in the graphite pores as an uncoupled two-phase diffusion in the matrix graphite is optional.⁷ In both fuel element and reflector graphite, the consideration of concentration dependent transport data is possible. Concerning the small activity inventory in the graphite grains and in the carbon buffer layer of defective particles, a release by the "slow" diffusive transport to the inner graphite surfaces (grain boundaries) is considered only for lower temperatures < 1250 °C. For higher temperatures, a spontaneous release of this inventory is assumed due to lack of data. Main input data for a FRESCO-I calculation are fuel temperature and coolant gas flow transients, coating failure rates from PANAMA-I, fission product diffusivities and sorption isotherms of fission products on graphitic materials.

The HRB code GETMIX for modeling fission product release during accident transients is a combination of GETTER as a 1D diffusion model describing the release from coated particles and spherical fuel elements and KONVEK describing the 2D convective transport with the coolant flow through the core. As a special feature, GETMIX includes fission product sorption on side reflector surfaces. It was found, however, to be of minor significance since its reduction potential was not more than a few percent in HTR-500 accident scenarios. The RADAX code is used for predicting cesium deposition in the top reflector graphite under accident conditions [45].

While the original version of the Integrated Failure and Release Model for Standard Particles from 1985 completely neglected a retention of cesium in the graphite of the spherical fuel element, the revised version has made the attempt to derive a relation between cesium inventory in the graphite and the fast neutron fluence from German heating experiments [26]. A dependence on fast fluence alone does not seem to be realistic since heating temperature and time are generally expected to play a major role in determining the transport behavior in graphite [46].

The calculational result of a very low cesium release from the core of small-sized HTGRs due to an almost complete retention by chemisorption in colder graphitic regions remains true, if the experimentally detected deviations from the Fickian diffusion model

⁷ The approach of regarding fission product transport in graphite grains and in graphite pores as used in many calculation models is not quite consistent with the fact that most of the fission product inventory is found in the binder component which is not strictly graphite. A diffusion coefficient for the binder material has not been evaluated so far. In this aspect, the diffusive transport in matrix graphite is still unclear.

[47, 48] are taken into account. Concentration profiles of cesium in graphites with steep gradients near the surface have been found indicating that the diffusion mechanism could not be explained by simple Fickian diffusion, but rather required a **trapping diffusion model**. The trap model does not only consider diffusion sites but also traps within the graphite.

$$\frac{\partial c_D(x,t)}{\partial t} = D \frac{\partial^2 c_D(x,t)}{\partial x^2} - \mu c_D(x,t) + b m(x,t) \quad (4-2)$$

$$\frac{\partial m(x,t)}{\partial t} = \mu c_D(x,t) - b m(x,t) \quad (4-3)$$

where

$c_D(x,t)$ is the local concentration on diffusion sites [mol/m³]

$m_D(x,t)$ is the local concentration on trapping sites [mol/m³]

D is the diffusion coefficient [m²/s]

μ is the trapping coefficient [s⁻¹]

$$\mu = \mu_0 * e^{-Q_\mu / (RT)}$$

Q_μ is the activation energy [J/mol]

b is the emission coefficient [s⁻¹]

$$b = b_0 * e^{-Q_b / (RT)}$$

Q_b is the activation energy [J/mol]

The trapping rate in graphite is given by:

$$\Phi_t = \mu c_D \quad (4-4)$$

where Φ_t is the trapping rate [mol/(m³ s)].

The emission rate from traps is given by:

$$\Phi_e = b m \quad (4-5)$$

where Φ_e is the emission rate [mol/(m³ s)].

Values for μ and b and the activation energies Q_μ and Q_b have been experimentally determined for cesium at low concentrations in A3-3 matrix material [47]. The diffusion coefficient D of the trap model is correlated to the effective diffusion coefficient D_{eff} of the Fickian model by:

$$D_{eff} = \frac{D}{1 + \mu/b} \quad (4-6)$$

Within this model, the sorption equilibria (represented by the Henry coefficient α) of cesium on graphite are given by:

$$\alpha = \frac{c_{\text{gas}}}{m + c_D} \quad (4-7)$$

where c_{gas} is the cesium concentration in gas [mol/m³].

Calculations of sorption kinetics on graphite (initial cesium burden in graphite = 0) have been performed with the trapping diffusion model in comparison with the Fickian model using D_{eff} of Eq. (A-6). The results indicated that due to the activation effect in trapping, the overall sorbed amount of cesium in graphite at beginning of sorption is smaller in the trapping diffusion model than in the Fickian model by a factor of

$$f_r = \frac{1}{\sqrt{1 + \mu/b}} \quad (4-8)$$

However, this difference decreases with increasing cesium burden and goes to zero under equilibrium conditions.

In order to examine the influence of the trapping effect on the overall cesium source term in core heatup events, FRESCO-calculations have been performed with and without the factor $1/f_r$ applied to the experimentally (evaluated from sorption isotherms) determined Henry coefficient α . The results show that the cesium release out of the core cavern in core heatup events of the HTR-MODUL design is larger by a factor of < 8 if diffusion trapping is taken into account [49]. This factor represents an upper limit of the influence of the diffusion trapping for these particular accidents. The overall cesium release out of the core cavern still remains $\ll 10^8$ even with this factor and the increase by trapping diffusion remains insignificant from a radiological point of view. Therefore, it may be concluded that the usually applied Fickian diffusion model in graphite is a reasonable tool for safety estimations of small HTGRs. The KFA code **FALLDIF** [50] has been developed to solve the above diffusion equations for cartesian and spherical geometries.

TRAP is an **HRB model** to investigate sorption kinetics under accident conditions. Under the assumption of instantaneous adsorption/desorption equilibrium, the code solves the coupled set of differential equations of the trap diffusion model and is in good agreement with experimental data as has been shown for cesium profiles in A3 matrix graphite [45].

A particularly high sorption capability was found for the ungraphitized binder component in fuel matrix graphite [51]. An experimental validation of this retention under accident simulation conditions for gas flow, temperature, and concentration is under way at KFA. The extremely high retention has been calculated only for small-sized HTGRs with their low fission product concentrations in graphite, whereas in medium-sized HTGRs, graphite saturation (Freundlich regime) and chemical reactions like formation of CsI are expected to occur [52]. A very effective sorption process could be demonstrated in a

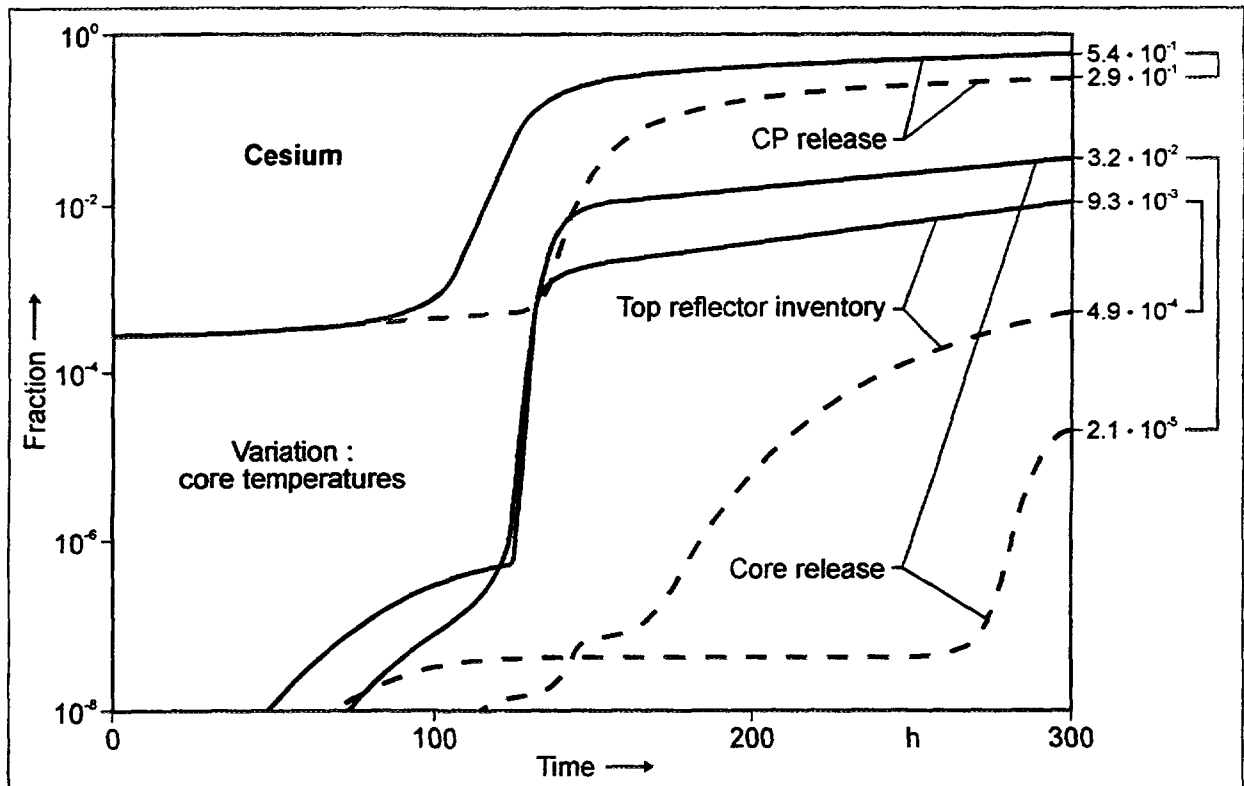


Fig. 4-19: Prediction of cesium behavior in the THTR-300 during a core heatup accident with a depressurization within 150 h. The variation of fuel temperatures was realized by assuming different decay heat functions in the thermodynamic calculations.

prediction of cesium behavior during a core heatup accident in the THTR-300 [53]. Fig. 4-19 shows the comparison of FRESCO-I calculations for two different accident temperature histories with maximum fuel temperatures of 2360 °C and 2080 °C, respectively. In the case of lower core temperatures, the matrix graphite provides a much higher potential of cesium sorption supported by the top reflector whose inventory gradually increases. This results in a significant cesium core release not until about 280 h into the accident. In contrast, for the case of higher core temperatures, the cesium concentrations in the graphite soon reach high levels such that sorption processes are not similarly effective to keep the core release level down.

Nevertheless, maximum accident temperatures up to 2000 °C might be possible without significant release of cesium and strontium from the core cavern up to 10 d into a core heatup accident, if credit is taken for this chemisorption [53]. This maximum temperature corresponds to a thermal power of about 600 MW [54]. Additional work on this question will be done in the future in order to optimize the concept of the HTR-MODUL.

With respect to iodine, only a limited potential for source term reduction by chemisorption on cold graphitic components exists in small HTGRs, as was indicated by FRESCO calculations using experimental sorption isotherms for the iodine/graphite system [55]. However, the extent of iodine sorption on graphite seems to be strongly influenced

by its impurity content [56]. Additional measurements are necessary in order to clarify the applicability of iodine sorption isotherms in HTR accidents.

A detailed description of fission product transport models for reactor graphite has been made in [57] including a proposition for an extended two-phase diffusion model comprising a concentration-dependent surface diffusion (see Appendix A.1.4.2.) and a gas phase diffusion which are coupled via sorption isotherms.

Models and data used for sorption on graphitic and metallic surfaces (as used in the FRESCO or SPATRA codes) can also be applied to calculations of temperature induced desorption from graphitic surfaces. Desorption from graphite is only important for the small amount of adsorbed iodine, whereas cesium and strontium are retained by the above outlined chemisorption on cold graphites. A core heatup accident does not lead to an overall increase but to an equalization of core temperatures. In most regions of temperature increase, the initial nuclide concentrations are far from saturation which, thus, does not lead to a major desorption.

4.1.2. Postirradiation Heating Tests in Japan

The performance of coated fuel particles and fuel compacts and the release behavior of fission products under accident conditions have been studied in Japan by means of out-of-reactor heating tests on unirradiated and irradiated samples [58, 59, 60, 61, 62, 63, 64], irradiation tests at very high temperatures [65, 66], and reactivity-initiated accident (RIA) tests in the Nuclear Safety Research Reactor (NSRR) [16, 66]. The heating tests on unirradiated [58, 59, 60] and trace-irradiated [61, 62] coated fuel particles and miniature fuel compacts revealed the behavior of the fuel at extremely high temperatures above 2000 °C, whose results and analyses were basis of the postirradiation heating tests. The postirradiation isothermal heating tests [63] were carried out to study the release behavior of fission products, whereas the postirradiation temperature ramp tests [64] were done to clarify the behavior of ultimate coating failure.

4.1.2.1. Equipment

The isothermal heating tests and the temperature ramp tests were done in a cold-wall graphite furnace installed in a hot cell, schematically shown in Fig. 4-20 [63]. The furnace is composed of a graphite heater, a graphite sample holder, graphite holder disks, and carbon insulators within a stainless steel vessel. The coated particles were individually placed in holes in the graphite disks. Each disk was X-ray microradiographed before and after heating. The temperature was read with a pyrometer viewing from the top and controlled with a programmable controller. The pyrometer readings were calibrated against the eutectics of palladium (1504 °C), platinum (1705 °C), molybdenum (2205 °C), and rhenium (2480 °C) with graphite [64].

During heating, the fission gas (Kr-85) release was monitored by an ionization chamber. It was confirmed that the number of burst events determined by the radioactivity measurement agreed with the number of failed particles determined by the X-ray micro-radiography after the heating [64].

4.1.2.2. Data of Fuel Samples

The TRISO coated UO₂ particles used in the tests were taken from two irradiated fuel compacts by electrolytic deconsolidation. The coated particles in both fuel compacts were fabricated in a batch. Table 4-7 [64] shows characteristics of the particles. One compact (sample A) was irradiated in a gas-swept capsule and the other (sample B) in a closed capsule in the Japan Materials Testing Reactor (JMTR). The irradiation conditions are shown in Table 4-8 [64]. The burnups of both fuels are 3.6 %FIMA which corresponds to the designed maximum burnup in the High Temperature Engineering Test Reactor (HTTR). The time-averaged irradiation temperature of sample B was 1510 °C which is higher than that of sample A (1250 °C). The release of short-lived noble gases was measured during irradiation in the gas-swept capsule (sample A); the release-to-birth ratio of Kr-88 was about

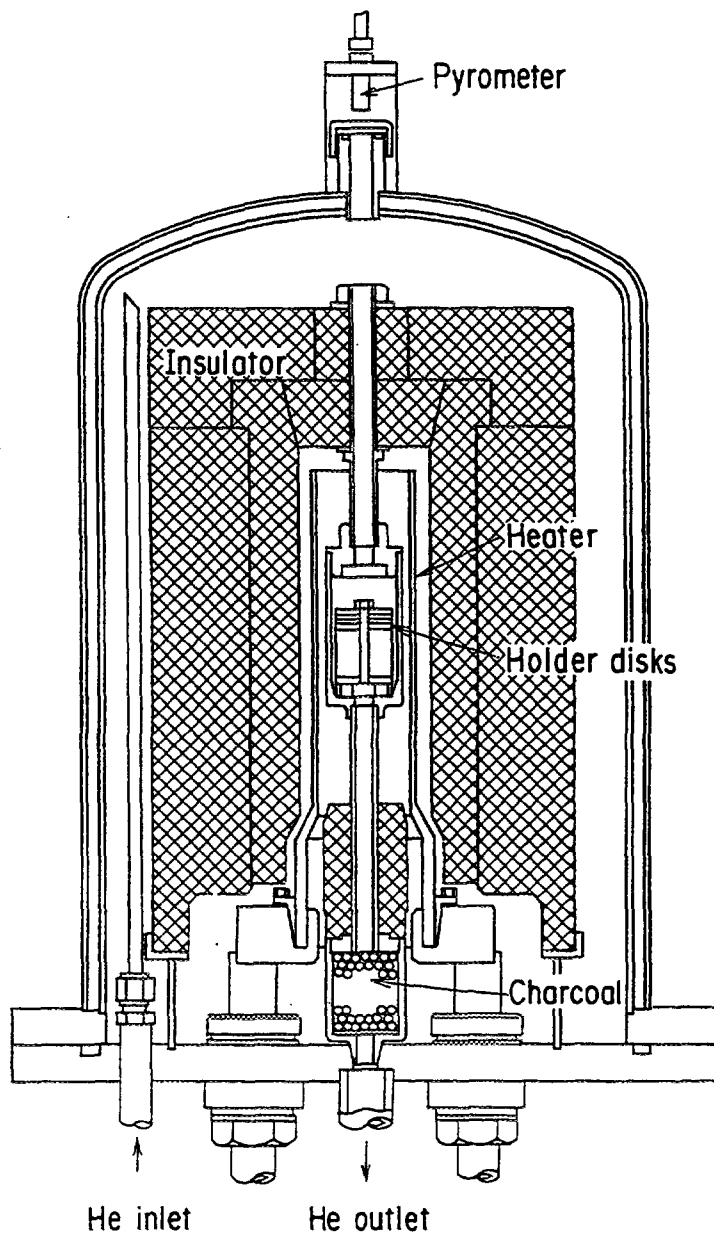


Fig. 4-20: Schematic representation of the furnace for postirradiation heating tests [63]

Table 4-7: Characteristics of coated fuel particles for postirradiation heating tests [64]

Particle	UO ₂ kernel		Buffer layer		Inner PyC layer		SiC layer		Outer PyC layer	
	Diameter [μm]	Density [Mg/m ³]	Thickness [μm]	Density [Mg/m ³]						
80FPC1	596 ± 34 ⁽¹⁾	10.5	59 ± 9 ⁽¹⁾	1.12	29 ± 4 ⁽¹⁾	1.86	24 ± 1 ⁽¹⁾	3.21	44 ± 6 ⁽¹⁾	1.83

(1) mean value ± standard deviation

Table 4-8: Irradiation conditions of samples for postirradiation heating tests [64]

Sample	Capsule	Compact	Irradiation conditions			
			Time [efph ⁽¹⁾]	Temperature [°C]	Burnup [%FIMA]	Fast fluence [10 ²⁵ m ⁻² , E>29 fJ]
A	80F-4A	80FP1A-1	1918	1250	3.6	2.6*10 ²⁵
B	80F-6A	80FP3A-7	2818	1510 ⁽²⁾	3.6	1.5*10 ²⁵

(1) Effective full power hours

(2) Maximum temperature was 1685 °C; irradiation above 1500 °C for 1512 h.

2×10^{-8} at the end of irradiation which indicates that the release was due to the contamination in the graphite matrix and no failed particle was contained in the fuel compact [67].

4.1.2.3. Results of Isothermal Heating Tests

The postirradiation isothermal heating tests were carried out at 1600 to 1900 °C. The heating conditions of the samples and experimental results are shown in Table 4-9 [63]. About 100 particles were heated in each test.

In all heating tests, no coating failure was detected by the Kr-85 release monitoring. X-ray microradiographs of the samples after the heating tests confirmed the results of the Kr-85 release monitoring. The ceramography of the samples showed that the coated particles heated at 1600 °C for 144 h were mechanically intact and the influence of the heating was hardly seen. It was seen, however, on the polished surface of the particles heated at 1800 °C for 48 h that the porous pyrocarbon layer was debonded from the inner PyC layer and the SiC layer was cracked in the radial direction at circumferential points; the cracks may have been introduced during polishing due to the release of the tensile stress in the SiC layer. No palladium attack and thermal decomposition of SiC was observed.

After each heating test, the graphite components of heater, sample holder and holder disks and carbon insulators were removed from the furnace and measured by γ -ray spectrometry to identify and evaluate the released metallic fission products. The nuclides of Cs-137, Cs-134, Eu-154, Eu-155 were detected. In some cases, Ag-110m was detected. Since the γ -ray analysis was conducted 6 - 9 years after the end of irradiation, relatively short-lived fission products could not be detected.

The measured fractional release for Cs-137 is shown in Fig. 4-21 [63] as a function of heating time and temperature. The diffusive release curves are also shown in the figure which were fitted to the measured points based on the diffusion model assuming a one-layer coated particle [68]:

$$F(t) = 1 - \left(1 + \frac{\gamma}{2}\right) \exp(-3\gamma D^* t) \quad (4-9)$$

where

F is the fractional release

t is the time

$\gamma = (R_o - R_i) / R_i$

R_o is the outer radius

R_i is the inner radius

$D^* = D / (R_o - R_i)^2$

D is the diffusion coefficient

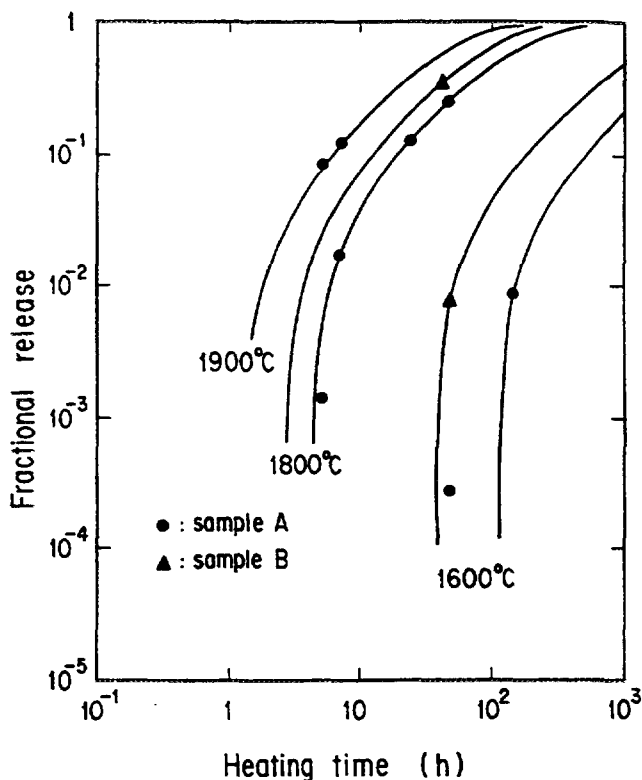


Fig. 4-21: Fractional release of Cs-137 during postirradiation heating as a function of heating time and temperature. Solid lines are diffusive release curves calculated by a simple diffusion model assuming a one-layer coated particle [63].

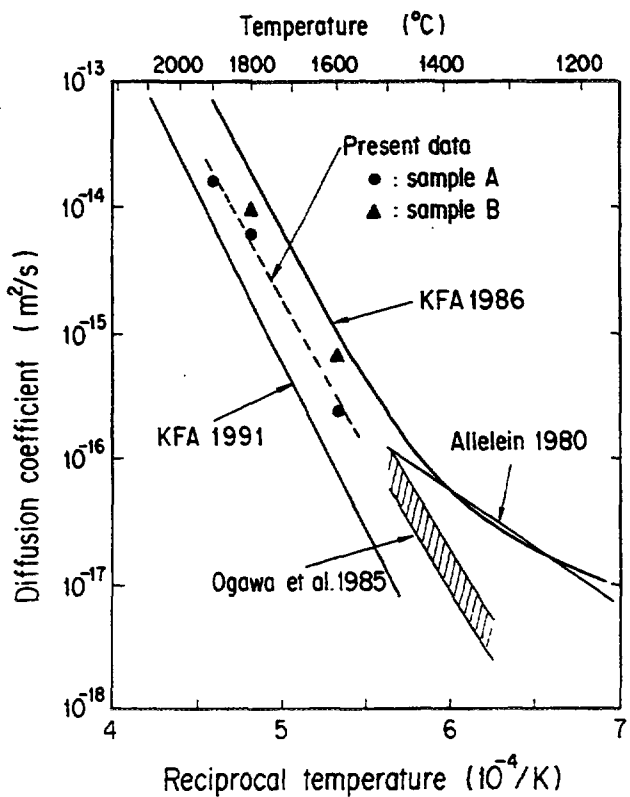


Fig. 4-22: Diffusion coefficient of Cs-137 in SiC as a function of temperature [63]. Data from literature are also presented for comparison; KFA 1986 [40], KFA 1991 [46, 69], Allelein 1980 [70], and Ogawa et al. 1985 [71].

Table 4.9: Results of accident simulation tests with irradiated coated fuel particles

UO ₂ TRISO coated particles	Burnup [%FIMA]	Fast fluence $[10^{25} \text{ m}^{-2},$ $E > 29 \text{ fJ}]$	Heating test		Fractional release			
			Temperature [°C]	Time [h]	Cs-137	Cs-134	Eu-154	Ag-110m
A	3.6	2.6×10^{25}	1600	5	1.7×10^{-4}	1.9×10^{-4}		
				48	2.8×10^{-4}	3.1×10^{-4}		
				144	8.2×10^{-3}	9.0×10^{-3}	6.7×10^{-3}	2.0×10^{-2}
			1700	5	2.3×10^{-4}	2.5×10^{-4}		
			1800	5	1.4×10^{-3}		6.7×10^{-4}	7.8×10^{-3}
				7	1.6×10^{-2}			
				24	1.3×10^{-1}	1.3×10^{-1}		
				48	2.7×10^{-1}	2.5×10^{-1}	4.4×10^{-2}	2.0×10^{-1}
			1900	5	8.6×10^{-2}	8.9×10^{-2}	1.4×10^{-2}	1.1×10^{-1}
				7	1.1×10^{-1}	1.2×10^{-1}		
B	3.6	1.5×10^{25}	1600	48	7.8×10^{-3}	7.3×10^{-3}	4.1×10^{-3}	1.7×10^{-2}
			1800	42	3.6×10^{-1}	3.8×10^{-1}	3.2×10^{-2}	

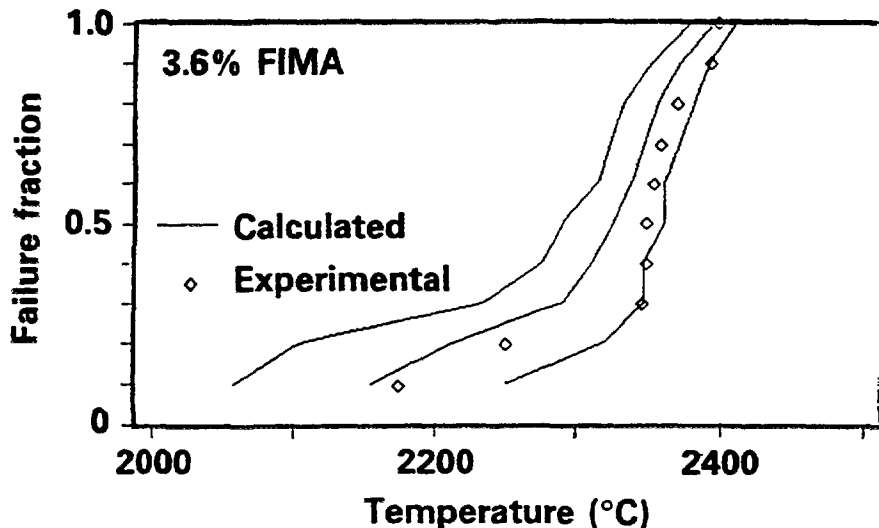


Fig. 4-23: Comparison of model predictions with a 1 °C/min ramp run on ten particles [64]

With this model analysis, a diffusion coefficient of Cs-137 in SiC was obtained as a function of temperature, as shown in Fig. 4-22 [63] where published data [40, 46, 69, 70, 71] are also presented for comparison. The resulting diffusion coefficient is described by

$$D_{SiC}(Cs\ 137) = 2.5 * 10^{-2} \ exp\left[-503 \frac{kJ}{mol} / (R T)\right] \frac{m^2}{s} \quad (4-10)$$

where R is the gas constant [8.3143 J/(mol K)] and T is the temperature [K].

The release of Ag-110m was measured only in the tests performed earlier after the end of the irradiation. The absence of Ag-110m in the other tests was partly attributed to the decay of Ag-110m ($T_{1/2} = 250.4$ d) below the detection limit. It is difficult to discuss the Ag-110m release behavior quantitatively, but it is safe to say that Ag-110m is released easier than Cs-137 at 1600 to 1900 °C.

4.1.2.4. Results of Temperature Ramp Tests

The postirradiation temperature ramp tests were performed at ramp rates of 1 and 5 °C/min. During the temperature ramp tests, the ultimate failure was judged by the burst of Kr-85 release, and the number of the burst events was confirmed by X-ray microradiography of the sample particles after the tests.

Fig. 4-23 [64] shows the result of a ten-particle run to 100 % failure at the ramp rate of 1 °C/min, where model-predicted curves are also shown for comparison. The upper and lower curves are one standard deviation above and below the mean. The model prediction agreed well with the experimental results.

Fig. 4-24 [64] shows the results of ramp tests at low failure fractions at a ramp rate of 5 °C/min. Sample B, irradiated at higher than normal temperatures, showed a slightly higher failure fraction than the prediction, but the difference is not considered significant in view of the error in the temperature measurement.

However, the agreement deteriorates for low failure fractions at a low ramp rate of 1 °C/min, as shown in Fig. 4-25 [64]. The experimental failure fraction was significantly lower than the model prediction. Inspection of the X-ray microradiographs and the ceramographic sections of the particles suggests that there was a significant delay between SiC failure and total coating failure. However, at higher temperatures, the expansion should be too rapid to give a noticeable delay. Hence, there was agreement between the calculation and experimental results in the ten-particle run shown in Fig. 4-23.

4.1.2.5. Modeling

4.1.2.5.1. Particle Failure

The **JAERI model** of simulating TRISO particle failure uses an approach similar to PANAMA-I with the SiC layer representing a pressure vessel [64]. The internal gas pressure is based on the Virial equations (expansion of the equation of state in terms of powers of T) describing non-ideal gases. In addition to fission gases, also alkaline earths, halogen, and tellurium species are expected to contribute to the pressure buildup in the particle. At the same time, fission-induced release of oxygen from UO₂ results in a large CO partial pressure. Free volume to take up the fission gases is made available by the porosity in the UO₂ kernel and in the buffer layer. The oxygen-to-uranium ratio which is dependent on the burnup, is estimated from thermodynamics resulting in a lower CO pressure than the theoretically maximum one. The stress induced by the internal gas pressure is compared with the SiC strength which follows Weibull statistics and failure occurs when they are equal. SiC strength is reduced by the porosity which is caused by thermal decomposition of the layer and is preferentially developed at grain boundaries of the SiC. A 4 % porosity in the SiC layer is considered to make it permeable to metallic fission products. The model includes the statistical variation of the normally-distributed particle fabrication parameters by adopting a random sampling method. SiC strength and thermal decomposition (or porosity increase) activation energy data for Japanese fuel particles have been derived from heating tests with both irradiated and unirradiated coated particles. These data exhibit much higher values than corresponding data for German and US fuel (see Appendix A.3.) which should be the subject of further detailed comparative analyses. Postheating examinations revealed a significant delay from the SiC failure to the total coating failure. Plastic deformation of the outer PyC layer after SiC failure results in a "ballooning" of the particle which reduces the inner gas pressure buildup, but makes the outer PyC permeable for fission gases at large stresses.

4.1.2.5.2. Fission Product Release

Two Japanese calculation codes are used to describe fission product release behavior under core heatup accident conditions. Besides the previously mentioned code **FORNAX** (see section 3.3.2.), the code **HTCORE** has been developed for HTTR safety evaluation purposes [72]. It is linked to thermohydraulics and nuclear design codes which provide

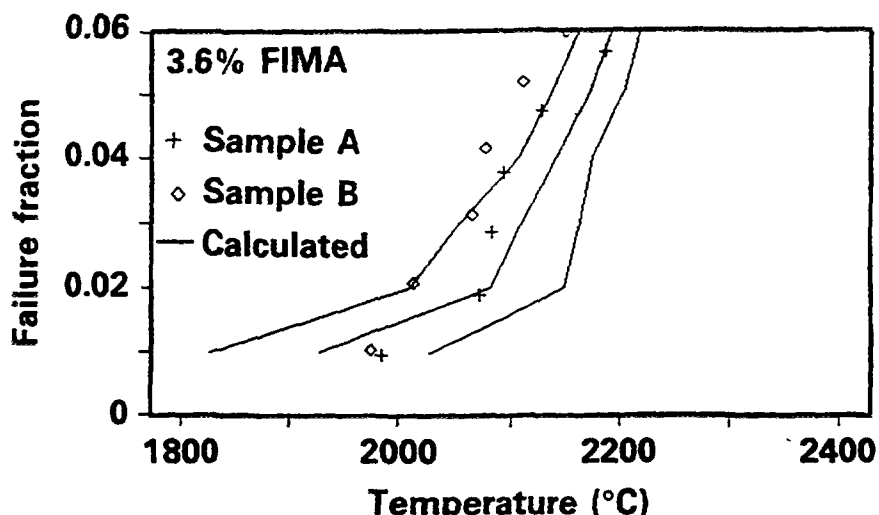


Fig. 4-24: Comparison of model predictions with 5 °C/min ramp runs on samples of about 100 particles each [64]

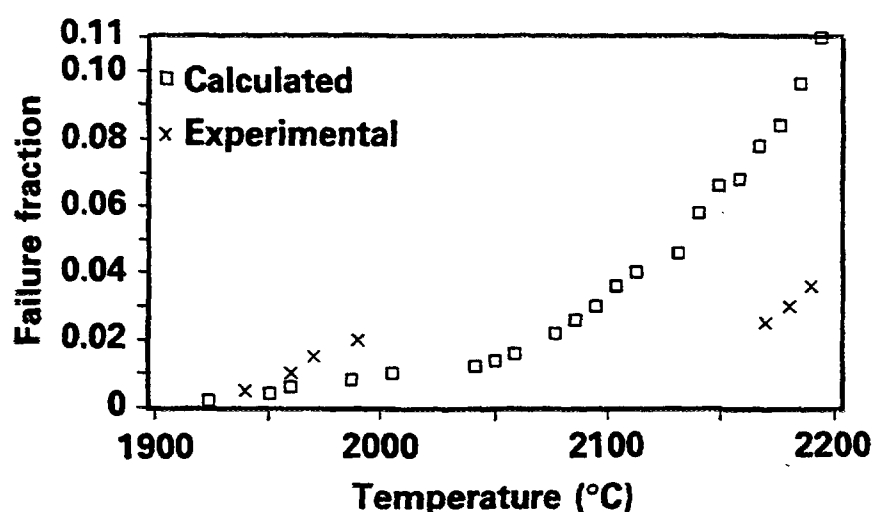


Fig. 4-25: Comparison of model predictions with a 1 °C/min ramp run on about 200 particles [64]

input data for fuel temperature and fission product inventories in the HTTR core. Empirical fission product release rates from the coated particles under HTTR depressurization accident conditions are taken from the GA code SORS as input data. Calculation steps of the HTCORE analysis are the release from the fuel region and diffusive transport through the graphite region into the coolant region. The comparison of model calculations for cesium with isochronal and isothermal heating test data up to 2200 °C have demonstrated a sufficient conservativeness of the code. A modification of the fuel region modeling is planned to allow for a more realistic approach. HTCORE is able to predict the noble gas

and iodine release from the HTTR core using the corresponding release rate functions from the SORS library.

4.1.3. Russian Federation

4.1.3.1. Experimental Work

The complex of post-reactor investigations is explained by the data given in Fig. 2-18 of chapter 2. Facilities for the annealing of irradiated fuel elements ("OSA") have been used for investigations, layer-by-layer scraping of the coated particle coating material, γ -scanning, etc. The results of some investigations are given in Figs. 4-26 - 4-33.

The influence of irradiation and heating simulating accident conditions on the tightness of coated particles has been experimentally investigated [73, 74]. Coated particles disintegrated from the fuel element which was irradiated in the PG-100 loop in helium containing oxidizing impurities (experiment KVG-3, 3 %FIMA, graphite corrosion loss \approx 80 g). have been examined up to UO₂ melting temperature (see Figs. 4-30, 4-31). After a layer by layer removal of the coating of the particles which had undergone postirradiation heating during 3 - 19 hours, it was observed that with increasing heating temperature the Cs-137 concentration in the SiC increased whereas it was reduced in the outer PyC layer (Fig. 4-32) [75].

4.1.3.2. Modeling

The **Russian Federation** employs a so-called "coated particle stress-strain state" model on a more empirical basis to calculate the circumferential stresses in the SiC layer which lead to its failure [76]. The analytical model equation includes dependencies on stresses upon the SiC layer from inside and outside, deformation, radiation shrinkage and elasticity. Experimental data on shrinkage and elasticity of matrix graphite as function of fast fluence and temperature are available from irradiation tests. Unknown model parameters such as shrinkage and elasticity of the outer PyC layer are formulated as polynomials whose constants are then obtained by correlating the equations with the experimental results.

A simple phenomenological model has been developed by the **Russian Federation**, called **activation model** [77]. Fission product release is treated as superposition of releases from two groups of species differing in the activation energy. The model is described in detail in section 3.3.1. and in Appendix B.

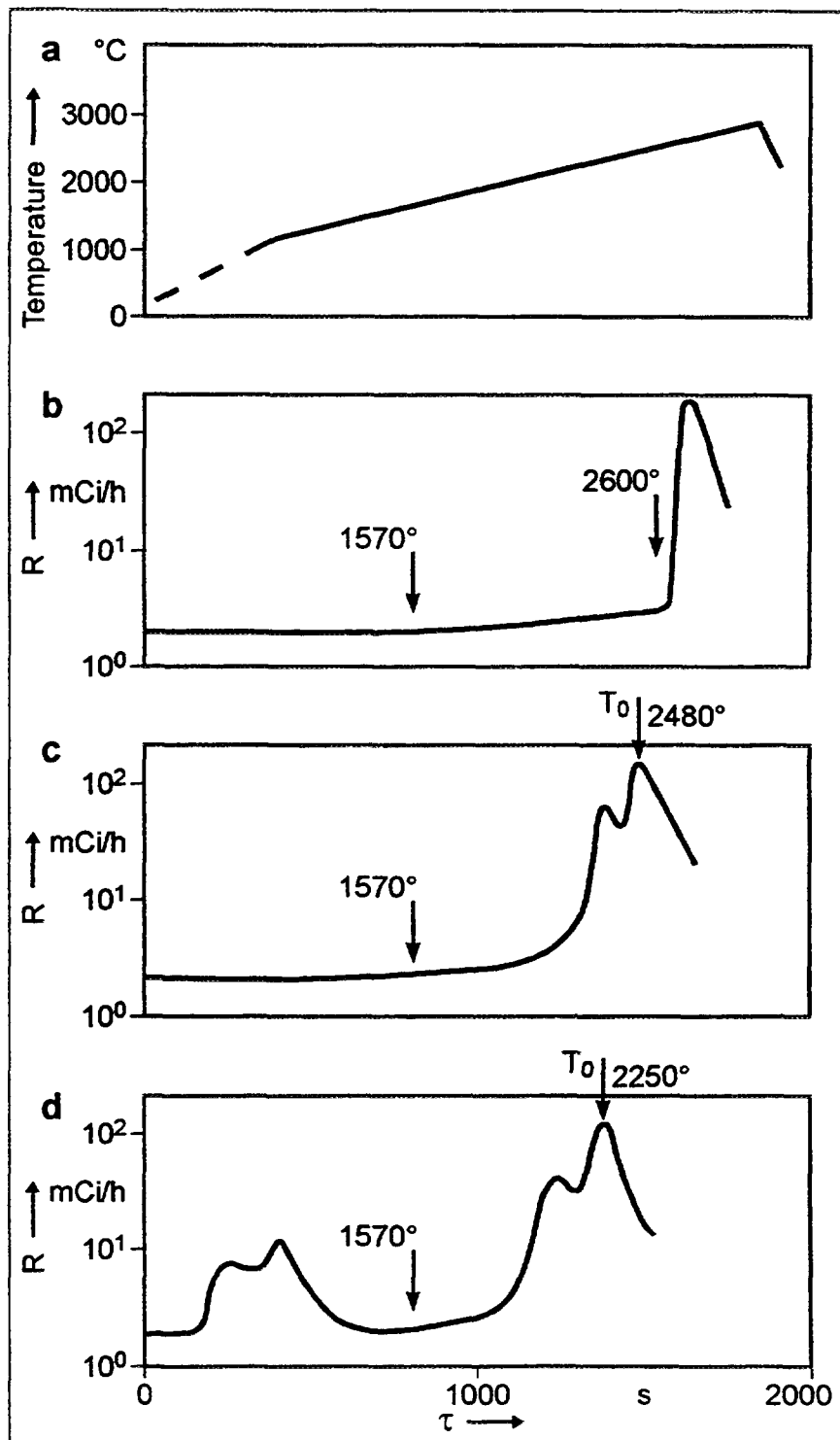


Fig. 4-26: Kr-85 release during the isochronous heating tests with coated particles (irradiated to a burnup of 3.8 %FIMA)

- Temperature regime
- Non-damaged coated particles
- Slightly damaged coated particles
- Severely damaged coated particles

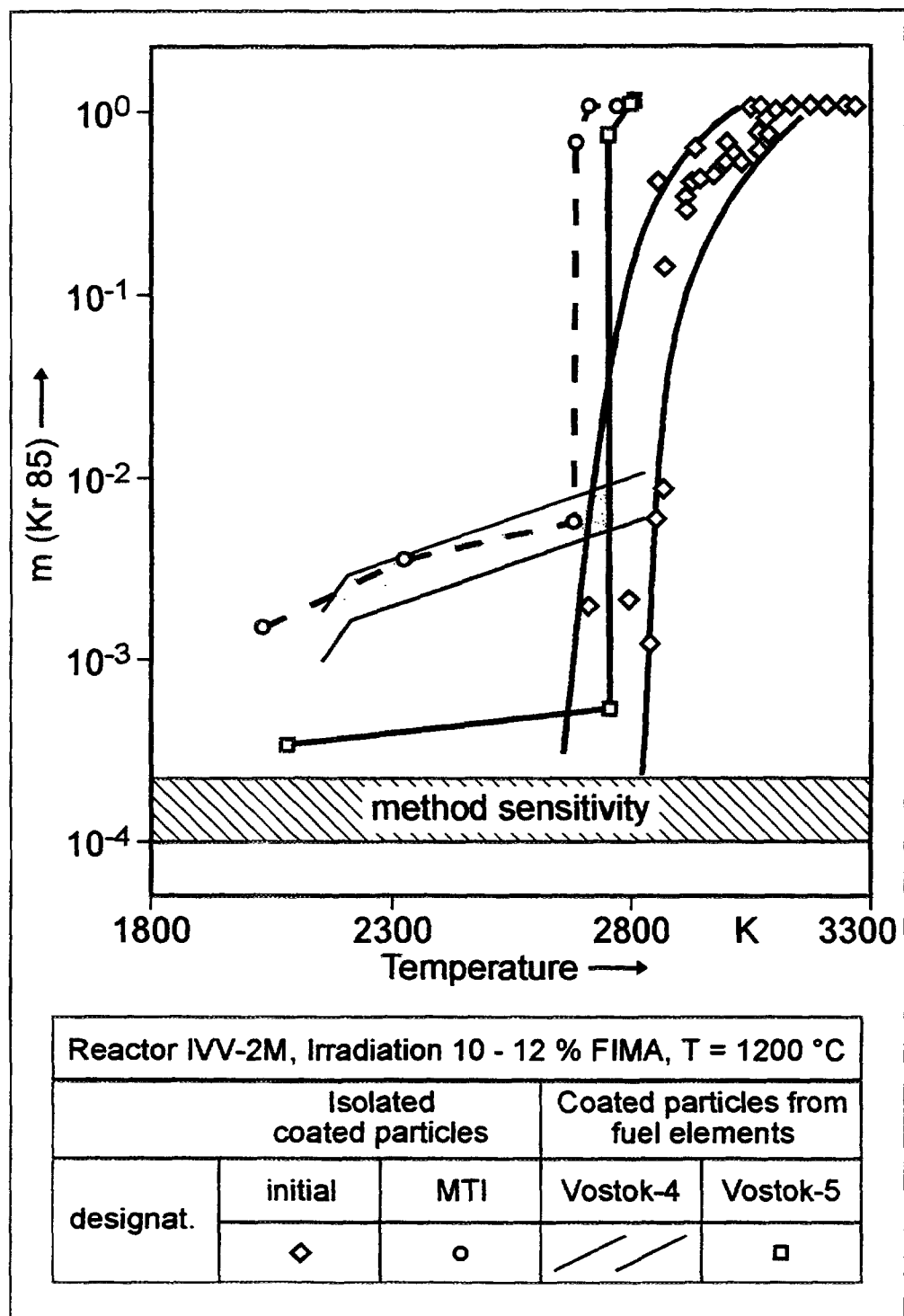


Fig. 4-27: Temperature dependence of Kr-85 release from coated particles

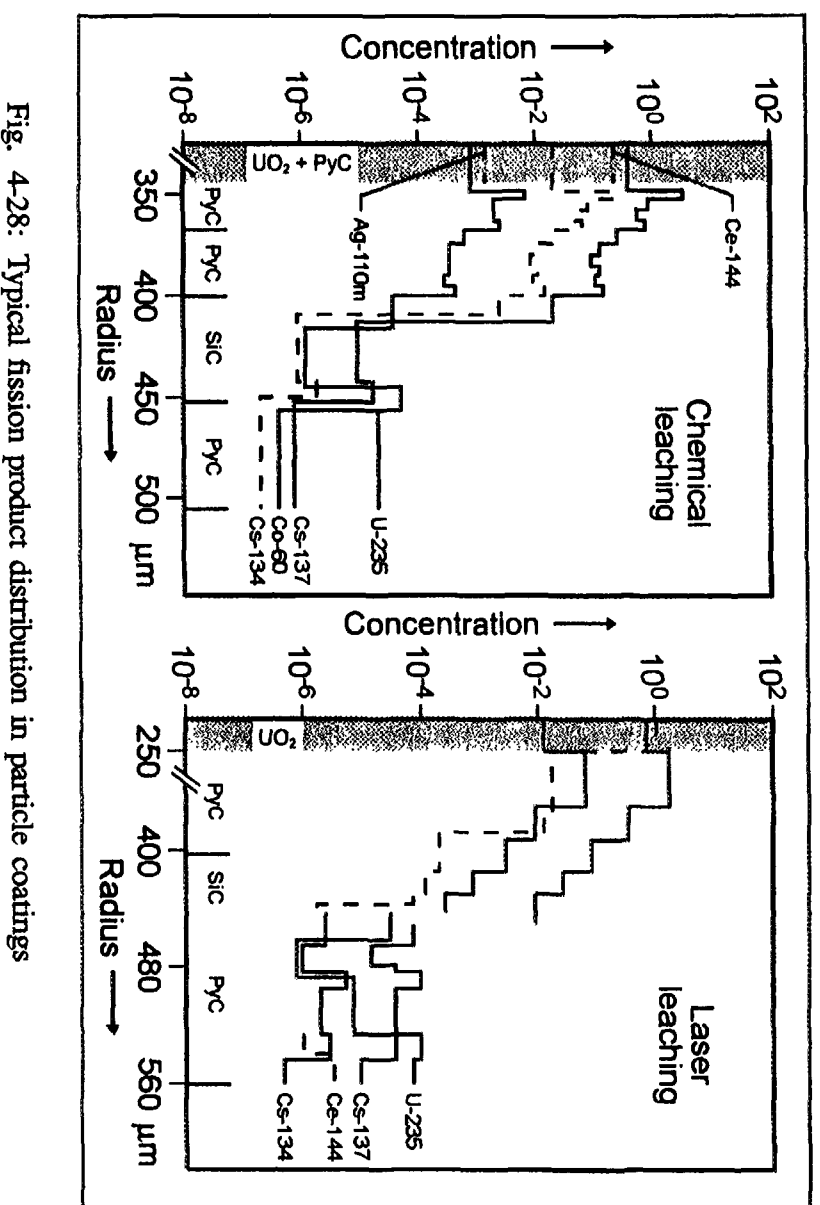


Fig. 4-28: Typical fission product distribution in particle coatings

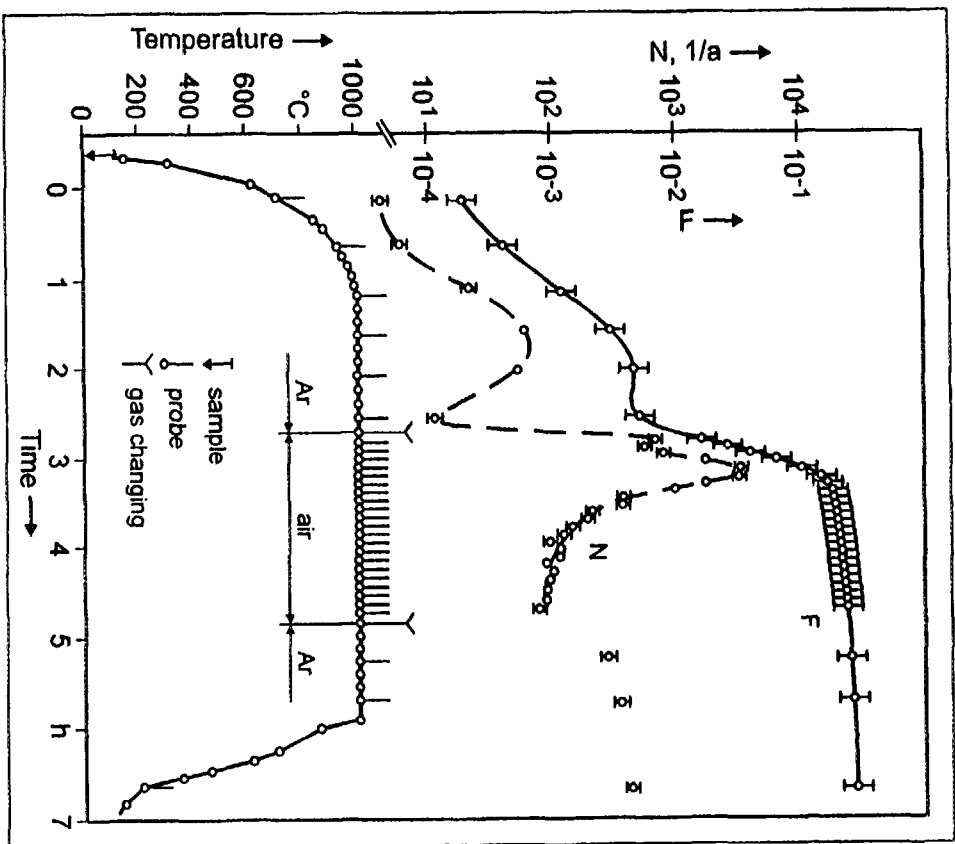


Fig. 4-29: Influence of air on the $\text{Xe}-135$ release from UO_2

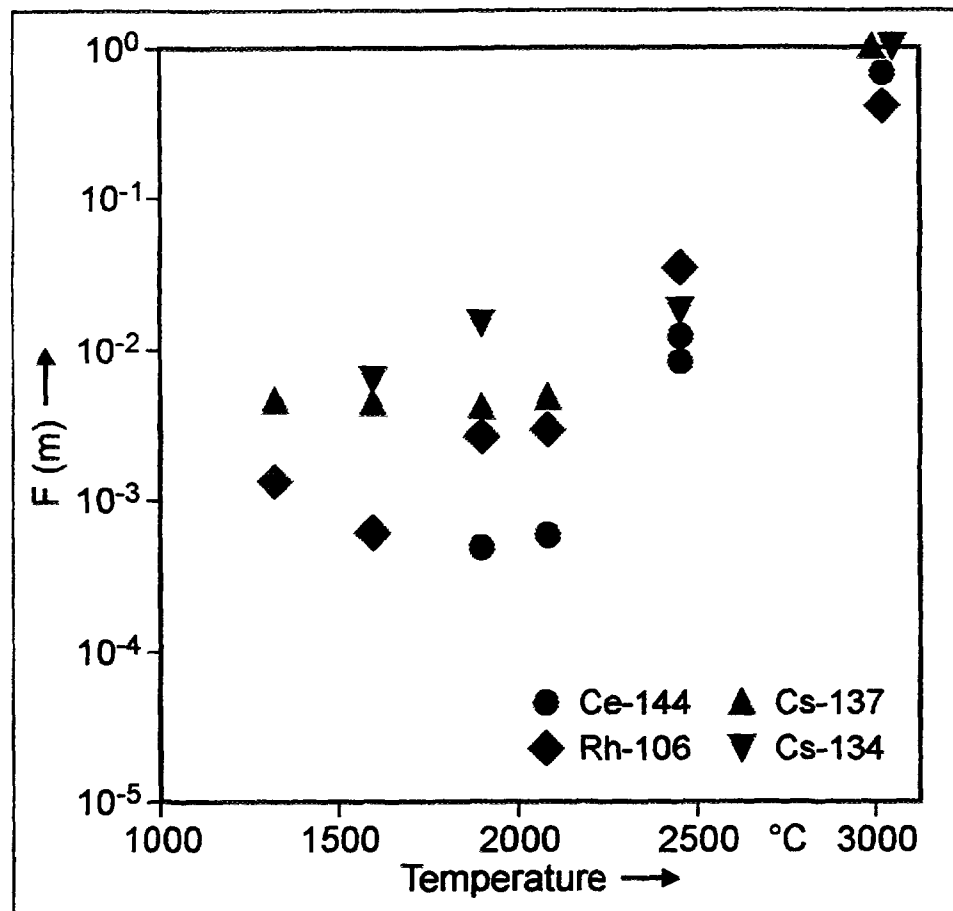


Fig. 4-30: Temperature dependence of metallic fission product release from coated particles

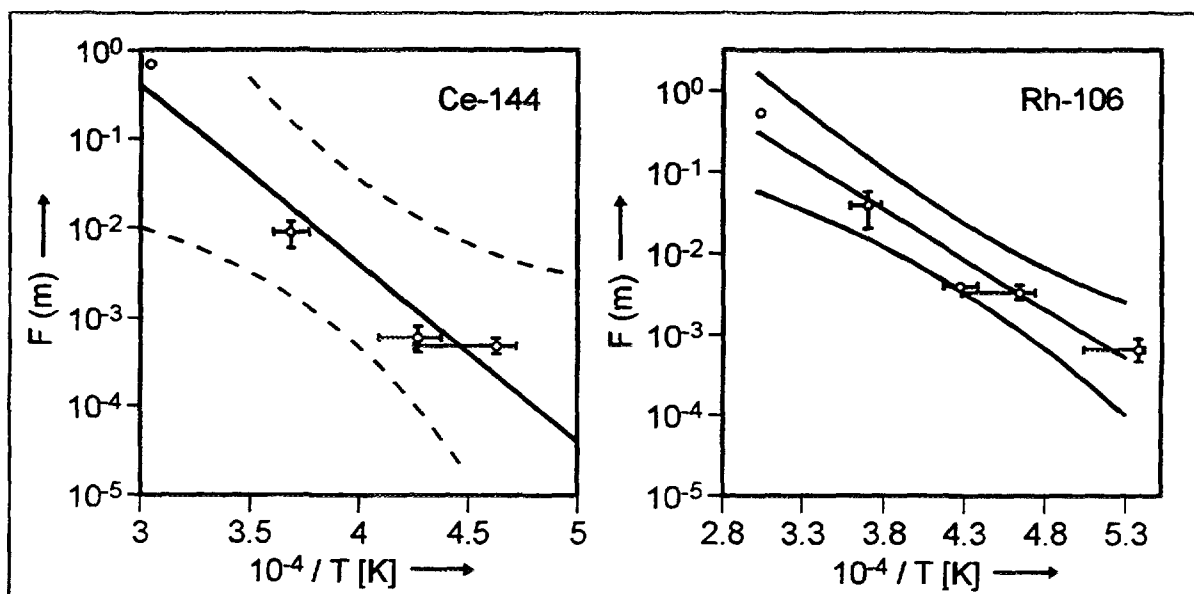


Fig. 4-31: Temperature dependence of metallic fission product release from coated particles

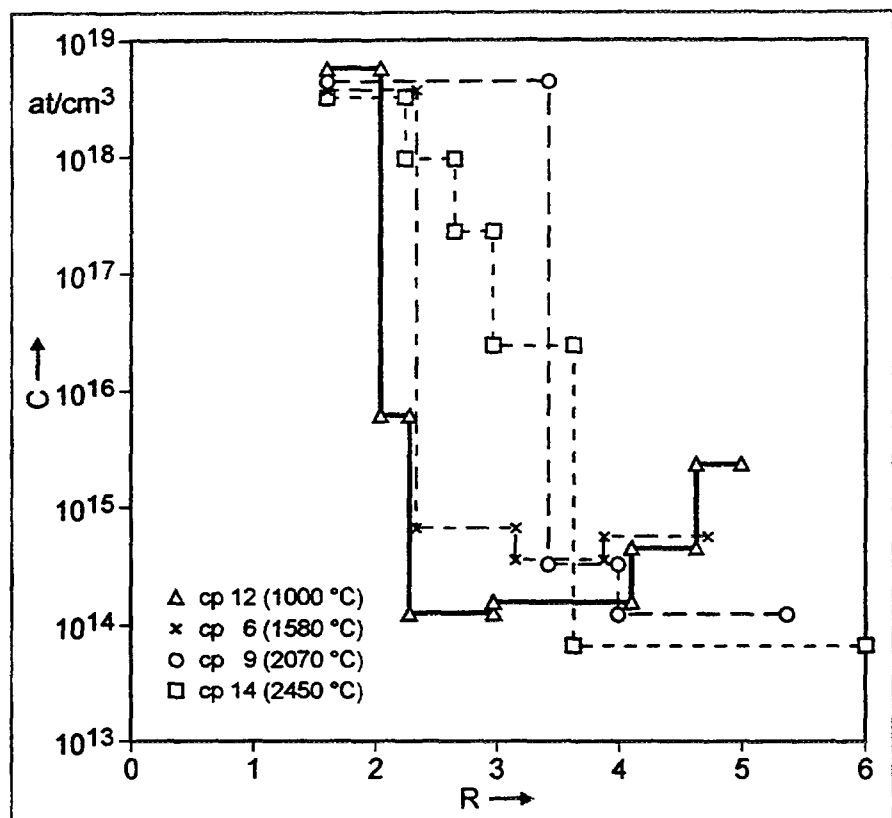


Fig. 4-32: Deformation of Cs-137 concentration profile after postirradiation heating

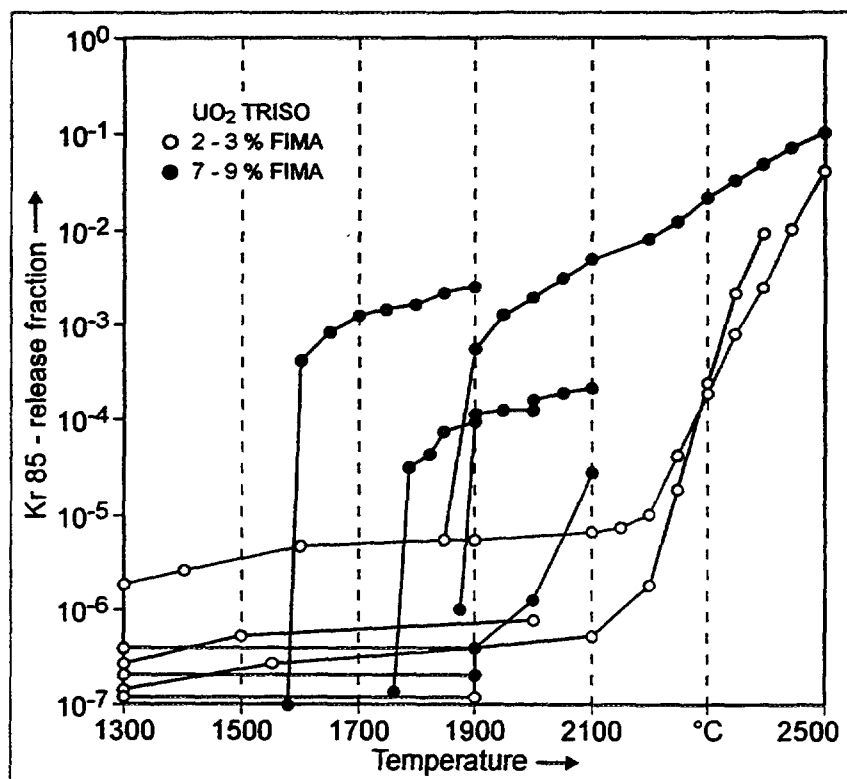


Fig. 4-33: Temperature dependence of Kr-85 release from coated particles [73]

4.1.4. Heating of Irradiated Particles in the USA

Work in the US related to the postirradiation heating of fuel particles has addressed the following: (1) design and construction of a high temperature furnace, (2) development of a model for transient fission gas release, and (3) postirradiation heating of intact particles to very high temperatures (2700°C).

4.1.4.1. The ORNL Core Conduction Cooldown Test Facility

A Core Conduction Cooldown Test Facility (CCCTF) was designed and constructed at ORNL in 1992. The CCCTF is essentially a high temperature (800 to 2000 °C) furnace in which the release of gaseous and condensable fission products from gas-cooled reactor fuel is measured. The facility can be used at present to simulate fuel response to core heatup accidents under non-oxidizing conditions. Alteration of the CCCTF for use under oxidizing conditions, i.e., in the presence of water vapor or air, can be made, and prototyped hardware for tests under these conditions has been fabricated. Components of the CCCTF [78, 79] as shown in Fig. 4-34 are:

- (1) A cylindrical furnace in a vertical orientation. A horizontal cross sectional view of the furnace would show a set of concentric tubular forms consisting of the water

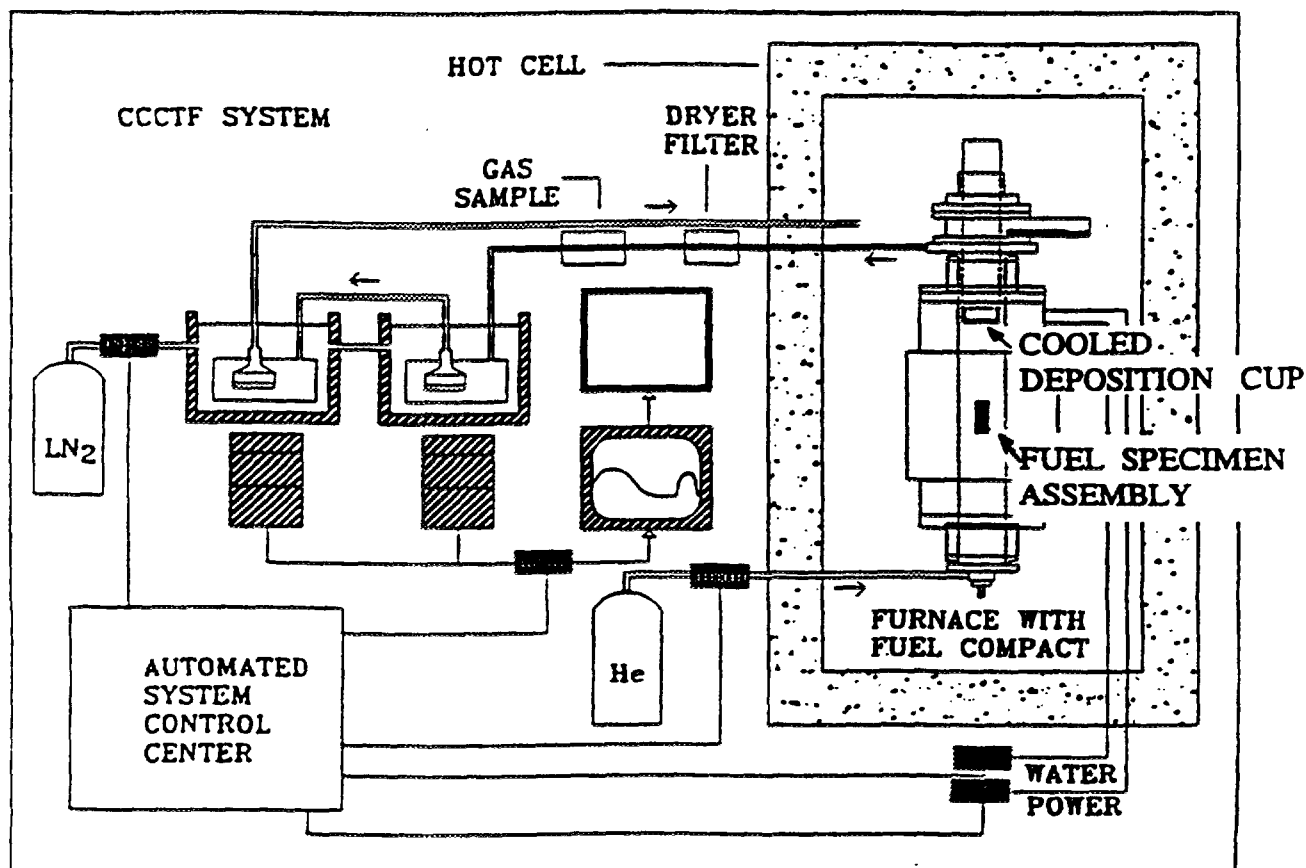


Fig. 4-34: Core Conduction Cooldown Test Facility (CCCTF) Remote Installation Layout

cooled, outer furnace wall and interior to it, followed in order by an insulation pack, a shield, the graphite heating element, and a muffle tube in which the test sample, graphite holder, and carrier gas feed lines are affixed.

- (2) A muffle tube with a tantalum liner was used in the ORNL tests of the CCCTF whereas a tantalum can hung from the top furnace flange was used in later experiments (see section 4.1.4.1.2.). As configured and installed, the tantalum can prevented escape of condensable fission products. The external temperature of the tantalum was monitored with a boron graphite thermocouple, BGT, and by an optical pyrometer sighting the surface through a furnace window. The BGT response is used in controlling furnace operation. The specimen temperature was monitored by a tantalum sheathed type C thermocouple located at the mid-plane of the fuel.
- (3) A cooled deposition cup assembly provided a copper surface at temperatures well below the specimen test temperature. The released, condensable fission products were primarily adsorbed on the cup. The deposition cup was attached to a water cooled support cylinder which was remotely raised and lowered to fixed positions. Thus, was the geometry of the cup with respect to the fuel specimen maintained. When removed from the furnace, installation and removal of the cup was by remote control rotation in one direction or the other to detach the exposed cup or to attach a new cup. During furnace operation, cups were removed and inserted with the aid of a radiation shielded hot cell and a remote handling system.
- (4) Outside the hot cell and downstream from the specimen, there are, in series, particulate filters, a moisture trap and two liquid nitrogen cooled charcoal traps; the latter two traps collect the released fission gas. The activity of the collected fission gas was measured using NaI(Tl) detectors and an associated electronic data handling system. Maintenance of specified trap temperatures by liquid nitrogen was also controlled by computer operation.
- (5) Helium, the carrier gas, flows through an upstream purifier to reduce O₂ concentrations to less than 1 ppm. Flow is then divided and directed along two paths: (1) through the tantalum assembly and (2) through the portion of the furnace exterior to the tantalum assembly and including the cold finger airlock assembly. Thereafter, the total flow passes through the particulate filter and the moisture and cold traps and is then returned to the hot cell for further processing.

Prior to operation with a fuel specimen, the CCCTF was thoroughly decontaminated. Calibration tests with radioactive sources were performed, following shake down tests [80] conducted to determine system performance. The facility has performed many tests with fuel at temperatures up to 1800 °C. The longest test was operated for 1000 hours continuously at 1600 °C with HTGR fuel in which all subsystems performed as designed. All tests were conducted with computer control for full automation requiring minimal interaction with operators. Overall control and online data collection within user-specified limits include sequencing from furnace initial conditions to purge and fill operations, temperature ramp rates and hold points to target temperature, generation of time profiles of temperature probe measurements, and continuous upgrade and display of operational data. Similar computer control of fission gas traps and data collection include a time record of fission gas collection using a dedicated multichannel analyzer and data collection and storage. Liquid nitrogen flow in the traps, and thus the temperatures were regulated

by computer control. The NaI detectors monitoring the traps have a dedicated computer and storage system. In addition, instrumented control of recirculated chilled water and carrier gas flows at selected locations were monitored. Also, a number of safety features independent of the experiment, such as termination upon power loss and over current limit control, are operator determined. Overall shielding of γ radiation is sufficient for heating specimens with a total activity of 3 Gy⁸.

4.1.4.1.1. Trial Experiments with the CCCTF

Two successful experiments [81] were conducted with the CCCTF on HRB-17 and HRB-18 HEU TRISO UCO unbonded, irradiated particles. Eighty particles each were heated at 1400 and 1600 °C for 300 and 100 h, respectively. In both experiments, there was initially a rapid transient release and thereafter a slow, roughly linear release of the Cs-137 and Cs-134. At 1400 °C the slow release was very small and difficult to measure. Also measured was Sr-90 release. No release of fission gases was detected. The transient release was ascribed to contamination of the particle coatings resulting from prior irradiation in a closed container with “designed-to-failed” particles.

4.1.4.1.2. JAERI Accident Condition Testing in the CCCTF

The following is a preliminary description and comments regarding the accident condition tests performed on fuel particles irradiated in experiment HRB-22 and conducted with the CCCTF.

Four accident condition tests were performed for JAERI in the CCCTF using Japanese fuels irradiated in experiment HRB-22 in the HFIR. The objectives of the tests were to study the release behavior of fission gas and metallic fission products at accident temperatures. Table 4-10 shows characteristics of the TRISO coated fuel particles used in the tests [82]. The fuels were irradiated in the form of annular fuel compacts of 26 mm in outer diameter, 10 mm in inner diameter and 39 mm in length. In the accident condition tests, samples used were as-irradiated fuel compact and unbonded fuel particles after electrolytic deconsolidation of the fuel compacts. Table 4-11 shows test conditions including burnups of the samples. Target temperatures in the tests were 1600, 1700, and 1800 °C. During the tests, fission gas release was monitored by the ratemeter and multichannel analyzer, and metallic fission products released were collected by deposition cups followed by γ spectrometry.

Since the accident condition tests, ACT, were performed 11 to 17 months after the end of the HRB-22 irradiation, the samples still contained a good amount of Ag-110m, whose halflife is 250 days. Especially in ACT 3 and ACT 4, the goal was to measure diffusion coefficients of Ag-110m through intact coating layers. Although Ag-110m has been reported to be released through intact SiC coating layers, conclusive evaluation of Ag-110m release behavior could not be made with the limited, available data [71, 83, 84, 85].

The data obtained from the accident condition tests showed that Cs-137, Cs-134, and Ag-110m were released from the intact coated fuel particles. For example, fractional

⁸ The new unit for the energy dose is 1 Gray (Gy) corresponding to 1 J/kg absorbed energy or, in the former unit, 100 rad (radiation absorbed dose).

Table 4-10: Characteristics of TRISO coated fuel particles for accident condition tests in the CCCTF

Particle components	Diameter or thickness [μm]	Density [Mg/m^3]
UO ₂ kernel	544	10.8
Buffer layer	97.4	1.10
Inner PyC layer	32.9	1.85
SiC layer	33.7	3.20
Outer PyC layer	39.3	1.85

Table 4-11: Test conditions in the CCCTF

Test	Sample	Burnup [%FIMA]	Temperature [°C]	Time at temperature [h]
ACT 1	100 unbonded particles	6.7	1600	73.6
ACT 2	annular fuel compact	6.7	1600	222.2
ACT 3	25 unbonded particles	4.8	1700	270
ACT 4	25 unbonded particles	4.8	1800	222

releases of Cs-137 and Ag-110m heated at 1700 °C for 270 h in ACT 3 were 6.9×10^{-2} and 4.7×10^{-1} , respectively. The fractional release of Ag-110m was larger than that of Cs-137 in each test. The analysis of the fractional release data is under way to obtain the diffusion coefficients of Ag-110m and Cs-137 in the SiC coating layer.

The surprising results in the present tests obtained by IMGA measurements was that the release behavior of Cs-137, Ag-110m, and Eu-154 was quite different from particle to particle. In ACT 3 and ACT 4, inventories of fission products, including Ag-110m, in each particle were measured by IMGA before and after heating, so that the amounts of released fission products from each particle were obtained precisely. The result showed that one particle retained Ag-110m very well, while another particle released a large amount of it. The results of this kind were also obtained in the release behavior of Cs-137 and Eu-154. To understand this nonuniform behavior of fission product release from the coated fuel particles, further experiments are to be made at JAERI after the particles are transported from ORNL.

4.1.4.2. The US Model for Transient Fission Gas Release

A generic model for transient fission gas release from particles with exposed fuel kernels was developed by **Myers and Morrissey** [86] to provide (1) a means for predicting kernel release under the conditions of a core heatup event, (2) a basis for understanding

the mechanisms of release, and (3) a framework for incorporating experimental results. The exposed kernels were made by drilling a hole from the particle surface to the kernel surface. About 5 % of the kernel surface was thus directly exposed.

The development of the model is based primarily on the results of isothermal experiments at three temperatures in the range 1250 to 2060 °C. These results were used to evaluate the parameters of the isothermal model. Additional non-isothermal experiments, temperature rise experiments, provided a test for the model but required a refinement in the evaluation of the parameters at temperatures not sampled in the isothermal experiments. Model parameters that can be used to describe the release of xenon, iodine, krypton, cesium, and tellurium from ThO₂ and UC₂ were evaluated. As the model is generic, it can be used for UO₂ and UO₂ + UC₂ as well, provided isothermal experiments are conducted and analyzed. In both isothermal and non-isothermal cases, a fractional release function was inserted into a set of three differential equations to account for the release and decay of a nuclide and if necessary, its precursor.

The central feature of the model is a fractional release function which describes the release as a function of time and temperature. This function, as developed, is semiempirical but, as shown [86], is practically identical to a fractional release function which can be derived from a diffusion equation which accounts for trapping and release from traps.

4.1.4.2.1. Characteristics of the Model

The fission product release model developed has the following characteristics:

1. The fission product atom population for each nuclide is divided into two subpopulations as follows, (a) a subpopulation which undergoes a rapid, transient release from the fuel and (b) a subpopulation which is slowly but steadily released. The distribution of the atom population between the two subpopulations changes with temperature.
2. Subpopulation 1(a) is further divided into a large number of independent subsystems, each containing a fixed number of the fission product atoms of a specific nuclide. The number of subsystems changes with temperature.
3. As the temperature rises, the subsystems sequentially begin to migrate from their initial locations in the fuel and the fractional release profile for each subsystem is unfolded in time.

The first characteristic is related to the fractional release observed in isothermal experiments. The second and third characteristics are related to the temperature dependence of components of the fractional release function.

4.1.4.2.2. The Fractional Release Function at Constant Temperature

The representative fractional release profile for constant temperature is shown in Fig. 4-35. One component reflects transient release and the other, steady state release. This profile can be reduced to two components as shown in the figure. These components can be described in terms of the profile parameters t_0 , $t_{0.8}$, f_β , and S . The $t_{0.8}$ is the time at which the fractional release minus the contribution of the linear component reaches 0.8 f_β .

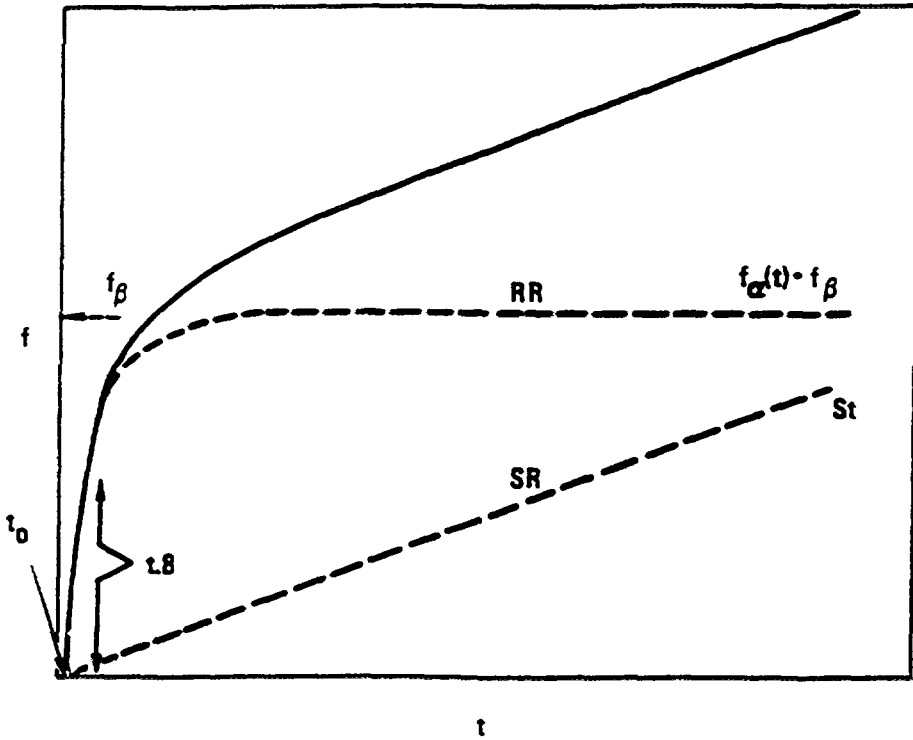


Fig. 4-35: Representative fractional release profile at constant temperature.

The component labeled RR in Fig. 4-35 represents a transient subpopulation (1(a) above) which is rapidly released from the fuel. This subpopulation is the fraction f_β of the total fission product atom population. The component RR is given by the product $f_\alpha(t)*f_\beta$ where $f_\alpha(t)$ is a function which describes the time dependence of the transient release fraction. The function $f_\alpha(t)$ is given by

$$f_\alpha(t) = \sqrt{1 - \exp\{-\alpha(t - t_0)\}} \quad (4-11)$$

where t_0 is the transit time from the furnace to the gas trap, and $\alpha = 1/t_{.8}$. Equation (4-11) has the limits $f_\alpha(0) = 0$ and $f_\alpha(\infty) = 1$. The functional form for f_α is justified by the solution of the diffusion equation including terms for trapping and release from traps [86]. The component labeled SR in Fig. 4-35 represents the subpopulation (of 1(b) above) which is slowly but steadily released. It is given by the product $S*t$ where S is the slope of the linear portion of the fractional release profile.

The sum of the components RR and SR gives the fractional release profile, i.e.,

$$f(t) = f_\alpha(t)f_\beta + St \quad (4-12)$$

4.1.4.2.3. The Temperature Dependence of the Fractional Release Function

The parameters of the fractional release profile f_β , α , and S have pronounced temperature dependencies. To represent the temperature dependencies of the fractional release profile functions, the following empirical functions have been used:

$$f_\beta = (1 - C) f_{\beta 1} + C f_{\beta 2} \quad (4-13)$$

$$f_{\beta i} = [1 + \exp \{ \beta_i (10^4/T - \tau_{\beta i}) \}]^{-1} \quad i = 1, 2 \quad (4-14)$$

$$S = S^\circ [\exp \{-\sigma/T\}] [1 - f_\beta] \quad (4-15)$$

$$\alpha = a_1 g_1 + a_2 (1 - g_1) \exp \{-\alpha_2/T\} \quad (4-16)$$

$$g_1 = (1 - C) f_{\beta 1} / f_\beta \quad (4-17)$$

$$\beta_i = Q_{\beta i} / 10^4 R \quad (4-18)$$

$$\sigma = Q_\sigma / R \quad (4-19)$$

$$\alpha_2 = Q_{\alpha 2} / R \quad (4-20)$$

where R is the gas constant.

The model parameters were evaluated on the basis of the temperature variation of the profile parameters by using Eqs. (4-13) through (4-17) and the profile parameter data from the isothermal experiments. Since the isothermal experiments were performed at only three temperatures, the temperature rise experiments were used to adjust the estimated values of two (C and $\tau_{\beta i}$) of the five model parameters associated with the profile parameter f_β . Also the quantity a_1 appearing in Eq. (4-16) may be temperature dependent; however, with isothermal experiments at just three temperatures, only the model parameters a_1 , a_2 , and α_2 could be evaluated. The values of the parameters are presented in Table 4-12.

The quantity f_β is fixed at constant temperature. This indicates that only a fixed number of atoms, called a subsystem above, can be released at that temperature by way of the mechanism governing the transient release fraction. If the temperature is incremented, f_β increases and then an additional fixed number of atoms becomes available for release. The increase in temperature provides the additional energy necessary to allow release of the atoms in the subsystem.

Subsystems which sequentially become available for migration are treated independently in the model and the release history is calculated for each subsystem. If, in the fuel material, the atoms are distributed similarly for each subsystem, then the release of the subsystems can be treated similarly except in accounting for the timing of release. In the model, such treatment is adopted.

4.1.4.2.4. Calculations of Release Based on the Model

The release is obtained by solving three differential equations in a form applicable to any nuclide and its precursor. Thus the equations can be written as:

$$\frac{d P_i}{dt} = -\lambda_p P_i - P_i \frac{df_p/dt}{1 - f_p} \quad (4-21)$$

$$\frac{d N_i}{dt} = \lambda_p P_i - \lambda_N N_i - N_i \frac{df_N/dt}{1 - f_N} \quad (4-22)$$

$$\frac{d N_r}{dt} = -\lambda_N N_r + \lambda_p P_r - N_r \frac{df_N/dt}{1 - f_N} \quad (4-23)$$

Table 4-12: Parameters of the fission product release model as a function of fission gas element, fuel material and burnup

Parameters		ThO ₂				UC ₂			
		1.4 %FIMA		15.7 %FIMA		23.5 %FIMA		74.0 %FIMA	
Profile	Model ⁽¹⁾	Xe	Kr	Xe	Kr	Xe	Kr	Xe	Kr
α	a_1	2.69	1.55	8.45	3.96	1.71	1.57	4.52	4.08
	a_2	6.03×10^5	5.57×10^5	3.36×10^6	1.12×10^6	1.82×10^{12}	7.02×10^{10}	1.0×10^{11}	3.09×10^{11}
	α_2	2.96×10^4	2.91×10^4	2.96×10^4	2.91×10^4	6.15×10^4	5.37×10^4	5.03×10^4	5.37×10^4
f_β	C	0.9917	0.976	0.94	0.94	0.99	0.985	0.99	0.98
	β_1	1.2	1.5	0.90	0.90	1.3	1.25	1.1	0.8
	τ_{β_1}	4.78	5.35	5.8	5.8	6.33	7.52	7.04	9.62
	β_2	11.81	11.81	11.81	11.81	10.3	10.3	10.3	10.3
	τ_{β_2}	4.51	4.59	4.69	4.66	5.35	5.41	5.41	5.47
S	S°	1.34×10^4	4.22×10^6	3.78×10^5	8.68×10^6	4.92×10^9	2.30×10^{12}	1.32×10^{10}	6.18×10^{12}
	σ	3.44×10^4	4.08×10^4	3.44×10^4	4.08×10^4	4.92×10^4	5.84×10^4	4.92×10^4	5.84×10^4

(1) The units of the model parameters are: [h⁻¹] for a_1 , a_2 , and S°; [K] for α_2 , β_1 , β_2 , and σ ; [10⁴/K] for τ_{β_1} and τ_{β_2} ; C is dimensionless

In the differential equations, N denotes a nuclide with a precursor P. If X represents either N or P then it follows that:

X is the atom population of the nuclide or the precursor nuclide in the kernel at time t

dX/dt is the rate of release of X [h^{-1}]

f_x is the fractional release at time t

df/dt is the rate of the fractional release

X_r is the atom population of the nuclide released from the kernel

dN/dt is the rate of release of X_r at time t

λ_x is the decay constant of the nuclide or its precursor [h^{-1}]

For the case of xenon release when the iodine precursor is important, the results of other experiments [86] are used; thus $f_N = f_P$.

The fractional release function enters into the solution of Eqs. (4-21), (4-22), and (4-23) through the evaluation of the quantity df/dt summed over the range $j=1$ to J. Thus

$$\frac{df}{dt} = \sum_j \left(\frac{df}{dt} \right)_{\alpha j} \Delta f_{\beta j} + S \quad (4-24)$$

where j is the subsystem index with values 1, 2, ... J,

$$\Delta f_{\beta j} = f_{\beta}(T_j) - f_{\beta}(T_{j-1}) \quad (4-25)$$

where $\Delta f_{\beta j}$ is the fraction of the fission product atom population in subsystem j; subsystem j is generated when the temperature is increased from T_{j-1} to T_j . The quantity $(df/dt)_{\alpha j}$ is evaluated on the basis of the expression, summed over k,

$$f_{\alpha j} = \sqrt{1 - \exp \left\{ - \sum \langle \alpha \rangle_{jk} \Delta t_k \right\}} \quad (4-26)$$

$$\langle \alpha \rangle_{jk} = [\alpha_j(T_k) + \alpha_j(T_{k-1})] / 2 \quad (4-27)$$

and k is the time step index with values 1, 2, ... K. The quantities f_{α} , α , f_{β} , and S of equations (4-24), (4-25), (4-26), and (4-27) have been defined in section 4.1.4.2.2. and Fig. 4-35.

In solving Eqs. (4-21), (4-22), and (4-23), the quantity $f_{\alpha j}(0)$ is set equal to a small, positive number to ensure a finite value of $df_{\alpha j}/dt$ at time zero. This quantity is set equal to zero when f exceeds 0.999 to avoid f values greater than 1.0.

The number of subsystems generated is related to the number of time steps in the computation (other methods are, of course, possible). For most of the calculations, a subsystem was generated for each time step; this corresponded to generating a subsystem for each 2 K rise in temperature when the model was used to predict fission gas release in the temperature rise experiments. The effect of generating a subsystem for larger temperature intervals has been examined [86].

4.1.4.2.5. Comparison of Model Prediction and Experimental Results

As an example, the agreement of the predictions and the experimental results is demonstrated in Fig. 4-36 for experiment 7240-78. Laser-drilled ThO₂ particles, having an exposed kernel surface area approximating the cross sectional area of the laser hole, were heated from 1250 to 2240 K in 4.83 h. The predicted and measured number of atoms released for the isotopes Kr-85m, Kr-87, and Kr-88 agree quite well. Furthermore, a mass balance is achieved. The measured number of atoms released and the number calculated as the difference between the initial inventory and the number of atoms not released are in agreement.

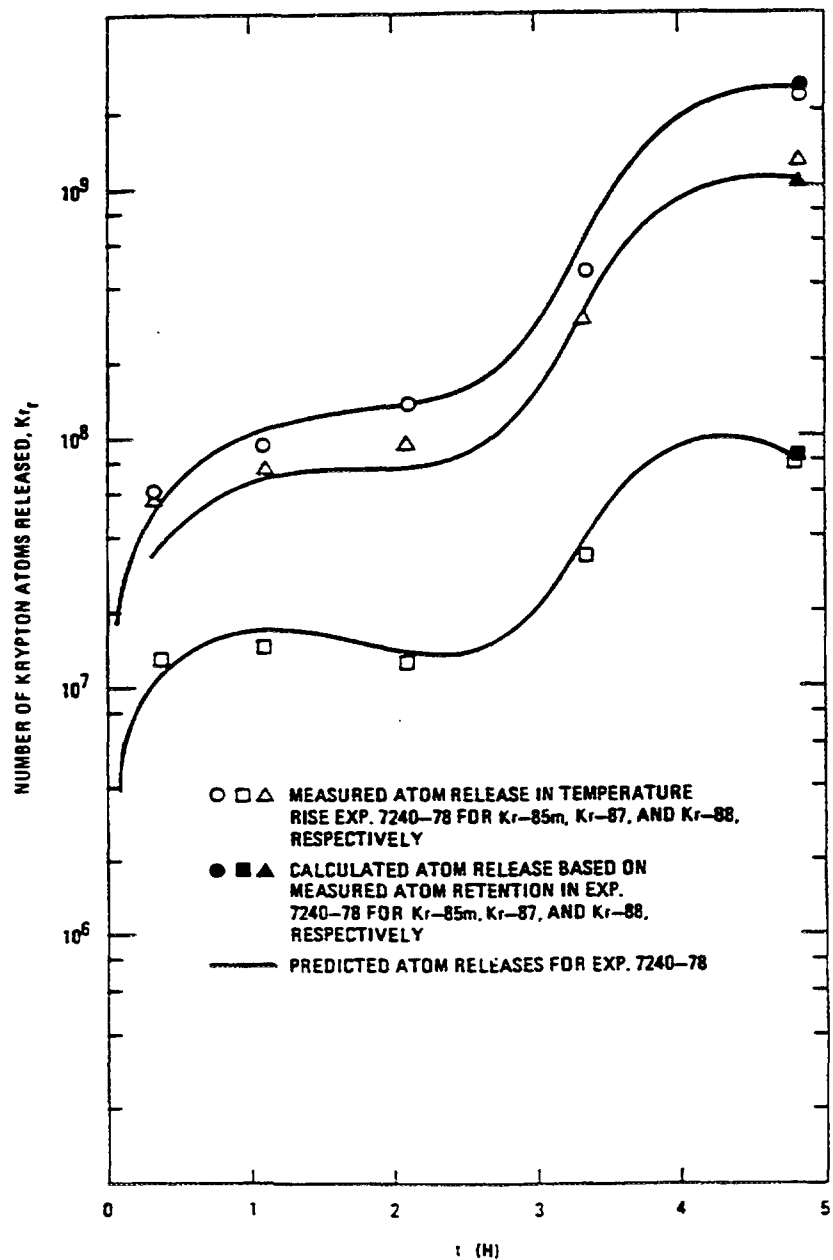


Fig. 4-36: Comparison of observed and predicted krypton release from laser-failed BISO ThO₂ particles with 15.7 %FIMA

4.1.4.2.6. Burnup

The experiments were conducted at only two burnups for each type of fuel. To determine the value of the model parameters at other burnups within the ranges of the set of two burnups, the parameters are grouped as (1) independent, (2) linearly dependent, and (3) non-linearly dependent on burnup. The necessary data are presented in Table 4-13.

4.1.4.2.7. The Theoretical Basis and Physical Interpretations

The diffusion equation with account of trapping and release from traps provided a strong basis for the physical interpretation of the experimental results. A number of physical interpretations were made [86]. As an example consider the following.

Comparison of the terms in the solution of the diffusion equation with account of trapping and release from traps with the semiempirical fractional release function, Eq. (4-11), leads to the correspondence

$$f_\beta \leftrightarrow 3L/a \quad (4-28)$$

where L is the diffusion trapping length and a is the radius of the fuel kernel, i.e., the characteristic diffusion length of the kernel. Thus f_β may be viewed as the ratio of the volume of a spherical shell of thickness L and the volume of the kernel. For $L \ll a$,

$$f_\beta = \frac{4\pi a^2 L}{4/3\pi a^3} = 3L/a \quad (4-29)$$

where f_β represents the fraction of the inventory in the kernel which lies in the spherical shell. Because escape from the spherical shell is facilitated by the lower probability of encountering traps in the shell, the release of fission products is perceived to have a transient component and also later, a significant steady state component.

4.1.4.3. The SHELL Model

The ORNL code **SHELL** [87] is a very simplified model describing the diffusive transport of fission products through a thin spherical shell for the case of a constant interior source of fission product(s). The model can be applied to intact fuel particles. When applied to irradiated fuel particles, the fission products already in the spherical shell and in locations exterior to the shell within the particle will affect the results. An analytical solution to the diffusion equation with an interior depleting source as well as a constant interior source is readily available [88]. Comparison of the two analytical solutions indicates the latter model is valid for fractional releases in the range 0.1 to 0.2.

Using the constant source model for the case of a SiC shell and cesium as the diffusant, coefficients agreeing with those derived from the much more complicated code FRESCO-II were derived.

4.1.4.4. The UT-KFA Model for Fission Product Release from Pebble Bed Fuel

The **UT-KFA model** was prepared as a cooperative effort between the Nuclear Engineering Department at the University of Tennessee (UT), Knoxville, TN, USA, and

Table 4-13: Recommended values of the model parameters

Parameters	ThO ₂				UC ₂			
	Xenon	Krypton	Xenon	Krypton				
<i>Independent of burnup, p = constant</i>								
α_2	$2.96 \cdot 10^4$	$2.91 \cdot 10^4$	$5.59 \cdot 10^4$ ⁽¹⁾	$5.37 \cdot 10^4$				
β_2	11.81	11.81	10.3	10.3				
σ	$3.44 \cdot 10^4$	$4.08 \cdot 10^4$	$4.92 \cdot 10^4$	$5.84 \cdot 10^4$				
<i>Linearly dependent on burnup, p = c + dF</i>								
	c	d	c	d	c	d	c	d
a ₁	2.13	0.403	1.31	0.169	0.403	$5.56 \cdot 10^{-2}$	0.402	$4.97 \cdot 10^{-2}$
a ₂	$3.33 \cdot 10^5$	$1.93 \cdot 10^5$	$5.02 \cdot 10^5$	$3.94 \cdot 10^4$	0.0	$1.84 \cdot 10^{10}$ ⁽²⁾	$6.15 \cdot 10^{10}$	$3.34 \cdot 10^9$ ⁽²⁾
C	0.9968	$-3.62 \cdot 10^{-3}$	0.980	$-2.52 \cdot 10^{-3}$	0.99	0.0	0.987	$-1.0 \cdot 10^{-4}$
β_1	1.23	$-2.10 \cdot 10^{-2}$	1.56	$-4.20 \cdot 10^{-2}$	1.39	$-3.96 \cdot 10^{-3}$	1.46	$-8.91 \cdot 10^{-3}$
$\tau_{\beta 1}$	4.68	$7.13 \cdot 10^{-2}$	5.31	$3.15 \cdot 10^{-2}$	6.00	$1.41 \cdot 10^2$	6.54	$4.16 \cdot 10^{-2}$
$\tau_{\beta 2}$	4.49	$1.26 \cdot 10^{-2}$	4.58	$4.90 \cdot 10^{-3}$	5.32	$1.19 \cdot 10^{-3}$	5.38	$1.19 \cdot 10^{-3}$
<i>Non-linearly dependent on burnup, S^o = S_o^o Fⁿ</i>								
S ^o	S _o ^o	n	S _o ^o	n	S _o ^o	n	S _o ^o	n
	$8.42 \cdot 10^3$	1.38	$3.82 \cdot 10^6$	0.298	$3.26 \cdot 10^8$	0.860	$1.51 \cdot 10^{11}$	0.862

(1) Average of values given in Table 4-12

(2) The value of a₂ at 23.5 %FIMA has been increased to avoid obtaining negative numbers with the recommended function for p (i.e., a₂)

the Institute for Safety Research and Reactor Technology at the Research Center Jülich (KFA, now FZJ), Germany. The UT effort consisted of the development and analysis of an improved fuel performance model for pebble bed reactor (PBR) fuels, while the KFA effort provided the fuel performance data, the initial version of the fuel performance model and its details, and extensive information concerning the experimental fuel tests, the results obtained, and their interpretation.

The UT effort consisted of two coordinated studies:

- (1) A study [28] which placed emphasis on: (A) Summarizing the detailed PBR fuel performance experiments and their results. (B) Developing a computer code for calculating the release of fission products arising from natural heavy metal contamination in the graphite matrix material (and applying it to the various fuel test results to determine the contamination required to give agreement between the calculated and the experimental results). (C) Studies with the FRESCO-II code to determine if relatively high diffusion coefficients associated with SiC coatings (equivalent to "intact" fuel particles plus a few particles with a high fission product diffusion coefficient) could account for the observed fuel performance; and (D) Applying the UT-KFA model to US MHTGR fuel particles and their associated testing results, to evaluate why the US fuel had poorer performance than the PBR fuel made in Germany.
- (2) A study [29] which placed emphasis on: (A) Revision of FRESCO-II to **FRESCO-R**, where a major difference was consideration of two types of PyC and SiC coatings in a batch of coated particles. Most of the coatings were treated as "intact", but a few coated particles had coatings with much higher diffusion coefficients. This could be broadened to treat a distribution of diffusion coefficients for a given coating material in a batch of fuel particles. (B) Revision of PANAMA-I to **PANAMA-R**, where major changes included treating a distribution of buffer and coating thicknesses in a batch of fuel particles; detailed analysis of SiC strength distributions and incorporating the distribution results in the pressure vessel failure model; and incorporating simplified diffusion calculations to estimate the diffusion of fission products through fuel coatings during heating tests. (C) Making use of the results obtained in the previous UT study to include the diffusion of fission products arising from matrix contamination; and (D) Extensive analyses of KFA experimental fuel performance data to determine how well the overall UT-KFA model could explain the experimental results.

The overall UT-KFA fuel performance model consists of three parts. Part I treats "contamination" effects, and calculates the fission gas release due to natural heavy metal contamination in the "grains" of the matrix graphite material, and to fuel contamination on or within the surface of the outer PyC layer. Part II calculates the fission gas release due to "pressure vessel" failure of the coated particles because of excessive gas pressure, including the effect of thickness variations in buffer and other coating layers on such failures. It also calculates diffusive release of krypton through Sic and outer PyC coatings during heating tests, based on simplified diffusion relations. It further calculates the effective "grain" contamination and effective grain diameter in matrix graphite required to give the time shape and level of Kr-85 release over birth ratio during the initial portion of the heating tests. Part III calculates the detailed diffusion release of fission products from the coated

fuel particles and from the fuel compacts. Diffusion through two classes of coated particles are treated: one class consists of "intact" coated particles, and the second class has high diffusion coefficient values in one more of the coating layers. The presence of only a few particles of defective layers (i.e., those with high diffusion coefficients) in a fuel batch containing nearly all "intact" coatings, can largely account for the observed release over birth behavior of fission products from a fuel element or compact.

Comparison of calculated and experimental results gave the following results: The release of fission products from the fuel elements / compacts during irradiation and during heating tests were controlled by: (1) The amount of defective fuel arising during fuel fabrication, (2) Diffusion of fission products through the coated fuel particles and through the matrix material; (3) Diffusion of fission products generated from natural uranium / thorium impurities in the graphite matrix material; and (4) Pressure vessel failures occurring during heating tests, particularly for AVR fuel exposed to very long irradiation times and high operating temperatures. SiC decomposition was not significant for nearly all tests; its effect was treated as a change in the thickness of the SiC layer. Kernel migration as a function of temperature gradients was also calculated, but found to be negligible for PBR fuels.

The UT-KFA model provides a technically sound, phenomenological basis for estimating the performance of Modular HTGR coated particle fuels under normal reactor and severe accident conditions, and was specifically applied to PBR fuel. For the PBR fuel, the model gave consistent agreement between calculations and experimental measurements over nearly all the broad range of parameters and test conditions evaluated in this study. Both SiC and PyC coating layers are important in obtaining high fuel performance. During reactor irradiation, the Kr-88 release is maintained at very low values by the integrity of the outer PyC coating layers. No pressure vessel type failures were observed during the irradiation tests. Very few pressure vessel failures of coatings were observed in the post-irradiation heating tests, and the number that occurred was consistent with the calculated number of failures using the UT-KFA model. The fractional release-to-birth (R/B) values of Kr-88 during irradiation were attributed to natural uranium / thorium contamination in the matrix graphite, and in some cases to fuel contamination of the outer PyC coating layers. The fractional release of cesium and strontium during reactor irradiation is attributed to high diffusion coefficients associated with one or perhaps a few SiC layers, which occurred because of either fabrication defects or damage during irradiation. During postirradiation heating tests, the fractional release of Kr-85, Cs and Sr is in general attributed to diffusion release; in a few cases, pressure vessel failure occurred and were in accordance with calculated values. The fast neutron fluence does not greatly reduce the mean strength of SiC, although there is a significant influence on the strength of the SiC "tails" (i.e., the relatively low fraction of coatings that have a relatively high probability of low strength). No significant interaction between the PBR graphite matrix and the coated fuel particles apparently occurred during irradiation and heating tests, for fuel having $< \approx 15\%$ coated particles by volume. Long fuel irradiation (≈ 3 years and longer) at high temperatures causes an increase in fission gas release from the fuel kernel during irradiation, giving pressure vessel failure in a number of coated particles during heating tests.

Further improvement in the UT-KFA fuel performance model should emphasize upgrading the FRESCO-R code to treat a distribution of defective SiC coatings within

a batch of coated particles.

Fuel R&D for further validation of the UT-KFA model should provide:

- detailed information on the nature of SiC coating defects occurring during fabrication;
- the performance of fuels irradiated for periods of time experienced in “real” PBRs;
- the strength distribution of outer PyC coatings in a large batch of coated particles, and the effects of fast neutron fluence on strength; and
- fission gas release of unfueled PBR spheres during irradiation and subsequent high-temperature heating, to confirm matrix contamination levels.

The relatively low performance of US MHTGR fuel appears to be due primarily to poor performance of outer PyC layers in US fuel, caused by excessive stresses in the outer PyC layers. A secondary reason is the lower strength of the “weak tails” for US SiC coatings relative to German SiC layers. There appears to be a need for substantially more R&D on US MHTGR fuel, in order to develop and validate fuel performance models.

4.2. IRRADIATION TESTING AT VERY HIGH TEMPERATURES (1500 – 2000 °C)

4.2.1. High Temperature Irradiation in Japan

The irradiation tests of fuel compacts at very high temperatures were performed to study the coating and fuel compact integrity under accident conditions.

4.2.1.1. Irradiation Capsules

The irradiation tests were carried out with three capsules (79F-1A, 80F-5A and 83F-2A) in the JMTR which were designed so as to make a temperature elevation during irradiation. In the capsule, a heat-transfer tube of metal (Nb-1%Zr) connected with a graphite tube in series could slide in the axial direction by gas pressure enforced from an outer equipment. During irradiation at normal temperatures, the graphite tube was located around the fuel compacts. At the last stage of the irradiation test, the graphite tube was replaced by the metal tube to make the temperature elevation.

4.2.1.2. Data of Fuel Samples

Model fuel compacts smaller than those to be used in the HTTR core were used in the irradiation tests. The compacts contained the TRISO coated UO₂ particles as well as the SiC-kerneled coated particles to adjust the linear heating rate. In each irradiation test, five fuel compacts were used.

4.2.1.3. Results of Irradiation Tests

The temperature history of the irradiation tests during the temperature transient is shown in Fig. 4-37 [65]. The fuel temperatures in 79F-1A and 80F-5A capsules were maintained at the average temperature of about 1200 °C under the normal condition, followed by temperature elevation up to about 1500 °C in the transient. In the 83F-2A

Table 4-14: Irradiation test conditions of samples at very high temperatures [65]

Capsule	Compact	Normal temp. [°C]	Transient temp. [°C]	Burnup [%FIMA]	Fast fluence [10^{25} m^{-2} , E>29 fJ]
79F-1A	79VHT	1197	1510	0.5	2.7×10^{23}
80F-5A	80VHT	1236	1520	1.0	9.7×10^{23}
83F-2A	83VHT	1373	2000	1.2	1.2×10^{25}

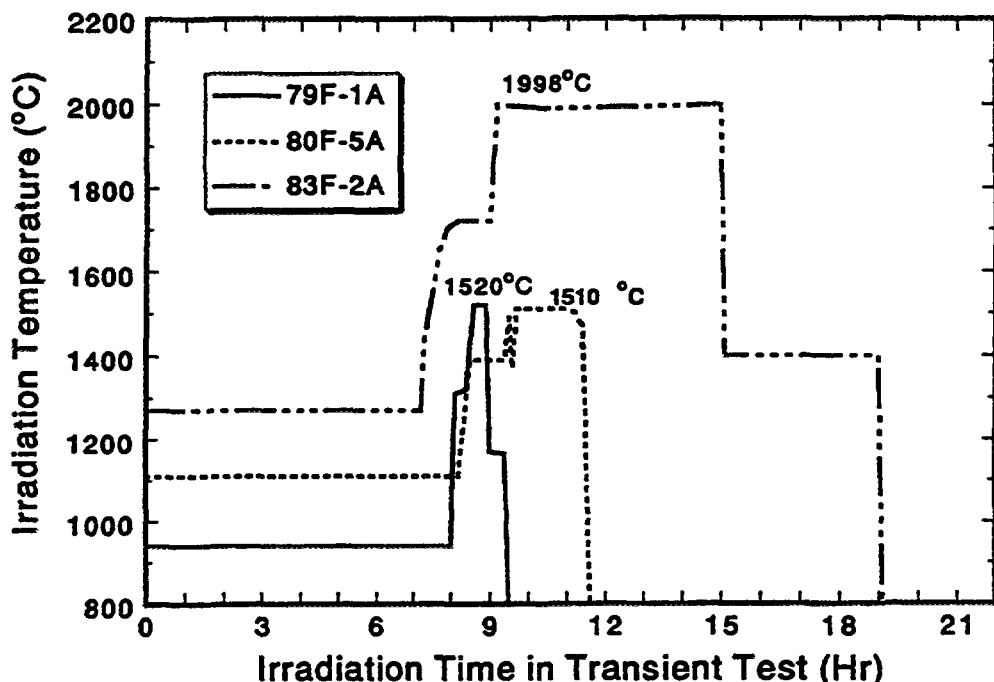


Fig. 4-37: Irradiation temperature history during temperature transient. The normal temperature shown before the transient is different from the normal temperature as listed in Table 4-14 because of very short duration [66].

capsule, the fuel temperature reached 2000 °C in the transient from the average temperature of 1373 °C under the normal condition. The irradiation conditions are summarized in Table 4-14 [65].

The visual inspection of the fuel compacts after the irradiation tests showed no change in the appearance of all the compacts. The dimensional change measurement of the fuel compacts indicated that the shrinkage of the fuel compacts was mostly in line with the previous results obtained from the normal temperature irradiation tests. Ceramography of the particles showed no intensive change. The pore formation in the SiC layer was not observed even in the particles of the 83F-2A irradiation test.

The failure fraction of the coated fuel particles was measured by electrolytical deconsolidation of the compacts followed by the acid leaching. Two or three compacts from each irradiation capsule were tested. In the 79F-1A capsule irradiation, the failure fraction after irradiation increased despite the fact that the transient temperature and duration were relatively low and short, respectively. The failure fraction was equivalent to one or two failed particles in each compact. This arose from the poor quality of the coated particles produced by an immature technology. Meanwhile, the particles in the 80F-5A capsule were not failed at all, implying the good performance under the transient condition tested. In the 83F-2A capsule irradiation, two failed particles were contained in each compact on the average which was obviously affected by the very high temperature.

4.2.2. High Temperature Irradiation in the USA

The behavior of intact, irradiated particles was studied during postirradiation heating from 1600 to 2700 °C as a function of burnup, neutron fluence and particle configuration for the isotopes of Cs, Ag, and Kr to yield a complete release profile [89].

4.2.2.1. Experimental Details

A simplified illustration of the experimental apparatus is shown in Fig. 4-38. The tests were conducted in flowing helium to ensure that released fission products were quickly transported to the traps. Mullite ($3\text{Al}_2\text{O}_3 \cdots 2\text{SiO}_2$) tubes were placed downstream of the test samples and maintained at 1100 °C to trap metallic fission products. As the helium and fission gases left the furnace, they passed through

1. a bed of copper oxide at 500 °C to convert tritium to water
2. a desiccant to remove the tritiated water
3. an activated charcoal bed to remove radon
4. ionization chambers
5. a liquid nitrogen cold trap to immobilize fission gases (xenon, krypton).

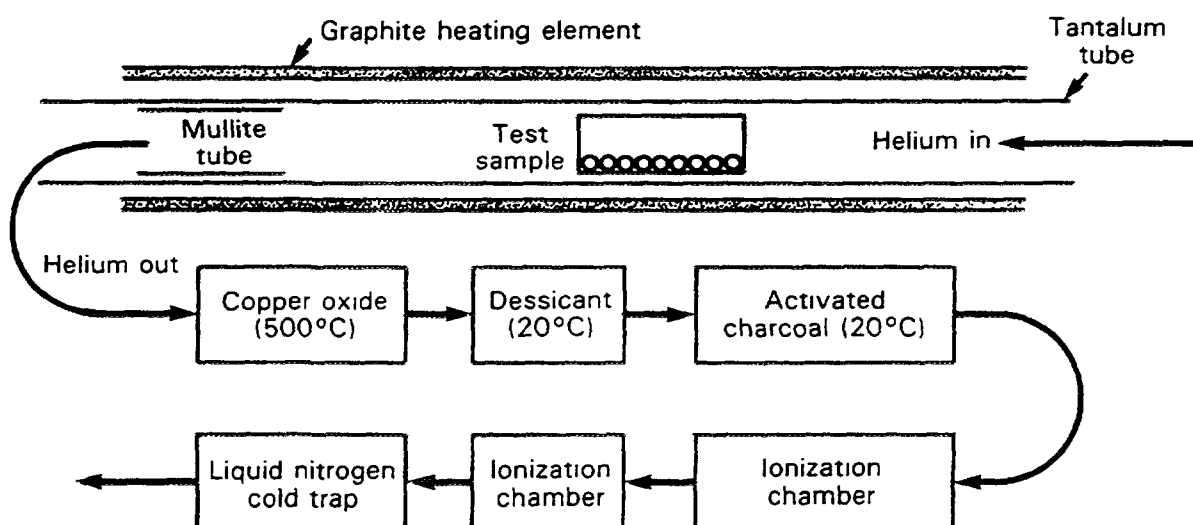


Fig. 4-38: Schematic of core heatup simulation test system used by GA to heat samples of 100 to 200 irradiated, unbonded particles

Upon completion of each test, the Kr-85 and metallic fission product release data were compared with pretest inventories to obtain the release fraction as a function of time and temperature. All of the tests were conducted many months after the end of irradiation, so only long-lived radionuclides were present.

4.2.2.2. Heating Test Results

Examples of fission product release results obtained at GA are shown in Fig. 4-39 with pertinent data given in Table 4-15. As discussed below, the evidence suggests that the controlling factor in the failure of TRISO particles subjected to the extreme conditions of these heating experiments is thermal decomposition of the SiC layer. This is consistent with the observations from heating of unirradiated particles at KFA, from heating of unirradiated fuel elements at HOBEG, and from heating of irradiated fuel elements at KFA.

Comparison of these release fractions from the individual GA ramp tests shows that performance is primarily dependent on time-at-temperature considerations and exhibits no significant correlation with other parameters routinely utilized to gauge the effects of irradiation damage upon fuel elements. For example, Fig. 4-40 examines the effect of kernel burnup on the performance of fuel particles with UC₂ kernels during ramp tests of three different heating rates, and no systematic correlation is observed. Likewise, Fig. 4-41 illustrates a similar comparison for ThO₂ fuels.

The lack of correlation of failure with burnup suggests a failure mechanism that is independent of the concentration of fission products in the kernel and of the internal pressure in the particle due to fission gases. This implies that failure does not occur by interaction of fission products with SiC or by a pressure-induced burst of coatings. Instead, failure under these extremely high-temperature conditions is dependent primarily on the thermal properties of the TRISO coating. Fig. 4-42 compares the relative performance of particles containing either oxide or carbide fuel kernels. The data are pooled together, disregarding the burnup and irradiation conditions as justified above. Fig. 4-43 illustrates a similar comparison between low-enriched uranium (LEU) (< 20 %) and highly enriched uranium (HEU) kernels. Considering that the kernel material controls a multitude of potential chemical effects within the particle that may influence the retention of fission products, the observed lack of systematic correlation strongly suggests that fission product retention is dependent only on the properties of the TRISO coating.

The above conclusion is supported qualitatively by postheating radiography and ceramography of the fuel particles. Contact X radiographs show the initially dense SiC layer being transformed into a low-density area as heating progresses (Fig. 4-44). The particles heated to high temperatures are characterized in the radiographs by dispersion of the fission products and/or heavy metal from the kernel into the buffer layer as well as thinning of the SiC. Ceramographic observations on the heated particles (Fig. 4-45) show that the intermediate stages of SiC failure are characterized by the development of a fairly uniform porosity throughout the SiC as well as cracks penetrating the entire layer. The outer PyC layers appear to be intact and, since pyrocarbon exhibits a slow diffusive release of fission gases, the particle is capable of retention of the radiologically important gaseous radionuclides even after SiC failure results in metallic fission product release.

Table 4-15: Data from irradiated TRISO-coated particles used in ramp tests to 2550 and 2500 °C (Release profiles are shown in Fig. 4-39)

Fuel Particle		LEU UCO TRISO with outer PyC	ThO ₂ TRISO without outer PyC
Irradiation Conditions	Burnup [%FIMA]	25.5	8.0
	Fluence [10 ²⁵ m ⁻²]	6.0	5.0
Heating Conditions	Temperature [°C]	2550	2500
	Time [h]	Ramp	Ramp
Fractional Release	Kr-85	1.0	1.0
	Cs-137	1.0	1.0
	Ag-110m	1.0	1.0
	Zr-95	0.28	0.28
	Ru-106	0.26	0.23

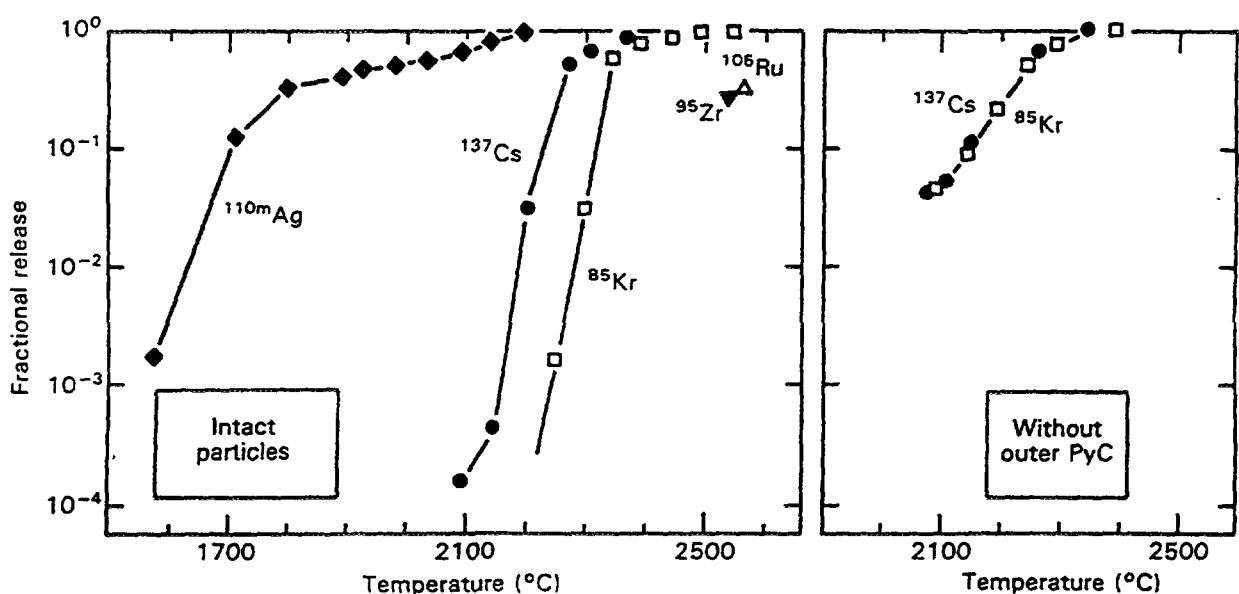


Fig. 4-39: Typical fission product release profiles during linear temperature ramp. In both cases, ≈ 200 irradiated particles were heated to 2500 °C. The left diagram shows intact particles, and the right diagram shows particles where the outer PyC layers had been removed.

4.2.2.3. Discussion of Experimental Results

As observed at GA in postheating radiography and ceramography, the crystalline material comprising the SiC layer of the TRISO coating has a reported tendency to

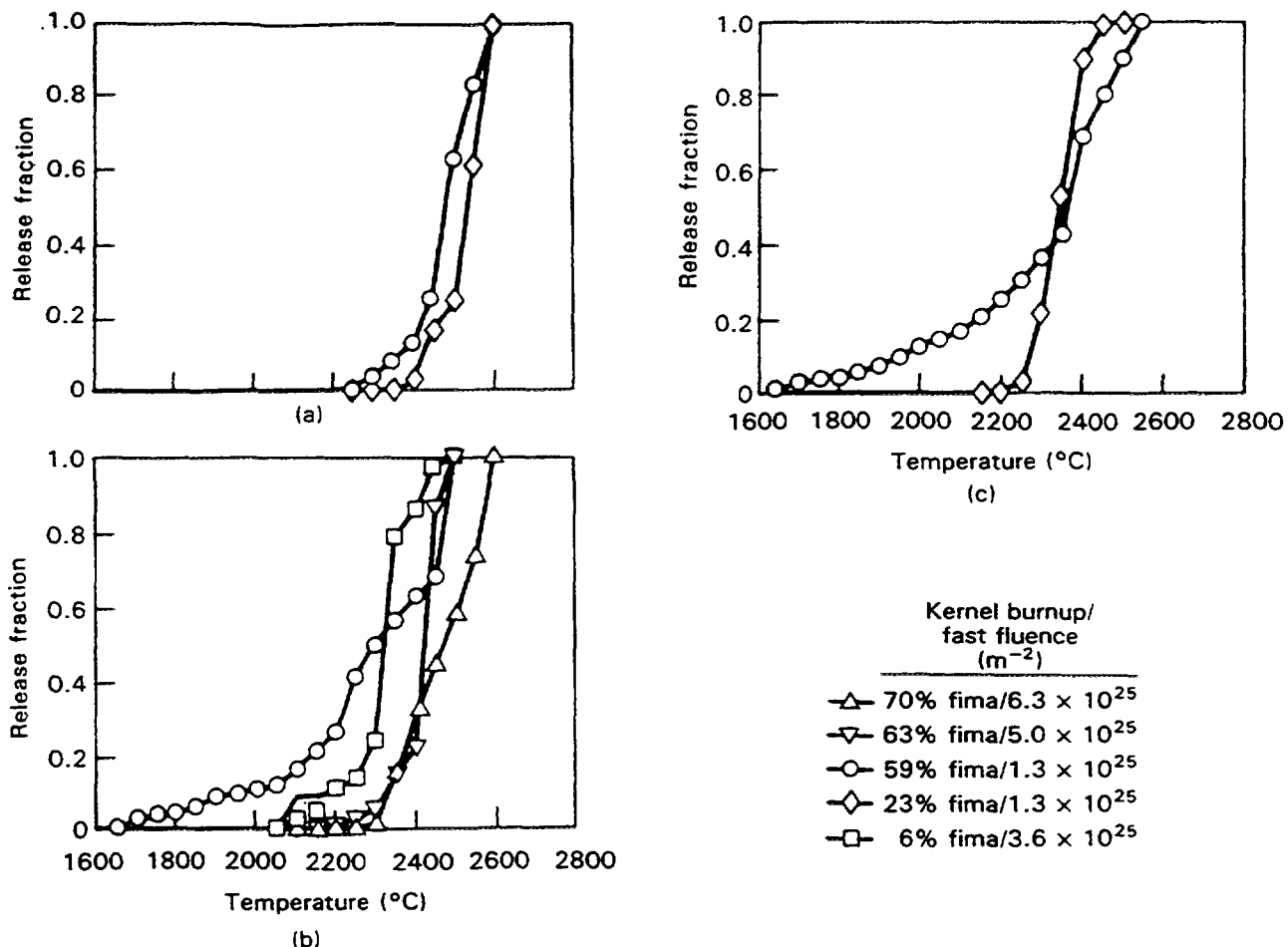


Fig. 4-40: Krypton release as a function of heating temperature during linear ramp tests, with heatup to 2600 °C in (a) 8 h, (b) 30 h, and (c) 80 h. No systematic trend of burnup dependence can be observed with the UC₂ TRISO particles used here.

decompose at high temperatures. Several studies have been performed on the phase transition of SiC at high temperatures. The transition temperatures of β -SiC (as-deposited) to α -SiC vary from 1600 to 2200 °C. As reported by Kurata et al. [61], coincident formation of small pores over the entire surface was observed, consistent with the results discussed above. Thus, under the temperature extremes considered herein, the ceramographic, radiographic, and fission product release data are consistent with the concept of a SiC failure mechanism initiated by a β - to α -SiC phase transition with consequent development of porosity and disordered material, followed at even higher temperatures by essentially complete thermal decomposition of the SiC layer of the TRISO coating.

The apparent lack of irradiation damage effects on the high-temperature stability of the SiC material remains a somewhat surprising observation, given the influence on crystal structure that bombardment of fast neutrons may cause. Effects of fast fluence and/or burnup may well be present, but are reduced by annealing [90] and are overshadowed (at least within the exposure conditions examined) by the variability in the performance

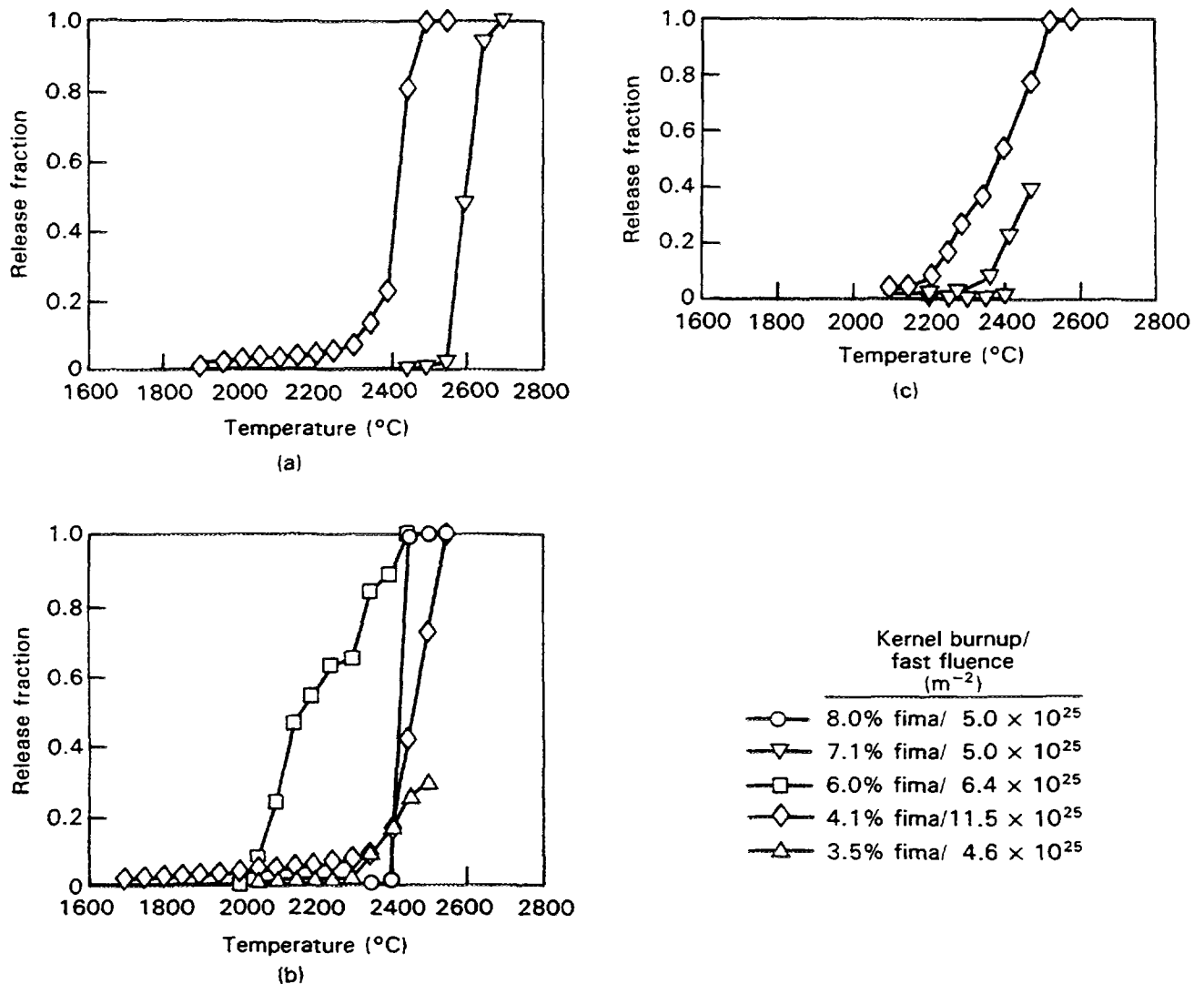


Fig. 4-41: Krypton release as a function of heating temperature during linear ramp tests, with heatup to 2600 °C in (a) 8 h, (b) 30 h, and (c) 80 h. No systematic trend of burnup dependence can be observed with the ThO₂ TRISO particles used here.

capability of the SiC layer due to normal variations in processing conditions that are allowed in fuel fabrication specifications.

4.2.2.4. Modeling

4.2.2.4.1. Particle Failure

A first step of modeling particle failure was to evaluate irradiation experiments and heating tests at elevated temperatures in order to find the lower and upper limits at which to expect zero failure or complete failure, respectively. Early US particle failure diagrams have defined failure isopleths in a burnup - fast fluence diagram under normal operating conditions [91] or regions for "no coating failures", "partial failures", and "100 % coating

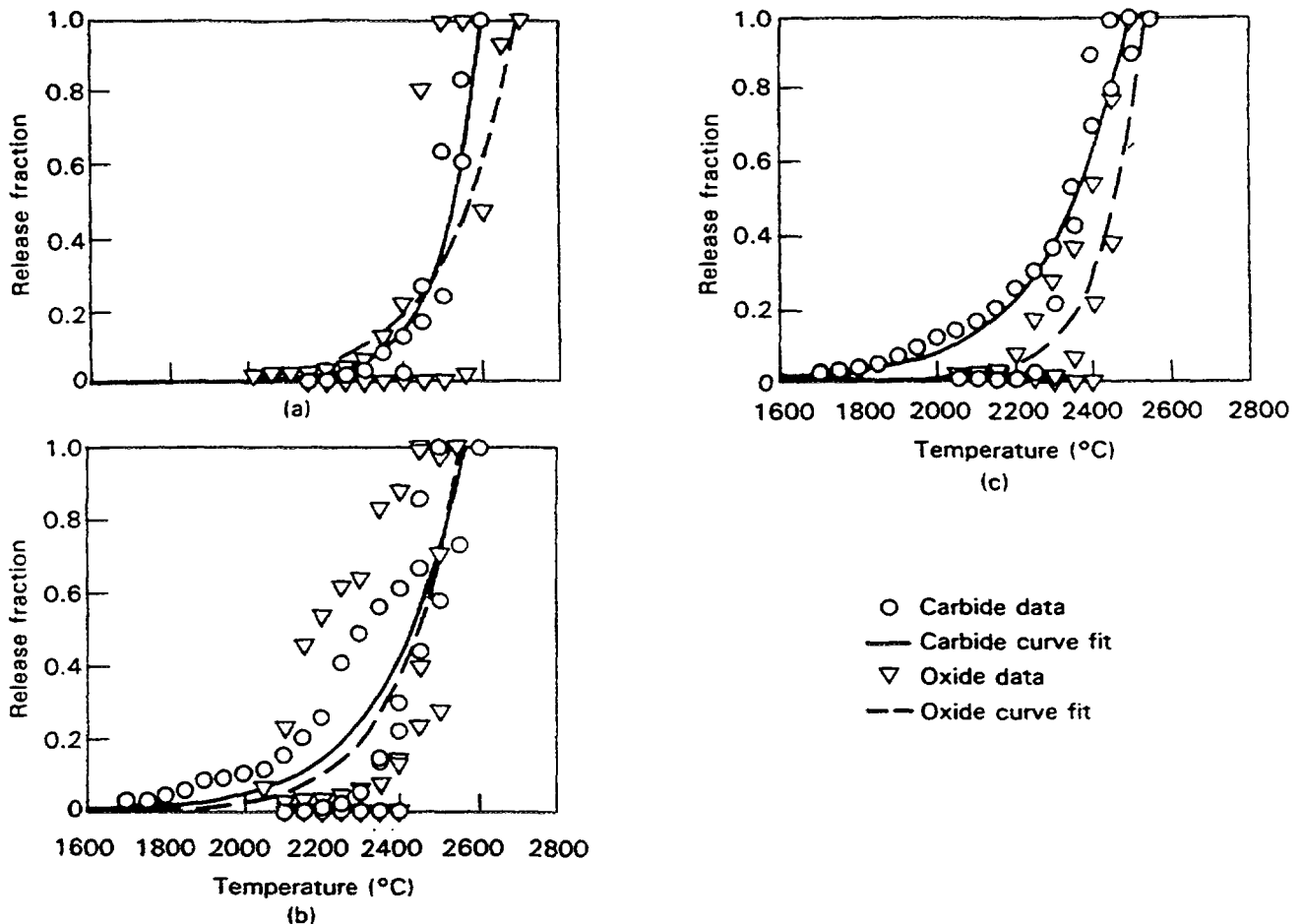


Fig. 4-42: Krypton release as a function of heating temperature during linear ramp tests, with heatup to 2600 °C in (a) 8 h, (b) 30 h, and (c) 80 h. A comparison of the oxide and carbide fuel performance at extreme temperatures shows no significant correlation with the chemical composition of the kernel.

"failures" as a function of irradiation time and fuel temperature under accident conditions [92]. Another simple approach was developed for TRISO particles in the early 1980s by Goodin [93], who derived from experimental data an exponential particle failure function dependent on fuel temperature or in a more complicated but still empirical way by adding a time dependence [94].

A modeling approach for a pressure vessel without adding a corrosion mechanism was made in the GA code **CONSTA** [95]. Calculational results with CONSTA were compared with experimental results with varying success. Using CONSTA results for US fuel specifications, the pressure vessel equation was converted into a simpler form dependent on temperature and with constants to be recommended for different types of particle configurations. The latter has become part of the GA code **SORS** [30]. Pressure vessel failure is not considered significant at temperatures > 1600 °C compared to other failure mechanisms, and is therefore not considered in this temperature range.

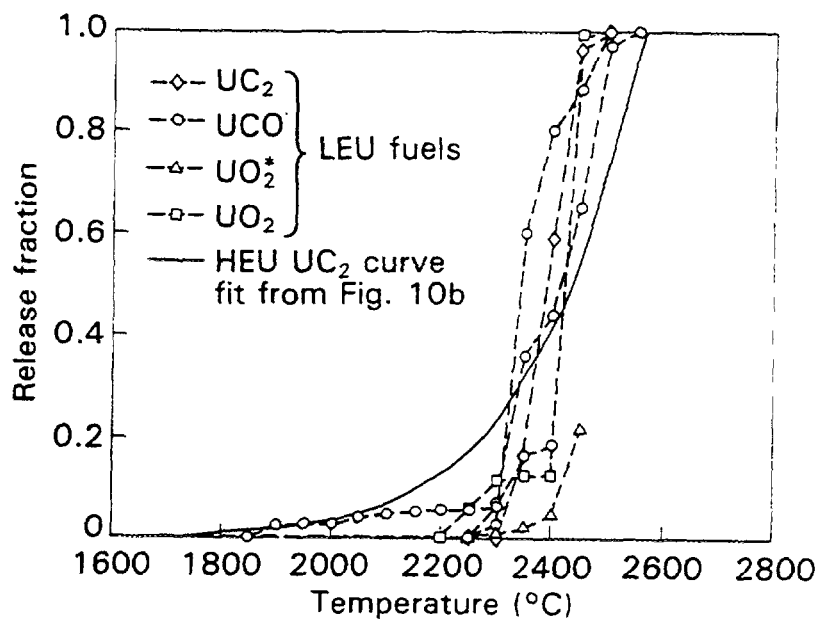


Fig. 4-43: Krypton release as a function of heating temperature during linear ramp tests. Release from low-enriched fuels is consistent with the average release obtained from high-enriched UC_2 TRISO particles.

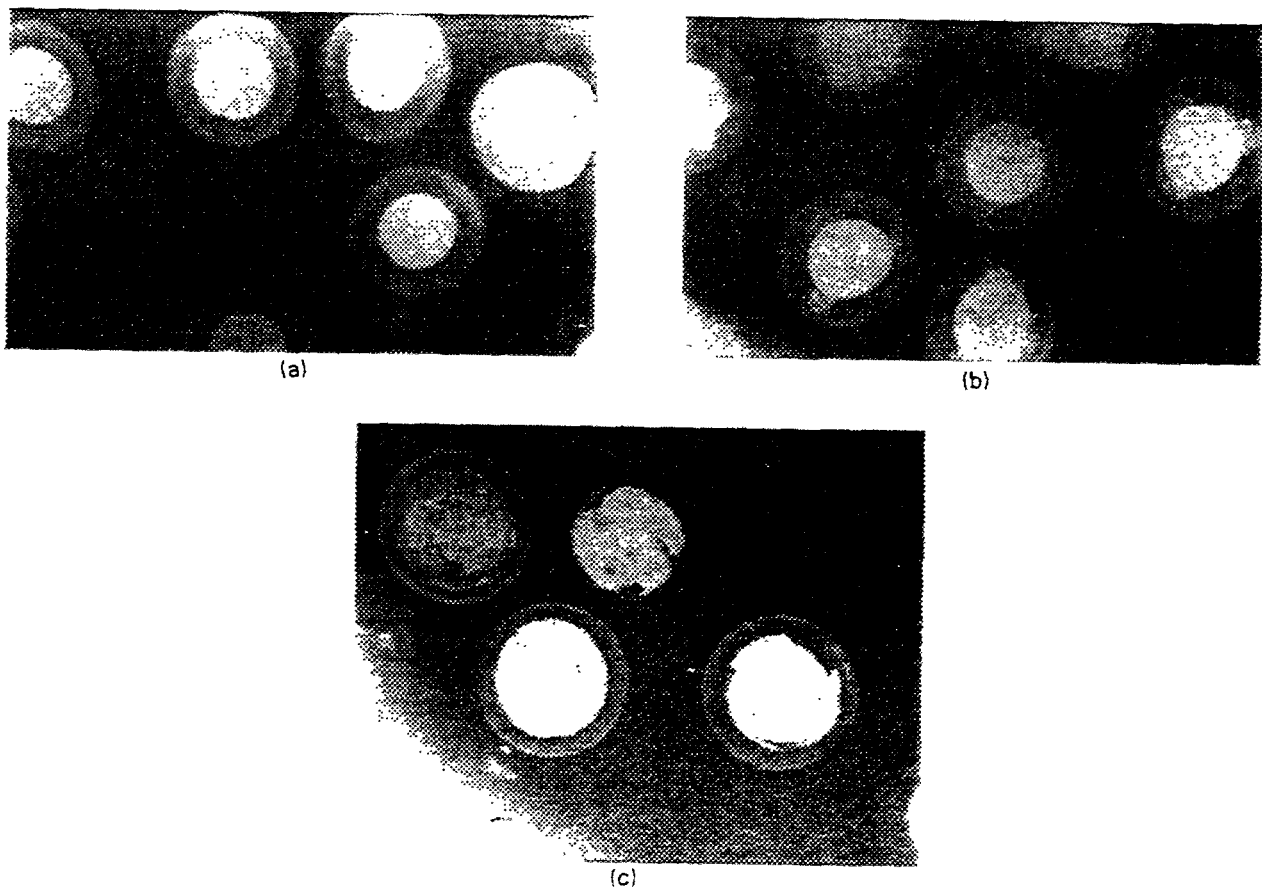


Fig. 4-44: Contact X radiographs showing representative particles (a) before heating, (b) after heating to 2059 °C, and (c) after heating to 2503 °C. Note the characteristic thinning of the SiC layer at high temperatures.

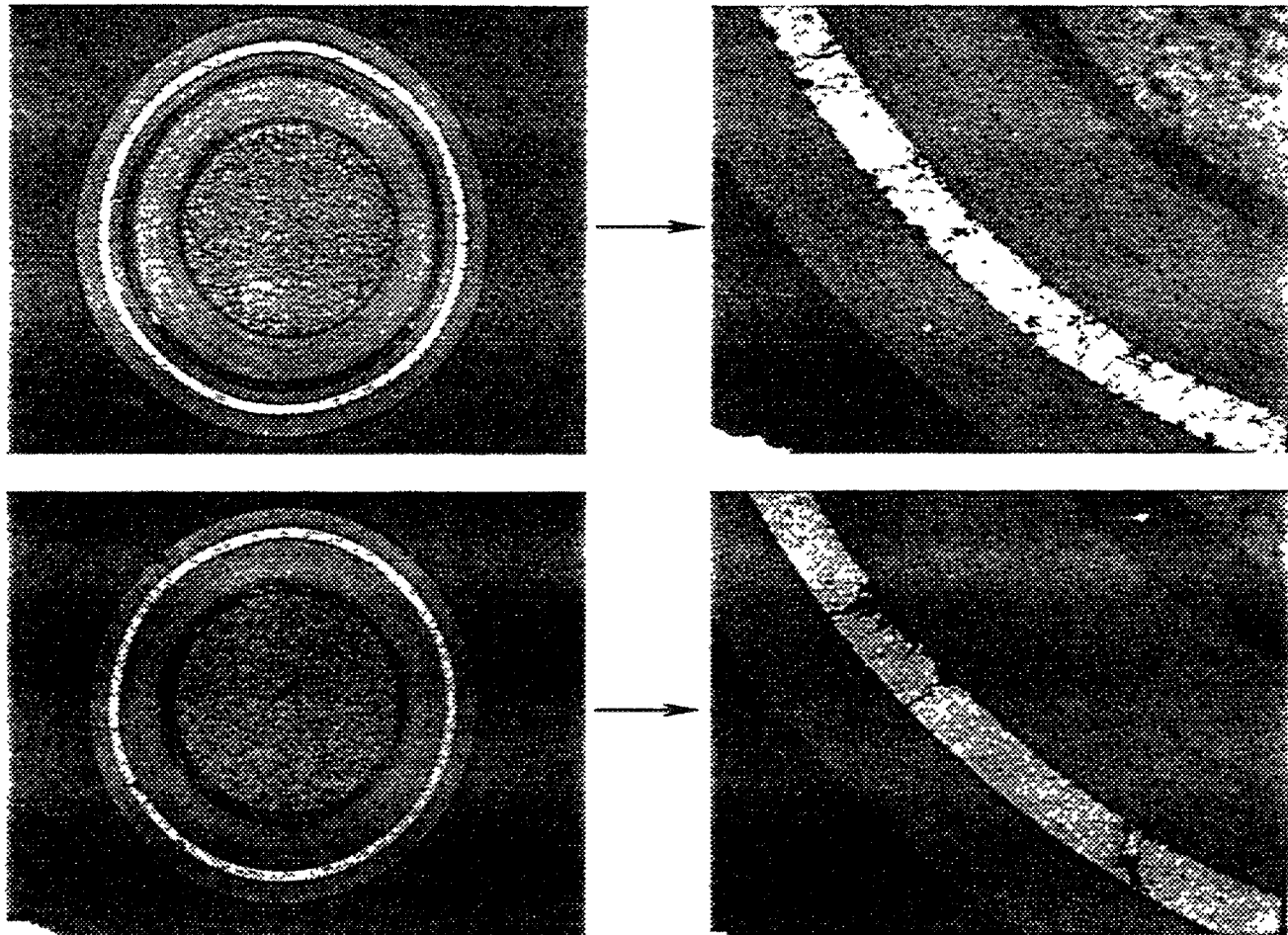


Fig. 4-45: Ceramography of TRISO ThO₂ particles irradiated to 4.1 %FIMA and heated at a rate of 20 °C/h to 2230 °C.

4.2.2.4.2. Fission Product Release

In the US fission product release modeling, the "Integrated Failure and Release Model for Standard Particles" [25, 96] is being applied in addition to the former diffusion model development. This statistical model uses the observed cesium release as indicator for a failure of the SiC layer as mentioned above (see previous section 4.1.1.4.), thus providing at the same time a cesium release fraction from the coated particles equal to the failure fraction. Since the model equations have been derived from heating tests with temperatures ≥ 1600 °C, the corresponding GA model coded in SORS assumes a certain fission product retention in the particle kernel at temperatures < 1600 °C using a diffusive transport mechanism [27].

The 1988 revision of this joint US/FRG statistical model has been developed as a replacement of the original version from 1985 as US reference radionuclide release model [26, 27]. By taking into account the retention capability of matrix graphite even at temperatures between 1600 and 1800 °C as observed in several heating experiments and using a larger experimental data base, the empirical equation for the cesium release from

the coated particles is a definite improvement compared to the original version. However, the derived empirical dependencies given in the pre-exponential factor for the Weibull distribution do not seem to represent a physical explanation for the observed release behavior.

4.3. REACTIVITY-INITIATED ACCIDENT TESTING

4.3.1. Pulse Tests in NSRR, Japan

Reactivity-initiated accident tests were performed in the Nuclear Safety Research Reactor (NSRR) using loose particles and fuel compacts. After the pulse irradiation, the samples were examined by ceramography and the failure fractions were measured.

4.3.1.1. Pulse Irradiation Conditions

The instantaneous reactivity insertion would not be considered in any HTGR design, but an event due to the reactivity insertion by rapidly drawing out the control rods was predicted in the HTTR design where energy deposition on the fuel was 1.26×10^4 J/(g UO₂) and the duration was about 8 s. The NSRR operation could not insert the reactivity in the HTTR fuel with fully simulating the design mode. The energy deposition in the tests ranged about 200 - 2300 J/(g UO₂) and the full width at half maximum power of the pulse used ranged about 10 - 30 ms. The pulse irradiation in the NSRR, however, gave interesting information.

4.3.1.2. Data of Fuel Samples

TRISO coated UO₂ particles were used in the tests. In total, ten pulse irradiation tests were performed which were divided into three groups with respect to the sample types:

- (a) unirradiated loose bed particles,
- (b) unirradiated fuel compacts, and
- (c) irradiated fuel compacts.

In each test, 2 - 4 kinds of U-235 enrichment (4 - 20 wt%) of the fuel were used to get various amounts of the energy deposition.

4.3.1.3. Results of RIA Tests

The ceramography of the unirradiated fuel compacts after the pulse irradiation showed that the central region of the UO₂ kernels of all the coated particles with energy deposition of 2300 J/(g UO₂) vaporized and a central void was formed. The observation by EPMA revealed that uranium vapor leaked through the cracks in the coating layers introduced by high inner gas pressure and it deposited near the boundary between the coated particles and the graphite matrix. The coated particles with the energy deposition less than 2300 J/(g UO₂) remained almost unchanged except for small cracking in the coating layers.

As for the appearance of the fuel compacts, only small cracks appeared on the surface even in the case of the energy deposition of 2300 J/(g UO₂), whereas no remarkable change

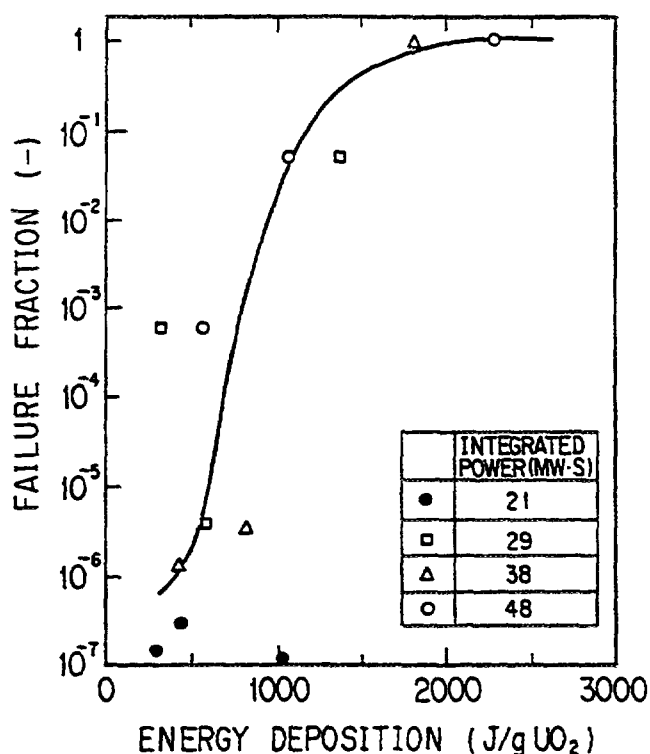


Fig. 4-46: Relation between failure fraction of the coated particles and energy deposition by NSRR irradiation [16]

was seen on the other fuel compacts with lower energy deposition. Fig. 4-46 [16] shows the relation between the failure fraction of the coated particles and the energy deposition. The failure fraction of the particles was about 1 % by the energy deposition of 1000 J/(g UO₂) and attained almost 100 % failure with the energy deposition of 1500 J/(g UO₂).

The examinations of the irradiated fuel compacts after the pulse irradiation test are under way. The analyses of temperature and stresses of the coated particles are needed to clarify the failure mechanisms. These analyses are also in progress.

4.3.2. Pulse Tests in HYDRA and IGR, Russia

Reactivity-initiated accidents (RIA) simulation tests were performed in the reactors of the HYDRA and the IGR, though the RIA of the modular HTGRs were not accurately reproduced in the tests. In the HYDRA tests, the pulse duration was shorter (1 - 2 ms) and the specific energy deposition was 100 - 1700 J/(g UO₂), whereas in the IGR tests, the duration was effective (1 - 30 s), but the specific energy deposition was higher (2×10^4 - 1×10^5 J/(g UO₂)). Besides the simulation tests, the modeling of behavior of the coated particles and the fuel elements was developed based on temperature and stress calculations.

Table 4-16: Characteristics of the coated fuel particles irradiated as loose particles and as tablets in the HYDRA tests

Coated particle batch U-235 enrich. [%]	Fuel kernel		Protective coating									
	UO ₂		PyC-1		PyC-2				SiC		PyC-4	
	Diameter [μm]	Density [g/cm ³]	Thickn. [μm]	Density [g/cm ³]	Thickness [μm]	Density [g/cm ³]	Thickn. [μm]	Density [g/cm ³]	Thickn. [μm]	Density [g/cm ³]	Thickn. [μm]	Density [g/cm ³]
1 KM 36	490	9.77	92	1.1	70	1.88	60	3.18	61	1.84		
2 KM 36	490	10.8	99	1.02	77	1.83	65	3.21	60	2.09		
3 KM ⁽¹⁾ 36	532	7.86	91	1.1	70	1.94	60	3.20	56	1.9		
<hr/>												
	UO ₂		PyC-1		PyC-2		SiC + PyC		SiC		SiC + PyC	
	Diameter [μm]	Density [g/cm ³]	Thickn. [μm]	Density [g/cm ³]	Thickn. [μm]	Density [g/cm ³]	Thickn. [μm]	Density [g/cm ³]	Thickn. [μm]	Density [g/cm ³]	Thickn. [μm]	Density [g/cm ³]
21-9X-84 21	900	9.1	105	1.1	14	1.5	91	2.4	100	3.18	56	2.4
36-27X-89 36	500	9.4	56	1.1	10	1.5	50	2.4	60	3.18	42	2.4

(1) Part of the samples of the 3 KM batch underwent irradiation after three hours of preliminary annealing at 1700 °C.

4.3.2.1. Tests Using the HYDRA Reactor

4.3.2.1.1. Pulse Irradiation Conditions

The pulse irradiation tests in the HYDRA were performed to study the dependence of the particle integrity on the energy deposition. The specific energy deposition was 100 - 1700 J/(g UO₂) and the pulse duration was 1 - 2 ms. In each test on the spherical fuel elements, four pulse irradiations were made.

4.3.2.1.2. Data of Fuel Samples

Three forms of fuel samples were used: loose particles, tablets, and spherical fuel elements. Table 4-16 shows the characteristics of five batches of the coated fuel particles irradiated as loose particles and as tablets. The tablets were made of the coated particles of 1 KM, 2 KM, and 3 KM batches with graphite powder which were about 10 mm in diameter and about 5 mm in thickness. The loose coated particles and the tablets were loaded in spherical graphite containers. The spherical fuel elements were 60 mm in diameter containing the coated fuel particles. The characteristics of the fuel elements and the coated fuel particles in the fuel elements are shown in Tables 4-17 and 4-18, respectively.

4.3.2.1.3. Results of RIA Tests Using the HYDRA

In the visual inspection of the loose coated fuel particles and the tablets, all the particles and the tablets, except one coating batch (36-27X-89), were intact. The thickness of the buffer layer of the particles of 36-27X-89 was 56 μm , whereas that of the particles of the other batches was > 90 μm . This resulted in smaller free volume in the particles of 36-27X-89 and higher internal pressure during irradiation which caused the coating failures.

The ceramography of the coated fuel particles after the pulse irradiation revealed that the kernels were intensively cracked without new structures at an energy deposition of < 1050 J/(g UO₂). At higher energy deposition (> 1300 J/(g UO₂)), two greatly different zones were observed in the kernels. In the external zone, no structure change occurred. The central zone with the pores may have melted.

Fig. 4-47 shows the dependence of the failure fraction of the coating layers on the specific energy deposition at a single pulse irradiation. The failure fractions after pulse irradiations were determined by the fission gas release after a short time of reactivation. Four pulse irradiations on the fuel elements with a specific energy deposition of 800 - 1300 J/(g UO₂) caused the increase in the fission gas release (Fig. 4-48).

4.3.2.2. Tests Using the IGR Reactor

4.3.2.2.1. Pulse Irradiation Conditions

The pulse irradiation tests were performed in the IGR reactor to study the behavior of spherical fuel elements under longer pulse duration than that in the HYDRA reactor. Two series of tests were carried out, as shown in Table 4-19. In the first series, irradiations of three pulses were made sequentially where the pulse durations were 1.6, 1.0, and 0.7 s,

Table 4-17: Characteristics of the fuel elements irradiated in the HYDRA tests

Purpose of experiments	Marking	Weight [g]	Density [g/cm ³]	U-235 loading [g]
1. Check of correctness of fluence value determination	GSP / - / 21 ^{(1), (2)}			
	X8-47	208	1.85	0.054
	X8-49	210	1.86	0.505
2. Study of irradiation time influence on fuel element performance (n τ =const, τ =var) series "C"	SPD / 100 / 20.5 ⁽¹⁾			
	11m	200	1.80	0.51
	14m	205	1.80	1.00
	15m	202	1.78	1.00
	GSP / 21-X-78 / 21 ^{(1), (3)}			
	X8-71	208	1.84	0.5
3. Study of specific energy deposition effect on radiation resistance and coated particle performance (n τ =var, τ =const) ⁽⁴⁾ series "B"	GSP / 36-X-80 / 35.4 ⁽¹⁾			
	X17-60	208	1.84	1.0
	X17-56	208	1.85	1.0
	X17-38	205	1.83	0.5
	X17-39 ⁽⁵⁾	206	1.83	0.5

(1) a / b / c with

a: Type of fuel element manufacturing

(GSP: graphite-bounded by pyrocarbon, SPD: sintering under pressure)

b: Coated particle batch

c: U-235 enrichment [%]

(2) Simulation of "failure": kernels (without coating) are placed in fuel elements

(3) Coated particles are located in fuel element in form of spherical layer

(4) Change of neutron fluence is provided by change of sample location at about the center of the core

(5) After performing of given testings, the fuel element was tested in the "KASHTAN-4" channel.

and the maximum energy deposition rates were 150, 300, and 620 kW per fuel element, respectively. In the second series, four successive pulses were made. The first pulse was low power by which the systems of measurement of neutron flux and temperature were checked. The durations of the subsequent three pulses were from 7 to 30 s, and the stationary energy deposition rate was 46 kW per fuel element. The surface temperature of the spherical fuel elements was measured by W-Re 5/20 thermocouples. The main purpose of the tests was to evaluate the integrity of the fuel elements, so a quantitative analysis of the coated fuel particle failure was not performed.

Table 4-18: Characteristics of the coated fuel particles contained in the fuel elements irradiated in the HYDRA tests

Batch	Kernel, coating	Density [g/cm ³]	Diameter, thickness [μm]
36-X-80	UO ₂	8.59	400 - 630
	PyC-1	1.1 ±0.1	20
	PyC-2	1.5	7
	PyC-3	1.1 ±0.1	15
	PyC-4	1.9	70
	SiC	3.2	140
	PyC-6	1.2	15
	PyC-7	1.7	56
100	UO ₂	9.8	560
	PyC-1	1.0	30
	PyC-2	1.5	67 (PyC-2 + PyC-3)
	PyC-3	1.8	
	SiC	3.0	60
	PyC-5	1.8	70
21-X-78	UO ₂	≈9.1	400 - 630
	PyC-1	≈1.1	30
	PyC-2	-	18
	PyC-3	≈1.6	35
	SiC	≈3.1	80
	PyC-4	≈1.75	84

4.3.2.2.2. Data of Fuel Samples

The spherical fuel elements of 60 mm in diameter containing the coated UO₂ particles were used for the tests. The enrichment of U-235 was 21 wt% and the U-235 loading in the fuel element was 2.5 g per fuel element. The characteristics of the coated fuel particles are shown in Table 4-20. The integrated free volume in the coated fuel particle used was 0.074 mm³.

4.3.2.2.3. Results of RIA Tests Using the IGR

No failure of the spherical fuel elements was observed after the pulse irradiations in the first series of the tests.

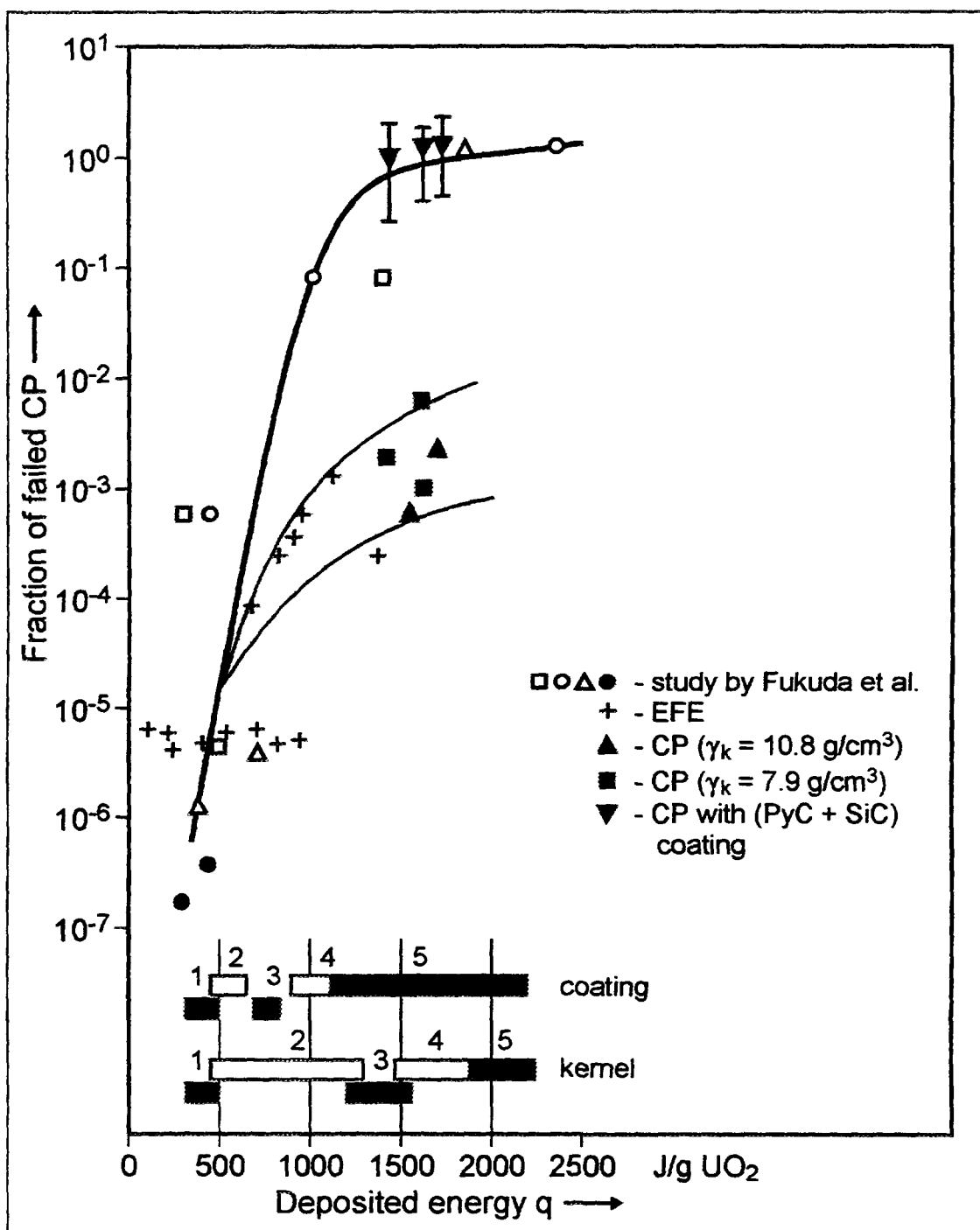


Fig. 4-47: Dependence of the failed coated particle fraction on specific energy deposition in the single irradiation. The stages:

- (1) Heating up to approx. $1500 - 1800^\circ\text{C}$
- (2) Heating up to approx. 2000°C ; kernel fuel dispersion
- (3) Heating up to melting; carbidization possible
- (4) Melting; carbidization possible
- (5) Evaporation; carbidization possible

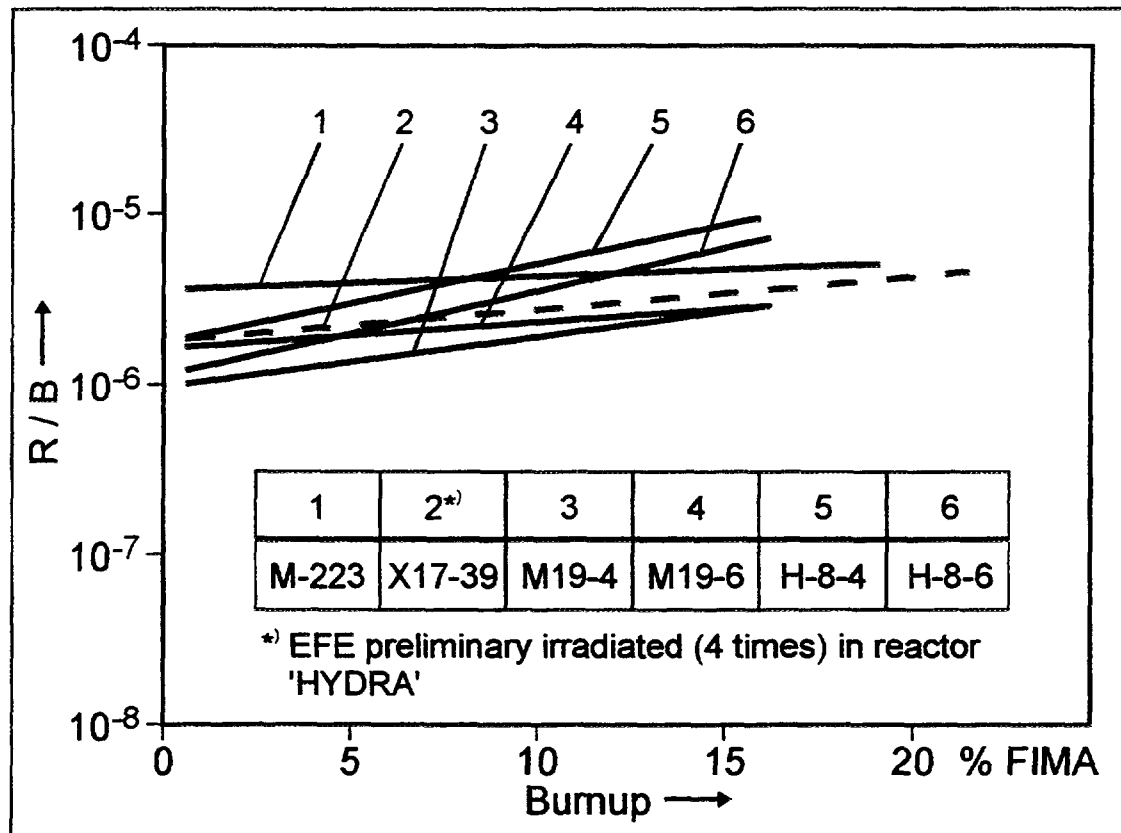


Fig. 4-48: Xe-135 relative release from spherical fuel elements irradiated in channel "KASHTAN-4", approximation by polynomial of degree 1

Table 4-19: Pulse irradiation conditions in the IGR tests

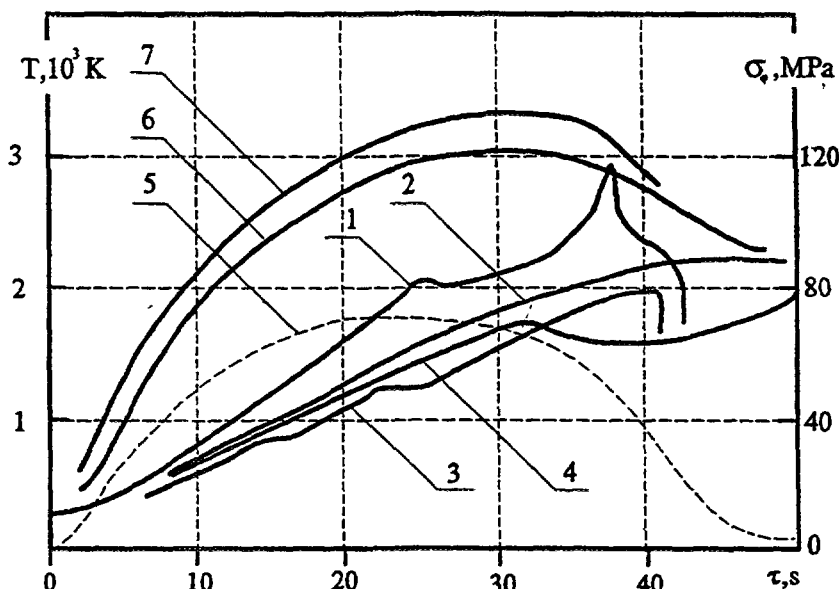
Characteristics	1st series	2nd series
Power [kW/fuel element]	620	46
Energy deposition [J/(g UO ₂)]	2.6*10 ⁴	9*10 ⁴
Pulse duration (on peak half-width)	0.7	30
Temperature [K]		
- spherical fuel element surface	860	2000 ±200
- spherical fuel element center	1490	3000
- kernel (in center of fuel element) ⁽¹⁾	3360	3200
Strain on surface of fuel element [MPa] ⁽¹⁾	70	70
Spherical fuel element state after testing	intact	Spherical fuel elements and particle coatings have failed

(1) Calculational data

Table 4-20: Characteristics of the coated fuel particles contained in the fuel elements irradiated in the IGR tests

	Kernel ⁽¹⁾	PyC-1	PyC-2	PyC-3	SiC-4	PyC-5
Size [μm]	520	100	20	65	45	70
Density [g/cm^3]	10.1	1.0	1.5	1.9	3.2	1.8

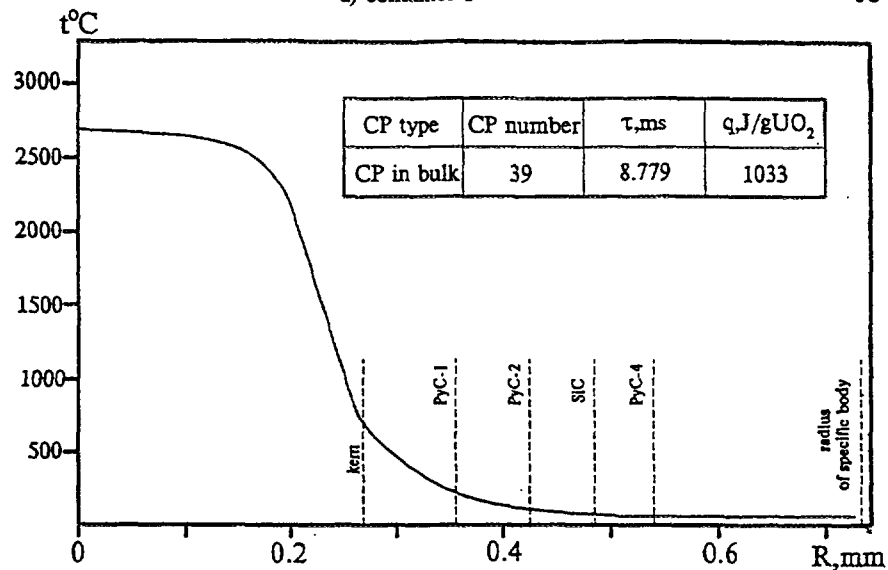
(1) Made on the basis of UO_2 with 21 % enrichment of U-235



- (1 - 4) Thermocouples readings in various points on the spherical fuel element surface
- (5) Circle tension on external surface of the spherical fuel element shell
- (6) Calculational temperature in the spherical fuel element center
- (7) Kernels maximum (calculational) temperature

Fig. 4-49: Temperatures and stresses of the fuel element at the fourth pulse irradiation in the second series of the IGR test.

In the second series of the tests, cracks were observed in the fuel-free zone of the fuel elements and part of the fuel element was split in 2 - 3 fragments. In the central zone of the fuel elements, traces of melting were observed. The ceramography of the fuel elements revealed delamination and thermal decomposition of the SiC layers and cracking of the PyC and SiC layers. Since the specific energy deposition was higher in the IGR tests than in the HYDRA tests by an order of magnitude, the coated particles were completely destroyed in the IGR tests though the free volume of the coated particles was about 0.07 mm^3 which was nearly the same as $0.06 - 0.08 \text{ mm}^3$ of the free volume of KM batches



b) container 2

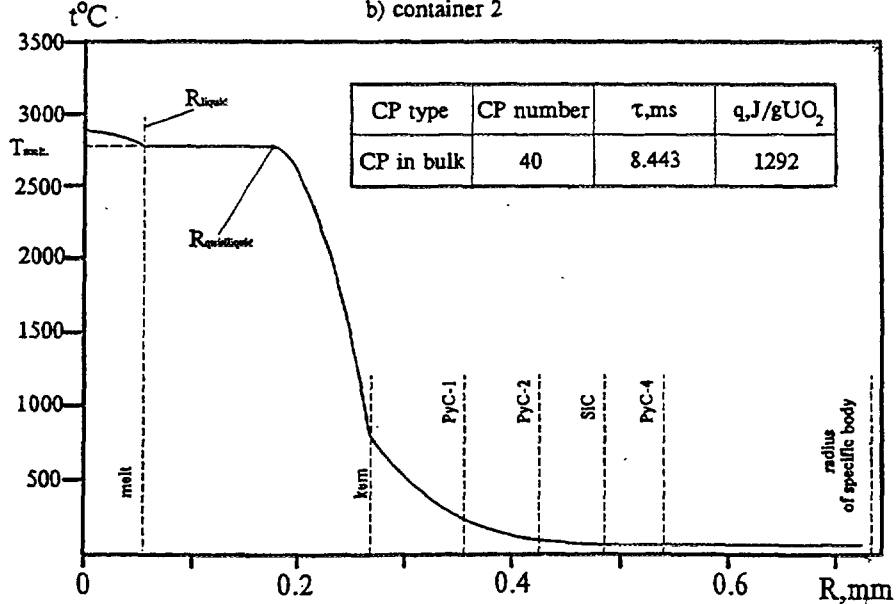


Fig. 4-50: Typical examples of the calculated temperature of the coated fuel particle pulse-irradiated in the HYDRA test

tested in the HYDRA. The destruction of the fuel-free zone of the spherical fuel elements was caused by thermo-elastic stresses inside which attained values of 60 - 70 MPa at the fourth pulse irradiation of the second series of the tests, as shown in Fig. 4-49.

4.3.2.3. Temperature and Stress Calculations

4.3.2.3.1. Temperature Calculation

In the mode of the pulse irradiation, an abrupt change of energy deposition in the fuel occurs where the fuel kernels are very hot or even melting surrounded by relatively cold coating layers and cold graphite matrix. The situation defines the processes of deformation

and destruction of the coated fuel particles and fuel elements. The quasi-stationary thermal analysis was carried out on the model coated fuel particle and the fuel element.

Typical results of the temperature calculation on the HYDRA tests are shown in Fig. 4-50. In Fig. 4-50 (top), the maximum fuel temperature is below the melting point whereas the central part of the fuel kernel is predicted to melt in Fig. 4-50 (bottom). The uncertainty of the thermal conductivity of the PyC coating layers slightly influenced the calculated melt zone size of the fuel kernel. The energy deposition of about 1000 J/(g UO₂) per pulse was the threshold of starting of kernel melt.

Fig. 4-51 shows the calculated radius of the melt zone and the quasi-melt zone of the fuel kernel as a function of the specific energy deposition where the HYDRA experimental results of the melt zone radius determined by ceramography are also presented for comparison. The radius of the quasi-melt zone was defined as the outer radius of the temperature area of $T = T_{melt}$. Although the experimental results of the melt zone radius were correlated with the calculated quasi-melt zone radius, the quantity of the experimental results was insufficient for reliable verification of the calculation code.

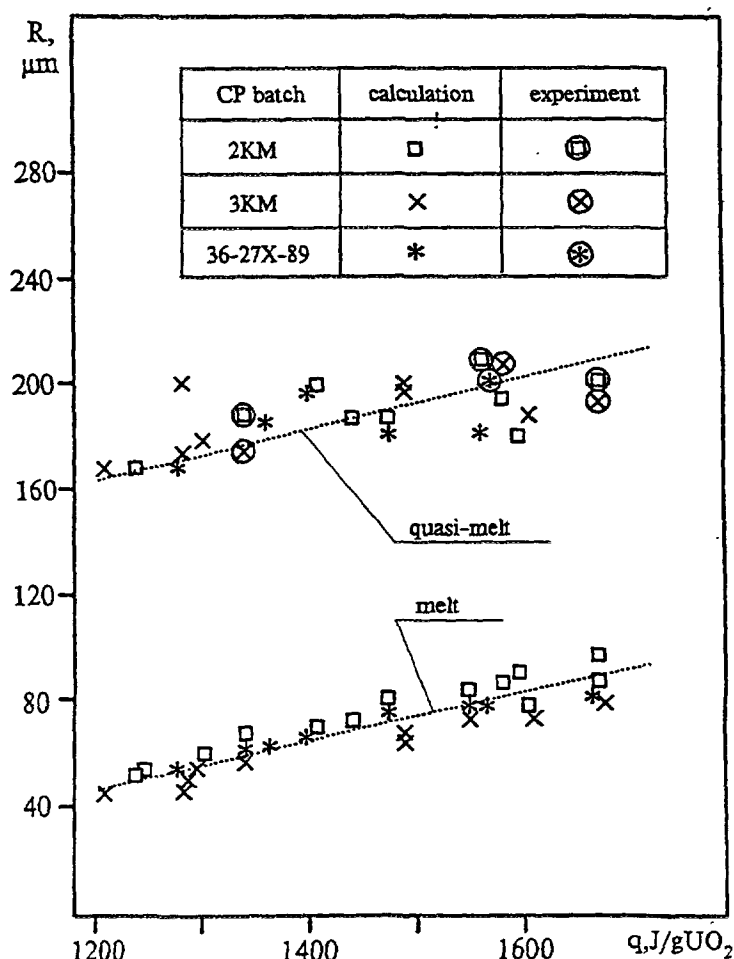


Fig. 4-51: Dependence of the radius of the melt zone and the quasi melt zone of the fuel kernel on the specific energy deposition in the HYDRA tests

4.3.2.3.2. Stress Calculation

After the temperature calculation, stress calculation in the coating layers and the fuel element was attempted. The thermal stresses in the SiC layer were calculated assuming a single-layer sphere or a three-layer sphere. However, the present model is insufficient. A number of effects has to be taken into account: thermal expansion of the kernel especially in the process of melting, deformation of the buffer layer, supporting effects of the graphite matrix, influence of parameters and properties of the kernel and the coating layers, etc.

4.4. SUMMARY OF CHAPTER 4

The highest temperatures and thus the greatest fission product release can occur in a **core heatup depressurization accident** (maximum temperature of 1620 °C predicted for the HTR-MODUL). For the simulation of a depressurization accident, spherical fuel elements were heated primarily at 1600 to 1800 °C in helium at a slight overpressure and the fission product release was measured. Measurements and additional model calculations have shown that the iodine release from defective coated particles is most significant from the safety engineering point of view.

The Kr-85 release fractions during the isothermal accident phase of the tests demonstrated that no particle damage occurs at 1600 °C. Kr-85 and thus also the iodine nuclides which behave similarly, are released with a fraction as small as $< 10^{-6}$. At 1800 °C, isolated pressure vessel failures and diffusive transport through still intact coatings lead to a further increase in krypton release. At 2100 °C, these effects are enhanced and, in addition, chemical decomposition begins to destroy the SiC layer.

The most important solid fission products have shown the following release behavior: Of all fissionable elements, cesium is most rapidly released internally from the fuel kernels, mainly into the buffer layer adjacent to the kernel. However, significant cesium release from the particles is only measured at 1800 °C; retention in the matrix graphite prevents rapid release from the fuel element. In contrast to cesium, strontium is very well retained in the oxide fuel kernels and in the matrix graphite, which almost completely prevents a release from the fuel sphere at 1600 °C. Strontium release amounts to the same level of cesium release at 1800 °C. The storage effect of the coating is relatively small for strontium. Silver is released from the fuel elements with the highest fraction, which is attributed to the large diffusivity of the comparably small atom size. Silver passes in particular through the matrix graphite very rapidly, whereas its retention in the particle kernel is even higher than that of cesium, and in the coating higher than that of strontium. Due to the small absolute inventory, however, its significance for the consequences of a core heatup accident is rather small.

The release behavior of metallic fission products from TRISO coated UO₂ particles was studied in Japan by postirradiation isothermal heating tests in the temperature range 1600 to 1900 °C. The fission gas release monitoring and the postheating examinations revealed that no pressure vessel failure occurred in the tests. The ceramographic observations showed no palladium attack and thermal decomposition of SiC. The diffusion coefficient of Cs-137 in the SiC layer was evaluated from the release curves based on a one-layer coated

particle model. Fractional release measurements suggested that the diffusion coefficient of Ag-110m in SiC be larger than that of Cs-137.

A model to predict the ultimate failure of TRISO coated fuel particles in hypothetical core heatup events was proposed. The features of the model allow treatment of the statistical variation of the number of particles and a thermodynamic estimation of the stoichiometry of irradiated UO₂ kernels and the equilibrium CO pressures. The model predictions agreed well with the results of the postirradiation temperature ramp tests. However, the model tended to overpredict at lower failure fraction at a low ramp rate. Inspection of the ceramographs and the X-ray microradiographs of the heated samples revealed the effect of thermal creep of the PyC layer in a range of temperatures around 2100 °C.

The ORNL Core Conduction Cooldown Test Facility, CCCTF, was designed and constructed to permit the study of the release of gaseous and condensable fission products from gas-cooled reactor fuel under simulated accident conditions either oxidizing or no-oxidizing. The system is operated with computer control for full automation requiring minimal interactions with operators and with remote handling for radioactive material.

Irradiation tests of the fuel compacts at **very high temperatures** were performed. No crack was observed on the low-burnup fuel compacts after high temperature irradiation. No deterioration of the SiC coating layer of the particles was found even after irradiation at 2000 °C, but a small fraction of the particles failed in the severest case of 2000 °C irradiation.

Reactivity-initiated accident (RIA) tests were carried out in Japan and in the Russian Federation. The coating failure fraction increased with the amount of energy deposition. The coating failure may have been caused by the internal high pressure due to UO₂ evaporation. To clarify the mechanisms of the coating failure, analyses of temperature and stresses of the coated particles are needed.

REFERENCES OF CHAPTER 4

- [1] SCHENK, W., NAOUMIDIS, A., NICKEL, H., The Behaviour of Spherical HTR Fuel Elements under Accident Conditions, J. Nucl. Mat. **124** (1984) 25-32.
- [2] PETERSEN, K., et al., The Fission Product Retention of Pebble-Bed Reactors in Ultimate Accidents, Nucl. Techn. **46** (1979) 306-311.
- [3] GOODIN, D.T., NABIELEK, H., SCHENK, W., Accident Condition Testing of US and FRG High-Temperature Gas-Cooled Reactor Fuels, Report JüL-Spez-286, Research Center Jülich, Report GA-A 17820, GA Technologies Inc. (1985).
- [4] SCHENK, W., Untersuchungen zum Verhalten von beschichteten Brennstoffteilchen und Kugelbrennelementen bei Störfalltemperaturen, Report JüL-1490, Research Center Jülich (1978).
- [5] SCHENK, W., Störfallsimulation an bestrahlten Brennelementen bei Temperaturen von 1400 °C bis 2500 °C, Report JüL-1883, Research Center Jülich (1983).
- [6] SCHENK, W., PITZER, D., NABIELEK, H., Fission Product Release Profiles from Spherical HTR Fuel Elements at Accident Temperatures, Report JüL-2234, Research Center Jülich (1988).

- [7] SCHENK, W., NABIELEK, H., Kugelbrennelemente mit TRISO-Partikeln bei Störfalltemperaturen (Zahlenwerk zum Bericht JüL-2091 und neue Ergebnisse von 1986 bis Oktober 1988), Report JüL-Spez-487, Research Center Jülich (1989).
- [8] NABIELEK, H., et al., Development of Advanced HTR Fuel Elements, Nucl. Eng. Des. **121** (1990) 199-210.
- [9] LOHNERT, G., Technical Design Features and Essential Safety-Related Properties of the HTR-Module, Nucl. Eng. Des. **121** (1990) 259-275.
- [10] SCHENK, W., GONTARD, R., NABIELEK, H., Performance of HTR Fuel Samples under High-Irradiated and Accident Simulation Conditions with Emphasis on Test Capsules HFR-P4 and SL-P1, Report JüL-2992, Research Center Jülich (1994).
- [11] SCHENK, W., NABIELEK, H., Iodine Retention in Spherical Fuel Elements under HTR MODUL Accident Conditions, (Proc. Jahrestagung Kerntechnik '90, Nürnberg, 1990), Inforum GmbH, Bonn (1991) 363-366.
- [12] KIRCH, N., IVENS, G., Results of AVR Experiments, AVR-Experimental High-Temperature Reactor, VDI-Verlag (1990) 90-105.
- [13] SCHENK, W., NABIELEK, H., Simulation of Steam and Water Ingress Accidents with Irradiated Fuel Elements, Response of Fuel, Fuel Elements and Gas Cooled Reactor Cores under Accidental Air or Water Ingress Conditions (Proc. IAEA Technical Committee Meeting, Beijing, 1993), IAEA-TECDOC-784, Vienna (1995) 37-44.
- [14] SCHENK, W., NABIELEK, H., High-Temperature Reactor Fuel Fission Product Release and Distribution at 1600 to 1800 °C, Nucl. Techn. **96** (1991) 323-336.
- [15] SCHENK, W., POTT, G., NABIELEK, H., Fuel Performance Testing for Small HTRs, J. Nucl. Mater. **171** (1990) 19-30.
- [16] FUKUDA, K., HAYASHI, K., SHIBA, K., Fuel Behaviour and Fission Product Release under HTGR Accident Conditions Fission Product Transport Processes in Reactor Accidents (Proc. Conf., Dubrovnik, 1989), (ROGERS, J.T., Ed.), Hemisphere Publ. Coop. (1990) 197-204.
- [17] SCHENK, W., NABIELEK, H., NICKEL, H., Die Spaltproduktrückhaltung im Brennelement, in: KUGELER, K., NEIS, H., BALLENSIEFEN, G. (Eds.), Fortschritte in der Energietechnik, Monographien des Forschungszentrums Jülich, Vol. 8, Research Center Jülich (1993) 321-328.
- [18] NABIELEK, H., et al., The Performance of High-Temperature Reactor Fuel Particles at Extreme Temperatures, Nucl. Technol. **84** (1989) 62-81.
- [19] PROKSCH, E., STRIGL, A., NABIELEK, H., Production of Carbon Monoxide During Burnup of UO₂ Kerneled HTR Fuel Particles, J. Nucl. Mater. **107** (1982) 280-285.
- [20] VERFONDERN, K., NABIELEK, H., PANAMA - Ein Rechenprogramm zur Vorhersage des Partikelbruchanteils von TRISO-Partikeln unter Störfallbedingungen, Report JüL-Spez-298, Research Center Jülich (1985).
- [21] WALLURA, E., et al., Siliciumcarbid-Hüllschichten von Kernbrennstoffteilchen - eine Charakterisierungsstudie, Report JüL-1871, Research Center Jülich (1983).
- [22] BENZ, R., Kinetics of Decomposition of CVD SiC in Modified TRISO-Coated Fuel Particles at Temperatures of 1600 to 2000 °C, Technical Note KFA-JRW-TN-124/82, Research Center Jülich (1982).

- [23] VERFONDERN, K., SCHENK, W., NABIELEK, H., Passive Safety Characteristics of Fuel for Modular HTR and Fuel Performance under Accident Conditions, Nucl. Techn. 91 (1990) 235-246.
- [24] NABIELEK, H., et al., Prediction of Temperature and Fission Product Release from HTR Fuel under Accident Conditions, Design and Safety of Advanced Nuclear Power Plants, (Int. Conf. ANP'92, Tokyo, 1992), OKA, Y., KOSHIZUKA, S. (Eds.), Atomic Energy Society of Japan (1992) P1.9-1 - P1.9-7.
- [25] NABIELEK, H., VERFONDERN, K., GOODIN, D.T., HTR Fuel: Prediction of Fission Product Release in Accidents, Fission Product Release and Transport in Gas-Cooled Reactors (Proc. IAEA Specialists Meeting, Berkeley, 1985), IAEA, IWGGCR/13, Vienna (1986) 155-169.
- [26] GOODIN, D.T., US/FRG Accident Condition Fuel Performance Models, Report DOE-HTGR-85107, General Atomics (1989).
- [27] VERFONDERN, K., DUNN, T.D., BOLIN, J.M., Comparison of US/FRG Accident Condition Models for HTGR Fuel Failure and Radionuclide Release, Report JüL-2458, Research Center Jülich (1991).
- [28] KASTEN, P.R., et al., Development of Correlations between Fuel Performance and Test Parameters in Modular High Temperature Gas-Cooled Reactors, Internal Report KFA-ISR-IB-9/94, Research Center Jülich (1994).
- [29] KASTEN, P.R., et al., Fuel Performance in Modular High Temperature Gas-Cooled Reactors, Internal Report KFA-ISR-IB-12/94, Research Center Jülich (1994).
- [30] SCHWARTZ, M.H., SEDGLEY, D.B., MENDONCA, M.M., SORS: Computer Programs for Analyzing Fission Product Release from HTGR Cores during Transient Temperature Excursions, Report GA-A12462, General Atomic Company (1974).
- [31] VERFONDERN, K., Code Development for Safety Assessments, MHTGR/HTR Fuel Performance under Accident Conditions (Proc. US/FRG Experts' Meeting, Oak Ridge, 1989), Internal Report KFA-HTA-IB-2/90, Research Center Jülich (1990) 289-339.
- [32] BALDWIN, C.A., KANIA, M.J., Fission Product Retention in TRISO Coated UO₂ Particle Fuels Subjected to HTR Simulated Core Heating Tests, Behaviour of GCR Fuel under Accident Conditions (Proc. IAEA Specialists' Meeting, Oak Ridge, 1990), IAEA, IWGGCR/25, Vienna (1991) 132-138.
- [33] VERFONDERN, K., Possible Explanation for HFR-K3/3 IMGA Results, Report ORNL/M-2248, Oak Ridge National Laboratory (1991).
- [34] MARTIN, R.C., Analysis of Fission Product Release Data for German Fuel Sphere HFR-K3/3, ORNL Draft Report (1991).
- [35] RÖLLIG, K., Capabilities of the Diffusion Model for Metallic Fission Products at Temperature Transients up to 1600 °C - Case: Cs-137 Release from Spherical Fuel Element R2-K13/1, Unification of Coated Particle Performance Models and Fission Product Transport Data for the HTR (IAEA Technical Workshop, Jülich, 1991).
- [36] CHRIST, A., Ausheizexperimente oberhalb 1600 °C, Technical Note HTR-5125-BF-GHRA 005058, HRB Mannheim (1987).
- [37] KROHN, H., Freisetzung von Spaltprodukten aus dem Core eines Kugelhaufenreaktors bei Störfällen mit Core-Aufheizung, Report JüL-1791, Research Center Jülich (1982).

- [38] KROHN, H., FINKEN, R., FRESCO-II: Ein Rechenprogramm zur Berechnung der Spaltproduktfreisetzung aus kugelförmigen HTR-Brennelementen in Bestrahlungs- und Ausheizexperimenten, Report JüL-Spez-212, Research Center Jülich (1983).
- [39] MARTIN, J.L., NABIELEK, H., Modelling of Fuel Element Heating Tests, Technical Note KFA-HBK-TN-4/88, Research Center Jülich (1988).
- [40] MOORMANN, R., VERFONDERN, K., Methodik umfassender probabilistischer Sicherheitsanalysen für zukünftige HTR-Anlagenkonzepte - Ein Statusbericht (Stand 1986), Band 3: Spaltproduktfreisetzung, Report JüL-Spez-388/Vol. 3, Research Center Jülich (1987).
- [41] BERGER-ROSSA, R., Rückhaltung und Umverteilung von Spaltprodukten im Core und im Primärkreislauf von Hochtemperaturreaktoren bei hypothetischen Störfallereignissen, Report JüL-2188, Research Center Jülich (1988).
- [42] KRANZ, L., Spaltprodukttransport im Hochtemperaturreaktor: Theorie, programmtechnische Umsetzung und Überprüfung an Experimenten, Report JüL-2463, Research Center Jülich (1991).
- [43] BATALAS, T.A., INIOTAKIS, N., VON DER DECKEN, C.B., Theoretische Untersuchungen zur Spaltproduktfreisetzung aus dem Core eines Hochtemperaturreaktors bei hypothetischen Coreaufheizungsstörfällen am Beispiel von Cäsium, Report JüL-2045, Research Center Jülich (1986).
- [44] CHRIST, A., Transiente Jodfreisetzung aus UO₂-Defektpartikeln, Technical Note HBK-5125-BF-GHRA 001785, HRB Mannheim (1986).
- [45] RÖLLIG, K., Weiterentwicklung von Rechenverfahren zur Spaltproduktfreisetzung und -ablagerung in HTR-Anlagen, Final Report HTR-5125-BA-GHRA 006887, Hochtemperatur-Reaktorbau GmbH (1992).
- [46] VERFONDERN, K., MÜLLER, D., Modeling of Fission Product Release Behavior from HTR Spherical Fuel Elements under Accident Conditions, Behavior of GCR Fuel under Accident Conditions (Proc. IAEA Specialists' Meeting, Oak Ridge, 1990), Report IWGGCR/25, IAEA, Vienna (1991) 45-55.
- [47] GAUS, H., et al., Untersuchungen zum Cs-Transport in Graphit, Report HMI-B 315, Hahn-Meitner-Institut Berlin (1979).
- [48] HILL, D.W., MYERS, B.F., Temperature, Pressure and Oxidation Effects on Cesium Diffusion in H-451 Graphite, Carbon: Extended Abstracts and Program (Proc. 16th Biennial Conference, San Diego, 1983), University of California San Diego (1993) 556-557.
- [49] MÜLLER, D., MOORMANN, R., Auswirkungen einer Adaption des Fallenmodells auf die Cs-Quellterme bei Kernaufheizung im HTR-Modul, Technical Note KFA-ISF-TN-16/90 II, Research Center Jülich (1990).
- [50] MOORMANN, R., REISCHLE, K., FALLDIF: Ein Rechenprogramm zur Lösung der durch Fallen gestörten Diffusionsgleichung, Technical Note KFA-ISF 14/90 II, Research Center Jülich (1990).
- [51] HILPERT, K., et al., Sorption of Cesium and its Vaporization from Graphitic Materials at High Temperatures, High Temperatures-High Pressures 20 (1988) 157-164.
- [52] MOORMANN, R., HILPERT, K., Chemical Behavior of Fission Products in Core Heat-up Accidents of High-Temperature Gas-Cooled Reactors, Nucl. Techn. 94 (1991) 56-67.

- [53] VERFONDERN, K., et al., Sensitivitätsstudien zur Spaltprodukt/Graphit-Wechselwirkung für Unfallabläufe mit Kernaufheizung mittlerer HTR, Spaltprodukt/Graphit-Wechselwirkungen im HTR (KFA/ISF Status Seminar, Jülich, 1989).
- [54] FRICKE, U., Untersuchungen zur Leistungssteigerung von inhärent sicheren HTR durch Optimierung der Coreauslegung, Report Jül-2155, Research Center Jülich (1987).
- [55] VERFONDERN, K., Rechnerische Untersuchung der Rückhaltefähigkeit des Graphits für Jod im Core des HTR-Modul, Technical Note KFA-ISF 14/85 I, Research Center Jülich (1985).
- [56] SCHOOPS, A., Die physikalischen Grundlagen der Absorption und Desorption von Jod in Reaktorgraphit, Diploma Thesis, RWTH Aachen (1989).
- [57] DANNERT, V., Mehrphasendiffusion von Spaltprodukten in Graphit - Ein Beitrag über die Sicherheit von Hochtemperaturreaktoren, Report Jül-2277, Research Center Jülich (1989).
- [58] IKAWA, K., KOBAYASHI, F., IWAMOTO, K., Failure of Coated Fuel Particles during Thermal Excursion above 2000 °C, J. Nucl. Sci. Techn. **15** (1978) 774-779.
- [59] KASHIMURA, S., IKAWA, K., Survival Temperature Limit of Unirradiated Coated Fuel Particles, Report JAERI-M 85-068, Japan Atomic Energy Research Institute (1985).
- [60] OGAWA, T., FUKUDA, K., Performance of the Model Fuel Pin of the Very High-Temperature Gas-Cooled Reactor at Temperatures above 2000 °C, Nucl. Eng. Des. **92** (1986) 15-26.
- [61] KURATA, Y., IKAWA, K., IWAMOTO, K., The Effect of Heat Treatment on Density and Structure of SiC, J. Nucl. Mater. **92** (1980) 351-353.
- [62] KURATA, Y., IKAWA, K., IWAMOTO, K., Fission Product Release from Triso-Coated UO₂ Particles at 1940 to 2320 °C, J. Nucl. Mater. **98** (1981) 107-115.
- [63] MINATO, K., et al., Release Behavior of Metallic Fission Products from HTGR Fuel Particles at 1600 to 1900 °C, J. Nucl. Mater. **202** (1993) 47-53.
- [64] OGAWA, T., et al., A Model to Predict the Ultimate Failure of Coated Fuel Particles during Core Heatup Events, Nucl. Techn. **96** (1991) 314-322.
- [65] FUKUDA, K., et al., Irradiation Behavior of HTGR Coated Particle Fuel at Abnormally High Temperature, Nucl. Eng. Des. **57** (1995) 221-230.
- [66] KASHIMURA, S., et al., HTGR Fuel Behavior at Very High Temperature, Report JAERI-M 86-046, Japan Atomic Energy Research Institute (1986).
- [67] OGAWA, T., et al., Release of Short-Lived Noble Gases from HTGR Fuel with Failed Coated Fuel Particles and Contaminated Matrix, Nucl. Eng. Des. **132** (1991) 31-37.
- [68] NABIELEK, H., Particle Release Model for Accident Calculations, Technical Note HBK-TN-5/85, Research Center Jülich (1985).
- [69] VERFONDERN, K., MARTIN, R.C., MOORMANN, R., Methods and Data for HTGR Fuel Performance and Radionuclide Release Modeling during Normal Operation and Accidents for Safety Analysis, Report Jül-2721, Research Center Jülich (1993).
- [70] ALLELEIN, H.J., Spaltproduktverhalten – speziell Cs-137 – in HTR-TRISO-Brennstoffteilchen, Report Jül-1695, Research Center Jülich (1980).

- [71] OGAWA, T., et al., Release of Metal Fission Products from Coated Particle Fuel – Swept-Gas Capsule 74F9J, 75F4A and 75F5A, Report JAERI-M 85-041, Japan Atomic Energy Research Institute (1985).
- [72] SAWA, K., et al., Analytical Method and Result of Fission Product Release from Core During a Depressurization Accident of HTTR, Behaviour of GCR Fuel under Accident Conditions (Proc. IAEA Specialists' Meeting, Oak Ridge, 1990), IAEA, IWGGCR/25, Vienna (1991) 117-123.
- [73] ZAKRZHEVSKAYA, I.V., et al., Radiation Investigations of HTGR Coated Particles at High Temperatures (up to 3000 °C), Presented at the 1st Research Coordination Meeting on Validation of Predictive method for Fuel and Fission Product Behaviour in Gas-Cooled Reactors, Vienna, Austria (1993).
- [74] GUDKOV, A.N., KASHPAROV, V.A., KHROULEV, A.A., Sampling Method for Distribution of Nuclear Fuel and its Fission Products in the HTGR Coated Particles, *Atomic Energy* **66** (1989) 185-188.
- [75] KHROULEV, A.A., PONOMAREV-STEPNOY, N.N., Release of Fission Products from High Temperature Fuel Materials, *Therm. Electr. Power Generation*, (3rd Int. Conf., Jülich, 1972).
- [76] GUSEV, A.A., et al., Experimental Data and Calculations to Analyze the Factors of HTGR Fuel Elements Service Life, Fuel and Graphite for HTR (Proc. 1st Soviet/German Seminar, Moscow, 1990), Internal Report KFA-HTA-IB-6/90, Research Center Jülich (1990) 455-472.
- [77] KHROULEV, A.A., et al., State of Works on Fuel Elements and Fission Products Transport for HTGR Radiation Safety Provision, Unification of Coated Particle Performance Models and Fission Product Transport Data for the HTR (IAEA Technical Workshop, Jülich, 1991).
- [78] MORRIS, R.N., et al., The Core Conduction Cooldown Test Facility. Current Status and Issues, Report ORNL/NPR-91/7, Oak Ridge National Laboratory (1992).
- [79] GABBARD, W.A., et al., Core Conduction Cooldown Test Facility (CCCTF): Overview and Description, Technical Note Unpublished, Metal and Ceramics Division, Oak Ridge National Laboratory (1992).
- [80] MORRIS, R.N., et al., Core Conduction Cooldown Test Facility Shakedown Tests, Report ORNL/NPR-91/25, Oak Ridge National Laboratory (1992).
- [81] MORRIS, R.N., et al., HRB-17 and HRB-18 HEU TRISO UCO Unbonded Irradiation Particle Core Conduction Cooldown Test, Report ORNL/NPR-92/9, Oak Ridge National Laboratory (1992).
- [82] MINATO, K., et al., Preirradiation Characterization of HTGR Fuel for HRB-22 Capsule Irradiation test, Report JAERI-Tech 95-056, Japan Atomic Energy Research Institute (1996).
- [83] AMIAN, W., Experimental Investigation on the Migrational Behavior of Silver in Coated Particle Fuel for High-Temperature Reactors, Report Jüll-1713, Research Center Jülich (1981).
- [84] NABIELEK, H., et al., Silver Release from Coated Particle Fuel, *Nucl. Technol.* **35** (1977) 483-493.
- [85] FÖRTHMANN, R., et al., Influence of Material Properties on the Retention of Fission Products by Silicon Carbide Coatings, *High Temp.-High Press.* **14** (1982) 477-485.
- [86] MYERS, B.F., MORRISSEY, R.E., Licensing Topical Report: The Measurement and Modelling of Time-Dependent Fission Product Release from Failed HTGR Fuel

- Particles under Accident Conditions, Report GA-A15439, General Atomic Company (1980).
- [87] MARTIN, R.C., Diffusion Modeling of Fission Product Release during Depressurized Core Conduction Cooldown Conditions, Behaviour of GCR Fuel under Accident Conditions (Proc. IAEA Specialists' Meeting, Oak Ridge, 1990), IAEA, IWGGCR/25, Vienna (1991) 77-84.
 - [88] CRANK, J., The Mathematics of Diffusion, Oxford At The Clarendon Press (1956).
 - [89] GOODIN, D.T., Accident Condition Performance of HTGR Fuels, Report GA-A 16508, GA Technologies Inc. (1983).
 - [90] KRAUTWASSER, P., BEGUN, G., ANGELINI, P., Raman Spectral Characterization of SiC Nuclear Fuel Coatings, *J. Am. Ceram. Soc.*, **66** (1983) 424-434.
 - [91] SMITH, C.L., Fuel Particle Behavior under Normal and Transient Conditions, Report GA-A12971, General Atomic Company (1974).
 - [92] TOKAR, M., Evaluation of High Temperature Gas Cooled Reactor Fuel Particle Coating Failure Models and Data, Report NUREG-0111, US Nuclear Regulatory Commission (1976).
 - [93] GOODIN, D.T., A Single Model for the Performance of HEU/LEU Fissile and ThO₂ Fertile Fuel under Hypothetical Accident Conditions, Report GA-A16291, General Atomic Company (1981).
 - [94] GOODIN, D.T., Accident Condition Performance of High-Temperature Gas-Cooled Reactor Fuels, Report GA-A16508, GA Technologies (1983).
 - [95] KOVACS, W.J., BONGARTZ, K., GOODIN, D.T., TRISO Coated HTGR Fuel Pressure Vessel Performance Models, Report GA-A16807, GA Technologies (1983).
 - [96] GOODIN, D.T., NABIELEK, H., The Performance of HTR Fuel in Accidents, Technical Note KFA-HBK-TN-19/85, Research Center Jülich (1985).

5. FUEL PERFORMANCE AND FISSION PRODUCT BEHAVIOR UNDER OXIDIZING CONDITIONS

Among the postulated accidents in the HTGR are those involving water and air ingress. These accidents can lead to extensive degradation of the core components, including the fuel elements, and to a significantly enhanced release of fission products. Water ingress can result from a breach of a steam generator tube and air ingress from breaches in the reactor system that link the internal and external gaseous atmospheres.

Although fuel performance is the central interest in this IAEA technical document, the oxidation of graphite components, other carbonaceous materials and the SiC carbide layer in the fuel particles can play an important role in governing fuel performance. The oxidation of graphite is of primary importance with respect to the structural integrity of the graphite. Much effort has been devoted to the consequences of graphite oxidation.

5.1. GENERAL COURSE OF THE ACCIDENTS

Given sources of water or air and the mixing of these with the coolant gas, mixtures of water vapor or air with helium circulate in the core passing fuel spheres in the pebble bed core or flowing through coolant channels in the prismatic core. Other graphitic components in the reactor vessel, such as core supports or reflector blocks, are also exposed to the circulating oxidants.

The effect of graphite oxidation depends on the penetration of the oxidant into the graphite as measured from the surface over which the oxidant-containing gases flow. The penetration will depend on the nature of the oxidant, its concentration or partial pressure, the temperature, the type of graphite and ultimately, the time. Decrement in the strength and structural integrity of the graphite core and support components will depend on the depth of penetration. For a given system and limited times, the penetration depth will decrease with increasing temperature and vice versa for limited times.

In the prismatic core as well as the pebble bed core, the oxidant must penetrate a graphite barrier, having about a 5 mm thickness, to reach the site of the fuel particles. In the prismatic core, the oxidant must penetrate radially outward in the US HTGR and radially inward in the Japanese HTTR. In the pebble bed core, the oxidant must penetrate radially inward through a 5 mm thick, fuel-free coating before encountering the fuel particles in the fuel element (pebble).

When the oxidant reaches the site of the fuel particles, oxidant-fuel interactions are possible along two general paths. Some particles may have failed during the course of the preceding irradiation or fabrication process in a manner that exposed the fuel kernels to the particle exterior. In this case, the oxidant can directly reach the fuel, induce oxidation, and alter the structure of the grains of fuel. The consequence is a significantly enhanced release of fission products. A second, more arduous, path involves the oxidation of the outer pyrocarbon coatings of the fuel particles, then oxidation of the more resistant SiC coatings and the inner pyrocarbon and buffer coatings. Frequently the latter two coatings are

fragmented; in this case, oxidation of the kernel occurs earlier than otherwise. The second path, more likely in the air ingress accident, could lead to a more serious degradation of the core and to a much larger fission product release than does the first path.

5.2. EXPERIMENTAL AND ANALYTICAL APPROACH TO THE ACCIDENTS

5.2.1. Experimental Efforts

Experiments relevant to the HTGR fuel performance during water and air ingress accidents have addressed the response of graphitic materials, coated fuel particles and fuel kernels to oxidants such as O₂, CO, and H₂O. The specific areas of interest include the oxidation of graphite, the structural properties of oxidized graphite, the oxidation of fuel particle coatings, particularly the SiC coating, and the oxidation of fuel. Representative of the many papers on graphite oxidation are references [1], [2], and [3]. The work on the oxidation of fuel and coated fuel particles is presented in this chapter.

5.2.2. Analytical Efforts

The analytical efforts, that is, the development of computer codes based on physical and chemical phenomena and models thereof, have been devoted largely to the area involving the oxidation of graphite and its consequences. The codes and corresponding references applying to graphite oxidation under water and air ingress accident conditions, entitled "Graphite Oxidation Codes", appear in Table 5-1. For the other areas listed in Section 5.2.1, little work has been done and no specific codes have been reported in the open literature.

5.3. WATER INGRESS ACCIDENTS

5.3.1. Particles with Exposed Fuel

The effect of water vapor on the release of fission gas from fuel has been investigated by injection of water vapor into carbonaceous systems containing particles with exposed fuel kernels. Such experiments have led to an understanding of the mechanisms of fission gas release in the presence of water vapor and of the dependence of the quantity released and the duration of release on the partial pressure of water vapor, the inventory and the temperature.

The interaction of water vapor with particles having exposed fuel kernels has been investigated both during and after irradiation. Although these types of experiments differ severally, they are potentially complementary. The data accumulated during irradiation indicate two general mechanisms. One reflects a strong dependence of fission gas release on the partial pressure of water vapor below 1 kPa and the other indicates a developing weakening dependence of release on the partial pressure of water vapor above 1 kPa. Such a sequence of dependency has been observed for the fuel UC₂ [13].

Table 5-1: Graphite oxidation codes: applications to water and air ingress conditions

	Code acronym	Ingress	Reference
Research Center Jülich	REACT/THERMIX	Air, Water	[4]
General Atomics, San Diego	OXIDE3	Air, Water	[5]
	GRAPHOX	Air	[6]
	REACT ⁽¹⁾	Water	[7]
	AIP	Air	[8]
Japan Atomic Energy Research Institute, Tokai	GRACE	Air	[9]
	OXIDE-3F	Air, Water	[10]
Institute of Nuclear Energy Technology, Beijing	OXIDE-RE	Air	[11]
	RETRAN	Water	[12]

(1) The acronym REACT is used in two codes. The REACT/THERMIX code consists of a thermohydraulic part strongly coupled to a module simulating chemical processes. The REACT code models steam-induced graphite corrosion but can be incorporated into the General Atomics code SURVEY which treats thermohydraulics and fuel performance.

5.3.1.1. Water Vapor Injection During Irradiation

Three irradiation experiments, HRB-17/18 [14], HFR-K6 [15, 16], and HFR-B1 [17], one in the ORNL high flux isotope reactor, HFIR, and the latter two in the Petten high flux reactor, HFR, have been conducted. In experiments HRB-17/18 and HFR-B1, the fuel element consisted of a cylindrical fuel compact, containing coated fuel particles dispersed in carbonaceous matrix material and surrounded by graphite. The kernels of a selected number of particles had only a thin pyrocarbon coating. The coating failed, as designed, shortly after irradiation began. Consequently, a known number of exposed kernels and therefore a known source of fission products were established. The exposed kernels initially consisted of 80 % UO₂ and 20 % UC₂. During irradiation, but before exposure to water vapor, the UC₂ content declined to 13 % as a result of fissioning and reaction with oxygen from UO₂ fissioning, and then to 0 % after exposure to water vapor (≈ 0.2 kPa) [18]. In experiment HFR-K6, there were four fuel spheres containing coated UO₂ particles dispersed in A3-3 matrix graphite and contained in three capsules. Two of the particles were defective and had exposed kernels.

The experiments were conducted by injecting water vapor, in a series of discrete tests, into the capsules containing the exposed fuel kernels. The sweep gas, having a known partial pressure of water vapor, flowed between a sleeve and the compacts in experiment HRB-17/18 and over the walls of the graphite blocks containing fuel compacts in experiment HFR-B1. Thus, in the former experiments, the water vapor diffused directly

into the fuel compact and, in the latter experiment, through the graphite wedge prior to entering the fuel compacts. The released fission gas was monitored for the quantity of the isotopes Kr-85m, Kr-87, Kr-88, Xe-133, Xe-135 and Xe-138 present.

The general sequential response of the exposed fuel kernels to the injection of water vapor consists of three distinct stages as shown in Fig. 5-1. These three stages are labeled 1, 2, and 3. Stage 0 represents the prehydrolysis reference stage. Stages 1, 2, and 3, respectively, consist of:

- (1) a transient release of fission gas with a concomitant increase in the steady-state release,
- (2) a period of constant steady-state release, and, upon cessation of water vapor injection,
- (3) a decline in the release to prehydrolysis values.

By expanding the time scale of Fig. 5-1 [18], the structure of stage 1 is clarified as shown in Fig. 5-2 for three of the measured isotopes, i.e., Kr-87, Kr-88, and Kr-85m. Stages 0 and 2 are represented by mean values of R/B, shown as thick line segments, both within and outside the time segment of Fig. 5-2. These R/B values have a standard deviation of 8 %. In stage 1, the fission gas release increases and then declines after reaching a peak 2 h after starting water vapor injection [14]. The decline in R/B during stage 1 suggests that the gas release in this stage comes from a limited source or availability of fission gas.

The length of stage 1, approximately 9 h in Fig. 5-2, is governed by the slow movement of water vapor to the sites of the exposed kernels in the fuel compact. This is confirmed by the series of 30 sequential $\text{UC}_2\text{-H}_2\text{O}$ reaction spikes appearing on the ionization chamber chart [14] and corresponding to the 30 particles with exposed kernels. Simultaneously, fission gas is also being released following the $\text{UO}_2\text{-H}_2\text{O}$ interaction albeit more slowly and over a long period of time for each kernel. The latter time period is 2 h and as shown [14, 18], accounts for the peak in R/B appearing 2 h after initiation of water vapor injection.

During the rise and decline of fission gas release in stage 1, there is an underlying increase in the fractional release between the regions of steady state fission gas release preceding and following stage 1. The time profile of the dashed curve is based on measurements of the time profile of Xe-135; the shape of the underlying curve has been assigned the same functional dependence on time as is observed for Xe-135. The justification for using Xe-135 data is presented below.

During the time interval represented by the data in Fig. 5-2, the fractional release for isotope i , $(R/B)_i$, is given to a good approximation by K/λ_i^n . K is a constant reflecting the essential constancy of experimental conditions in the time interval addressed, λ_i is the decay constant for isotope i and n , a constant, is a measure of the relative fractional concentrations of the isotopes of a given element in a gas sample. A zero value of n corresponds to identical values of the fractional concentrations. As n increases, the fractional concentration of a longer-lived isotope also increases relative to a shorter-lived isotope.

The stages in the response of fuel kernels to the injection of water vapor are distinguished not only by the R/B profiles but also by the profiles of n . This is shown in Fig. 5-3. The mean values of n before and after stage 1 are ≈ 0.35 and n has a peak value of ≈ 1.1 in stage 1. Note that fission gas, diffusively released from particles with

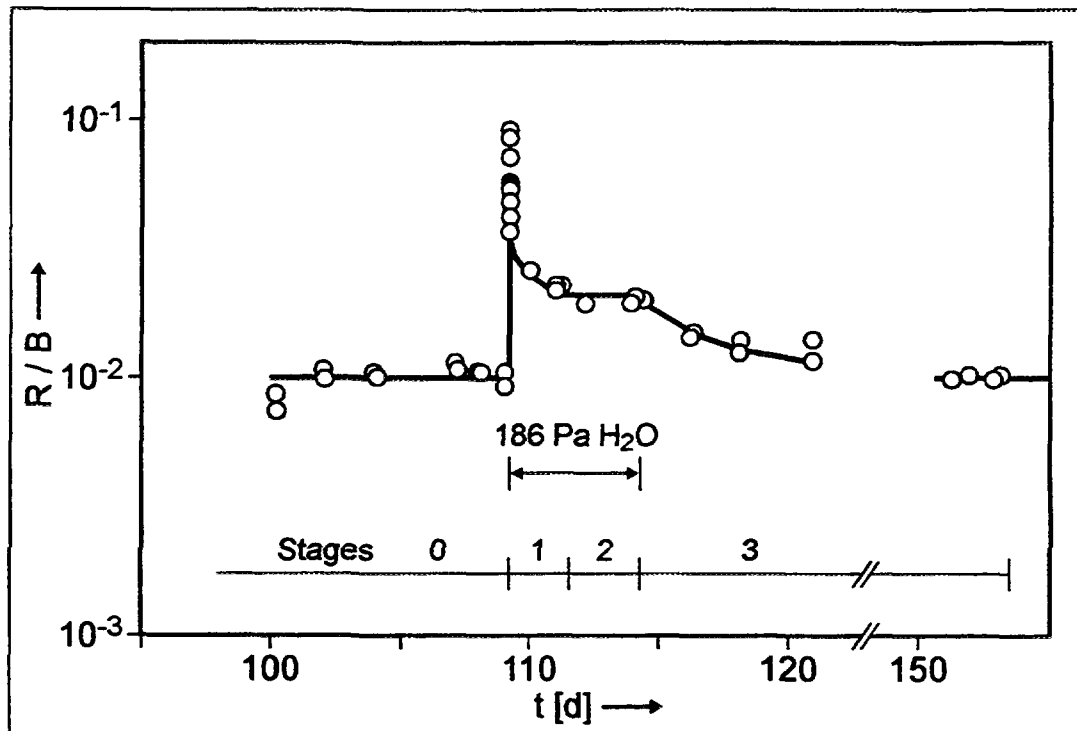


Fig. 5-1: R/B-time profile for Kr-85m before, during, and after a water vapor injection test with 186 Pa of water vapor at 755 °C

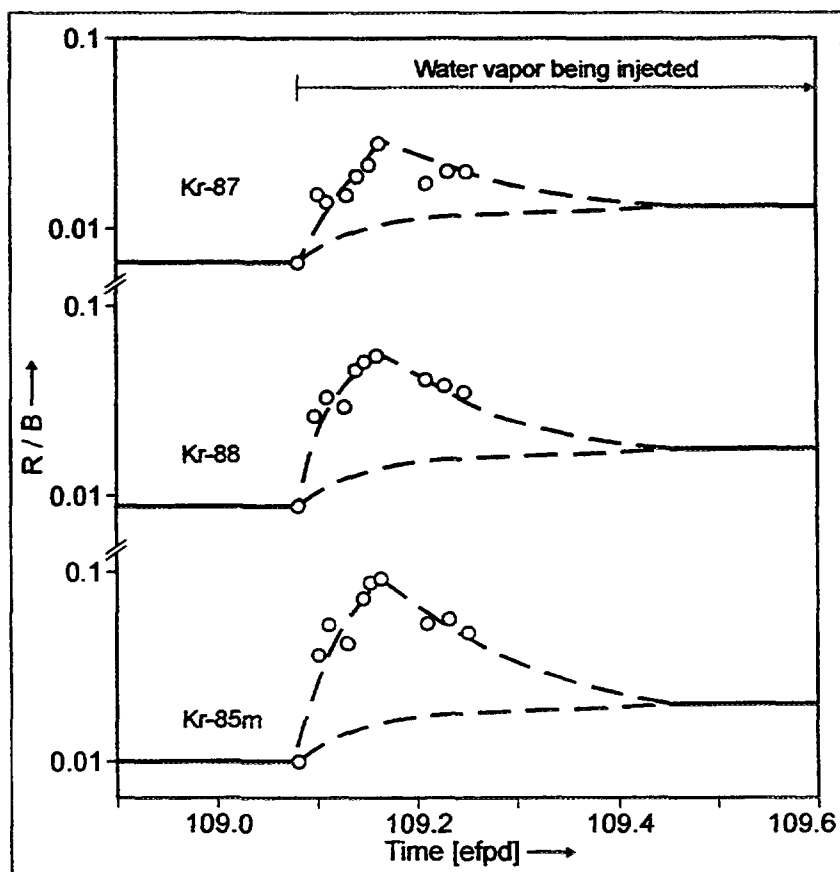


Fig. 5-2: R/B profiles in the early portion of the water vapor injection test at a partial pressure of 186 Pa and at 755 °C in experiment HRB-17

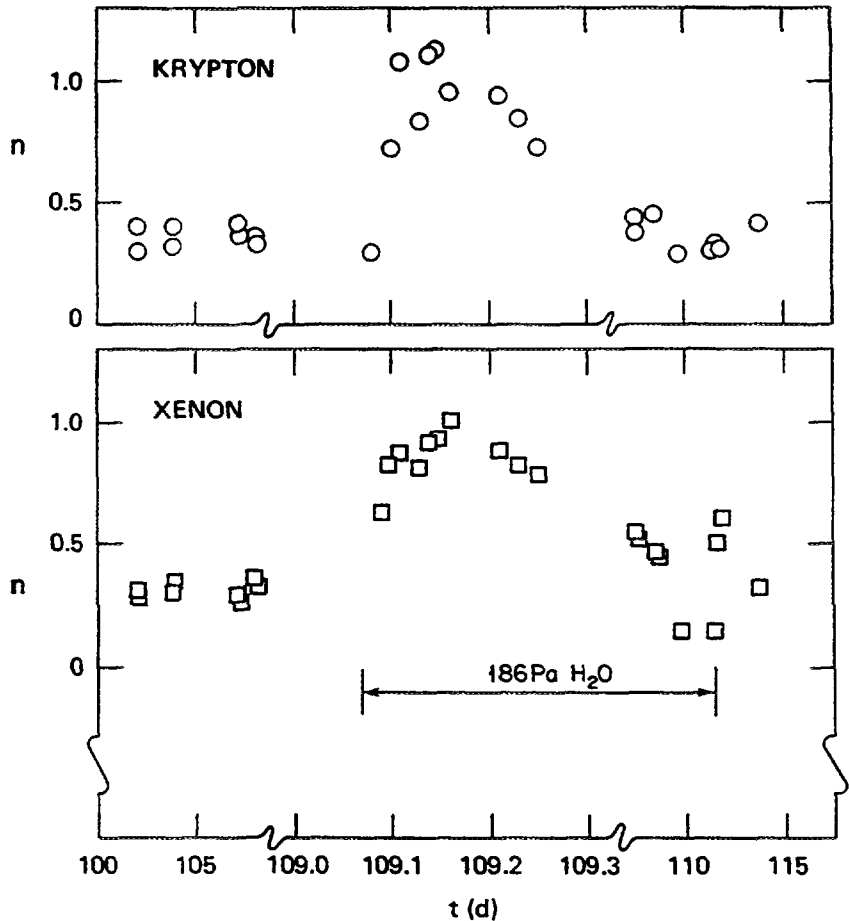


Fig. 5-3: A measure of the relative concentration of isotopes of an element before and during water vapor injection at 755 °C with 186 Pa of water vapor

exposed kernels, has n values in the range ≈ 0.2 to ≈ 0.5 and gas collectives have values of n in the range ≈ 1 to ≈ 1.5 . Thus before and after stage 1, the n values of Fig. 5-3 are consistent with diffusive release and during stage 1 are consistent with the predominate release of gas collectives following a breaching of gas bubbles or closed pores.

The curves of Fig. 5-2 can be used to separate the contributions of gas collectives and interstitial fission gas atoms to the quantity of gas released. The Xe-135 release curve on which the underlying curve in stage 1 region is based, represents only diffusive release. There was no stored Xe-135. Because of the (n,γ) reaction of Xe-135, the effective decay constant was large enough to prevent the accumulation of this isotope in storage during irradiation. Thus the underlying dashed curve in stage 1 represents the continuation of diffusive release in stage 1. The total profile of diffusive release is then established.

The quantity of gas released from collectives, hereinafter referred to as "stored" gas, is determined by summing the differences in R/B values in stage 1 over small increments of time [17]. The data [17] from experiment HFR-B1, over a range of partial pressures of water vapor and temperatures, were used in a preliminary analysis. The model function previously used [14] was generalized to include a dependence on temperature as well as on the partial pressure of water vapor. This yielded [17] the relation:

$$f = k p^{m(T)} \exp\{-Q/(RT)\} \quad (5-1)$$

where

- f is the fraction of inventory released as stored gas
- k is a constant [Pa^{-m}]
- $m(T)$ is a temperature dependent exponent, $m(T) = \alpha + \beta T^{-1}$
- α, β are constants
- Q is the activation energy for release of stored gas [J/mol]
- R is the gas constant, $R = 8.314 \text{ J/(mol K)}$
- T is the temperature [K]

Eq. (5-1) is an empirical relation which is meant to describe simply the complicated interplay of the effect of water vapor pressure and temperature on the release of fission gas from exposed fuel kernels. The simplification is centered in the function $m(T)$ which represents the effective declining relative contribution of water vapor to release as the temperature increases. Eq. (5-1) is only valid within the water vapor pressure and temperature ranges of the experimental data [17]. To evaluate the parameters and constants of Eq. (5-1), excepting $m(T)$, preliminary data [17] from experiment HFR-B1 were used. The temperatures varied from 820 to 1040 °C and the partial pressures of water vapor varied from 2.8 to 1051 Pa during irradiation in HFR-B1. Data [14, 17] from experiments HRB-17 and HFR-B1, respectively, were used to evaluate the constants α and β of $m(T)$. The results of the evaluations are given by the equation:

$$f = 2.13 * 10^{13} p^{-4.353+6503/T} \exp\{-4.7257(10^4/T)\} \quad (5-2)$$

The values of α , β , k , and Q are, respectively, -4.353, 6503., $2.13*10^{13}$, and 392.9 kJ/mol. As for Eq. (5-1), Eq. (5-2) is only valid within the water vapor and temperature ranges of the experimental data [17]. Note that isorelease curves [17], i.e., curves of constant release on a plot of water vapor pressure, $P(\text{Pa})$, versus the reciprocal temperature, $10^4/T(\text{K})$, can be deduced from Eq. (5-2).

The dependence of the release of stored gas, as a fraction of the inventory, on the partial pressure of water vapor at 770 °C is shown in Fig. 5-4 whereon the calculated and measured values are presented. There is a linear relation between the logarithms of the stored fission gas releases and the partial pressures of water vapor; this persists over at least three powers of ten in the partial pressure. Extrapolation of the calculated line in Fig. 5-4 would indicate complete release of the stored fission gas at a water vapor pressure of $\approx 2 \text{ kPa}$ assuming the amount of stored fission gas to be a large fraction of the gaseous inventory.

Bearing on the matter of the extrapolation of the calculated line of Fig. 5-4 are results from experiment HFR-K6 [15, 16]. In this experiment, two fuel particles in the fuel sphere of Capsule C significantly contributed to release; they were judged to have kernels effectively exposed to the particle exteriors [16].

A preliminary analysis of HFR-K6 [19] yielded three data representing the relative releases of stored fission gas at water vapor pressures of 0.2, 0.5, and 2.0 kPa. As shown

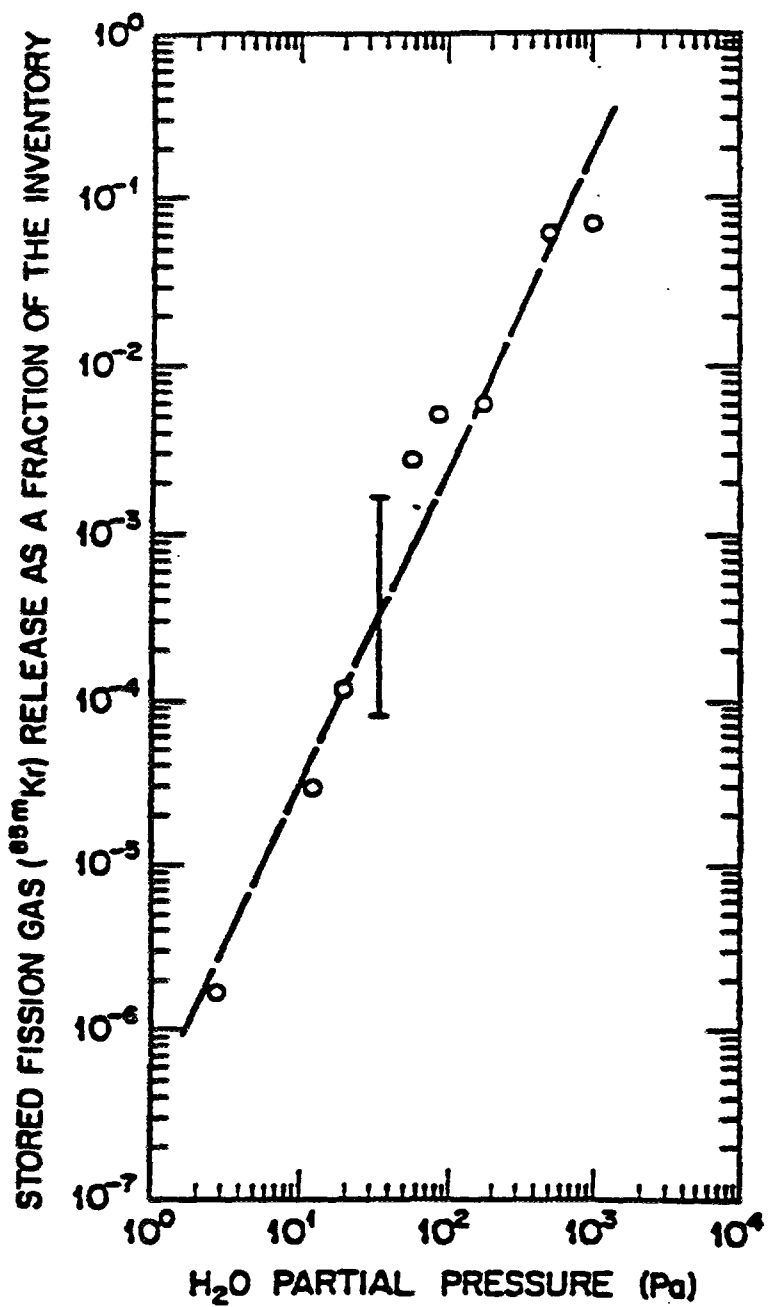


Fig. 5-4: The dependence of the release of stored fission gas on the partial pressure of water vapor at 770 °C derived from experiments HFR-B1 and HRB-17

in Fig. 5-5, the datum at the lowest pressure was normalized to the calculated line at 0.2 kPa and the other data were placed on the figure using their relative values and the corresponding water vapor pressures.

For Figs. 5-4 and 5-5, note the temperature difference. This difference accounts for the slightly different release values of the data and plotted curves on these figures, particularly so, given the large activation energy, 393 kJ/mol, for the release of stored fission gas.

Two features of the HFR-K6 data on Fig. 5-5 are of interest: (1) The data at 0.2

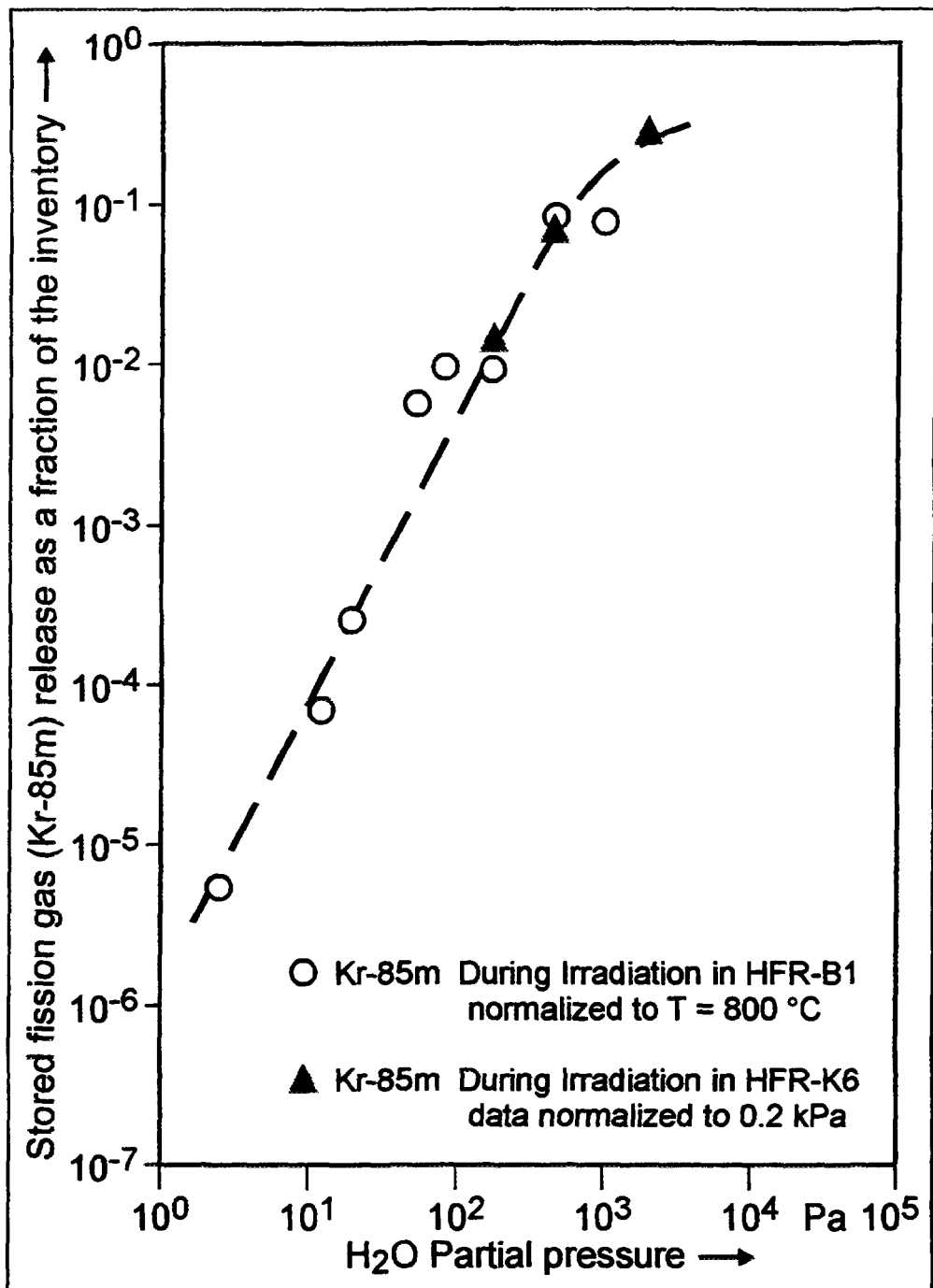


Fig. 5-5: The fractional transient release of stored fission gas as a function of the partial pressure of water vapor at $800\text{ }^\circ\text{C}$ based on experiments HFR-B1 and HFR-K6 during irradiation

and 0.5 kPa fall on the calculated line and are therefore consistent with the representation of the HFR-B1 data. (2) The datum at 2.0 kPa indicates that the slope of the calculated line must begin to significantly decline with increase in the partial pressure of water vapor above $\approx 0.5\text{ kPa}$. At 2 kPa , the HFR-K6 datum lies a factor of ≈ 4 below the datum reached by extrapolation of the calculated line.

The change in the slope of the dependence of the release of fission gas on the partial pressure of water vapor has been observed [13] in the case of release from UC₂ fuel. Of

Table 5-2: Values of h_o as a function of water vapor pressure and element

	$h_o = (R/B)_{i2} / (R/B)_{i0}$			
Partial pressure of water vapor [Pa]	20.6	64.8	186.	199.
Krypton	2.1	2.0	2.0	2.5
Xenon	2.5	2.5	2.7	3.1

course, further experimentation and analysis are required before a tolerable uncertainty is established.

The examination of the dependence of the release of stored fission gas on the partial pressure of water vapor was confined, thus far, to one isotope. However, experiments [14] have decisively shown that the release of stored fission gas as a fraction of the inventory is the same for all isotopes of a given element and the same for the elements Kr and Xe provided the contribution of the xenon precursor, I-133, is taken into account. The range of the partial pressures of water vapor in these experiments was ≈ 20 to ≈ 200 Pa. Nevertheless, the common fractional release of stored fission gas for all isotopes is strong evidence for the release of fission gas atoms in collectives and would be expected at pressures outside the foregoing range to an extent yet to be determined.

The mechanism(s) leading to the activation energy of ≈ 393 kJ/mol in Eq. (5-2) has(have) yet to be identified. It is perhaps worth noting that this activation energy is only 34 % larger than the activation energy, 293 kJ/mol, attributed [20], but with caution, to intrinsic diffusion of rare gas atoms in UO_2 .

Stage 2 begins after the cessation of the transient release of stored fission gas. In stage 2, the fractional, steady-state, diffusional release $(R/B)_i$ (the ratio of the release rate to the birth rate for isotope i), remains constant for UO_2 fuel provided the temperature and the partial pressure of water vapor are held constant. This has been demonstrated in experiments [21] over time periods of 3 to 11 h. Stage 2, for UO_2 fuel, is characterized by the ratio

$$h_o = (R/B)_{i2} / (R/B)_{i0} \quad (5-3)$$

where the subscripts represent the isotope (i) and the stages (0) and (2). This applies to UO_2 fuel for which, under the experimental conditions of interest here, there is no irreversible change induced by interaction with water vapor.

The use of Eq. (5-3) yields the data presented in Table 5-2 showing that (1) the values of h_o in columns 2, 3, and 4 are sensibly constant for krypton and xenon over a range of water vapor pressures; (2) the values of h_o in column 5 are larger by ≈ 20 % than the element average of the other columns, and (3) the values of h_o for xenon are larger than those for krypton by a factor of nearly 1.3 on the average.

To account qualitatively for the data in Table 5-2, consider a distance of order $(D\tau)^{1/2}$ which is represented hereinafter by $\sqrt{D\tau}$. D is a diffusion coefficient (m^2/s) and $\tau(s)$ is the lifetime of an isotope (defined as a time by which only a specified small fraction remains radioactively undecayed). The qualitative accounting of the data of Table 5-2 is as follows:

1. If an isotope is within a distance $\sqrt{D\tau}$ of a surface, it can escape from the fuel kernel otherwise it will decay radioactively before escape. When the water vapor interacts with the fuel, the fuel density decreases and D can increase. Consequently the quantity of the isotope escaping will increase by a factor independent of the particular isotope of an element. Furthermore, if increasing the partial pressure of water vapor only increases the depth beneath the surface to which the enhanced D extends, rather than increasing D, then $\sqrt{D\tau}$ remains unchanged as does the quantity of an isotope escaping.
2. When carbide is present and is significantly hydrolyzing, as is the case only in the test with 199 Pa of water vapor, the distortion of the fuel structure is greater than otherwise and D would be expected to increase beyond that observed for an H_2O-UO_2 interaction.
3. For any decrease in the density of the fuel, the effect on diffusivity could be greater for xenon than for krypton atoms because of the larger atomic radius of xenon atoms. Note [22] that the ratio of the atomic volumes of xenon to krypton, 1.3, is nearly the same as the corresponding average ratio of the h_o values from Table 5-2.

For Xe-133, the h_o values are about twice as large as for the other isotopes [14]. This reflects the contribution to $(R/B)_{Xe}$ from the radiodecay of the xenon precursor I-133 [14]. The ratio of n_2/n_o for the experiments of Table 5-2 has the average value and standard deviation of 1.1 ± 0.09 . The slight increase in n in going from stage 0 to stage 2 may reflect a change in the fuel surface topology.

Stage 2 observations provide data on the temperature dependence of $(R/B)_i$ in the presence of water vapor [19]. For UO_2 fuel kernels, the activation energy is 65.8 kJ/mol before exposure to water vapor [14] and is 23.6 kJ/mol under a constant partial pressure of water vapor, 1051 Pa, during stage 2 [17]. The latter activation energy accounts for the different values of h_o measured at temperatures of 680 and 767 °C in experiments HFR-K6 and HRB-17, respectively. The mean value of h_o in experiment HFR-K6 is 1.55 [19]. By using the activation energy of 23.6 kJ/mol and a temperature of 767 °C, the predicted value of h_o for experiment HRB-17 becomes 2.0 which is also the value measured in experiment HRB-17 at 767 °C. This result indicates a consistency among experiments HRB-17, HFR-B1, and HFR-K6 and is in accord with the deductions that h_o is independent of element, isotope, and the partial pressure of water for UO_2 fuel. (Note that 767 °C, not 755 °C [14] is the statistically corrected average temperature (see Table E.1 in [21].)

Stage 3 begins with the cessation of water vapor addition to the fuel system. The R/B smoothly declines from the stage 2 value to that in stage 0 as shown, for example, in Fig. 5-1. This change implies that the fuel returns to a structure equivalent in release to the structure existing prior to water vapor addition. The decline is characterized by a quantity δ in the relation

$$(R/B)_{id} = (R/B)_{i0} [1 + (h_o - 1) \exp\{-\delta(t - t_T)\}] \quad (5-4)$$

where the subscripts id and i0 represent, respectively, the declining R/B and the R/B in stage 0 for isotope i, and the subscript T represents the time of terminating water vapor addition. The quantity h_o is defined by Eq. (5-3). Eq. (5-4) is valid only for UO₂ fuel systems. The value of δ was found to be independent of the isotope, element, and water vapor pressure in experiment HRB-17 [14]. The time at which the approach to $(R/B)_{i0}$ is 95 % complete, Δt_{95} , is given by the relation:

$$\Delta t_{95} \approx 3 / \delta \quad (5-5)$$

For the data gathered from the experiment HRB-17, $\Delta t_{95} \approx 7$ d.

Similar behavior of the fission gas release after cessation of water vapor addition was also observed in experiments HFR-B1 [17] and HFR-K6 [19]. This is shown in Figs. 5-6a and 5-6b for times greater than 7.5 and 100 d. The curves corresponding to the declining R/B values represent the fittings of Eq. (5-4) to the data points. This has resulted in a δ value of 0.109/d and an h_o value of 2.3 for both experiments. It is necessary to note that the h_o values arise from the fittings. Deriving h_o values from the experimental data is difficult. In experiment HFR-B1, water vapor injections were generally made randomly between stage 2 and stage 0 rather than waiting until the near completion of stage 3 with one exception. In experiment HFR-K6, the water vapor injections were made cumulatively thus obscuring stages 1 and 2.

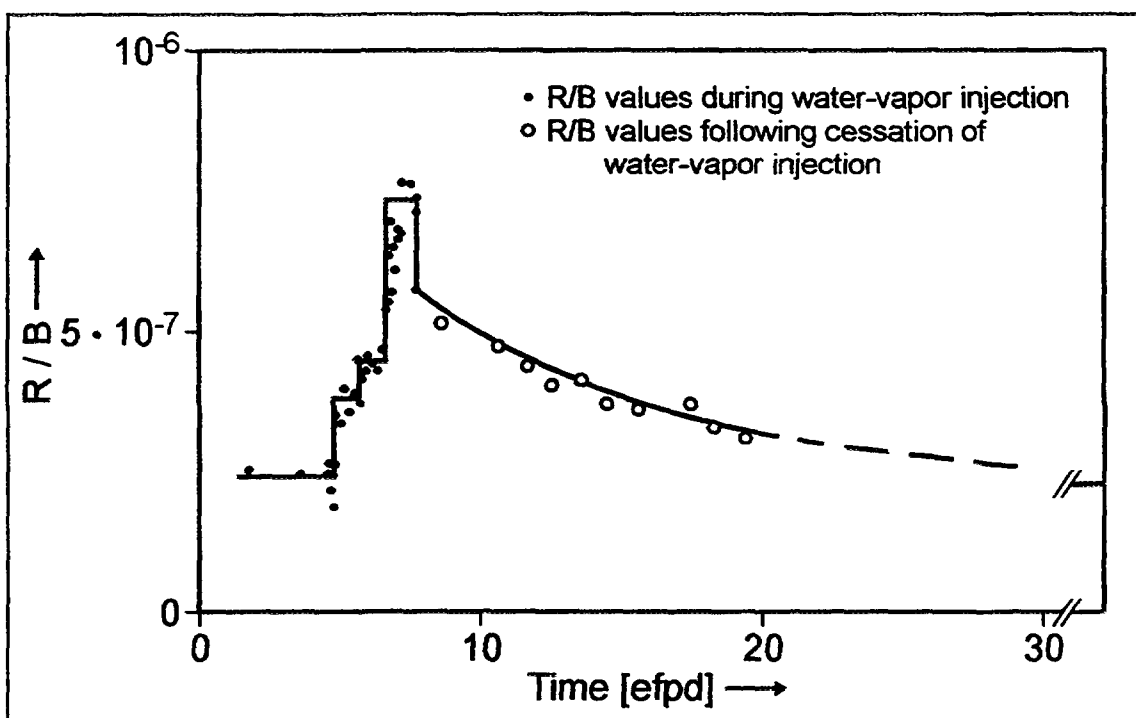
The values of Δt_{95} are a function of the fast neutron flux, f , as shown in Fig. 5-7. The time measure, Δt_{95} , is shown as a function of $Q(f)$ which is linear in f . The function $\Delta t_{95} = Q(f)$ is only very roughly established. On the abscissa scale, the value 2 crudely represents the flux spectrum in the Petten high flux reactor (HFR) during experiments HFR-B1 and HFR-K6, and the value 6 crudely represents the flux spectrum in the ORNL high flux isotope reactor (HFIR) during experiment HRB-17. The value zero here represents the post irradiation experiments in the Research Center Jülich (KFA) corrosion apparatus (KORA) with compacts from experiment HFR-B1 [23].

In experiment HRB-17, following cessation of the water vapor addition, the initial decline of R/B was more rapid for a small period of about 15 h than subsequently. For the isotopes Kr-85m, Kr-87, Kr-88, and Xe-138, the slope of the initial decline was the same. For Xe-133 the slope was larger. The radioactive decay of I-133 accounted for the difference between the slope for Xe-133 and that common to Xe-138 and the krypton isotopes.

If the fuel consists of a mixture of UO₂ and UC₂, as is the case for the US fuel kernel, the presence of water vapor induces two events: (1) the UC₂ portion of the kernel is irreversibly oxidized and this contributes to an increase in $(R/B)_i$; (2) in the UO₂ portion of the kernel, interaction with water vapor also induces an increase in $(R/B)_i$ as considered above. For such a mixed kernel composition, stage 2 can be characterized by the ratio:

$$H_c = h_o c_p \quad (5-6)$$

(a)



(b)

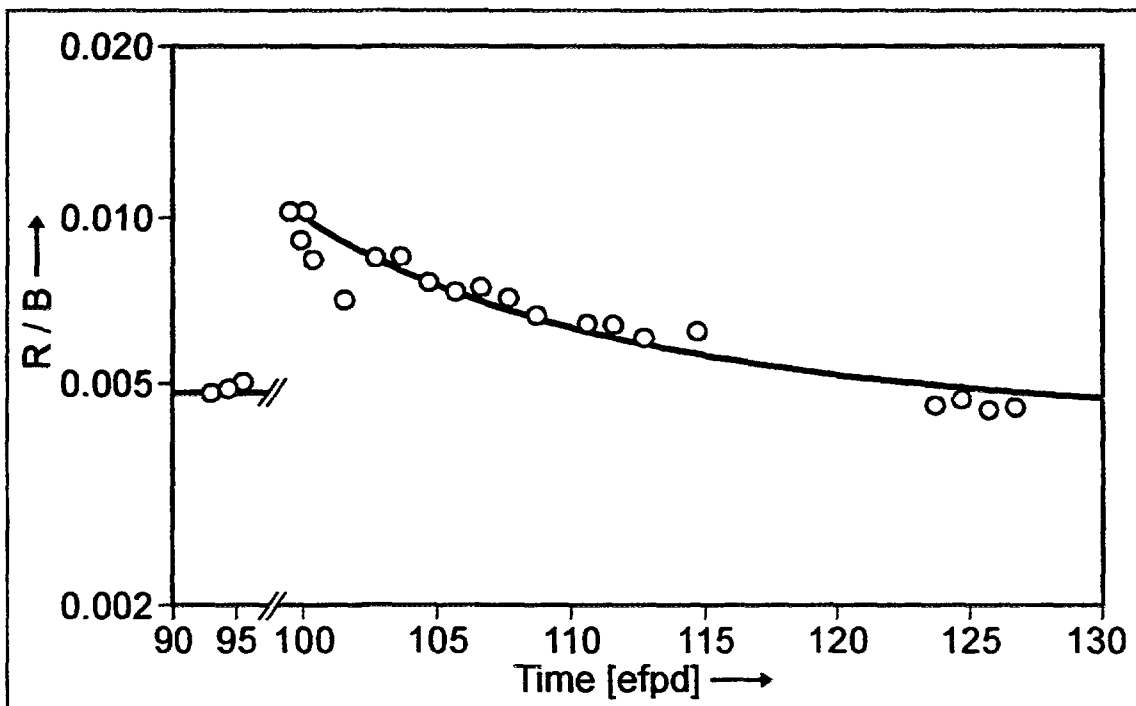


Fig. 5-6: The decline of R/B following the cessation of water vapor addition in
(a) experiment HFR-K6, Cycle 25 at $680\text{ }^{\circ}\text{C}$
(b) experiment HFR-B1, Cycle 88.10, test 5 at $925\text{ }^{\circ}\text{C}$

The relevant data are represented by open circles and the curve is derived from the equation $(R/B)_{id} / (R/B)_{i0} = 1 + 1.3 \exp\{-\delta(t - t_T)\}$ with $(R/B)_{i0} = 2.4 \times 10^{-7}$, $\delta = 0.109/d$ and t in units of days (d).

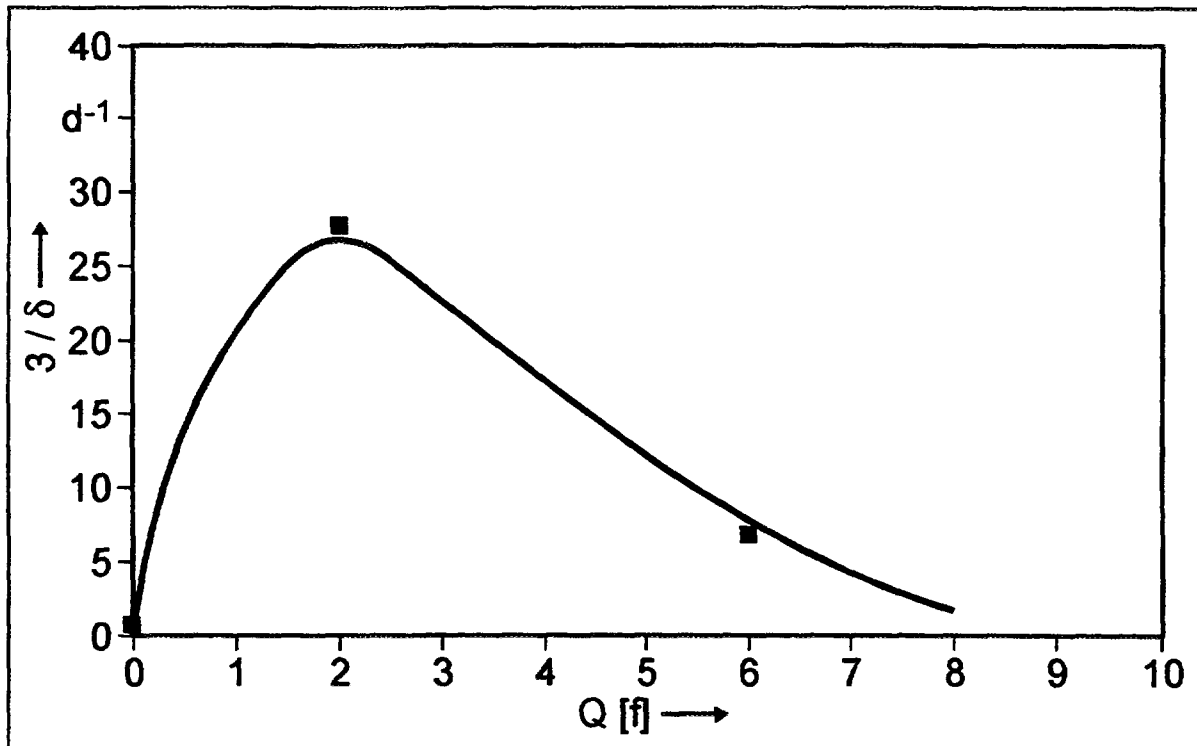


Fig. 5-7: The recovery to within 95 % of the prehydrolysis value of R/B following cessation of water vapor injection into the fuel element system as a function of the fast neutron flux, f

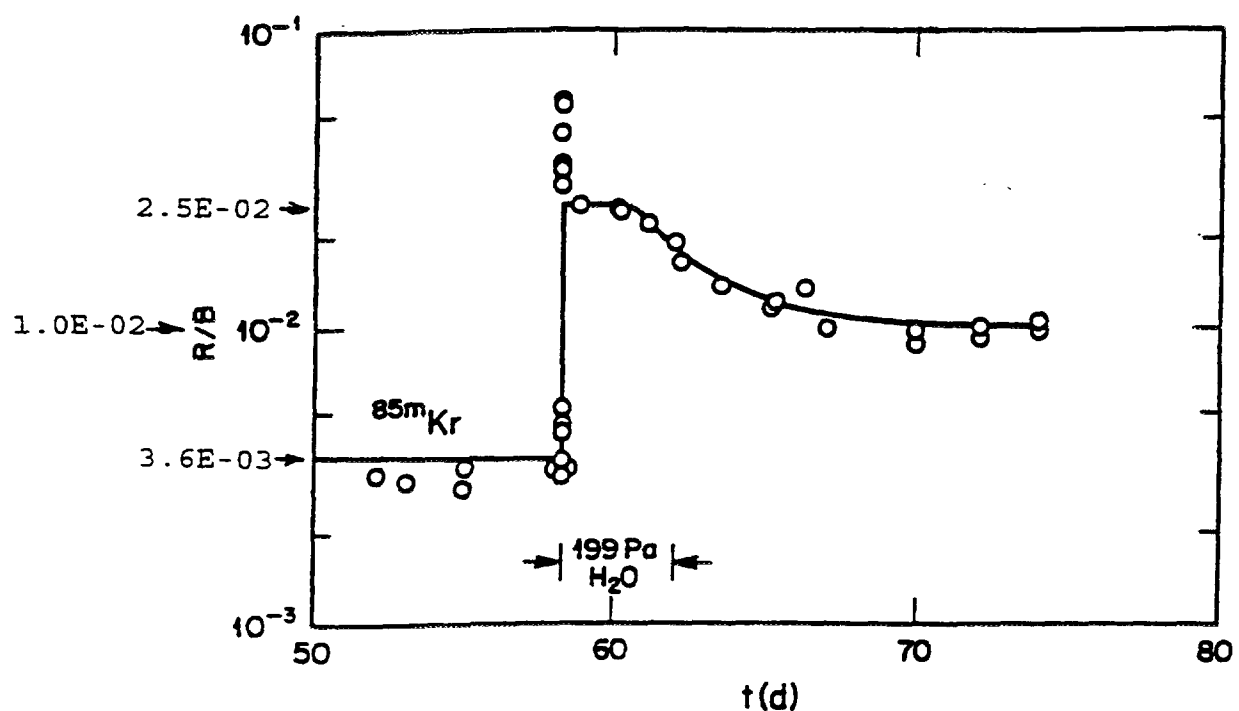


Fig. 5-8: R/B time profile for Kr-85m before, during, and after a water vapor injection test at 199 Pa of water vapor and 779 °C into fuel with an initial composition of 90 % UO_2 and 10 % UC_2

The quantity h_o , given by Eq. (5-3), applies to the UO_2 portion whereas the quantity c_p accounts for the increase in $(R/B)_i$ resulting from the irreversible oxidation of UC_2 by the water vapor, c_p depends on the fraction of UC_2 , the temperature, and the water vapor pressure. For example, in a kernel of composition $\text{UC}_{0.2}\text{UO}_{1.8}$ (10 % UC_2 and 90 % UO_2), $c_p = 2.78$ for the UC_2 portion under a vapor pressure of 199 Pa and a temperature of 779 °C (see Fig. 5-8). The corresponding H_c values for krypton and xenon, using h_o values from Table 5-2 below, are 6.94 and 8.71, respectively. The measured values of H_c differ by less than 1.2 % from these calculated values.

In the case of stage 3 for a fuel with a mixture of UO_2 and UC_2 , the right-hand side of Eq. (5-4) must be multiplied by the factor c_p . Thus:

$$(R/B)_{id} = (R/B)_{i0} c_p [1 + (h_o - 1) \exp\{-\delta(t - t_T)\}] \quad (5-7)$$

where $(R/B)_{i0} = 3.6 \times 10^{-3}$, $c_p = 2.78$, $h_o = 2.5$, $\delta = 0.425$, and $t_T = 60.5$ d. The application of Eq. (5-7) is shown in Fig. 5-8 to a fuel with 90 % UO_2 and 10 % UC_2 . Note that the presence of UC_2 in the fuel leads to an onset of the decline in R/B before the cessation of water vapor addition unlike the response to cessation where the fuel is solely UO_2 .

5.3.1.2. Changes in Kernels Exposed to Water Vapor During and After Irradiation

5.3.1.2.1. During Irradiation

As shown in Figs. 5-1, 5-6a, and 5-6b after the cessation of water vapor injection, the R/B declines to the value measured just prior to the initiation of water vapor injection. This behavior was observed [17, 21, 25] in experiments HFR-B1, HRB-17, and HFR-K6, respectively. These observations imply that the structures of the kernels, just prior to initiation, and those asymptotically reached, following the cessation of water vapor injection, are equivalent with regard to the release of fission gas, i.e., they yield essentially the same R/B value. On the large scale, the structures are apparently similar.

The kernels in HRB-17 and HFR-B1 that interacted with the injected water vapor, resided initially in designed-to-fail particles. Such particles have only a single pyrocarbon coating of 22.8 μm thickness; the coating fails shortly after irradiation begins [24] and thus expose the kernels, as intended. In HFR-K6, manufacturing defects in two of the particles resulted in exposing their kernels [25]. The postirradiation examination of the exposed kernels involves a laborious and difficult search due principally to the sparsity of exposed kernels, the accompanying work of grinding and impregnation, and the few attempted examinations permitted by the available funding.

With regard to kernel intactness, diameter, and sphericity, the similarity of the kernels prior to initiation of water vapor injection and those asymptotically reached following the cessation of water vapor injection is realized in one successful attempt [26] at locating an exposed kernel. Fig. 5-9 displays the postirradiation photomicrograph of compact HRB-17-8. The intactness of the kernel is evident and, extensive, considering that the kernel was subjected to four water vapor injection tests. The length of a northwest-southeast oriented

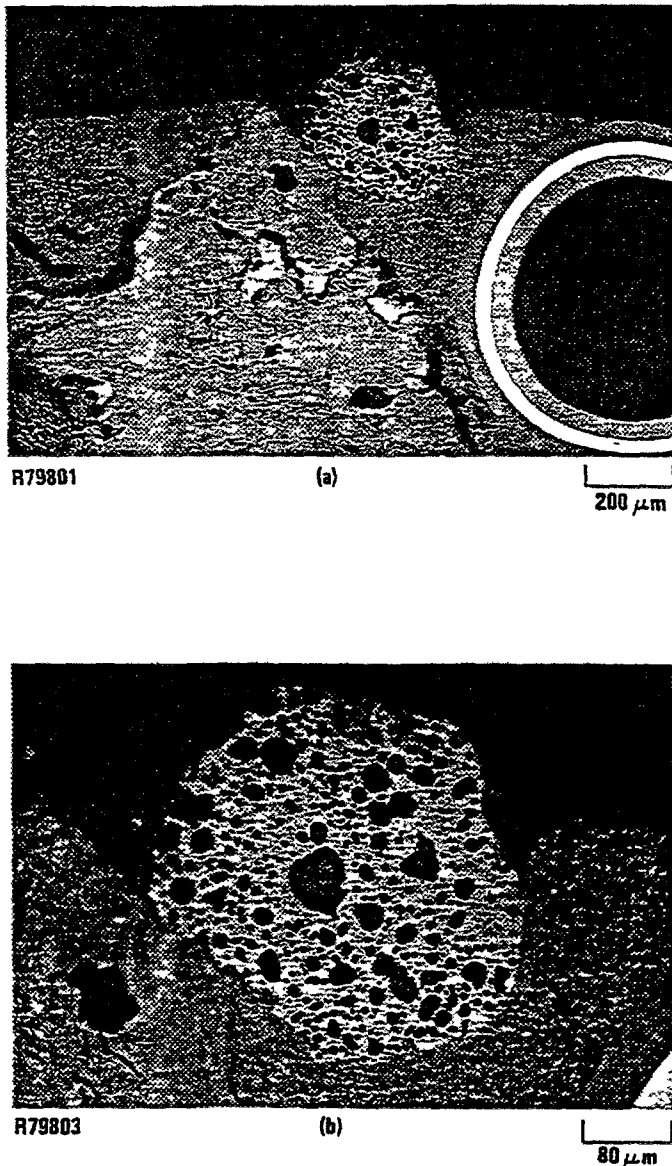


Fig. 5-9: Metallographic section of compact 8 from experiment HRB-17 [26]

diameter for the kernel shown in Fig. 5-9, is within a few percent of the pre-irradiation value ($347 \mu\text{m}$). The segments of the perimeter intersected by the northwest-southeast oriented diameter indicate a significant degree of sphericity.

5.3.1.2.2. After Irradiation

A second successful attempt [21, 26] at locating an exposed kernel is shown in Fig. 5-10 by the postirradiation photomicrograph of compact HRB-18-11. This compact was held at approximately 760°C during irradiation for 122 d. The compact was then removed from the reactor and held for 27.6 d at 200°C in a helium flow containing 1.85 kPa of water vapor. Thereafter, water vapor injection was terminated and the capsule was re-inserted into the reactor after a delay of 1.7 d. This led to the re-establishment of a steady state release of fission gases within a time period small compared to the time periods for stage

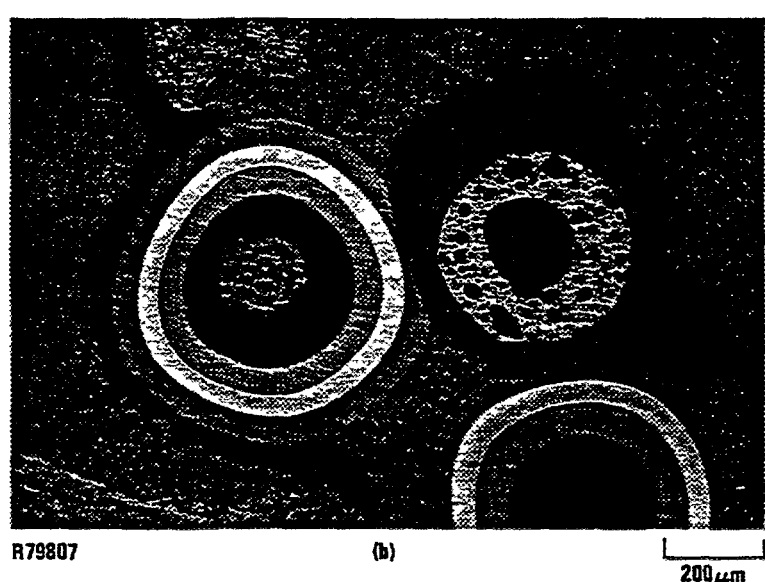
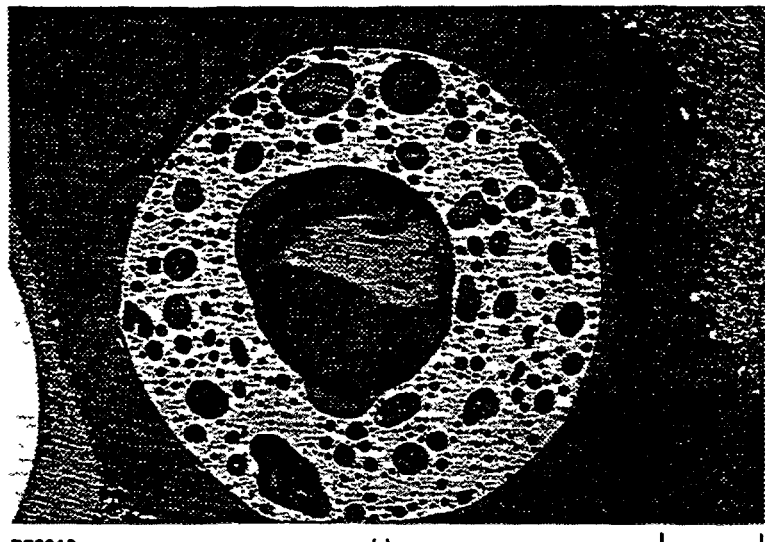


Fig. 5-10: Metallographic section of compact 11 from experiment HRB-18 [26]

3 in Figs. 5-1, 5-6a, and 5-6b. The steady state release was the same as measured prior to the injection of water vapor.

The central void in Fig. 5-10 is attributable to the oxidation of UC_2 during water vapor injection. The kernel had an initial composition of 20 % UC_2 and 80 % UO_2 . The UC_2 was essentially confined to a central sphere representing 56 % of the kernel volume. Under the experimental conditions there was sufficient time for water vapor to oxidize the UC_2 thus accounting for the location of the void.

With regard to kernel intactness, sphericity, and diameter, Fig. 5-10 demonstrates that intactness and sphericity are evident and that the outer diameter of the fuel mass corresponds to a volume enlargement between 6 and 11 %. The contribution of the oxidation of UC_2 to this enlargement and to the magnitude of the central void has yet to be determined.

5.3.1.2.3. Irradiation Effects

In regard to the two exposed kernels located, one was exposed to water vapor during irradiation and the other to water vapor only after termination of irradiation. In the former case, the R/B declined slowly after cessation of water vapor injection and in the latter case the response was rapid after a brief period of re-irradiation to establish a steady state release for fission gases (Xe-135, Xe-138, Kr-87, Kr-88, and Kr-85m).

In comparing the two cases, the brief re-irradiation is assumed to have negligible structural effects in the kernel. The assumption is substantiated on the large scale by the equality of the R/B values before and after the exposure to water vapor. The ratio of the duration during the brief re-irradiation to that during the continued irradiation in stage 3 of Figs. 5-1, 5-6a, 5-6b has the range 0.003 to 0.23.

To account for the overall effect, the following postulate is proffered. Irradiation of the kernel during exposure to water vapor results in a strong binding of water-derived species in the kernel. The strong binding sites are created by large energy transfer to the kernels during the slowing down of neutrons traversing them. In the absence of irradiation, binding of the water-derived species involves only smaller energies of the magnitude associated with chemical reactions. Therefore, in the absence of water vapor, releasing the water-derived species from the kernels requires the energy magnitudes associated with the respective strengths of binding. The latter is observed.

5.3.1.2.4. In the Absence of Water Vapor

Changes in the designed-to-fail particles, in the absence of water vapor, occurred in capsules 1 and 2 of experiment HFR-B1. An example is shown in Fig. 5-11 for compact HFR-B1-012100 in capsule 1 [27]. After the start of irradiation, the pyrocarbon coatings failed within 20 days. The status of a designed-to-fail particle after 444 effective full power days is shown in Fig. 5-11. The post-test diameter of the kernel is within 5 % of the initial value of 347 μm . A rough measurement of the thicknesses of the coating fragments shown, yields a value between 25 and 30 μm , depending on the fragments orientation. This is regarded as consistent with the pre-irradiation value of 23 μm .

5.3.1.3. German Postirradiation Water Vapor Injection

As there was only a limited possibility to examine fuel under water ingress conditions in Material Test Reactors, the **Corrosion Furnace (KORA)** was developed in the Research Center Jülich. The KORA was built in 1991 to study the effect of the moisture-induced increase in fission product release as a function of the partial pressure of water vapor and temperature using different fuel samples.

In general, only the long-lived isotope Kr-85 can be measured in post-irradiation heating experiments, whereas the short-lived fission gas and iodine nuclides in the test samples have already decayed. Since Kr-85 with a half-life of 10.8 y is continuously built-up during irradiation and no production/decay equilibrium is established, only an R/N value, where R is the release rate [s^{-1}] and N is the inventory [atoms], can be specified. In contrast to in-pile experiments [14], there is no birth rate of fission gases. Consequently the



Fig. 5-11: Postirradiation Metallographic section of compact -12100 capsule 1 of experiment HFR-B1 [27]

Table 5-3: Properties and irradiation history of fuel samples used in the water-vapor injection tests in KORA

Sample properties				Irradiation condition		
Fuel samples	Type of sample	Kernel	Defective particles [%]	Burnup [%FIMA]	Fast fluence [$10^{25} \text{ m}^{-2}, E > 16 \text{ fJ}$]	Irradiation temperature [°C]
AVR 89/30	Sphere	UO ₂	< 2*10 ⁻⁴	9.0	2.6	Maximum surface temperature 1000 - 1280
AVR 92/8				9.0	2.6	
AVR 92/7				9.2	2.7	
AVR 73/8		UO ₂	100	4.7	0.8	
AVR 92/29				9.2	2.7	
HFR-B1, 2.2.1+2	Compacts	UCO ⁽¹⁾	9	21.6	6.6	880 - 1230
HFR-B1, 3.2.1+2				19.6	5.1	820 - 1050
HFR-B1, 3-7a	Kernels	UCO ⁽¹⁾	100	19.6	5.1	820 - 1050
HFR-B1, 3-7b				19.6	5.1	820 - 1050

(1) UCO is only an acronym that represents a particle with a fuel kernel composed of a mixture of UO₂ and UC₂. Irradiated compact samples from capsule 3 have kernels which are unlikely to contain any UC₂. During irradiation and water vapor injection, the UC₂ will be completely and irreversibly oxidized.

source of Kr-85 decreases during the heating test. Therefore, the first water vapor injection is most important whereas results of the following injections are difficult to interpret.

Of particular significance for licensing of an HTGR is the release of iodine nuclides. Iodine could not be measured directly, but it has been demonstrated that noble gas release is similar to iodine release [28].

5.3.1.3.1. Apparatus

The corrosion apparatus, KORA, enables different samples (particles, compacts, spherical fuel elements) to be studied with less effort than is required in irradiation experiments (Fig. 5-12). Fuel samples up to the size of spherical fuel elements can be heated in helium with a water vapor content of more than 80 kPa, and also in other gases such as air, up to a maximum temperature of 1600 °C. It is thus possible to achieve higher water vapor concentrations than in previous reactor experiments (0.02 - 2 kPa). In extreme cases, however, with an accident in the HTR-MODUL under full pressure, the H₂O partial pressure can amount, for example, to 500 kPa, and the depth of water vapor penetration into the graphite decreases with increasing system pressure [29]. In contrast, the KORA experiments are operated at atmospheric pressure.

5.3.1.3.2. Results

The fuel samples subjected to water vapor injections in KORA are listed in Table 5-3 together with selected properties and their irradiation histories. The spherical fuel elements are of the AVR GLE-3 type envisaged for modern HTGRs. The associated irradiation data correspond to HTR-MODUL target values. The bare kernels provided samples for comparison. The five UO₂ kernels, with different accumulated burnups, were obtained from cracked particles after deconsolidation of two fuel elements (AVR 73/8 and AVR 92/29). Also two sets of five intact particles from cell 3 of experiment HFR-B1 were cracked to recover the kernels which had a composition mainly of UO₂. The intact particles provided samples with relatively high Kr-85 inventories.

The samples were all investigated at 800 °C with the intermittent addition of a low level of water vapor (1 kPa) followed by a high level (50 kPa). A temperature of 800 °C was selected for this first series of experiments, because it is an HTGR operating temperature and, moreover, is in the boundary region of temperatures at which the diffusion of water vapor into the matrix graphite is still significant.

As burn-leach investigations have shown, modern spherical fuel elements with UO₂ TRISO particles contain on average one fabrication-related defective particle for every two spherical fuel elements [30]. However, no damaged particles were found in the majority of the fuel elements, whereas three were found in some of the fuel elements. For the three heated AVR GLE-3 fuel elements with UO₂ TRISO particles, moisture-induced Kr-85 release occurred in only two of the elements as shown in Figs. 5-13 and 5-14. No release was detected from fuel element AVR 92/8 (Table 5-4). The figures show the measured release and release rate relative to the total inventory of the spherical fuel elements.

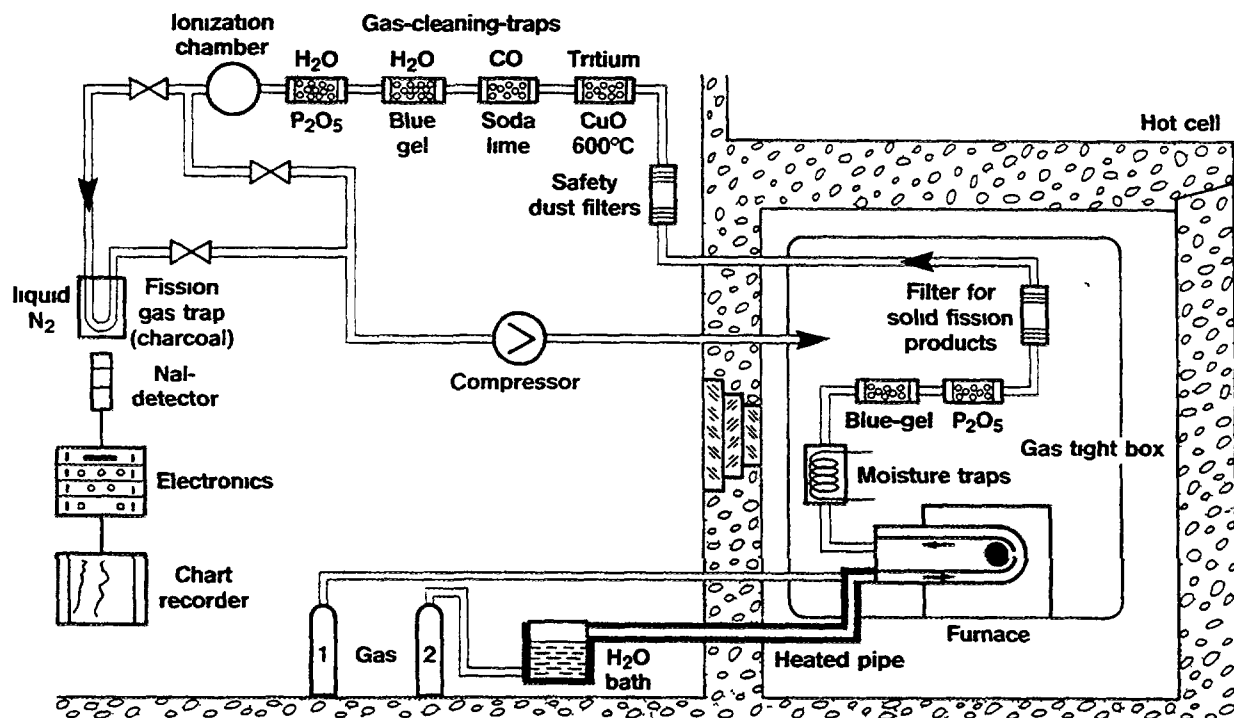


Fig. 5-12: The sweep gas circuit of the corrosion apparatus KORA, including the moisturizing equipment

Table 5-4: Kr-85 release from modern fuel elements during intermittent water injection

Fuel element	Burnup [%FIMA]	Kr-85 release fraction			Failed particles
		At test before 1st injection	1st injection ⁽¹⁾ 1 kPa water vapor at 800 °C	2nd injection ⁽¹⁾ 50 kPa water vapor at 800 °C	
AVR GLE-3 89/30	9.0	3.67×10^{-6}	3.70×10^{-5}	2.15×10^{-6}	1 or 2
AVR GLE-3 92/8	9.0	1.30×10^{-8}	-	-	-
AVR GLE-3 92/7	9.2	7.00×10^{-8}	-	1.20×10^{-5}	1

(1) without equilibrium release

Since extensive reactor experiments with modern TRISO fuels like AVR GLE-3 have shown that irradiation-induced particle defects do not occur [30], the Kr-85 releases in Fig. 5-13 and 5-14 are attributed to particle damage caused during fabrication. Furthermore some of the kernels of these defective particles may have been carburized during the

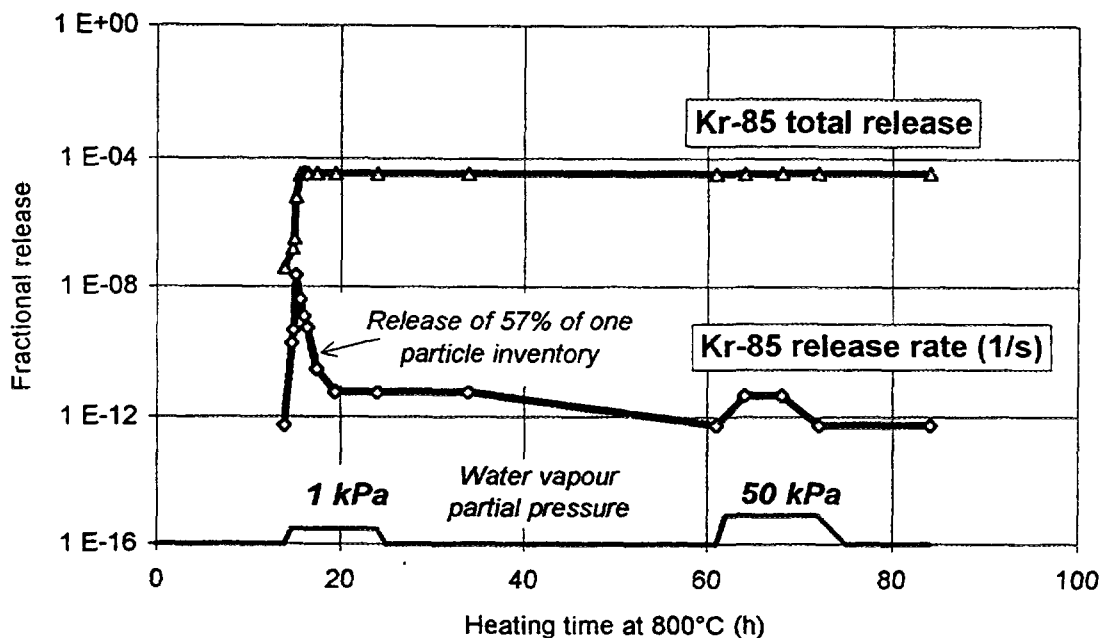


Fig. 5-13: Kr-85 release from a fuel sphere (AVR 89/30, type GLE-3, 9.0 %FIMA) during heating at 800 °C

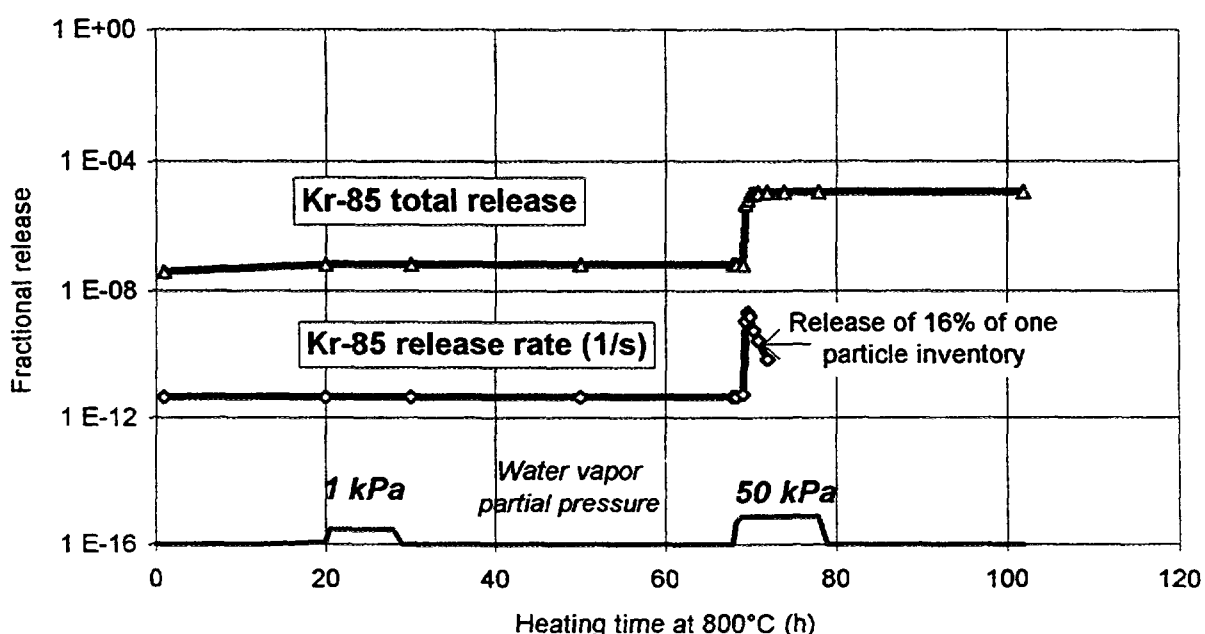


Fig. 5-14: Kr-85 release from a fuel sphere (AVR 92/7, type GLE-3, 9.2 %FIMA) during heating at 800 °C

fabrication process in the final heat treatment at 1950 °C, which may have led to a changed release behavior under water vapor influence.

Fig. 5-13 shows the typical course of fission gas release from fuel kernels under the influence of water vapor during postirradiation heating . The release fraction during the first water vapor injection corresponds to 57 % of a particle inventory. However, it still remains unclear whether one, two or even three defects have caused the Kr-85 release measured.

Two defects are probably involved leading to an average moisture-induced release of 28 % of the particle kernel inventory. Moisture-induced increase in Kr-85 release from fuel sphere AVR 92/7 only occurred with the second, higher-level injection, as can be seen in Fig. 5-14. During the first 10 hours injection of water vapor at 1 kPa partial pressure, the water probably did not diffuse deeply enough into the matrix graphite to reach the exposed fuel kernels. Although the release is similar in comparison to the fuel element in Fig. 5-13, it is significantly smaller amounting to only 16 %. In this case it is not clear what has caused the release.

To better understand the relation between the number and types of defects and specific moisture-induced fission gas release events, UO₂ fuel kernels obtained by cracking particles from deconsolidated fuel elements were also investigated. The result of an experiment with five kernels with a burnup of 4.7 %FIMA is shown in Fig. 5-15. In this figure, one can see that Kr-85 is released within 4 hours in a burst during heating at 800 °C. Relative to the sample inventory, 4 % of the Kr-85 was released; this corresponds to 19 % of a particle inventory. During the first injection of water vapor, only 2.6 % of the inventory in the five UO₂ kernels is released for a brief period of time at a high rate. The two subsequent injections with a high water vapor level show a relatively small release effect. In order to balance the total Kr-85 inventory, the sample was heated in a different apparatus for 2.5 h at 2060 °C following the 800 °C test. In this experiment, the residual inventory of 90 % was heated out of the fuel samples. Table 5-5 gives a survey of the Kr-85 fractional release during the heating experiments with fuel kernels.

The Kr-85 release profile from three experiments with kernels having different burnups is shown in Fig. 5-16. The curves prove that water vapor-induced fission gas release increases with burnup for Kr-85. Though the Kr-85 release through the dry heating phase of the 9.2 %FIMA kernels is lower than from the 4.7 %FIMA fuel, the release during the water vapor injection is higher. Another difference between these two samples is the significant prior Kr-85 release. As a consequence of high irradiation temperatures that possibly had prevailed in the AVR, only 43 % of the computed kernel inventory at the beginning of the experiment was left in the 9 %FIMA kernels. The release during the first water vapor injection is 16.6 instead of 38.6 % relative to the available Kr-85. The significance of this value, however, has to be evaluated by further investigations. The significant release values from the UCO kernels, which were also obtained by cracking intact particles, are obviously attributable in all cases to the simultaneous bursting of kernels due to high internal gas pressure.

The burnup dependence of Kr-85 release under the influence of water vapor can thus be correlated with the appearance pattern of fuel kernels with different burnups (Fig. 5-17). The kernel structure is observed to have significantly changed with increasing burnup and, in particular, gas bubbles are increasingly formed as a consequence of increasing fission gas inventory. The formation of gas bubbles and possibly also the changed chemical composition seem to be major reasons for the fact that fission gas release from the UCO (UO₂) kernels is almost complete during irradiation and in the heating test at corresponding temperatures and/or moisture levels.

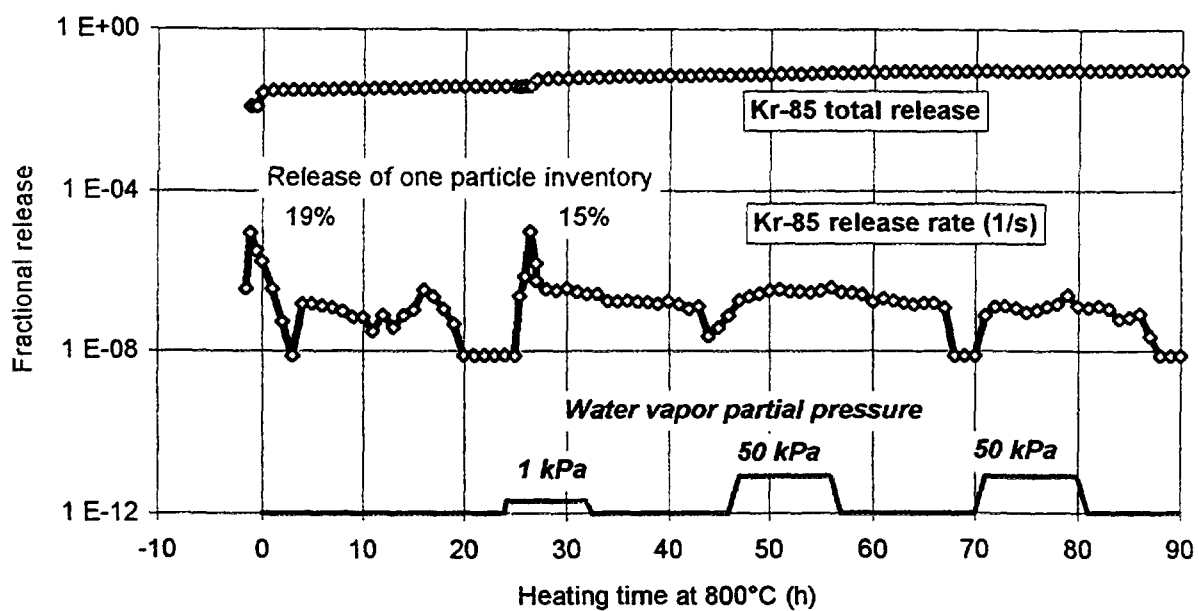


Fig. 5-15: Kr-85 release from five UO₂ kernels (AVR 73/8a, type GLE-3, 4.7 %FIMA) during the 800 °C heating

Table 5-5: Total Kr-85 release from fuel kernels in KORA and in heating experiments

Fuel kernels	Fuel type	Burnup [%FIMA]	Kr-85 release fraction [%]				A.-test at 2060 °C
			Before test (internal release ⁽¹⁾)	At test before 1st injection	1st injection 1 kPa water vapor at 800 °C	2nd injection 50 kPa water vapor at 800 °C	
AVR 73/8a	UO ₂	4.7	-	3.9	2.6	1	89.6
AVR 73/8b	UO ₂	4.7	-	4.7	0.4	0.6	94.2
AVR 92/29a	UO ₂	9.2	57	0.7	16.6	0.3	24.7
HFR, tr. 3-7a	UCO	19.5	-	29.1	65.6	1.6	2.5
HFR, tr. 3-7b	UCO	19.5	-	78.4	16.9	no inj.	2.1

(1) "Internal release" means release during irradiation from the kernels of intact particles.

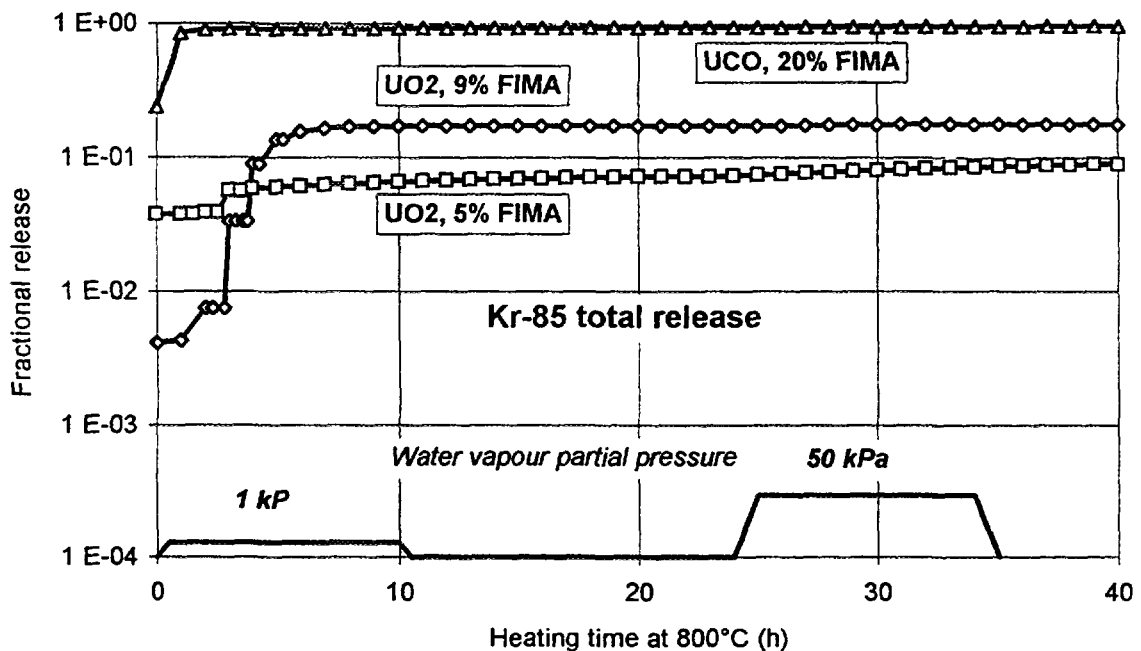


Fig. 5-16: Kr-85 release from specimens with five fuel kernels each with different burnup during the 800 °C heating

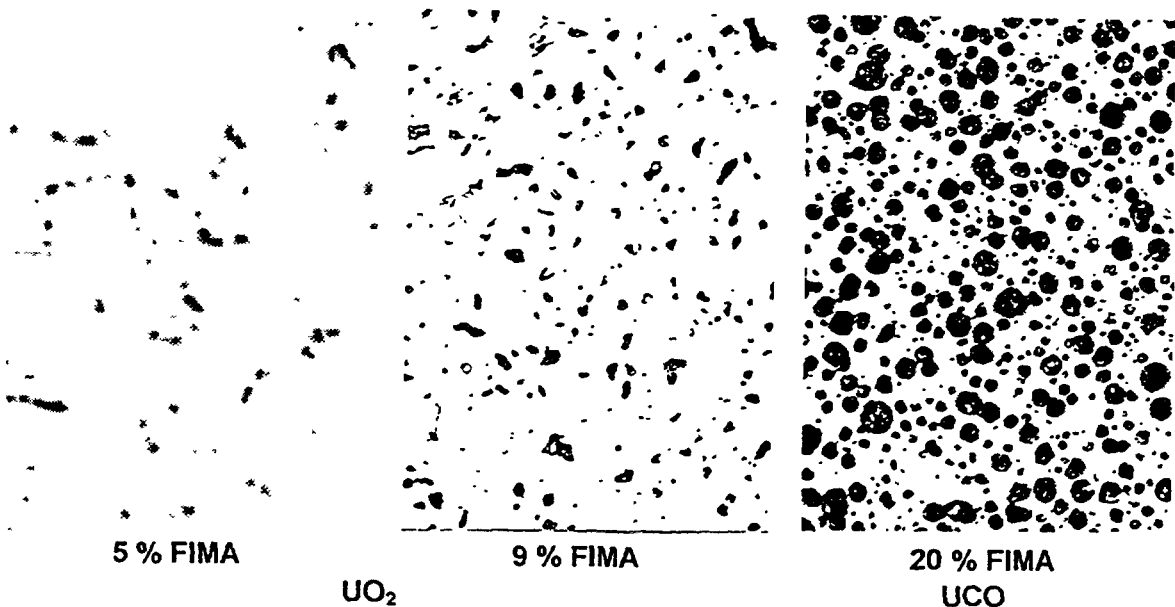


Fig. 5-17: Kernel sections from different burnup fuel particles

5.3.1.3.3. Evaluation and Comparison of Results

Heating experiments with fuel samples already containing defective particles during irradiation are indispensable for evaluating the influence of water vapor on fission gas and iodine release, although the interpretation of measured values poses problems since only long-lived Kr-85 is measured. It is evident that the increase in Kr-85 release from the spherical fuel elements examined is attributable to particle defects (Fig. 5-13), but it cannot

be stated how much of the Kr-85 inventory was still contained in the defective particles and what fraction was released from how many defective particles.

The results from the experiments with five fuel kernels obtained by cracking intact particles are a valuable aid for interpretation, because the final high-temperature test causes complete Kr-85 release and enables mass balancing. However, kernels from fabrication-related defective particles may differ from these kernels, which may influence the release behavior induced by water vapor. The results from all tests with fuel kernels are compiled in Table 5-5.

As shown in this table, moisture-induced release clearly increases with burnup for Kr-85. The highest Kr-85 release for kernels with an average burnup of 5 %FIMA (the HTR-MODUL target value is 9 %FIMA) was measured during the heating process and in the initial 800 °C phase, whereas the increase in release due to water vapor is comparatively small. In the case of fuel kernels from the fuel element AVR 92/29, only 43 % of the calculated inventory was still present in the kernel at the beginning of the experiment due to high internal Kr-85 release. Release during the first water vapor injection is 16.6 instead of 38.6 % relative to the available Kr-85.

The high release from the UCO kernels which were also obtained by cracking intact particles, are apparently attributable in all cases to simultaneous bursting of the kernels due to high internal gas pressure. It is not clear whether kernels of the designed-to-fail particles in the HFR-B1 compacts also bursted during irradiation.

5.4. AIR INGRESS ACCIDENTS

Most of the effort leading to an understanding of the consequences of air ingress accidents has been devoted to the formulation and application of computer models and experimental studies of graphite reaction with oxygen or air. Sections 5.1 and 5.2 touch lightly on these matters while including a listing of codes. Typically the codes address thermohydraulics, graphite structure, and chemical processes. The latter encompasses the reactions of oxygen and CO₂ with carbon and oxygen with CO.

Limited and severe air ingress accidents have been addressed by using the codes. In the limited case, one is said to have oxidation of graphite whereas in the severe case, one is said to have "burning" (which is usually self sustained). On a diagram of heat power versus graphite temperature [14], the curves of heat production and heat removal, which are, respectively, S-shaped and nearly straight [14], intersect at three points, the central one of which depends on a selected graphite starting temperature (T_g). At these points, heat production and heat removal are in balance. At temperatures above T_g production exceeds removal and below, removal exceeds production. As a consequence the system is heated in the former case and cooled in the latter until a balance is restored. The high temperature balance is characterized as burning. Contributing to heat production and oxidation and decay heat and to heat removal are convection, conduction, and radiation. In addition, mass transfer control mitigates the rise in heat production in the higher temperature regions. The relative contributions of these processes [14] depend on a variety of quantities and conditions such as flow rate, oxygen concentration, temperatures, thermal gradients, localization of chemical heating, and local and global burning.

The consequences of air ingress for coated fuel particles has not been adequately addressed to date. The principal concern is the formation and behavior of SiO_2 . The latter is presently thought of as providing a protective barrier to the oxidation of fuel kernels and of fuel spheres. The SiO_2 coatings are to be derived by oxidation of the SiC as well as the outer pyrocarbon coatings in the as-fabricated fuel particles and of the SiC coatings on the surfaces of fuel spheres. However, conditions for the ideal oxidation and for the stability of the oxidative resistance of SiO_2 are not necessarily found during air ingress accidents [14]. Exposed SiC in an atmosphere of sufficient oxygen is converted to SiO_2 while in an atmosphere with a deficit of oxygen it is converted to the volatile SiO above ≈ 1300 °C. At even higher temperatures, the viscous nature of SiO_2 may promote diffusion of oxygen through the particle. Other concerns include the supposedly greater susceptibility of irradiated SiC coatings and derived coatings to ingress-induced damage and the stability of SiO_2 in the presence of oxides of carbon at high temperatures.

Fortunately, work is underway on the effects of oxygen on fuel particles and fuel spheres in regard to fuel and fission product behavior. Contributions from JAERI and the Research Center Jülich are presented below.

5.4.1. Response of Graphite and Carbonaceous Material

For a postulated accident in which a primary coolant pipe is ruptured and air invades the core, the graphite components react with the air to the exclusion of the fuel contained. Consequently reaction with the fuel is suppressed and the burnout of the fuel is small. In a safety analysis of the HTTR at JAERI, air ingress resulted in the burning of the graphite sleeve thereby reducing the thickness of the sleeve from 10 to 6.4 mm. No oxidation of the fuel compacts occurred for irradiation temperatures less than 1500 °C. However, for particles in which coating failure occurs under air ingress conditions, the fuel could be completely burned. This case would be placed in the category "Beyond Design Base" [31].

Tests were conducted on non-irradiated coated fuel particles and fuel compacts in an atmosphere of air over a range of temperatures between 900 and 1400 °C. Fig. 5-18 depicts a decrease in the relative weight of a compact with the heating time in air flow at 1400 °C. Between 0 and 20 h, the weight decreased gradually to 42 %, and was constant between 20 and 40 h. The significant decrease is attributable to the burning of carbonaceous materials such as the graphite matrix of the fuel compacts and the outer pyrocarbon coating of the fuel particles. Once the exterior SiC surface was exposed, following the complete burning of the outer pyrocarbon coating, the fuel would not oxidize, while the SiC coating is intact. If, however, the SiC is failed, then fuel oxidation may occur.

Table 5-6 summarizes the burning tests with the fuel particles and the fuel compacts and gives the failure fractions of the SiC coating. The failure fraction of the SiC layer in the fuel compacts is relatively high compared with those of the coated particles; the fraction was highest for those fuel compacts heated at 900 °C. Burning the graphite matrix is exothermic so that the temperature at oxidizing local points might be far higher than 900 °C. This would enhance the failure of the SiC layer. Therefore the particle failure in the fuel compacts during burning might not be strongly dependent on the general temperature.

Table 5-6: Coated particle failure of non-irradiated fuel under air at high temperatures

	Sample	No. of coated particles tested	Test conditions		No. of failed coated particles	Failure fraction of SiC layer
			Temperature [°C]	Time [h]		
1	Coated particles	3151	900	40	1	$2.3 \cdot 10^{-4}$
2	Coated particles	3127	1000	40	0	$5.1 \cdot 10^{-6}$
3	Coated particles	3136	1200	40	0	$1.0 \cdot 10^{-6}$
4	Coated particles	3123	1300	600	2	$5.4 \cdot 10^{-4}$
5	Coated particles	3114	1400	40	1	$3.2 \cdot 10^{-5}$
6	Fuel compact	10461	900	54	13	$1.2 \cdot 10^{-3}$
7	Fuel compact	10599	1400	20	8	$6.9 \cdot 10^{-4}$

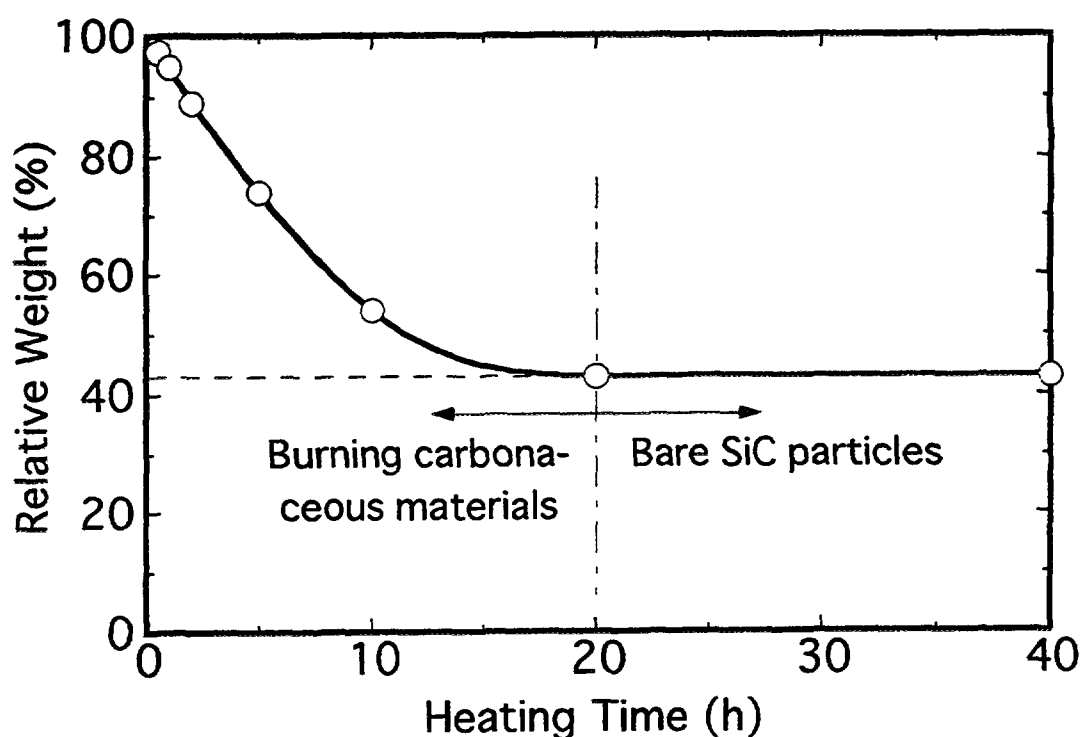


Fig. 5-18: Weight change of a fuel compact during air oxidation at 1400 °C

5.4.2. Response of Coated Fuel Particles

5.4.2.1. German Postirradiation Heating, Introduction

Long term air ingress with graphite burning [32] is possible only by natural convection (chimney draught) from two leaks in the top and bottom positions of the pressure vessel and an additional leak in the inner core container, i.e., one large-sized leak in pressure vessel and core container or, in case of the HTR-MODUL, a complete rupture of the coaxial duct. In addition, there must be a path between the leak(s) in the pressure vessel and the environment [33], meaning that the reactor building does not act as a significant barrier against gas exchange. Accident scenarios leading to such a hypothetical configuration are hard to imagine. It was calculated that under extreme conditions (chimney draught, open reactor building), half of the fuel sphere is corroded after 38 hours so that the particles are set free. The temperature in the bottom region of the core then rises to a maximum less than 1300 °C [34]. The important question is: Does the SiC interlayer withstand the corrosion process given by the chemical reaction



The experimental equipment, the corrosion apparatus (KORA), is the same as has been used for heating fuel samples under moisture influence and as has been described previously.

5.4.2.2. Postirradiation Heating Results

Experiments with UO₂ TRISO particle specimens and spherical fuel elements in air at a flow rate of 30 l/h and a pressure of about 0.13 MPa were carried out in KORA (Table 5-7) [35]. First of all, batches of 10 UO₂ TRISO particles each from two disintegrated AVR fuel elements with different burnups were heated. Only one particle failed after 397 hours at 1400 °C, whereas defects occurred in all 10-particle batches at 1500 °C irrespective of burnup. When heated up to 1620 °C, damage started at 1613 °C. This shows that the oxidation of the SiC layer, before failing, proceeds slowly at temperatures around 1400 °C and more rapidly as the temperature approaches 1600 °C.

Table 5-7 also includes the results from tests with three spherical fuel elements. At 1300 °C, only one of the 16,400 particles of the fuel sphere failed after 258 hours, followed by three further particle failures in the period up to 410 hours. In the 1400 °C experiments, individual defects began shortly after the heatup phase, but it is remarkable in this case that not more than about 0.1 % of the particles were damaged in the further course of the experiment.

Fig. 5-19 shows the release of the gas activity and of Kr-85 from a fuel sphere during heating in air. A temperature of 1100 °C was first selected. At this temperature particle defects are not induced and corrosion of the matrix graphite and the outer pyrocarbon coating of the particles proceeds rather rapidly. Increased initial release is first observed, which is essentially attributed to tritium contamination on the sphere surface from the sweep gas circuit of the AVR reactor. Subsequent steady release of H-3 and C-14 results

Table 5-7: Heating tests with intact particles and fuel spheres in air (UO_2 TRISO)

Fuel sample	No. of particles	Burnup [%FIMA]	Test conditions			Kr-85 release		
			Heatup [h]	Max. temp. [°C]	Time [h]	1st failed particle after	No. of failed particles	Fraction of failed particles
92/29, 12	10	9.2	14	1400	400	397 h	1	0.1
73/8, 11	10	4.7	15	1500	25	8 h	10	1
92/29, 13	10	9.2	15	1500	25	3 h	10	1
92/29, 11	10	9.2	28	1620	1	at 1613 °C	10	1
AVR 89/12	16,400	9.4	13	1300	410	258 h	4	$2.4 \cdot 10^{-4}$
AVR 92/22	16,400	8.8	14	1400	140	1 h	20	$1.2 \cdot 10^{-3}$
AVR 89/14	16,400	9.0	14	1400	70	2 h	12	$7.3 \cdot 10^{-4}$

from graphite combustion at an air flow rate of 30 l/h. This combustion is completed after about 100 hours. Following this experimental phase, the particles which were all intact, i.e., gastight up to then, were heated to 1400 °C. During the 140 h treatment at 1400 °C, about 20 of the 16,400 particles failed. Fig. 5-20 shows particles of this test after heating.

Fig. 5-21 contains the results of the tests with fuel spheres and of one test at 1500 °C with 10 particles (92/29, 13). The curves indicate a temperature/time dependence of the particle failure fraction.

5.4.2.3. Prediction of Particle Failure During Air Ingress

A model for predicting particle failure during air ingress has been developed by Nabielek [36].

For experiments at constant temperatures, the fractional failure is given by:

$$F = 1 - \exp \left\{ -(kt)^2 \right\} \quad (5-9)$$

where

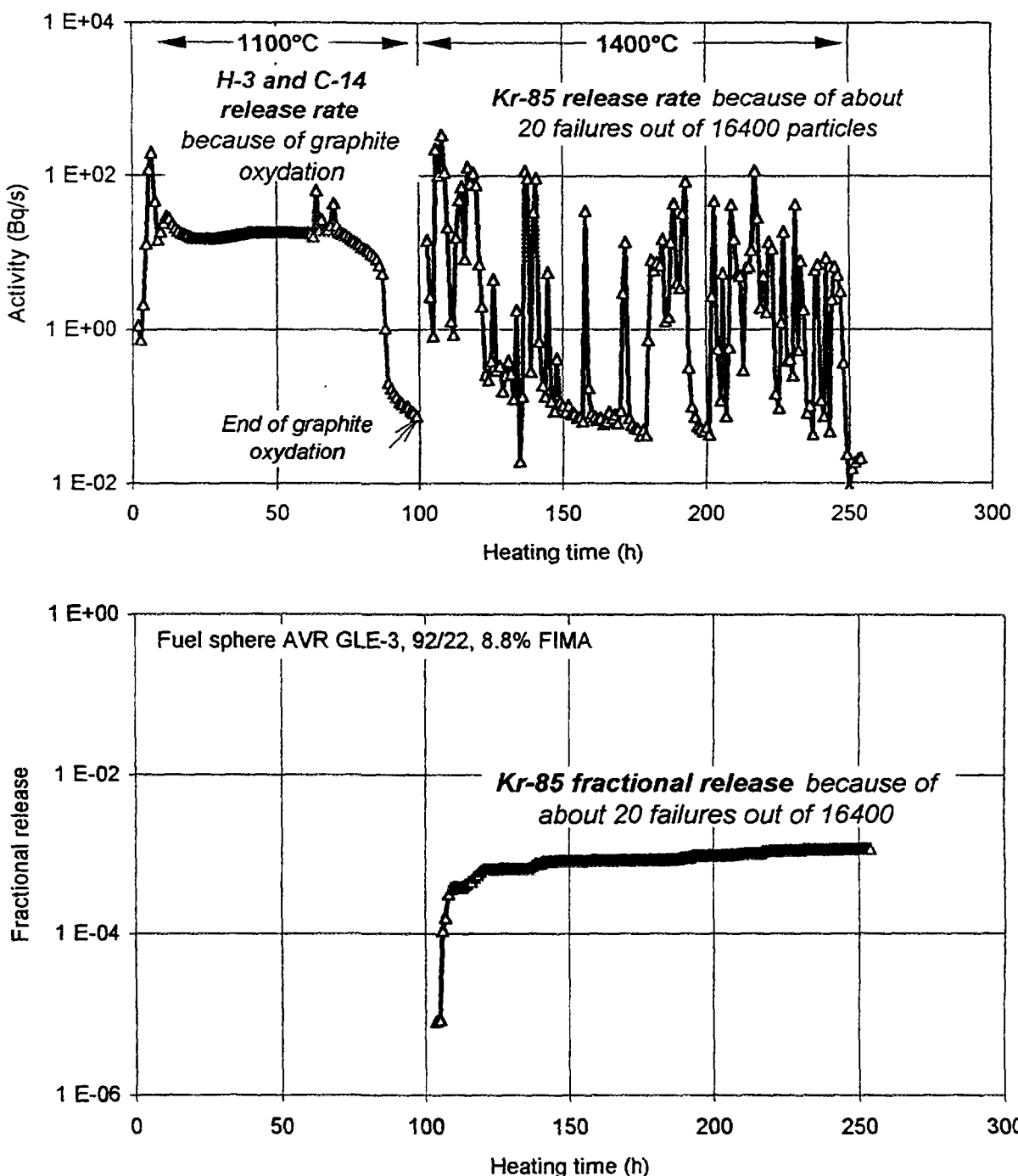


Fig. 5-19: Oxidation of a fuel sphere in air
 (top) AVR 92/8, 9 %FIMA (bottom) AVR 92/22, 8.8 %FIMA

F is the fractional failure

t is the time [s]

is the reaction rate coefficient [s^{-1}]

k $k = k_0 \exp\{-Q/(RT)\}$

k_0 is a constant [s^{-1}]

Q is an activation energy [J/mol]

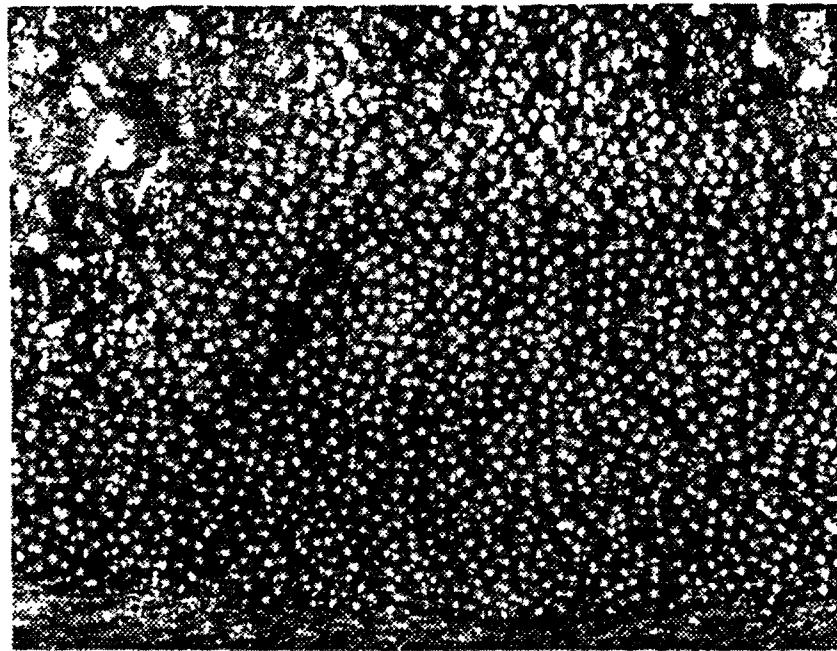


Fig. 5-20: Particles of fuel sphere AVR 92/8 after the heating test in air at 1400 °C

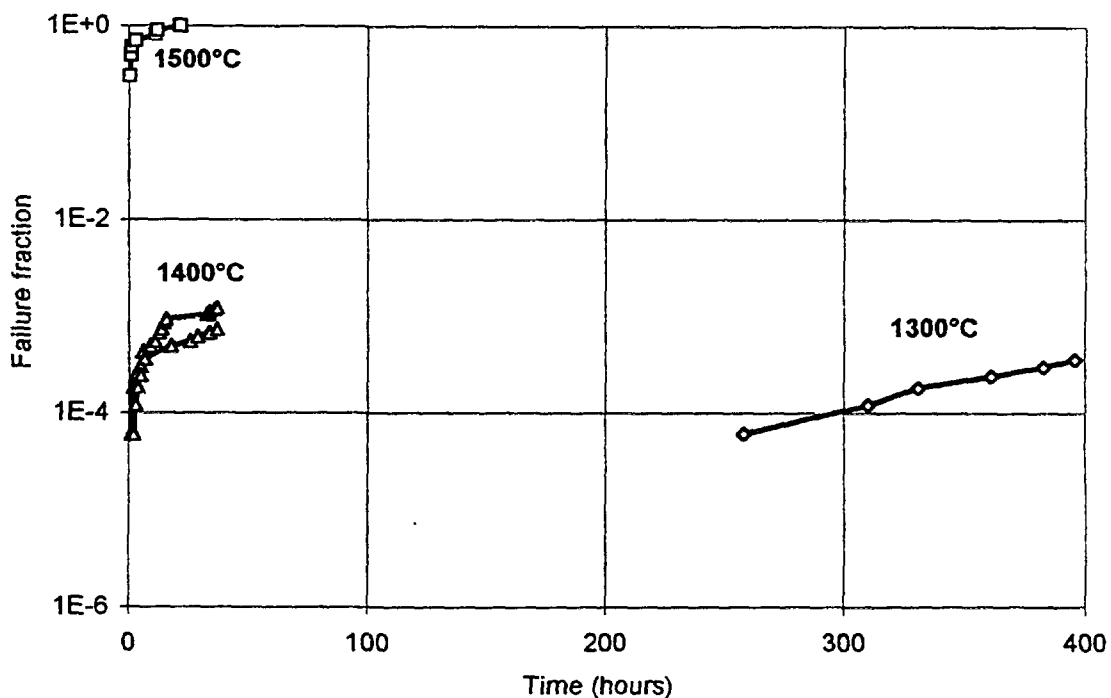


Fig. 5-21: Failure fraction of fuel particles within fuel spheres during heating in air at 1300 °C and of 10 intact, unbonded particles at 1500 °C

R is the gas constant, $R = 8.314 \text{ J}/(\text{mol K})$

T is the temperature [K]

There are two parameters to be evaluated using the experimental results, i.e., k_0 and Q . If the data from the constant temperature experiments at 1300 and 1400 °C [35] are used to evaluate these parameters, the model then underpredicts the experimental results

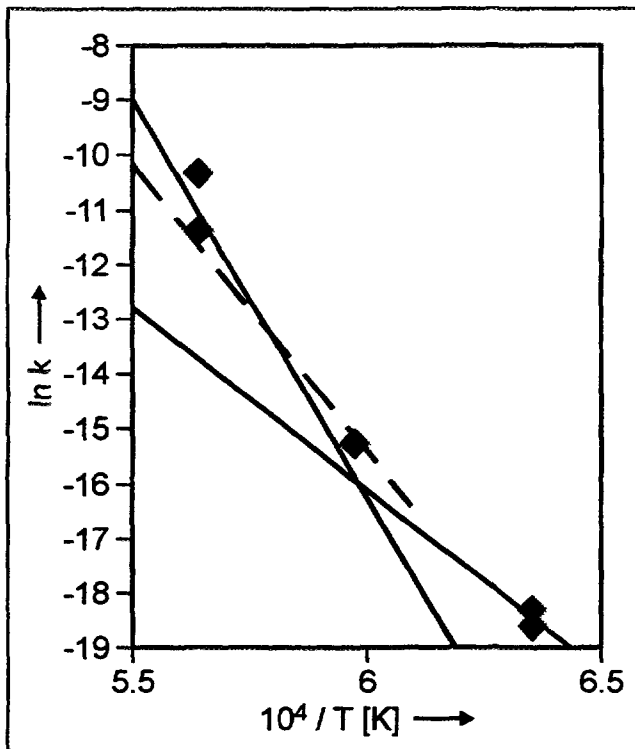


Fig. 5-22: Temperature dependence of air ingress reaction rate coefficient, k [s^{-1}]

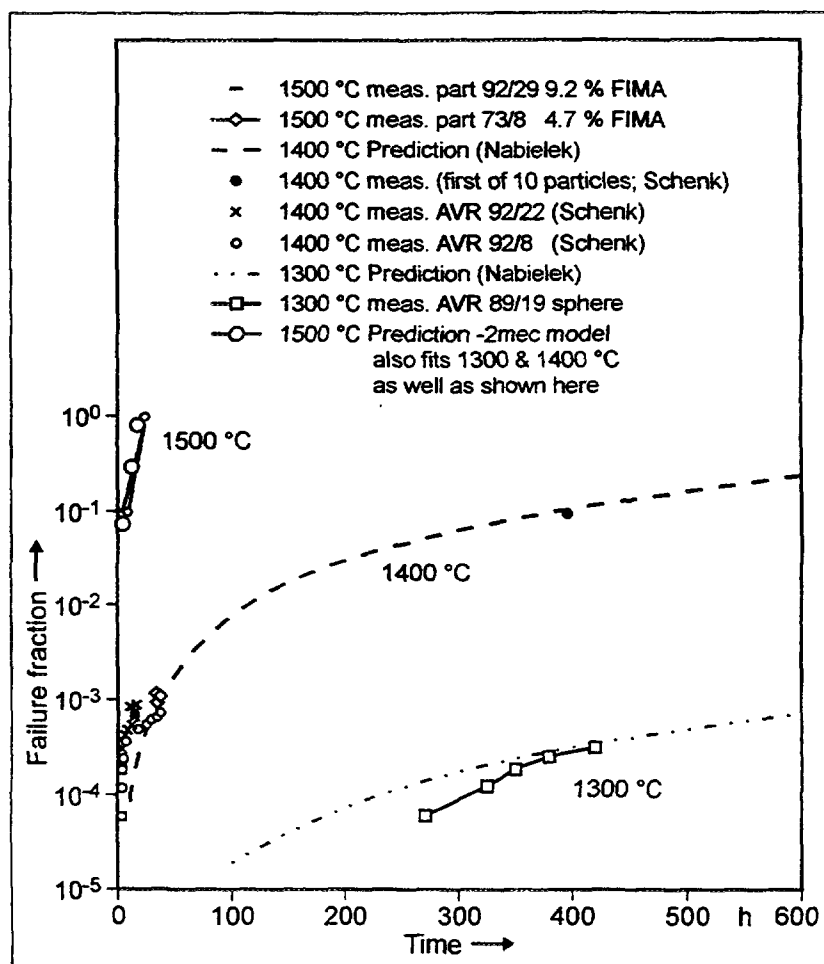


Fig. 5-23: Particle failure fraction during air ingress at constant temperatures

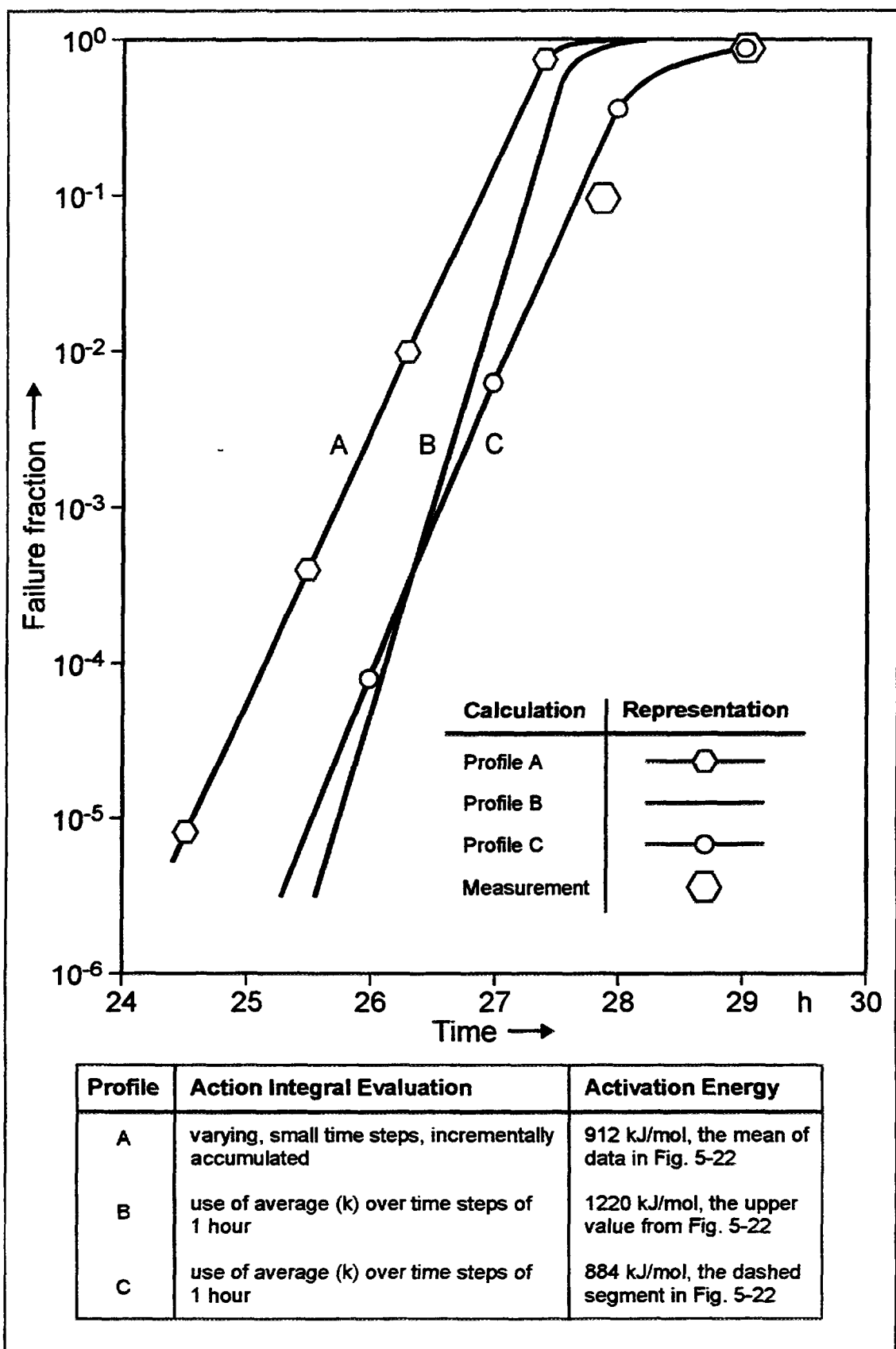


Fig. 5-24: Particle failure fraction during air ingress and rising temperatures

at 1500 °C by a factor of about 10. By the following line of thought, this matter can be mitigated. In the model, the single value of Q indicates that there is one mechanism of failure. However, if one postulates in the present case two mechanisms of failure and alters the model accordingly, then this version of the model [37] predicts quite well the measurements at 1300, 1400, and 1500 °C [35]. In Fig. 5-22 is shown not only the data at the foregoing temperatures but also the dependence of ln k as a function of $10^4/T(K)$ for the two mechanisms. Each mechanism is represented by one of the continuous line segments and the sum of the continuous line segments over the range of temperatures yields a smooth curve which matches the data or an average of data. The deduced activation energies are 1221 and 555.5 kJ/mol. The ratio of these activation energies is larger than 2, a ratio seemingly large enough to justify the postulate of two mechanisms. The corresponding values of k_0 are 1.467×10^{31} and 2.508×10^{10} , respectively.

Comparison of experimental results and of predictions are shown in Fig. 5-23. In the legend, the abbreviation "2-mec model" refers to the version of the model altered to include two mechanisms of failure. It applies equally well to the 1300 and 1400 °C.

For experiments in which the temperature varies with time, the quantity, k_t , of Eq. (5-9) must be replaced by an action integral [36], i.e., $\int k(T(t')) dt'$ with lower and upper integration limits of t_1 and t_2 . For the "2-mec" case, the average value of k , i.e., $\langle k \rangle$, over a specific time interval was evaluated using the relationship [37]:

$$\langle k \rangle = \frac{k_2 T_2 F_2 - k_1 T_1 F_1}{T_2 - T_1} \quad (5-10)$$

where

$$F_i = 1 - x_i \exp\{x_i\} E_i(x_i) \quad (5-11)$$

with

$$x_i = (Q_i/(RT))$$

i is 1 or 2

$E_i(x_i)$ is an exponential integral.

There is available, at present, one experiment during which the temperature rose linearly with time from room temperature to 1620 °C in 28 h and thereafter was constant at 1620 °C for one hour. The test was performed with 10 particles from fuel element AVR 92/29. The first particle failed at 1613 °C after 27.88 h into the ramp. All 10 particles were failed by the end of the experiment. Three model calculations, shown in Fig. 5-24 as profiles A, B, and C, demonstrate the strong dependence of the fractional release on activation energy, Q. With decreasing Q, the linear slope of the profiles also decreases. As evident in Fig. 5-22, a maximum and minimum value of Q in the range 5.5 to $6.1 \times 10^4/T$ can be determined. It is clear, based on Figs. 5-22 and 5-24, that sufficient data to provide a reliable mean and variance for Q must be obtained before an adequate test of the models can be conducted. At present, the model version corresponding to profile C at least overpredicts the datum at 27.88 h.

5.5. SUMMARY OF CHAPTER 5

Among the postulated accidents in gas-cooled reactors are those of water and air ingress. These accidents, involving oxidation of exposed fuel kernels, graphitic and carbonaceous materials, SiC and ZrC, can lead to a significantly enhanced release of fission products and to extensive degradation of the core components. Recent experiments have focused mainly on the effect of water vapor on exposed fuel kernels; the focus is now shifting to the effect of oxygen on fuel particles.

The interaction of water vapor with particles having exposed fuel kernels has been investigated both during and after irradiation. Although these types of experiments differ severally, they are potentially complementary. Thus far, no attempts to relate the data from irradiation and postirradiation tests has been made. Here, the summary of the irradiation experiments is followed by the summary of the postirradiation tests.

Three irradiation experiments, HRB-17/18, HFR-B1, and HFR-K6, have been conducted. Prior to water vapor injection, in each experiment there were a small but known number of particles with exposed kernels. These provided a known source of fission products subject to release from the kernels. The kernels were of UO₂ except in the former two experiments where the kernels contained 20 % UC₂ initially; however, the UC₂ was completely oxidized in the first water vapor injection at \approx 200 Pa or more. A discrete series of tests was conducted with water vapor at partial pressures in the range 0.003 to 2 kPa. The released fission gas was monitored for the isotopes Kr-85m, Kr-87, Kr-88, Xe-133, Xe-135, and Xe-138.

The general sequential response of the exposed fuel kernels consists of three stages:

1. a rapid transient release of fission gas with a concomitant smooth increase in the steady state release,
2. a period of constant steady state release, and
3. a decline in the release to prehydrolysis values upon cessation of water vapor injection.

During stage 1, collectives (bubbles and closed pores containing gas atoms) and interstitial gas atoms are the sources of released fission gas. These sources were identified and evaluated on the basis of the slope n ($= -\partial \ln(R/B) / \partial \ln(\lambda)$); here R/B is the fractional fission gas release of the monitored isotopes and λ the corresponding decay constants. Note that interstitial fission gas, diffusively released from particles with exposed kernels, yields n values in the range \approx 0.2 to \approx 0.5 and gas collectives have values of n in the range \approx 1 to \approx 1.5. Thus before and after stage 1, the slopes are consistent with diffusive release and during stage 1 are consistent with the predominate release of gas collectives following a breaching of gas bubbles or closed pores.

In stage 1, the contribution to fission gas release of gas collectives (hereinafter referred to as stored gas) was delineated and the release of stored gas as a function of the partial pressure of water vapor and the temperature determined. The functional relation, Eq. (5-1), is empirical and is meant to describe simply the complicated interplay of the effect of water vapor pressure and temperature on the release of fission gas from exposed fuel kernels. The relation is only valid within the water vapor pressure and temperature ranges of the experimental data. The temperatures varied from 820 to 1040 °C and the partial

pressures of water vapor varied from 2.8 to 1051 Pa. At a fixed temperature, the logarithms of the release of stored gas and the water vapor pressure at ≤ 1 kPa are linearly related. Above 1 kPa, the dependence of stored gas release on the water vapor pressure weakens significantly. This could indicate the onset of a transport-limiting mechanism.

During stage 2, which begins after completion of the transient release, interstitials are diffusively released. This stage is characterized by the ratio $h_o = (R/B)_{\text{stage 2}} / (R/B)_{\text{stage 0}}$. The ratio is constant in time, depends on the temperature, but is independent of P_{H2O} (at least for $P < 0.2$ kPa) and of isotopic variation. The latter is also theoretically expected. The ratio differs for the elements Kr and Xe to the same extent as do their atomic volumes. The activation energies of R/B in the presence and absence of water vapor are, respectively, 65.8 kJ/mol and 23.6 kJ/mol.

During stage 3, which begins after the injection of water vapor ceases, the fractional release declines to $(R/B)_{\text{stage 0}}$, i.e., to a fuel structure equivalent in release to the fuel structure existing before water vapor was injected. The characteristic time, Δt , for decline to within 5 % of $(R/B)_{\text{stage 0}}$, is equal to $3/\delta$. The governing parameter in the corresponding exponential function is δ . At zero neutron flux, δ is essentially zero, but with increasing neutron fluence, δ increases and passes through a maximum.

Initial postirradiation experiments on fuel samples with UO_2 and UCO kernels and designed-to-fail particles at 800 °C in a special heating apparatus (KORA) revealed that Kr-85 release is increased if water vapor is added. In contrast, intact particles are not damaged even by extremely long water vapor injections. UO_2 kernels obtained by cracking particles from spherical fuel elements, which would correspond to irradiation-induced failures, showed the following release fractions at 800 °C after repeated injections of water vapor:

for medium burnup of 5 %FIMA	release of 0.4 - 2.6 % of Kr-85 inventory
for high burnup of 9 %FIMA	release of 17 % of Kr-85 inventory

Complete moisture-induced release was observed from high burnup particles and designed-to-fail particles with more than 20 %FIMA. Together with the knowledge that unirradiated UO_2 kernels show practically no changes due to moisture, the moisture-induced fission gas release, and similarly the iodine release, from fuel kernels is a burnup-dependent effect. Both the changed structure of the kernel and the chemical composition may be of significance.

In the case of fabrication-related damage to UO_2 TRISO particles in spherical fuel elements which would dominate the release in an HTR-MODUL, some of the free fuel may have been carburized in the fabrication process during final heat treatment at 1950 °C which could lead to the changed release behavior of fission gases and iodine. Further studies will have to show whether the release due to the influence of water vapor is similar to that from UO_2 kernels or possibly higher.

The prerequisite for a massive ingress of air, e.g. in a modular HTGR, is a very large leak, for instance after a rupture of the connecting vessel between reactor core and steam generator. Only then can excessively high graphite corrosion occur due to sufficient

oxygen supply. Even under extreme circumstances (open cell, open reactor building), it will still take 1 - 2 days until corrosion of the fuel-free zone of the spheres has progressed such that the first fuel particles were uncovered, and it is then of significance how long the SiC coating of the particles will withstand.

Samples of fuel spheres were heated in an air stream of 30 l/h. At 1100 °C, complete burning of the graphite takes 70 to 100 hours in heating tests with spherical fuel elements. During subsequent treatment at elevated temperatures, the first SiC layers of particles were damaged at 1300 °C, although not after less than 10 days. At 1400 °C, the fraction of particle failures increases to 1.2×10^{-3} after 140 hours.

In Japan, burning tests were conducted on non-irradiated fuel particles and fuel compacts in an atmosphere of air and a temperature range of 900 to 1400 °C. The test revealed that the burning of fuel compacts even at a temperature as low as 900 °C resulted in a higher fraction of failed SiC layers than the burning of coated particles at higher temperatures.

REFERENCES OF CHAPTER 5

- [1] VELASQUEZ, C., HIGHTOWER, G., BURNETTE, R.D., The Oxidation of H-451 Graphite by Steam, Report GA-A14851, General Atomic Company (1978).
- [2] HINSEN, H.K., KATSCHER, W., MOORMANN, R., Kinetik der Graphit/Sauerstoff-Reaktion im Porendiffusionsbereich: Teil II; Graphite V483T, ASR-1RS, ASR-1RG und ATR-2E, Report JüL-2052, Research Center Jülich (1986).
- [3] FULLER, Jr., E.L., et al., Microgravimetric Analysis of Corrosion of H-451 Graphite by Coolant Impurities: Preliminary Report of Kinetics and Mechanisms, Report ORNL/GCR-90/3, Rev. 0, Oak Ridge National Laboratory (1992).
- [4] MOORMANN, R., PETERSEN, K., REACT/THERMIX, ein Rechenprogramm zur Ermittlung der störfallbedingten Graphitkorrosion in Hochtemperaturreaktoren, Report JüL-1782, Research Center Jülich (1982).
- [5] PEROOMIAN, M.B., BARSELL, A.W., SAEGER, J.C., OXIDE-3: A Computer Code for Analysis in HTGR Steam or Air Ingress Accidents, Report GA-A12493, General Atomic Company (1974).
- [6] RICHARDS, M.B., et al., A Computational Model for Graphite Oxidation Under Nuclear Reactor Conditions, Heat Transfer, (24th National Conference), AIChE Symp. Series, No. 257, Vol. 83 (1987).
- [7] RICHARDS, M.B., Reaction of Nuclear-Grade Graphite With Low Concentrations of Steam in the Helium Coolant of an MHTGR, Energy 15 (1990) 729-739, and RICHARDS, M.B., Software Design Description and User's Manual for REACT Graphite Corrosion Computer Code, Report CEGA-002695, Rev. 0, CEGA Corporation (1993).
- [8] RICHARDS, M.B., TANGIRALA, V., AIP Software Design Description and User's Manual for REACT Graphite Corrosion Computer Code, Report CEGA-002695, Rev. 0, CEGA Corporation (1993).
- [9] KAWAKAMI, H., Air Oxidation Behavior for Carbon and Graphite Materials for HTGR, Tanos 126 (1986) 26-33.

- [10] MARUYAMA, S., et al., Evaluation of Graphite Oxidation During Water Ingress Accidents in HTTR, Response of Fuel, Fuel Elements and Gas-Cooled Reactor Cores Under Accidental Air and Water Ingress Conditions (Proc. IAEA Technical Committee Meeting, Beijing, 1993), IAEA-TECDOC-784, Vienna (1995) 97-103.
- [11] GAO, Z., et al., Transient Analysis of Air Ingress From Broken Pipe into the HTR-10 Reactor Pressure Vessel, Response of Fuel, Fuel Elements and Gas-Cooled Reactor Cores Under Accidental Air and Water Ingress Conditions (Proc. IAEA Technical Committee Meeting, Beijing, 1993), IAEA-TECDOC-784, Vienna (1995) 69-72.
- [12] GAO, Z., et al., Transient Analysis of Water Ingress into the HTR-10 High Temperature Gas Cooled Test Reactor, Response of Fuel, Fuel Elements and Gas-Cooled Reactor Cores Under Accidental Air and Water Ingress Conditions (Proc. IAEA Technical Committee Meeting, Beijing, 1993), IAEA-TECDOC-784, Vienna (1995) 92-96.
- [13] MONTGOMERY, F.C., Test Report on Hydrolysis of HTGR Carbide Fuel: Chemical Reactions and Consequences, Report GA-904929-1, General Atomic Company (1980).
- [14] MYERS, B.F., Effect of Water Vapor on the Release of Fission Gases from Uranium Oxycarbide in High-Temperature, Gas-Cooled Reactor Coated Fuel Particles, *J. Am. Ceram. Soc.* **75** (1992) 686-693.
- [15] RÖLLIG, K., Transiente Edelgasfreisetzung, Report HTR-M-0210-BF-GHRA 006904, Asea Brown Boveri AG (1992).
- [16] NABIELEK, H., CONRAD, R., RÖLLIG, K., MYERS, B.F., Fuel Irradiation Experiments HFR-K6 and HFR-B1 with Intermittent Water Vapor Injections, Response of Fuel, Fuel Elements and Gas-Cooled Reactor Cores Under Accidental Air and Water Ingress Conditions (Proc. IAEA Technical Committee Meeting, Beijing, 1993), IAEA-TECDOC-784, Vienna (1995) 17-24.
- [17] MYERS, B.F., Experiment HFR-B1: A Preliminary Analysis of the Water Vapor Injection Experiments in Capsule 3, Report ORNL/TM-11846, Oak Ridge National Laboratory (1991).
- [18] MYERS, B.F., A Review of Selected Aspects of the Effect of Water Vapor on Fission Gas Release from Uranium Oxycarbide, Report ORNL/TM-12641, Oak Ridge National Laboratory (1994).
- [19] MYERS, B.F., The Effect of Water Vapor on the Release of Fission Gas from the Fuel Elements of High-Temperature, Gas-Cooled Reactors: A Preliminary Assessment of Experiments HRB-17, HFR-B1, HFR-K6 and KORA, Report ORNL/M-4294, Oak Ridge National Laboratory (1995).
- [20] TURNBULL, J.A., et al., The Diffusion Coefficients of Gaseous and Volatile Species During the Irradiation of Uranium Dioxide, *J. Nucl. Mat.* **107** (1982) 168-184.
- [21] MYERS, B.F., The Effect of Water Vapor on the Release of Gaseous Fission Products from High-Temperature, Gas-Cooled Reactor Fuel Compacts Containing Exposed Uranium Oxycarbide Fuel, Report ORNL-6610, Oak Ridge National Laboratory (1991).
- [22] KITTEL, C., Introduction to Solid State Physics, 5th Edition, John Wiley & Sons, Inc. (1976), p. 100.
- [23] SCHENK, W., KNAUF, H., PITZER, D., Spaltgasfreisetzung aus Brennstoffproben unter dem Einfluß von Feuchte, Internal Report KFA-IRW-IB-6/93, Research Center Jülich (1993).

- [24] MYERS, B.F., The First Water Vapor Injection Tests in HFR-B1, Report ORNL/GCR-87/4, Oak Ridge National Laboratory (1987).
- [25] MYERS, B.F., A Comparison of the Effect of Water Vapor in HFR-K6 with that in HRB-17 and HFR-B1, Unpublished Report (1995).
- [26] KETTERER, J.W., MYERS, B.F., Capsule HRB-17/18 Final PIE Report, Report DOE-HTGR-86-083, GA Technologies (1987).
- [27] DERZ, H., FLOßDORF, T., Ceramographic Examination of Coated Particles in Fuel Rods for Capsule 1 of HFR-B1, Technical Note KFA-IWE-1/HZ-TN-37/94, Research Center Jülich (1994).
- [28] SCHENK, W., PITZER, D., NABIELEK, H., Fission Product Release Profiles from Spherical HTR Fuel Elements at Accident Temperatures, Report JüL-2234, Research Center Jülich (1988).
- [29] LOENISSEN, K.-J., HINSEN, H.-K., KATSCHER, W., MOORMANN, R., Graphitkorrosion durch Wasserdampf in HTRs bei Störfällen mit hohem Systemdruck, (Proc. Jahrestagung Kerntechnik '87, München, 1987), Inforum GmbH, Bonn (1987) 171-174.
- [30] NABIELEK, H., et al., Development and Qualification of Modern TRISO Fuels for the HTR, Design and Safety of Advanced Nuclear Power Plants (Proc. Int. Conf., Tokyo, 1992).
- [31] KIKUCHI, K., HAYASHI, K., FUKUDA, K., Air Oxidation Behavior of Fuel for the High Temperature Engineering Test Reactor (HTTR), Report JAERI-M 92-114, Japan Atomic Energy Research Institute (1992).
- [32] MOORMANN, R., KATSCHER, W., Examination on Graphite 'Burning' in HTGRs, Nuclear Reactor Severe Accident Chemistry, (Proc. 2nd Int. Symp., Toronto, 1988).
- [33] MOORMANN, R., Air Ingress and Graphite Burning in HTRs: A Survey on Analytical Examinations Performed with the Code REACT/THERMIX, Report JüL-3062, Research Center Jülich (1995).
- [34] HAQUE, H., LOHNERT, G., Auswirkungen und Abläufe bei massiven Lufteinbrüchen in den HTR-MODUL, (Proc. Jahrestagung Kerntechnik '92, Karlsruhe, 1992), Inforum GmbH, Bonn (1992) 179-182.
- [35] SCHENK, W., POTT, G., Brennelemente mit hoch abgebrannten beschichteten UO₂-Brennstoffpartikeln in Luft, (Proc. Jahrestagung Kerntechnik '95, Nürnberg, 1995), Inforum GmbH, Bonn (1995) 348-351.
- [36] NABIELEK, H., Prediction of Particle Failure During Air Ingress, Memorandum, Research Center Jülich (1996).
- [37] MYERS, B.F., Assumption of Two Failure Mechanisms in Prediction of Particle Failure During Air Ingress, Memorandum, Oak Ridge National Laboratory (1997).

NEXT PAGE(S)
left BLANK

6. EX-CORE FISSION PRODUCT TRANSPORT DURING NORMAL AND ACCIDENT CONDITIONS

As shown schematically in Fig. 6-1, the HTGR radionuclide containment system is comprised of five principal release barriers: (1) fuel kernel, (2) particle coatings, (3) matrix/graphite, (4) primary coolant pressure boundary, and (5) reactor building/containment structure; also shown are the various phenomena which challenge the retention capabilities of these barriers. The first three barriers were addressed in previous sections; the latter two are addressed in this section.

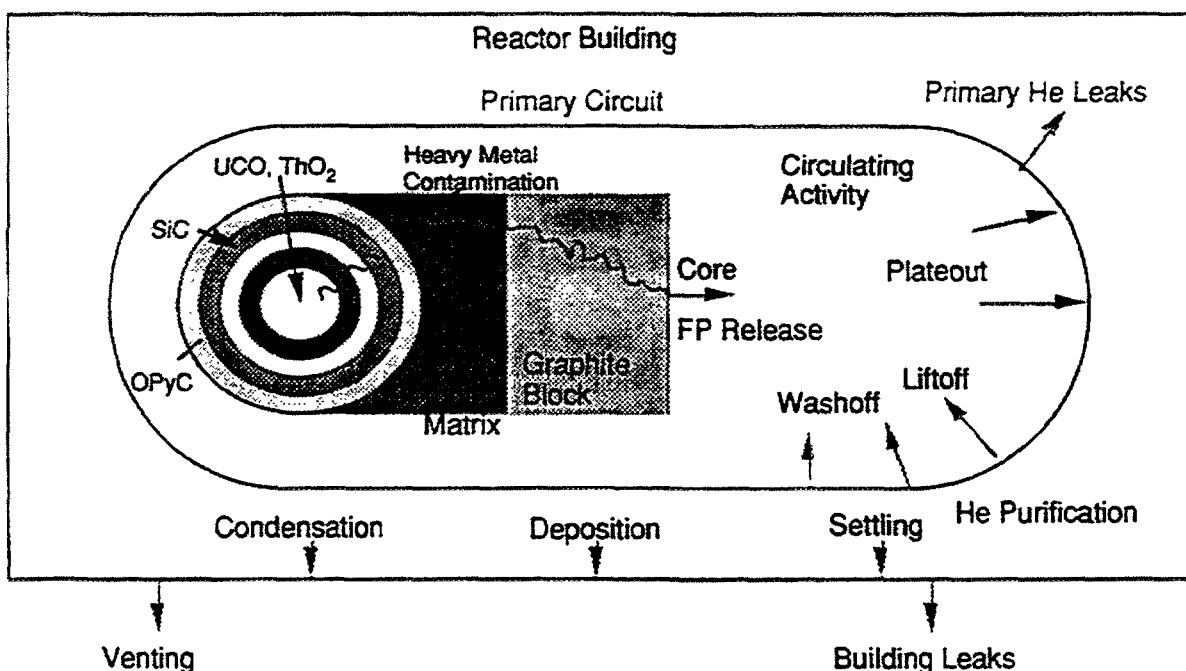


Fig. 6-1: Schematic of release barriers

The effectiveness of the individual barriers in containing radionuclides depends upon a number of fundamental factors, including the chemistry and half-lives of the various radionuclides, the service conditions, and irradiation effects. The effectiveness of these release barriers is also event specific; for example, the attenuation of iodine release to the environment by the reactor building is much higher during core conduction cooldown events than during rapid depressurization events.

The fourth release barrier in the HTGR is the primary coolant pressure boundary. Once the fission products have been released from the core into the helium coolant, they are transported throughout the primary circuit. The helium purification system removes both gaseous and metallic fission products from the primary coolant at a rate determined by the gas flow through the purification system. However, for the condensable fission products, the dominant removal mechanism is deposition, or "plateout", on the various helium-wetted surfaces in the primary circuit. The plateout rate is determined by the mass

transfer rates from the coolant to the fixed surfaces, by the sorptivities of volatile fission products on the various materials of construction, and by the temperature of operation.

The circulating and plateout activities in the primary coolant circuit are potential sources of release into the environment in the event of primary coolant leaks or as a result of the venting of primary coolant in response to overpressuring the primary circuit, e.g., in response to significant water ingress. The fraction of the circulating activity lost during such events is essentially the same as the fraction of the primary coolant that is released, although the radionuclide release can be mitigated by pumpdown through the helium purification system if the leak rate is sufficiently slow.

A small fraction of the plateout may also be reentrained, or "lifted off", if the rate of depressurization is sufficiently large. The amount of fission product liftoff is expected to be strongly influenced by the amount of particulate matter in the primary circuit as well as by the presence of friable surface films on primary circuit components which could possibly spall off during a rapid depressurization.

Other mechanisms which can potentially result in the removal and subsequent environmental release of primary circuit plateout activity are "steam-induced vaporization" and "washoff". In both cases, the vehicle for radionuclide release from the primary circuit is water which has entered the primary circuit. In principle, both water vapor and liquid water could partially remove plateout activity (these two removal mechanisms are subsequently referred to as "steam-induced vaporization" and "washoff", respectively). However, even if a fraction of the plateout activity were removed from the fixed surfaces, there would be environmental release only in the event of venting of helium/steam from the primary circuit. For all but the largest water ingress events the pressure relief valve does not lift. Moreover, the radiologically important nuclides such as iodine and cesium are expected to remain preferentially in the liquid water which remains inside the primary circuit.

The reactor building/containment structure is the fifth barrier to the release of radionuclides to the environment. Its effectiveness as a release barrier is highly design and event-specific. The US GT-MHR design utilizes a Vented Low-Pressure Confinement (VLPC), and the German modular HTGRs designs utilize similar containment concepts. In contrast, the Japanese HTTR has a high-pressure steel containment building. Since fission product transport phenomena are more important for the low-pressure vented designs, this section will emphasize that concept.

The VLPC and similar confinement vented designs may be of limited value during rapid depressurization transients; however, they can be of major importance during core conduction cooldown transients. Under such conditions, the natural removal mechanisms occurring in the reactor building, including condensation, fallout and plateout, are expected to attenuate the release of condensable radionuclides, including radiologically important iodines, by at least an order of magnitude.

6.1. FISSION PRODUCT TRANSPORT IN PRIMARY COOLANT CIRCUIT

6.1.1. Fission Product Transport and Deposition during Normal Operation

6.1.1.1. Plateout Models and Computer Codes

A number of different transport models and computer codes have been developed to predict plateout in the primary coolant circuits of HTGRs; typically, the utility of the more sophisticated models has been limited by unavailability and/or unreliability of the material property data required as input to these codes.

6.1.1.1.1. FRG Contribution

Plateout distribution of fission products in the primary circuit under normal operating conditions is calculated at the Research Center Jülich [1] with the codes SPATRA or PATRAS which combine ad-/desorption behavior and mass transfer, as it was first proposed for HTGR plateout calculations by Kress and Neill [2]. In the **SPATRA code** [3], the ad-/desorption equilibrium partial pressure on metals is approximated by:

$$p_i = p_o \exp[-\Delta H_{des}/(RT)] \frac{\sigma}{\sigma_o} \quad (6-1)$$

where

p_i is the partial pressure of nuclide i [Pa]

p_o is an empirical constant, $p_o \approx 10^8$ [Pa]

σ is the concentration of fission products with respect to the geometrical surface [mol/m²]

σ_o is the monolayer concentration on the geometrical surface [mol/m²]

ΔH_{des} is the desorption enthalpy in the sub-monolayer regime [J/mol]

R is the gas constant, R = 8.3143 [J/(mol K)]

T is the temperature [K]

This equation is easily obtained by equating the rate of collisions of nuclides onto the geometrical surface with the desorption rate. The latter is proportional to the lattice vibration frequency and to an Arrhenius factor containing the desorption enthalpies. As shown in Appendix C of Ref. [1] in more detail, the assumption of an ad-/desorption equilibrium is a reasonable approach, because the desorption process is much faster than the diffusion process into the metal.

Introducing Eq. (6-1) into the mass transfer equation

$$\frac{1}{F} \frac{dn}{dt} = \beta (c_{gas} - c_{gr}) \quad (6-2)$$

where

- F is the area [m²]
- n is the number of moles
- β is the mass transfer coefficient [m/s]
- c_{gas} is the concentration in coolant [mole/m³]
- c_{gr} is the concentration in graphite [mole/m³]

leads to:

$$\frac{d\sigma}{dt} = \frac{\beta}{R T} (p_{i,BULK} - 10^8 \exp[-\Delta H_{\text{des}}/(RT)] \frac{\sigma}{\sigma_0}) \quad (6-3)$$

where $d\sigma/dt$ is the deposition rate [mol/(m²s)].

Eq. (6-3) which is solved (in a more complicated form) in SPATRA is valid only for a low fission product fractional coverage on surface layers which is usually true for the normal operating reactor. In case of higher surface concentrations saturation effects must be taken into account, meaning that fission product concentrations cannot be considered independently of their adsorption behavior. Coverage of effective surfaces approaching a monolayer also leads to a significant decrease of desorption enthalpies. However, due to surface roughness, effective surfaces in HTGRs may be at least one order of magnitude larger than the geometrical surfaces.

Values of desorption enthalpies as derived from various deposition experiments (a.o., LAMINAR, VAMPYR) are in the range 220 - 260 kJ/mol for cesium and silver and 110 - 180 kJ/mol for iodine, depending on the adsorbent and its surface conditions [1]. Cesium desorption enthalpies seem to be larger on oxidized surfaces than on clean metallic surfaces, whereas iodine desorption enthalpies are especially small on oxidized surfaces. A quantitative relation between surface conditions and desorption enthalpies, however, is not available up to now.¹ One should keep in mind that the desorption enthalpy is part of the exponent in Eq. (6-3), thus the data range of ΔH_{des} given above translates into sorption isotherm differences of up to several orders of magnitude.

Strontium plateout behavior is less well known. Thermochemical estimations have indicated that strontium in the presence of oxide layers may be converted into SrO or into another oxidic phase. In that case, Eq. (6-1) is not applicable, and the usual vapor pressure equations for pure oxidic strontium must be assumed. Vapor pressures of oxidic strontium compounds, however, are extremely low. Vapor pressure equations for pure compounds may also be applied in case of iodine plateout under conditions of solid FeI₂ formation, i.e. for less oxidized metal surfaces at low temperatures [4]. Because of their relevance for source term estimations in water ingress accidents, the knowledge concerning desorption and vaporization enthalpies under reactor conditions must be improved by additional experiments.

¹ However, a qualitative explanation might be provided by an atom's electronegativity (affinity for acquiring electrons) and oxidation state. Because metals (Cs, Sr, etc.) readily give up electrons and oxygen prefers electrons, they are compatible. But iodine and oxygen would compete for electrons and thus be less compatible. This interpretation is consistent with the observed desorption enthalpies.

SPATRA also contains a simplified model for consideration of absorption processes. A partition coefficient is assumed between adsorbed and absorbed state. The transport into the adsorbing material is regarded as simple Fickian diffusion. Absorption effects are experimentally confirmed to some extent for cesium [5]; they are, however, not well understood up to now. Mechanisms such as volume diffusion, diffusion in the micropore or grain boundary system of the oxide layers and growing of oxide layers must be taken into consideration. There are experimental arguments for absorption: diffusion profiles of cesium have been found within the oxide layers of metals for a depth of some μm ([6], [7], [8]) at temperatures of 600 - 800 °C for diffusion times on the order of hundreds to thousands of hours.

Besides diffusion within the micropore system of the oxide layer, some real absorption (i.e. irreversibility relative to ad-/desorption equilibrium) with inclusion of cesium into the metal or oxide volume may also occur. Although absorption hinders remobilization of plated-out fission products, it is conservatively not considered in safety analyses up to now because of the uncertainties. An overview of models concerning absorption is found in [9].

As mentioned above, the Jülich code PATRAS [10, 11] is similar to SPATRA with respect to adsorption but considers a temperature independent penetration coefficient (which is identical to the absorption probability of a gas atom colliding with the surface) and a re-evaporation of the absorbed nuclides as soon as solubility limits are reached. Some experimental facts conflicting with a simple absorption/penetration model will be given in this chapter. In addition, from a physical point of view, it is difficult to explain the absorption probability of a gas atom colliding with a surface to be independent of temperature (or kinetic energy of the gas atom) and rather depends for a given nuclide on some (temperature independent) material properties only. All transport processes into the volume (volume diffusion, grain boundary or micropore diffusion) are coupled to a significant activation energy which necessarily requires a temperature dependence of that penetration coefficient. Although the penetration coefficient is an empirical factor without a definite physical meaning, it can be shown that this model provides reasonable results for plateout problems, in particular for low fission product concentrations (where the above mentioned solubility limits do not play any role). The overestimation of the penetration effect in PATRAS may be due to the fact that it is based on interpretation of plateout data on titanium which, however, shows, in contrast to most other HTGR metals, a rapidly growing oxide layer that would completely include absorbed fission products [1].

HRB codes to describe the deposition behavior in a primary circuit are NESSIE and RADAX which have been applied in THTR-300 licensing procedure. The RADAX model contains transport mechanisms such as convection in the flowing coolant, turbulent mass transport to the surface, adsorption/desorption at the surface, solubility/diffusion in the wall material. A main feature similar to the PATRAS code, is the subdivision of the sorption rate into a surface-related adsorption rate and a volume-related solubility rate which is a linear function of the penetration coefficient [12].

The plateout codes SPATRA and PLATO [13] also contain the penetration model as an option. An improvement of the penetration model of PATRAS (and the other codes) should contain the option of a temperature dependent penetration coefficient.

Input for the calculation models for estimation of the fission product distribution at accident initiation are basically taken from best estimate data of irradiation experiments with fuel elements [14], of reactor experience ([15], [16], [17], [18]), and, in case of plateout calculations, of laboratory experiments ([5], [19], [20]).

While in safety analyses best estimate values of desorption enthalpies are used to estimate the plateout distribution, their lower boundaries are taken to calculate the equilibrium coolant gas activities. This procedure leads to lower limits for the relative plateout per pass and to upper limits of the atomic or molecular coolant gas activities. Since the plateout activities for iodine and metallic fission products are larger than the atomic/molecular gas-borne activities, the different handling of gas-borne and plateout activity does not lead to conflicting mass balances. The equilibrium activity of noble gases must be calculated by considering sinks like primary circuit leakages and gas purification systems.

6.1.1.1.2. Japanese Contribution

JAERI has developed the **PLAIN code** [21] to predict plateout distributions in gas circuits and have used it extensively to model plateout in the OGL-1 loop and in the HTTR. PLAIN is based on the PATRAS code model developed by Iniotakis [10, 11] but has a modified component model for fission product penetration into the wall material. Three regions are considered: flowing gas, wall surface, and wall interior. In the gas regime, fission products are mixed with the flowing coolant and transported to the wall by convective mass transfer. On the surface, fission products adsorb with certain probabilities, and adsorbed fission products desorb by the thermal excitation of the metal surfaces of the components. In the wall, the fission products migrate into the base metal from the surface according to the excitation of the lattice vibration, and diffused fission products sublime from the wall material when the gas-phase partial pressure becomes sufficiently low. Mass balances are written for each region, and the resulting set of coupled partial differential equations are solved by Laplace transforms.

6.1.1.1.3. US Contribution

GA has extensively used the **PADLOC code** [22, 23], a one-dimensional, transient, convective mass transfer code, to calculate the circulating- and plateout activity distributions of condensable fission products. Fission product deposition on primary circuit surfaces may be modelled as irreversible sorption or reversible adsorption as described by nonlinear sorption isotherms. Primary circuit components are represented by an equivalent number of parallel tubes, and a library of mass transfer correlations is available within PADLOC to accommodate a wide variety of geometries and flow regimes. An advanced version of the code **PADLOC/INDIF** models indiffusion of plated out activity into the interior of structures as well [24], but this advanced version is not yet available as a production code. (In principle, PADLOC/INDIF is very similar to the above described JAERI PLAIN code.)

6.1.1.2. Aerosol ("Dust") Effects

Perhaps the most difficult aspect to understanding and modeling the behavior of condensable fission products in the primary coolant circuit is the potential effects of **aerosols**, or "dust", that may be present therein. Conceptually, it is evident that if the concentrations of circulating and deposited dust in the circuit are very low (e.g., such that the collisions between fission product atoms and circulating particulates are infrequent compared to collisions between fission product atoms and helium atoms and/or fixed surfaces), then dust effects should be unimportant. In the other extreme, if the concentrations of dust are very high, then dust effects should play a dominant role in determining the transport, deposition and reentrainment behavior of condensable fission products.

Wichner, in his review of HTGR plateout and liftoff phenomena [25], provides a good summary of the available experimental data and the numerous attempts to model aerosol transport effects. In certain cases, including the Peach Bottom HTGR and the AVR, rather high concentrations of dust were observed in the primary coolant circuit; however, it is not at all clear that these data are representative of what should be expected for future modular HTGRs, especially those with prismatic fuel elements. Based upon limited FSV data, one might speculate that future HTGRs, especially those with magnetic-bearing circulators or turbocompressors, would be characterized by relatively low levels of dust, once the original construction debris, etc., were removed by prolonged action of helium purification system.

It is also noteworthy here that there is an extensive amount of open-literature data related to aerosol formation, transport, deposition and reentrainment, but it is not apparent that any of it relates directly to the circumstances expected in the primary circuit of an HTGR. In fact, it is not currently possible to state with confidence the nature or concentrations of dust in future HTGR primary circuits which implies large uncertainties in fission product transport behavior will persist until there is significant operating experience with a specific standardized reactor design.

6.1.1.2.1. British Contribution

There are British data on the transport of metal-oxide aerosols in AGRs (e.g., [26]), but no data on the effects of such aerosols on fission product transport.

6.1.1.2.2. FRG Contribution

In a pebble-bed HTGR, graphite dust forms resulting from abrasion during fuel balls recirculation and represents a major transport medium for fission products besides the coolant itself. The **AVR** reactor has been used to conduct several experiments for investigation of atomic or molecular radionuclides in the coolant flow as well as transport and deposition with graphitic or metallic dust [27]. Besides the VAMPYR-I and VAMPYR-II installations which will be explained in section 6.1.1.3.2., the cold gas filter and the dust experiments have been carried out.

The experience with the **cold gas filter** is based on 45 tests since 1970 where a coolant

Table 6-1: Operating Conditions and activity measurements of dust experiments in the AVR, from [29].

Run ⁽¹⁾	Time [h]	Total coolant throughput in branch 2 [Nm ³]	Average gas tempe- rature [°C]	Dust collected on SFs [mg] branch 1 / branch 2	Specific dust activity [10 ⁶ Bq/g]		Coolant activity [Bq/Nm ³]	
					Cs-137	Ag-110m	Cs-137	Ag-110m
S ₁	146	5,287	846	81.9 / 119.4	1.13 / 1.64	0.057 / 0.054	17.8 / 37.0	0.89 / 1.22
S ₂	764	27,820	850	42.6 / 46.6	1.27 / 9.45	0.11 / 0.32	1.85 / 15.9	0.17 / 0.52
S ₃	432	15,539	850	1.1 / 4.3	31.1 / 41.9	3.16 / 2.06	2.22 / 11.5	0.22 / 0.59
S ₄	288	10,452	850	3.5 / 3.0	6.94 / 29.4	0.78 / 1.57	2.22 / 8.51	0.26 / 0.44
S ₅	430	15,451	950	7.4 / 6.7	13.3 / 96.1	1.24 / 4.39	6.29 / 41.8	0.59 / 1.92
S ₆	431	15,222	950	5.3 / 12.0	16.7 / 50.3	1.88 / 2.90	5.92 / 39.6	0.67 / 2.29
S ₇	432	15,314	950	4.8 / 8.6	15.2 / 61.5	1.84 / 3.76	4.81 / 34.4	0.59 / 2.11
S ₉	288	9,975	950	5.4 / 4.2	2.48 / 25.0	0.64 / 2.37	1.48 / 10.4	0.33 / 1.00
S ₁₀	744	26,062	950	2.5 / 8.4	13.1 / 28.3	4.31 / 4.08	1.48 / 9.25	0.41 / 1.33
S ₁₁	188	6,604	900	5.9 / 7.5	31.2 / 98.2	15.3 / 54.3	27.8 / 112.	13.7 / 61.7
S ₁₂	680	24,015	950	4.3 / 17.2	28.3 / 29.0	11.0 / 7.46	5.18 / 20.7	1.96 / 5.33
S ₁₃	668	24,434	950					
S ₁₄	722	26,138	935					
S ₁₅	275	10,155	933					

(1) Test runs S₁ and S₂ were conducted with an irradiated Te-130 powder as I-131 source which did not properly work due to tellurium iodide formation. The source type was therefore changed to I-131 on an I-127 carrier.

(2) Due to the low surface concentration, the specific activity of the source was varied after this test.

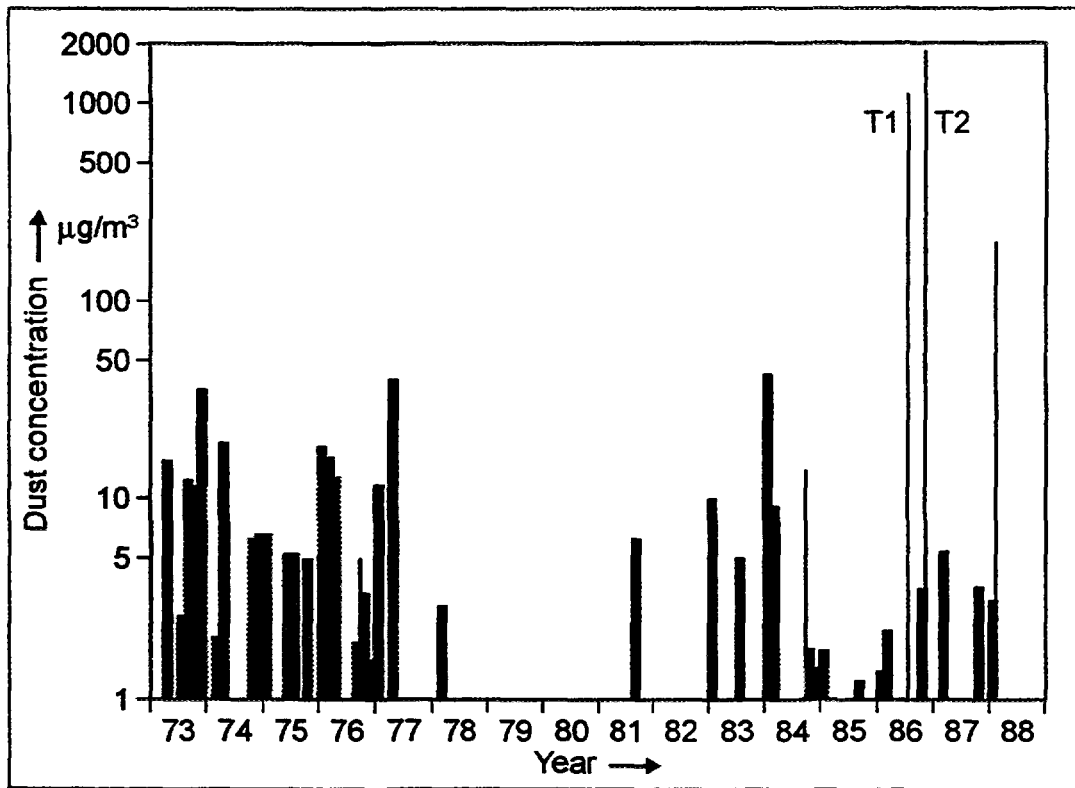


Fig. 6-2: Measured dust concentration in the coolant of AVR during steady-state operation conditions, transient operating conditions are marked with T1 and T2, from [27].

flow of $8 \text{ Nm}^3/\text{h}^2$ was bypassed through filters of quartz paper which allowed retention of dust particles down to $0.3 \mu\text{m}$ diameter with an efficiency of 50 %. Results are given in Fig. 6-2. It can be stated that dust concentrations during stationary, undisturbed operation were in the range of $1 - 2 \mu\text{g}/\text{m}^3$ superposed by concentration peaks that can be higher by some orders of magnitude. The average dust concentration in the AVR over the final operation years was about $5 \mu\text{g}/\text{m}^3$ [28].

Main goal of the **dust experiment** (Fig. 6-3) was the measurement of vapor-phase and dust-borne metallic fission product activities in the coolant, activities reversibly and irreversibly bound to dust, and the determination of the amount of dust and its grain size distribution. In these tests, a helium bypass in the cold gas region was routed through a sampling tube of 2.5 m length followed by a cooler and a special sequence of dust and fission product filters arranged in two parallel lines. The gas inlet temperature was in the range of 50 - 270 °C. Table 6-1 lists the operating conditions for the dust experiments in the AVR and presents measurement results of dust and coolant activities from branch 2 of the setup [29]. In Table 6-2 the detailed figures of activities measured at the single dust filters (SF) and fission product filters (SPF)³ of both branches are given [30]. The relative distribution as measured in the branch 2 components in dust experiment S₃ is given in Table 6-3 [31].

² Nm^3 means m^3 at standard conditions of temperature (298 K) and pressure (0.1 MPa)

³ The fission product filters (SPF) deployed in the AVR experiments were designed by Iniotakis based on the idea that the in-diffusion into the metal walls is dominant compared (high penetration coefficient). These filters basically offered a large metal surface. Experimental data, however, revealed that they did not work as expected [1].

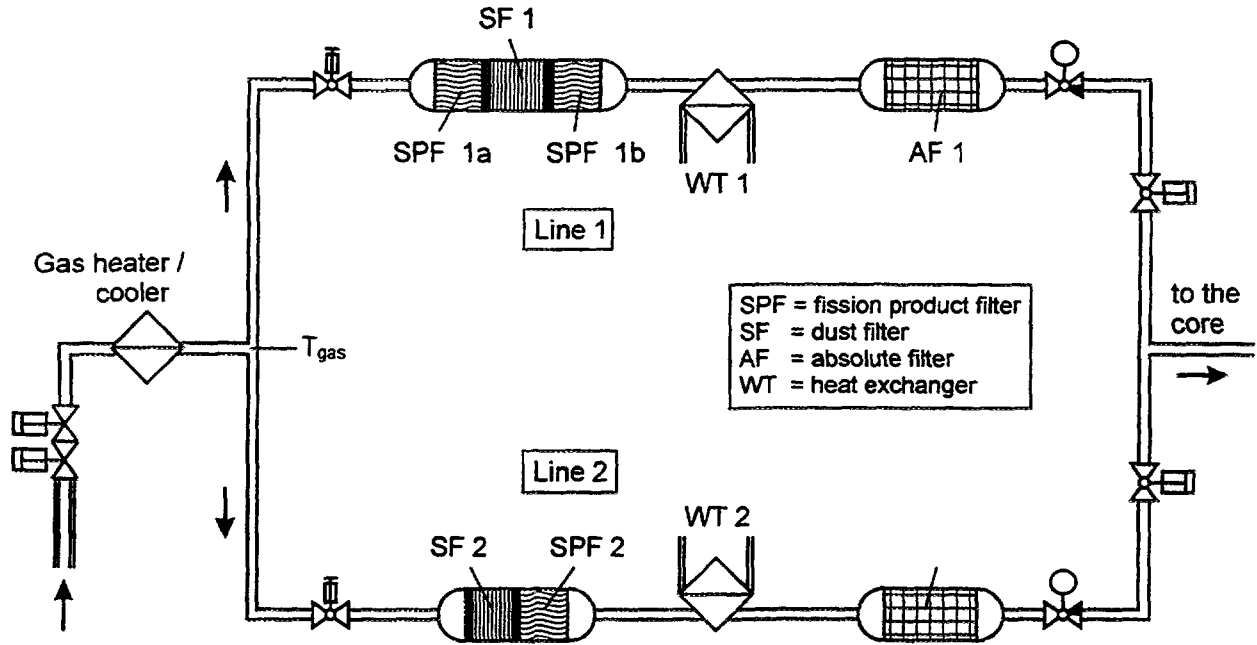


Fig. 6-3: Dust experiment at the AVR reactor

Table 6-2: Cesium and iodine activities [Bq] measured in the single components of dust experiment S₁, from [30]

Branch 1			Branch 2		
Location	Cs-137	I-131	I-131	Cs-137	Location
SPF1a	$3.6 \cdot 10^5$	$4.1 \cdot 10^3$			
SF1 (2μ)	$7.0 \cdot 10^4$	$1.9 \cdot 10^2$	$1.4 \cdot 10^3$	$2.0 \cdot 10^5$	SF2 (2μ)
SF1 (QF)	$1.6 \cdot 10^4$	$7.0 \cdot 10^1$	-	$4.8 \cdot 10^4$	SF2 (QF)
SF1 (P)	$7.0 \cdot 10^3$	$4.1 \cdot 10^1$	-	$1.9 \cdot 10^4$	SF2 (P)
SPF1b	$9.6 \cdot 10^3$	$2.0 \cdot 10^2$	$8.1 \cdot 10^2$	$9.3 \cdot 10^4$	SPF2

Table 6-3: Relative activity distribution of some nuclides in the single components of branch 2 of the dust experiment S₃, from [31]

Branch 2 component	Cs-134 [%]	Cs-137 [%]	Ag-110m [%]	I-131 [%]
SF2 + SPF2	94.4	95.8	88.4	1.7
Paper filter	4.8	4.2	11.6	0.1
Absolute filter	0.8	-	-	98.2
Absolute Activity [Bq]	$6.7 \cdot 10^4$	$2.8 \cdot 10^5$	$1.1 \cdot 10^4$	$3.6 \cdot 10^5$

The dust experiments, in general, have shown that the dust mass in the AVR primary circuit has steadily decreased. The dust collected was much finer ($< 2 \mu\text{m}$) than expected. The specific dust activities for cesium and strontium in branch 2 were found to be higher by a factor of 2.5 - 5 than in branch 1 meaning that it is basically in the filters where the dust was loaded with activity [32].

Dust samples collected in the VAMPYR-II [33, 34, 35, 36] in fine dust filters preceding the fission product filters, contain a significant amount of metallic particles as shown in Table 6-4. The small dust mass collected in run VII,4 is due to the fact that another dust filter (SF1) preceding the test tube was active. VAMPYR-II is described in further detail in section 6.1.1.3.2.

Table 6-4: Dust samples collected in the dust filter SF2 in the experiment VAMPYR-II, from [35, 36]

Test	Dust [mg]				
	C	Fe	Ni	Cr	Total
VII,3	88.9	8.7	9.4	3.0	110
VII,4	18.1	6.8	1.8	0.9	27.6

For the AVR reactor, the dust production rate was estimated to be about 3 kg per operating year with a total dust inventory in the primary circuit of about 60 kg at the end of 1988. As shown in Fig. 6-2, dust concentrations in the coolant can vary over several orders of magnitude with peak values achieved when during transient operation conditions dust is remobilized due to changes in the coolant flow (see also section 6.1.2.2.). From such transients, it could be concluded that a fraction of 0.5 - 2 % of the gas-borne dust is deposited per recirculation.

The measurements of Cs-137 activities in graphite dust collected in the THTR-300 from the moisture sensors were taken to assess the fine dust production in 300 days full power operation [37]. The estimated range was 13 - 400 kg with an expected value of 25 kg. The distribution of dust within the primary circuit depending on particle size, coolant velocity, and geometry is, as expected, dominant in the cold gas area. The specific activity is relatively high, $2 \times 10^8 \text{ Bq/g}$ maximum, mainly caused by the radionuclides Co-60, Sr-95, Hf-181, and Pa-235 [38] due to the enhanced particle failure from fuel element fracture. The measurements for the radiologically relevant cesium and silver isotopes were $1.1 \times 10^6 \text{ Bq/g}$ for Cs-137, $5.7 \times 10^5 \text{ Bq/g}$ for Cs-134, $5.0 \times 10^5 \text{ Bq/g}$ for Ag-110m [37]. The increase of the Cs-137 activity to $4.7 \times 10^6 \text{ Bq/g}$ half a year later, however, is not that strong as would have been expected from the higher burnup [39].

According to a prediction made by SIEMENS for the HTR-MODUL, dust will accumulate to 500 - 1000 kg after 32 years of operation. This prediction is based on experience with AVR and on results from experiments with a fuel element feeding system. The experiments led to an estimate of 10 mg abrasion per transit [40]. For the medium-sized HTR-500, a reduced mechanical impact can be expected because of the OTTO ("Once

"Through Then Out") loading scheme. The expected dust production rate is 10 kg per operation year which increases after 25 years due to side reflector abrasion [41].

The uncertainties with respect to dust effects are remarkably high. In pebble bed HTGRs, most of the dust seems to be produced by friction of fuel element pebbles and mechanical erosion as a result of pebble recirculation, in particular in the fuel handling system, and, therefore, consists mainly of carbon. In addition, some metallic dust has been found containing iron and cobalt and their oxides. Also carburization may play a role in production of some small-sized dust. With respect to dust depletion during normal operation, two different effects must be considered:

- dust transport to surfaces mainly by turbulent diffusion and sticking by adhesion
- sedimentation of (probably larger) dust particles in quiescent coolant regions

It is a well known fact that adhesively bound particles of diameter $< 50 \mu\text{m}$ are not easy to remove by shear forces [42]. The average size of AVR dust seems to be significantly smaller as indicated by a typical distribution of particle numbers [16, 43]. A typical size distribution of fine dust particles collected from the AVR during a VAMPYR-I experiment and independent of sampling location and time is presented in Fig. 6-4 [44]. This number-weighted distribution indicates an average dust particle diameter of about $0.6 \mu\text{m}$ which corresponds to a median diameter of about $5 - 10 \mu\text{m}$ for a particle volume-weighted distribution. The size distribution of AVR dust seems to be similar for all filter experiments. One should keep in mind, however, that an agglomeration of individual dust particles on surfaces cannot be excluded especially for high dust concentrations, which could produce particle sizes which are more easily lifted-off by depressurization induced shear forces. Adhesively bound dust can change the plateout behavior of primary circuit surfaces.

The modeling of **dust-borne activity** can currently not be treated because of major uncertainties concerning production, deposition and interaction with gas-borne or plated out fission products.

Radionuclide activities borne on the dust are significantly dependent on where the dust is located as indicated by the measurement data in Table 6-5. Assuming half of the dust inventory to be deposited in the fuel cycle system and the other half uniformly distributed between steam generator and cold gas zone, an estimated fraction of 8 % for Cs-137 and of 11 % for Sr-90 out of the totally released activity is bound to dust [27].

With respect to the dust-borne activity in the AVR, dust from filter experiments was estimated to contain about 10 % of the amount of Cs-137 and Sr-90 released from the core during normal operation [45]. Because of the greatly reduced amount of dust expected for modern HTGR concepts such as the HTR-MODUL, in particular due to dust filtering in the fuel element handling system, the dust-borne fraction of the primary circuit activity is assumed to be smaller by a factor of about 5 for these nuclides. Significant activities of Ag-110m were also found in the AVR dust [45]. In the past, the I-131 content in dust was thought to be nearly negligible. However, recent on-line examination of dust during blower transient experiments has indicated that the AVR dust mobilized during the transient contains concentrations of I-131 as large as 3.5 GBq/kg. The total amount of iodine in the AVR primary circuit is on the order of 25 GBq. This means that iodine

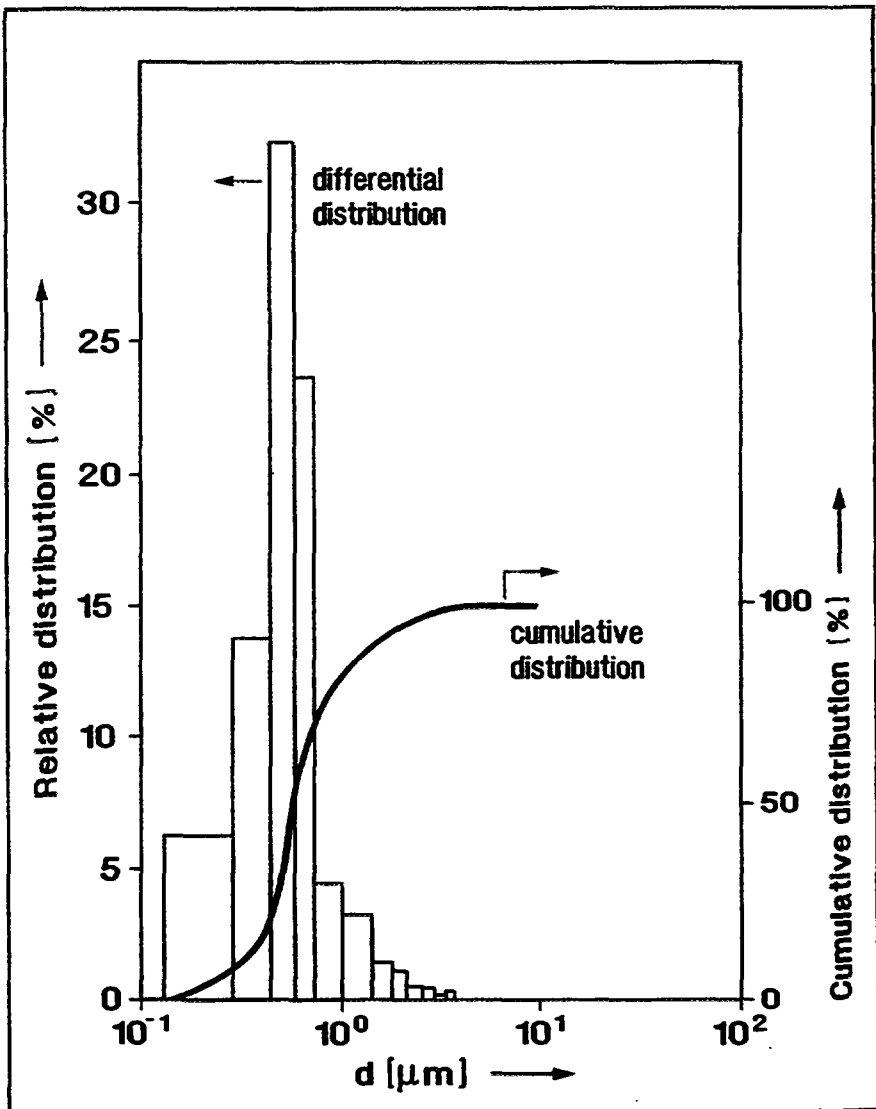


Fig. 6-4: Typical number-weighted distribution of dust particles sizes in the AVR coolant as measured in V41 of VAMPYR-I, from [1, 44].

Table 6-5: Activity concentrations of collected AVR dust samples at different locations, from [27].

Point of extraction	Year	Concentration [Bq/g dust]			
		Co-60	Ag-110m	Cs-137	Sr-90
Fuel Element Surfaces	1978	1.8×10^6	5.4×10^4	1.0×10^6	2.7×10^6
	1988	3.0×10^4	5.1×10^3	1.3×10^5	9.0×10^5
Steam generator	1986	5.1×10^6	2.7×10^7	7.4×10^7	3.6×10^8
Cold gas zone	1978	6.7×10^5	1.6×10^6	3.0×10^7	2.5×10^8
	1988	1.6×10^6	6.4×10^5	5.9×10^6	5.0×10^7
Fuel cycle system	1978	7.4×10^4	9.3×10^4	1.5×10^5	-
Shutdown rod	1987	4.3×10^5	1.9×10^5	1.3×10^7	-

is inhomogeneously distributed on the dust in the primary circuit and that, in particular, the dust which contains large concentrations of iodine is preferentially mobilized during transients. A possible reason is that the outer layers of the sedimented dust which come into direct contact with the gas flow contain equilibrium fission product concentrations. Considering nuclear decay, there will be a concentration gradient toward the bottom dust layers which settled earliest, especially for short-lived nuclides. The outer dust layers seem to be preferentially mobilized. There is no information available about the activity gradient within the settled dust. Therefore, the dust-borne fraction of the radiologically important iodine nuclides cannot be quantified at this time.

It is important to note that the examination of dust specimens removed by wiping from AVR primary circuit surfaces has shown remarkable differences in the specific activities [45]. In particular, dust from fuel element surfaces has a significantly smaller specific activity than dust depleted or adhesively bound on primary circuit components. This was confirmed by the postexamination of irradiated AVR fuel elements, with specific activities on fuel element surfaces [46] found to be one to two orders of magnitude smaller than dust activities [45]. Since dust formation is assumed to proceed mainly by friction of fuel elements, it is not sufficient to consider only the activity on fuel element surfaces as a source of the dust activity.

Interaction of dust with molecular gas-borne or plated-out activity must also be taken into account. This is, however, difficult to correlate with another observation in the AVR: dust from quiescent coolant regions obtained during blower transients has about the same specific activity as adhesively bound dust; i.e., much higher activities than found on fuel element surfaces. A significantly larger fission product loading of dust in quiescent coolant regions is hard to imagine because of the small mass transfer efficiency in this area. This observation can obviously be explained only by the assumption of a (slow) dust particle exchange between areas with sedimented and adhesively bound dust during reactor normal operation. Local flow turbulence [47] in combination with the above mentioned growth of adhesively bound particles by agglomeration is possibly responsible for such an activity exchange. These interpretations, however, are highly speculative and cannot be used as a basis for accident calculations.

6.1.1.2.3. US Contribution

The available data on the effects of dust on fission product transport in the primary coolant circuit are largely from reactor surveillance measurements made at Peach Bottom and, to lesser extent, Fort St. Vrain. Significant quantities of carbonaceous dust were observed in the **Peach Bottom** primary coolant circuit [48, 49, 50] as a result of periodic ingresses of lubricating oil from a leaking purified helium transfer compressor [51]. Perhaps surprisingly, the presence of this particulate matter, which was predominately bound to fixed surfaces, appeared to have little influence on the cesium plateout distribution in the primary circuit other than increasing the effective sorptivity of the hottest metal surfaces [52].

The particulate matter in the **Fort St. Vrain** primary coolant circuit was not as extensively characterized as that in Peach Bottom. The available data are largely from the examination of several circulators that were removed for repair (e.g., [53]) and from the removal and radiochemical analysis of two plateout probes [54, 55]. Based upon these data,

it appears that the concentration of particulate matter in FSV was relatively low, certainly much lower than in Peach Bottom or AVR, and that it was comprised of metallic oxides, predominantly Fe_3O_4 , and had a carbon content of < 10%. Presumably, the friable metallic oxides in the primary circuit resulted from the chronic water-ingress problems associated with the water bearings used in the helium circulator.

Limited semi-quantitative data are also available from the GA deposition loop program [56]. In one test, a quantity of graphite powder was added to the out-of-pile loop, and the result was to alter the plateout distribution of the Cs-137 and Sr-90 and to increase significantly the amount of liftoff observed in *ex-situ* blowdown tests.

6.1.1.3. Integral Plateout Data

The validity of the methods used to predict plateout distributions in the primary coolant circuit during normal operation have been assessed by applying them to predict integral plateout data measured in out-of-pile loops, in-pile loops and operating HTGRs with mixed results. In certain cases, excellent agreement has resulted, but in other cases order-of-magnitude discrepancies were observed.

6.1.1.3.1. British Contribution

Extensive plateout distribution data were obtained by examining components removed from the **Dragon HTGR**. GA has evaluated these data and has used its reference plateout methods to predict the plateout of Cs, Sr and I isotopes in the Dragon primary circuit; in general, the agreement was quite good [57]. Typical comparisons between measured and predicted plateout distributions in the Dragon primary heat exchanger are shown in Fig. 6-5; however, it should be noted that the peak wall temperature was only ≈ 350 °C so this good agreement is primarily an indication of an accurate prediction of the convective mass transfer coefficients.

British researchers have also investigated the plateout behavior of condensable fission products in the primary circuits of their CO_2 -cooled Advanced Gas Reactors (e.g., [58] and [59]). However, the extent to which these AGR data are applicable to HTGRs has not been systematically evaluated.

6.1.1.3.2. FRG Contribution

In Germany various reactor and laboratory experiments were used to analyze the behavior of fission and activation products available as either free or dust-borne activity in the cooling gas or as activity deposited in the HTGR primary circuit. Their goal was the description of transport, plateout, interaction and release processes by physical models and the establishment of a data bank for nuclide and material specific parameters. In close cooperation between AVR and KFA, the in-pile experiments VAMPYR-I and VAMPYR-II were conducted for the purpose of investigating deposition under normal operating conditions. Additional experiments were conducted in the out-of-pile facilities SCAFEX and SMOC (the latter is, because of its major relevance for desorption behavior under accident conditions, described in section 6.1.2.1.2.). Furthermore HRB operated another out-of-pile deposition loop LAMINAR at the Research Center Jülich. Within the frame of

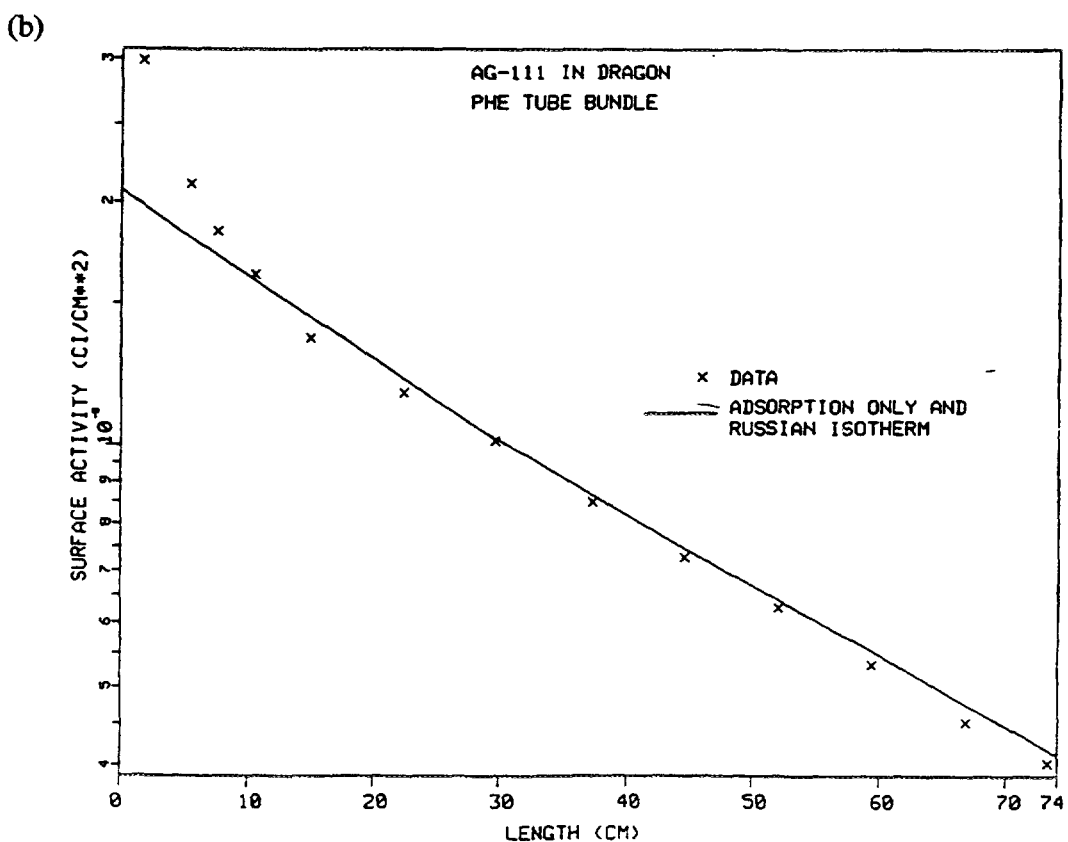
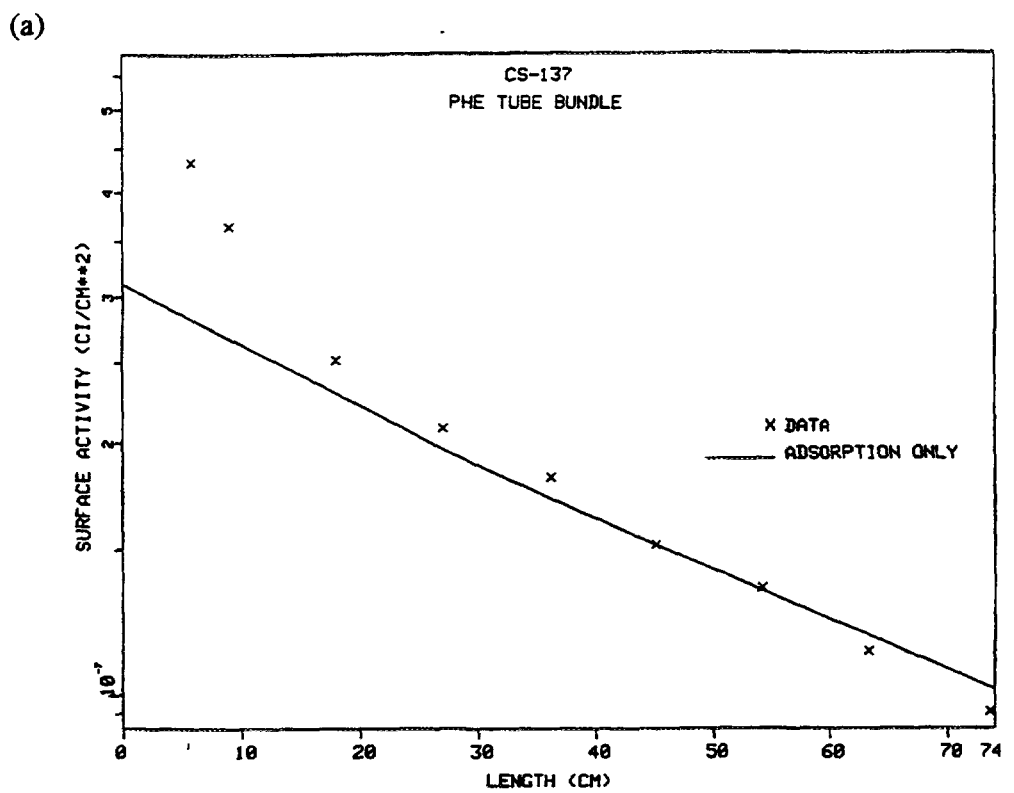


Fig. 6-5: Predicted and measured plateout distributions in DRAGON [57],
(a) Cs-137 profile along primary heat exchanger
(b) Ag-111 profile along primary heat exchanger

international cooperation, in-pile experimental data were gathered from the British Dragon Hot Gas Duct experiment and from the loop SAPHIR in the French Pegase reactor.

Out-of-Pile Loop Data

HRB Deposition Loop Facility LAMINAR

HRB operated a closed-cycle **helium loop facility LAMINAR** for cesium and iodine deposition experiments with the goal of fixing relevant design parameters and to test the HRB deposition model RADAX [19]. The essential measurement section consisted of a sample tube of 2.4 m length with heaters outside to adjust the axial wall temperature profile (300 - 900 °C). A helium mass flow was circulated at a rate of 18 kg/h under a pressure of 0.3 MPa. The helium inventory in the circuit was 18 g. Reynolds numbers were in the range of 6000 - 10000. The fluid was loaded with either Cs-134 or I-131. The vapor pressure of these elements was adjusted by the temperature of the source through which the fluid passed. Partial pressures $< 10^{-6}$ Pa at normal operation conditions were possible. After passing the test tubes (20 - 27 mm outer diameter, 2 - 2.9 mm wall thickness), the flow was cooled and passed through absolute filter blocks. The materials of the test tubes investigated were the high-temperature alloys Incoloy 800 and Inconel 617 plus, for iodine, 10CrMo910 and 15Mo3.

During operation, the temperature was raised (or lowered) to a specified value and the experiment continued after equilibrium was established. The operation was sometimes interrupted by desorption periods with the source disconnected. The surface activity accumulated on the test tubes was continuously measured by four NaI detectors. After each test, the sample tube was cut into 15 cm long sections which were γ -scanned and then leached. Also thickness and structure of the oxide layers formed were determined.

The number of deposition experiments conducted was 10 with Cs-134 and 5 with I-131. Operating conditions and measurement results are summarized in Table 6-6 for cesium and in Table 6-7 for iodine. The experimental data of deposited activities for all cesium tests are plotted in Fig. 6-6. The decrease in the final deposition profiles with increasing wall temperatures is as expected. The curves 1, 2 and 3, 4, respectively, indicate the degree of reproducibility.

The cesium measurement data have been used to derive a set of plateout parameter for the respective materials. For Incoloy 800, the desorption energy was estimated to be $Q = 234 \pm 13$ kJ/mol in the temperature range 600 - 800 °C and the penetration coefficient to be $1 \times 10^{-6} - 2 \times 10^{-5}$. The respective figures for Inconel 617 are $Q = 230 \pm 8$ kJ/mol ($T = 700$ °C) and $Q = 268 \pm 8$ kJ/mol ($T = 900$ °C) for the desorption energy and $1 \times 10^{-7} - 4 \times 10^{-6}$ for the penetration coefficient. As an example, the application of the above Incoloy 800 data to test run 4 with the HRB code RADAX is presented in Fig. 6-7 [19].

The basic ideas of the **iodine experiments** in the LAMINAR loop were [60], on one hand, to obtain samples representative of normal operation (10^{-5} Pa I-131, 250 - 500 °C) for use in subsequent steamoff/washoff experiments, and also to examine iodine deposition under core heatup conditions ($10^{-2} - 10^{-1}$ Pa I-131, 300 - 700 °C). Another goal was pre-oxidation of the test tube in an $H_2O/H_2/He$ atmosphere to obtain representative oxide layers.

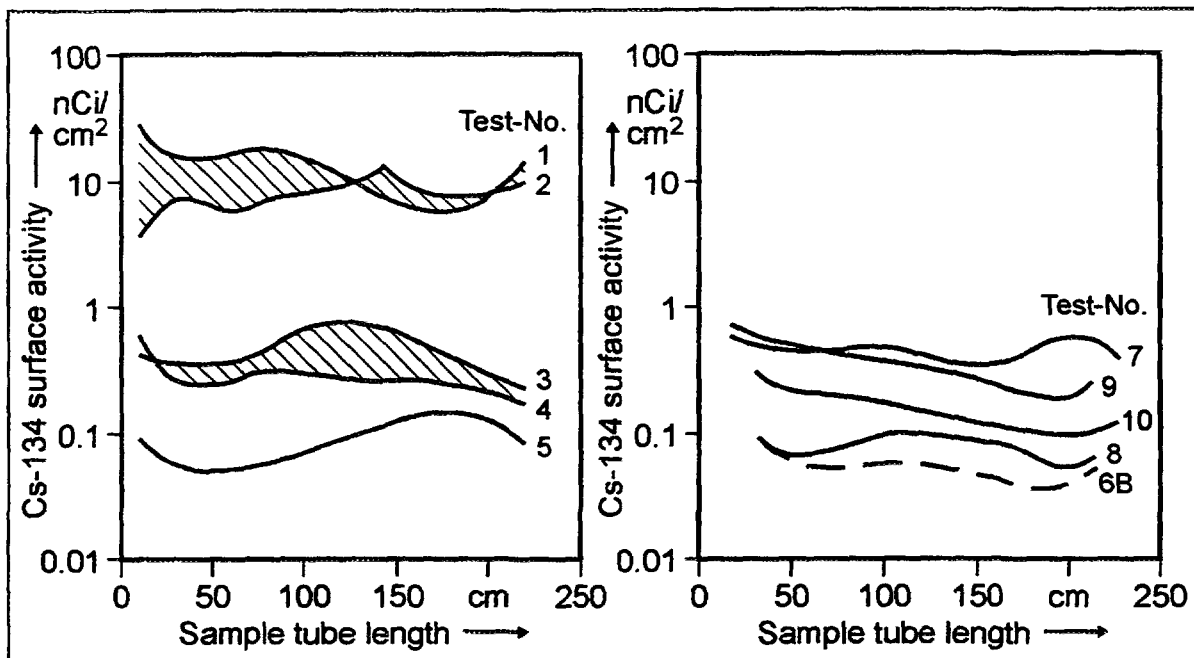


Fig. 6-6: Measurement of Cs-134 plateout profiles in LAMINAR, from [19] (left) on Incoloy 800, (right) on Inconel 617

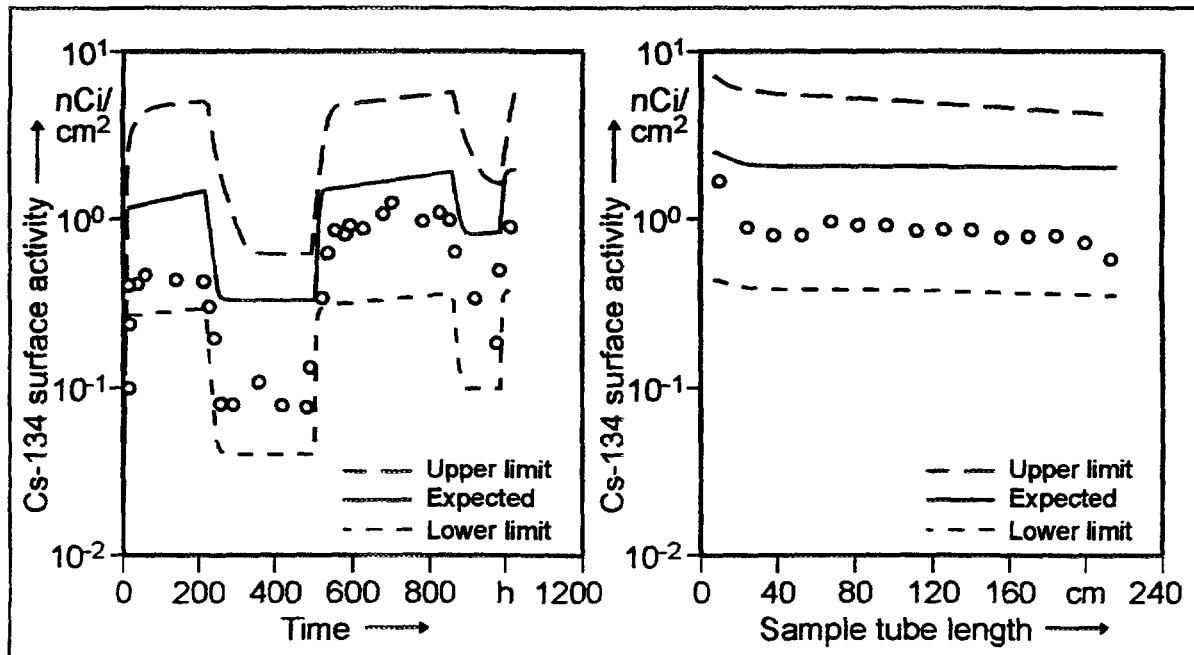


Fig. 6-7: Calculated and measured Cs-134 activities deposited on Incoloy 800 of LAMINAR test run 4, from [19] (left) vs. time at position 1.5 m, (right) vs. tube length after 50 d

Table 6-6: Operating Conditions and activity measurements of cesium experiments in the LAMINAR loop, from [19].

Run	Time [d]	Gas temperature inlet / outlet [°C]	Wall temperature inlet / outlet [°C]	Partial pressure [Pa]	Activity deposited [Bq /cm ²]
<i>Cs-134 on Incoloy 800</i>					
1	23	627 / 605	620 / 590	$3.4 \cdot 10^{-7}$	296 - 740
2	43	628 / 600	618 / 590	$4.1 \cdot 10^{-7}$	148 - 518
3	50	706 / 668	697 / 707	$16 \cdot 10^{-7}$	74 - 167
4	50	720 / 698	693 / 704	$13 \cdot 10^{-7}$	26 - 56
5	27	854 / 758	800 / 750	$1.1 \cdot 10^{-7}$	1 - 3
<i>Cs-134 on Inconel 617</i>					
6 A	22	725 / 691	700 / 700		11 - 26
6 B	2.4	818 / 784	800 / 800		4 - 7
7	46	710 / 692	710 / 694	$14 \cdot 10^{-7}$	185 - 333
8	31	823 / 785	808 / 804	$14 \cdot 10^{-7}$	37 - 74
9	60	811 / 793	803 / 799	$40 \cdot 10^{-7}$	370 - 925
10	35	893 / 881	906 / 902	$21 \cdot 10^{-7}$	111 - 148

Table 6-7: Operating Conditions and activity measurements of iodine experiments in the LAMINAR loop, from [60].

Run ⁽¹⁾	Time [d]	Specific activity [Bq/g]	Source rate [MBq/h]	Wall temperature inlet/outlet [°C]	Material	Activity deposited [Bq/cm ²]
<i>I-131</i>						
III.3	9	3.8×10^8	1.0	300 - 20	1.7380, 10 CrMo 910	$23^{(2)}$
III.4	13	7.4×10^9	5.4		10 CrMo 910	3.7×10^3
III.5	11		6.3 / 2.7	300 - 450	15 Mo 3	2.6×10^3
III.6	18	7.4×10^9		200 - 500	Incoloy 800	2.3×10^3
III.7	30	3.7×10^9		300 - 500	5415	1.4×10^4

(1) Test runs III.1 and III.2 were conducted with an irradiated Te-130 powder as I-131 source which did not properly work due to tellurium iodide formation. The source type was therefore changed to I-131 on a I-127 carrier.

(2) Due to the low surface concentration, the specific activity of the source was varied after this test.

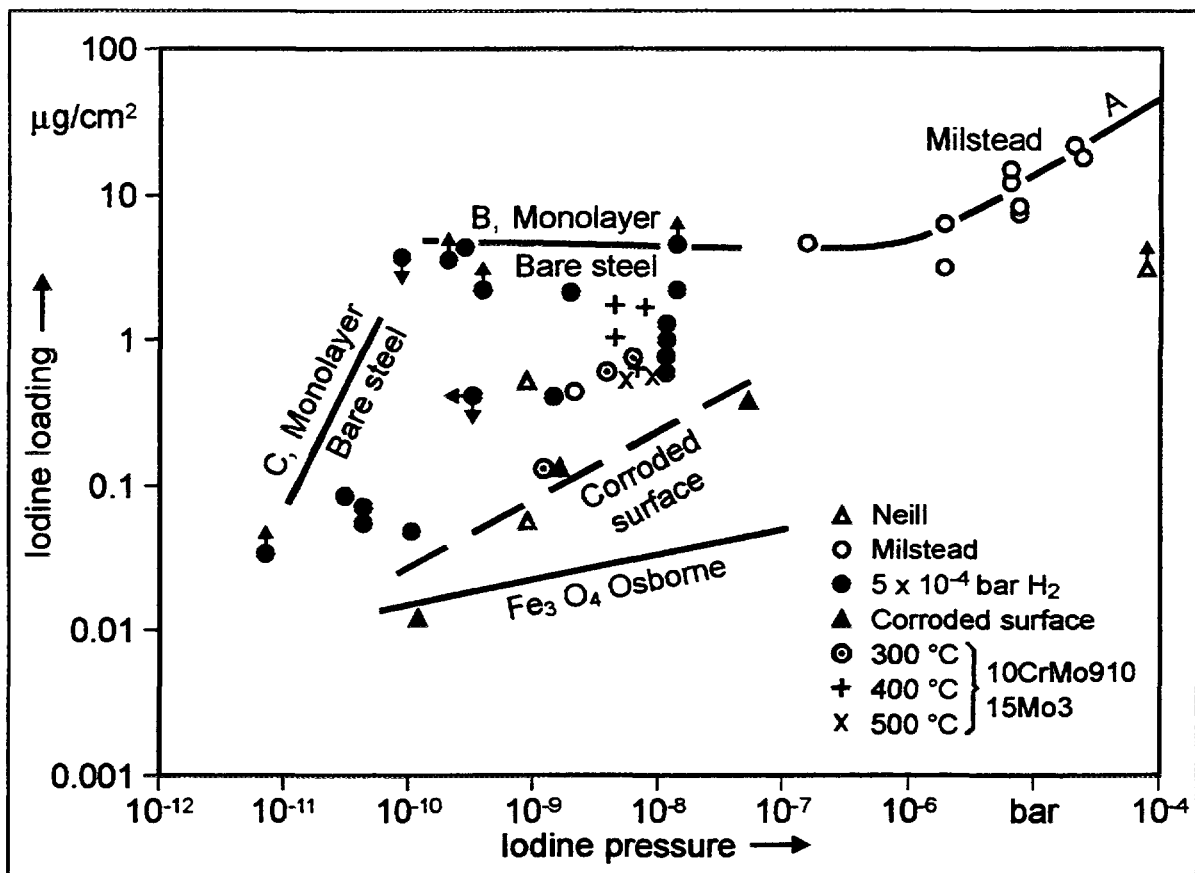


Fig. 6-8: Iodine sorption isotherms, from [60].

Results of iodine sorption isotherms are summarized in Fig. 6-8. The weak temperature dependence for both 10CrMo910 and 15Mo3 which is surprising for concentrations up to an order of magnitude below a mono layer, seems to confirm the tendency found by Osborne to reach a monolayer [61, 60].

Leach results from both the iodine and cesium plateout experiments are presented in section 6.1.2.3.2.

Laboratory Circuit SCAFEX

In the once-through **laboratory circuit SCAFEX**, the goal was to study different source concepts (as preparatory step for the SMOC experiments, see section 6.1.2.1.2.) and source control for the species Cs, Ag, I, and Sr, and to test different filter geometries and structures. It was also taken to examine silver deposition on metallic surfaces. A laminar or turbulent helium flow at a rate of 2 - 12 m³/s (< 3.6 g/s) at a system pressure between 0.2 - 0.6 MPa was loaded with a source and introduced into the test section. The gas inlet temperature was 100 °C. In SCAFEX, 1 - 8 tubes of various lengths and inner diameters could be examined. A schematic of SCAFEX is given in Fig. 6-9.

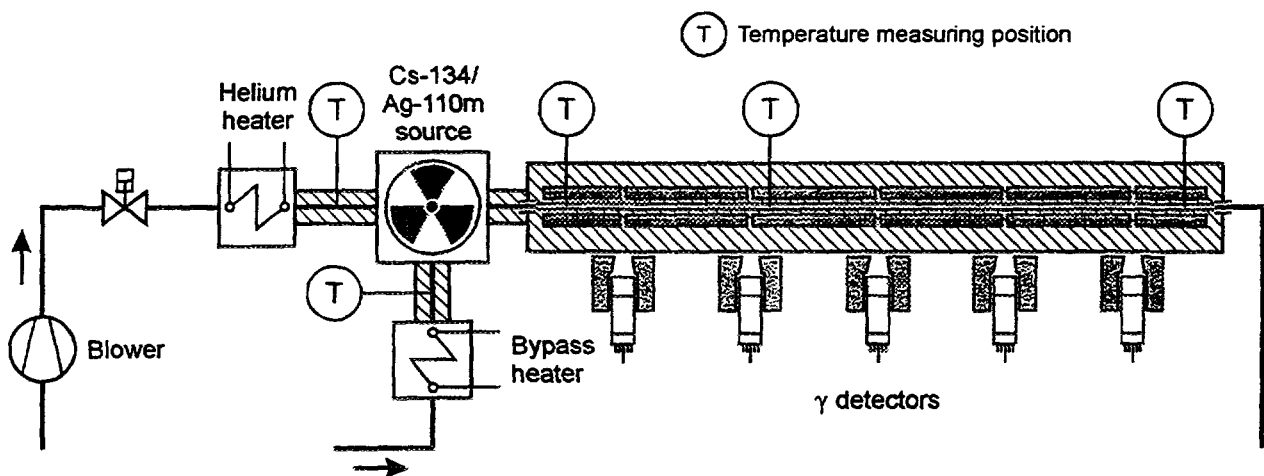


Fig. 6-9: Schematic of the laboratory circuit SCAFEX at the Research Center Jülich

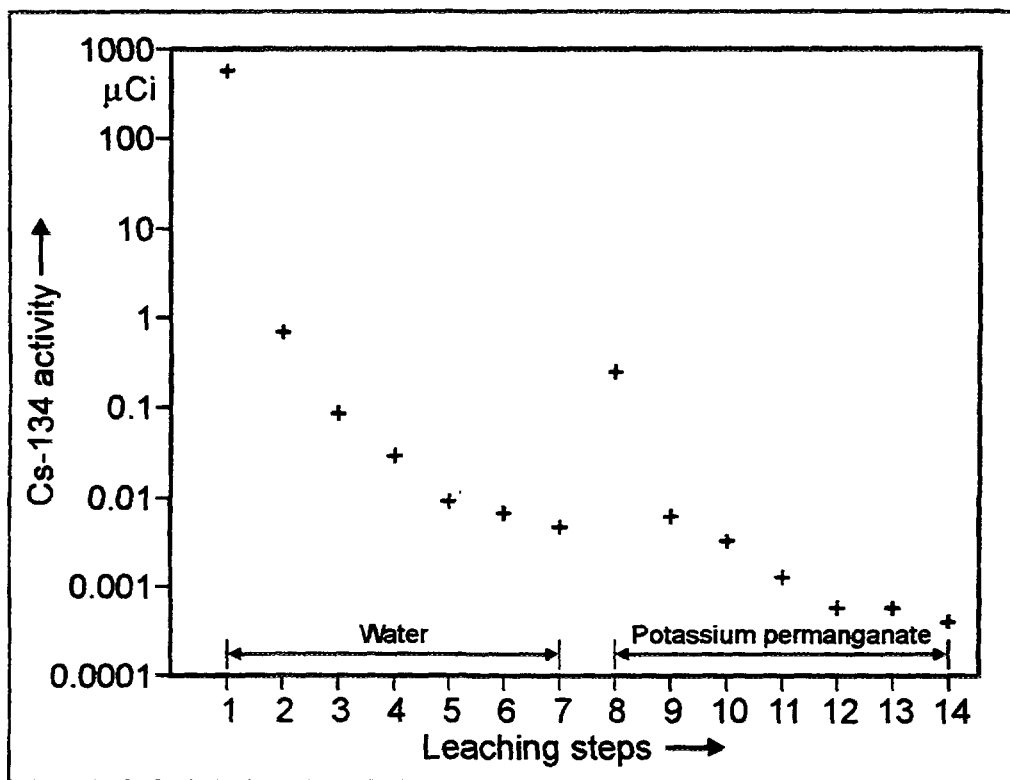


Fig. 6-10: SCAFEX test SX-1 decontamination, from [62].

In the first successful SCAFEX runs, SX-1 and SX-2, only measurements of deposited Cs-134 and the investigation of its removal by treatment with water (7 steps) and afterwards with potassium permanganate solution (7 steps) as shown in Fig. 6-10 were made. One test in 1983 served the purpose on examining the influence of the Reynolds number on the deposition behavior. It varied between 1500 and 4000 for a bundle of 3 parallel tubes.

A significantly reduced deposition was found at $Re \approx 2300$ [63]. In the test SX-2, the influence of gas temperature and moisture (> 3 ppm) on the concentrations of deposited cesium was studied [63].

In the late 1980s, SCAFFEX tests with silver were conducted. The operational conditions for the successful test with stable silver were a helium mass flow of 1.2 g/s at 0.6 MPa flowing through a titanium test tube. With a gas temperature of 350 °C at the entrance (wall temperature ≈ 400 °C), silver deposition during the operation time of 95 h was measured to have an average of $0.22 \mu\text{g}/\text{cm}^2$ forming a layer with a weight of 665 mg and with a thickness of $80 \mu\text{m}$ [64]. The source was found to release silver at a source temperature of 700 °C. After this test, the SCAFFEX series was terminated.

Hot Gas Sampling Tube VAMPYR-I

The **Hot Gas Sampling Tube VAMPYR-I** was installed in the AVR reactor in 1972 in one of the tubes available above the core in order to obtain diffusion profiles of deposited fission products on various materials under laminar flow conditions as well as concentrations of condensed fission and activated products in the hot gas to examine the influence of dust on deposition and, last but not least, to test fission product filters at operating temperatures of 850 - 900 °C [65]. The test tube had a length of 2.2 m and an inner diameter of 20 mm. To determine fission product concentrations in the helium, a portion of the helium flow was diverted into the tube and then into an absolute filter. The rate was approx. 15 Nm³/h at a pressure of 1.1 MPa (0.7 g/s). Materials investigated were Ti, 15Mo3, 4541, 4961, ST35.8, and 10CrMo910. A schematic of VAMPYR-I is given in Fig. 6-11. The

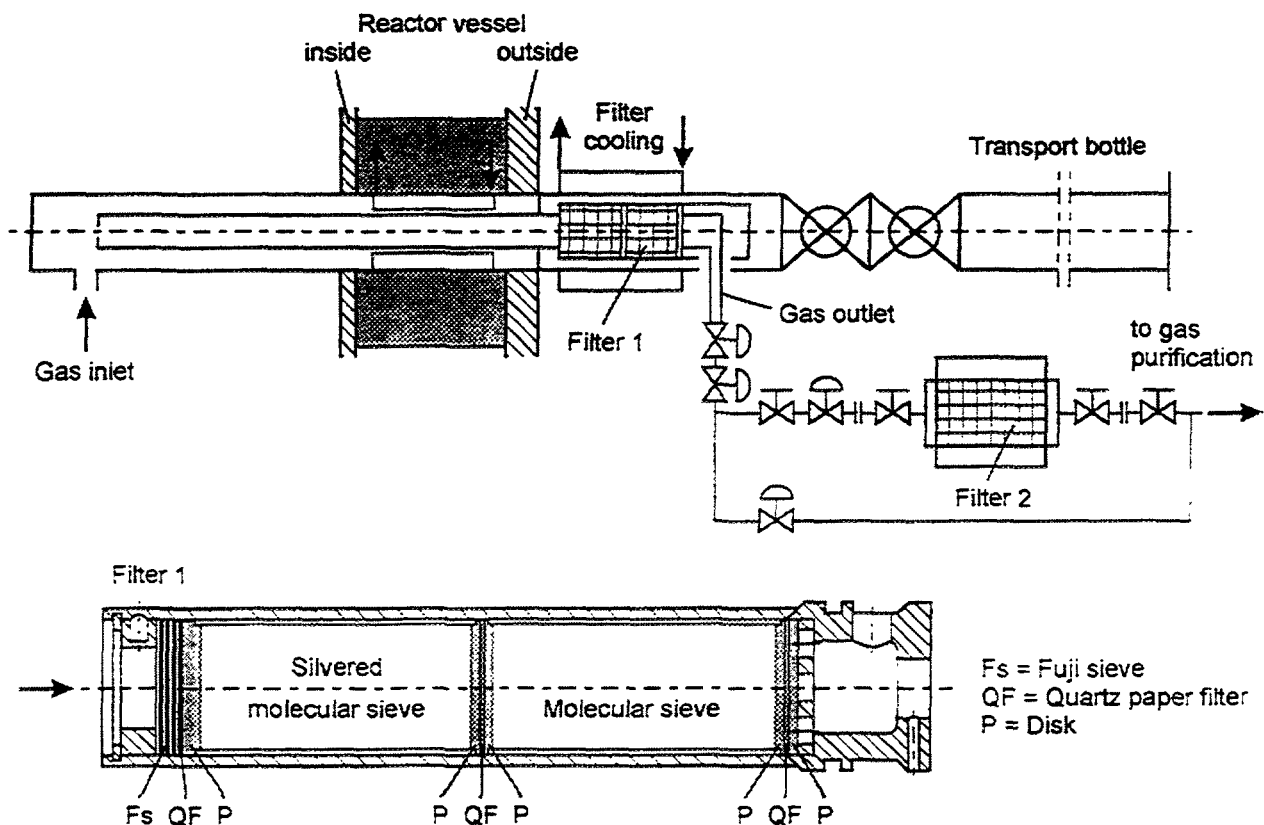


Fig. 6-11: Schematic of the hot gas sampling tube VAMPYR-I in the AVR reactor

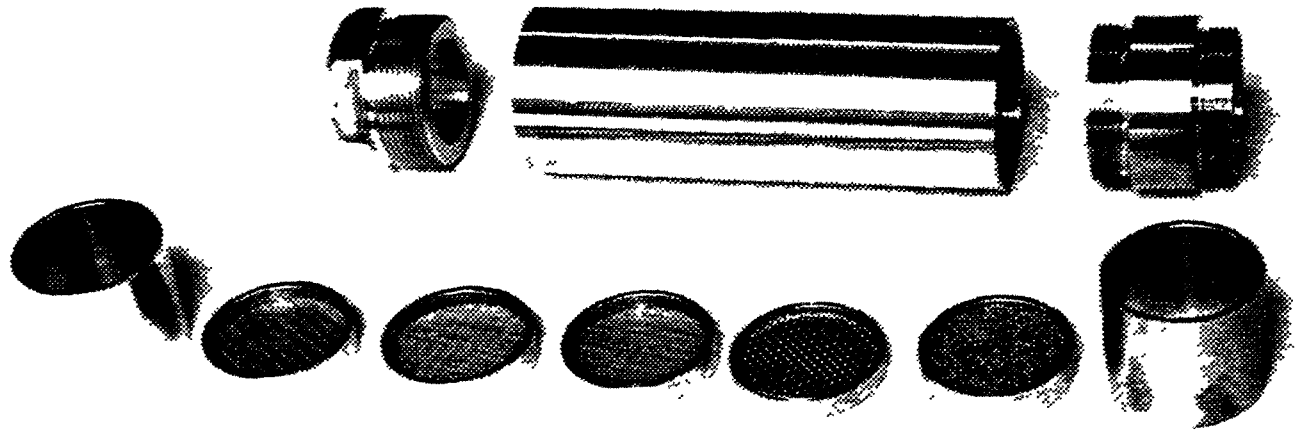


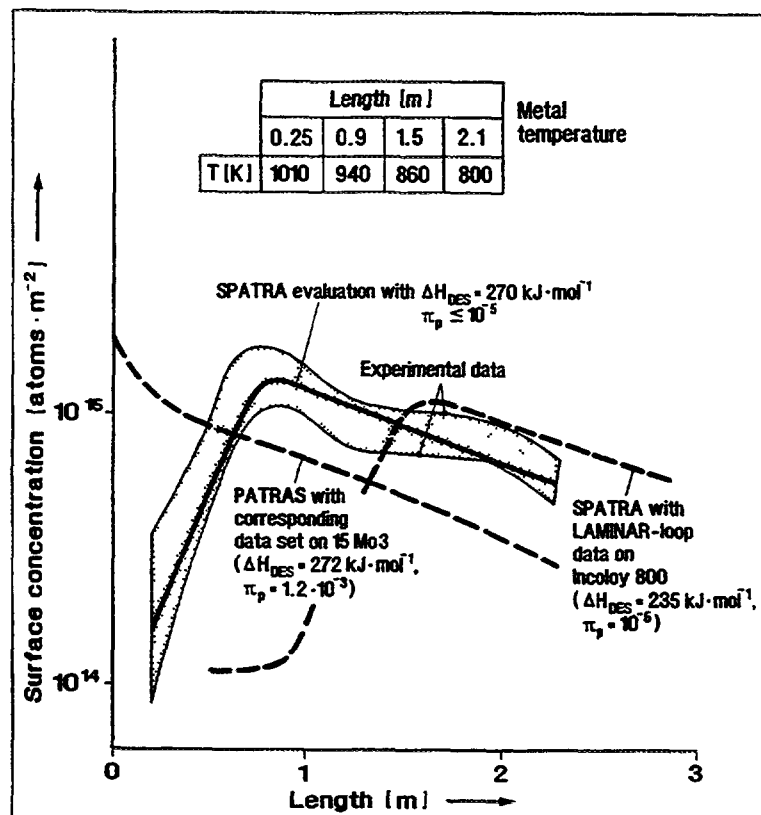
Fig. 6-12: Photograph of filter 1 body and components as used in the VAMPYR experiments

photograph in Fig. 6-12 shows the single components of a dust filter. A total of 49 runs some of which failed have been conducted. Operating conditions and measured activities for the successful ones are given in Tables 6-8 and 6-9, respectively.

It should be noted that during the long period of time in which VAMPYR-I has been operated (1972 - 1988), many improvements have been made with respect to both measurement techniques and evaluation methods, and the core composition changed as well.

In the VAMPYR-I experiment, the increase of the gas exit temperature from the core from 850 to 950 °C has obviously caused an increase of fission product concentrations in the coolant. The influence of dust on the cesium plateout profiles does not appear to be as strong as that observed in VAMPYR-II [16]. The adsorbent metals, at least in the high-temperature part of this experiment, however, are not representative for the HTGR primary circuit. In addition, considerable neutron activation occurred in the high temperature part of VAMPYR-I influencing in particular the Ag-110m concentrations. Flow conditions in this loop differ significantly from those in VAMPYR-II. Iodine plateout in the VAMPYR-I loop is obviously controlled by ad-/desorption equilibrium and mass transfer only [16] and can therefore be easily handled by the plateout model SPATRA. A comparison of experimental data with calculations is presented in Fig. 6-13 for Cs-137 and I-131 plateout on 15Mo3 in test run V09 of VAMPYR-I. The SPATRA calculation results in desorption enthalpies on 15Mo3 of 170 kJ/mol for iodine and 270 kJ/mol for cesium. The cesium plateout calculation with PATRAS and its corresponding data base reveals that, in contrast to the SPATRA calculation, the penetration is overestimated and a strong reduction of the penetration coefficient to $\leq 10^{-5}$ is required for a reasonable interpretation of the measurements [1].

(a)



(b)

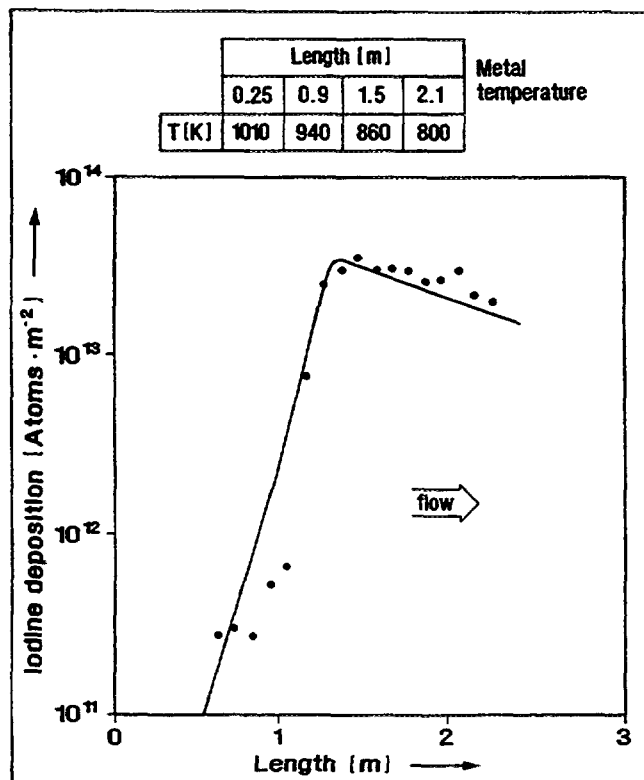


Fig. 6-13: Evaluation of activity plated out along the test tube on 15Mo3 in VAMPYR-I test V09 with the SPATRA code, from [1].

(a) Cs-137, (b) I-131

Table 6-8: Operating Conditions and activity measurements of the hot gas sampling tube VAMPYR-I, from various AVR and KFA-IRB(IEV) technical notes and internal reports, e.g., [66, 67]

Run	Time [h]	Gas temperature average inlet / outlet [°C]	Wall temperature inlet / outlet [°C]	Total coolant throughput [Nm³]	Material 1st tube, 2nd tube
V01	548	810 /		7,124	Ti
V02	737	810 / 100		11,055	Ti
V03	739	810 / 100	775 / 160	11,078	Ti
V04	784	810 / 110	770 / 160	11,525	Ti
V06	1029	755 / 110	740 / 160	16,310	Ti
V07	817	800 / 100	780 / 170	12,263	Ti, 4541
V08	799	780 / 110	765 / 170	11,980	Ti, 4541
V09	799	780 / 110	755 / 160	11,985	15Mo3
V10	885	780 / 102	755 / 160	13,268	15Mo3
V11	952	770 / 100	740 / 160	14,276	15Mo3
V12	821	900 / 94	870 / 130	12,319	Ti
V13	938	900 / 113	870 / 130	14,070	Ti, 4541
V14	2306	880 / 102	850 / 130	35,966	Ti, 4541
V15	2219	900 / 100	870 / 130	32,838	Ti, 4541
V16	986	975 ⁽¹⁾ /		14,790	AS2-500, 4541
V18	1997	980 ⁽¹⁾ /		29,959	Ti, St35.8
V19	991	885 / 100	840 / 130	14,865	Ti, 15Mo3
V20	655	870 / 100	840 / 130	9,829	Ti, St35.8
V21	747	870 / 120	840 / 130	10,899	Ti, 4961
V22	937	760 / 95		14,055	Ti, St35.8
V24	1934	900 / 95	870 / 130	29,010	Ti, 10CrMo910
V26	912	840 / 105		15,498	Ti, 10CrMo910
V27	861	840 / 108		14,637	Ti, 13CrMo44
V28	572	890 / 84		7,868	Ti
V30	866	900 / 105		11,085	Ti

Table 6-8: Operating Conditions and activity measurements of the hot gas sampling tube VAMPYR-I, from various AVR and KFA-IRB(IEV) technical notes and internal reports, e.g., [66, 67] (continued)

Run	Time [h]	Gas temperature average inlet / outlet [°C]	Wall temperature inlet / outlet [°C]	Total coolant throughput [Nm³]	Material
V31	335	900 / 105		5,079	Ti
V32	405	720 / 98		5,775	Ti
V33	763	840 / 91		11,543	Ti
V34	720	840 / 90		8,810	Ti
V35	860	900 / 48		12,289	Ti
V36	610	900 / 89		9,333	Ti
V37	743	900 / 80		11,294	Ti, 4541, 15 Mo 3
V38	901	900 / 80		13,515	Ti
V40	668	900 / 80		9,352	Ti
V42	721	900 / 77		10,191	Ti
V43	644	850 / 92		9,156	Ti
V45	713	750 / 102		10,183	Ti
V47	491	705 ⁽¹⁾ / 113		7,028	Ti
V48	1252	706 ⁽¹⁾ / 96		17,510	Ti
V49	623	723 ⁽¹⁾ / 80		8,756	Ti

(1) Core outlet temperature

Table 6-9: Activity measurements of the hot gas sampling tube VAMPYR-I, from various KFA-IRB(IEV) technical notes and internal reports, e.g., [66, 67]

Run	Concentration in coolant ⁽¹⁾ [Bq/Nm ³]					Range of activity deposited [Bq/cm ²]		
	Cs-134	Cs-137	Sr-90	Ag-110m	I-131	Cs-137	Ag-110m	I-131
V03	8.1×10^0	2.0×10^1	7.8×10^{-1}	1.4×10^2	3.7×10^2	7.4×10^0 - 8.1×10^2	1.4×10^2 - 1.4×10^3	1.4×10^{-1} - 5.9×10^2
V04	8.9×10^0	4.1×10^0		1.2×10^2	3.6×10^2	1.0×10^0 - 4.4×10^2	4.1×10^2 - 9.3×10^2	1.2×10^1 - 6.3×10^2
V06	8.1×10^0	5.2×10^0	9.6×10^{-1}	3.2×10^1	1.3×10^2	8.1×10^{-1} - 2.0×10^3	4.8×10^1 - 3.2×10^2	1.2×10^1 - 3.3×10^2
V07	1.0×10^1	1.0×10^1	2.6×10^{-1}	1.1×10^2	1.0×10^2	1.3×10^1 - 5.9×10^1	4.1×10^1 - 1.4×10^3	3.2×10^0 - 1.0×10^3
V08	7.8×10^0	3.4×10^0	5.6×10^{-1}	8.9×10^1	2.4×10^2	8.5×10^0 - 1.7×10^1	5.2×10^1 - 4.8×10^2	5.9×10^0 - 5.9×10^2
V09	1.4×10^1	8.9×10^0	5.2×10^{-1}	6.7×10^1	7.8×10^2	4.1×10^1 - 1.2×10^2	2.6×10^2 - 7.4×10^2	2.7×10^1 - 3.5×10^3
V10	1.0×10^1	6.3×10^0	3.0×10^0	5.9×10^1	7.8×10^2	2.4×10^1 - 8.9×10^1	2.3×10^2 - 3.3×10^3	4.4×10^0 - 3.2×10^3
V11	1.1×10^1	6.7×10^0	2.2×10^0	5.2×10^1	6.3×10^2	2.0×10^1 - 5.2×10^1	3.5×10^1 - 4.1×10^2	2.1×10^1 - 2.3×10^3
V12	7.0×10^1	3.5×10^1	1.2×10^1	6.3×10^2	1.0×10^3	2.8×10^2 - 5.6×10^2	5.2×10^1 - 7.0×10^3	5.6×10^1 - 3.7×10^3
V13	8.9×10^1	4.4×10^1	2.3×10^2	4.8×10^2	1.3×10^3	1.9×10^2 - 4.8×10^2	1.3×10^3 - 5.2×10^3	4.1×10^1 - 5.2×10^3
V14	2.0×10^2	1.4×10^2		5.6×10^2	1.3×10^2	1.3×10^2 - 4.1×10^3	5.9×10^3 - 2.2×10^4	2.1×10^2 - 4.4×10^3
V15	4.1×10^2	4.4×10^2		3.0×10^3	1.2×10^3	5.6×10^2 - 1.1×10^4	8.5×10^1 - 3.5×10^4	9.6×10^2 - 4.4×10^4
V16	1.0×10^3	1.3×10^3		2.2×10^2	1.4×10^3			
V18	1.0×10^4	1.2×10^4		2.7×10^2		8.9×10^3 - 2.6×10^5	2.0×10^2 - 8.9×10^3	

(1) Activity collected in the filters in relation to coolant flow through VAMPYR-I

Table 6-9: Activity measurements of the hot gas sampling tube VAMPYR-I, from various KFA-IRB(IEV) technical notes and internal reports, e.g., [66, 67] (continued).

Run	Concentration in coolant ⁽¹⁾ [Bq/Nm ³]					Range of activity deposited [Bq/cm ²]		
	Cs-134	Cs-137	Sr-90	Ag-110m	I-131	Cs-137	Ag-110m	I-131
V19	1.2×10^3	1.4×10^3		1.3×10^2	4.1×10^2	2.0×10^3 - 2.9×10^4	4.4×10^2 - 2.0×10^3	2.7×10^3 - 7.0×10^3
V20	6.7×10^2	8.5×10^2		1.1×10^2	4.1×10^2	1.0×10^3 - 1.0×10^4	2.2×10^2 - 9.3×10^2	1.4×10^2 - 3.5×10^3
V21	4.4×10^2	5.6×10^2		1.1×10^2	7.4×10^2	1.8×10^3 - 4.1×10^3	4.1×10^2 - 1.1×10^3	5.2×10^1 - 7.8×10^3
V22	5.2×10^2	7.4×10^2		1.0×10^2	1.4×10^2	1.7×10^3 - 7.0×10^3	5.6×10^1 - 1.1×10^3	9.6×10^1 - 1.5×10^3
V24	3.5×10^3	4.1×10^3		3.3×10^2	2.3×10^3	1.3×10^4 - 9.6×10^4	1.2×10^2 - 9.6×10^3	1.1×10^3 - 7.8×10^4
V26	2.4×10^2	4.1×10^2		7.4×10^1	1.0×10^2			
V27	1.6×10^2	3.2×10^2		8.5×10^1	2.7×10^1	9.6×10^2 - 6.7×10^3	1.8×10^2 - 2.0×10^3	2.2×10^2 - 6.9×10^2
V28	2.9×10^2	5.2×10^2		2.3×10^2	1.3×10^2	4.4×10^2 - 1.7×10^4	3.7×10^2 - 2.7×10^3	9.9×10^1 - 1.2×10^3
V30	9.0×10^2	5.9×10^2		1.2×10^2	3.1×10^2	1.6×10^3 - 4.1×10^3	1.2×10^2 - 3.5×10^2	1.2×10^2 - 4.1×10^3
V31	2.9×10^2	5.6×10^2		3.3×10^2	3.2×10^2			
V32	1.2×10^2	3.4×10^2		1.4×10^2	1.8×10^1	1.8×10^2 - 4.1×10^3	1.3×10^2 - 9.6×10^2	2.0×10^1 - 1.2×10^2
V33	2.4×10^2	6.3×10^2		7.3×10^1	8.3×10^1	9.1×10^2 - 7.4×10^3	9.8×10^1 - 2.5×10^3	3.6×10^1 - 1.2×10^2
V34	1.8×10^2	5.0×10^2		5.2×10^1	1.3×10^2	6.7×10^2 - 6.4×10^3	5.1×10^1 - 1.2×10^3	3.9×10^1 - 1.8×10^2
V35	7.9×10^1	2.3×10^2		4.6×10^1	5.0×10^1	6.9×10^1 - 5.1×10^3	6.8×10^0 - 9.0×10^2	4.0×10^1 - 1.3×10^3

(1) Activity collected in the filters in relation to coolant flow through VAMPYR-I

Table 6-9: Activity measurements of the hot gas sampling tube VAMPYR-I, from various KFA-IRB(IEV) technical notes and internal reports, e.g., [66, 67] (continued).

Run	Concentration in coolant ⁽¹⁾ [Bq/Nm ³]					Range of activity deposited [Bq/cm ²]		
	Cs-134	Cs-137	Sr-90	Ag-110m	I-131	Cs-137	Ag-110m	I-131
V36	1.4×10^2	3.1×10^2		9.1×10^1	2.5×10^2	6.8×10^2 - 2.4×10^3	2.4×10^2 - 1.1×10^3	4.6×10^1 - 1.4×10^3
V37	1.1×10^2	2.5×10^2		8.8×10^1	1.8×10^2	7.6×10^0 - 3.1×10^3	2.6×10^2 - 1.3×10^3	2.2×10^2 - 3.2×10^3
V38	1.2×10^2	1.8×10^2		1.0×10^2	2.2×10^2	3.7×10^2 - 2.4×10^3	9.08×10^1 - 1.2×10^3	3.6×10^2 - 3.1×10^3
V40	1.1×10^2	2.0×10^2		8.2×10^1	3.1×10^2	2.8×10^2 - 2.4×10^3	1.5×10^2 - 1.1×10^3	1.1×10^2 - 2.9×10^3
V42						5.5×10^2 - 8.6×10^3	2.3×10^2 - 1.0×10^3	4.6×10^2 - 1.4×10^3
V43						2.0×10^2 - 1.1×10^3	6.1×10^1 - 6.1×10^2	8.1×10^1 - 5.3×10^2
V45						1.5×10^2 - 6.7×10^2	2.4×10^1 - 2.4×10^2	2.2×10^4 - 2.9×10^4
V47						2.4×10^0 - 9.9×10^1	9.7×10^{-2} - 1.2×10^0	
V49						8.7×10^1 - 1.1×10^3	7.6×10^0 - 1.1×10^2	

(1) Activity collected in the filters in relation to coolant flow through VAMPYR-I

Deposition Loop VAMPYR-II

The **deposition loop VAMPYR-II** [68] was installed in the AVR in the upper layer of the top reflector in order to avoid two major drawbacks of VAMPYR-I. One drawback was the higher neutron fluence to which the test tube of VAMPYR-I was exposed; the other one was the imprecise determination of the test tube wall temperature. The location of VAMPYR-II had a lower neutron fluence level which reduced the activation of the materials tested thus allowing for examining more materials in the temperature range of interest above 550 °C. Furthermore, thermocouples for direct wall temperature measurements were included and a heating section for temperature variation was installed both of which could not be realized in VAMPYR-I due to space restrictions.

The main goals of VAMPYR-II were the study of the metallic fission product deposition behavior on realistic HTGR materials (Incoloy, Inconel) and of the influence of dust in the temperature range 850 - 400 °C under turbulent flow conditions, the test of dust filter concepts, and the acquisition of a model specific set of plateout parameters. Samples of the deposition tube were also to be used for investigation of washoff and steamoff effects. A schematic of VAMPYR-II is presented in Fig. 6-14.

Hot helium gas was extracted from the main AVR flow and routed at a flow rate of 50 Nm³/h to an insulated tube of 5.4 m length and 30 mm inner diameter which contained the exchangeable test section. The test section itself consisted of a cylindrical tube (length 3.62 m, outer diameter 16 mm, wall thickness 1 mm) of Incoloy 800H with an inner centrally arranged rod (length 3.59 m, outer diameter 9 mm, composed of 35 interconnected pieces) of Inconel 617. The test section is preceded by a dust filter (optionally) and followed by 5 fission product filters. After leaving the test section, the helium passed through a cooler and two absolute filters.

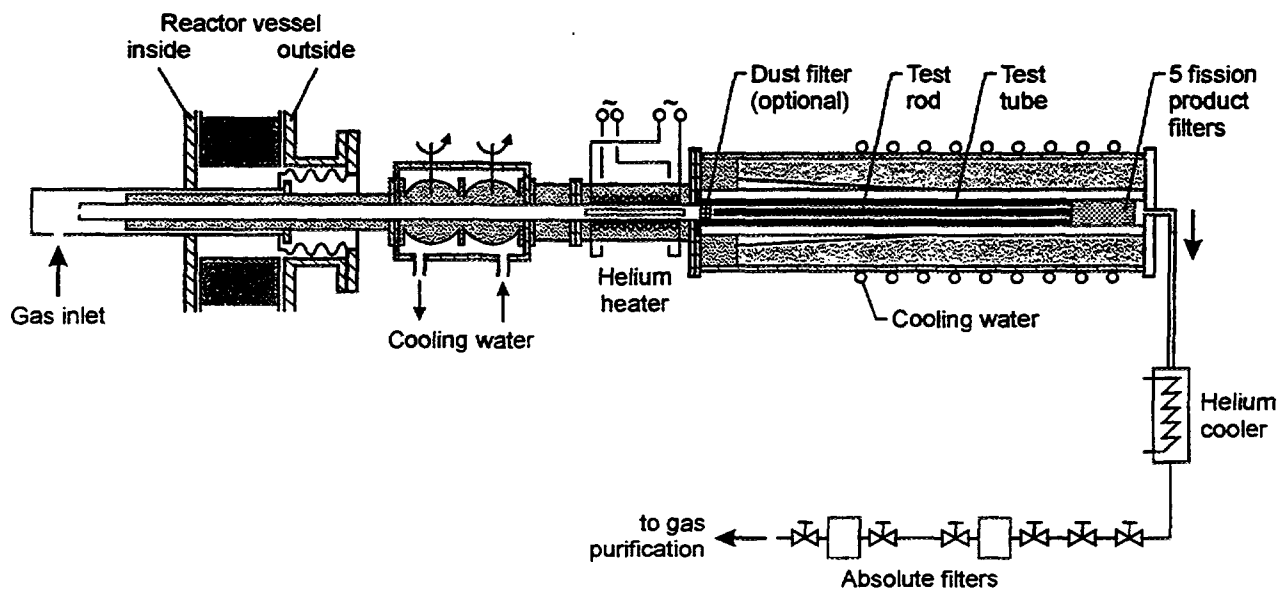


Fig. 6-14: Schematic of AVR deposition loop VAMPYR-II

Table 6-10: Operating Conditions and activity measurements of the deposition loop VAMPYR-II, from [33, 34, 35, 36].

Run	Time [h]	Gas temperature inlet / outlet [°C]	Wall temperature inlet / outlet [°C]	Total coolant throughput [Nm³]	Material	Dust [mg]
VII,1	1305	811 / 357	725 / 430	65,319	Incoloy 800 H Inconel 617	-
VII,2	528	810 / 365	725 / 425	26,615	Incoloy 800 H Inconel 617	-
VII,3	526	764 / 320	685 / 405	26,373	Incoloy 800 H Inconel 617	110 (SF2) ⁽²⁾
VII,4	1252	775 / 300	660 / 395	62,682	Incoloy 800 H Inconel 617	313.5 (SF1) ⁽¹⁾ 27.6 (SF2) ⁽²⁾

(1) Dust filter preceding the test tube

(2) Dust filter following the test tube and preceding the fission product filters

Table 6-11: Relative activity distribution in the deposition loop VAMPYR-II, from [33, 34, 35, 36].

Location ⁽¹⁾	VII,1			VII,2		VII,3		VII,4	
	Cs-137	Ag-110m	I-131	Cs-137	Ag-110m	Cs-137	Ag-110m	Cs-137	Ag-110m
SF1	-	-	-	0.2	1.0	-	-	4.7	2.4
Tube	6.8	76.7	82.5	26.5	69.4	27.4	52.3	15.2	70.3
Rod	2.9	21.6	17.5	8.8	20.4	9.8	27.8	5.1	18.1
SF2	-	-	-	-	-	52.9	19.3	59.4	7.9
SPF1	24.6	0.1		9.0	4.7	3.5	0.2	6.7	0.5
SPF2	17.9	0.1		9.1	1.8	2.9	0.1	4.9	0.3
SPF3	17.8	0.3		12.6	1.1	1.8	0.1	1.5	0.2
SPF4	17.7	0.3		16.7	0.9	1.0	0.1	0.9	0.1
SPF5	12.3	0.9		17.1	0.7	0.7	0.1	1.6	0.2
Σ (Σ in Bq)	100 (2.62×10^7)	100 (8.22×10^6)	100 (8.64×10^6)	100 (2.96×10^6)	100 (1.26×10^6)	100 (1.50×10^6)	100 (1.34×10^5)	100 (3.43×10^6)	100 (2.17×10^5)

(1) For the position of the single components see schematic in Fig. 6-14

Four VAMPYR-II experiments were planned, two eventually completed followed by another two with a modified experimental program. Operating conditions are listed in Table 6-10. Postexaminations comprised γ -measurements of test tube and rod as well as fission product filters, leaching of selected pieces, removal of oxide layer, size distribution of dust particles. The global distribution of Cs-137 and Ag-110m in all 4 runs and of I-131 which was measured only in test run VII,1 is summarized in Table 6-11. Plateout activities of Cs-137 and Ag-110m measured both on the Incoloy 800H test tube and the Inconel 617 test rod over the tube length are plotted in Fig. 6-15.

Silver plateout measurements made in the VAMPYR II loop are of particular interest since there is a paucity of Ag plateout data, especially at high surface temperatures on gas-turbine alloys. As shown in Fig. 6-16 (a), the VAMPYR-II data from test run VII,1 appear to indicate that the accumulation of Ag plateout will be limited by sorption effects at temperatures $> \approx 550$ °C which implies that the amount of Ag plateout within a gas turbine HTGR might be significantly limited. The postcalculation with the PATRAS code, also shown in Fig. 6-16, leads to a temperature independent plateout curve in contrast to the experimental data.

However, there is another potentially important consideration here. The duration of the VAMPYR II tests was only in the range of 20 - 50 days. During the typical 7-year residence time of a gas turbine in a direct-cycle HTGR, the Ag isotopes deposited on the turbomachinery may diffuse from the surface layers into the bulk of the structural metals, thereby, increasing the effective sorptivity of the metal. Since significant "in-diffusion" would preclude effective decontamination prior to turbine maintenance, this eventuality is of considerable importance to the design of a direct-cycle HTGR.

In the same experiment, **cesium plateout** is small and shows an unusually small temperature dependence (Fig. 6-16 (b)). Plateout curves remain flat even in the low temperature range. One possible interpretation of this behavior is the influence of dust in cesium plateout. However, the deployment of dust filters through which the helium coolant was flowed before it entered the test section, (test run VII,4), did not change the cesium deposition profiles. There is no reasonable interpretation for this behavior of cesium at this moment [1]. Fig. 6-16 (b) contains also the cesium plateout curves postcalculated with the codes PATRAS (as described in Ref. [69]) and SPATRA. The assumption of a comparably high penetration coefficient of 7×10^{-4} in PATRAS leads to a very high plateout in the upper temperature range. In contrast, the SPATRA reference calculation based on a lower penetration coefficient of 1×10^{-5} reproduces well the measured Cs data at higher temperatures, however fails in the lower temperature range. An optimized fit with SPATRA for the whole plateout profile is feasible, if the desorption enthalpy of cesium is reduced from 235 to 180 kJ/mole as given in curve 3 of Fig. 6-16 (b). Nevertheless, the theoretical evaluation of the VAMPYR-II experiments as well as these with VAMPYR-I may be considered a partial validation of the plateout model SPATRA [1].

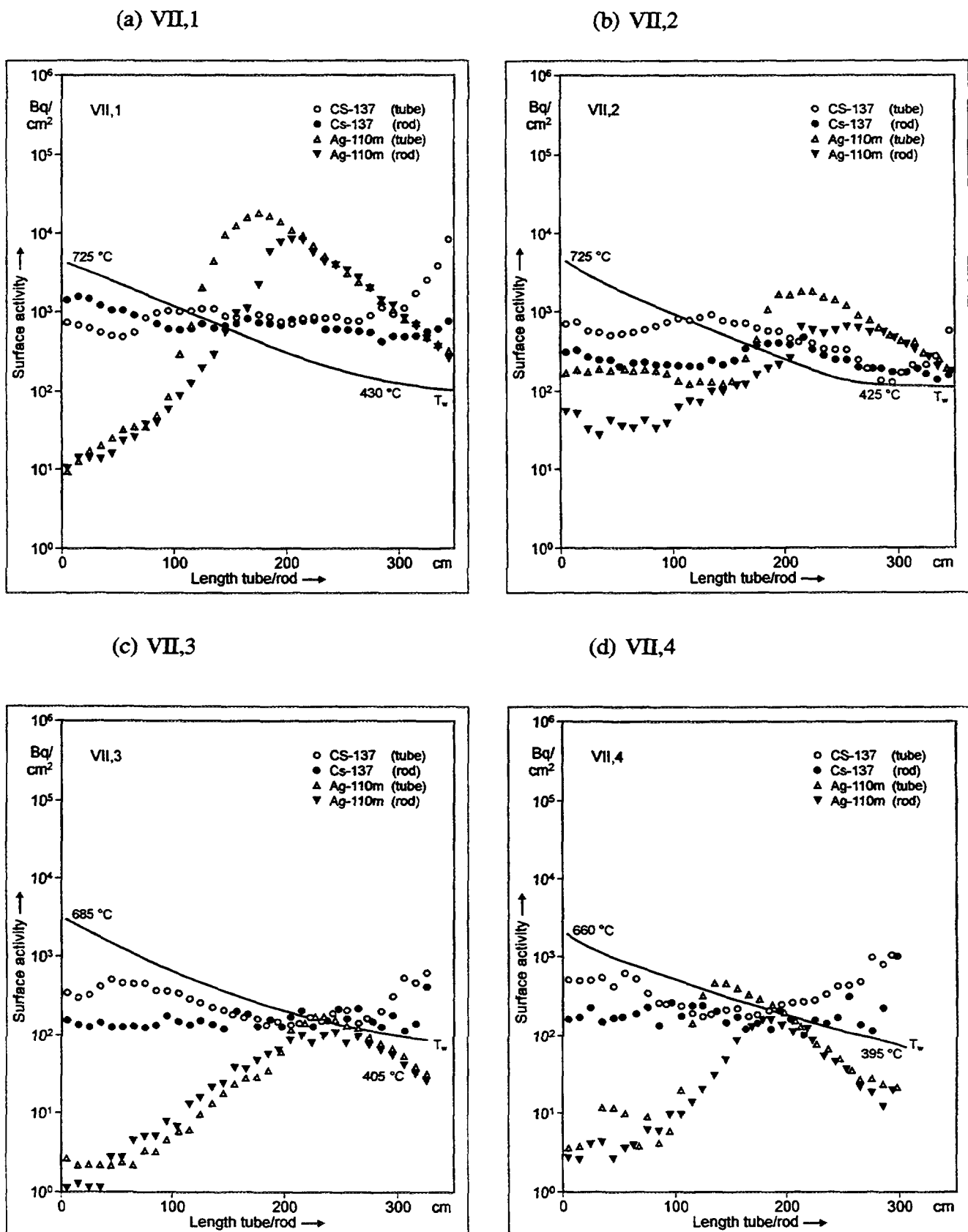


Fig. 6-15: Measured surface concentration profiles of Cs-137 and Ag-110m activities on test tube and test rod for VAMPYR-II experiments, from [33, 34, 35, 36].

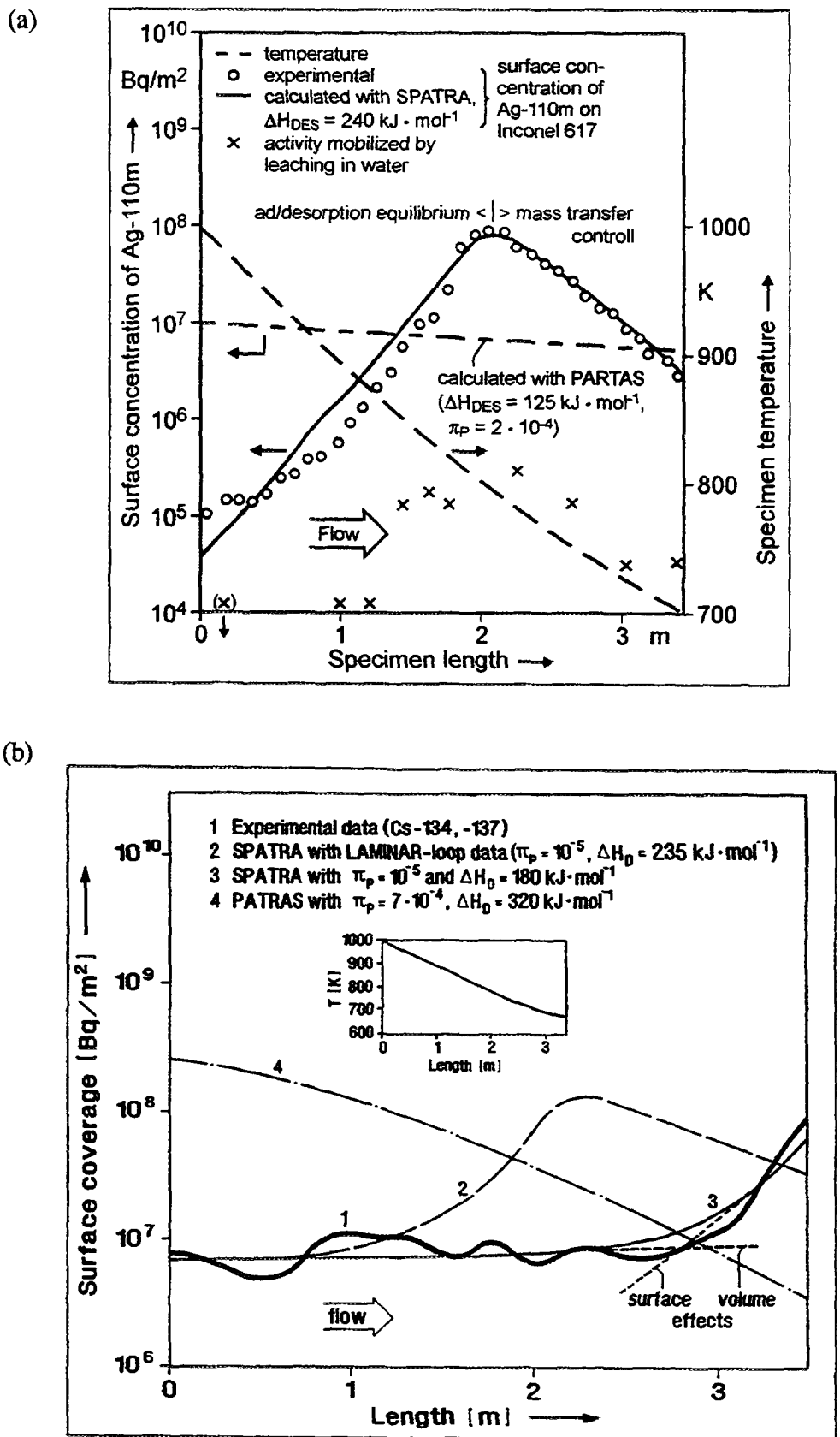


Fig. 6-16: Plateout experiment VAMPYR-II (AVR), test run VII,1: Measured and calculated plateout profiles, from [1]
(a) for Ag-110m on Inconel 617 (rod), (b) for Cs-137 on Incoloy 800 (tube)

In-Pile Loop Data

KFA-sponsored plateout experiments were conducted in 1970 - 1975 in the **in-pile loop SAPHIR** in the reactor **PEGASE** in Cadarache, France. Its test section consisted of an insulated graphite sleeve containing 14 HTGR spherical fuel elements, an exchangeable test tube of 2 m length and 30 mm inner diameter, and a connection tube ending with filters. A turbulent helium flow at 4.3 MPa transported the fission products released from the fuel spheres into the tube. After each run, test tubes and filters were quantitatively analyzed by γ -spectrometry, surface leaching, removal of oxide layer, electrolytical removal of bulk material. The materials investigated as well as the operating conditions and measured activities for some of them are given in Table 6-12; test runs P01 - P04 were considered pre-tests and are not listed. Run P09 reaching for the first time a wall temperature as high as 725 °C, could not be fully evaluated because of an unexpected Sb contamination of the test section. For run P11, the setup was modified to allow for higher wall temperatures [70].

Some results for test run P11 are given in Fig. 6-17 [71]. In the first half of the test section with high wall temperature, the influence of different materials and their sorptivities, respectively, can be seen. In the low temperature section, mass transfer effects are dominant revealing the bend positions as locations of enhanced deposition. Examples of Cs-137 diffusion profiles in the wall material are presented in Fig. 6-18, where the experimental data as indicated by the step curves were taken to derive diffusivities in both oxide layer and bulk material and to obtain information on oxide layer growth [72]. A dense oxide layer creates a considerable diffusion barrier thus influencing the decontamination.

The measured water leach values are strongly dependent on the physical surface conditions; low values do not necessarily mean a high fraction diffused into the wall [19].

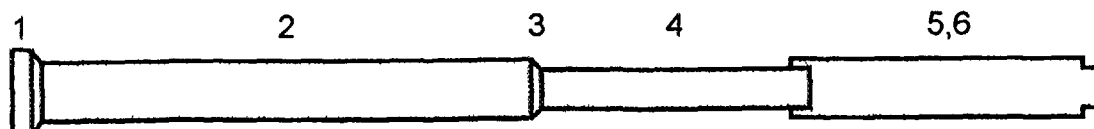
Table 6-12: Operating Conditions and activity measurements of the in-pile loop SAPHIR in the PEGASE reactor, from [70].

Run	Time [h]	Gas temperature inlet / outlet [°C]	Medium wall temperature (segment 1 / segment 2) [°C]	Gas flow [g/s]	Partial pressure [Pa]	Material ⁽¹⁾ (2)	Activity deposited [µBq Cs-137/cm²]
P05	1991	835 / 585	530 / 560	12.2		b-b-b-b-d-l	
P06	1676	822 / 590	520 / 550	12.2	-	a-a-a-a-d-l	a: 74 - 222
P07	1334	810 / 590	525 / 560	12.0		a-a-a-b-d-l	
P08	1336	795 / 595	485-570 / 540	12.3		a-c-a-a _{ox} -d-l	
P09	1246	850 / 630	700-530 / 530-565	13.0		d-e-d-f-b-b	
P10	1176	830 / 635	720-480 / 485-585	12.0		a-g-d-b-m-m	b: 740
P11	3193	970 / 720	810-685 / 685-610	11.0	2.2*10 ⁻⁸	h-i/j-k-b-m-m	b: 3-19*10 ³ i: 5.6-6.3*10 ³ j: 15-26*10 ³

(1) The given string of letters corresponds to the following positions in the test section (see scheme below): 1 – Inlet, 2 – Segment 1 ($d_i=30\text{mm}$), 3 – Cone (30/20), 4 – Segment 2 ($d_i=20\text{mm}$), 5 – Connection to filter, tubes, 6 – Connection to filter, bends.

The letters are equivalent to the following materials:

- | | | | |
|---------------------|--------------------|-----------------------|------------------|
| a: 15 Mo 3 | b: 4541 | c: 2.4811 Hastelloy | d: Z8-CNDT 18-12 |
| e: Graphite AL2-500 | f: Nimonic 75 | g: Graphite AS2-500 | h: Inconel 600 |
| i: Inconel 625 | j: Nimocast 713 LC | k: NS30 Z15 CNS 25-20 | l: Z3-CND 1812 |
| m: 4961 | | | |



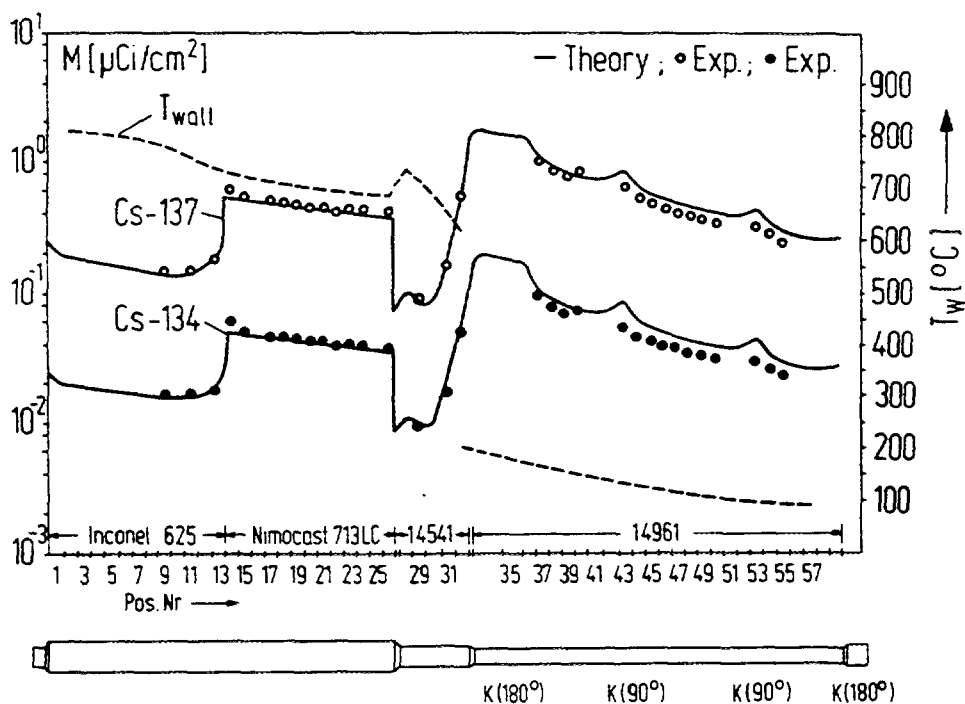


Fig. 6-17: Measured concentration profiles of Cs-134 and Cs-137 in P11 of the PEGASE series along the deposition tubes (whose schematic is given below) and comparison with PATRAS calculation. The K's indicate the position of bends with the angle in parentheses, from [71].

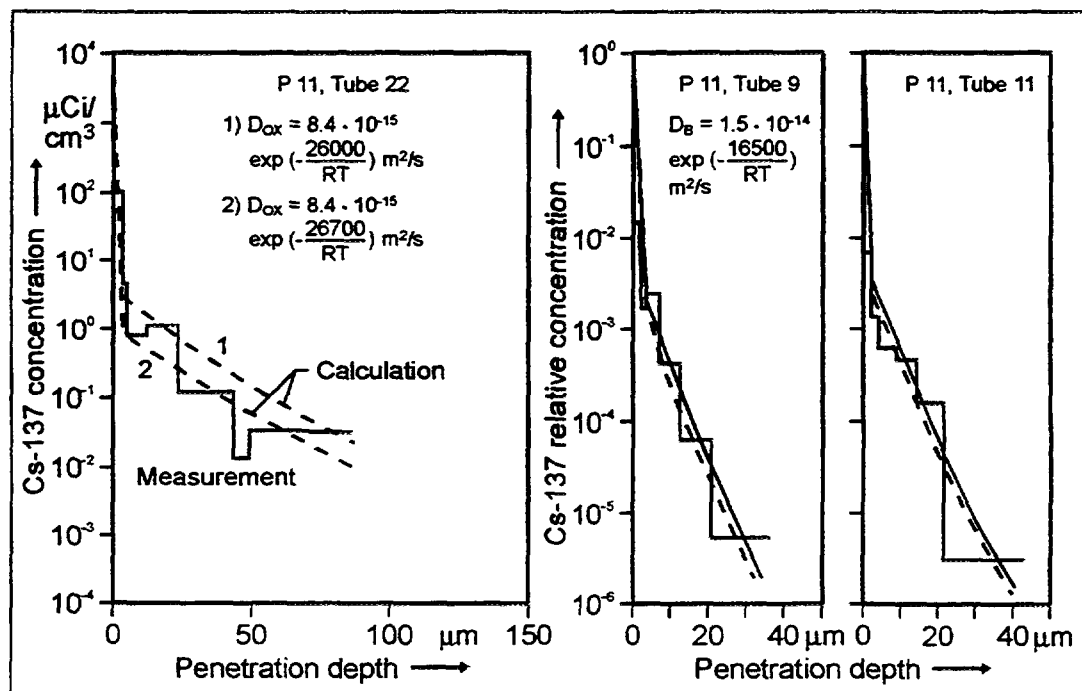


Fig. 6-18: Measured diffusion profiles of Cs-137 in test run P11 of the PEGASE series, (left) in Nimocast 713LC, (right) in Inconel 625, from [72]

The contamination of primary circuit surfaces in the AVR reactor was estimated by GA [73] assuming a relatively simple power and temperature history. Fig. 6-19 shows the calculated results along with measurements during decontamination of the blowers after the steam generator leakage. With regard to the simple assumptions made, the agreement is quite satisfactory.

As part of the HHT-Project, one long-term deposition experiment (1973 - 1975) with the goal of investigating metallic foil hot gas isolations was conducted in the **Dragon reactor** (Duct F). The tube that was flowed by the gas (inner liner of the hot gas duct) with a total length of 3.11 m, an inner diameter of 194 mm, a wall thickness of 1.6 mm and consisting of different materials was exposed for 490 days to an almost isothermal outlet gas temperature of 700 °C and a wall temperature of 680 °C. The gas flow rate was 1.6 kg/s at a pressure of 2 MPa. In the postexamination program conducted by the Research Center Jülich and the EIR in Switzerland, the tube was cut to 10 cm pieces for γ -analysis

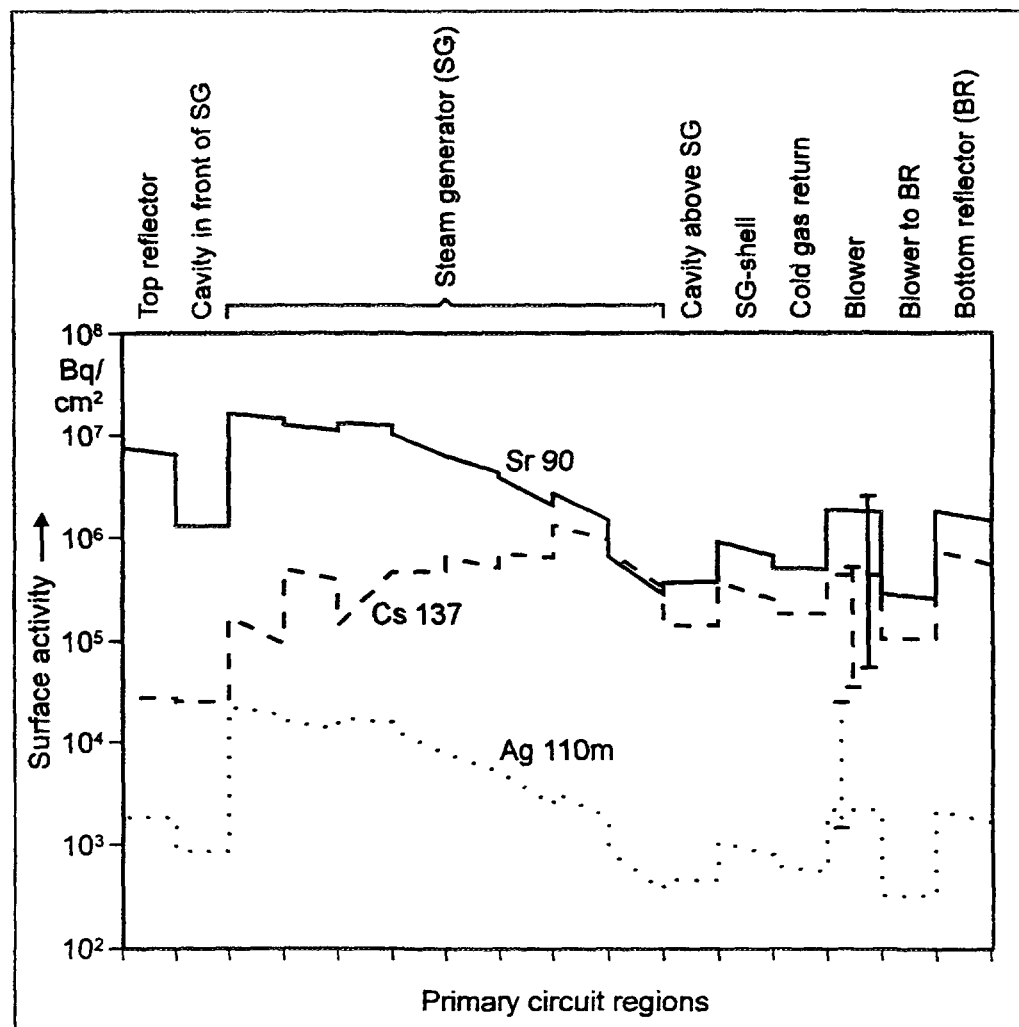


Fig. 6-19: Estimated specific activities of metallic fission products on AVR primary system surfaces and corresponding measurements in the blower area, from [27]

Table 6-13: Operating Conditions and activity measurements of the hot gas duct experiment in the DRAGON reactor, from [8, 19, 70].

Time [d]	Gas temperature [°C]	Wall temperature [°C]	Gas flow [g/s]	Partial pressure [Pa]	Material	Activity deposited [Bq Cs-137/cm²]
490	700	680	1600	$7.7 \cdot 10^{-10}$	4981, Incoloy 800, AISI 347, AISI 316, Inconel 625	$3.7 - 11 \cdot 10^3$

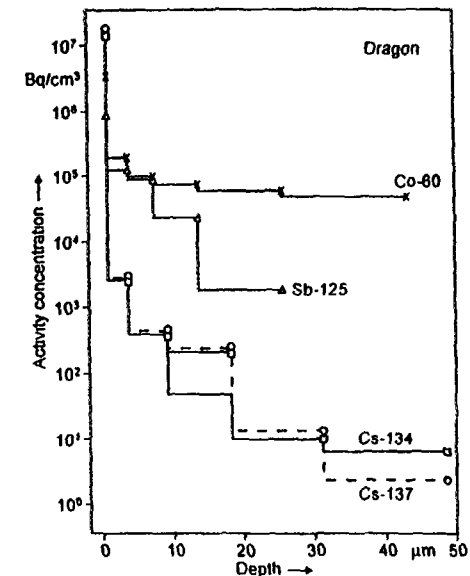
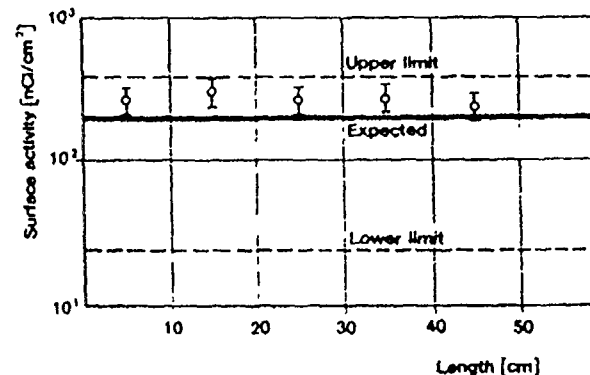
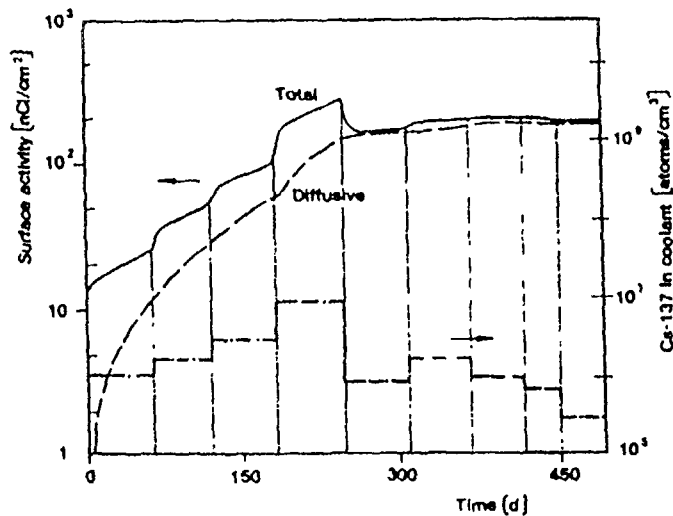


Fig. 6-20: Dragon hot gas duct experiment, from [8, 19], (left) RADAX calculation of Cs-137 deposition behavior, (middle) RADAX calculation and measurement of final profile after 480 d, (right) Measurements of in-diffusion profiles

to obtain deposition profiles and for decontamination investigations. Table 6-13 lists again the operating conditions and the measured Cs-137 concentration range.

In the postexamination program, various methods were applied comprising chemical treatment to remove oxide layers and an electrolytical removal of inner surfaces. The depth of the removed layers was determined from weight loss measurements. As an example, the measured diffusion profiles for Cs-134, Cs-137, Sb-125, and Co-60 are plotted in Fig. 6-20 (c). Some results from the postexamination program are that the austenitic steel AISI 316 was found to be inappropriate for temperatures ≥ 700 °C since appearances of material degradation were observed. Corrosion effects on Incoloy 800 were detected up to a depth of 25 μm meaning that it is not recommended for decontamination and subsequent reuse [8].

Fig. 6-20 shows the measured and calculated Cs-137 deposition as a function of operation time (a) and as the final profile along the tube (b). Plateout parameters were derived from the LAMINAR tests and applied to the Dragon test conditions in the RADAX code. One can see from the figures that the results from the LAMINAR loop can be applied to simulate long-term operation under realistic HTGR conditions [19]. On the other hand, the application of the PATRAS model to the Dragon test [71] is successful only if based on a severe underestimation of the cesium source; a reestimation of the source has shown that the penetration effect is much smaller and better agrees with a coefficient of about 10^{-5} [1].

6.1.1.3.3. Japanese Contribution

Fission product plateout data were obtained in **Oarai Gas Loop No. 1 (OGL-1)** which was installed in the Japan Materials Testing Reactor (JMTR) in JAERI [74]. The OGL-1 simulates the primary cooling system conditions of an HTGR. In the OGL-1, the plateout distribution has been measured from the outside of the primary pipes after every operational cycle using a Ge-detector. The range of helium gas temperature was from 1000 °C at fuel exit to room temperature. Flow condition was turbulent. A flow diagram of the

Table 6-14: Main plateout conditions of OGL-1

Parameter	Experimental condition	HTGR condition
Materials	Stainless steel Hastelloy-X	Stainless steel (PWC heat tube) Hastelloy-XR (Inner pipe, IHX heat pipe) Cr-Mo steel (Annulus of heat exchanger, RPV)
Coolant temperature	950 °C - RT ⁽¹⁾	950 °C - 395 °C
Wall temperature	950 °C - RT ⁽¹⁾	950 °C - 160 °C
Helium gas pressure	3 MPa	4 MPa
Helium gas velocity	10 m/s - 60 m/s	20 m/s - 40 m/s

(1) Room temperature

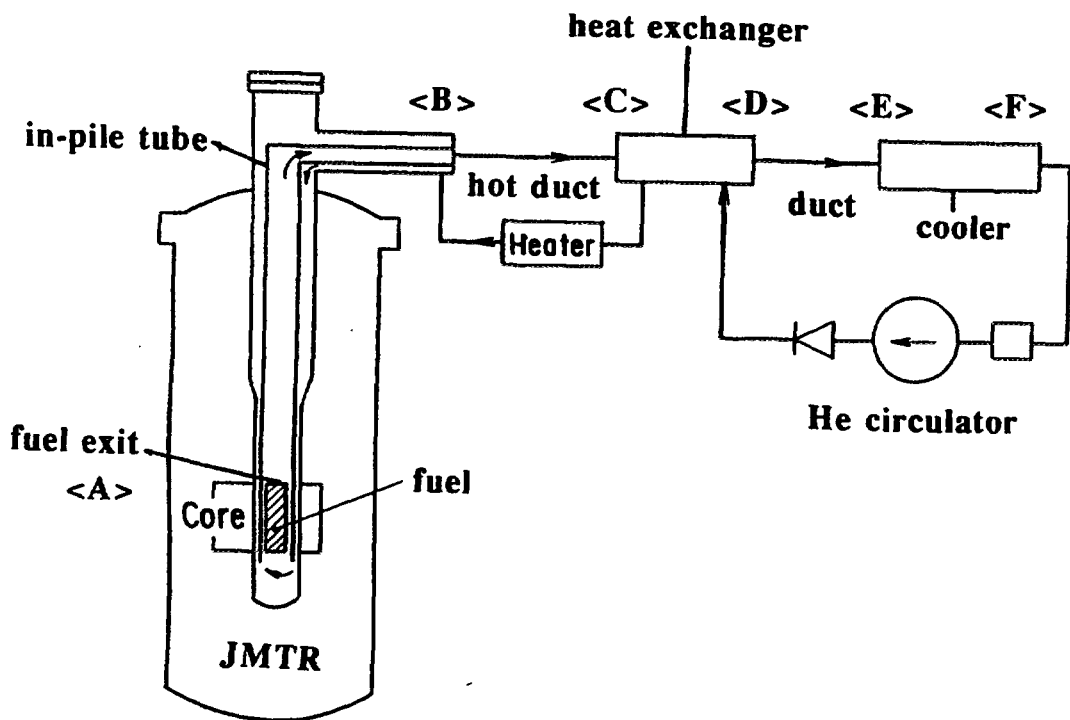


Fig. 6-21: Flow diagram of primary cooling system of OGL-1

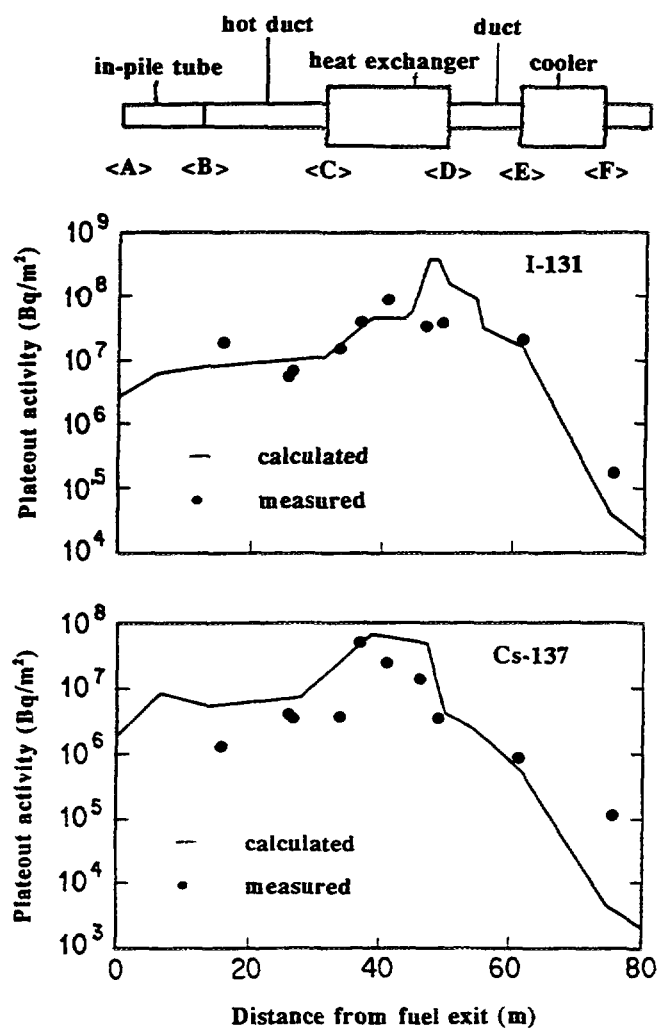


Fig. 6-22: Measured and calculated plateout distribution in OGL-1

primary cooling system of OGL-1 is shown in Fig. 6-21. The main plateout conditions in OGL-1 are given in Table 6-14 and compared with those of HTTR [75].

Geometrical parameters of the OGL-1 are shown in Table 6-15, operational conditions are given in Table 6-16. Measured plateout densities of I-131 and Cs-137 are tabulated in Tables 6-17 and 6-18.

JAERI carried out verification works of plateout analysis code by comparing the calculated fission product plateout distribution with experimental data obtained in the OGL-1 loop [76].

Examples of verification results for I-131 and Cs-137 are shown in Fig. 6-22. In the plots, black circles and lines show measured and calculated plateout densities, respectively. Since Cs-137 has a long half-life (about 30 years), it is accumulated during the operation cycles. The calculations of plateout distributions of Cs-137 were carried out considering the operational history of OGL-1. From the results, though about an order of difference is locally observed between measured and calculated values, the calculated plateout profiles show good consistency with the measured ones as a whole. It was concluded that the analytical model and the physical constants were applicable to predict the plateout distributions in the primary cooling system of HTGRs.

Table 6-15: Geometrical parameters of OGL-1

Location	Length [m]	Inlet gas and wall temp. [°C] ⁽¹⁾	Outlet gas and wall temp. [°C] ⁽¹⁾	Hydraulic diameter [m]	Flow area [m ²]	No. of flow channels	Material
In-pile tube	6.50	T ₁	T ₂	0.08	5.027*10 ⁻³	1	Hastelloy-X
Duct	6.85	T ₂	T ₃	0.059	2.734*10 ⁻³	1	Hastelloy-X
Duct	18.25	T ₃	T ₄	0.0446	1.562*10 ⁻³	1	Hastelloy-X
Heat exchanger	7.52	T ₄	T ₅	0.0119	1.112*10 ⁻³	22	Hastelloy-X
Duct	4.55	T ₅	T ₅	0.0527	2.181*10 ⁻³	1	SUS
Heat exchanger	6.87	T ₅	T ₆	0.0127	1.267*10 ⁻³	22	SUS
Duct	11.53	T ₆	T ₆	0.0527	2.181*10 ⁻³	1	SUS
Cooler	12.21	T ₆	T ₇	0.0214	3.597*10 ⁻³	6	SUS
Duct	8.32	T ₇	T ₇	0.0527	2.181*10 ⁻³	1	SUS

(1) The values of T₁, ..., T₇ in each cycle are shown in Table 6-16.

Table 6-16: OGL-1 operating cycle dependent input data

Cycle	Press. [MPa]	Power [kW]	Coolant flow [g/s]	Gas temperature [°C]								Test dura- tion [h]	Concentration [m ⁻³]	
				T ₁	T ₂	T ₃	T ₄	T ₅	T ₆	T ₇	T ₈		I-131	Cs-137
46	3.0	36.9	39.0	839	551	523	466	377	170	30	130	467		2.00*10 ¹¹
47	3.0	37.7	45.0	763	509	465	428	266	169	30	130	509		1.78*10 ¹¹
48	2.9	73.6	80.2	823	583	528	503	326	215	30	130	512		3.26*10 ⁸
49	3.0	73.7	80.0	785	539	480	457	300	201	30	131	462		3.28*10 ⁸
50	2.9	76.1	80.3	806	520	497	473	312	205	30	131	497		3.37*10 ⁸
51	3.0	72.6	80.0	-	521	497	472	286	222	30	130	401		3.23*10 ⁸
52	2.9	65.3	73.4	872	623	575	548	357	227	30	131	475		6.64*10 ¹¹
53	3.0	65.7	74.2	886	633	541	516	340	216	30	130	450		6.61*10 ¹¹
54	3.0	69.9	74.5	846	567	458	438	302	203	30	130	521		7.00*10 ¹¹
55	3.0	70.2	80.0	794	527	461	445	307	216	35	130	519		6.55*10 ¹¹
56	3.0	62.9	76.7	851	606	563	540	356	231	35	129	458		6.12*10 ¹¹
57	3.0	63.5	77.3	842	595	545	524	347	227	35	129	468		6.13*10 ¹¹
58	3.0	63.2	76.2	827	583	532	511	338	226	35	129	525		6.19*10 ¹¹
59	3.0	40.6	48.0	841	585	528	493	297	182	33	129	525		3.01*10 ⁸
60	3.0	67.4	80.4	837	582	520	496	326	221	35	130	465		3.76*10 ¹¹

Table 6-16: OGL-1 operating cycle dependent input data (continued)

Cycle	Press. [MPa]	Power [kW]	Coolant flow [g/s]	Gas temperature [°C]								Test dura- tion [h]	Concentration [m ⁻³]	
				T ₁	T ₂	T ₃	T ₄	T ₅	T ₆	T ₇	T ₈		I-131	Cs-137
61	3.0	63.3	80.7	855	620	567	541	348	230	36	130	469		3.51*10 ¹¹
62	3.0	64.8	84.2	664	430	359	344	249	192	34	130	-		-
63	3.0	62.1	79.9	862	633	581	554	355	233	36	130	458		3.48*10 ¹¹
64	3.0	45.8	55.0	878	645	480	449	280	185	27	130	275		5.30*10 ¹¹
65	2.5	45.8	55.1	857	632	442	415	268	189	27	130	486		5.29*10 ¹¹
66	2.5	46.7	68.0	884	632	590	559	350	231	30	130	519		4.37*10 ¹¹
67	3.0	42.3	59.6	891	664	548	514	310	193	28	130	524	6.53*10 ¹⁰	5.80*10 ¹¹
68	3.0	42.7	60.1	876	642	531	499	309	188	28	130	526	6.54*10 ¹⁰	5.81*10 ¹¹
69	3.0	40.3	58.5	881	657	558	523	320	191	29	130	472	6.34*10 ¹⁰	5.63*10 ¹¹
70	3.0	40.7	59.6	872	640	550	517	321	193	30	129	481	6.28*10 ¹⁰	5.58*10 ¹¹
71	3.0	43.2	64.8	823	612	465	441	288	187	30	129	514	6.13*10 ¹⁰	5.45*10 ¹¹
72	3.0	41.7	64.9	825	623	470	447	291	187	30	129	467	5.91*10 ¹⁰	5.25*10 ¹¹
73	3.0	41.7	63.9	831	627	469	446	290	186	30	129	484	6.00*10 ¹⁰	5.34*10 ¹¹

Table 6-17: Measured plateout concentrations of I-131

Cycle	I-131 concentration [10^7 Bq/m ²] at location [m] (distance from fuel exit)											
	13.4	17.0	33.1	33.8	35.3	39.8	42.8	45.8	51.4	54.2	65.7	78.0
67	2.1	0.41	2.1	1.4	1.4	3.5	1.8	8.1	21.	13.	8.1	0.26
68	2.2	0.41	1.3	1.7	3.0	2.6	6.7	14.	6.7	6.7	NM	NM
69	NM	1.8	0.52	0.63	1.4	NM	1.3	3.5	7.8	3.0	3.4	0.017
70	1.3	0.28	1.2	1.5	2.4	1.9	6.7	13.	4.4	4.1	NM	NM
71	3.0	0.56	2.3	2.7	4.1	4.1	7.8	18.	7.8	7.4	3.7	0.056
72	1.9	0.35	1.9	2.2	4.1	4.1	8.5	18.	4.4	4.4	NM	NM
73	3.7	0.85	2.7	3.1	4.8	5.6	9.3	16.	5.9	7.4	2.7	0.052

NM = not measured

Table 6-18: Measured plateout concentrations of Cs-137

Cycle	Cs-137 concentration [Bq/m ²] at location [m] (distance from fuel exit)											
	13.4	17.0	33.1	33.8	35.3	39.8	42.8	45.8	51.4	54.2	65.7	78.0
46	8.9×10^5	3.5×10^5	NM	NM	5.2×10^5	NM	NM	6.3×10^4	NM	NM	NM	NM
47	2.6×10^6	7.8×10^5	1.1×10^6	1.5×10^6	9.6×10^5	NM	NM	8.5×10^4	NM	NM	NM	NM
48	4.4×10^4	NM	6.3×10^4	3.3×10^4	1.1×10^5	NM	NM	8.5×10^5	NM	NM	8.5×10^4	1.3×10^3
49	1.6×10^5	3.5×10^4	1.3×10^5	1.3×10^5	3.6×10^5	NM	NM	7.0×10^5	NM	NM	1.6×10^4	1.2×10^4
50	2.7×10^5	5.2×10^4	1.9×10^5	2.3×10^5	2.6×10^5	NM	NM	9.6×10^5	NM	NM	2.9×10^4	1.5×10^4
51	3.6×10^5	5.9×10^4	2.5×10^5	3.2×10^5	3.1×10^5	NM	NM	9.6×10^5	NM	NM	3.0×10^4	6.7×10^3
52	4.1×10^5	8.9×10^4	5.2×10^5	4.1×10^5	4.8×10^5	NM	NM	2.1×10^6	NM	NM	4.8×10^4	3.7×10^2
53	7.0×10^5	1.0×10^5	7.4×10^5	5.2×10^5	7.8×10^5	NM	NM	4.1×10^6	NM	NM	6.3×10^4	2.7×10^3
54	7.4×10^6	1.2×10^6	4.4×10^6	4.8×10^6	3.7×10^6	NM	NM	4.4×10^6	NM	NM	8.9×10^4	1.2×10^4
55	1.1×10^7	2.6×10^6	5.6×10^6	5.9×10^6	4.4×10^6	NM	NM	3.6×10^6	NM	NM	NM	NM
56	2.8×10^6	5.6×10^5	2.6×10^6	3.1×10^6	4.4×10^6	NM	NM	9.6×10^6	NM	NM	2.3×10^5	3.7×10^4
57	8.1×10^6	1.4×10^6	5.2×10^6	6.3×10^6	5.9×10^6	NM	NM	1.1×10^7	NM	NM	1.9×10^5	5.2×10^3
58	8.9×10^6	2.1×10^6	7.8×10^6	1.0×10^7	8.9×10^6	NM	NM	1.8×10^7	NM	NM	6.7×10^5	4.8×10^4
59	2.7×10^6	5.9×10^5	4.1×10^6	3.7×10^6	4.8×10^6	NM	NM	2.3×10^7	NM	NM	3.5×10^5	5.6×10^4
60	9.3×10^5	1.7×10^5	1.9×10^6	8.1×10^5	3.4×10^6	NM	NM	2.4×10^7	NM	NM	5.2×10^5	1.7×10^4

NM = not measured

Table 6-18: Measured plateout concentrations of Cs-137 (continued)

Cycle	Cs-137 concentration [Bq/m ²] at location [m] (distance from fuel exit)											
	13.4	17.0	33.1	33.8	35.3	39.8	42.8	45.8	51.4	54.2	65.7	78.0
61	4.8*10 ⁵	1.9*10 ⁵	1.5*10 ⁶	3.6*10 ⁵	3.5*10 ⁶	NM	NM	2.5*10 ⁷	NM	NM	5.2*10 ⁵	8.5*10 ⁴
62	5.2*10 ⁵	1.5*10 ⁵	1.5*10 ⁶	3.3*10 ⁵	3.4*10 ⁶	NM	NM	2.7*10 ⁷	NM	NM	NM	NM
63	3.0*10 ⁵	1.9*10 ⁵	1.5*10 ⁶	3.3*10 ⁵	3.7*10 ⁶	7.0*10 ⁵	4.1*10 ⁷	2.9*10 ⁷	9.6*10 ⁶	3.0*10 ⁶	6.7*10 ⁵	7.0*10 ⁴
64	4.1*10 ⁵	2.2*10 ⁵	1.8*10 ⁶	4.4*10 ⁵	4.1*10 ⁶	4.8*10 ⁵	5.2*10 ⁷	2.8*10 ⁷	1.2*10 ⁷	3.0*10 ⁶	8.9*10 ⁵	6.7*10 ⁴
65	4.4*10 ⁵	2.3*10 ⁵	1.8*10 ⁶	4.1*10 ⁵	3.7*10 ⁶	9.6*10 ⁵	5.2*10 ⁷	2.8*10 ⁷	1.2*10 ⁷	3.1*10 ⁶	NM	NM
66	7.0*10 ⁵	4.4*10 ⁵	2.7*10 ⁶	4.4*10 ⁵	4.1*10 ⁶	4.8*10 ⁵	4.8*10 ⁷	3.0*10 ⁷	1.3*10 ⁷	3.5*10 ⁶	1.0*10 ⁶	1.1*10 ⁵
67	1.2*10 ⁶	5.9*10 ⁵	2.6*10 ⁶	1.0*10 ⁶	4.4*10 ⁶	8.5*10 ⁵	4.8*10 ⁷	2.3*10 ⁷	1.3*10 ⁷	3.4*10 ⁶	9.6*10 ⁵	1.2*10 ⁵
68	3.0*10 ⁶	1.1*10 ⁶	3.2*10 ⁶	2.0*10 ⁶	5.2*10 ⁶	1.9*10 ⁶	4.8*10 ⁷	2.2*10 ⁷	1.3*10 ⁷	3.4*10 ⁶	NM	NM
69	NM	1.2*10 ⁶	4.1*10 ⁶	3.5*10 ⁶	5.9*10 ⁶	3.7*10 ⁶	4.8*10 ⁷	2.3*10 ⁷	1.3*10 ⁷	2.9*10 ⁶	8.1*10 ⁵	1.2*10 ⁵
70	4.4*10 ⁶	3.5*10 ⁵	4.8*10 ⁶	4.8*10 ⁶	7.0*10 ⁶	4.8*10 ⁶	4.8*10 ⁷	2.3*10 ⁷	1.3*10 ⁷	2.7*10 ⁶	NM	NM
71	1.1*10 ⁷	4.1*10 ⁶	6.3*10 ⁶	5.9*10 ⁶	7.4*10 ⁶	6.7*10 ⁶	5.2*10 ⁷	2.6*10 ⁷	1.4*10 ⁷	3.4*10 ⁶	8.1*10 ⁵	1.5*10 ⁵
72	2.3*10 ⁷	8.9*10 ⁶	7.4*10 ⁶	8.1*10 ⁶	8.9*10 ⁶	7.8*10 ⁶	5.2*10 ⁷	2.3*10 ⁷	5.9*10 ⁶	1.9*10 ⁶	NM	NM
73	4.1*10 ⁷	1.5*10 ⁷	1.0*10 ⁷	1.1*10 ⁷	1.1*10 ⁷	8.9*10 ⁶	5.2*10 ⁷	2.1*10 ⁷	1.3*10 ⁷	3.7*10 ⁶	8.1*10 ⁵	2.0*10 ⁵

NM = not measured

6.1.1.3.4. US Contribution

The validity of the methods used to predict plateout distributions in the primary coolant circuit during normal operation have been assessed by applying them to predict the plateout distributions observed in out-of-pile loops, in-pile loops and operating reactors. The bulk of the experimental data were generated by the various US HTGR programs, but considerable Dragon data (see section 6.1.1.3.1) and German data have also been analyzed at GA.

Out-of-Pile Loop Data

The **GA deposition loop** [56] was constructed to study plateout under conditions approaching those in the evaporator-economizer sections of an HTGR steam generator (the temperatures in the intercoolers and precooler of a gas-turbine HTGR are comparable). High-pressure helium (≈ 20 atm) circulated in fully developed turbulent flow ($Re \approx 12,000$) in a closed loop. Loop surface temperatures ranged from a low of about 50°C when a water-cooled chill block was clamped to an exterior portion of the T2 (0.5 % Cr, 0.5 % Mo chromaloy steel) tubing to a high of about 500°C when the chill block was omitted.

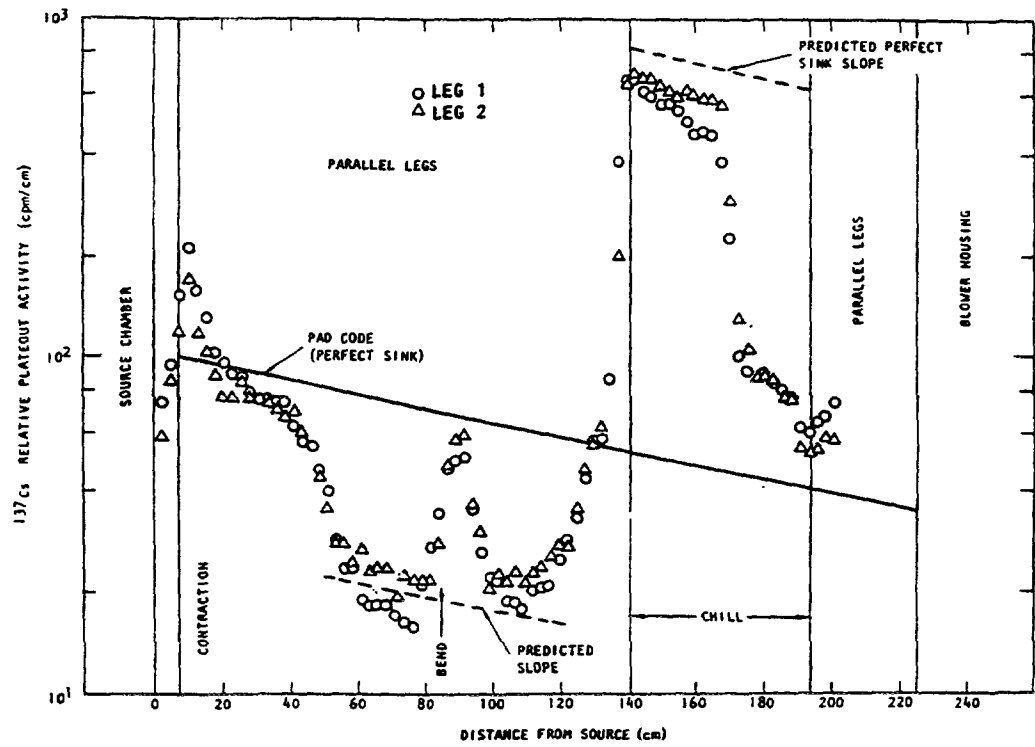
Five experiments were performed; typical results for cesium and iodine are shown in Fig. 6-23, respectively. Because of the chill block, surface temperatures in both tests were quite low ($\leq 260^\circ\text{C}$). Also shown in the figures are the deposition profiles predicted with the PAD code⁴ [77] using reference sorption isotherms. Because of the low temperatures and surface concentrations, perfect sink behavior is predicted for both cesium and iodine - hence, the monotonic decrease in specific activity with increasing distance from the source.

Inspection of Fig. 6-23 (a) shows large discrepancies between the predicted and measured cesium profiles in Test #1. The slope of the experimental profile over the first 50 cm of tubing is much steeper than predicted, yet at other locations (see dotted lines) the slope is about as expected. Far more disconcerting, however, is the large but unpredicted increase of plateout levels in the chill section. The cause of this dramatic increase remains unknown some two decades after the data were obtained as is the reason for the abrupt decrease in activity, which occurs about half-way through the chill section.⁵ Test #2, a strontium experiment, gave quantitatively similar results. In marked contrast, the iodine plateout profile obtained in Test #3, as shown in Fig. 6-23 (b) is in good agreement with the predicted profile. The iodine profile is most interesting when compared to the cesium profile from Test #1. The operating conditions in these tests were quite similar. Surprisingly, the chill section seems to have had much less effect on iodine than on cesium or strontium - a strange effect indeed since iodine is the most volatile. In Test #4, another cesium experiment, the chill block was eliminated in order to obtain higher surface temperatures (350 - 450°C); in this case, the measured profile exhibited the expected perfect sink behavior.

⁴ PAD [77] is a precursor to the PADLOC code which solves the same equations as the PADLOC code [22] but employing a much less efficient numerical solution technique.

⁵ In fact, these data are included here primarily because they appear remarkably different from cesium plateout data obtained at modestly higher temperatures.

(a)



(b)

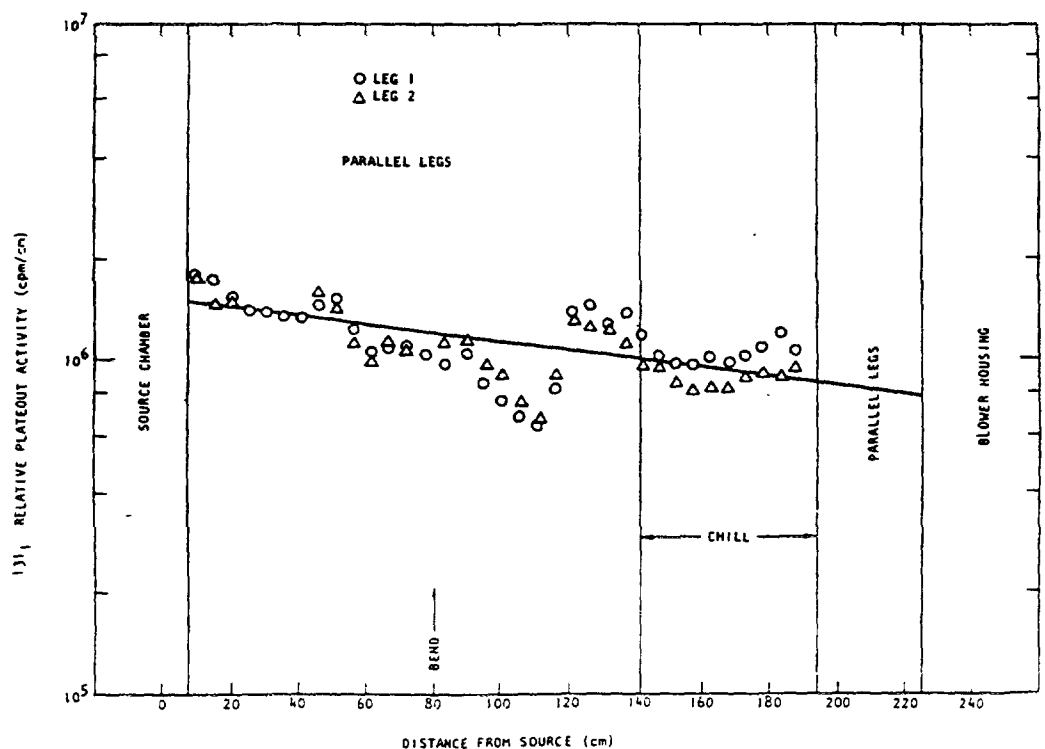


Fig. 6-23: Comparison of measured and predicted plateout profiles in GA deposition loop [56]

(a) PAD code simulation of loop #1, (b) PAD code simulation of loop #3

In-Pile Loop Data

GA has collaborated with the Commissariat l'Energie Atomique (CEA) to perform six in-pile fission product transport tests. The first five in-pile tests, the four CPL-2 in PEGASE and the SR1 test in COMEDIE, were part of a private cooperative program for HTGR development between CEA and GA in the 1970s. The last BD-1 test in COMEDIE was sponsored by the USDOE via a subcontract from ORNL to CEA.

CPL-2 Test Program

The **CPL-2 test program** was a series of four in-pile loop tests in the **PEGASE** materials test reactor in Cadarache, France. The essential features of the CPL-2 loop were a fuel element (representative of a prismatic block), reflector element, and a counter-current, shell-and-tube heat exchanger-recuperator. Selected fuel compacts contained 1 - 4 % bare UO₂ kernels in addition to TRISO-coated driver particles to provide a well defined fission product source. Four tests were performed in the CPL-2 program. Tests CPL-2/1 [78], CPL2/1-Bis [79], and CPL-2/3 [80] were characterized by variable coolant chemistries during the two-month irradiations with the latter test operating with up to 100 ppm total oxidants for most of the irradiation. CPL-2/4 [81] was an *in-situ* depressurization test: the loop was operated under nominal conditions for 60 days and then rapidly depressurized with the effluent passing through a series of traps to recover the radionuclides released from the loop.

The CPL-2 test program generated a broad spectrum of fission product transport data, including an extensive amount of plateout data from the tubes of the heat exchanger-recuperator. The heat exchanger consisted of 186 tubes, 4 mm inside diameter and 1.25 m long, arranged in a close-packed array. Several different types of steels, both in an as-received and pre-oxidized state were used to fabricate the tubes; included were the French equivalents of Incoloy 800, Hastelloy B, SS-347, SS-410 and T22 (2.25 % Cr, 1 % Mo chromaloy steel). During loop operation, helium at ≈ 750 °C entered the tube side of the exchanger where it was cooled to ≈ 350 °C by a counterflow of cold helium returning from the loop blower. A detailed, thermal/fluid dynamic analysis of the heat exchanger determined that the temperature distributions and flow fields within the exchanger were non-uniform and very complex, which added to the complexity of interpreting the plateout distributions.

Upon removal from the loop, the plateout distributions were determined by γ scanning and by leaching followed by radiochemical analysis. Radionuclides identified included I-131, Te-127m, Cs-134, Cs-137, Sr-89, Sr-90, and Sb-125 as well as certain activation products which generally tracked the neutron flux distribution in the exchanger. Most of the fission products exhibited perfect sink deposition profiles, but the cesium and iodine isotopes concentrated in the cold part of the exchanger. Typical results for Cs-137 and I-131 are shown in Figs. 6-24 [82]; also shown are PAD code calculations using sorption isotherms measured by CEA (e.g., [83]).

These sorption measurements were made on the actual materials of construction and in the actual temperature range, but they were taken in a partial pressure range some three

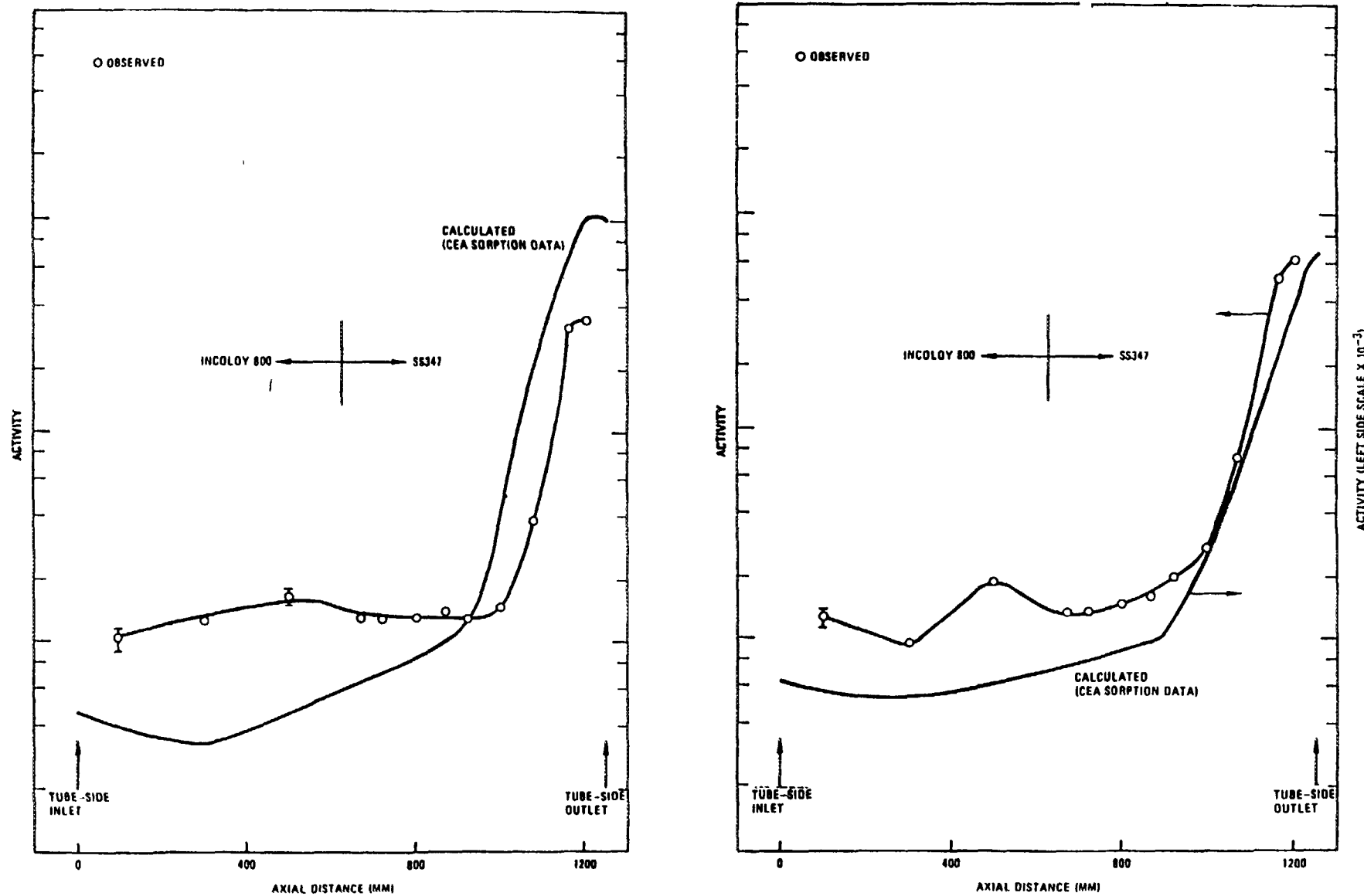


Fig. 6-24: Comparison of measured and predicted (with original isotherms) plateout profiles (arbitrary units) for tube B-31 from CPL 2/1 heat exchanger [82], (left) Cs-137 (right) I-131

to four orders of magnitude higher than that which prevailed in the CPL-2 loops (It is virtually impossible to perform pseudoisopiestic sorption measurements at pressures much less than 10^{-11} atm). The data were fit with a Freundlich isotherm and extrapolated to lower partial pressures. Inspection of the figures indicates good agreement between the measured and predicted cesium profile; the shape of the iodine profile (i.e., the temperature dependence) is correct, but the absolute magnitude is grossly underpredicted. This pattern was consistently seen among tubes of varying material type, initial oxidation state, and temperature distribution when using the CEA iodine sorption isotherm.

In the mid-1980s a comprehensive reanalysis of the extensive fission product transport data sets from the four CPL-2 tests was completed [84, 85, 86]. In this reanalysis, the reference GA iodine isotherm, which was derived from ORNL sorption measurements on T22 [61], was utilized, and the agreement between measurement and prediction improved dramatically [86] (not shown in Fig. 6-24).

COMEDIE Test Programs

The **CEA COMEDIE loop** is an in-pile test facility in the **SILOE** materials test reactor in Grenoble, France [87]. This loop was designed with the specific goal of characterizing the release, transport, deposition and liftoff of fission products in HTGRs during normal operation and during rapid depressurization transients. The loop is capable of providing engineering scale, integral test data under realistic reactor operating conditions to validate the methodology used to predict HTGR source terms.

The loop consists of an in-pile section and an out-of-pile section. The in-pile section includes a fuel element which is the source of fission products and also produces nuclear heating to operate the loop components at the desired temperatures. The fuel element (representative of a prismatic fuel element) contains fuel compacts seeded with a known fission product source (e.g., "designed-to-fail" particles, fuel kernels with a thin PyC seal coat) and coated-particle driver fuel. Immediately downstream of the fuel element is a graphite block, simulating a core reflector element, to determine the deposition of condensable fission products on core structural graphite. The reflector block is followed by a plateout section where condensable fission products are deposited. The plateout section is a straight tube, counter-flow, gas-to-gas heat exchanger/- recuperator simulating the steam generator and the other metallic components in the primary circuit of an HTGR. Downstream of the plateout section is a full-flow filter to trap condensable radionuclides, including iodines, and any circulating particulate matter. The loop also includes a 60 kW electrical heater to control the temperature of the gas to the inlet of the in-pile section.

The out-of-pile section contains additional filters, a helium cooler, a blower and facilities for gas analysis, gas purification and controlled injection of desired impurities. The instrumentation of the loop provides for measurement of temperature, gas flow rate, gas pressure and analysis of noble fission gases. Analysis of noble fission gases provided a measure of the time-dependent, fission product release during the steady-state part of the irradiation during which a typical plateout profile was established prior to the blowdown tests.

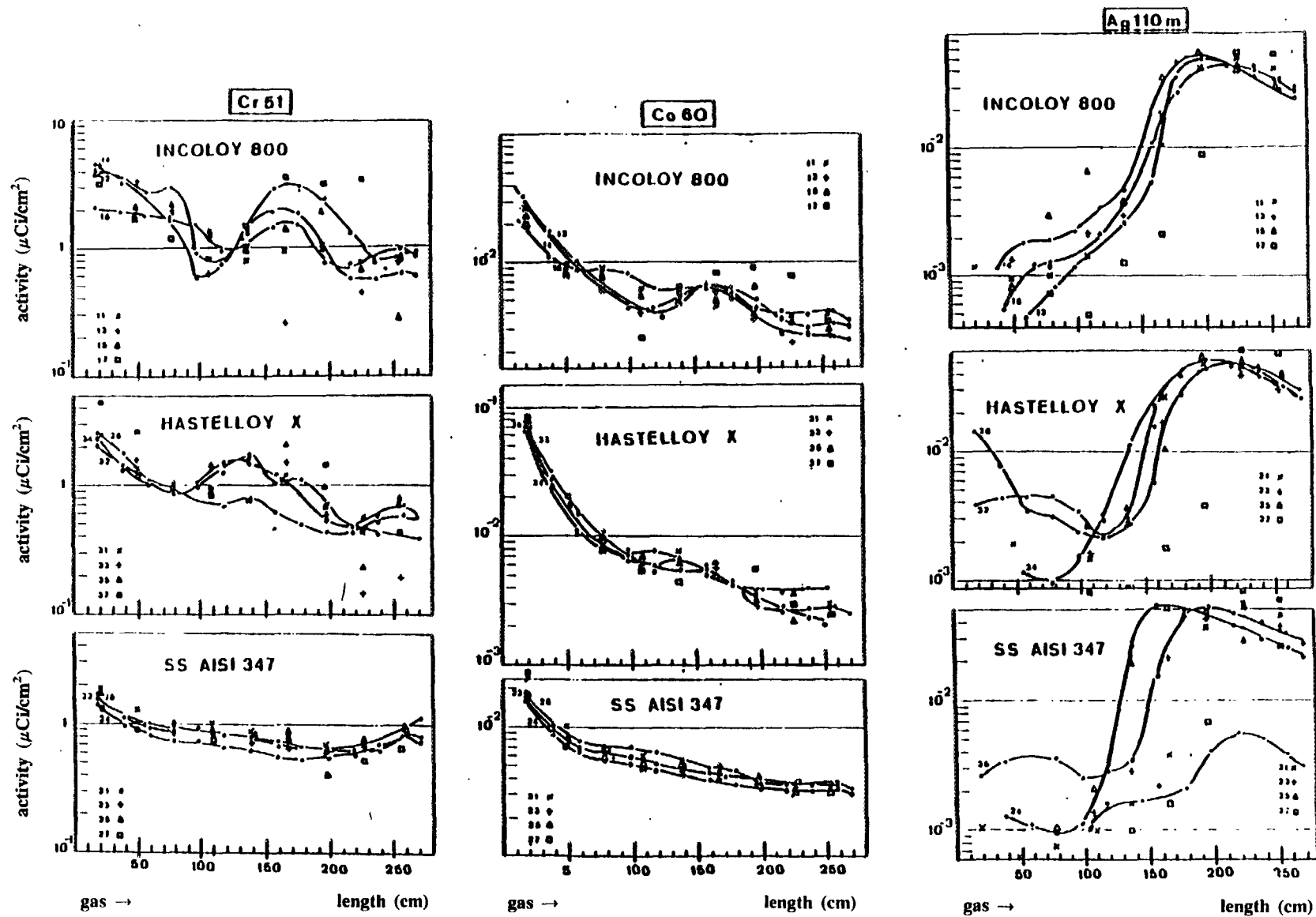


Fig. 6-25 (a): Measured plateout profiles in COMEDIE SR1 heat exchanger [87]

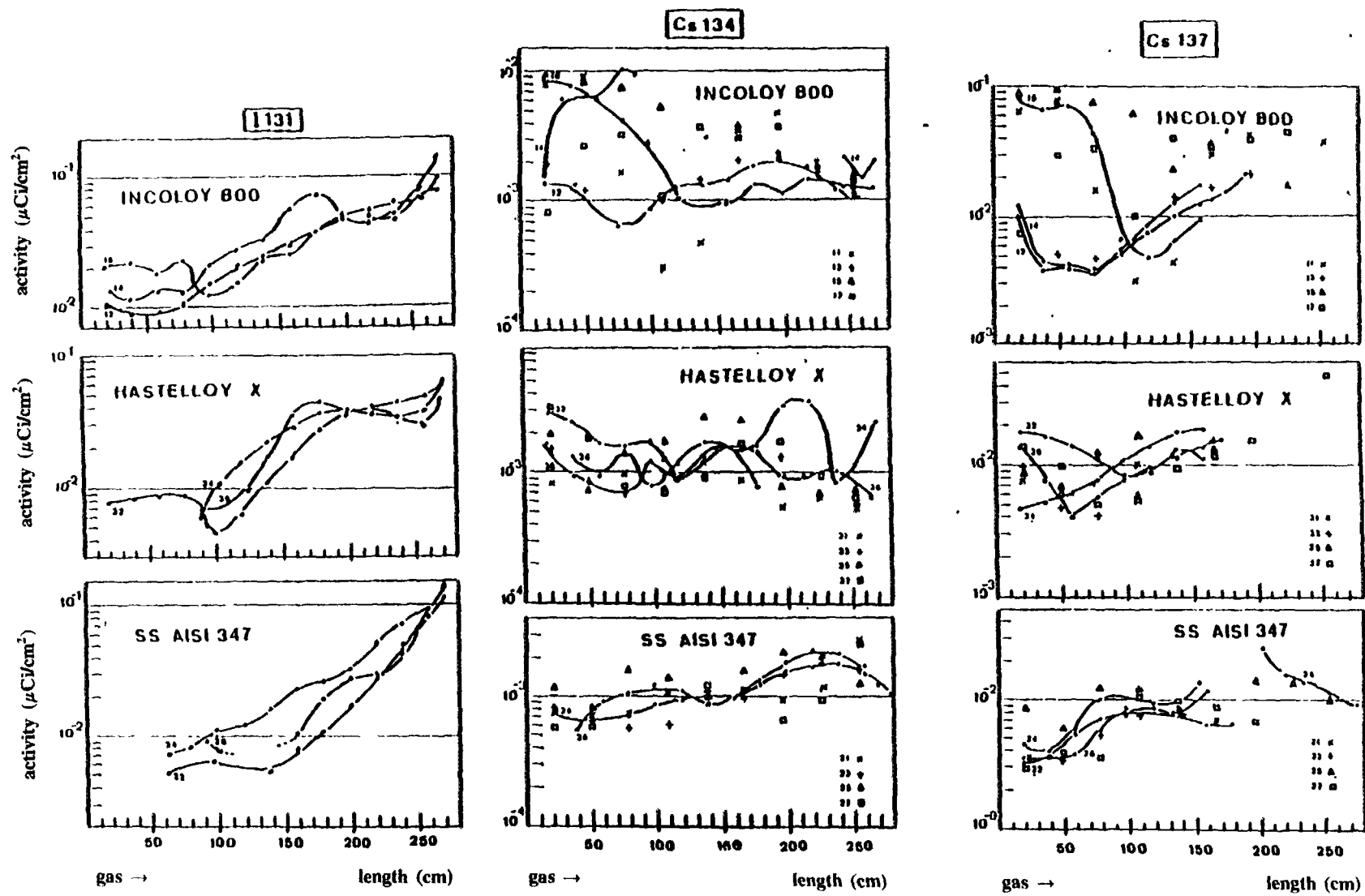


Fig. 6-25 (b): Measured plateout profiles in COMEDIE SR1 heat exchanger [87]

A series of COMEDIE loop tests, referred to as the SR program [88], were planned in this facility under the former GA/CEA Accord. The first two tests were completed, prior to the termination of the CEA HTGR program in 1978. The first in the series, called SR0, was a cold unfueled shakedown test to determine the operating characteristics and capabilities of the loop. The second test, called SR1, was a hot fueled shakedown test. These two tests demonstrated the operational reliability of the loop. In addition, the procedures for rapid measurement of the deposition profiles of various fission products (Ag-110m, I-131, Cs-134 and Cs-137) as well as activation products (Cr-51 and Co-60) in the loop were demonstrated. The plateout distribution data from SR1 have been discussed previously [87] (see Figs. 6-25 (a) and (b)), but limited quantitative analysis has been performed to date. These plateout data, especially the high-temperature Ag-110m data, merit further evaluation.

The **BD-1** test in COMEDIE was conducted to obtain integral test data to validate the methods and transport models used to predict fission product release from the core and plateout in the primary coolant circuit of a steam-cycle HTGR and liftoff during rapid depressurization transients. The design of the loop was similar to that of SR1 except that the loop was operated to obtain lower wall temperatures in the heat exchanger. After a 62-day steady-state irradiation, the loop was subjected to a series of *in-situ* blowdowns at shear ratios⁶ ranging from 0.7 to 5.6. Typical plateout profiles in the loop exchanger are shown in Fig. 6-26 [89]. In general, the Cs isotopes showed perfect sink plateout. Ag-110m also exhibited perfect sink plateout except for highest wall temperatures near the heat exchanger inlet (i.e., for wall temperatures $> \approx 525$ °C). As expected, the I-131 plateout occurred preferentially in the coldest part of the heat exchanger. The BD-1 plateout distributions have been analyzed in detail and compared with PADLOC code predictions [90].

Gas-Cooled Reactor Data

Peach Bottom Unit 1 was a 40 MW(e) prototype HTGR with a two-loop primary coolant circuit comprised of a steel reactor vessel, vertical U-tube steam generators, electric motor-driven oil-lubricated compressors, and interconnecting piping. After seven years of commercial operation, the reactor was shut down for decommissioning because of its perceived uneconomically small size. An extensive end-of-life R&D program was conducted to verify reference GA design methods with emphasis on fission product transport and alloy Incoloy 800 material performance [51]. Considerable plateout distribution data were obtained by a combination of *in-situ* γ scanning and radiochemical analysis of destructively removed samples.

⁶ Shear ratio is the ratio of the wall shear stress during blowdown to that during steady-state operation (see Section 6.1.2.2.1.)

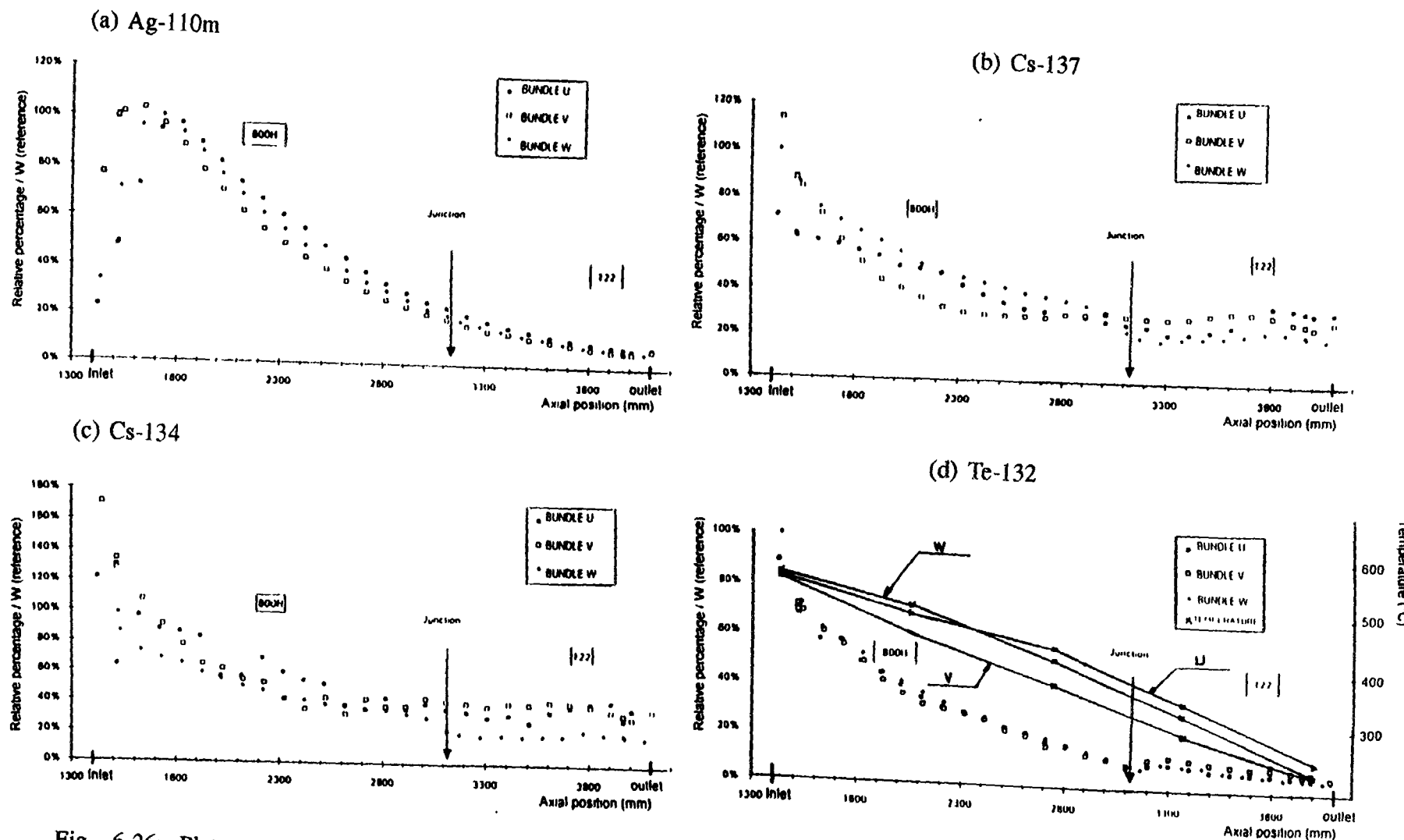


Fig. 6-26: Plateout profiles in COMEDIE BD-1 heat exchanger [89]

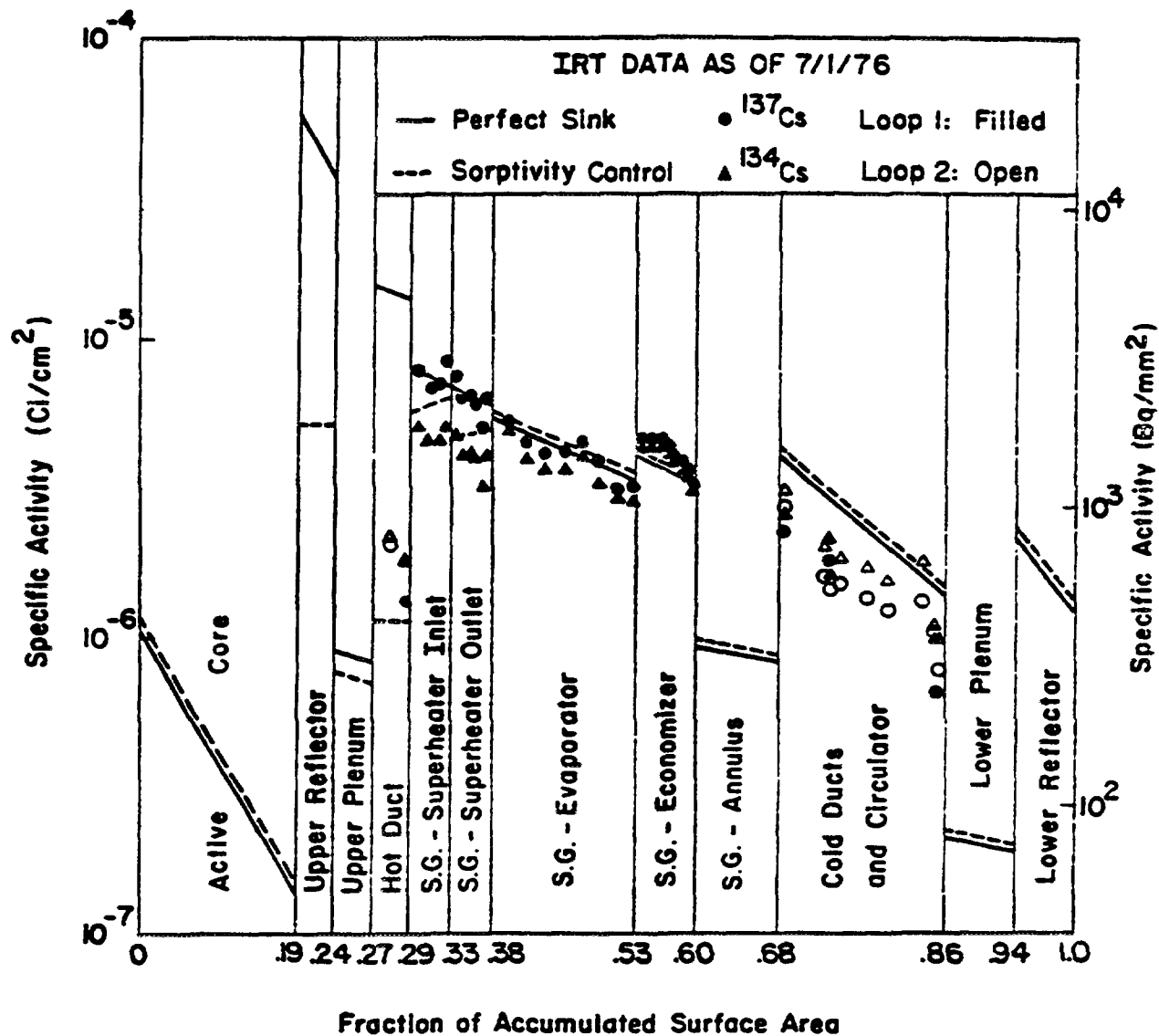


Fig. 6-27: Plateout distribution of Cs-137 and Cs-134 in Peach Bottom HTGR [51]

The dominant γ -emitting nuclides were Cs-137 and Cs-134; their plateout distributions were similar. Radioassay of the destructively removed samples confirmed the specific cesium activities determined by the *in-situ* scanning; Sr-90 was also measured, but the specific strontium activity was about 1/1000 that of cesium. Somewhat surprisingly, neutron activation analysis of leach samples failed to detect any I-129 or Te-126.

The predicted and experimental cesium plateout distributions are compared in Fig. 6-27. Two PAD code calculations are shown: (1) mass transfer control (i.e., the surfaces are perfect sinks for cesium) and (2) sorptivity control. Inspection of the figure indicates that the mass transfer control case (solid lines) resulted in good agreement everywhere except in the hot duct leading from the reactor vessel to the steam generator. Here, the specific cesium activity is over-predicted by an order of magnitude. Since the flow geometry is simple (a circular duct), prediction of the mass transfer coefficient should be reasonably

accurate. Thus, the logical conclusion is that the deposition rate in the hot duct was not limited by mass transfer effects but rather by the high surface temperature.

The major difficulty in predicting cesium plateout in Peach Bottom was the choice of isotherms to describe the sorptive capacity of the surface. The hot-duct cladding was constructed of SS-304 for which sorption data are available [91]. For SS-304 the oxidation state of the surface has a large effect with oxidation favoring increased sorption. Another complication was that all exposed surfaces in the primary circuit were covered with a carbonaceous deposit produced by cracking of lubricating oil leaked periodically into the primary circuit. This carbon deposit was likely a significant sink for cesium. Conceivably, the plateout surfaces may be more appropriately characterized as carbonaceous rather than metallic. Since the cesium sorptivity of this carbon deposit was unknown, it was evaluated parametrically assuming that the deposit had a sorptivity ranging from that of graphite to petroleum-derived, fuel-compact matrix.

In summary, the experimentally observed cesium plateout distribution in Peach Bottom can be predicted almost exactly, providing appropriate sorption isotherms are employed. However, the observed sorption behavior is consistent with either assuming that the primary cesium sink is a relatively oxide-free SS-304 surface or assuming that the carbon deposit has a cesium sorptivity intermediate to that of graphite and matrix. These assumptions seem equally feasible; in reality, both probably contributed to the total sorptive capacity of the surface. With the exception of the hot duct which experienced surface temperatures of ≈ 700 °C, cesium deposition throughout the primary circuit was likely mass transfer controlled; moreover, the deposition profiles indicate that cesium was transported primarily in atomic form despite the ubiquitous presence of carbonaceous dust in the primary circuit.

The Fort St. Vrain plateout data were obtained from the plateout probe measurements and the radiochemical analysis of a circulator removed after reactor operation [92, 93]. The plateout probes, one in each steam generator loop, were designed to monitor vapor and aerosol-borne condensable fission products released from the reactor core. The plateout probes were inserted through nozzles in the PCRV and into a penetration through the wall of the steam generator. Each probe withdrew four sample streams from the hot helium at the inlet to the steam generator and a fifth sample stream from the cold return helium in the lower plenum prior its return to the core inlet. Probes were removed after cycle 3 and at the end of FSV operations, and the accumulated plateout inventories calculated from the probe data.

The measured EOL plateout inventories of metallic fission products (Sr-90, Cs-134 and Cs-137) are compared to the inventories calculated by TRAFIC in Section 3.5.3. The FSV Final Safety Analysis Report (FSAR) Expected (allowable) plateout inventory levels are also listed. TRAFIC predictions of the metallic fission product inventories for the three isotopes are in reasonable agreement with measurements and consistently conservative.

The EOL Sr-90 plateout distributions for the FSV primary circuit components predicted with the PADLOC code [22] are presented in Fig. 6-28, which also shows the predicted and measured activities for the circulator C2105 which had been in service since the beginning of cycle 3 and which remained in service for 450 effective full power days (efpd).

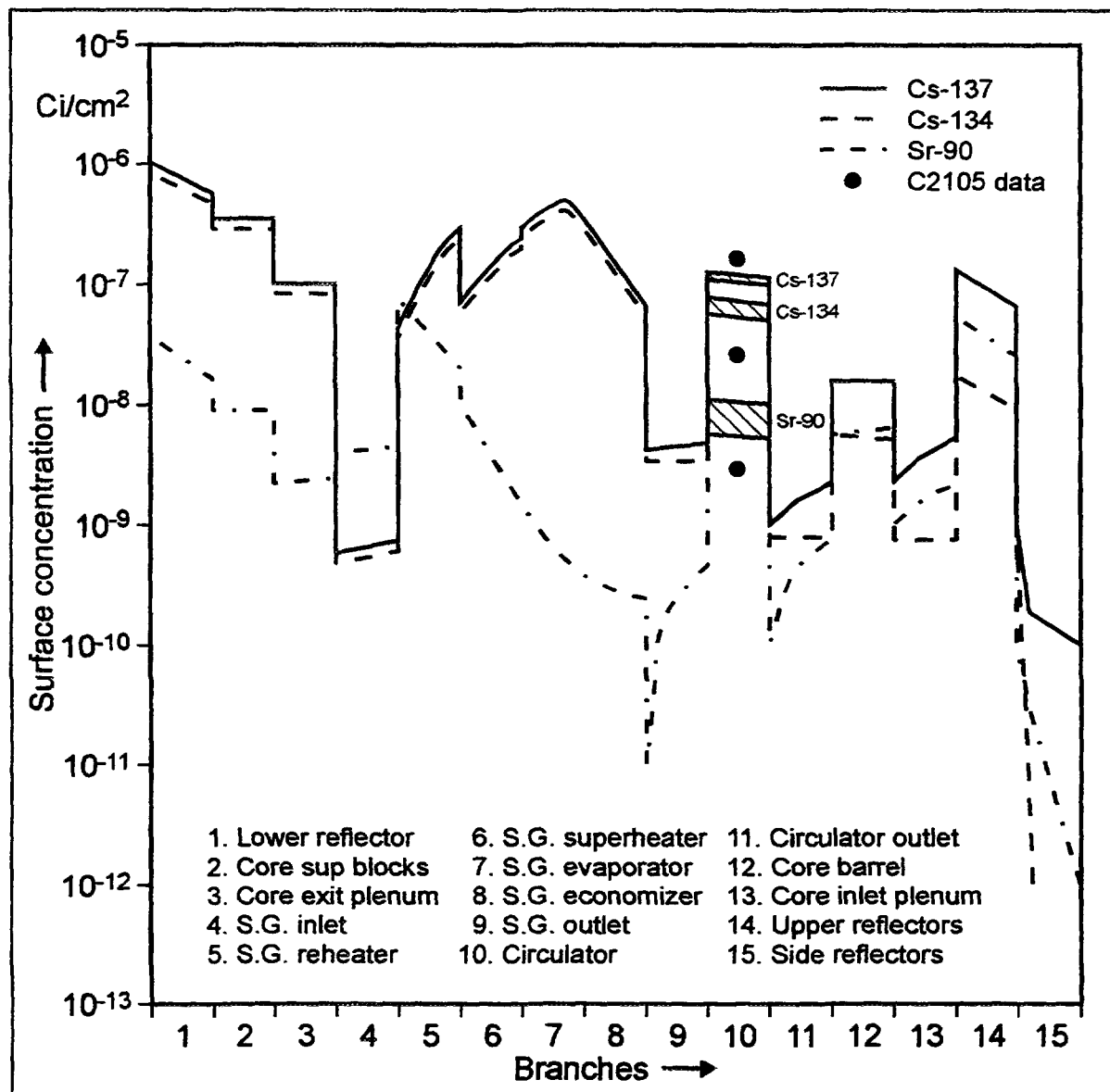


Fig. 6-28: Comparison of predicted plateout profiles for Cs-134, Cs-137, and Sr-90 and of measurements from circulator C2105 in Fort St. Vrain

The C2105 circulator was removed when the reactor was shut down on July 5, 1988 and radiochemically examined at GA. Considering the accuracy in HTGR fission metal release calculations and the additional uncertainties in the plateout distribution calculations (e.g., sorption isotherms), the agreement between the predicted and measured plateout activities for the circulator C2105 is quite good. The Sr-90 data were overpredicted by a factor of 1.8. This good agreement reflects the good agreement with the data for the main source (the precursor Kr-90 decay). However, the Cs-137 data were underpredicted by a factor of 1.4, while the Cs-134 data were overpredicted by a factor of 2 [92].

While this reasonably good agreement for the circulator plateout is encouraging, the circulators represented a small fraction of the total surface area in the FSV primary circuit; the most important plateout location is the steam generator tube bundles, and they were not examined. In fact, the amount of plateout distribution data available from FSV is limited because the primary circuit components were confined within the Prestressed Concrete

Reactor Vessel (PCRV) which restricted their accessibility for *in-situ* γ scanning. Moreover, no EOL R&D program was conducted at FSV, and no radiochemical examinations were made when the primary circuit components, including the steam generators, were removed as part of the plant decommissioning which is now complete. From a scientific point of view, a great opportunity to obtain operating reactor data to validate HTGR design methods, including fuel performance and fission product transport methods was missed. The primary reason was a lack of the requisite funding. It remains to be seen if this experience will be repeated when the AVR and THTR are decommissioned in the relatively near future.

6.1.1.4. Fission Product Distribution at Initiation of the Accident

Table 6-19 summarizes the distribution of fission product inventory as estimated for the German 200 MW(th) HTR-MODUL after 30 years of operation (expected values) [1]. The values of the first four lines of the table are exclusively determined by the fuel quality to define the source term from the active core. The other data concerning plateout are basically best estimate values derived from reactor experience and laboratory experiments.

In actual safety analyses, the adhesively bound dust-borne activity is assumed to be equally distributed over all surfaces of the primary circuit. Since adhesion forces tend to show only a slight temperature dependence, this assumption is not incorrect as long as the surface structure within the primary circuit is more or less homogeneous. The amount of adhesively bound dust is roughly assumed to be half of the total dust amount. The other half is considered to be sedimented dust. AVR data are the basis for the dust-borne fractions of the overall activity given in Table 6-19. For long-lived nuclides, these values consider a smaller relative dust production rate in the HTR-MODUL compared to the AVR due to a dust filter in the refueling system. Sufficient AVR data for iodine do not exist. The relative iodine sorption capacity of dust is roughly assumed to be 50 % of that of the long-lived metals. This value considers both the weaker iodine sorption on graphite and its stronger sorption on metallic dust. A reduction of the dust-borne fraction of iodine due to the smaller dust formation rates in modern HTGRs compared to the AVR is not taken into account for short-lived nuclides because their interaction with dust seems to be restricted to the dust layers in contact with the coolant.

With respect to the empirical modeling of dust, the uncertainties concerning its production, settlement and interaction with gas-borne or plateout activities are high. The radionuclide activity values given in Table 6-19 are upper limits of the uncertainty scatter which may be reduced with increasing knowledge. In connection with dust contributions to the equilibrium cooling gas activities, it was found that an equilibrium like dust concentration in the coolant is obtained only for uniform flow conditions. Based on experimental evidence from the AVR, a fraction of 10^{-7} of the total mass of dust within the primary circuit is assumed to be gas-borne under equilibrium conditions. For the 200 MW(th) HTR-MODUL, this fraction will contain about 5×10^{-9} of the Cs-137 inventory released from core into the primary circuit (or 5×10^{-13} of the overall reactor inventory).

Table 6-19: Fractional distribution of some fission products in the 200 MW(th) HTR-MODUL following a 30 y operation, from [1].

Inventory in	Cesium-137	Strontium-90	Iodine-131	Xenon-133
Particles with intact coatings	> 0.9998	0.9999	> 0.9999	> 0.9999
Kernels of particles with defective coatings	5×10^{-5}	5×10^{-5}	5×10^{-5}	5×10^{-5}
Carbon buffer layer of particles with defective coatings	1×10^{-6}	1×10^{-6}	1×10^{-6}	1×10^{-6}
Grains of matrix graphite (recoil from uranium contamination into matrix material)	$< 1 \times 10^{-6}$	$< 1 \times 10^{-6}$	$< 1 \times 10^{-6}$	$< 1 \times 10^{-6}$
Inner surfaces of matrix and reflector graphites (chemisorbed during diffusion from coolant or coated particles into the porous graphite)	2×10^{-5}	1×10^{-5}	(4×10^{-7})	-
Metallic primary circuit components (plateout)	5×10^{-5}	2×10^{-6}	2×10^{-7}	-
Settled dust a) primary circuit b) purification system	a) 1×10^{-6} b) $< 2 \times 10^{-8}$	a) 4×10^{-8} b) $< 8 \times 10^{-10}$	a) 1×10^{-8} b) 2×10^{-10}	-
Coolant	$< 1 \times 10^{-11}$	$< 1 \times 10^{-12}$	$< 1 \times 10^{-10}$	$< 6 \times 10^{-7}$
Overall Inventory [GBq]	1.7×10^7	1.4×10^7	2.1×10^8	4.5×10^8

Conclusions from Table 6-19 are that for the HTR-MODUL:

- less than 2×10^{-4} of the inventory is found outside intact coated particles,
- the equilibrium activity within the coolant is extremely low due to low release from the fuel and due to plateout on primary circuit component surfaces,
- the inventories of defective particles and the plateout on the metallic primary circuit surfaces represents most of the activity outside intact coated particles.

6.1.2. Fission Product Transport during Accidents (Reentrainment)

The condensable radionuclides which are plated out in the primary circuit may be partially retrained and released to the reactor building during rapid depressurization transients. In the simplest case, volatile fission products that are chemisorbed on primary circuit surfaces could simply desorb; however, since most postulated depressurization transients are characterized by decreasing surface temperatures (i.e., because helium-side heat transfer coefficients are decreasing and feedwater flow is maintained), this removal mechanism is generally perceived to be unimportant. A potentially more significant removal mechanism, especially during rapid depressurizations, is mechanical reentrainment of deposited particulate matter contaminated by plateout and/or spallation of friable surface films; this mechanical reentrainment is traditionally referred as "liftoff."

6.1.2.1. Chemical Desorption

6.1.2.1.1. Physical Models and Computer Codes

FRG Contribution

Desorption of Plateout Activity due to Temperature Increase

The previously described calculation models FRESCO and SPATRA can be used to determine the **temperature-induced desorption** of radionuclides plated out on graphitic or metallic surfaces. Data for sorption isotherms are given in Appendix A, sections A.2 (graphite) and A.5 (metal), respectively.

Cesium and strontium continue to be strongly bound to cold graphite by chemisorption, whereas a desorption of the small amount of iodine on graphitic surfaces, should not be neglected. With respect to metallic surfaces, a desorption is considered small, because fission product concentrations are small compared to the capacity of the surface for adsorbed fission products [1].

Desorption of Plateout Activity due to Pressure Drop

Desorption from primary circuit surfaces as one source of activity in a **depressurization accident** is caused by the diminishing partial pressure of fission products in the coolant. If an ad-/desorption equilibrium is assumed for all gas/surface interlayers of the primary circuit, a pressure drop by Δp leads to an increase of the molecular gas-borne

activity after equilibrium is established by a factor f_p :

$$f_p = \ln\left(\frac{p_o}{p_o - \Delta p}\right) \frac{p_o}{\Delta p} \quad (6-4)$$

where p_o is the system pressure at depressurization start. For a complete depressurization assumed in the HTR-MODUL ($p_o = 6$ MPa), the factor f_p is around 4.2.

Calculations using the Jülich code SPATRA, however, indicate that under typical HTGR normal operating conditions, most of the plateout is controlled by mass transfer effects. This means that the surfaces act as a nearly perfect sink and that surface concentrations are far from equilibrium, as calculated from the AVR experiment VAMPYR-II. Nevertheless, due to the comparably small increase in the very low molecular fission product concentration in the cooling gas induced by a pressure drop ($f_p < 5$), the above equation is used in safety analyses to define an upper limit of the molecular contribution to the depressurization source term.

According to SIEMENS modeling [40], it is assumed that the equilibrium distribution factor M expressing the ratio of deposited over gas-borne activity, is

$$M = \frac{f_{po}}{\lambda} [1 - \exp(-\lambda t)] \quad (6-5)$$

where

f_{po} is the plateout constant [s^{-1}]

$f_{po} = 0.0062$ based on a design value for the plateout rate of 10 % per cycle
(the expected value is 90 % per cycle)

t is the reactor operation time [s]

λ is the decay constant [s^{-1}]

For example, $M = 4.4 \times 10^6$ for the nuclide Cs-137 (assumed 32 full power years) and is still as high as 6200 for the short-lived I-131. These M values indicate that remobilization of even small portions of plateout activity in a depressurization accident could significantly contribute to the released activity.

The factor M as resulting from normal operation remains constant during (isothermal) depressurization because of the rapid process of desorption. The released activity, A_F , resulting from the desorption, can then be treated as a multiple of the steady-state coolant activity, A_K :

$$\frac{A_F}{A_K} = (M + 1) (1 - e^{-x})$$

with $x = \left(\ln \frac{P_o}{P_1} \right) (M + 1)$

$$\approx \ln \frac{P_o}{P_1} \quad \text{for } x \ll 1 \quad (6-6)$$

where

A_F is the released activity [Bq]

A_K is the steady-state coolant activity [Bq]

P_0 is the system pressure before depressurization [Pa]

P_1 is the system pressure after depressurization (atmospheric pressure) [Pa]

Applied to the case of a depressurization in the HTR-MODUL (operated for 32 years) from 6 MPa to atmospheric pressure, the released fission product activity is about 4 times the coolant activity.

Japanese Contribution

In general, plated-out fission products on the metal surface will be lifted-off mainly by desorption when the change of flow condition is mild; normal operating condition or small-scale pipe rupture accident (i.e., the maximum shear ratio is nearly one and depressurization continues several ten seconds). Chemical desorption of plate-out fission products is treated by the PLAIN code as described in 6.1.1.1.2.

US Contribution

Chemical desorption is modeled in the PADLOC code as reversible desorption of deposited fission products as described by the same sorption isotherms used to predict deposition (see Appendix A.5.). Wichner has also derived a chemical sorption model for plateout [25].

6.1.2.1.2. Single-Effects Data

British Contribution

British researchers at Harwell performed cesium desorption experiments with contaminated steam-generator tube specimens removed from the Peach Bottom HTGR as part of the postmortem R&D program. The observed cesium desorption profiles were complex, implying the presence of several different sorbed Cs species with significantly different volatilities and/or a population of sorption sites with a broad range of enthalpies of adsorption [94].

FRG Contribution

Deposition Circuit SMOC at the Research Center Jülich

The main goal of the **out-of-pile circuit SMOC** (Fig. 6-29) was the systematic investigation of fission product transport and deposition mechanisms under conditions characteristic for an HHT plant. Temporal behavior of deposition profiles were measured under the turbulent flow conditions of a depressurization accident in order to establish a set of plateout parameters for a wide range of test conditions. Its central feature was a test section of 6 m length and an inner diameter of 30 mm. A specified amount of Cs-133 and

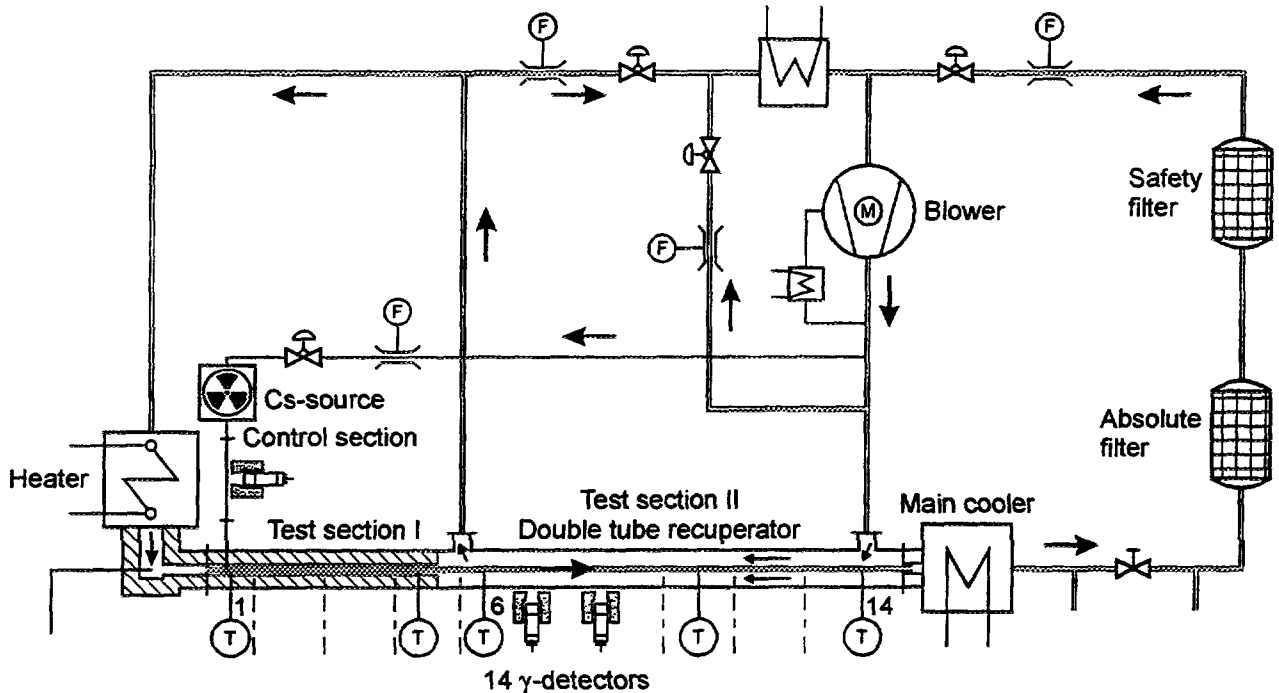


Fig. 6-29: Schematic of the out-of-pile circuit SMOC

Cs-134 was injected into the helium flow. The helium was at a pressure varying between 0.5 and 8 MPa. A wide range of gas temperatures (200 - 900 °C) and wall temperatures (150 - 900 °C) as well as of the mass flow rate (40 - 240 g/s) was used in the experiments. The activity plated out along the tube was measured by 15 NaI detectors. Filters at the end of the test section were operating at a temperature of 100 °C. Operating conditions are given in Table 6-20.

In the first run, Sm-2, of the test series (after pre-testing to qualify the cesium source in Sm-1), the influence of the coolant flow and the temperature on the local desorption kinetics of cesium from the stainless steel 4541 was investigated. Temperatures and mass flow rates were varied in several steps as indicated in Fig. 6-30 [95]. The basic results from this test were that desorption was observed only at temperatures > 410 °C, that there was only a small influence of the velocity ($< v^{0.75}$, that no desorption was observed by velocity change only, and that a part of the activity was found to be locally bound by diffusion into the bulk. Cs-134 activity measurements are depicted in Fig. 6-30.

Fig. 6-31 presents the measured activities of cesium on the HTGR materials Incoloy 800 (Sm-8) and Inconel 617 (Sm-9) at three different positions of the test tube as function of time. A strong desorption was observed in Sm-8 after disconnecting the cesium source; it is even increased after raising the wall temperature to the 650 - 700 °C level. In Sm-9 the lower temperature during the first loading did not allow a desorption after cutting off the source. The wall temperature at sensor #14 was at an almost constant level as low as some 300 °C implying a loading only expressed in a steadily increasing activity [97]. As a result from the "dry" SMOC tests, Incoloy 800 and Inconel 617 showed about the same desorption characteristics with higher desorption energies compared to the stainless steel 4541. The temperature required to desorb deposited cesium in the isothermal section of

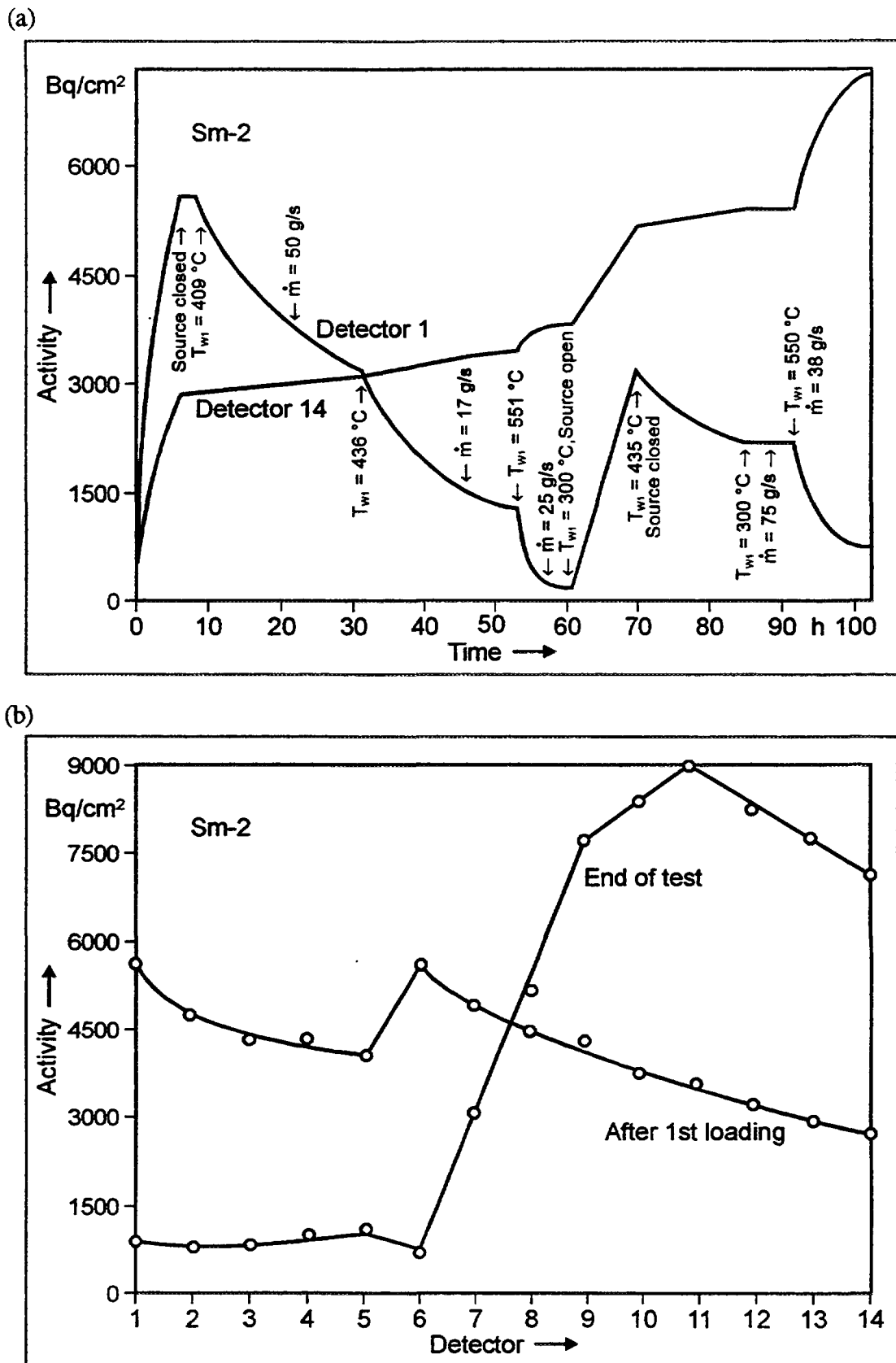


Fig. 6-30: Cs-134 activity measurements in SMOC test run Sm-2, from [95].

(a) vs. time at detectors 1 (inlet) and 14 (outlet)

(b) vs. detector position (tube length) after 1st loading and at test end

Table 6-20: Operating Conditions and activity measurements of the deposition loop SMOC, from [32, 95, 96, 97].

Run	Time [h]	Gas temperature inlet / outlet [°C]	Wall temperature [°C]	Gas flow [g/s]	System pressure [MPa]	Material
Sm-1		325 / 409	max 403	26		4541
Sm-1a		max 611	max 579	max 36.1		4541
Sm-2		308	300	25	1	4541
Sm-3 ⁽¹⁾	100		max 560	50 - 150	2	4541
Sm-4	120		max 570	max 150	2	4541
Sm-5	120		max 560	max 112	1.5	4541
Sm-6	93	max 588 / max 425	max 570	49.1 - 143.8	2	4541
Sm-7	98	max 574 / max 498	max 570	37.6 - 114.9	1.5	4541
Sm-8	96	max 715 / max 485	max 701	24.2 - 72.4	1	Incoloy 800
Sm-9	99	max 735 / max 485	max 702	23.9 - 73.9	1	Inconel 617
Sm-9/2	103					Inconel 617
Sm-10	120	max 700		25		Inconel 617
Sm-10e	72					Inconel 617
Sm-11		max 700		25		Incoloy 800

(1) Cs-134 source did not work properly

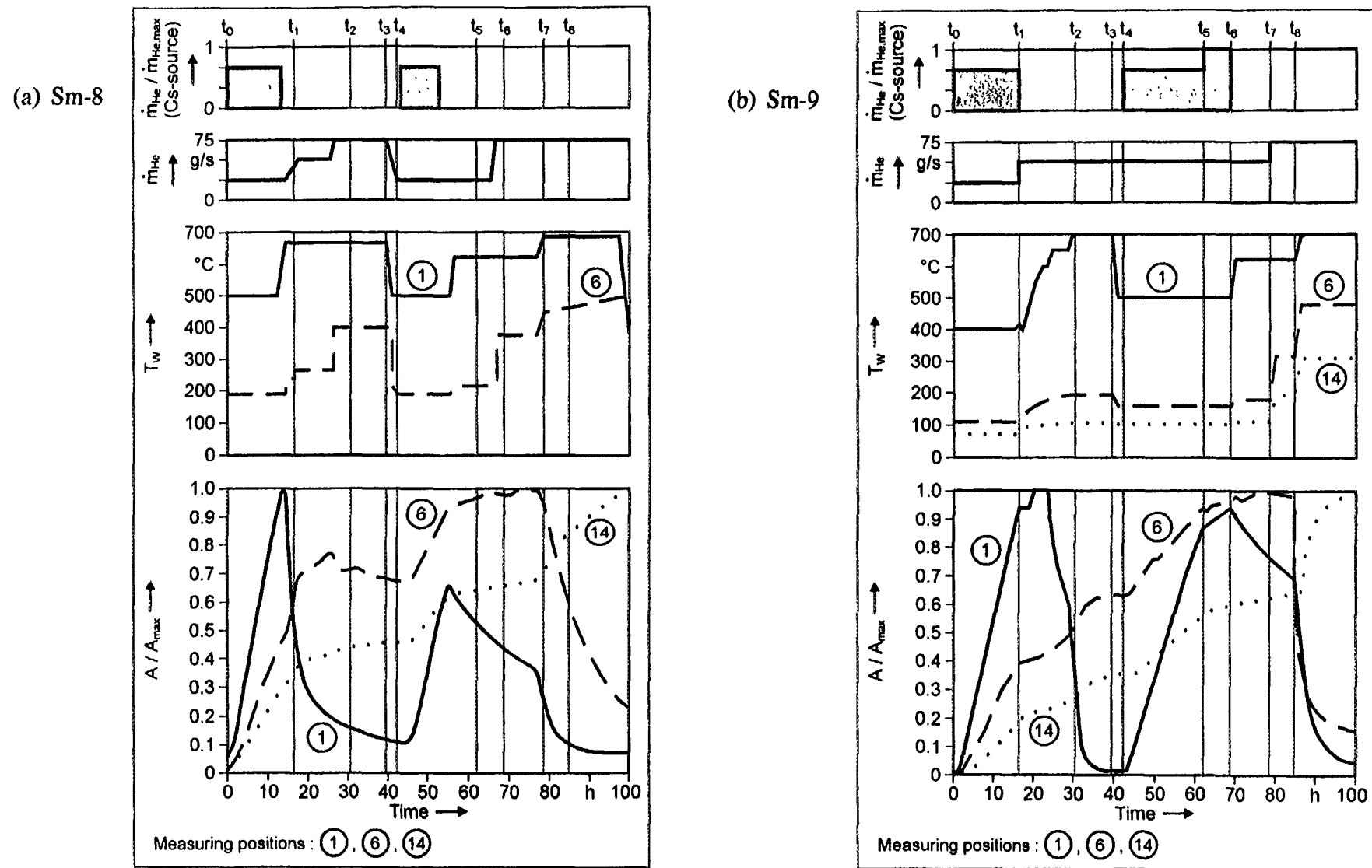


Fig. 6-31: Cs-134 activity measurements in SMOC, from [97].

SMOC was determined to be ≥ 410 °C for 4541 and ≥ 500 °C for Incoloy 800, while in the colder recuperator part the temperatures were ≥ 300 °C and ≥ 440 °C, respectively. Due to the small test times, only a small amount of cesium diffused into the material [63].

After the dry SMOC tests, the first and only tests with radioactive cesium Cs-134 with moist primary gas were conducted, Sm-10 (+Sm-10e) and Sm-11. The loading was made under dry conditions followed by an injection of water vapor at various partial pressures in the range 500 - 10,000 Pa. A nitrogen injection in Sm-10e indicated only a slight influence by co-adsorption on the cesium deposition behavior. After these tests in 1985, the SMOC facility was dismantled [32].

6.1.2.1.3. Integral Data

US Contribution

A significant desorption and redistribution of I-131 plateout was observed in the **COMEDIE BD-1 test** [89] although it was most likely an artifact of the experimental operating procedures. After the irradiation phase of the test was completed, the loop cold leg was allowed to cool to ≈ 150 °C, and the He pressure was allowed to fall in response to these lower temperatures while preparations for the blowdown testing were completed. By design, the blowdown tests were conducted without nuclear heating, and the thermal power was provided by in-pile and out-of-pile electrical heaters. In preparation for the first blowdown, the first blowdown filter was put on-line immediately after isolating bundle W (one of three parallel tube bundles) and prior to beginning the loop heatup on the electrical heaters. Several hours were required to return the loop to the temperatures required for the blowdown tests. During the destructive postirradiation examination it was determined that ≈ 55 % of the I-131 plateout had desorbed from the two unisolated tube bundles and redeposited in the colder out-of-pile sections of the loop during the reheating phase.

6.1.2.2. Mechanical Reentrainment ("Liftoff")

The correlations for predicting the degree of reentrainment, or "liftoff," during depressurization transients were determined empirically. The liftoff data base was obtained largely from *ex-situ* blowdown tests wherein the blowdown specimens were mechanically removed from the loop or reactor in which the plateout activity was originally deposited. These *ex-situ* blowdown data exhibit considerable scatter and have been shown to be, in general, excessively conservative.

6.1.2.2.1. Physical Models and Computer Codes

Wichner provides a comprehensive overview of a number of candidate reentrainment models in his review of plateout and liftoff in HTGR primary circuits [25]. While the more complicated liftoff models may be more intellectually appealing than the simple empirical correlations, all liftoff models are plagued by the lack of definitive experimental data, and the more sophisticated models suffer the most.

British Contribution

In AGRs, a series of experiments has been performed to investigate the remobilization of dust-borne activities [98]. Flow increase by a factor of 2 has been found to raise the level of gas-borne Fe-59, Co-58, and Mn-54 by about four orders of magnitude. These nuclides are assumed to be mainly fixed on dust. In addition, dust particles of 2, 5, and 17 μm diameter labelled with Fe-59 have been injected into the primary circuit. The dependence of depletion and remobilization behavior on the diameter of dust particles allows some conclusions to be reached about the physical mechanisms. The impact of dust on surfaces seems to be one important depletion mechanism which, however, is reduced by a bouncing-off effect being proportional to particle size and to flow rate. Adhesion sites on the surfaces show a broad distribution of interaction energies with the dust particles due to surface inhomogeneities. This causes remobilization and redepletion of particles until more energetically favorable sites are occupied.

FRG Contribution

Sedimented dust is partly lifted-off during fast depressurizations as indicated by AVR experiments with blower transients. Changing the flow rate leads to an increase of the gas-borne dust (which in equilibrium is very low, $< 5 \mu\text{g/Nm}^3$) by up to three orders of magnitude [99] as mentioned already in section 6.1.2.2. and will be described in more detail in section 6.1.2.2.3. The increase is probably due to flow disturbances during the change of the flow rate. After these disturbances are gone, the dust concentration declines by depletion within a few hours. Flow disturbances are also expected during or preceding depressurization events.

The comparably large liftoff in the Peach Bottom steam generator tube experiments (see next section 6.1.2.2.) raises the question whether a surface erosion with dust formation may occur in the course of HTGR primary circuit depressurizations. Such an erosion could also lead to a partial liftoff of the plated-out activity. With respect to this problem, some cesium plateout and desorption experiments in the loop SMOC at the Research Center Jülich are noteworthy. These experiments included a variation of the mass flow [100]. In contrast to the Peach Bottom steam generator tube tests, no significant liftoff was observed after a flow rate increase. The amount of dust in SMOC is believed to be very small.

Experiments have also been performed to study dust settling in quiescent coolant regions behind an obstacle [101]. Graphitic dust particles with an average diameter of 50 μm have been used. Additional experiments indicated that settled dust is partly lifted off in case of a reversal of the flow direction.

Summing up the above outlined experience on dust and liftoff, there is no sufficient physical-based assessment available up to now allowing for a reliable description of dust behavior in HTGRs.

For the **modeling of dust remobilization**, both a deterministic and a statistical approach have been adopted. The first approach is characterized by a critical parameter, e.g., a force (van der Waals, electrostatic, friction), depending on adhesion distance and surface

roughness. If this force is exceeded by comparison with fluid dynamic (shear) forces, then liftoff occurs. The evaluation of dust deposition experimental data have confirmed that the van der Waals force appears to be a satisfactory liftoff criterion. In the statistical approach, liftoff starts at about the critical velocity, but reentrainment occurs within a relatively wide range of velocities even for mono-sized dust particles.

HRB has developed a **calculation model RADAX-3** based on the liftoff criterion

$$\text{fluid dynamic shear force} \geq \text{van der Waals force}$$

with statistically distributed forces [41]. The probability β for a dust particle to adhere to the surface is given according to Weibull statistics by

$$\beta(d, v) = \exp\{-\ln 2 * (av/v_{crit}(d))^m\} \quad (6-7)$$

where

d is the diameter of dust particles [m]

v is the fluid velocity [m/s]

$v_{crit}(d)$ is the critical liftoff velocity (mean value) for particles with diameter d [m/s]

a, m are the Weibull distribution parameters

The derivation of the Weibull distribution parameters a and m from experimental data resulted in

$$\begin{aligned} a &= 1. \\ m &= v_{crit} / 10 + 2. \end{aligned} \quad (6-8)$$

(see Fig. 6-32).

The saturation dust coverage is determined by multiplying a monolayer coverage with β meaning that there is a 50 % monolayer for a critical velocity. For the HTGR circuit, the critical velocity is calculated by equating adhesion force with shear force in tube flows yielding

$$v_{crit} = 0.277 \left(\frac{1}{\alpha_p} \frac{1}{\rho} \frac{d_h}{\nu} \frac{E_W}{z^2} \right)^{4/7} \quad (6-9)$$

where

α_p is the adhesion coefficient for particles with diameter d

ρ is the density of fluid

d_h is the hydraulic diameter

ν is the kinematic viscosity of fluid

E_W is the van der Waals energy (= 5 eV)

z is the adhesion distance (= $2.5 \times 10^{-2} \mu\text{m}$)

For velocities ≤ 10 m/s, particles with $d \leq 3 \mu\text{m}$ will almost completely be deposited (as long as no monolayer is existent), whereas for velocities > 50 m/s, only particles with

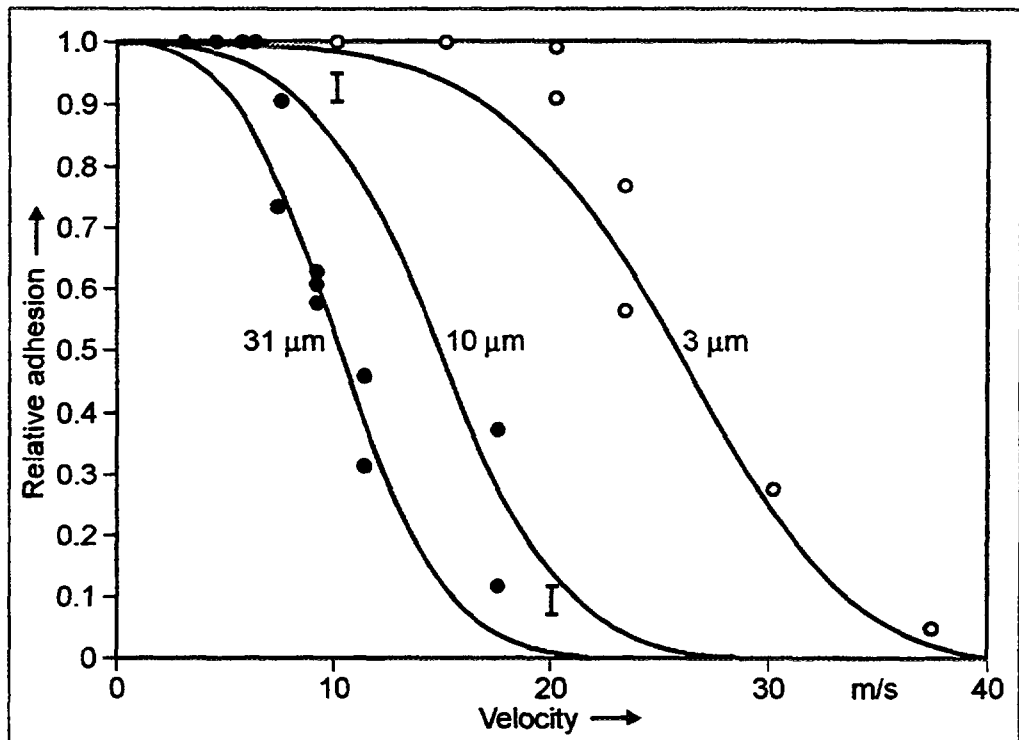


Fig. 6-32: Comparison of calculated (according to Weibull statistics) and measured probability of dust adhesion as function of coolant velocity, from [41]

$d < 1 \mu\text{m}$ will be able to deposit. A verification of RADAX-3, however, requires more experiments with HTGR specific materials and boundary conditions [41].

In case of a depressurization, the dust in areas with shear forces larger than under normal operating conditions is assumed in safety analyses to be completely lifted-off. With respect to the release of dust settled in quiescent coolant regions by sedimentation, 1 % of this dust inventory is additionally assumed to be lifted-off in case of depressurizations where flow disturbances in these regions cannot explicitly be excluded. This value is at least a factor of 5 larger than observed in experiments with blower transients (AVR, CAGR), but has been chosen because of the inadequate knowledge about the liftoff effect of settled dust. The concentrations of long-lived nuclides are assumed to be equally distributed in the dust settled by sedimentation, whereas short-lived iodine isotopes are conservatively assumed to be completely sorbed in the mobilized dust fraction. Part of the adsorbable activity entering the gas purification system is sorbed on dust particles collected on filters. In safety analyses, 20 % of all adsorbable activities reaching the purification system is assumed to be dust-borne at the beginning of a depressurization accident. These inventories, whose absolute values also depend on the cleaning capacity of the particular purification system, are significant in depressurizations with rapid, reverse flow in the purification system (depressurization via a leak).

According to the SIEMENS prediction for the HTR-MODUL, flow dynamics are merely changed if a “reference leak” in the steam generator occurs except for the immediate vicinity of the leak. Therefore no additional activity liftoff will be expected in the area of

the steam generator. It is assumed, however, that in the course of a design basis accident 1 kg dust will be remobilized and released [40].

Japanese Contribution

In the safety evaluation for the HTTR, the liftoff fractions of fission products, which are released to the containment vessel during a depressurization accident caused by a large-scale pipe rupture, were determined on the basis of the experimental results [102] as a function of shear ratio as shown in Fig. 6-33. In this accident, it was evaluated that the liftoff fractions of I-131 and Cs-137 were 60 and 30 %, respectively [103].

US Contribution

GA has traditionally employed an **empirical shear ratio (SR)** model for correlating liftoff data. While there are many valid criticisms of this simplistic model, the currently available liftoff data do not appear to justify a more complicated one. For fully turbulent flow in a circular duct, it can be easily shown that the shear ratio, or the ratio of the wall shear stress during blowdown to the steady-state wall shear stress, is a simple function of the readily measured quantities of pressure, velocity, and temperature (e.g., [56]).

$$SR = \left(\frac{P_B}{P_N} \right)^{0.75} \left(\frac{V_B}{V_N} \right)^{1.75} \left(\frac{T_N}{T_B} \right)^{0.58} \quad (6-10)$$

where

SR is the shear ratio

P is the pressure

V is the velocity

T is the temperature [K]

and subscript "B" signifies blowdown conditions and subscript "N" signifies normal conditions.

GA has developed the **POLO** code [104] to calculate the integral fission product liftoff in the primary coolant circuit during a depressurization transient. POLO contains an empirical correlation which gives the fractional liftoff as a function of shear ratio. The initial plateout distribution is obtained from the PADLOC code, and the shear ratio distribution in the primary circuit as a function of time and space is obtained from a transient thermal/fluid dynamics code, such as RATSAM. POLO integrates the transient shear ratio distribution over the initial plateout distribution to predict the cumulative release from the primary circuit. (POLO also contains a simple washoff model for the analysis of wet depressurization transients.)

6.1.2.2.2. Single-Effects Data

Japanese Contribution

In Japan, the safety evaluation of a large-scale pipe rupture accident was required to confirm the potential safety features of an HTGR facility. When the guillotine rupture

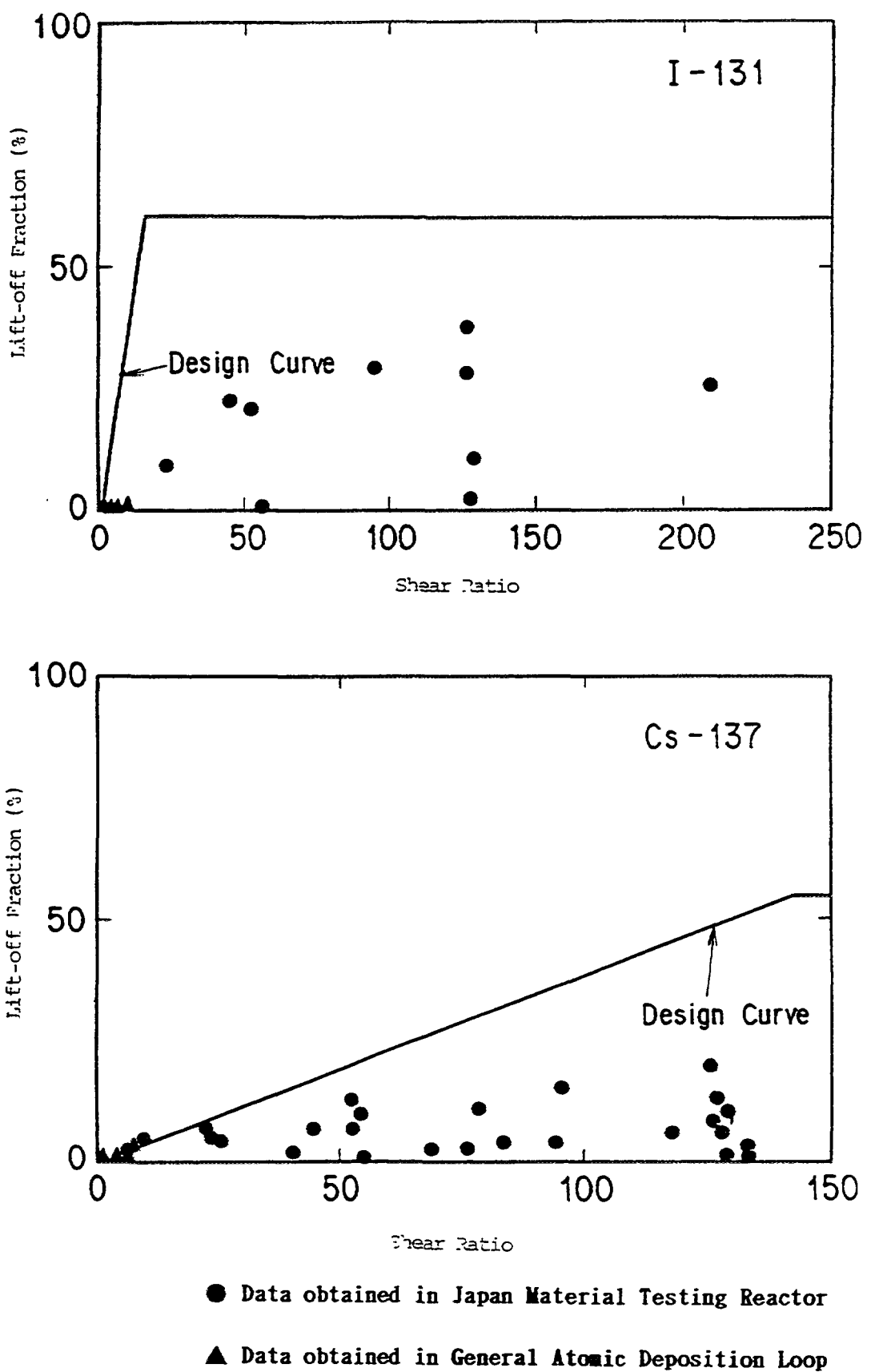


Fig. 6-33: Measurements of liftoff fractions as a function of shear ratio, from [102]

Table 6-21: Plateout conditions of test specimens

Materials	Stainless steel (SUS-316) Hastelloy-XR Incoloy-800
Temperature [°C]	
9th irradiation test	670
10th irradiation test	675°C
12th irradiation test	630 °C
Helium gas pressure [MPa]	3 MPa
Plateout duration [d]	
9th irradiation test	120 d
10th irradiation test	100 d
12th irradiation test	150 d
Helium gas velocity [m/s]	
9th irradiation test	60 m/s
10th irradiation test	50 m/s
12th irradiation test	50 m/s

of the co-axial double pipe of High Temperature Engineering Test Reactor (HTTR) is assumed, for example, the maximum gas velocity and shear ratio exceeds 800 m/s and 100, respectively. In order to investigate the behavior of fission products under the conditions of a rapid depressurization caused by large-scale pipe rupture, blow down, wipe off, and leaching tests were carried out [105].

In the **blow down test**, helium gas at high speed was blown on the surface of test specimens, on which fission products were plated out, to simulate the flow conditions during a large-scale pipe rupture accident. In the **wipe off test**, test specimens were directly wiped off by cloth to remove the fission products from the test specimen surface by mechanical force. The **leaching test** was divided into two types; water washing test and chemical leaching test. In the water washing test, test specimens were washed by hot water to obtain the fraction of fission products plated out on the surface which were not removed by dry depressurization. Fission products borne on dust particles adhering on the surface of the test specimen, were also removed by the water washing method if dust particles were present. In the chemical leaching test, test specimens were leached to determine the fraction of fission products contained in the oxide film of the test specimen surface. In these tests, in order to simulate plateout conditions of the primary cooling system of HTGRs, test specimens were prepared in OGL-1 installed in the Japan Materials Testing Reactor. Plateout conditions of the test specimens are summarized in Table 6-21.

The liftoff fractions obtained by the blow down test are shown in Fig. 6-34 as a function of the shear ratio, which is defined as the ratio of wall shear stress in the

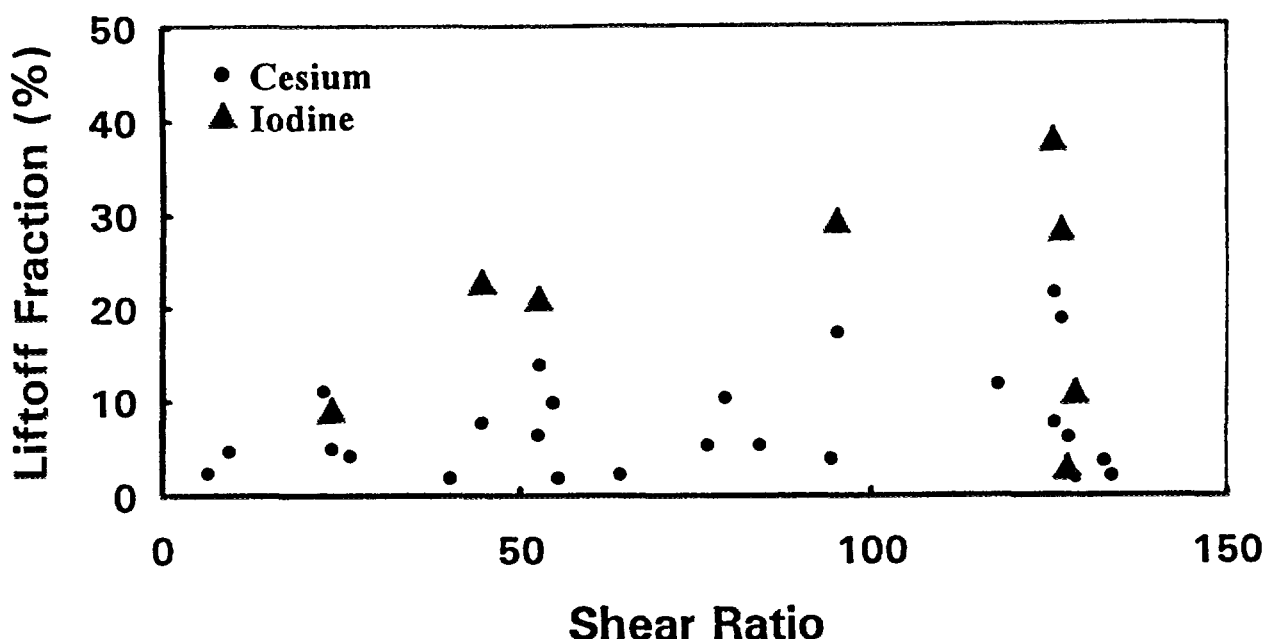


Fig. 6-34: Liftoff fractions in blowdown test

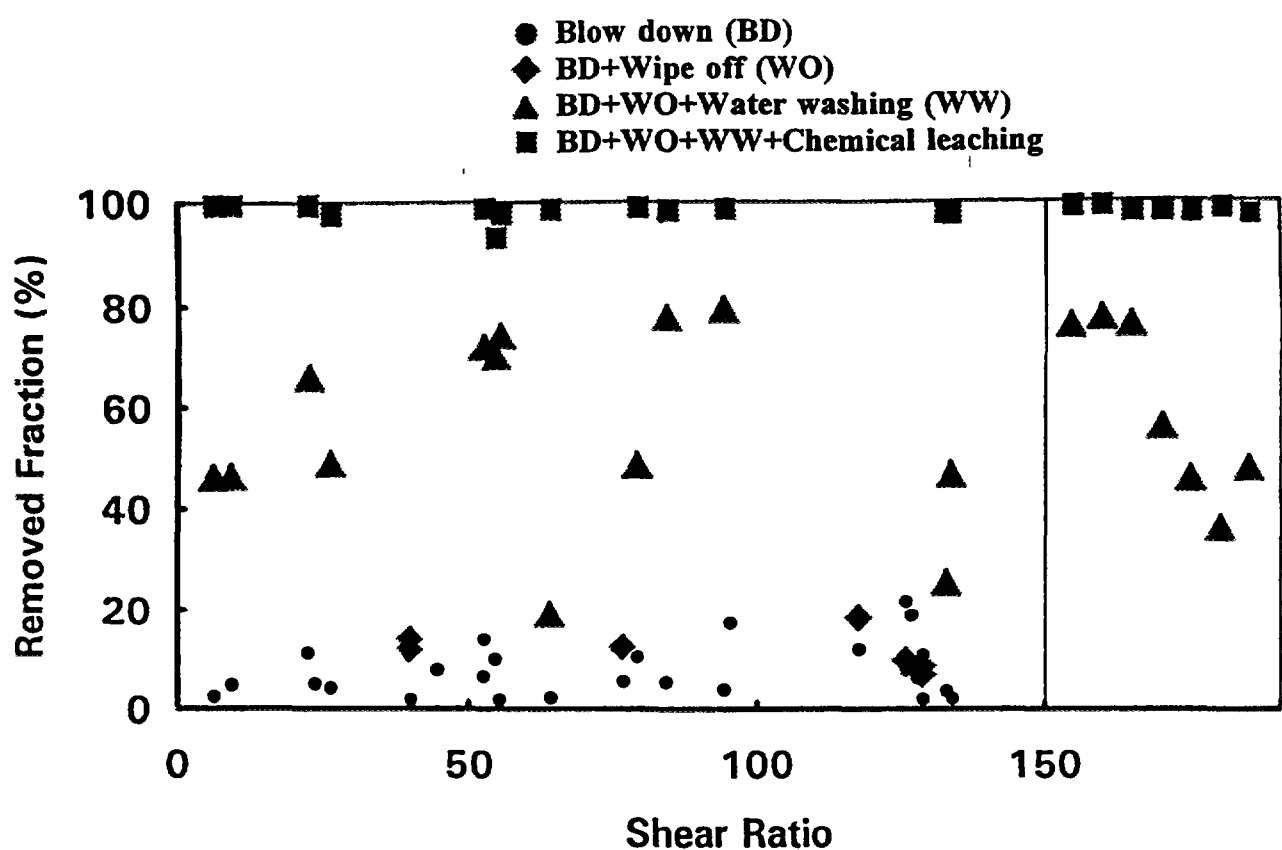


Fig. 6-35: Summary of test results

blow down to the normal condition. The result of wipe off, water washing, and chemical leaching tests for cesium are shown in Fig. 6-35 together with the blow down test result. The following conclusions were derived from the test results.

1. The difference of liftoff fractions between iodine and cesium was observed. It is caused by not only by the difference in their desorption properties but also by the difference in plateout mechanisms. Therefore, in the case of a depressurization caused by large-scale pipe rupture, the liftoff fractions should be estimated not only by equilibrium sorption on the metal surface but also by accounting for mechanical phenomena such as breakup of the oxide film microstructure on the surface of materials.
2. Though the liftoff fraction increases with the shear ratio up to 130, data are largely scattered. Therefore, it is difficult to affirm that the shear ratio is the main parameter to describe the liftoff fraction in the region of large shear ratios.
3. Under dry depressurization conditions, the plated out fission products are not completely removed, and the liftoff fractions decrease with increasing migration of fission products into the oxide film.

From the results described above, it could be concluded that even in a large-scale pipe rupture accident, plated out fission products would not be completely removed from the metal surfaces, and the liftoff of dust particles [106] is still as important as in a small-scale pipe rupture accident.

US Contribution

The current liftoff data base is composed of results from four experiments: (1) the GA In-Pile Loop (GAIL IV), (2) The GA Deposition Loop Program, (3) The CPL-2 test program and (4) the blowdown tests with Peach Bottom steam generator tube samples. The first two tests were performed at GA, the CPL-2 tests were performed in France as part of the GA/CEA Accord, and the blowdown tests with Peach Bottom tube samples were performed by the same CEA researchers under separate contract with GA.

Blowdown tests fall into two distinct categories: *ex-situ* and *in-situ* blowdown tests. In *ex-situ* tests, fission products are first plated out on a test specimen, the specimen is then removed from the test apparatus by destructive means and reinstalled in a blowdown apparatus for blowdown testing. In contrast, in *in-situ* testing, the test specimen is blown down in place without removal from the plateout apparatus. A summary of the liftoff data base from the four experimental programs is given in Reference [107].

GAIL IV Results

Specimens of piping taken from the GAIL IV in-pile loop were blown down *ex-situ*, and the fractional fission product reentrainment was correlated as a function of shear ratio. The GAIL IV loop contained a full flow filter, which removed some circulating particulate matter and, possibly, caused the liftoff measurements to be biased low. In summary, the degree of liftoff increased in an approximate linear fashion with increase in shear ratio. About 48 % of Ce-144, 28 % of Sr-90 and 3 % of Cs-137 were retrained at a maximum shear ratio of 7.5. This is an indication that Cs-137 is more tightly held at the surface.

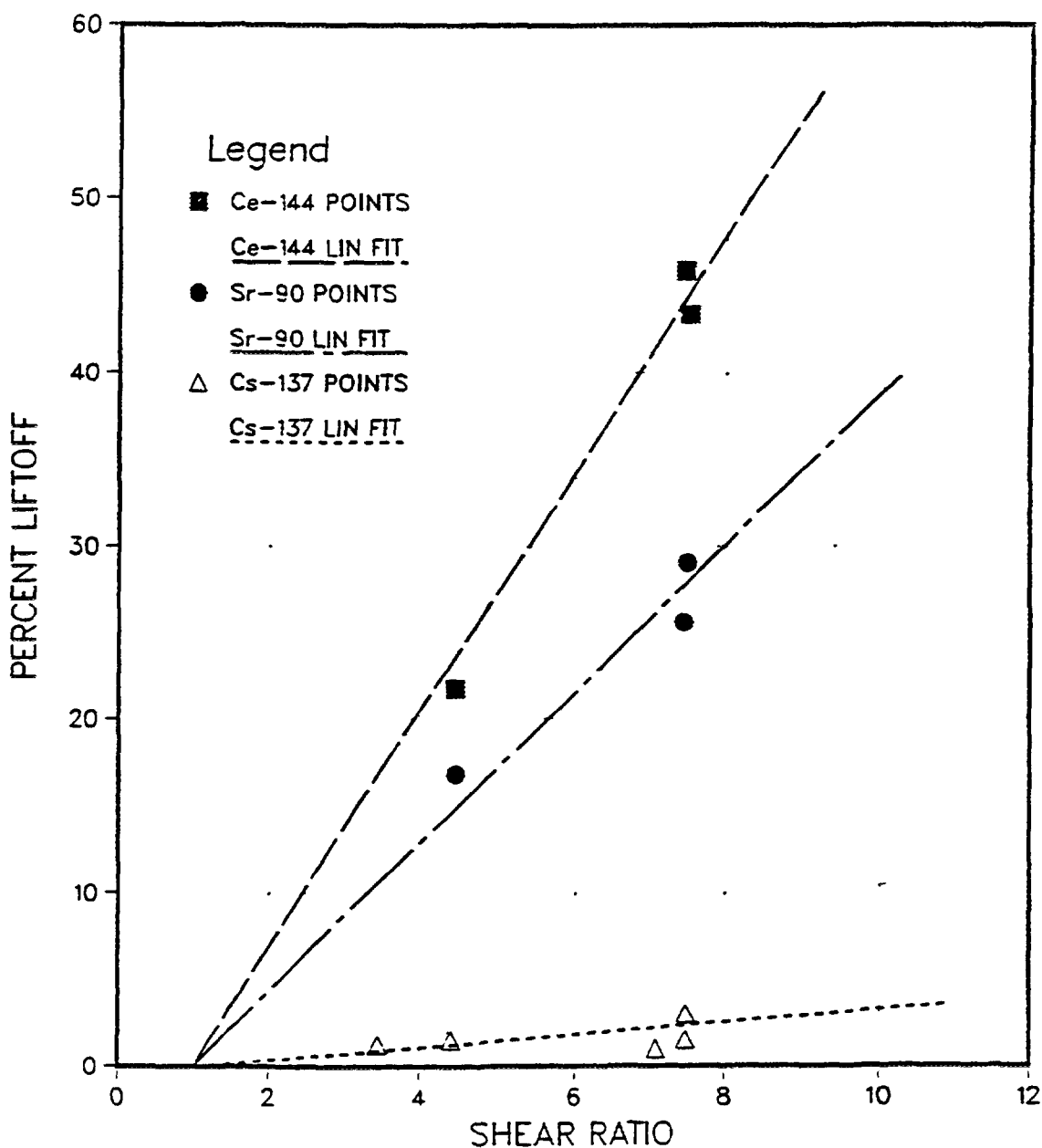


Fig. 6-36: Composite GAIL IV liftoff results [56]

Iodine data was not obtained because the iodine had decayed away prior to the tests. These tests were conducted *ex-situ* with the attendant uncertainties associated with that method. The results are shown in Fig. 6-36.

GA Deposition Loop Results

The GA deposition loop tests [51] were conducted to both confirm and extend the data base obtained from GAIL IV tests. The deposition loop tests were designed to simulate

conditions in the evaporator-economizer section of the steam generator of a HTGR. The fission product source was graphite powder impregnated with radioactively tagged cesium or strontium or tagged PdI_2 crystals encapsulated in porous graphite crucibles. Upon heating in the loop, evaporation of the nuclides from the tagged source represented a realistic fission product source. After plateout, the tube samples were destructively removed and were blown down in the same apparatus as used in the GAIL IV blowdown tests.

Figure 6-37 shows the Cs-137 and I-131 liftoff data from GA Deposition Loop tests. Since the maximum shear ratio during a design basis depressurization accident is < 1.1 , these data imply very modest liftoff. However, in separate strontium tests, a quantity of graphite dust was also deliberately added, resulting in increased fractional liftoff and significantly increased data scatter. These data are questionable because of the *ex-situ* blowdown technique and the uncertainties introduced by out-of-pile deposition tests.

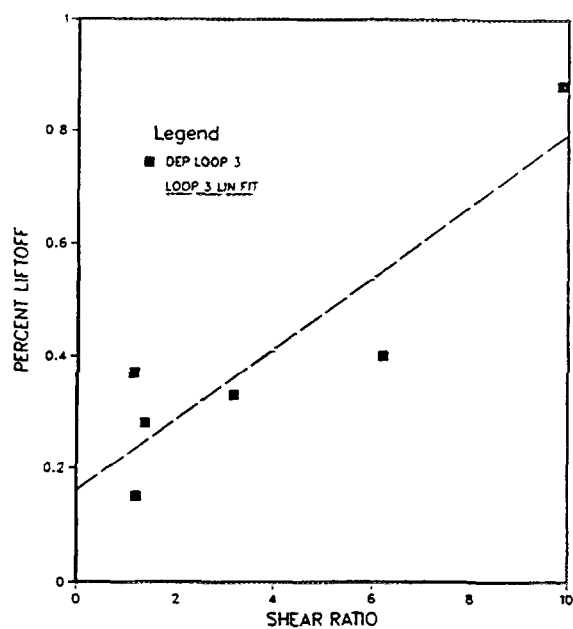
CPL-2 Test Program Results

The CPL-2 *ex-situ* blowdown tests examined the effects of shear ratio, temperature, humidity and surface condition on liftoff of various fission products from tube specimens cut from the heat exchangers of each of the four loops [107]. Excessive scatter in the data prevented any definitive conclusions. Significant liftoff was observed at shear ratios less than unity, which indicates that the test specimens had been compromised, e.g., by the dislodging of deposited particulate matter and the spallation of friable surface films by the vibration associated with loop disassembly, tube cutting, and exposure to ambient air.

Peach Bottom Steam Generator Tube Samples

The Peach Bottom steam generator tubes were subjected to *ex-situ* blowdown tests by the same CEA researchers that performed the CPL-2 tests. The results [87] indicated liftoff is independent of water content in the helium and of temperature from 30 to 400 °C. Both Alloy 800 and carbon steel tube specimens were blown down. Alloy 800 results showed less scatter, probably due to the higher oxidation resistance of this material resulting in a more coherent surface film; typical results are shown in Fig. 6-38. The only unequivocal conclusion that could be drawn was that liftoff increased with increasing shear ratio.

I-131 LIFTOFF FOR DEPOSITION LOOP NUMBER 3



Cs-137 LIFTOFF FOR DEPOSITION LOOP NUMBER 4

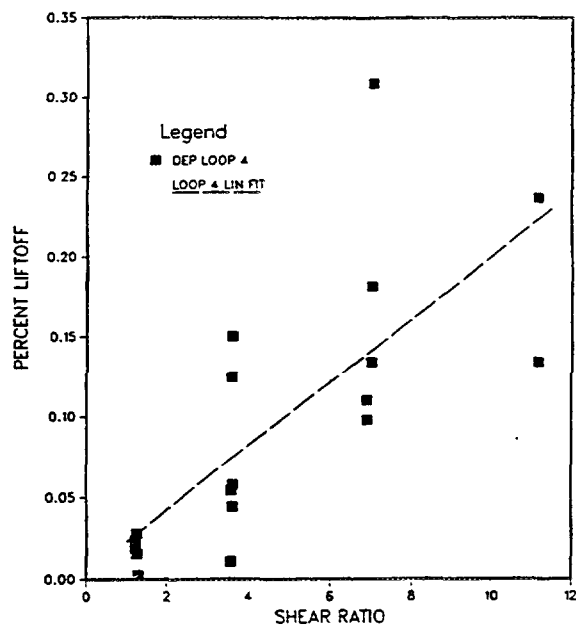


Fig. 6-37: Liftoff results from GA deposition loop program [56]

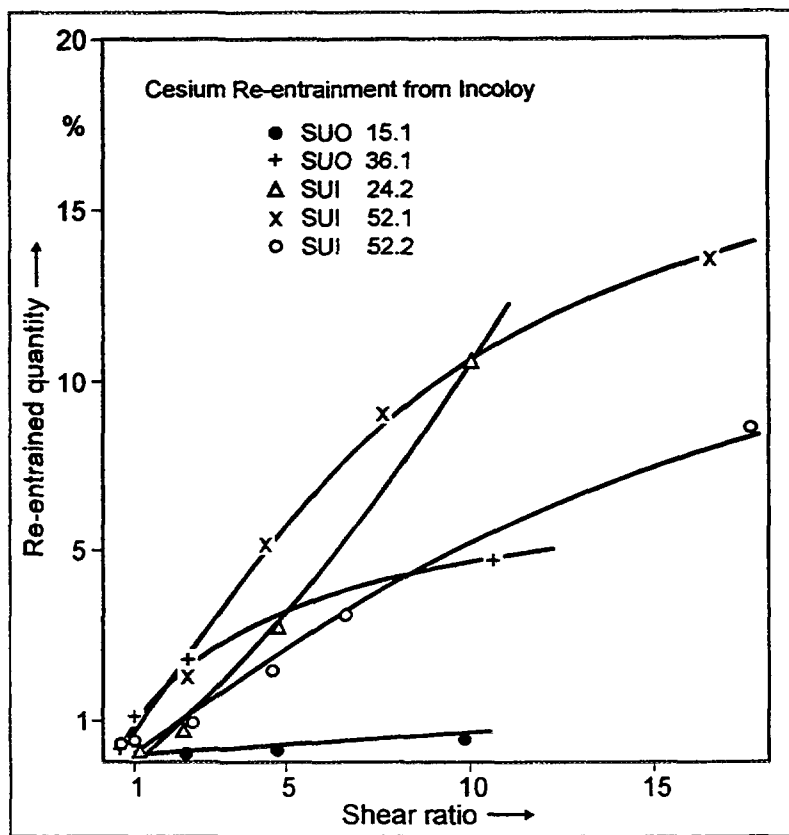


Fig. 6-38: *Ex-situ* blowdown results for Peach Bottom steam generator tube samples [87]

6.1.2.2.3. Integral Data

FRG Contribution

Blower transient tests have been conducted at the AVR reactor within the experimental program HTA-14 to investigate remobilization of deposited dust [99]. Not until these tests were conducted, was a sufficient amount of dust obtained that allowed further examination, i.e., the determination of a particle size distribution. All transient tests were done in the shutdown reactor with an isothermal core temperature of ≈ 110 °C. Sudden changes in coolant flow which increased the shear forces acting upon the deposited dust particles were caused by a variation of the blower speed. It was increased from 1500 up to about 4000 rev/min at a rate of about 40 (rev/min)/s and then kept constant until a stationary state was reached. The installations of both the dust experiment and VAMPYR-I and the cold gas filter operated at a constant flow rate, were used to simultaneously collect the remobilized dust. A detailed schematic of the dust filter as used in the VAMPYR-I facility is given in Fig. 6-39. In the dust experiment, continuous γ -measurements were made to examine the transient dust deposition behavior.

Measured dust concentrations in the coolant are shown in Fig. 6-40 indicating a decay behavior after a sharp increase by several orders of magnitude. Results of fission product activities found in the dust and dust masses collected are listed in the Tables 6-22 and 6-23. Further details of the tests are given in Table 6-24. The maximum dust concentrations were found to be 3 orders of magnitude higher compared to those under steady-state flow conditions. A particle size distribution analysis of samples taken under transient or steady-state conditions revealed that the size distribution is independent of location and flow speed. In all cases, the maximum of the particle size distribution curve is around 1 μm [99].

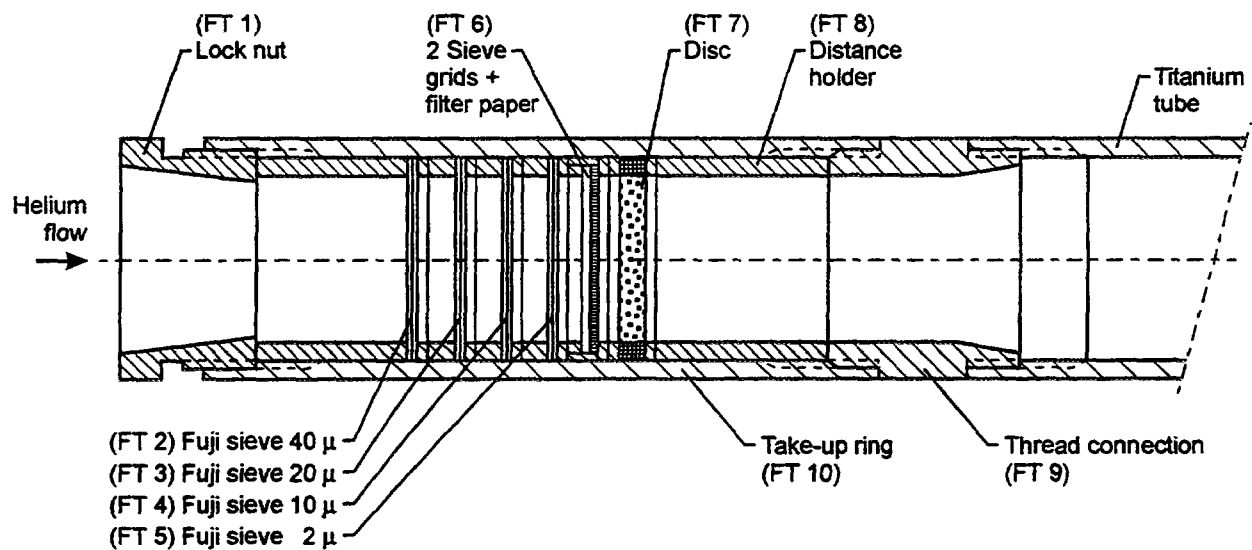


Fig. 6-39: Schematic of the dust filter preceding the VAMPYR-I test tube in the transient tests (see also Fig. 6-12)

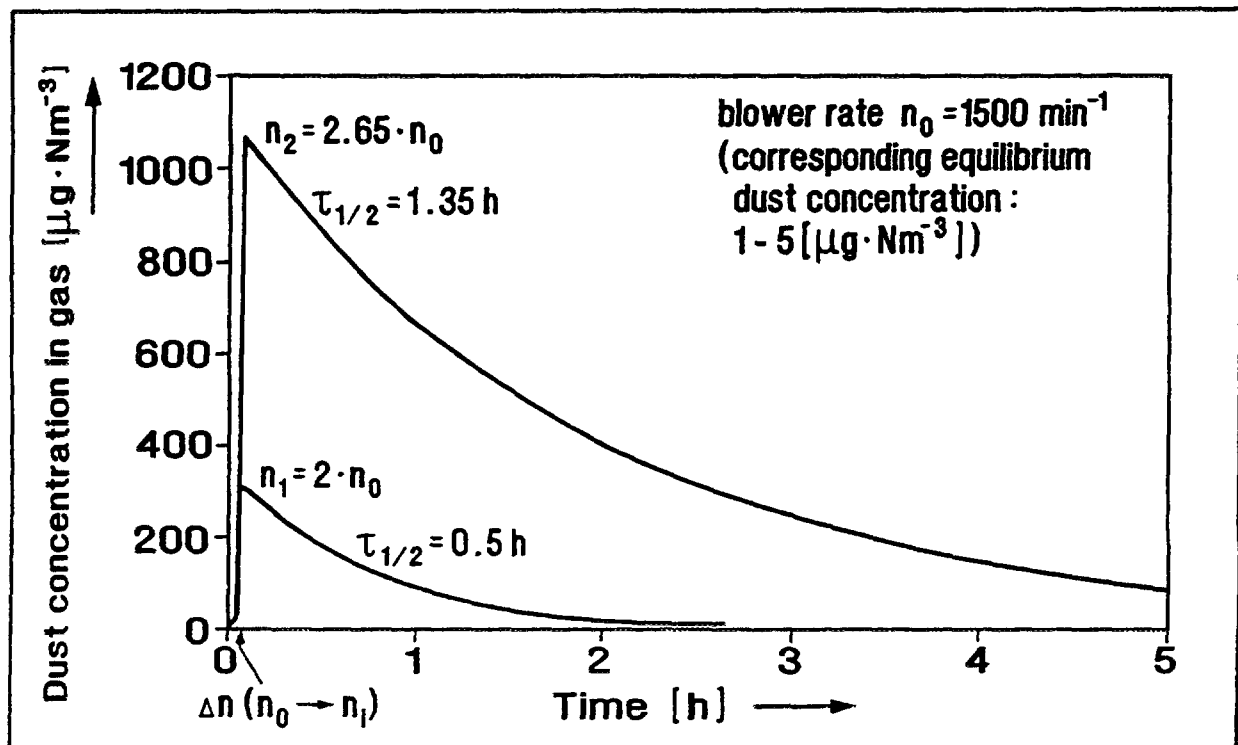


Fig. 6-40: Influence of blower speed variation on dust concentration in AVR coolant, from [99].

Table 6-22: Fission product activities on dust samples from different positions (see Fig. 6-39), from [108, 109, 110].

Position	Dust mass [mg]	Cs-137		Ag-110m		I-131	
		[Bq]	[%] ⁽¹⁾	[Bq]	[%] ⁽¹⁾	[Bq]	[%] ⁽¹⁾
<i>Transient Test T2 (VAMPYR-I, V41) [108]</i>							
FT1	69.0						
FT2	28.7	8.81×10^4	8.2	3.10×10^4	7.2		
FT3	5.9	1.73×10^5	16.2	6.94×10^4	16.2		
FT4	2.7	2.18×10^5	20.4	9.37×10^4	21.8		
FT5	3.6	2.60×10^5	24.3	1.06×10^5	24.6		
FT6	3.5	3.16×10^5	29.6	1.24×10^5	28.8		
FT7	1.0	1.36×10^4	1.3	5.80×10^3	1.4		
FT8-10	12.2						
<i>Transient Test T4 (VAMPYR-I, V44) [109]</i>							
FT1	2.6						
FT2	4.1	1.49×10^5	22.9	4.54×10^4	23.2		
FT3	2.4	1.47×10^5	22.5	4.43×10^4	22.6		
FT4	2.7	1.48×10^5	22.7	4.65×10^4	23.7		
FT5	1.8	1.07×10^5	16.4	3.34×10^4	17.0	6.52×10^3	100
FT6	1.4	7.83×10^4	12.0	2.00×10^4	10.2		
FT7	1.8	2.31×10^4	3.5	6.55×10^3	3.3		
FT8-10	12.2						
<i>Transient Test T5 (VAMPYR-I, V46) [110]</i>							
FT1	19.1						
FT2	4.9	1.89×10^5	19.1	4.54×10^4	19.3		
FT3	2.6	1.94×10^5	19.6	4.59×10^4	19.5		
FT4	3.9	2.46×10^5	24.8	5.73×10^4	24.3	6.08×10^3	86.8
FT5	2.5	1.91×10^5	19.3	4.51×10^4	19.1		
FT6	1.4	1.39×10^5	14.0	3.36×10^4	14.3	4.65×10^2	6.6
FT7	1.1	3.24×10^4	3.2	8.20×10^3	3.5	4.58×10^2	6.6
FT8-10	16.0						

(1) normalized to the sum of activities of FT2 - FT7, others' contributions are considered insignificant.

Table 6-23: Dust activity measurements of the AVR transient tests, from [111].

Nuclide	Activity [MBq/g]								
	T1	T2-1	T2-2	T3-1	T3-2	T4-1	T4-2	T5-1	T5-2
Cs-134	16.24	36.48	37.09	24.58	30.98	24.32	27.76	16.25	16.99
Cs-137	62.57	94.77	90.71	55.41	73.92	82.04	96.03	75.20	78.94
Ag-110m	22.24	38.75	36.78	33.67	43.28	25.04	28.86	15.73	16.47
I-131	-	2.50	2.67	1.30	1.53	-	-	-	-
Co-60	4.29	6.27	5.97	7.39	7.96	5.86	6.72	5.76	5.81

- : below detection limit

Table 6-24: Operating Conditions and activity measurements of the AVR transient tests, from a.o. [108, 109, 110].

Run	Time [h]	blower speed increase [rev/min]	AVR power [MW] / gas outlet t [g C]	Gas flow [Nm ³ /s]	Material	Dust collected [mg]
T1 (V39)	24	2000 - 4050	45 / 850	17.1	Ti, 4541	163
T2 (V41)	1.5	2000 - 4000	45 / 950-890	17.1	Ti, 4541	127
T3			22 / 950			
T4 (V44)	11.5		45 / 880-860	16	Ti	29
T5 (V46)	12.5	1500 - 4000	42 / 810	16	Ti	52

Japanese Contribution

Description of Japanese *ex-situ* blowdown tests using test specimens from the OGL-1 loop [102, 112]; as shown in Fig. 6-41, these tests are of particular significance because they include test results for very high shear ratios (> 100) since they were intended for use in analyzing a postulated guillotine failure of the HTTR crossduct.

US Contribution

CPL-2/4 Loop Blowdown Test

In the *in-situ* blowdown test of the CPL 2/4 in-pile loop, $< 0.5\%$ liftoff of the plateout activity resulted [107]. This *in-situ* loop blowdown was an integral test and, therefore, was intended to be a model validation test. However, the CPL 2/4 loop was shown to contain relatively high concentrations of a metallic oxide aerosol resulting from the spallation of friable surface films; these surface films developed during the irradiation as a result of corrosion of the heat-exchanger tubes by a residue of a sulfur-containing die lubricant that was not properly removed during loop fabrication. The implication is that these CPL 2/4 *in-situ* blowdown results are also biased high.

COMEDIE BD-1 Blowdown Tests

As discussed in Section 6.1.1.3.2., four *in-situ* blowdown tests were performed at the end of the 62-day irradiation at successively higher shear ratios of 0.72, 1.7, 2.8, and 5.6; these different shear ratios were imposed by varying the blower speed and maintaining it at a constant level for 2 minutes. A rapid depressurization from 60 bar to 6 bar was then effected after each of the four holding periods. In each blowdown test, the reentrained activity was trapped by a dedicated full-flow filter. The measured cumulative liftoff fractions are summarized in Table 6-25.

From inspection of the table, it is apparent that fractional liftoff in the COMEDIE BD-1 was quite low. The I-131 liftoff data are different from all the other radionuclide in that 60 % of the total reentrained iodine activity occurred during the first blowdown at a SR = 0.72. As discussed in Section 6.1.2.1.3., this behavior is likely due to chemical desorption during prolonged thermal conditioning of the loop with electrical heaters prior to performing the first blowdown; in any case, the total I-131 reentrained during the four blowdowns was $< 1\%$ of the total I-131 plateout inventory in the loop.

6.1.2.3. Removal by Liquid Water ("Washoff")

6.1.2.3.1. Physical Models and Computer Codes

FRG Contribution

A simple approach was adopted at the Research Center Jülich for an estimation of **iodine desorption** from steam generator surfaces under the influence of moisture [113]. Starting from an equilibrium state disturbed by the presence of moisture, the temporal

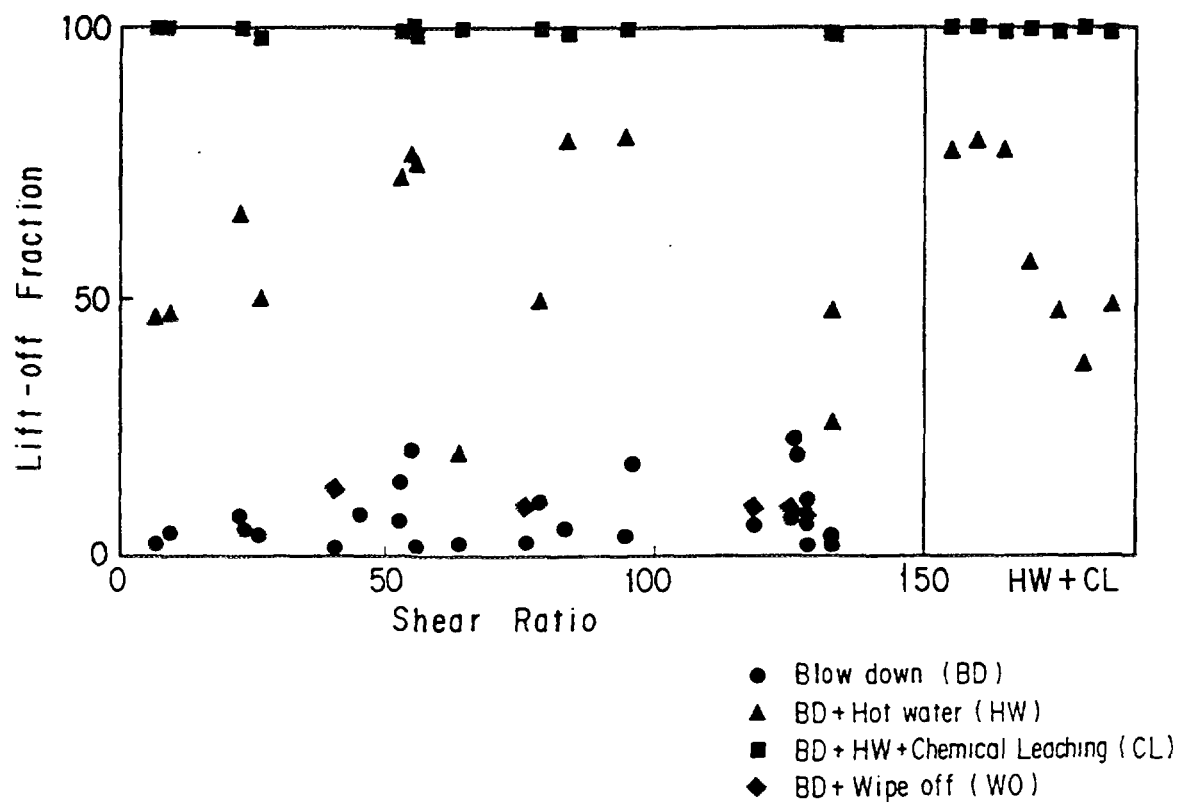
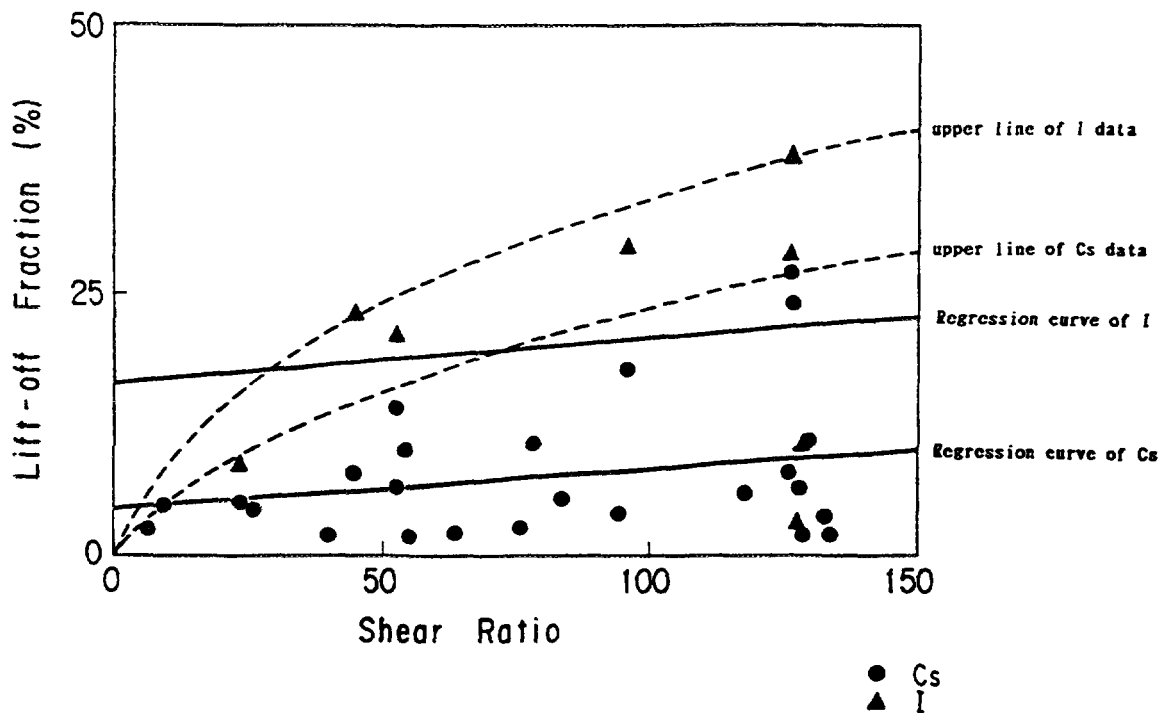


Fig. 6-41: Results of JAERI liftoff tests [112]

Table 6-25: COMEDIE BD-1 liftoff fractions [89]

Nuclide	Measured cumulative liftoff fractions			
	SR = 0.7	SR = 1.7	SR = 2.8	SR = 5.6
I-131	7.7×10^{-4}	1.0×10^{-3}	1.1×10^{-3}	1.3×10^{-3}
Cs-137	1.4×10^{-4}	2.1×10^{-4}	3.0×10^{-4}	1.1×10^{-3}
Cs-134	1.5×10^{-4}	2.0×10^{-4}	2.8×10^{-4}	9.6×10^{-4}
Ag-110m	1.5×10^{-4}	1.9×10^{-4}	4.3×10^{-4}	2.3×10^{-3}
Sr-89	3.9×10^{-4}	8.7×10^{-4}	1.4×10^{-3}	1.8×10^{-3}
Sr-90	1.6×10^{-3}	3.6×10^{-3}	5.6×10^{-3}	7.4×10^{-3}
Te-132	4.7×10^{-6}	6.3×10^{-6}	9.3×10^{-6}	4.2×10^{-5}
Ba-140	5.7×10^{-4}	1.8×10^{-3}	3.4×10^{-3}	4.1×10^{-3}

change of plated out activity is given by

$$\frac{dA}{dt} = -\lambda A - K(T(t)) A \quad (6-11)$$

where

A is the plateout activity before moisture ingress [Ci]

K is the iodine desorption coefficient [s^{-1}]

λ is the decay constant [s^{-1}]

T is the temperature [K]

t is the time [s]

It is assumed that the reactor has been shut down and that the desorption process is independent of the iodine concentration on the surfaces. The accumulated iodine activity desorbed is

$$A_{des}(t) = \int_0^t K(T(t')) A(t') dt' \quad (6-12)$$

with the solution

$$A_{des}(t) = A(0) \frac{K}{\lambda + K} [1 - \exp\{-(\lambda + K)t\}] \quad (6-13)$$

The data of an experiment conducted at ORNL [114] were taken to derive the desorption constant of iodine as function of temperature. In these tests, iron powder loaded with I-131 and exposed to a helium flow was heated up from 200 to 600 °C and the iodine left was measured. Parameters varied were the addition of moisture to the helium (3 % H₂O in run #2 and #3) and an increase of the flow rate (2.2 l/min in run #1, 2.4 l/min in run #2, 4.3 l/min in run #3). The only adequate data for the desorption coefficient derived for iodine are for the case of no moisture:

$$K(T) = F/F_o \cdot 68.13 \exp\{-20,910/(RT)\} \quad (6-14)$$

and for the cases of 3 % moisture content

$$K(T) = F/F_o \cdot 0.0332 \exp\{-8,022/(RT)\} \quad (6-15)$$

where

F/F_o is a factor depending on mass flow, $F_o = F(1 \text{ l/min})$

R is the gas constant [cal/(mole K)], R = 1.987

T is the temperature [K]

Thermochemical equilibrium considerations indicate that leaching with liquid water nearly quantitatively dissolves cesium and strontium which has deposited on metallic/oxidic surfaces (washoff). Cesium plateout data given in [19, 115] ($\Delta H_{des} = 234 \text{ kJ/mol}$) lead to the following equilibrium for chemisorption in the sub-monolayer regime on Incoloy 800H in presence of liquid water:



with the equilibrium constant

$$\begin{aligned} K &= [CsOH] \sqrt{p_{H_2}^o} \\ &= \frac{\sigma}{\sigma_o} \exp\left[\frac{5410}{T} + 3.62\right] \end{aligned} \quad (6-17)$$

where

... expresses an adsorptive bonding

[] is the molality [mol/kg_{solution}]

σ / σ_o is the fractional coverage of geometrical surface with cesium

The cesium washoff reaction is slightly exothermic (-45 kJ/mol). This is not necessarily true for silver because of its noble character. The sorption of silver on metals has sorption enthalpies similar to the sublimation enthalpy of the element (270 kJ/mol), which

suggests that silver sorption is more like a physi-sorption; i.e., its elemental character probably remains unchanged. Measurements of silver leaching indicate that about 1 % of the deposited amount is dissolved. Nevertheless, a silver dissolution of 10 % is conservatively assumed in safety analyses. A total dissolution is postulated for iodine because of its comparably low sorption enthalpy and its complex chemical behavior in a liquid solution.

Leaching experiments in the temperature range 25 - 90 °C have indicated that there is a kinetic hindrance of dissolution with time constants of some minutes [19, 115, 116]. Similar to the behavior in graphite, this may be caused by the slow transport of water into the pore system of oxide surface layers. This kinetic hindrance is not taken into consideration in safety analyses, because of much higher water temperatures in accidents compared to those in the experiments and because of the poor knowledge with respect to the actual distribution of sorbed fission products within the oxide layer and metal.

Besides dissolution and chemical attack of liquid water on sorbed fission products, mechanical effects (erosion) due to a high speed water jet from a tube rupture must also be taken into consideration. The directly impacted surface (some m²) is conservatively assumed to be completely decontaminated.

The fission product content of liquid water is expected to be released mainly by (fast) evaporation of the water (bubbling and droplet formation), followed by volatilization of the residue after complete water evaporation and transport of the gas-borne activity into the environment. In addition, an equilibrium partition of fission product between steam and liquid water is assumed which is influenced by solubilities in steam [117]. In the German HTGR safety analyses, it has been conservatively postulated so far that the dissolved fission products are transferred into the gas phase proportional to the degree of water evaporation. There is some evidence, however, that this might be a significant overprediction [118], at least for metallic fission products. High gas flow rates with significant water suspension within the gas may have the same effect as evaporation.

In addition, leaching with water removes only on the order of ten percent of the plated-out cesium [5, 7, 19], especially in the high-temperature deposition area. Plateout of cesium sometimes shows a remarkably small dependence on temperature which has often been explained by (temperature independent) absorption. It is an effect visible at a relatively high temperature level where desorption is high and the absolute amount of sorbed fission products low.

In many cases, however, mass transfer may have diminished the temperature dependence. Simple absorption or penetration mechanisms are in conflict with the following fact: at deposition temperatures > 400 °C, the water leach yield does not show a clear temperature dependence. If adsorption decreases in favor of absorption with increasing temperatures, as assumed in simple absorption models, a remarkable decrease of the leach yield must be expected. In addition, diffusion profiles have been measured also at low temperatures (< 150 °C) and were found both in mass transfer controlled plateout regions and in ad-/desorption controlled regions, the latter sometimes showing no significant deviations from simple ad-/desorption profiles. This might be explained by cesium diffusion along the inner oxide surfaces/grain boundaries with a rate which is fast compared to the rate constants of cesium desorption into the gas phase. From a physical point of view this is

Table 6-26: H₂O leach fractions for cesium and iodine in the LAMINAR tests, from [19, 60]

Cs-134		I-131	
Run	H ₂ O leach fraction	Run	H ₂ O leach fraction
1	0.48 - 0.64	III.3	0.85
2	0.40 - 0.54	III.4	0.878
3	0.19 - 0.22	III.5	0.864
4	0.38 - 0.41	III.6	0.31
5	0.22 - 0.40	III.7	0.779
6B	0.01 - 0.04		
7	0.41		
9	0.03 - 0.05		
10	0.40 - 0.64		

possible, because in surface diffusion, cesium atoms do not completely leave the attraction range of the surface and the corresponding activation energies of diffusion are much smaller than desorption energies. This explanation is compatible with the low leach yield, because penetration of water into the oxide layer micropore system is strongly impeded.

US Contribution

The US has few data on water induced removal of fission products adsorbed on the primary circuit alloys. The removal of adsorbed cesium, based on limited data, is estimated to be 50 % of the sorbed cesium. The same factor is assumed to apply to all other fission products in the absence of supporting data [119].

6.1.2.3.2. Single-Effects Data

FRG Contribution

The activity leached by H₂O, i.e., the activity that is accessible and dissolved in the water, is considered representative for the adsorptive fraction of the total surface activity. Leach tests were conducted with 80 °C demineralized water for 15 - 50 h from both cesium and iodine deposition experiments in the **HRB loop LAMINAR**. The results are summarized in Table 6-26. The small leach fraction found for Cs-134 is explained by the injection of 5 Pa CO into the helium loop which caused a more compact oxide layer of 4 - 6 μm thickness leading to a better inclusion of the activity [120].

Tube specimens from the iodine plateout experiments in LAMINAR were leached with an alkaline water solution of 25 °C. Leach time in run III.5 was twice as long as in run III.3. The figures indicate that a fraction of about 15 % of the final deposition is probably not bound by adsorption [60].

Samples of titanium and steel from VAMPYR test tubes were also taken to apply the H₂O leach procedure. Results are given in Figs. 6-42 and 6-43 [72], where the decontamination factor, i.e., the fraction as a percent of the Cs-137 activity leached by the water, is given as function of leach time and of deposition temperature, respectively. The shape of the curve in Fig. 6-42 gives evidence that only a certain, the adsorptive, fraction of the cesium is removed from the surface by the water treatment. The last data point indicates another significant fraction of cesium vanishing with the complete removal of the oxide layer by chemical treatment. Long term leaching of steel and titanium tube samples with 80 °C water is shown in Fig. 6-43. The distinct jump between steel and Ti data indicates differences in the adsorption capacity of both materials for Cs-137.

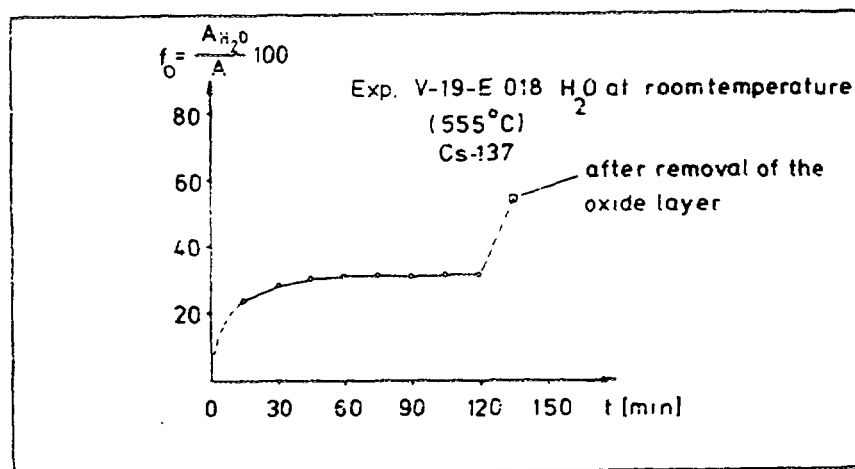


Fig. 6-42: Decontamination factor of Cs-137 deposited on ferritic steel at 550 °C in test run V19 as a function of the duration of water treatment, from [72]

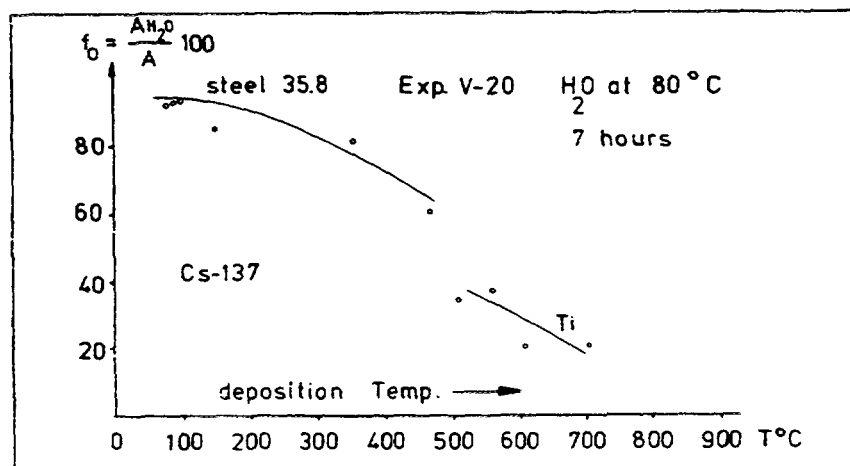


Fig. 6-43: Decontamination factor of Cs-137 deposited on ferritic steel and titanium in test run V20 as a function of the deposition temperature, from [72]

US Contribution

As part of the GA/CEA Accord in the 1970s, Puccini performed a number of leaching experiments with contaminated heat-exchanger tube specimens from the four CPL-2 loops using various solvents including water and mineral acids [121]. While the primary purpose of his work was to estimate fission product penetration profiles into the base, his data may be of interest in estimating washoff fractions as well.

A series of washoff tests in a high-pressure autoclave was initiated at ORNL in the late 1980s. Preliminary results for iodine were obtained in the temperature range of 250 to 300 °C which indicated ≈ 60 % washoff [122]. Additional iodine and cesium washoff experiments were planned; unfortunately, the test program was abruptly canceled, so little actual data were generated by this promising program.

While there have been few direct measurements of the "washoff" characteristics of key radionuclides deposited on HTGR primary circuit metals, the considerable LWR data on the behavior of fission products in steam-water systems should be largely relevant to HTGRs (e.g., [123]). In particular, the data and correlations for the partitioning of key radionuclides, including iodine, between the vapor and liquid phases in steam-water mixtures appear to be applicable to HTGRs.

6.1.2.3.3. Integral Data

There are no integral measurements of fission product washoff during steam ingress accidents which are presently available to the US program. LWR data on the behavior of fission products in steam-water systems may be relevant to HTGRs (e.g., [123]).

6.1.2.4. Steam-Induced Vaporization ("Steamoff")

6.1.2.4.1. Physical Models and Computer Codes

FRG Contribution

There are few experimental data available on removal of chemisorbed fission products from metals by an attack of steam (steamoff) or air. In addition, the data scatter is remarkably high. Fig. 6-44 shows two sets of steamoff rate measurements for cesium plated out on HTGR relevant metals. Differences in the data are four orders of magnitude and more.

Thermochemical estimations lead to the following equilibrium relationship for cesium steamoff on Incoloy 800H:



with the equilibrium constant

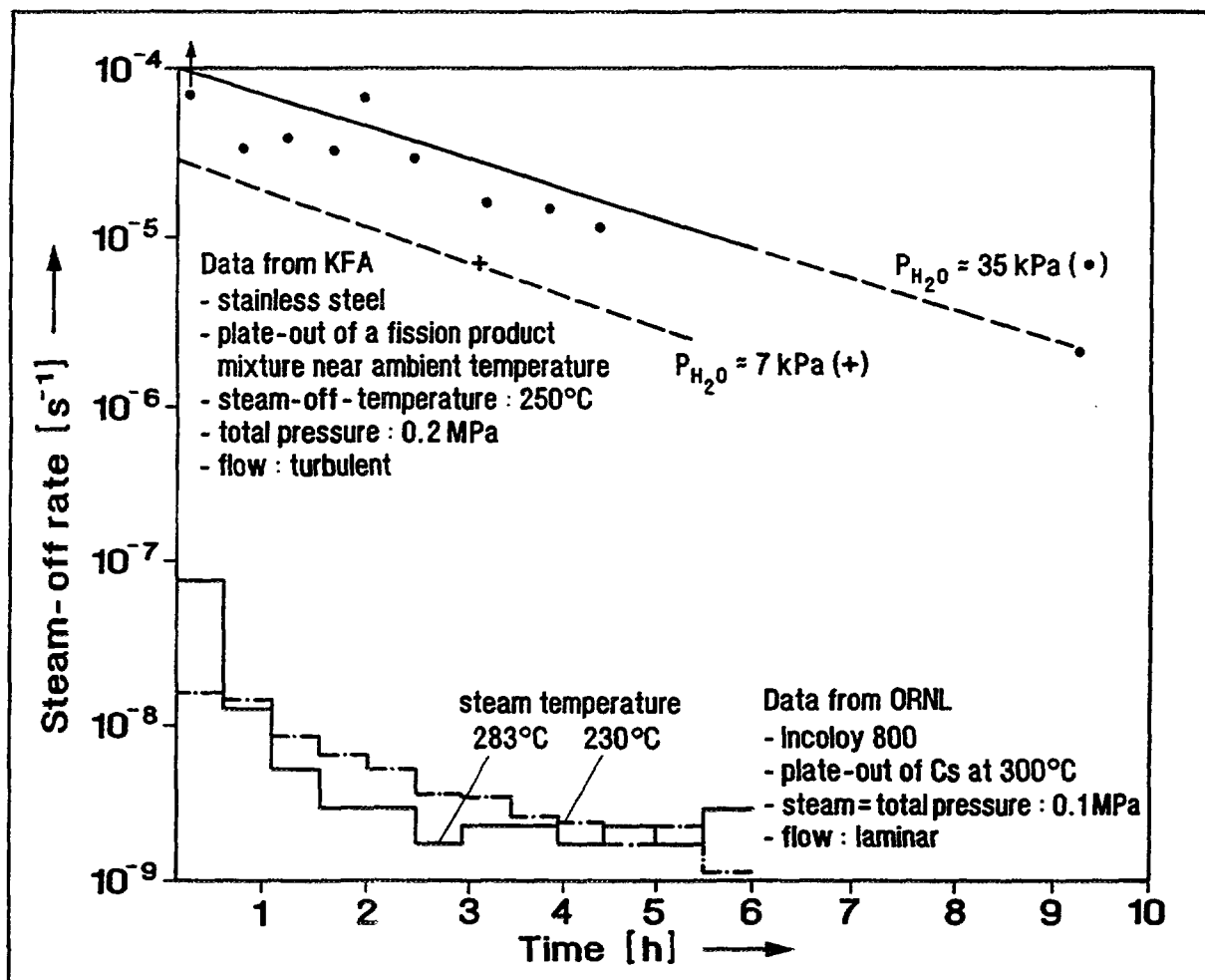


Fig. 6-44: Steamoff release rates for cesium [124, 125] plated out on metal surfaces, from [1].

$$\begin{aligned}
 K &= p_{CsOH}^o \frac{\sqrt{p_{H_2}^o}}{p_{H_2O}^o} \\
 &= \frac{\sigma}{\sigma_o} \exp \left[-\frac{16750}{T} - 4.42 \right]
 \end{aligned} \tag{6-19}$$

where ... expresses an adsorptive bonding and σ / σ_o is the fractional coverage of geometrical surface with cesium.

The reaction enthalpy of the above reaction is endothermic (+139 kJ/mol). With the assumptions of $p_{H_2}^o = 0.001 * p_{H_2O}^o$, $T = 523 \text{ K}$, and $p_{H_2O}^o = 0.5 \text{ Pa}$, the equilibrium partial pressure of CsOH is calculated to be on the order of $4 * 10^{-10} * \sigma / \sigma_o \text{ Pa}$. An additional increase by CsOH_g/steam interaction is not expected under these conditions [117]. In comparison with values of Eq. (6-1) (no oxidants present), this is equivalent to an increase of cesium containing species in the gas phase in equilibrium by more than six orders of

magnitude due to the presence of steam. If also chemisorption of steam or hydrogen on sorption sites previously occupied by cesium (displacement adsorption) is taken into account, an additional increase is expected which, however, cannot be sufficiently quantified due to lack of data. A still larger increase occurs, if oxidation of metallic sorption sites proceeds simultaneously with the chemical conversion of cesium to CsOH. However, mass transfer in combination with the small partition coefficient between gas and chemisorbed phase significantly limits the relative steamoff rate τ . Under the assumption that sorption is an unactivated process (i.e., there is no further activation energy beyond the desorption energy), the ad-/desorption step itself cannot be a rate limiting factor; i.e., a spontaneous ad-/desorption equilibrium on the surface/gas boundary must be expected [117] and is considered in the following equation:

$$\tau = \beta \frac{p_{CsOH}}{R T \sigma} \quad (6-20)$$

where

- τ is the relative steamoff rate [s^{-1}]
- β is the mass transfer coefficient [m/s]

One should keep in mind that in this equation p_{CsOH} for the gas bulk is assumed to be zero leading to an upper limit of the mass transfer rate for a given equilibrium partial pressure. Mass transfer coefficients for laminar flow in tubular geometry are on the order of 0.01 m/s which leads from the above given $p_{CsOH} = 4*10^{-10}*\sigma/\sigma_0$ Pa and $\sigma_0 = 10^{-5}$ mole/m² to relative steamoff rates of $1*10^{-10} s^{-1}$; i.e., a value just below the lower boundary of that found in [116]. This underestimation of the measured steamoff rate might be caused by uncertainties in experimental desorption enthalpies. A decrease of the desorption enthalpy by 5 % increases the relative steamoff rate by more than one order of magnitude. Uncertainties in mass transfer coefficients and hydrogen partial pressure might also contribute to these deviations. The interpretation given for the steamoff data in [116], leads to the somewhat surprising result of decreasing steamoff rates with increasing temperatures, and cannot be used in safety analyses without a convincing experimental validation.

The drastically higher steamoff rates of [126] are partially caused by a larger mass transfer coefficient in these experiments, which may be responsible for an increase of as much as two orders of magnitude. Another rate increasing factor may be a lower sorption enthalpy of cesium on the type of stainless steel as regarded in [126] due to its composition and surface conditions or due to a fission product burden near its saturation limit. In addition, displacement adsorption or metal oxidation, as outlined above, might play a role in steamoff acceleration. The significant uncertainties in this field require additional experiments. Besides measurements of steamoff rates, the accurate determination of the desorption enthalpies (i.e. the thermochemical stability of the sorbed cesium) is necessary.

In safety analyses, the above outlined calculation method is recommended to be used for estimating the steamoff rates for cesium. Considering the uncertainties in chemical behavior, especially the above mentioned influence of displacement adsorption/adsorbent oxidation, an uncertainty factor of 1000 should be applied to the equilibrium partial pressure of CsOH. For strontium and silver, cesium steamoff rates reduced by a factor of 0.1 could

be used. This procedure seems to be highly conservative, in particular for strontium. The chemical state of strontium on oxidized metal surfaces is probably not only a chemisorbed one but may be an oxidic phase with volatilities which remain very low even if interaction of its gaseous phase with steam is taken into consideration [117]. The lack of experimental data with respect to strontium, however, requires this conservativism.

Cesium mobilization on contact with dry air is small because of the low stability of cesium oxides in comparision with CsOH. In air containing moisture, the reaction



is highly favored [117]. For strontium and silver in air, a similar procedure as that in steam is applied.

Iodine does not form compounds in reaction with steam or air which are significantly less volatile than the element. On the other hand, its chemisorption enthalpies are low and release by displacement adsorption of H₂O or oxygen and by adsorbent oxidation might be possible. Evaluation of iodine mobilization in steam/air mixtures indicates that at temperatures > 160 °C a total mobilization can be expected [4]. Experiments in helium containing a H₂O partial pressure of 3000 Pa show that iodine desorption rates at 300 °C increase by about a factor of 20 compared to pure helium [127]. The dependence of the desorption rate on flow velocity found in these experiments leads to the conclusion that mass transfer within the boundary layer is rate determining and not the partition kinetics between gas and solid. Accordingly, the rate increase factors may reflect also the change in equilibrium which will probably be proportional to the steam partial pressure. This effect must be considered in safety analyses, too. Because iodine and steam sorption enthalpies may depend on surface conditions in a different way, a larger increase is expected for other surface conditions than those in the experiments. Therefore, an additional uncertainty factor of 5 is assumed for the above given experimental data leading to the following relation between sorption isotherms in dry and moist helium:

$$p_{I,moist}^o = p_{I,dry}^o (1 + 3500 p_{H_2O}^o) \quad (6-22)$$

These isotherms are combined with mass transfer correlations in a similar way as shown above for cesium in steam. One should keep in mind that this handling of iodine steamoff contains significant conservatism which should be reduced by additional experiments. An indication of this conservatism may be found in results for the AVR water ingress [128]. The above mentioned model postulates a nearly complete steamoff for iodine in that accident scenario, whereas only about 15 % of the steam generator contamination was found within the water removed from the primary circuit. Substituting p^o_{H₂O} by p^o_{O₂}, the above equation may be used also for calculating iodine mobilization by air.

US Contribution

The US has few data on steam induced removal of fission products adsorbed on the primary circuit alloys. The removal of adsorbed iodine, based on limited data, is estimated

to be 60 % of the sorbed iodine. The same factor is assumed to apply to all other fission products in the absence of supporting data [119].

6.1.2.4.2. Single-Effects Data

Steam could also cause the most volatile of the plated out fission products to partially desorb by competing for adsorption sites (subsequently referred to as "steam-induced vaporization" or "steamoff").

Scoping "steam-induced vaporization" (no liquid phase) measurements for iodine on T22 (2.25 % Cr - 1 % Mo chromaloy steel) were made at GA in 1985. These tests demonstrated that the amount of I revaporized was strongly dependent upon surface oxidation state with the fraction removed varying from 0 to 0.60 [129].

In an out-of-pile **vapor leach experiment** [130], the remobilization of radioactivity from metallic surfaces by superheated steam under accident conditions was investigated. A photograph of this laboratory experiment is presented in Fig. 6-45. Water vapor is produced in a round flask (No. 1) and superheated up to a temperature of 200 °C (No. 2). The water vapor is then led onto the test tube (No. 8) which is contained in a furnace

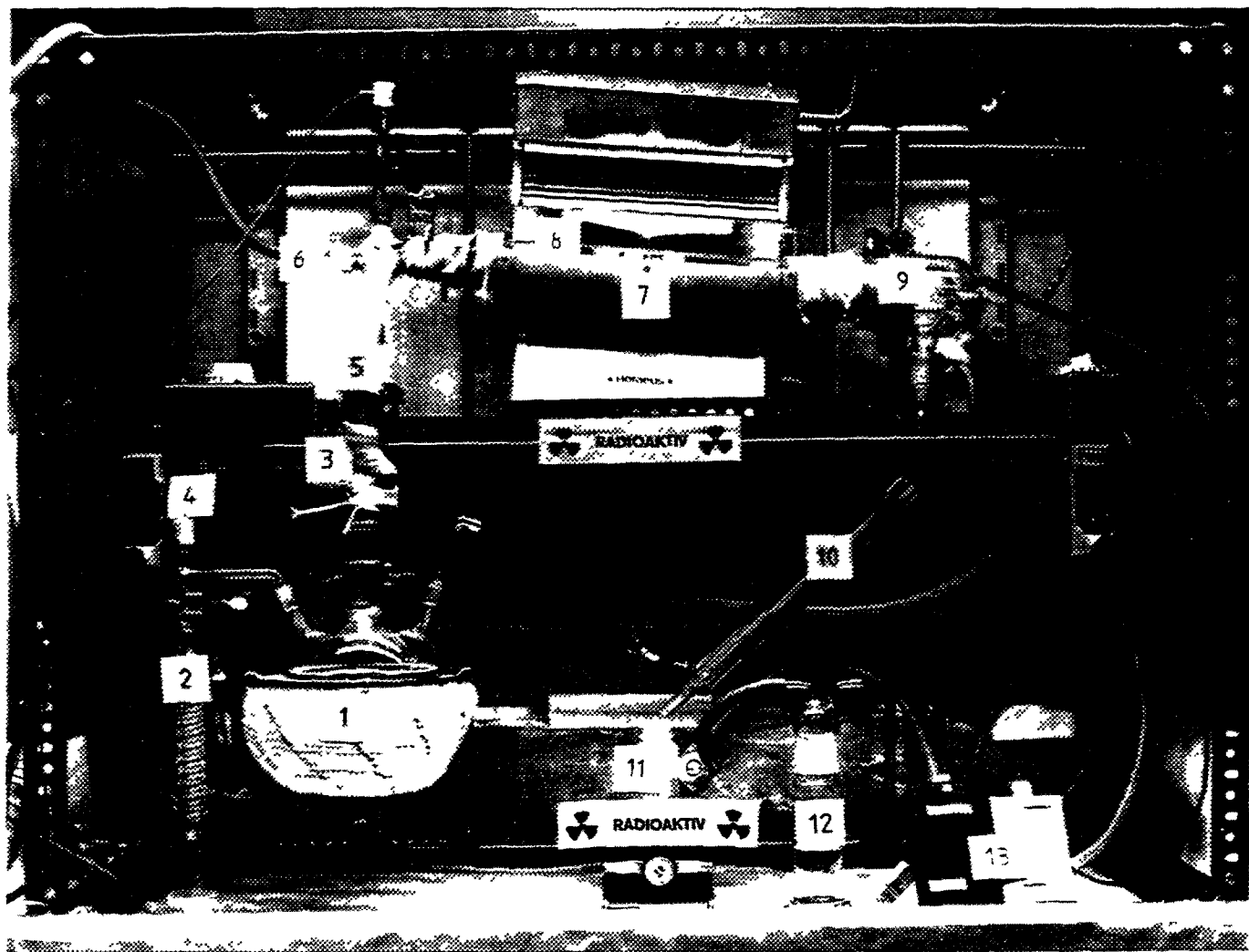


Fig. 6-45: Water vapor leach experiment at the Research Center Jülich, from [130].

Table 6-27: Leach measurements from Sm-9 segments, from [131].

Sm-9 segment	Activity before leach [10^3 Bq/cm 2]	Max. operation temperature [°C]	Temp. of leach solution [°C]	ΔT [°C]	Relative activity of leach solution [%]		
					Water	Water + Alkaperm	Water vapor
1 ⁽¹⁾	4.1	702	80	622	32	95	
5 ⁽¹⁾	3.7	686	80	606	39	97	
3 ⁽¹⁾	4.4	694	80	614	38		
2 ⁽¹⁾	4.4	698	200	498			$5.6 \cdot 10^{-4}$
4 ⁽¹⁾	4.1	690	200	490			0.
14 ⁽²⁾	18.1	202	80	122	99		
9 ⁽²⁾	22.9	292	200	92			$1.6 \cdot 10^{-3}$
10 ⁽²⁾	23.7	273	250	23			$1.1 \cdot 10^{-2}$
11 ⁽²⁾	22.2	254	120	134			$2.5 \cdot 10^{-3}$
12 ⁽²⁾	21.5	236	230	6			$8.7 \cdot 10^{-3}$
13 ⁽²⁾	19.6	218	169	49			$2.8 \cdot 10^{-2}$
15 ⁽²⁾	16.7	186	120	66			$3.6 \cdot 10^{-3}$

- (1) Inner tube surface oxidized
 (2) Inner tube surface non-oxidized

(No. 7) at a temperature between 120 and 500 °C. The activity removed from the test specimens is transported with the water vapor to be condensed in a cooler (No. 10) and is measured by γ -spectroscopy.

Test specimens investigated were from SMOC runs [131]. Tube segments from Sm-9 were leached both with water and with water plus Alkaperm⁷ and with water vapor. Results of the measurements are given in Table 6-27. The leaching process was conducted in 10 steps preceded and followed by flushing with helium (see Fig. 6-46).

A simplified relation for the velocity of the reaction between cesium and H₂O is [132]:

$$\bar{r}_j = \frac{1}{\Delta t_j} \frac{\Delta A_j (\Delta t_j)}{A_{ot}} \quad (6-23)$$

⁷ Alkaperm is an acronym for an alkaline potassium permanganate solution.

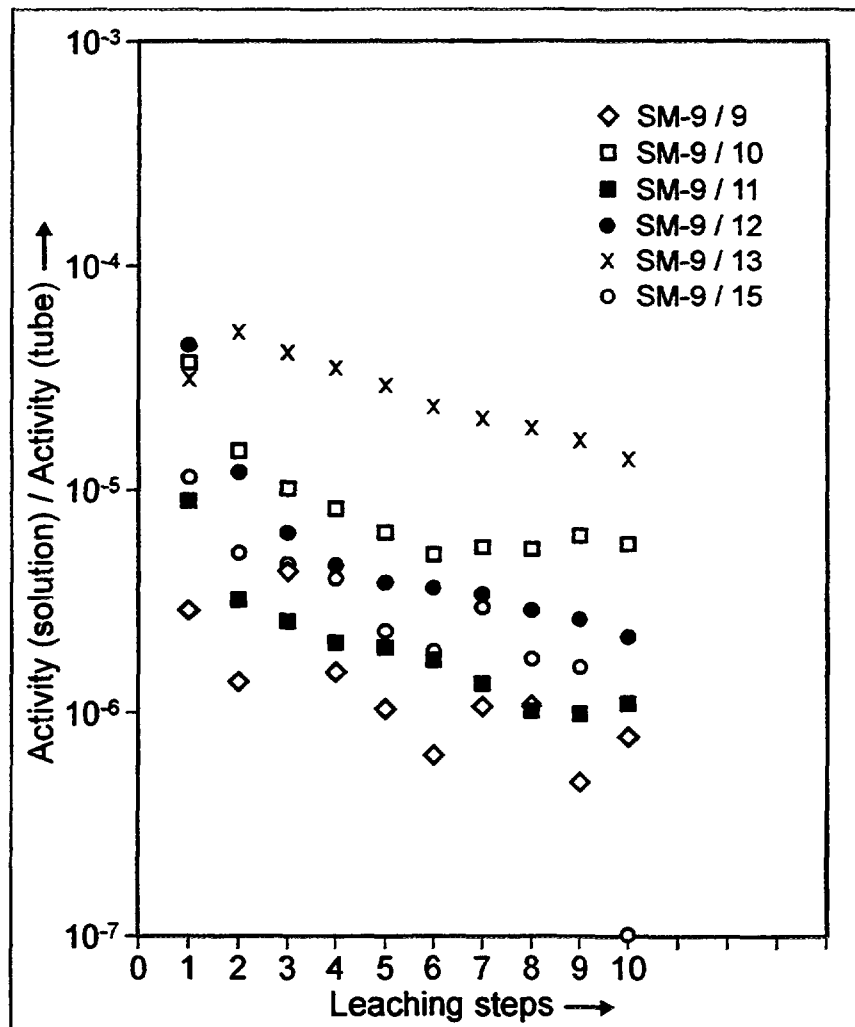


Fig. 6-46: Leaching process in SMOC test Sm-9 for various Inconel 617 tube segments, from [131]

where

Δt_j is the j th time interval

A_{ot} is the total activity sorptively bound to the surface at time $t = 0$

ΔA_j is the activity transported with the water vapor within Δt_j

was taken to obtain Fig. 6-47 with the reaction velocities as function of time for different tube segments.

The presumed influence of the loading temperature on the reaction velocity could not be verified. From other tube segments operated at the maximum SMOC temperature of 700 °C in Sm-9, no activity could be leached by water vapor resulting in the conclusion that oxidation of the surface induces a decrease of the reaction velocity by at least a factor of 5 [132].

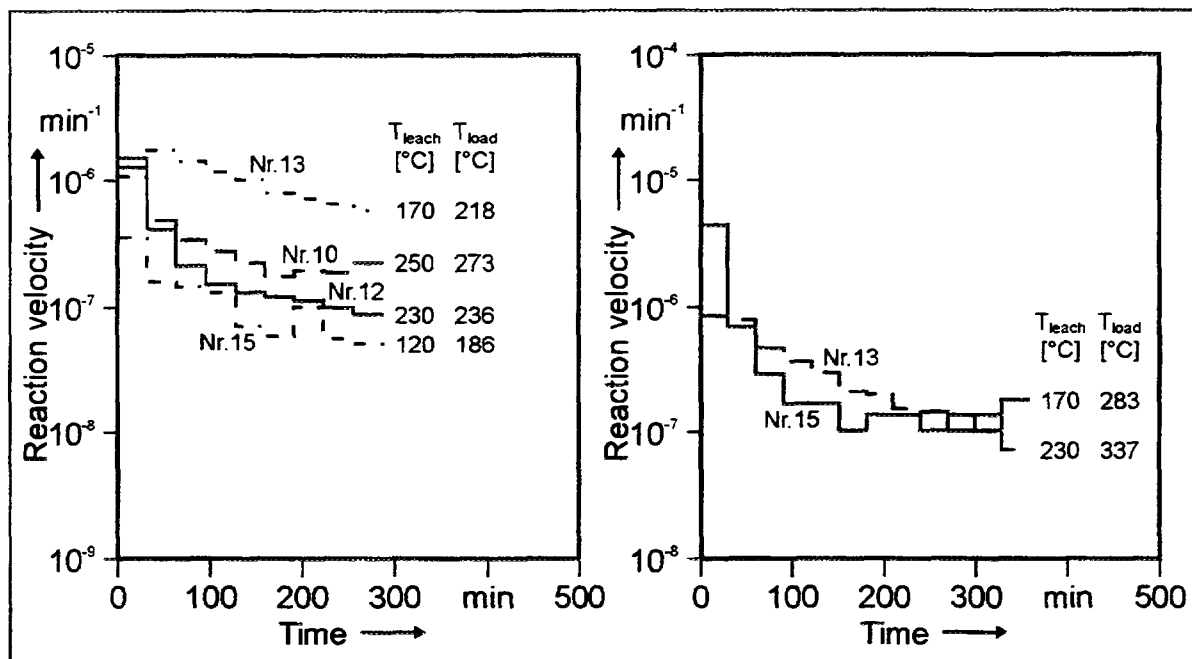


Fig. 6-47: Time-dependent reaction velocity between cesium and water vapor at different vapor leach temperatures, from [132]
 (left) Inconel 617 tube segments from Sm-9
 (right) Incoloy 800 tube segments from Sm-8.

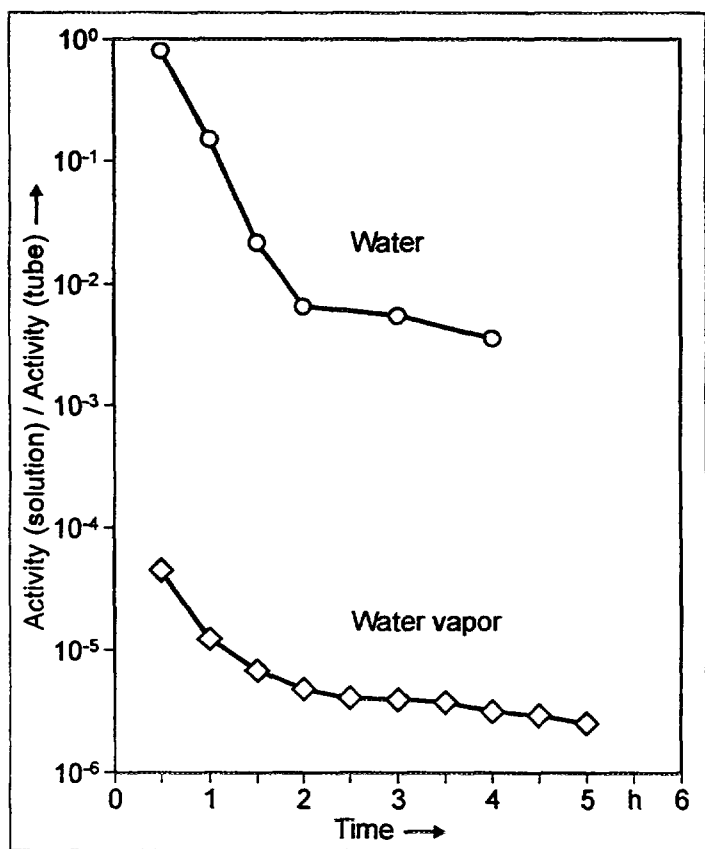


Fig. 6-48: Comparison of activity removal of cesium by water and water vapor, respectively, in the vapor leach apparatus

The measured activity removed by water vapor in comparison to liquid water is shown in Fig. 6-48 showing that the activity removal with liquid water is by far more effective than with water vapor.

6.1.2.4.3. Integral Data

There are no integral measurements of fission product release during steam ingress accidents which are presently available to the US program. LWR data on the behavior of fission products in steam-water systems may be relevant to HTGRs (e.g., [123]).

6.2. DECONTAMINATION OF PRIMARY CIRCUIT COMPONENTS

6.2.1. Introduction

During normal operation of a HTGR, condensable fission products released from the core are transported by the helium coolant and plate out or deposit in the primary circuit. As this plateout activity accumulates in the primary circuit, it becomes a radiological hazard during normal plant operation and maintenance as well as a potential source for offsite release during depressurization accidents. One possible option for mitigating the radiological hazard posed by plateout, especially the hazard to plant workers, is decontamination of primary circuit components either *in-situ* or when they are changed out for periodic maintenance.

This decontamination option is of particular interest for direct-cycle, gas-turbine HTGRs, such as the GT-MHR, because the turbine in these plants is typically designed to undergo planned maintenance approximately every seven years. Moreover, metallic fission products, especially cesium and silver, are expected to preferentially plate out on the turbine during normal operation, resulting in a significant radiation dose which could complicate turbine maintenance.

As discussed in Section 6.1, these plated out fission products (primarily silver, cesium, iodine, and tellurium) may diffuse into the surface, i.e., into the surface oxide and/or into the bulk alloy. There is also the possibility of the fission products becoming attached to dust particles. These dust particles may then get transported around the primary circuit (aerosol transport) and may deposit on various component surfaces independent of the temperature. Thus, the surface contamination may be in three different forms: (1) incorporated within the oxide layer, (2) plated out on the metallic surfaces, or (3) in the form of dust particles loosely bound or tightly attached to the surfaces. Each form of surface activity may require a different method of decontamination.

Considerable decontamination data are available from diverse sources, including gas-cooled power reactors. The information reviewed this section for its applicability to the HTGR with emphasis on gas turbine maintenance in direct-cycle HTGRs.

6.2.2. Decontamination Experience

Many methods have been devised for the decontamination of primary circuit components. These include mechanical methods, such as wiping, water jet blasting, grit added to

the water jet blasting, chemical methods such as alkaline and acidic chemical treatments, and electrochemical etching or polishing of the contaminated surface. Mechanical methods are designed for the removal of loosely adhering contamination. Chemical and electrochemical methods are designed to react with the deposits and some cases dissociate the surface oxide layer to remove the contamination.

Mechanical methods range from gentle to aggressive cleaning processes. The simplest mechanical method is to wipe the surface using an alcohol-moistened kleenex or rags. This method will remove any loosely attached surface contamination, typically yielding small decontamination factors of 2 to 4. This method is only suitable for hands-on decontamination efforts and probably will not be of use for a gas turbine. Another mechanical method is the use of a high pressure water jet. This method may be enhanced by the addition of ceramic grit to the water jet providing some amount of scrubbing capability. Surface damage may result from aggressive grit blasting. Grit blasting may result in work hardening of the surface with possible effects on mechanical properties of the component. This method was extensively used in the Three Mile Island (TMI) cleanup of contaminated walls. Typically these methods result in decontamination factors of 10 or less.

Chemical methods include various chemical cleaning agents/etchants (both oxidizing and reducing agents), and electrochemical cleaning methods to remove diffused fission products. Chemical methods used in the decontamination of the primary circuits of water reactors result in the reduction of the oxide scale and removal of contamination associated with scale. Many of these methods have been commercialized utilizing proprietary chemicals and processes.

Electrochemical methods were developed for the decontamination of the primary circuit of the French G2 CO₂-cooled reactor. They have used electrolytes such as sulfuric and phosphoric acids and sodium hydroxide with success.

Decontamination methods developed to date typically belong to two different categories. The first category was developed to decontaminate components as part of the decommissioning of the reactors that were taken out of service. With these methods, one need not be particularly concerned with affecting the mechanical or structural properties of the components alloys, since these components are being permanently removed from service. The primary consideration is to remove activity from the surface such that the component can be released for public usage as scrap, or at least be disposed of as low level radioactive waste. An additional concern is to minimize the amount of radioactive waste generated during the decontamination process.

The second category of decontamination methods was developed to reduce the surface activity of the component such that normal maintenance work could be performed with minimum radiation exposure of the workers. An additional constraint was that the methods should not degrade the mechanical/structural properties of the components, such that the component could be returned to service. In some cases, this type of decontamination is utilized to reduce the activity of the primary circuits in an attempt to reduce operating personnel radiation exposure in light water reactors (LWRs).

A significant number of decontamination methods [133, 134, 135, 136, 137, 138, 139,

140] to aid in the decommissioning of reactors taken out of service were developed under the aegis of the IAEA. A majority of the work was done on LWR components and circuits, although some gas-cooled reactor work was also performed. Additional methods were developed following the TMI accident. Some research was also conducted in support of the direct-cycle High-Temperature Reactor with Helium Turbine (HHT Project) in Germany [141, 143, 144, 145]. This was specifically aimed at the gas turbine, and provided insight into the contamination and decontamination aspects of the turbine equipment.

6.2.2.1. Light Water Reactor Decontamination Experience

Most components in the primary circuits of LWRs exhibit oxide layers. The fission or activation products released from the reactor core are transported to the site by flowing coolant and deposit on the oxide layer. During the process of deposition, the oxide layer is also growing, resulting in the mixing of the fission products with the oxide layer. A majority of the radioactive contamination of LWR components is on or in the oxide layer.

Many decontamination methods utilizing proprietary chemical reagents have been developed by the LWR industry. Successful decontamination by chemical methods typically requires the removal of oxide layers. The oxide layer is chemically dissolved to achieve the removal of the contamination. The dissolution process liberates the radioactive constituents of the oxides, facilitating the removal of the activity from the system undergoing decontamination. The composition of the surface oxide determines the difficulties involved and the effective decontamination factors that can be achieved.

A great deal of work on the characterization of the surface activity and decontamination surfaces of LWR components [139] has been performed by CEGB in the UK. A series of examination methods was investigated to characterize radioactive deposits on the surfaces. The techniques used include γ spectrometry, α spectrometry, scanning electron microscopy and wet chemical analysis.

Decontamination of circuit components *in-situ* in operating power reactors in an effort to reduce reactor operations personnel exposure was the reason for development of the CEGB process [139]. The methods were successfully utilized in at least a dozen reactors, in both boiling water reactors (BWR) and pressurized water reactors (PWR). Significant reduction of the surface radioactivity and personnel dose was achieved using these methods. The process is a commercial product and has been used in the US. Typical contamination factors in the US BWR and PWR applications between 4 and 25 have been reported.

The methods developed for decontamination of LWR components include: (a) oxidizing systems, NP (nitric permanganate) and the POD (PWR oxidative decontamination) procedure, and (b) reducing systems, LOMI (low oxidation state metal ion) reagents. These methods have been successfully used on entire reactors and on components being returned to service. Multistage cyclic processes using dilute reagents (a CEGB process) have resulted in measured decontamination factors of 100 or more. The process was used for decontamination of the steam generating heavy water reactor (SGHWR) coolant circuits and fuel rods. The decontamination process was found to be more efficient on stainless steel components than on Inconel 600 components presumably operating at relatively low temperatures. A majority of the decontamination was achieved by the removal of the oxide

layer bearing the radioactive isotopes. This is clear indication of the effect of surface condition on the decontamination factor that can be achieved. The use of these processes has resulted in significant savings (up to 2000 man-rem estimated) of radiation exposure to the operating personnel.

The CEGB processes have also been utilized for decommissioning purposes, where concern over corrosion of circuit materials are reduced and aggressive reagents such as strong mineral acids could be employed. However, the problems of treating the radioactive waste solutions remain. An alternative method is to use the dilute reagents in a multistage cycling process analogous to that used for operating plants. Commercial reagent combinations were tested with decontamination factors exceeding 100 for stainless steel specimens. The Inconel steam generator specimens were more difficult with decontamination factors of less than 30. These low decontamination factors were thought to be due to penetration of the oxide, hence the radionuclides, into grain boundaries.

6.2.2.2. French Gas-Cooled and Sodium-Cooled Reactor Decontamination Experience

The French have used a gel spraying and/or foam decontamination of the components in the G2 gas-cooled reactor decommissioning [138, 139, 140]. The coolant in the reactor was carbon dioxide, and the primary contaminant on the reactor component surfaces was Co-60. The primary circuit was made from ferritic steels. Spraying and foams were extensively tested in the laboratory and were used in the final decontamination. These techniques were aggressive, with some amount of surface corrosion and possible impact on the mechanical properties of the components.

Gel Spraying: Initially, laboratory experiments were performed using small scale samples (mild steel) from a carbon dioxide loop, followed by experiments on larger scale samples to determine decontamination factors. Finally *in-situ* mockup tests were performed. The technique uses a spray of sodium hydroxide gel for about 30 minutes followed by an acidic gel spray containing sulfuric and phosphoric acids. The surface is finally rinsed.

The following procedure was used for decontamination of a large section of pipe:

- Soda gel spraying NaOH (3 moles/liter) for 30 minutes,
- Rinsing,
- Acid gel spraying:
 - a. H_3PO_4 3 moles/liter
 - b. H_2SO_4 3 moles/liter
 - c. Silica 16 %
- Rinsing

Decontamination factors achieved after the above treatment ranged from 60 to 200. Final surface activity was less than 1 disintegration/(s cm^2), i.e. less than background, and low enough for the components to be recycled as scrap metal.

Foam Decontamination: This technique is suitable for decontamination of large objects with complex shapes. Spraying or gel spraying does not reach internal surfaces evenly due to preferential flow patterns. Immersion systems are not practical as the reactants

are ineffective in large volumes because of boundary layer problems and the excessive reactant volume requirements. Mechanical means cannot reach all the internal surfaces, and recovery of abrasion residues is difficult.

In contrast, foam has many advantages. These include foam expansion which helps the reagent to reach interstitial gaps of the component, foam mobility and continuous renewal on component walls eliminating boundary layer effects, small liquid volume requirements, and the option to use stronger reactants. The foam used consists of a gas, usually air, dispersed in a liquid in proportions such that the mixture density more closely approximates that of a gas than a liquid. Suitable surfactants are added to lower the surface tension of the liquid containing chemical decontaminants and thus facilitate the formation of foam. The foam is recirculated continuously for periods of several hours. Application of this method for the decontamination of large valves resulted in decontamination factors from 60 to 200. Final surface activity was less than 1 disintegration/(s cm²) (background), again low enough for the components to be recycled as scrap metal. This process has some interesting possibilities, for decontamination of complex shapes using small quantities of chemical reagents and could be conceivably used for decontamination of a gas turbine.

An industrial application of the foam decontamination process to large volume components is described in [146]. Laboratory tests were first performed to optimize the chemical formulation of the foams. Pilot tests were then conducted to study the hydrodynamic features of the fluids and to adapt a technique of permanent foam circulation. With these tests completed, it was essential to validate the foam process on an industrial scale and on a representative nuclear component. The objective to demonstrate an effective *in-situ* decontamination process for the example of a graphite-gas cooler representing a developed area of 1000 m² was successfully achieved. Results were quite convincing since the residual activity of the component was lowered below 1 Bq/cm² and a decontamination factor of 180 was obtained [146].

6.2.2.3. Rapsodie Reactor Decommissioning

Rapsodie was a sodium cooled reactor with a primary circuit fabricated from stainless steel. The primary surface activities were from Cs-137, Co-60 and Mn-54 with activity levels of more than 2200 dps/cm².⁸

Laboratory studies were performed to select a decontamination process with the least hazards and difficulty. A large fraction of the surface activity was removed during the first step of washing with a sodium hydroxide solution. The final process chosen for pilot plant tests used sulfo-nitric acid at about 85 °C.

The surface condition in a sodium cooled reactor is different from water cooled or gas cooled reactors. Typically, the surfaces do not exhibit oxide layers. The decontamination data from this reactor do not appear to apply to the HTGR.

⁸ dps = disintegrations per second, 1 dps = 1 Bq

6.2.2.4. AVR Helium-Cooled Reactor Decontamination Experience

The AVR [137] was a German pebble-bed HTGR which was placed in service in 1967. The primary loop consisted of a gas circulator, the core with fuel spheres and graphite components, and the steam generator. The coolant gas, helium, entered the core at 270 °C and achieved a maximum outlet temperature up to 950 °C. The reactor was operated at a power level of 46 MW(th) and 15 MW(e).

The most reliable data from the AVR decontamination experience were from a circulator, which operated at low temperatures (about 270 °C) prior to the decontamination. In May 1978, water ingressed into the primary loop because of steam generator damage. After removal of the water, test runs indicated damage to a circulator. The reactor had operated for about 10 years prior to the water ingress. At this time it was decided to remove the circulator for repair. This provided an opportunity to measure plateout behavior of fission products and activation products on the circulator inlet, the circulator wheel, and the wheel cap. These measured activities could then be compared to predictions. In addition, the repair of the circulator necessitated its decontamination to reduce the radiation exposure to personnel. The decontamination effort was broad based with AVR, BBC Baden and EIR Würenlingen (now the Paul Scherrer Institute) involvement, whereby different and complementary methods were investigated. Significant data on radiation levels and decontamination methods were obtained during this effort.

By the time the circulator was removed from the reactor, about 300 days had elapsed after reactor shutdown. All the short lived radioactive isotopes had decayed away. Only long half-life fission products remained and contributed to the measured radiation dose rate from the circulator components. Of the fission products, Sr-90 (β decay) represented the greatest specific activity, followed by γ -emitting radionuclides Cs-137 and Cs-134 and Ag-110m. The β activity is a primary concern for skin dose and inhalation doses.

Radiation dose rates were measured using thermo-luminescence dosimeters placed in contact with the surface of the components. In addition, manual measuring devices were used to measure radiation dose rates. They also used wipe samples, scrape samples, microscopic samples using a polisher, and samples using an electrolytic method. The methodology for each of these sampling techniques is described in [137, 136]. Activity measured on the surface was dominated by Cs-137 and Cs-134. Cs-137 activity on the surface was about 0.7 $\mu\text{Ci}/\text{cm}^2$. The dose rates on contact measured were in the range of 10 to 40 rad/h γ radiation and 100 to 400 rad/h β radiation. (Such high radiation dose rates were due to the large fission product plateout as a result of operating a core containing > 50 % BISO fuel at outlet temperatures of 950 °C.)

Decontamination treatments were constrained such that only standard media without strong chemical agents could be used to prevent any damage to the mechanical properties of the components which were going to be returned to service. Many decontamination agents were utilized, and the decontamination factors were measured. The wheel cap was fabricated from St 330 A and was not nickel plated. Decontamination of the wheel cap using OX-24 and R-6 solutions provided a decontamination factor of ≈ 75 for cesium and 160 for Ag-110m. The OX-24 and R-6 solutions are commercially available, proprietary chemical reagent mixtures.

The circulator wheel was fabricated from steel 24 Ni 12, and was nickel plated using a chemical process, although the plating in some areas was defective. Initial high pressure spray of hot water provided a decontamination factor of about 2.4 for γ dose rate and 3.3 for β dose rates. The decontamination factors increased for both β and γ activities to about 5.6 after the OX-24 and R-6 treatments. Once again a higher decontamination factor for Ag-110m as compared to cesium isotopes was observed.

These data clearly show that the material composition is an important parameter in the ability to decontaminate a reactor component. The nickel-plated surfaces were harder to decontaminate than the non-plated surfaces, where the removal of the rust on the surface was easier and decontamination was more effective. At low temperatures, it appears that it is easier to remove silver from the surface than cesium.

Applicability of this data for the HTGR gas turbine decontamination is limited. The low temperature of operation of the AVR circulator may have resulted in an easily removable form of contamination as compared to the GT-MHR, where significant in-diffusion of the plateout activity is possible. In addition, the presence of large quantities of carbonaceous dust in the AVR primary circuit may have facilitated decontamination, since this dust was generally easily removed by mechanical means.

6.2.2.5. Fort St. Vrain Helium Circulator Decontamination

Fort St. Vrain (FSV) was a prismatic HTGR operated by Public Service Company (PSC) of Colorado. PSC was contacted regarding their experience on circulator removal and decontamination [147]. The first two circulators removed and sent to GA were decontaminated using a liquid cutting compound known as Mystic Metal Mover. This is a mineral spirit. After this treatment, the surfaces were wiped down with rags. Surface activity in the circulator interior was reduced from 500 dpm/cm²⁹ to less than 10 dpm/cm². This represents a decontamination factor of about 50. The surface activity outside the of the compressor was typically reduced from 100 to 200 dpm/cm² to background. This is a clear indication of removal of loosely attached (particulate) form of contamination.

After about 1987, an initial on-site decontamination was conducted by wiping the surface with Maslin (a commercially available cloth material impregnated with a surface decontamination agent). The resulting decontamination factors were estimated to be at least a factor of 10 and in some cases a factor of 100.

As a part of a continuing surveillance program at FSV, the helium circulator C2105 was examined radiochemically for plateout activity when it was removed for repair. The circulator had accumulated a total of 450 efpd of operation prior to removal and shipment to GA for refurbishment. The active parts of the circulator were decontaminated prior to reassembly. The decontamination was performed at the GA hot cell [148].

Prior to shipment to GA, initial surface cleaning/wiping of the circulator was performed at the Fort St Vrain site [147]. At GA the circulator was γ scanned using a Ge(Li) detector before and after decontamination. The initial γ scans of the circulator showed

⁹ dpm = disintegrations per minute, 60 dpm = 1 Bq

surface contamination from fission product isotopes Cs-134, C-137, Ba-140, I-131, and Ag-110m.

The circulator was decontaminated as follows: The circulator inlet duct areas were wiped using moistened laboratory wipes, scrubbed using moist silicon carbide powder and a brush, and finally wiped with wet tissues. This procedure removed about 22 % of the contamination. (The water wipe removed an average of 13 % of the contamination and the SiC powder scrubbing removed an additional 9 %). This is a clear indication that the contamination was strongly bound and not easily removed.

The rotor, insulator cover, inlet duct and stator were cleaned by high pressure hot water followed by scrubbing with steel wool pads and Micro detergent. This procedure removed an average 40 % of the contamination. It was noted that the high impact areas such as an inlet duct and the rotor were more difficult to decontaminate using the above cleaning procedures.

These data indicate that only a small fraction of the circulator activity was loosely bound and easily removed by simple techniques. However, since loosely bound activity is an inhalation hazard and prevents easy hands on maintenance, removal of this loosely bound activity is important.

6.2.2.6. Peach Bottom HTGR Component Samples Decontamination

Data from the Peach Bottom HTGR component samples are described in detail in [149]. The component samples were obtained from the primary coolant duct and steam generator tube bundle as part of the End-of-Life R&D program for the Peach Bottom HTGR. These samples were subjected to γ counting, leach tests, and decontamination tests.

Decontamination tests were conducted to determine the effectiveness of selected chemical agents for decontaminating the surfaces of steam generator tube samples. The decontamination procedure used the following sequence of chemicals:

- a. 1,1,1-trichloroethane
- b. 1N NaOH
- c. Turco 4501-A
- d. Turco 4502
- e. 4N HNO₃, followed by
- f. Detergent

Using this technique, total removal of cesium contamination from the mild steel evaporator and economizer tube samples was obtained. Less than half the cesium was removed from the alloy 800 superheater tube samples. This different removal efficiencies were attributed to the differences in the materials rather than the operating temperature of the tubes.

6.2.2.7. Decontamination of CAGR Gas Circulator Components

CAGR is a CO₂ cooled reactor in the UK. The development and demonstration of two practical methods for removal of radioactive surface contamination are described in [150]. The methods are particle impact cleaning (PIC) and an electropolishing technique, referred as electro-swabbing. The particle impact cleaning method used 75 to 125 μm glass beads with an impact velocity of 50 m/s. More than 99 % of the surface activity was removed with the original black surface appearance changing to bright metal finish. The decontamination appears to be the result of the removal of the surface film. The surface damage resulting from the treatment was negligible in terms of weight loss, and dimensional change was of the order of 3 μm or less. The beads had a peening effect on the surface and rather than being detrimental to the treated surface, were considered advantageous in improving fatigue life of components placed back in service after decontamination and repair. The decontamination required the removal of a black surface film, which was probably caused by the CO₂ coolant in this type of reactor.

The other method utilized was electrochemical swabbing. Electrochemical cleaning has the advantage of rapid decontamination with minimal base metal removal. It has a further advantage of producing a smooth, polished surface which may show increased resistance to recontamination.

6.2.2.8. Decontamination of Gas Turbine Materials

A summary of analytical and experimental results of fission product behavior and turbine decontamination studies performed in support of the HHT project is provided in [141]. The HHT project found that high decontamination factors can be achieved using aggressive chemical means. Removal of about 20 μm of the surface is required to achieve a decontamination factor of about 100. A potential disadvantage of such aggressive decontamination methods is that the surface removal may lead to selective corrosion, i.e., grain boundary attack, which may have deleterious effects on the fatigue and creep rupture properties of the components. There have not been sufficient data collected on the mechanical behavior of turbine components after the aggressive decontamination to determine whether or not the components are adversely affected.

Limited data on the decontamination of turbine materials such as molybdenum TZM and alloy Nimocast 713LC (the GT-MHR reference turbine alloy) have been generated by BBC, KFA, and EIR [142, 143]. This effort was based on the desire to minimize radiation exposure during maintenance and inspection work, particularly in view of the possible limitation of the service life of the turbine components. Alloy coupons representing alloys of interest to the HHT Project were exposed to Dragon reactor coolant at 720 °C for 60 days. Decontamination was performed by EIR using techniques developed specifically for this purpose. Decontamination required removal of significant amounts of the base metal. At a removal depth of ≈ 20 μm, a decontamination factor of 100 was achieved for isotopes of cesium. These data suggest that the fission product of interest in this case, cesium, diffuses into the bulk material to a depth of at least 20 μm and the only way decontamination can be achieved is by removal of this layer by aggressive chemical means.

Although, the surface removal (20 μm) was considerable, concerns about selective

corrosion attack (i.e., grain boundary attack) during the chemical decontamination treatment were not considered in this effort. It is well known that mechanical and chemical properties of the materials can be affected by the treatment. Creep rupture and fatigue behavior could be affected by the chemical corrosion treatments of the turbine components. The recontamination behavior, i.e., sorption of the fission products on the surface, may also be deleteriously affected by the chemical treatment. A materials testing program to determine the effect of the treatment as well as to determine the recontamination behavior would be required to qualify this technique for decontamination of a gas turbine.

6.2.2.9. Dragon Reactor Decontamination Experience

The contamination and decontamination behavior of Incoloy 800 samples were studied by Schenker et al. [144]. The samples were exposed to Dragon reactor coolant at 700 °C in the hot duct for a period of 480 days of operation of the reactor. The primary contamination was from Cs-134 and Cs-137. Smaller amounts of Mn-54, Sb-125 and Co-60 were also detected. Ag-110m was not at detectable levels because the fuel in the core at the time was primarily uranium and thorium.

The decontamination procedures included:

- a. γ spectrometry of samples,
- b. treatment with demineralized water for 1 hour at 60 °C,
- c. Ox-24 treatment at 80 °C for 16 hours,
- d. R-6 solution treatment for 8 hours at 80 °C followed by
- e. γ spectrometry.

Decontamination factors greater than 150 were achieved for cesium isotopes. The decontamination factor for Co-60 was about 3. It is believed that the low decontamination factor for cobalt was due to the fact that the cobalt activity was associated with *in-situ* activation of the samples, i.e., it was in the bulk of the sample and not at the surface. The process of decontamination removed the oxide layer which was highly enriched in chromium and manganese, depleted in iron and nickel and was relatively thin ($< 1 \mu\text{m}$) on one side and about 1 to 4 μm on the other side. Chromium rich oxides are stable oxides and typical of gas-cooled reactors. The decontamination treatment removed chromium and manganese preferentially, leaving behind the aluminum oxide, and leading to an impoverishment of Cr and Mn near the surface. Material loss was measured by gravimetry and the analysis of the solutions. Material loss was determined to be about 1.5 mg/cm^2 . This is equal to the removal of about $2 \mu\text{m}$ of the surface. The effects of this material loss on the mechanical properties of the samples were not determined.

6.2.2.10. Fission Product Behavior in OGL-1 and HENDEL Loop Tests

Experiments on the behavior of plated out fission products in the OGL-1 and the HENDEL loops were reported in [151]. These experiments were to simulate a large scale pipe rupture accident with very high gas velocities and high shear ratios to determine liftoff and dust behavior. Tests were conducted on stainless steel 316, Hostel-XR and Incoloy-800 tubing exposed to fission products at temperatures in the range of 630 to 675 °C for up to 150 days. After blowdown, liftoff fractions in the range of 10 to 20 % were measured.

Additional experiments were performed after the initial blowdown tests. These included: (a) wipe off, (b) water washing, and (c) chemical (acid) leaching. After each additional step the activity removal from the surface was measured. Water washing resulted in removal of up to 80 % of the cesium contamination. This is equivalent to a decontamination factor of about 5. Additional decontamination was achieved after the chemical leaching. No data on the extent of chemical leaching and the decontamination factor achieved were provided in this reference. The accompanying plot showed 100 % removal of cesium from the surface.

6.2.3. Conclusions

There are extensive data on the decontamination of reactor primary circuit components. These data suggest that an effective decontamination protocol can be developed for the GT-MHR turbine if needed to reduce personnel radiation exposure during maintenance operations. Selection of a method for decontaminating the turbine and other components will require detailed knowledge of the chemical and physical form of the contamination, the isotopic content, the depth of penetration by diffusion into the bulk material, and any deleterious effects of the decontamination procedures on the mechanical properties of the construction materials.

A majority of the current decontamination data is from LWRs components undergoing decommissioning. Mechanical methods, including high pressure water jet with abrasive grit, do not provide decontamination factors greater than 2 to 4. More aggressive decontamination techniques were developed to obtain high decontamination factors and minimize radioactive waste streams. Decontamination factors of > 100 were achieved by the removal of the oxide layer and some base metal. These methods may have limited applicability for turbine decontamination.

Other methods were developed to reduce the activity of the LWR primary circuit components which were to be reused. The CEGB has commercialized a process which uses mild oxidizing and reducing proprietary reagents to achieve decontamination factors of up to 100. This process could be of use for a gas turbine.

Most gas-cooled reactor decontamination data are for Alloy 800 and mild steel components exposed to reactor coolants at relatively low temperatures (well below 700 °C). Even in this case, decontamination factors of greater than 10 may be achieved only by removal of oxide films and some base metal. Applicability of this data to a gas turbine is uncertain.

Decontamination data from samples exposed to the Dragon reactor coolant for about 60 days at 720 °C are probably the most relevant to the GT-MHR. In this case, turbine alloys, TZM and alloy 713LC were tested. To obtain high decontamination factors, in the range of 50 - 100, base metal removal up to a depth of 20 μm was required. The effect of such metal removal on the mechanical behavior of the components has not been determined. Use of such a method will require additional testing to develop mechanical behavior data for decontaminated components.

6.3. FISSION PRODUCT TRANSPORT IN REACTOR BUILDING

6.3.1. FRG Contribution

6.3.1.1. Fission Product Release into the Reactor Building

In the **German** modeling of fission product transport into the reactor containment through a leak (e.g., a safety valve) in case of a depressurization accident, two different phases are considered: (i) release with the coolant during depressurization and (ii) further escape due to thermal expansion of coolant, if the average primary circuit temperature is still rising [152].

The escape rate during the **depressurization phase** (i) is given by:

$$\frac{d M(t)}{d t} = - \frac{1}{\tau} M(t) \quad (6-24)$$

where $M(t)$ is the helium mass inventory in the primary circuit at time t and $\tau = M / \dot{M} = \text{const}$ is characterized by the leak size. A balance of fission product activity in the coolant, $C(t)$, thus becomes

$$\frac{d C(t)}{d t} = P(t) - \frac{1}{\tau} C(t) \quad (6-25)$$

with the solution

$$I(t) - C(t) = \frac{1}{\tau} \exp(-t/\tau) \int_{t_0}^t I(\Theta) \exp(\Theta/\tau) d\Theta \quad (6-26)$$

where

$P(t)$ is the rate of activity release from the core at time t

$I(t)$ is the activity release from the core accumulated up to t

t_0 is the moment of start of release into reactor building

For the **thermal expansion phase** (ii), the ideal gas law is applied leading to

$$\frac{d M(t)}{d t} = - \frac{1}{\tau} \frac{M}{T} \frac{dT}{dt} \quad (6-27)$$

with the coolant activity balance

$$\frac{d C(t)}{d t} = P(t) - \frac{1}{T} \frac{dT}{dt} C(t) \quad (6-28)$$

and the solution

$$I(t) - C(t) = \left[I(t_o) - C(t_o) + \int_{t_o}^t I(\Theta) \frac{\dot{T}(\Theta)}{T_o} d\Theta \right] \frac{T_o}{T} \quad (6-29)$$

where $I(t_o) - C(t_o)$ is the activity released into the reactor building in the time up to t_o .

The general mathematical treatment of activity transport in the SIEMENS code ATM is given by [40]:

$$\frac{d A_p}{dt} = A_{tot} \dot{F}(t) e^{-\lambda t} - [\dot{L}_p(t) + \lambda] A_p(t) \quad (6-30)$$

$$\frac{d S_{RBcum}}{dt} = A_p(t) \dot{L}_p(t) f_{ret} \quad (6-31)$$

where

A_{tot} is the core inventory [Bq]

A_p is the primary circuit inventory [Bq]

\dot{F} is the relative release rate from the core [h^{-1}]

λ is the decay constant [h^{-1}]

t is the time [h]

\dot{L}_p is the leakage rate from primary circuit [h^{-1}]

S_{RBcum} is the accumulated source rate from the primary circuit into the reactor building

f_{ret} is the retention factor for activity in primary circuit

(In SIEMENS safety analyses, the retention potential of all graphitic and metallic surfaces was expressed by $f_{ret} = 10$ [40]. This assumption is considered conservative for metallic fission products, however, it seems to overestimate the iodine retention.)

6.3.1.2. Deposition Constants and Escape Probabilities

The fission product transport paths are schematically summarized in Fig. 6-49.

In general, the deposition of fission products in the reactor containment is calculated by using the following simple approach

$$-\frac{dc_g}{dt} = v_d \frac{F}{V} c_g \quad (6-32)$$

or

$$\frac{dn_s}{dt} = v_d F c_g \quad (6-33)$$

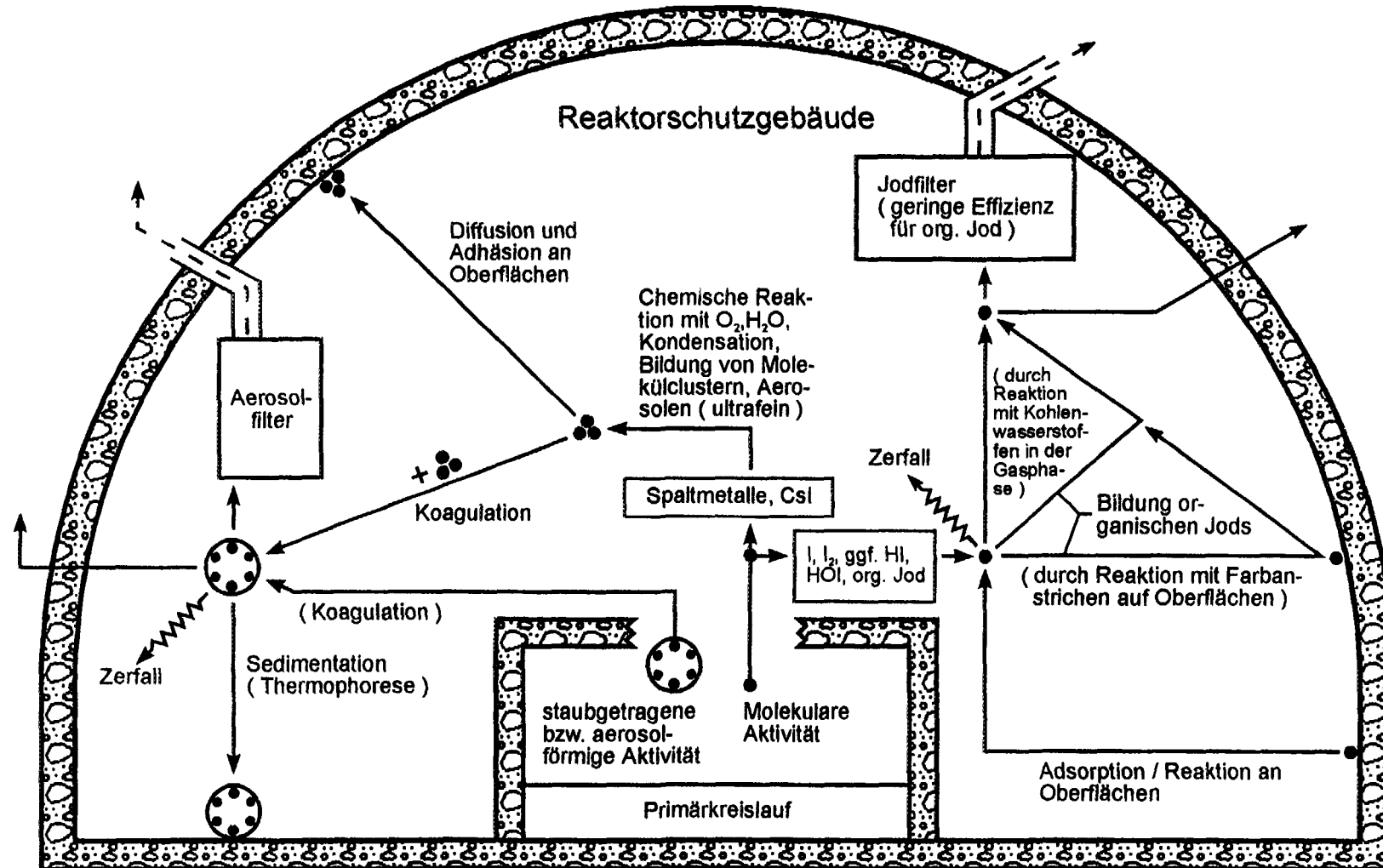


Fig. 6-49: Fission product behavior and release paths in the reactor building during accidents, from [153].

where

c_g is the particle concentration in gas phase [m^{-3}]

v_d is the deposition velocity of particles / molecules [m/s]

F/V is the surface / volume ratio of containment [m^{-1}]

n_s is the number of particles / molecules deposited on surface

This approach is applied to both molecular and aerosol-type species no matter what mechanism is responsible for the deposition. The use of the above equation requires the knowledge of v_d under accident conditions. For aerosols, v_d is strongly dependent on the particle size. For molecular iodine, v_d is primarily influenced by the type of surface. The expression $v_d * F/V$ is called deposition constant.

In general, **aerosol evolution** depends on particle size, composition, shape, charge effects, spatial inhomogeneities, environmental conditions, and thermohydraulics. It can be stated that sufficiently large particle concentrations and residence times in the containment cause the growth of the particles by coagulation and, thus, the increase of their deposition velocity. Such coagulation processes can be simulated with the **PARDISEKO code** [154].

The **GA code CARCAS** [155] for the description of the containment thermodynamics contains a submodel for simulating iodine deposition processes (sorption on protective paint coats, diffusion into concrete, deposition in connection with water vapor condensation on surfaces, filtration). Its applicability in future HTGR safety analyses should be assessed.

Other containment codes have been basically created for LWR applications. In the computer code **CONTAIN** [156, 157], the chemical, physical, and radiological behavior of aerosols and fission products as well as the thermohydraulics in the containment are modeled. Four aerosol deposition mechanisms are considered: (i) gravitational settling, (ii) turbulent diffusion to surfaces, (iii) thermophoresis, and (iv) diffusiophoresis, where the first two are the most important ones. All mechanisms are treated separately, corresponding deposition rates are summed.

The advanced containment code **GOTHIC** [158] simulates a multicompartiment structure by a network of control volumes and flow connections in which simplified time-dependent Navier-Stokes equations are solved [159]. The code includes a three-phase submodel (drops, liquid, vapor) which makes it applicable to a wide range of 3D containment analysis problems such as hydrogen dispersion and water, steam, or superheated steam blowdown.

In the trend analysis for the HTR-MODUL [160], the reactor containment has not been taken into account to serve as a sink for fission products. An assessment of iodine retention in the HTR-MODUL confinement, however, has been made later [161]. The deposition constants of gaseous iodine used in the trend analysis for the HTR-500 [152] originate from a SANDIA study [162] revealing a large uncertainty range; the value taken was 0.3 h^{-1} . For cesium and strontium (aerosols), corresponding data have been estimated by using PARDISEKO calculations. No more accurate data have yet been obtained. Note that iodine in the form CsI influences the deposition behavior.

The particle size distribution is of great importance for evaluating the deposition behavior in the containment of medium and large-sized HTGRs under core heatup accident conditions. In order to support the predictive calculations with PARDISEKO, experiments were performed at the Research Center Jülich to determine the particle size distribution of cesium aerosols. The heart of this **aerosol experiment ALEX** is a test tube of 1.5 m length and 0.18 m diameter through which air is blown with a maximum velocity of 1 m/s. Another tube inside is used to centrally feed a flow of helium loaden with cesium vapor (partial pressure range 0.5 - 5 kPa) into the test tube. The evolved aerosols are collected in a filter for further electron-microscopy evaluation. The results have shown that cesium aerosols typical for medium-sized HTGRs under accident conditions, basically had a spherical shape with a size remaining in the range of $\leq 1 \mu\text{m}$ (mean diameter $0.3 \mu\text{m}$) [163].

With respect to the use of deposition constants in future safety analyses, the following recommendations are given:

- For medium and large-sized HTGRs, a deposition constant of 0.1 h^{-1} for cesium, silver, and strontium as has been used in the trend analysis for the HTR-500 should be applied. A significant retention effect due to aerosol sedimentation has not been found under the conditions of that study. Due to the still very large uncertainty range of the deposition constants (cesium and strontium: 5×10^{-5} to 0.5 h^{-1} for a particle diameter of 0.01 and $1 \mu\text{m}$, respectively, estimated due to its sedimentation velocity), their influence on fission product release cannot be shown without having defined specific accident conditions. Thermodynamic equilibrium calculations have shown that, with respect to iodine, even in the containment it can be available as CsI and, thus, as an aerosol for many core heatup accident sequences. The highly uncertain data situation requires the deposition constant of the aerosols to also apply to iodine, if it is less than the corresponding value derived from the SANDIA study [162]. Also in the BMI "Calculation Guide Lines for the Assessment of the Design of PWR Nuclear Power Plants Pursuant to § 28.3 of the Radiological Protection Ordinance" [164], a starting point for some accident sequences is the assumption of 90 % aerosol-type iodine and only 10 % elementary iodine. During the dispersion in the environment, however, the behavior of aerosol-type iodine with its smaller deposition velocity is more likely to be ingested compared to elementary iodine. As far as aerosol coagulation may influence the deposition processes in the reactor containment, the PARDISEKO code should be applied. In case future analyses will demonstrate a reduction of fission product release into the containment of a medium-sized HTGR down to the same level as calculated for the HTR-MODUL in the trend analysis ($< 10^{-5}$ of the total activity in the core) [160], the calculational procedure for small-sized HTGRs as described below should be taken over for medium-sized HTGRs.
- For small-sized HTGRs, iodine is recommended to be treated in agreement with [161], i.e. by applying a deposition constant of 0.1 h^{-1} which is by a factor of 3 smaller than that used in the HTR-500 trend analysis. Due to the probably very small concentrations of cesium and strontium in the reactor containment, these nuclides which are available as CsOH , Cs_2CO_3 , and SrO , SrCO_3 , respectively, are depositable only if they can be combined with other present aerosols of different composition. The lack of reliable data, however, does not allow one to take credit of these effects. A deposition by diffusion, thermophoresis, or if applicable, diffusiophoresis on humid containment walls is probable. However, the same is true that due to poor data it is not possible yet to

take account of these mechanisms. Therefore, cesium, silver, and strontium deposition in the containment of small-sized HTGRs is neglected at present. However, it should be checked in future analyses whether metallic fission products are to be treated in the same way as iodine.

A deposition of "organic iodine" is not to be assumed. In addition, dust-borne iodine as found in the AVR reactor has to be considered.

For determination of escape probabilities of fission products, the gas volume flow released from the containment is of significance as well as the deposition constant and the fission product source term. A method for calculating the gas flow has been presented in the HTR-500 trend analysis, based on depressurization velocities, thermal gas expansion, and volume sources in the primary circuit [152]. As an extension of this model, the gas exchange processes caused by atmospheric pressure variations are recommended to be considered in addition in future safety analyses.

6.3.1.3. Filter Efficiencies

For some of the core heatup sequences of present HTGR designs, the gas is released from the containment via filters. Filter efficiencies of 99.99 % for elementary iodine and 99.9 % for aerosol-type cesium and strontium (according to the data given by the manufacturer) have been assumed in agreement with LWR figures for accident condition filters (BMI guide lines [164]).

It is intended to investigate the effect of iodine, a 10 % fraction of which consists of methyl iodine (CH_3I) with a filter efficiency of 99 % and compare the results with the analysis of 100 % inorganic iodine. A fraction of 1 % "organic iodine" is assumed in LWR risk analyses of core melting. The BMI guide lines anticipate for some cases fractions of up to 50 % "organic iodine" of the total gas-borne iodine activity. It should be noted, however, that the problems of "organic iodine" for LWRs and HTGRs have not been solved yet. Furthermore, deposition velocities of "organic iodine" with respect to fallout and washout in the environment are, according to the BMI guide lines, smaller by two orders of magnitude compared to elementary iodine. Therefore, the lower filter efficiency of "organic iodine" is partially compensated, with respect to ingestion, by a more favorable behavior during the dispersion in the environment. Since a certain fraction of iodine can be available as aerosol (CsI) in medium and large-sized HTGRs, the smaller efficiency of the aerosol filters should be considered in a conservative manner, if an efficient aerosol deposition in the containment does not take place. It is recommended to select the alternative leading to the higher release values.

Under certain experimental conditions (humid atmosphere, solvent containing protective paint on the simulated containment surfaces), unknown, highly penetrating iodine compounds with a filter efficiency of 50 % have been found. At present, these penetrating compounds should not be considered as has been done in the Deutsche Risikostudie (DRS) Phase B [165].

With respect to the aerosol filters (cesium, strontium, silver), it is deemed ascertained that the filter efficiencies are valid even for the extremely small particle diameters as

probably encountered in an HTGR. Filters efficiencies have been determined by applying an unfavorable particle size (diameter $\approx 0.3 \mu\text{m}$). The efficiency increases towards smaller particle sizes due to diffusion processes, and towards larger particle sizes due to inertia forces.

6.3.2. Japanese Contribution

In the safety analysis of a depressurization accident of HTTR, the amount of fission products released to the atmosphere was evaluated by a release path model, as shown in Fig. 6-50 [103]. In the depressurization accident, fission products are released from the primary cooling system to a containment vessel through a break in a coaxial double pipe, along with the primary helium gas coolant. Fission products released to the containment vessel are leaked to a service area, which surrounds the containment vessel, according to elevation of the containment vessel pressure. Based on a simple analysis, it is assumed that a half of condensable fission products plate out on the inner surface of the containment vessel [166]. In the analysis, 1 % of the fission products is released from the service area to the atmosphere on the ground level. The ground level release fraction was calculated on the basis of the pressure elevation of the service area. When the service area pressure becomes lower than the atmospheric pressure by means of a ventilation system of an emergency air cleaning system, fission products are released from the stack to the atmosphere via a filter of the emergency air cleaning system.

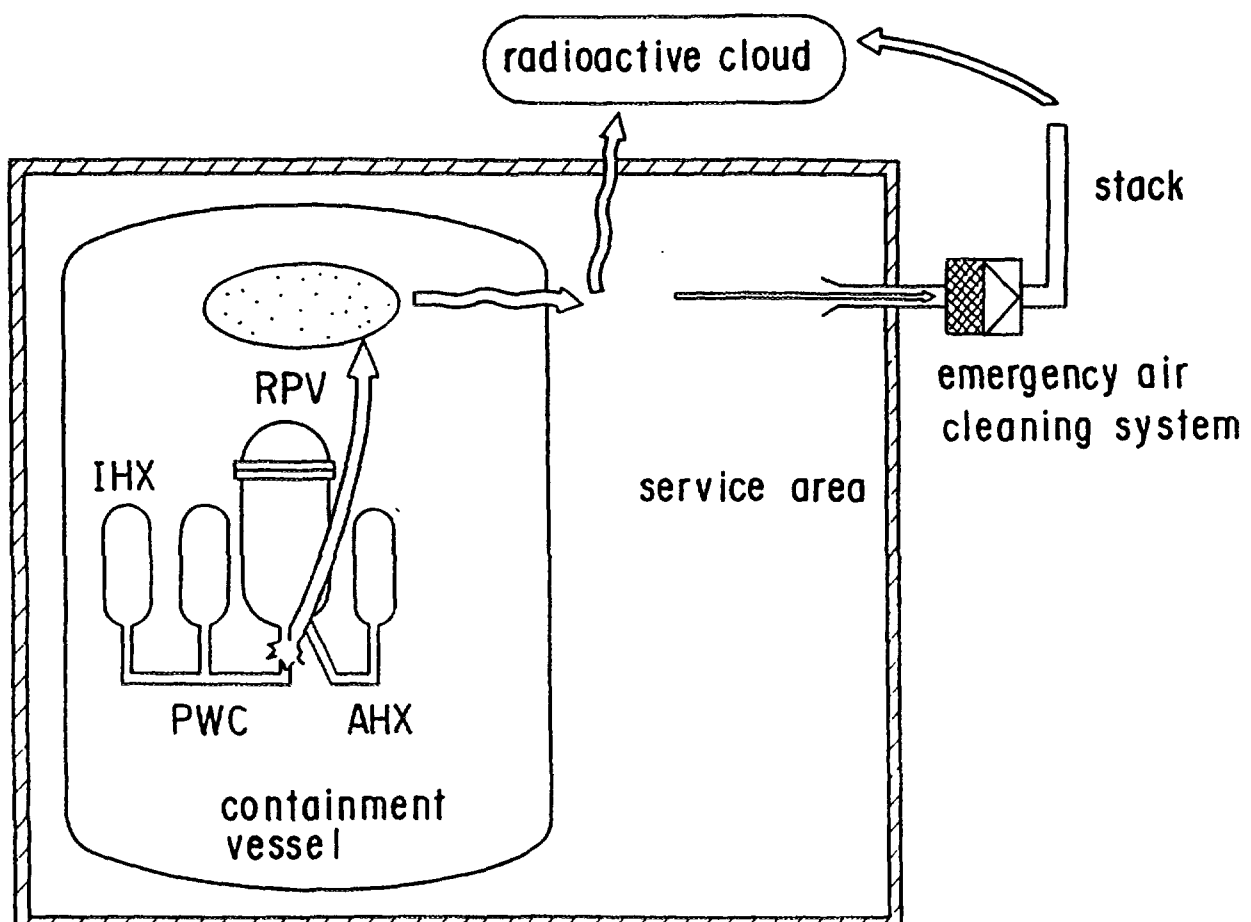


Fig. 6-50: Release path model for the HTTR [103]

6.3.3. US Contribution

Reference [167] concludes that the existing experimental data, primarily from the LWR technology base, should be sufficient to ascertain what phenomena dominate aerosol deposition under the conditions of interest in an HTGR reactor building and to estimate appropriate ranges for the input parameters into retention models. Moreover, the low concentrations of radionuclides released into the building during HTGR depressurization events may allow certain simplifications in areas where the data are insufficient, such as the chemical species of iodine within the building. Nevertheless, there is a paucity of data for the specific conditions expected in an HTGR reactor building during postulated accidents (Reference [168] is an important exception). Consequently, it should be anticipated that regulatory authorities will ultimately require experimental confirmation that certain LWR data and transport models can be applied to the HTGR with confidence.

Some general conclusions which can be drawn from the available data (e.g., [167, 168, 169, 170, 171, 172, 173, 174, 175, 176, 177, 178, 179, 180]) are summarized below:

Operating GCR Reactor Data:

- The concentration of graphite dust in a pebble bed HTGR is likely significantly higher than in a prismatic HTGR as a consequence of pebble recirculation in the former.
- The size, concentration, and material composition of particles in GCRs are dependent upon the structural materials and operating history of the reactor.
- Measurements indicate that dust concentrations circulating within the MHTGR will likely be low. Particles will be composed of graphite and metallic oxides and are expected to be less than 1 mm in diameter.

Small-Scale Laboratory Tests:

- Loop test results indicate that reentrained particulates will be approximately $0.1 \mu\text{m}$ in diameter and confirm that the size, shape, and concentration of particles impact radionuclide transport and release from the vessel.
- Chemical species are also important for modeling radionuclide transport, but insufficient data are available to discern the chemical form of elements such as iodine in the reactor building. However, scoping calculations indicate that the impact of iodine species upon building retention may be negligible for the MHTGR because of the low quantities of iodine released.

Large-Scale Integral Tests:

Parameters found to influence aerosol retention in large- scale tests include:

- Thermodynamic and Flow Conditions

Thermodynamic conditions, flow rates, and humidity levels significantly impact aerosol agglomeration and deposition rates in several experiments. The addition of moisture in tests caused aerosols to form more spherical, tightly-packed agglomerates (aerosols in dry environments form loosely compacted webs of branched chains).

- Aerosol Physical Characteristics

The concentration, size, shape, and physical form of aerosols as a function of time impacted the retention rates in several tests.

- **Aerosol Chemical Properties**
Several tests utilized multiple species of aerosols, concrete and metallic oxides, soluble and insoluble, etc. Soluble species exhibited higher deposition rates. For mixtures of aerosols, deposition rates varied depending upon the species selected.
- Results provide particulate and vapor depletion rate data as a function of building flowrate, humidity level, aerosol concentration, and physical and chemical properties of the aerosols. MHTGR retention models can be applied to integral test conditions to test the model accuracies for these conditions.
- Results show that in most cases, the assumption of a well-mixed gas volume is valid if the thermodynamic conditions are well-defined.

Further codes to describe the fission product behavior in an HTGR containment are:

- TDAC (General Atomics) [181] is a one-compartment model which takes into account sedimentation as aerosol deposition mechanism as well as filtration. Leakage rates as input data are taken to determine the release of radioactivity into the environment. An essential part of the model deals with the desorption of the decay of short-lived radionuclides via 65 decay sequences.
- LEAF (Los Alamos) [182] is similar to TDAC.
- SCIMCA (MIT) [167] is a multi-compartment model still in the process of development. It takes account of nuclear decay, sedimentation of aerosols, and filtration. The modeling of activity release into the environment is similar to that in TDAC.

6.4. SUMMARY OF CHAPTER 6

Numerous experimental and theoretical efforts have been made to examine plateout distribution of fission products in the primary circuit both under normal operating and accident conditions. **In-pile and out-of-pile deposition loops** were operated in Germany (LAMINAR, VAMPYR-I and -II, SMOC), Japan (OGL-1), France (SAPHIR, COMEDIE), the UK (Dragon), and the USA (GA deposition loop, CPL-2 tests) to study systematically the ad-/desorption behavior of fission product on metallic surfaces as function of temperature and gas flow. The obtained experimental data as well as the measurements from the gas-cooled reactors AVR, THTR-300, Peach Bottom, Fort St. Vrain were taken to derive plateout parameters such as desorption energy or penetration coefficient to be used in corresponding calculation models. The most important computer codes which were tested and more or less successfully validated, are SPATRA (Germany), PLAIN (Japan), and PADLOC, TRAFIC (USA).

The AVR reactor has been used in Germany to conduct experiments for the investigation of deposition phenomena. Cold gas filter and dust experiments provided fission product and dust concentrations in the coolant gas since 1970. During stationary, undisturbed operation, dust concentrations happened to be in the range of $1 - 2 \mu\text{g}/\text{m}^3$ with a production rate of 3 kg per operating year and a total dust inventory of 60 kg at the end. With $< 2 \mu\text{m}$ the dust particle size was much smaller than expected. The dust was estimated to contain about 10 % of the amount of Cs-137 and Sr-90 released from the core during normal operations. Available data from Fort St. Vrain revealed much lower dust concentrations than in Peach Bottom and AVR and it was comprised of mainly metallic oxides with a carbon content of $< 10 \%$.

The knowledge of the distribution of radionuclides in the primary circuit during normal operations is essential for the assessment of activity transport and release by remobilization during accidents. Remobilization of fission products deposited in the primary circuit occurs during accident sequences by desorption due to temperature increase and/or due to system pressure drop by liftoff of dust-borne activities. In SMOC different kinds of steels were tested under a variety of test conditions characteristic for a future direct-cycle HHT plant to find out the temperature ranges in which cesium desorption takes place.

From the **blowdown tests** in COMEDIE, iodine was found to be significantly desorbed and redistributed. Gathered liftoff data were deemed excessively conservative. The AVR blower transient experiments showed an increase of the gas-borne dust by up to three orders of magnitude. More blowdown tests were conducted in British AGRs and in the Japanese OGL-1 loop. Computer models were developed to calculate liftoff fractions. The German RADAX-3 code is based on a liftoff criterion with statistically distributed forces, while in the US POLO code, an empirical shear ratio model for correlating liftoff data is applied.

Various tube samples have been taken from deposition experiments to investigate the removal of cesium and iodine from metal surfaces by washoff and steamoff in leaching experiments at ORNL and at the Research Center Jülich. It is both dissolution and chemical attack in water and mechanical effects in case of a high speed water jet, by which accessible fission products are released in water ingress accidents. However, on the order of 10 % only of the plated-out cesium is being removed during water leaching probably due to the slow transport of water into the pore system of oxide surface layers. Steamoff rate measurements were found to vary over several orders of magnitude. An influence of the loading temperature on the water-fission product reaction velocity could not be verified.

The **decontamination of primary circuit components** from plated-out activity is an option to mitigate radiological hazards to plant workers which is of particular interest for direct-cycle gas turbine HTGRs. It is also used for decommissioning purposes. Different forms of surface activities (in-diffusion into oxide layer, adsorption on metallic surface, deposited dust) may require different methods of decontamination encompassing mechanical, chemical, or electrochemical processes. The material composition was found to be an important parameter.

Most of the decontamination work was dedicated to LWR components and circuits. CEGB has commercialized an own process and applied to at least a dozen reactors. HTGR-related decontamination work was performed in Germany with the AVR circulator by means of wiping, scraping, polishing, and applying an electrolytic method. For the circulator wheel cap, decontamination factors of 75 for cesium and 160 for silver were obtained. Also Fort St. Vrain's circulators were subject to decontamination treatment. The helium circulator C2105 was examined radiochemically for plateout activity and then decontaminated by wiping, scrubbing, brushing, and wet-wiping, removing not more than about 22 % of the decontamination. In the Japanese OGL-1 loop, wipeoff, water washing, and chemical leaching tests were conducted to remove plated-out activity. A 100 % removal of cesium from the surface was reported.

The modeling of the behavior of fission products released into the **reactor building** takes account of both the depressurization phase and the subsequent thermal coolant gas

expansion phase. Sedimentation, condensation, coagulation, adhesion on and diffusion into the surface, chemical reaction, and decay are the pertinent processes in the containment. Certain assumptions for the deposition constant and filter efficiencies have been defined to assure a conservative approach in safety analyses. Experience from LWR-related tests can also be applied to HTGRs with confidence.

REFERENCES OF CHAPTER 6

- [1] MOORMANN, R., Source Term Estimation for Small-Sized HTR's, Report JüL-2669, Research Center Jülich (1992).
- [2] KRESS, T.S., NEILL, F.H., A Model for Fission Product Transport and Deposition under Isothermal Conditions, Report ORNL-TM-1274, Oak Ridge National Laboratory (1965).
- [3] MOORMANN, R., MEISTER, G., Spaltproduktablagerung auf Metallen und der Code SPATRA, Spaltproduktverhalten in Kernreaktoren (Proc. Seminar, Rossendorf, 1991), Report ZFK-747, FZ Rossendorf (1991) 56-60.
- [4] HOINKIS, E., A Review of the Adsorption of Iodine on Metal and its Behaviour in Loops, Report ORNL-TM-2916, Oak Ridge National Laboratory (1970).
- [5] CHRIST, A., HAASE, F.W., WIEDMANN, J., Experimentelle Untersuchungen zur Cäsium-Ablagerung auf Hochtemperatur-Werkstoffen (Proc. Jahrestagung Kerntechnik '85, München, 1985), Inforum GmbH, Bonn (1985) 175-178.
- [6] MATZKE, H.J., PICKERING, S., Diffusion of Cesium in Stainless Steel and Possible Implications for Cs Depletion and Mobility, J. Nucl. Sci. Techn. **20** (1983) 237-245.
- [7] HAMMEKE, K., Experimentelle Ergebnisse der Ablagerungs- und Diffusionsmessungen von Spalt- und Aktivierungsprodukten beim Bestrahlungsexperiment Saphir 11 am Reaktor PEGASE in Cadarache, Internal Report KFA-IRB-IB-22/83, Research Center Jülich (1983).
- [8] PETERSEN, I., Zusammenstellung aller experimentellen Ergebnisse der Plate-out Untersuchungen an dem Gasführungsrohr des KFA-Heißgas-isolierungsexperiments im DRAGON-Reaktor, Internal Report KFA-IRB-IB-12/84, Research Center Jülich (1984).
- [9] HERION, J., Der Einfluß der Wandmaterialien auf die Ablagerung von Cs in HTR-Kühlkreisläufen, Report JüL-1155, Research Center Jülich (1975).
- [10] INIOTAKIS, N., Rechenprogramm PATRAS; Programmbeschreibung, Internal Report KFA-IRB-IB-7/84, Research Center Jülich (1984).
- [11] INIOTAKIS, N., MALINOWSKI, J., MÜNCHOW, K., Initial Results of Investigations into Fission Product Deposition in In-Pile Experiments, Nucl. Eng. Des., **34** (1975) 169-180.
- [12] RÖLLIG, K., Spaltproduktablagerungsversuche - Auswertung der HRB-Kreislaufversuche, Spaltproduktverhalten in Kernreaktoren, (Proc. Seminar, Rossendorf, 1991), ZfK Dresden-Rossendorf (1991).
- [13] EHRHARDT, K.D., PLATO, ein Programm zur Berechnung der Spaltproduktablagerung, Report JüL-Spez-135, Research Center Jülich (1981).
- [14] NABIELEK, H., et al., Development of Advanced HTR Fuel Elements, Nucl. Eng. Des. **121** (1990) 199-210.

- [15] RÖLLIG, K., The THTR Coolant Gas Activity, an Indicator of Fuel Performance, Behavior of GCR Fuel under Accident Conditions (Proc. IAEA Specialists' Meeting, Oak Ridge, 1990), IAEA, IWGGCR/25, Vienna (1991) 99-108.
- [16] BIEDERMANN, P., SACKMANN, B., Labor- und Reaktorversuche zur Ablagerung von Spaltprodukten im HTR-Primärkreislauf, Report JüL-Conf-64, Research Center Jülich (1988) 72-87.
- [17] HANSON, D.L., BALDWIN, N.L., STRONG, D.E., Fission Product Behaviour in the Peach Bottom and Fort St. Vrain HTGR's, Coolant Chemistry, Plate-out and Decontamination in Gas-Cooled Reactors (Proc. IAEA Specialists Meeting, Jülich, 1980), IAEA IWGGCR/2, Vienna (1981) 49-54.
- [18] STEWART, K.P., Final Summary Report on the PEACH BOTTOM End of Life Program, Report GA-A14404, General Atomic Company (1978).
- [19] RÖLLIG, K., et al., Cesium Deposition on HTR Primary Circuit Materials, Fission Product Release and Transport in Gas-Cooled Reactors (Proc. IAEA Specialists Meeting, Berkeley, 1985), IAEA IWGGCR/13, Vienna (1986) 329-350.
- [20] HANSON, D.L., Results of the General Atomic Deposition Loop Program, Report GA-A13140, General Atomic Company (1976).
- [21] BABA, O., TSUYUZAKI, N., SAWA, K., [PLAIN Code Description], Report JAERI-M 88-266 (1989) (in Japanese).
- [22] HUDRITSCH, W.W., SMITH, P.D., PADLOC, A One-Dimensional Computer Program for Calculating Coolant and Plateout Fission Product Concentrations, USDOE Report GA-A14401, General Atomic Company (1977).
- [23] HUDRITSCH, W.W., PADLOC, A One-Dimensional Computer Program for Calculating Coolant and Plateout Fission Product Concentrations, Part II, USDOE Report GA-A14401, General Atomic Company (1981).
- [24] HUDRITSCH, W.W., Plateout Code Development, [PADLOC/INDIFF], GA Document 906395, Rev. 1, GA Technologies Inc. (1982).
- [25] WICHNER, R.P., Fission Product Plateout and Liftoff in the MHTGR Primary System: A Review, Report NUREG/CR-5647 (ORNL/TM-11685), Oak Ridge National Laboratory (1991).
- [26] GARLAND, J.A., WELLS, A.C., HEDGEBOCK, J.B., Behaviour of Particles in a Commercial Advanced Gas-Cooled Reactor, Fission Product Release and Transport in Gas-Cooled Reactors (Proc. IAEA Specialists Meeting, Berkeley, 1985), IAEA, IWGGCR/13, Vienna (1986) 250-261.
- [27] VON DER DECKEN, C.-B., WAWRZIK, U., Dust and Activity Behavior, in: ASSOCIATION OF GERMAN ENGINEERS (VDI) (Ed.), AVR – Experimental High-Temperature Reactor, 21 Years of Successful Operation for a Future Energy Technology, VDI-Verlag Düsseldorf (1990) 259-275.
- [28] WAWRZIK, U., Staub im AVR-Reaktor; eine Analyse der Kaltgasfilterversuche, (Proc. Jahrestagung Kerntechnik '87, Karlsruhe, 1987), Inforum GmbH, Bonn (1987) 315-318.
- [29] PETERSEN, I., Zusammenstellung der experimentellen Ergebnisse von Staubablagerungsversuchen im AVR-Kreislauf, Technical Note KFA-IRB-TN-20/86, Research Center Jülich (1986).
- [30] BIEDERMANN, P., BLICK, H., LENNARTZ, T., γ -spektrometrische Nachuntersuchung des Staubexperimentes S1, Technical Note KFA-IRB-TN-2/85, Research Center Jülich (1985).

- [31] JUMPERTZ, P., γ -spektrometrische Auswertung des Staubexperimentes S3 (80,18), AVR Technical Note H5-X4/Jum/Ga (1985).
- [32] KFA-HTA, HTA Jahresbericht 1985, Internal Report KFA-HTA-IB-3/86, Research Center Jülich (1986).
- [33] BIEDERMANN, P., BLICK, H., LENNARTZ, T., SEIFERT, J., Zur γ -spektrometrischen Nachuntersuchung des Experimentes VAMPYR-II/V01 (Vorläufige Meßwerte), Technical Note KFA-IRB-TN-10/87, Research Center Jülich (1987).
- [34] BIEDERMANN, P., BLICK, H., LENNARTZ, T., SEIFERT, J., Zur γ -spektrometrischen Nachuntersuchung des Experimentes VAMPYR-II/V02, Technical Note KFA-IRB-TN-08/89, Research Center Jülich (1989).
- [35] BIEDERMANN, P., BLICK, H., LENNARTZ, T., SEIFERT, J., Zur γ -spektrometrischen Nachuntersuchung des Experimentes VAMPYR-II/V03, Technical Note KFA-IRB-TN-01/91, Research Center Jülich (1991).
- [36] BIEDERMANN, P., BLICK, H., LENNARTZ, T., SEIFERT, J., Zur γ -spektrometrischen Nachuntersuchung des Experimentes VAMPYR-II/V04, Technical Note KFA-IRB-TN-03/91, Research Center Jülich (1991).
- [37] WAHSWEILER, H.G., THTR-300, F+E Teilverhaben: Graphitstaub, 2. HJ 1988, Technical Note HRB-419-040-BH 0029, Hochtemperatur-Reaktorbau GmbH (1989).
- [38] BÄUMER, R., KALINOWSKI, I., THTR Commissioning and Operating Experience, Energy **16** (1991) 59-70.
- [39] WAHSWEILER, H.G., THTR-300, F+E Teilverhaben: Graphitstaub, 1. HJ 1989, Technical Note HRB-419-040-BH 0034, Hochtemperatur-Reaktorbau GmbH (1989).
- [40] SIEMENS-INTERATOM, Aktivitätsfreisetzung und Strahlenexposition bei der HTR-Modul-Kraftwerksanlage, Teil II: Störfälle, Technical Information for Audit Talks No. 76.00561.4, Siemens/Interatom (1987).
- [41] RÖLLIG, K., Weiterentwicklung von Rechenverfahren zur Spaltproduktfreisetzung und -ablagerung in HTR-Anlagen, Final Report HTR-5125-BA-GHRA 006887, Hochtemperatur-Reaktorbau GmbH (1992).
- [42] HINDS, W.C., Aerosol Technology, Wiley, New-York (1982) Chap. 6.
- [43] HANSON, D.L., BALDWIN, N.L., STRONG, D.E., Fission Product Behaviour in the Peach Bottom and Fort St. Vrain HTGR's, Coolant Chemistry, Plate-out and Decontamination in Gas-Cooled Reactors, (Proc. IAEA Specialists Meeting, Jülich, 1980), IAEA IWGGCR/2, Vienna (1981) 49-54.
- [44] GOTTAUT, H., KRÜGER, K., Results of Experiments of the AVR Reactor, Nucl. Eng. Des. **121** (1990) 143-153.
- [45] WAWRZIK, U., VON DER DECKEN, C.B., Staub- und Aktivitätsverhalten, VDI-Berichte 729 (1989) 239-254.
- [46] IVENS, G., WIMMERS, M., Der AVR als Testbett für Brennelemente, VDI-Berichte 729 (1989) 161-176.
- [47] SKYRME, G., Attachment of Gaseous Fission Products to Aerosols, Fission Product Release and Transport in Gas-Cooled Reactors, (Proc. IAEA Specialists Meeting, Berkeley, 1985), IAEA IWGGCR/13, Vienna (1986) 262-274.
- [48] BUSCH, D.D., The Nature of Condensable Fission Products in an HTGR Environment, USAEC Report GA-6957, Gulf General Atomic (1966).

- [49] CRAIG, G.T., The Behavior of Particulate Matter in High-Temperature Gas-Cooled Graphite Reactor Primary Coolant Systems, GA Report GA-A13402, General Atomic Company (1975).
- [50] DYER, F.F., et al., Distribution of Radionuclides in the Peach Bottom HTGR Primary Circuit during Core 2 Operation, USERDA Report ORNL-5188, Oak Ridge National Laboratory (1977).
- [51] STEWARD, K.P., Final Summary Report on the Peach Bottom End-of-Life Program, DOE Report GA-A14404 (1978).
- [52] HANSON, D.L., et al., Fission Product Behavior in the Peach Bottom and Fort St. Vrain HTGRs, DOE Report GA-A16154, General Atomic Company (1980).
- [53] BALDWIN, N., Radiochemical Examination of Fort St. Vrain Circulator C2105, GA Document No. 909776, General Atomics (1988).
- [54] BURNETTE, R.D., Radiochemical Analysis of the First Plateout Probe from the Fort St. Vrain High-Temperature Gas-Cooled Reactor, Report GA-A16764, GA Technologies Inc. (1982).
- [55] AKERS, D.W., Examination and Analysis of the Second Plateout Probe from the Fort St. Vrain High-Temperature Gas-Cooled Reactor, Report EGG-NPR-9441, EG&G Idaho (1991).
- [56] HANSON, D.L., Results of the General Atomic Deposition Loop Program, USERDA Report GA-A13140, General Atomic Company (1976).
- [57] BECKER, C., Cs, I, Ag and Sr Plateout in Dragon, GA Document 906017/1, General Atomic Company (1981).
- [58] PHILLIPS, M.E., Modelling of Caesium Deposition in CAGR Reactor Circuits, Fission Product Release and Transport in Gas-Cooled Reactors (Proc. IAEA Specialists Meeting, Berkeley, 1985), IAEA, IWGGCR/13, Vienna (1986) 299-317.
- [59] CLOUGH, P.N., HOOD, E.M., Modelling of Iodine Chemistry and Plate-out in a CAGR, Fission Product Release and Transport in Gas-Cooled Reactors (Proc. IAEA Specialists Meeting, Berkeley, 1985), IAEA, IWGGCR/13, Vienna (1986) 318-328.
- [60] HEIM, ?, PNP Project Progress Report, BBC-HRB Final Report 1987, PNP-1200-BC-GHRA 005465, BBC Brown Boveri AG, Hochtemperatur-Reaktorbau GmbH (1988).
- [61] OSBORNE, M.F., BRIGGS, R.B., WICHNER, R.P., Iodine Sorption on Low-Chromium Alloy Steel, USDOE Report ORNL/TM-7755, Oak Ridge National Laboratory (1982).
- [62] KFA-HTA, HTA Jahresbericht 1982, Internal Report KFA-HTA-IB-3/83, Research Center Jülich (1983).
- [63] KFA-HTA, HTA Jahresbericht 1983, Internal Report KFA-HTA-IB-1/84, Research Center Jülich (1984).
- [64] KFA-HTA, HTA Jahresbericht 1987, Internal Report KFA-HTA-IB-1/88, Research Center Jülich (1988).
- [65] MÜNCHOW, K., et al., Experimental Facilities for Plate-out Investigations and Future Work, (1980) 26-34.
- [66] BIEDERMANN, P., DEDERICHS, H., Vampyr-I / V03 - V32, Eine Zusammenstellung von Spaltprodukt-Konzentrationen im Kühlgas des AVR, Internal Report KFA-JRB-IB-5/84, Research Center Jülich (1984).

- [67] MALINOWSKI, J., Vergleich einiger Ergebnisse der Vampyr-Experimente, Internal Report KFA-IRB-IB-2/83, Research Center Jülich (1983).
- [68] GOTTAUT, H., Summary of Experiment HTA-12 in the AVR Investigation Programme VAMPYR-II, Final Report, Research Center Jülich (1990).
- [69] SCHREIBER, D., Siemens/Interatom, Personal Communication (1988).
- [70] PETERSEN, I., FRONING, D., Theoretische Auswertung und Interpretation des Ablagerungsversuchs P-06 aus der Pegase-Serie, Internal Report KFA-IRB-IB-10/86, Research Center Jülich (1986).
- [71] INIOTAKIS, N., VON DER DECKEN, C.-B., RÖLLIG, K., SCHLESINGER, H.J., Plate-out of Fission Products and its Effect on Maintenance and Repair, Nucl. Eng. Des. **78** (1984) 273-284.
- [72] INIOTAKIS, N., MALINOWSKI, J., GOTTAUT, H., MÜNCHOW, K., Results from Plate-Out Investigations, Coolant Chemistry, Plate-out and Decontamination in Gas-Cooled Reactors (Proc. IAEA Specialists Meeting, Jülich, 1980), IAEA IWGGCR/2, Vienna (1981) 35-43.
- [73] GENERAL ATOMICS, Pretest Analyses in Support of AVR Depressurization Program, GA Report DOE-HTGR-88120/0, General Atomics (1988).
- [74] TSUYUZAKI, N., MATSUMOTO, M., Report JAERI-M 88-225, Japan Atomic Energy Research Institute (1988) (in Japanese).
- [75] SAWA, K., MURATA, I., SAIKUSA, A., SHINDO, R., et al., Prediction of Nongaseous Fission Products Behavior in the Primary Cooling System of High Temperature Gas-Cooled Reactor, J. Nucl. Sci. Technol. **31** (1994) 654-661.
- [76] SAWA, K., BABA, O., The Verification of Fission Products Plate-out Analysis Code for HTGR -PLAIN-, Report JAERI-M 91-084, Japan Atomic Energy Research Institute (1991) (in Japanese).
- [77] VANSLAGER, F.E., MEARS, L.D., PAD: A Computer Code for Calculating the Plateout Activity Distribution in a Reactor Circuit, GA Document No. 10460, Gulf General Atomic (1971).
- [78] LHIAUBET, G., Dossier Experimental de L'Experience CPL 2/1 Dans la Pile Pegase Du Centre D'Etudes Nucleaires de Cadarache, Report EMT/78/228, Commissariat L'Energie Atomique (1978).
- [79] LHIAUBET, G., Dossier Experimental de L'Experience CCPL 2/3 Dabs la Pile Pegase Du Centre D'Etudes Nucleaires de Cadarache, Report EMT/78/272, Commissariat L'Energie Atomique (1978).
- [80] LHIAUBET, G., Dossier Experimental de L'Experience CCPL 2/1 Bis Dabs la Pile Pegase Du Centre D'Etudes Nucleaires de Cadarache, Report EMT/SYST/79/008, Commissariat L'Energie Atomique (1979).
- [81] LHIAUBET, G., Dossier Experimental de L'Experience CCPL 2/4 Dabs la Pile Pegase Du Centre D'Etudes Nucleaires de Cadarache, Report EMT/SYST/79/095, Commissariat L'Energie Atomique (1979).
- [82] GENERAL ATOMIC COMPANY, HTGR Fuels and Core Development Program, Quarterly Progress Report for Period Ending May 31, 1976, Report GA- A13941, General Atomic Company (1976).
- [83] ABASSIN, J., et al., Etude des Isothermes d'Adsorption de Cesium sur Hastelloy B, Incoloy [sic] et Inox SS347, Compte Rendu DMG No. 40/46, Centre d'Etude Nucleaire de Grenoble (1976).

- [84] DOWNEY, K., KRICH, R., CPL 2 Analysis: Fission Product Release, Plateout and Liftoff - Summary Report, Report HTGR-85-058 (1985).
- [85] JOVANOVIC, V., MCCORD, F., Reanalysis of Iodine Plateout in CPL 2 Inpile Loop, GA Document 909054/0, GA Technologies (1986).
- [86] JOVANOVIC, V., Reanalysis of Cesium Plateout in CPL 2 Inpile Loop, GA Document 909620, GA Technologies (1986).
- [87] BLANCHARD, R.J., In Pile Helium Loop 'COMEDIE', Fission Product Release and Transport in Gas-Cooled Reactors (Proc. IAEA Specialists Meeting, Berkeley, 1985), IAEA, IWGGCR/13, Vienna (1986) 57-73.
- [88] STRONG, D., Summary of SR Experiments in COMEDIE Loop, GA Document 904151, Issue 1, General Atomic Company (1980).
- [89] GILLET, R., et al., COMEDIE BD-1 Experiment: Fission Product Behaviour during Depressurization Transients, Design and Development of Gas-cooled Reactors with Closed Cycle Gas Turbines (IAEA Technical Committee Meeting, Beijing, 1995).
- [90] MEDWID, W., GILLESPIE, A., COMEDIE BD-1 Test Evaluation Report, DOE-HTGR-88552, Rev. 0, General Atomics (1993).
- [91] MILSTEAD, C.E., ZUMWALT, L.R., Cesium Deposition on Stainless Steel, USAEC Report GA-7433, Gulf General Atomic (1966).
- [92] JOVANOVIC, V., WOOD, D., HOOKS, F., MATTIS, E., FSV Plateout Probe Analysis for Decommissioning Study, Report GA-909658, Rev. B, General Atomics (1992).
- [93] BAXTER, A.M., et al., FSV Experience in Support of the GT-MHR Reactor Physics, Fuel Performance, and Graphite, Report GA-A21925, General Atomics (1994).
- [94] CLARK, M.J., The Desorption of Cesium from Peach Bottom HTGR Steam Generator Tubes, Report AERE-R8949, Atomic Energy Research Establishment, Harwell (1979).
- [95] INIOTAKIS, N., VON DER DECKEN, C.-B., DEDERICHHS, H., Verhalten von Spaltprodukten bei der Simulation von Druckentlastungsstörfällen im Kreislauf SMOC (Versuch Sm-2), Internal Report KFA-IRB-IB-3/83, Research Center Jülich (1983).
- [96] DEDERICHHS, H., SACKMANN, B., Versuche Sm-6 und Sm-7 am Experiment SMOC, Internal Report KFA-IRB-IB-3/84, Research Center Jülich (1984).
- [97] DEDERICHHS, H., SACKMANN, B., Versuche Sm-8 und Sm-9 am Experiment SMOC, Internal Report KFA-IRB-IB-4/84, Research Center Jülich (1984).
- [98] GARLAND, J.A., et al., Experimental Study of the Deposition of Iodine and Other Fission Products in a Coolant Circuit of a CAGR, Thermal Nuclear Reactor Safety, (Proc. 5th Int. Meeting, Karlsruhe, 1984), Report KfK-3880, Nuclear Research Center Karlsruhe (1984) 1423-1431.
- [99] WAWRZIK, U., BIEDERMANN, P., OETJEN, H.F., Staub im AVR-Reaktor, Verhalten bei transientes Strömungsbedingungen, (Proc. Jahrestagung Kerntechnik '88, Travemünde, 1988), Inforum GmbH, Bonn (1988) 171-174.
- [100] INIOTAKIS, N., et al., Verhalten von Spaltprodukten bei der Simulation von Druckentlastungsstörfällen im Kreislauf SMOC", (Proc. Jahrestagung Kerntechnik '83, Berlin, 1983), Deutsches Atomforum, Bonn (1983) 219-222.

- [101] GRIEMERT, R., Staubablagerung in Gebieten abgelöster Strömung, Report Jülich 1985, Research Center Jülich (1985).
- [102] SAWA, K., et al., A Study of Plateout Fission Product Behavior during a Large-Scale Pipe Rupture Accident in a High-Temperature Gas-Cooled Reactor, Nucl. Technol. **106** (1994) 265-273.
- [103] SAWA, K., Radiation Exposure in Depressurization Accident of HTTR, Nuclear Safety **32** (1991) 222-228.
- [104] BOLIN, J.M., POLO Users Manual, DOE-HTGR-88332, Rev. 0, General Atomics (1989).
- [105] SAWA, K., MURATA, I., SHIOZAWA, S., MATSUMOTO, S., A Study of Plateout Fission Product Behavior during Large-scale Pipe Rupture Accident of High Temperature Gas-Cooled Reactor, Nucl. Technol. **106** (1994) 265-273.
- [106] SAWA, K., NISHIMOTO, T., MIYAMOTO, Y., Experimental Study of Dust Behavior during Depressurization, J. Nucl. Sci. Technol. **29** (1992) 1018-1025.
- [107] DOWNEY, K., Summary of Fission Product Liftoff Data Base, GA Document 908332/0, GA Technologies Inc. (1985).
- [108] BIEDERMANN, P., BLICK, H., LENNARTZ, T., SEIFERT, J., Zur γ -spektrometrischen Nachuntersuchung des Experimentes VAMPYR-I/V41 (Transientenversuch T2), Technical Note KFA-IRB-TN-05/87, Research Center Jülich (1987).
- [109] BIEDERMANN, P., BLICK, H., LENNARTZ, T., SEIFERT, J., Zur γ -spektrometrischen Nachuntersuchung des Experimentes VAMPYR-I/V44 (Transientenversuch T4), Technical Note KFA-IEV-TN-09/90, Research Center Jülich (1990).
- [110] BIEDERMANN, P., BLICK, H., LENNARTZ, T., SEIFERT, J., Zur γ -spektrometrischen Nachuntersuchung des Experimentes VAMPYR-I/V46 (Transientenversuch T5), Technical Note KFA-IEV-TN-10/90, Research Center Jülich (1990).
- [111] JUMPERTZ, P., HTA-14 Versuche zur Staubremobilisierung, Gebläsetransiente T5, AVR Technical Note H5-X4/Jum/Ga, Arbeitsgemeinschaft Versuchsreaktor GmbH (1988).
- [112] SAWA, K., et al., Evaluation of Lift-off Fraction in Accident Condition of HTGR, Report JAERI-M 91-207, Japan Atomic Energy Research Institute (1991) (in Japanese).
- [113] MÜLLER, A., Zur Jod-Desorption bei Wassereinbruch in den HTR-Primärkreis, Internal Report KFA-ISF-IB-1/79, Research Center Jülich (1979).
- [114] DE NORDWALL, H.J., Fission Product Technology, Chapter 13 in Report ORNL-4975, Oak Ridge National Laboratory (1974).
- [115] CHRIST, A., HAASE, F.W., WIEDMANN, J., Experimentelle Untersuchungen zur Cäsium-Ablagerung auf Hochtemperatur-Werkstoffen, (Proc. Jahrestagung Kerntechnik '85, München, 1985), Inforum GmbH, Bonn (1985) 175-178.
- [116] INIOTAKIS, N., VON DER DECKEN, C.B., Radiological Consequences of a Depressurization Accident Combined with Water Ingress in an HTR Modul-200, Nucl. Eng. Des. **109** (1988) 299-306.
- [117] MOORMANN, R., Source Term Estimation for Small-Sized HTR's, Report Jülich 2669, Research Center Jülich (1992).

- [118] BORKOWSKI, R., BUNZ, H., SCHÖCK, W., Resuspension of Fission Products During Severe Accidents in LWR's, Report KfK-3987, Nuclear Research Center Karlsruhe (1985).
- [119] GA TECHNOLOGIES, Fuel Design Data Manual, Report GA-901866, Issue F, GA Technologies Inc. (1987).
- [120] HEIM, ?, PNP Project Progress Report, BBC-HRB Final Report 1986, PNP-1200-BC-GHRA 005066, BBC Brown Boveri AG, Hochtemperatur-Reaktorbau GmbH (1987).
- [121] PUCCINI, F., Contribution l'Etudes des Depots de Produits de Fission et de Leur Reentrainment, Thesis, L'Institut National Polytechnique de Grenoble (1976).
- [122] BEAHM, E.C., SHOCKLEY, W.E., Fission Product Washoff from Structural Alloys: Preliminary Tests, Report ORNL/NPR-90/45, Oak Ridge National Laboratory (1991).
- [123] NRC, Technical Bases for Estimating Fission Product Behavior during LWR Accidents, NRC Report NUREG-0772, US Nuclear Regulatory Commission (1981).
- [124] BREITUNG, W., Oxygen Self and Chemical Diffusion Coefficients in $\text{UO}_{2\pm x}$, J. Nucl. Mater. 74 (1978) 10-18.
- [125] KUHLMANN, W.C., Treatment of UO_2 with Water Vapor at High Temperatures, Report MCW-103, (1948).
- [126] ORNL, GCR Program, Semiannual Progress Report for Period Ending Sept. 30, 1966, ORNL-4035, Oak Ridge National Laboratory (1967) 124-126.
- [127] ORNL, GCR Program, Annual Progress Report 1973, ORNL-4975, Oak Ridge National Laboratory (1975) Chap. 13.
- [128] ASHWORTH, F.P.O., Information from Water Ingress Accident on AVR, Report JüI-Spez-43, Research Center Jülich (1979).
- [129] PSID Safety Analysis Supplement: Safety Methods and Consequence Description for the Standard MHTGR, DOE-HTGR- 87009, Rev. 0 (1987).
- [130] OETJEN, H.F., Beschreibung einer Apparatur zur Behandlung radioaktiv kontaminierte Rohre mit überhitztem Wasserdampf, Technical Note KFA-IRB-TN-3/84, Research Center Jülich (1984).
- [131] BIEDERMANN, Gammaspektroskopie von Proben aus SMOC SM9-Wasser bzw. Dampfbehandlungen, Technical Note KFA-IRB-TN-8/86, Research Center Jülich (1986).
- [132] INIOTAKIS, N., Einfluß des Wassers bzw. Wasserdampfes auf die Remobilisierung von an Metallocerflächen angelagertem Cäsium, Internal Report KFA-IRB-IB-3/85, Research Center Jülich (1985).
- [133] ANS-CNA, Decontamination of Nuclear Facilities, (Int. Joint Topical Meeting, ?, 1982).
- [134] IAEA, Decontamination and Decommissioning of Nuclear Facilities, Final Report IAEA-TECDOC-511, International Atomic Energy Agency, Vienna (1989).
- [135] IAEA, Decontamination and Decommissioning of Nuclear Facilities, Phase II: 1989-1993, Report IAEA-TECDOC-716, International Atomic Energy Agency, Vienna (1993).
- [136] HANULIK, J., SCHMIED, H., WAHL, J., Plate-out Measurements and Decontamination of a Component of the AVR Reactor at Jülich, Plate-out and Decontamination in Gas-Cooled Reactors, (Proc. IAEA Specialists Meeting, Jülich, 1980), IAEA IWGGCR/2, Vienna (1981) 99-106.

- [137] HANULIK, J., et al., Plateout Measurements and Decontamination Work on AVR Reactor Component Parts in Jülich, Report EIR No. 384, Eidgenössisches Institut für Reaktorforschung (1980) and Report GA-905755, General Atomic Company (1981).
- [138] LURIE, R., Decontamination of the Main Circuits of the G2 Gas-Graphite Reactor, Decontamination and Decommissioning of Nuclear Facilities, Final Report IAEA-TECDOC-511, International Atomic Energy Agency (1989).
- [139] PICK, M.E., Summary of Work on Characterization of The Radioactive Deposits on PWR Primary Circuit Surfaces, Decontamination and Decommissioning of Nuclear Facilities, Decontamination and Decommissioning of Nuclear Facilities, Final Report IAEA-TECDOC-511, International Atomic Energy Agency (1989).
- [140] COURTOIS, C., GAUCHON, J.P., COSTES, J.R., LORIN, ?, Decontamination Techniques for Dismantling, Decommissioning Policies, (Proc. Int. Seminar, Paris, 1991).
- [141] ETZEL, K.T., HHT Fission Product Behavior and Decontamination, Memo to F.A. Silady 647:KTE:010.93, General Atomics (1993).
- [142] GOTTAUT, H., MALINOWSKI, J., Einige Ergebnisse der Bestimmung von Diffusionsprofilen in HTR-Werkstoffen, Internal Report KFA-IRB-IB-2/79, Research Center Jülich (1979).
- [143] JAKOBET, J., PFEIFER, J.-P., ULLRICH, G., Evaluation of High-Temperature Alloys for Helium Gas Turbines, Nucl. Technol. 66 (1984) 195-206.
- [144] SCHENKER, E., ULLRICH, G., LÖWENSCHUSS, H., HANULIK, J., Contamination and Decontamination of Incoloy 800 Samples from the KFA Experimental Duct of the Dragon Reactor, in: BETTERIDGE, W. , et al., (Eds.), Alloy 800, North Holland Publishing Co. (1978).
- [145] ULLRICH, G., SCHENKER, E., Mechanical Properties of Incoloy 800 from the KFA Experimental Duct at 700 oC and 480 d in The Dragon Reactor, Before and After Decontamination, in: BETTERIDGE, W. , et al., (Eds.), Alloy 800, North Holland Publishing Co. (1978).
- [146] FAURY, M., Decontamination of a Gas Cooler Using Foams Containing Chemical Reagents, Decommissioning of Nuclear Installation, (Proc. 3rd Int. Conf., Luxembourg, 1994), Report CEA-CONF-12073, CEA Centre d'Etudes de Cadarache (1994).
- [147] ALBERSTEIN, D., Fort St. Vrain Circulator Decontamination Experience, Memo to D.L. Hanson 866-DA-019-95, General Atomics (1995).
- [148] BALDWIN, N., Radiochemical Examination of Fort St. Vrain Helium Circulator C2105, Report GA-909776, Issue N/C, General Atomics (1988).
- [149] BALDWIN, N.L., et al., Radiochemical Examination of Peach Bottom HTGR Component Samples, Report GA-A14495, General Atomic Company (1978).
- [150] ROGERS, L.N., HOOPER, A.J., Decontamination of CAGR Gas Circulator Components, Fission Product Release and Transport in Gas-Cooled Reactors (Proc. IAEA Specialists Meeting, Berkeley, 1985), IAEA, IWGGCR/13, Vienna (1986) 385-401.
- [151] SAWA, K., Fission Products and Dust Behaviours in Depressurization Condition, Presented at the 2nd Research Coordination Meeting on Validation of Predictive method for Fuel and Fission Product Behaviour in Gas-Cooled Reactors, Tokai, JAERI (1994).

- [152] NABBI, R. (Ed.), Sicherheitstechnische Untersuchungen zum Störfallverhalten des HTR-500, Report JüL-Spez-240, Research Center Jülich (1984).
- [153] MOORMANN, R., VERFONDERN, K., Methodik umfassender probabilistischer Sicherheitsanalysen für zukünftige HTR-Anlagenkonzepte - Ein Statusbericht (Stand 1986), Band 3: Spaltproduktfreisetzung, Report JüL-Spez-388/Vol. 3, Research Center Jülich (1987).
- [154] BUNZ, H., PARDISEKO, Ein Computerprogramm zur Berechnung des Aerosolverhaltens in geschlossenen Behältern, Report KfK-3545, Nuclear Research Center Karlsruhe (1983).
- [155] LANDONI, J.A., Containment Atmosphere Response (CAR) Program Status Report, DOE Report GA-A14699, General Atomic Company (1978).
- [156] MURATA, K.K., et al., User's Manual for CONTAIN 1.1: A Computer Code for Severe Nuclear Reactor Accident Containment Analysis, Report NUREG/CR-5026, SAND87-2309, Sandia National Laboratories (1989).
- [157] FERNANDES, A., LOYALKA, S.K., Modeling of Diffusive Gravitational Aerosol Deposition in CONTAIN, Nucl. Technol. 113 (1996) 155-165.
- [158] GEORGE, T.L., THURGOOD, M.J., WILES, L.E., WHEELER, C.L., Containment Analysis with GOTHIC, Heat Transfer (Proc. Nat. Conf., Minneapolis, 1991), American Society of Mechanical Engineers (1991).
- [159] FISCHER, K., Qualification of a Passive Catalytic Module for Hydrogen Mitigation, Nucl. Technol. 112 (1995) 58-62.
- [160] MERTENS, J. (Ed.), Sicherheitstechnische Untersuchungen zum Störfallverhalten des HTR-Modul, Report JüL-Spez-335, Research Center Jülich (1985).
- [161] MOORMANN, R., SCHWARZER, K., Abschätzung zur Jodrückhaltung im Confinement des HTR-Modul beim Druckentlastungsstörfall, Technical Note KFA-ISF-AN-11/85 III, Research Center Jülich (1985).
- [162] ZAK, B.D., RUSSO, A.J., Core Meltdown Experimental Review, Report SAND 74 - 0382, Sandia National Laboratory (1974) Chapter 8.
- [163] KATSCHER, W. STAUCH, B., Experimental Investigations on Aerosol Formation from Metallic Fission Products under Hypothetical Accident Conditions in High-Temperature Gas-Cooled Reactors, (Proc. European Aerosol Conf., Vienna, 1989), Paper 087.
- [164] GESELLSCHAFT FÜR REAKTORSICHERHEIT (Ed.), Incident Calculation Bases for the Guide Lines Issued by the BMI for the Assessment of the Design of PWR Nuclear Power Plants Pursuant to § 28.3 of the Radiological Protection Ordinance, GRS Quantitative Examination, Gesellschaft für Reaktorsicherheit (1983).
- [165] GESELLSCHAFT FÜR REAKTORSICHERHEIT (Ed.), Deutsche Risikostudie Kernkraftwerke Phase B, Report GRS-72, Gesellschaft für Reaktorsicherheit (1989).
- [166] SAWA, K., et al., Siting Evaluation of the High Temperature Engineering Test Reactor, Report JAERI-Research 91-158, Japan Atomic Energy Research Institute (1996) (in Japanese).
- [167] MANEKE, J.L., Review of Radionuclide Retention Models and Data Applicable to the Reactor Building of the MHTGR, Report DOE-HTGR-88236 (1988).
- [168] SCHLENGER, B.J., Investigation of Fission Product Aerosol Behavior in an HTR Containment Building during Severe Core-Heatup Accidents using PARDISEKO IV, Internal Report KFA-ISF- IB-1/88, Research Center Jülich (1988).

- [169] POSTMA, A.K., SHERRY, R.R., TAM, P.S., Technical Bases for Models of Spray Washout of Airborne Contaminants in Containment Vessels, Report NUREG/CR-0009 (1978).
- [170] NRC, Technical Bases for Estimating Fission Product Behavior during LWR Accidents, Report NUREG-0772, US Nuclear Regulatory Commission (1981).
- [171] RASTLER, D.M., Suppression Pool Scrubbing for Postulated Boiling Water Reactor Accident Conditions, Report NEDO-25420, General Electric (1981).
- [172] PARSLY, L.F., Calculation of Iodine-Water Partition Coefficients, Report ORNL-TM-2412, Part IV, Oak Ridge National Laboratory (1970).
- [173] BELL, J.T., CAMPBELL, D.D., LIETZKE, M.H., TOTH, L.M., Aqueous Iodine Chemistry in LWR Accidents, NRC Report NUREG/CR-2493, Oak Ridge National Laboratory (1982).
- [174] KANZLEITER, T., et. al., DEMONA Experiments Investing Aerosol Behavior within a Containment, Source Term Evaluation for Accident Conditions (Proc. IAEA International Symposium, Columbus, OH, 1985) IAEA-SM-281/1 (1985).
- [175] WRIGHT, A.L., PATTERSON, W.L., Summary of TRAP-MELT2 Results for Aerosol Transport Test A105 and A106, Report ORNL/NRC/LTR-86/9, Oak Ridge National Laboratory (1986).
- [176] RAHN, F.J., COLLEN, J., WRIGHT, A.L., Aerosol Behavior Experiments on Light- Water Reactor Primary Systems, Nucl. Techn. 81 (1988) 158-182.
- [177] SCHÖCK, W., et al., Large-Scale Experiments on Aerosol Behavior in Light Water Reactor Containments, Nucl. Techn. 81 (1988) 139-157.
- [178] COLLEN, J., et al., The MARVIKEN Experiments - Fifth Series Large Scale Aerosol Transport Tests, Summary Report, MXE-301, Studsvik Energiteknik AB (1985).
- [179] RAHN, F.J., Summary of the LWR Aerosol Containment Experiments (LACE) Program, Report LACE-TR-012 (1987).
- [180] LIDSKY, L., Survey of Commercial CDF Software with Specific Reference to GT-MHR Design Problems, Final Report for Purchase Order No. SC L411801, Massachusetts Institute of Technology (1995).
- [181] BUCKLEY, D.W., TDAC – An Analytical Computer Program to Calculate the Time-Dependent Radiological Effects of Radionuclide Release, unpublished, General Atomic Company (1976).
- [182] LEE, C.E., APPERSON, C.E., FOLEY, J.E., LEAF, A Computer Program to Calculate Fission Product Release from a Reactor Containment Building for Arbitrary Radioactive Decay Chains, Report LA-NUREG-6570-MS, Los Alamos National Laboratory (1976).

7. ADVANCED FUELS

In the past 25 years, the coated particle fuels have been evolved through various improvements after the first application in the Dragon Reactor, and to date two types of the fuel elements, the spherical fuel and the block fuel using TRISO-coated particles are available for the HTGRs in the world. Meanwhile, the HTGR fuels in the next generation are required for a higher temperature utilization and an enhanced safety. To ensure these demands, many attempts have been made so far, and these will be continued in future.

For the higher temperature utilization of the HTGR fuels, a key issue is an adoption of a more refractory carbide than silicon carbide (SiC) used as the coating layer in the conventional coated fuel particles. Since zirconium carbide (ZrC) is one of the promising materials to meet this requirement, the development works on the ZrC coating layer have been conducted in the United States, Japan, and Russia. In the United States, ZrC was also tested as a fission product and oxygen getter inside the coated particles, by depositing over the fuel kernel or dispersing through the buffer layer.

Another attempt to reduce the fuel temperature without any reduction of the cooling gas temperature has been made in Japan for the block fuel containing fuel rods following the works at Dragon Project. The standard fuel design for the Japanese HTGR (so-called HTTR) contrives the fuel rod consisting of the fuel compacts and the graphite tube (sleeve). For aiming at a better heat transfer between these components, the monolithic fuel rod consolidating these components in one body has been examined.

On the other hand, a significant safety requirement arose for protecting the spherical fuel elements from the corrosion by air or steam ingress in case of reactor accidents. For meeting this requirement, the protective layer composed of SiC as a principal ingredient as well as the corrosion resistant matrix have been developed in countries which are relevant to the development of the spherical fuel elements as Germany, Russia, and China. This chapter deals with performance of the advanced fuel on the basis of these attempts.

7.1. ZrC-COATED FUEL PARTICLES

Zirconium carbide (ZrC) is known as a refractory and chemically stable compound, having a melting point of 3540 °C, and melts eutectically with carbon at 2850 °C [1]. SiC sublimes at temperatures of about 1800 °C [2]. ZrC is a candidate to replace the SiC coating layer of the Triso-coated fuel particles. The resulting particles are termed ZrC-TRISO coated fuel particles.

The evaluation of ZrC as a coating material for VHTR fuels is part of a recently published study prepared by Kasten et al. [2]. They summarized pertinent portions of the available literature on the ZrC coating layers and proposed an R&D program for developing high quality ZrC-TRISO coated particle fuels. It was mentioned that the use of the ZrC-TRISO coated particles has several potential advantages. A primary one is the potential for improved fission product retention at very high temperatures, such that the peak fuel

temperature permissible under operating and accident conditions would increase while still retaining a very high degree of inherent safety. An associated feature would be the ability to operate at relatively high core power densities while maintaining a very high degree of safety. Also, use of ZrC coatings instead of SiC coatings could increase the temperature at which fuel matrix material can be carbonized during the fabrication process, could result in increased thermal conductivity of the fuel matrix material, and could reduce fuel operating temperatures for a given reactor-outlet coolant temperature [2].

7.1.1. Fuel Particle Design

In the United States, several coating designs have been tested [3, 4]: ZrC-TRISO coated particles, ZrC-TRISO type coated particles without outer pyrocarbon (PyC) layer, ZrC-coated particles with ZrC-doped outer PyC layer, and ZrC-coated particles with graded C-ZrC layer(s). In the graded C-ZrC layer, the compositions are changed gradually from the pure pyrocarbon through the C-ZrC alloy and into the pure ZrC. The graded layer was applied to either inside or outside of the ZrC layer. Propylene was used to produce the pure pyrocarbon and to provide the carbon for the graded portion of the co-deposited carbon and ZrC.

Although most of the work reported on the use of ZrC in coated fuel particles has been directed towards the development to replace the SiC barrier layer, ZrC was also tested as a fission product and oxygen getter [5, 6], where ZrC was deposited over the fuel kernel or ZrC was dispersed throughout the buffer layer. The primarily interesting design was the UO₂ kernel coated by the ZrC layer which was denoted as UO₂^{*}, followed by the standard SiC-TRISO coatings. The original purpose of the ZrC layer in this design was to provide a getter that would react with the oxygen released by the fissions in the UO₂ kernel to form ZrO₂, thereby reducing gas pressure buildup from CO generation and gas-pressure-driven kernel migration [7].

In Japan, ZrC-coated fuel particles have been developed since the early 1970s at JAERI [1]. The first generation of the ZrC-coated fuel particles was characterized by a thick ZrC layer with composition C/Zr > 1.0 and by the absence of the outer PyC layer. The ZrC was called "Zirconium-Carbally" meaning ZrC-C alloy. Later it was found that the retention of metallic fission products, especially Sr-90, by the Zr-Carbally was rather poor [8], presumably owing to a short circuit through free carbon phase. And it was also felt from the irradiation experiences that the presence of the outer PyC was essential for the mechanical integrity of the coated fuel particles. Hence, in the second generation, the emphasis was placed on the development of the ZrC-TRISO coated particles with the ZrC composition C/Zr=1.0.

7.1.2. Coating Processes

Coating layers of ZrC and ZrC-C alloy were prepared by the chemical vapor deposition, where the reaction of zirconium halide with hydrocarbon was used in principle. Two methods have been developed for supplying zirconium halide to the coater: sublimation of ZrCl₄ [4, 9, 10, 11] and *in-situ* generation of zirconium halide vapor [12, 13, 14, 15, 16, 17, 18, 19].

At Los Alamos Scientific Laboratory (LASL), the chemical vapor deposition of ZrC has been studied using a gas mixture of CH₄, H₂, ZrCl₄ and Ar [4, 9, 10, 11]. A key development in the ZrC coating project proved to be the ZrCl₄ powder feeder for metering ZrCl₄ into the coater. ZrCl₄ is a solid at room temperature, and sublimes at 352 °C. In this process, the ZrCl₄ powder was supplied from the powder feeder, whose rate was controlled by the auger speed and metered by the output of the load cell on which the powder feeder was hung. The powder was swept by Ar to the coater base where it was mixed with the other coating gases supplied from a gas manifold. The ZrCl₄ powder in the gas stream was vaporized in the coater base before entering the coating chamber [10].

Wagner et al. [10] studied effects of varying CH₄ and H₂ concentrations, and particle bed area on the coating rate, the appearance, and the composition of the ZrC, using the ZrCl₄ powder feeder in which the mass flow rate of the powder could be varied and controlled accurately. Increases in CH₄ and H₂ concentration were effective in increasing the linear coating rate of ZrC. Increases in the ratio of CH₄ over ZrCl₄ in the coating gas resulted in a decreased metallic appearance of the coating and an increase in the C/Zr in the deposit. Increases in H₂ inhibited these effects.

Hollabaugh et al. [11] have prepared ZrC coating using a gas mixture of C₃H₆, H₂, ZrCl₄ and Ar with the same coater and ZrCl₄ powder feeder as those used by Wagner et al. [10]. In general, ZrC coatings made with CH₄ and C₃H₆ were similar and were similarly affected by variations in the hydrocarbon and hydrogen concentrations. The coatings made using the ZrCl₄-C₃H₆ reaction were more sensitive to changes in hydrogen concentration than those made using CH₄.

At INET, China, the ZrC coating process was recently examined [20], which was the same as the one described in [11]. The ZrC coatings derived from the process were characterized, and the oxidation behavior was discussed.

At JAERI, on the other hand, the coating processes based on the *in-situ* generation of zirconium halide vapor have been investigated in order to avoid the handling of highly hygroscopic halide powder [1]. Ikawa et al. [12, 13, 14, 15, 16, 17] and Ogawa et al. [18, 19] studied several processes: the chloride process [12], the methylene dichloride process [13], the iodide process [14, 15], and the bromide process [16, 17, 18, 19]. Among these processes, the bromide process proved to be the most convenient and reliable. Fig. 7-1 [21] shows the experimental apparatus for depositing ZrC by the bromide process. In this process, the bromine which is liquid at room temperature, was carried by argon onto the heated zirconium sponge to generate the bromide vapor, and the vapor was mixed with methane and hydrogen to be fed into a spouted bed of fuel particles.

Ogawa et al. [19] studied effects of gas composition and temperature on the chemical vapor deposition of ZrC within a spouted bed by the bromide process. The feed gas was a mixture of ZrBr₄, CH₄, H₂ and Ar. The results of the deposition experiment were compared with the calculated chemical equilibria in the Zr-C-H-Br system. The thermochemical analysis predicted that the methane determined the deposition in the ZrC monophase region and that the ZrBr₄ concentration diminished the C/Zr ratio of the deposit to 1.0. It was found that the weight and composition of the deposit could be calculated by thermochemical analysis after correcting the supply of methane for its pyrolysis efficiency.

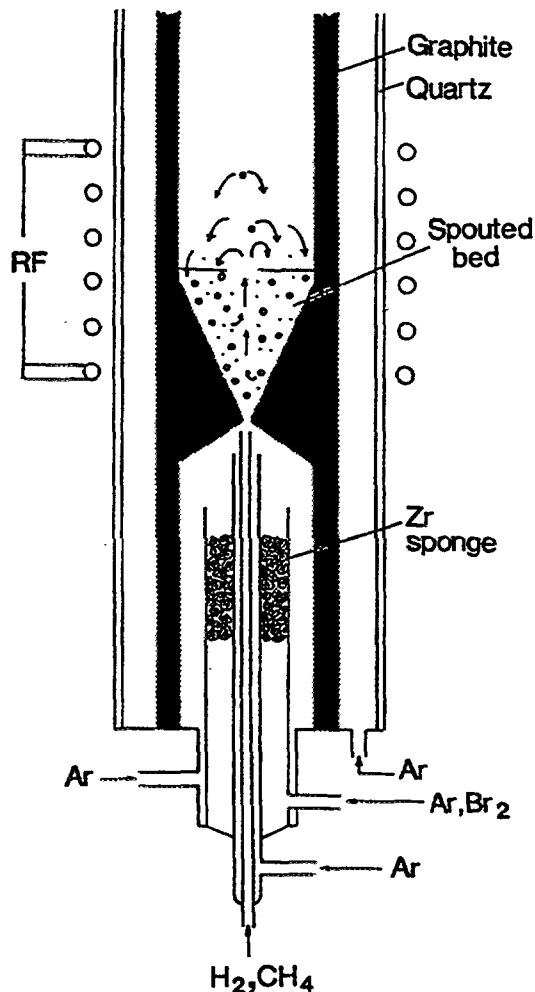


Fig. 7-1: Experimental apparatus for depositing ZrC by the bromide process [21]

Predominant reactions presumably occurring were derived by a mass balance consideration on the calculated equilibrium species. A simplified model of the ZrC deposition was proposed [19].

7.1.3. Characterization Techniques

In the case of the SiC-TRISO coated particles, the PyC layers are burnt off to recover the SiC fragments for characterization such as density, composition, strength measurements, etc. However, it was almost impossible to separate the ZrC from the PyC layers by the same method, since ZrC, in contrast with SiC, does not form a protective oxide layer, resulting in oxidation of ZrC to ZrO₂ when exposed to air at high temperatures [21].

Ogawa et al. [21] have developed the method for obtaining the ZrC fragments from the coating layers containing the PyC. They found that the ZrC is virtually unaffected by plasma oxidation. Fig. 7-2 [21] shows the plasma oxidation apparatus, where low-pressure oxygen is ionized by high-frequency induction coupling at 75 MHz. Plasma reaction was monitored by a color analyzer and an optical power meter. The color changed from pale violet of pure oxygen to pale blue during vigorous oxidation of free carbon, and again to

pale violet when the PyC was completely removed and a very thin oxide scale was formed on the ZrC. The brightness also changed dramatically during the reaction. It was confirmed by Raman spectroscopy and X-ray diffraction that the bulk of the ZrC remained unaffected by the plasma oxidation [22].

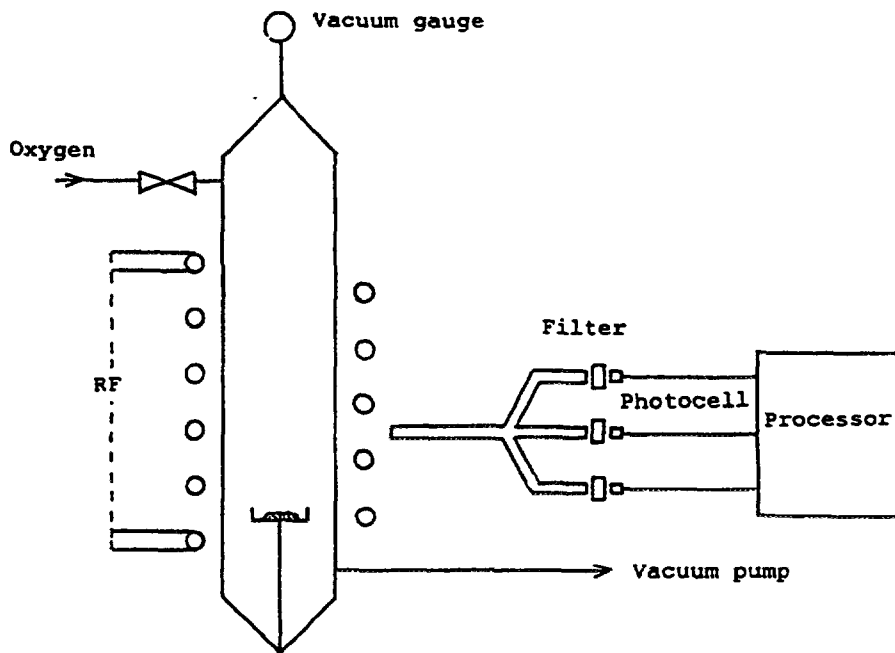


Fig. 7-2: Plasma oxidation apparatus for removing PyC layers from ZrC [21]

Plasma oxidation with emission monitoring was also applied to the quantitative analysis of free carbon in ZrC powder [23]. The analysis of the free carbon is important for the quality control of the ZrC coating. The emission was monitored with an optical color analyzer and was calibrated with standard samples of ZrO_2+C mixtures. Oxidation rates of the free and the combined carbons are so different that it is possible to estimate the amount of the former from the emission. With powdered ZrC of about 10 mg, the free carbon of less than 1 wt% could be easily determined. Without this method, the composition of the ZrC was estimated by burning the ZrC and PyC together, weighing ZrO_2 and CO_2 , and subtracting the contribution of PyC from the total amount of CO_2 [21].

7.1.4. Fuel Performance during Normal Operation

Although systematic irradiation experiments have not been completed on the ZrC-coated fuel particles, some promising data were obtained. The ZrC layer is less susceptible to chemical attack by fission products and fuel kernels, and the ZrC-coated fuel particles perform better than the SiC-TRISO coated particles at high temperatures, especially above 1600 °C. Some early irradiation tests showed poor performance of the ZrC-coated particles which may be attributed to the fact that the fabrication conditions had not been optimized.

Irradiation tests on the LASL-made ZrC-coated particles [24, 25, 26, 27] were carried out in the High Flux Isotope Reactor (HFIR) and the Oak Ridge Research Reactor (ORR).

Table 7-1 summarizes the irradiation conditions. Prior to the tests on the fuel-kerneled coated particles, carbon-kerneled inert coated particles were tested to determine the stability of the ZrC at high temperature and fluence [24, 25]. The irradiation results of the inert coated particles were encouraging. In the tests of the fuel-kerneled particles, it was found that the graded coatings in the OF-2 capsule were cracked and it was postulated that the cracking was associated with the low PyC deposition rate and was not related to the ZrC [26]. Metallographic examination showed that the performance of the ZrC-coated particles in the HRB-12 capsule appeared to be poor in comparison with the SiC-coated particles. However, there was no evidence of palladium attack on any of the ZrC layers [27].

GAC-made ZrC-TRISO coated fuel particles were irradiated in HFIR [28, 29, 30]. The irradiation conditions are listed in Table 7-2 [28, 29, 30]. The performance of the ZrC-TRISO coated particles was very favorable. However, there was evidence that ZrC might not be as effective in retaining fission products as SiC. Microprobe analysis showed rare-earth fission products on the outside of the ZrC coating, whereas all cesium was retained within the coating [28]. The ZrC layers in the ZrC-TRISO coated UO₂ and UC₂ particles in the HRB-15A capsule suffered no fission product attack, while the standard SiC-TRISO coated fuel particles showed some degree of SiC-fission product interaction. The ZrC-TRISO coated UC₂ particles, however, showed poor retention of silver and europium, with large variety from particle to particle in this respect [29].

Reynolds et al. [31] performed irradiation tests of ZrC-coated fuel particles in the Siloe test reactor. Table 7-3 shows the irradiation conditions [31]. Postirradiation stereoscopic, metallographic and electron-beam microprobe examinations of the particles showed that the ZrC possessed exceptional resistance to chemical attack by fission products and good mechanical stability under irradiation. No chemical attack of the ZrC was found even in the case where the ZrC was adjacent to the UC₂ kernel.

Irradiation tests on the SiC-TRISO coated UO₂* particles which had a ZrC layer applied to the UO₂ kernel [29, 30, 32, 33], were carried out in HFIR. The irradiation conditions are listed in Table 7-4 [29, 30, 32, 33]. No detrimental irradiation effects were ceramographically found, except for carbon that precipitates near the outer edge of the kernels, which may result from the gettering action of the ZrC. The kernel migration was not observed in the SiC-TRISO coated UO₂* particles but in the standard SiC-TRISO coated UO₂ particles in the HRB-15A and HRB-16 capsules. The absence of kernel migration in the SiC-TRISO coated UO₂* particles was good evidence that this potentially detrimental phenomenon in oxide fuels can be controlled by the addition of oxygen getters [33]. There also appeared to be a reduction in fission product corrosion of the SiC layers even in cases where ZrC layer eventually fails [34]. The improved silver retention of the SiC-TRISO coated UO₂* particles during irradiation was found in the measurements of the inventories by "Irradiated Microsphere Gamma Analyzer" (IMGA). The best evidence was that the particles irradiated in the HRB-16 capsule retained silver at or near 100 % during irradiation [34]. It was not necessary to maintain an intact ZrC layer throughout irradiation to achieve improved silver retention. The key to the improved irradiation performance seemed to be the better quality SiC layer obtained in these particles which could be made possible by

- (1) less heavy metal contamination of the SiC layer as a result of better retention of kernel material during coating process because of the presence of an intact ZrC layer during SiC deposition, and by

Table 7-1: Irradiation conditions of LASL-made ZrC-coated particles [24, 25, 26, 27]

Capsule	Sample type	Temperature [°C]	Burnup [%FIMA]	Fast fluence [m ⁻² , E > 29 fJ]
HT-28	C-kernel, no outer PyC	900	0	3.5*10 ²⁵
	C-kernel, ZrC-TRISO			
	C-kernel, graded C-ZrC	1250	0	7.5*10 ²⁵
	C-kernel, double-graded			
HT-29	C-kernel, no outer PyC	900	0	9.4*10 ²⁵
	C-kernel, ZrC-TRISO			4.4*10 ²⁵
	C-kernel, graded C-ZrC			9.0*10 ²⁵
	C-kernel, double-graded			10.7*10 ²⁵
				4.4*10 ²⁵
				9.0*10 ²⁵
				10.7*10 ²⁵
HT-31	C-kernel, ZrC-doped outer PyC	1250	0	8.65*10 ²⁵
				8.89*10 ²⁵
				9.00*10 ²⁵
OF-2	UC ₂ , double-graded C-ZrC-C	1150	73	5.6*10 ²⁵
		1350	80	8.4*10 ²⁵
HRB-12	UC _{4.6} O _{1.1} , ZrC-TRISO	—	84	4.40*10 ²⁵
		1250	86	6.90*10 ²⁵
	UC _{4.6} O _{1.1} , ZrC-doped outer PyC	1100	85	4.94*10 ²⁵
		—	87	7.14*10 ²⁵
	UC _{4.6} O _{1.1} , graded C-ZrC and ZrC-doped outer PyC	1260	85	5.40*10 ²⁵
		—	87	7.36*10 ²⁵

(2) reduced corrosion of the SiC layer from chemical reactions with fission products during irradiation because of the shortened reaction time remaining subsequent to ZrC failure [34].

At JAERI, irradiation experiments have been made on the ZrC-coated UO₂ particles characterized by the Zr-Carballyo layer without the outer PyC [1] and the ZrC-TRISO coated UO₂ particles [35].

Table 7-2: Irradiation conditions of GAC-made ZrC-coated fuel particles [28, 29, 30]

Capsule	Sample type	Temperature [°C]	Burnup [%FIMA]	Fast fluence [m^{-2} , $E > 29 \text{ fJ}$]
HRB-7	UC_2 , ZrC-TRISO, rod	1225	84.4	4.50×10^{25}
				5.92×10^{25}
HRB-15A	UC_2 , ZrC-TRISO, rod	1125	28.1	6.2×10^{25}
	UC_2 , ZrC-TRISO, tray	1130	26.7	5.8×10^{25}
		1055	24.9	4.9×10^{25}
	UC_2 , ZrC-TRISO, wafer	1125	28.3	6.3×10^{25}
		1065	27.4	5.7×10^{25}
	UO_2 , ZrC-TRISO, rod	1075	27.2	6.0×10^{25}
	UO_2 , ZrC-TRISO, tray	1125	27.6	6.1×10^{25}
		1100	27.6	6.1×10^{25}
	UO_2 , ZrC-TRISO, wafer	1125	28.8	6.2×10^{25}
HRB-16	UC_2 , ZrC-TRISO, tray	1080	20.9	4.1×10^{25}
	UC_xO_y , ZrC-TRISO, tray	1160	20.3	3.8×10^{25}

Table 7-3: Irradiation conditions of ZrC-coated fuel particles by Reynolds et al. [31]

Sample type	Temperature [°C]	Burnup [%FIMA]	Fast fluence [m^{-2} , $E > 29 \text{ fJ}$]	
UC_2 / buffer / ZrC / PyC	1200	70	5×10^{25}	
UC_2 / ZrC / buffer / PyC				
(8Th,U) O_2 / buffer / ZrC / PyC		8		
(8Th,U) O_2 / ZrC / buffer / PyC				

The first generation of the ZrC-coated UO_2 particles were charged into four capsules and irradiated in the Japan Materials Testing Reactor (JMTR), as summarized in Table 7-5 [1]. In all cases, the particles were placed in a multi-hole graphite holder containing also the SiC-TRISO coated particles as the reference. The particles in the 73F-12A and 73F-13A capsules experienced very high temperatures exceeding 1600 °C. The failure fractions of the ZrC-coated particles were rather high, though they were on a par with those of the SiC-TRISO particles or below. Ceramographic examination showed the UO_2 kernels came in contact with the Zr-Carballyo layers by the amoeba effect in the particles which

Table 7-4: Irradiation conditions of TRISO-coated UO₂^{*} particles [29, 30, 32, 33]

Capsule	Sample type ⁽¹⁾	Temperature [°C]	Burnup [%FIMA]	Fast fluence [m ⁻² , E > 29 fJ]
HRB-15A	UO ₂ [*] , SiC-TRISO, rod	1040	22.0	4.4*10 ²⁵
		1110	28.5	6.1*10 ²⁵
		1120	29.0	6.5*10 ²⁵
	UO ₂ [*] , SiC-TRISO, wafer	1050	22.8	4.6*10 ²⁵
		1095	28.2	6.0*10 ²⁵
		1125	29.1	6.5*10 ²⁵
	UO ₂ [*] , SiC-TRISO, tray	1080	22.8	4.6*10 ²⁵
		1125	28.2	6.0*10 ²⁵
HRB-15B	UO ₂ [*] , SiC-TRISO, tray	860	23.8	5.4*10 ²⁵
		860	24.0	5.5*10 ²⁵
		905	26.6	6.6*10 ²⁵
		915	26.7	6.5*10 ²⁵
		1080	19.0	3.7*10 ²⁵
HRB-16	UO ₂ [*] , SiC-TRISO, rod	1086	20.0	4.2*10 ²⁵
		1148	25.1	5.6*10 ²⁵
		1175	26.9	6.1*10 ²⁵
		1175	27.3	6.3*10 ²⁵
		1212	27.6	6.3*10 ²⁵
		1210	26.7	5.9*10 ²⁵
		1120	22.0	4.7*10 ²⁵
	UO ₂ [*] , SiC-TRISO, tray	1180	25.5	6.3*10 ²⁵
		1190	25.3	6.3*10 ²⁵
		1140	21.6	4.4*10 ²⁵

(1) UO₂^{*} is the UO₂ kernel coated by a ZrC layer.

experienced irradiation above 1600 °C. However, there seemed to be no reaction except a little roughening of the inner surface of the Zr-Carballyo, showing better performance than the SiC layer against chemical attack. The results of fission product inventory measurements suggested that the ZrC layer containing little free carbon could retain Cs-137 better than the SiC layer.

Table 7-5: Irradiation conditions of JAERI-made Zr-Carballoy-coated fuel particles [1]

Capsule	Sample type	Temperature [°C]	Burnup [%FIMA]	Fast fluence [m^{-2} , $E > 29 \text{ fJ}$]
72F-6A	UO ₂ , ZrC-TRISO type, no outer PyC	1197 - 1427	2.5	$1.4*10^{25}$
72F-7A	UO ₂ , ZrC-TRISO type, no outer PyC	1287	0.1	$0.06*10^{25}$
73F-12A	UO ₂ , ZrC-TRISO type, with thin outer PyC	697 - 1177	2.0	$0.8*10^{25}$
		927 - 1807	3.2	$1.4*10^{25}$
	UO ₂ , ZrC-TRISO type, no outer PyC	927 - 1807	3.2	$1.4*10^{25}$
73F-13A	UO ₂ , ZrC-TRISO type, with thin outer PyC	647 - 1197	2.5	$1.9*10^{25}$
		957 - 1627	4.1	$3.1*10^{25}$
	UO ₂ , ZrC-TRISO type, no outer PyC	957 - 1627	4.8	$3.1*10^{25}$

The irradiation tests on the ZrC-TRISO coated UO₂ particles were done in JMTR and the Japan Research Reactor-2 (JRR-2). Irradiation conditions are summarized in Table 7-6 [35]. Except for the capsules denoted "VOF", the particles were irradiated in the form of annular compacts. The VOF capsules were designed to give a steep temperature gradient on the fuel particles. The release-to-birth ratio (R/B) of Kr-88 was measured during irradiation in the 80F-4A capsule which showed no failure through this irradiation test. After irradiation, the particles were examined by visual inspection with stereomicroscopy, X-ray microradiography, and acid leaching. No failure was detected for all samples using these inspection techniques. The particles in the VOF-14H capsule were irradiated at 1600 °C for 3330 h in the steep temperature gradient. The ceramographs of the particles from the VOF-14H showed carbon accumulation at the colder end of the fuel kernel, which accompanied kernel migration up the temperature gradient. In the TRISO coated fuel particles, the palladium attack of the SiC was occasionally found at the colder side of the particle [36]. However, there was no indication of coating deterioration in the ZrC coating.

The better performance of the ZrC than the SiC against the chemical attack has also been demonstrated in the out-of-pile experiments [37]. The ZrC-TRISO and SiC-TRISO coated particles were heated in either vapor or powdered palladium. Morphology of the reaction was observed metallographically, and the reaction products were identified by X-ray diffraction and electron-probe microanalysis. In addition, reactions in the mixture of SiC, ZrC, Pd and C, and the reaction of ZrC with an Ag-Pd alloy were studied. It is known that ZrC reacts with Pd to form ZrPd₃ and C [38]. When the ZrC-TRISO coated particles were heated in the palladium powder, ZrPd₃ and C were formed as expected. However, no reaction was found on the ZrC-TRISO coated particles heated in Pd vapor at

Table 7-6: Irradiation conditions of JAERI-made ZrC-TRISO coated fuel particles [35]

Capsule	Sample type	Temperature [°C]	Burnup [%FIMA]	Fast fluence [m^{-2} , $E > 29 \text{ fJ}$]
78F-4A	UO ₂ , ZrC-TRISO, compacts	1100	4.0	2.2×10^{25}
80F-4A		900	1.5	1.2×10^{25}
ICF-26H		1400 - 1500	1.8	1.0×10^{25}
VOF-8H	UO ₂ , ZrC-TRISO, disks	1370 (15 °C/mm)	1.6	$(< 1 \times 10^{25})$
VOF-14H		1600 (15 °C/mm)		

temperatures ranging from 1557 to 1877 °C, while the SiC layers were severely attacked and completely penetrated. The different reaction behavior of ZrC with Pd was discussed in terms of the Pd activity; if the Pd activity exceeded 0.12, ZrC should react with Pd. After heating the mixture of SiC, ZrC, Pd and C at 1250 °C for 7 h, only Pd₂Si was formed as a reaction product but there was no formation of ZrPd₃. It was concluded that ZrC was less susceptible to Pd attack than SiC [37].

7.1.5. Fuel Performance during Accidents

7.1.5.1. Non-Oxidizing Conditions

Postirradiation heating test of the ZrC-TRISO coated fuel particles has been performed at JAERI [35]. The heated particles were sampled from an irradiated fuel compact after electrolytic disintegration, which were irradiated to 4 %FIMA at 1100 °C. The postirradiation heating was made in a cold-wall furnace with a graphite heater which has been used in the tests of the standard SiC-TRISO-coated particles [39]. The particles were individually contained in holes of thin graphite disks. The ZrC-TRISO coated fuel particles were heated to 2400 °C at 1 °C/min. During heating, radioactivity in flowing helium was monitored with an ionization chamber. The activity was due mostly to Kr-85. An activity burst occurred only after keeping the particles at 2400 °C for about 6000 s. The activity burst corresponded to one failure among 101 particles heated. This interpretation was confirmed by the X-ray radiographs of the particles after heating. Fig. 7-3 [35] compares this result with the result on the JAERI standard SiC-TRISO coated particles [39]. The figure shows the failure fraction when reaching the given temperature.

The different behavior of the ZrC-TRISO coated fuel particles at high temperatures compared to that of the standard SiC-TRISO coated fuel particles was discussed with the post-heating ceramographs [35]. There was a significant difference in behavior of the ZrC from that of the SiC at such high temperatures: while the SiC is brittle in nature, the ZrC

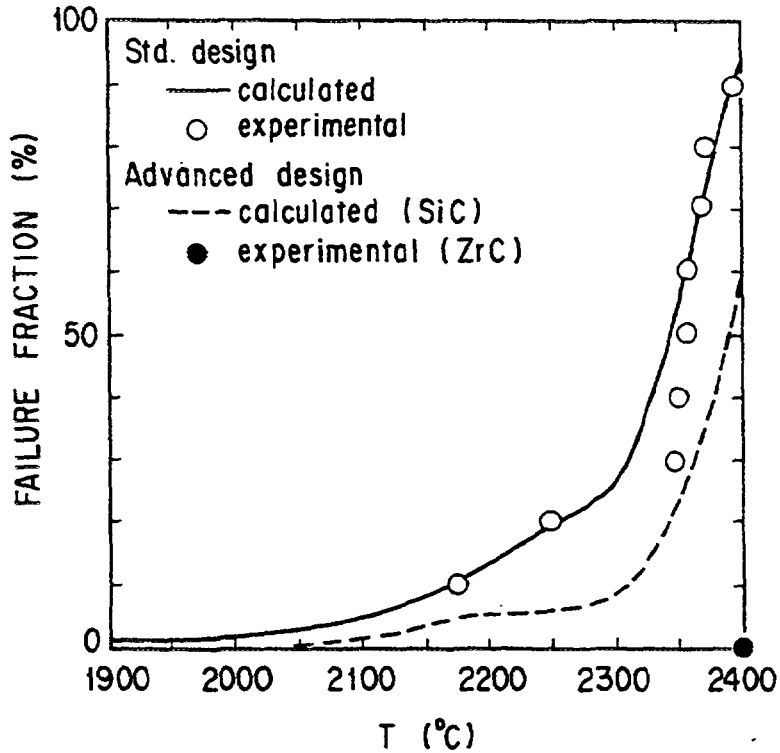


Fig. 7-3: Comparison of failure fraction of the ZrC-TRISO coated fuel particles with the reference SiC-TRISO coated particles with SiC. Dashed line gives model prediction for the SiC-TRISO coated particles which have the same dimensions as the ZrC-TRISO coated particles in this study [35].

can sustain a very large strain. The high plasticity is explained by the fact that resistance of the ZrC crystal lattice to the dislocation motion became very weak above 2200 °C [40].

In this heating test, the particles have been heated in a loose condition without the mechanical support from the surrounding graphite matrix of the fuel compact. The presence of graphite matrix could offset the coating expansion and would further reinforce the integrity of the ZrC-TRISO coated fuel particles [35].

7.1.5.2. Oxidizing Conditions

No experimental work was found in the literature on the performance of the ZrC-coated fuel particles under accidental oxidizing conditions.

Thermodynamic analysis has been performed on the system of ZrC-C-(O₂ or H₂O)-He at JAERI [41]. The analysis showed that there were two kinds of oxidation behavior of ZrC which was similar to that of SiC, as shown in Fig. 7-4 [41]: active oxidation and passive oxidation. While a loss in mass occurs in the active oxidation, the passive oxidation results in a net mass increase. The active-to-passive transition of oxidation occurred depending on temperature and initial O₂ or H₂O pressure.

Under most of the accidental air or water ingress conditions, the passive oxidation of

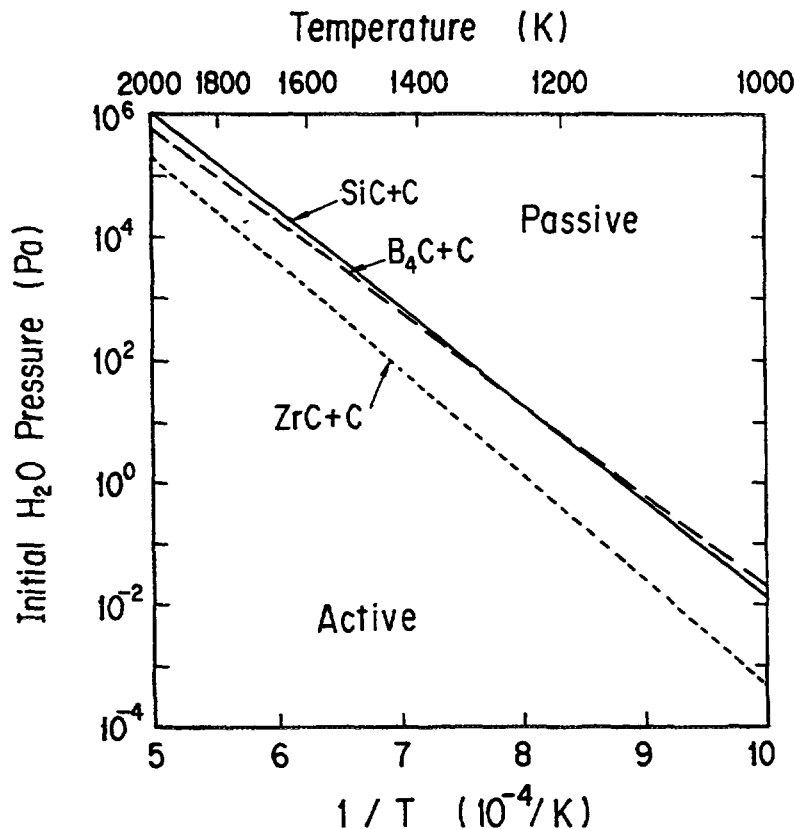


Fig. 7-4: Active-to-passive oxidation transitions for ZrC+C, B₄C+C and SiC+C calculated in the (ZrC, B₄C or SiC)-C-H₂O-He system as a function of temperature and initial H₂O pressure [41].

ZrC was expected to occur. According to the experiment on the passive oxidation of ZrC at temperatures of 857-1887 °C [42], a protective layer of ZrO₂ would not be formed on the ZrC, in contrast with the case of SiC. The preferential oxidation along grain boundaries occurred in the ZrC. Between 857 and 1287 °C, this preferential oxidation resulted in intergranular fracture due to grain boundary stresses. At higher temperatures, stresses were apparently sufficiently released so that the samples remained intact [42]. From this point of view, ZrC is not a retentive layer in air or water ingress accidents.

7.1.6. Fission Product Retentiveness

Several authors have investigated the potential of ZrC coating layer for retaining metallic fission products though the data is limited compared with that on SiC.

Stark [43] has performed cesium infusion experiments on ZrC powder and ZrC coated graphite. The diffusion coefficient of Cs in ZrC was estimated to be 10⁻¹⁸ - 10⁻¹⁶ m²/s over the temperature range 1212 - 1623 °C with the activation energy of about 50 kJ/mol.

Fukuda et al. [8] have studied the diffusion behavior of Cs-137, Sr-90, and Ce-144 in Zr-Carballyo (C/Zr=1.3) by measuring concentration profiles in the ZrC and PyC layers of the coated particles and the release from the particles during postirradiation annealing. The particles used were irradiated to 2.48 %FIMA at 1260 °C. The diffusion coefficient for Cs-137 obtained from the analysis of the concentration profiles in ZrC_{1.3} was 2.3*10⁻⁷*exp{

$3.18 \times 10^5 / RT \} \text{ m}^2/\text{s}$ in the temperature range 1260 - 1600 °C. The diffusion coefficients for Sr-90 and Ce-144 at 1600 °C were estimated to be 1.5×10^{-15} and 2.0×10^{-16} , respectively.

Ogawa et al. [44] have made two types of experiments: strontium soaking experiments and postactivation annealing experiments. In the soaking experiments, the ZrC-TRISO coated UO₂ particles were annealed in graphite powder containing 0.2 wt% Sr as nitrate tagged with Sr-85. After annealing at 1400 °C for 146 h in flowing helium, the outer PyC layer was removed stepwise to measure the Sr content. The diffusion coefficient of Sr in ZrC_{1.0} was estimated to be $2 \times 10^{-18} \text{ m}^2/\text{s}$ at 1400 °C. In the postactivation annealing experiments, short-lived fission products were generated within the ZrC-TRISO coated UO₂ particles by short-term neutron irradiation. After annealing at 1400 °C for 216 h in flowing helium, the concentration distributions of fission products within the ZrC layer were determined. Based on these experiments, the diffusion coefficients were estimated to be $1.2 \times 10^{-16} \text{ m}^2/\text{s}$ for Ru-103 and $2.9 \text{--} 4.6 \times 10^{-18} \text{ m}^2/\text{s}$ for Ba-140 in ZrC_{1.0} at 1400 °C.

Chernikov et al. [45] have investigated diffusion behavior of solid fission products in ZrC coating layer by annealing experiments. The nuclides Ba-133, Ag-110m and Pm-147 were deposited on the surface of unirradiated ZrC-coated particles from the solution. After annealing of the particles, the distribution of the nuclides in the ZrC coating layer was determined by removing the ZrC stepwise. Two kinds of diffusion coefficients for each nuclide were presented: the migration along short-circuit diffusion paths and the migration in the grain volume. The temperature range investigated was about 1700 - 2200 °C. They [45] also estimated the diffusion coefficients for Ba-133 and Ce-144 using irradiated ZrC-coated fuel particles. Based on the distribution of the nuclides in the ZrC measured by removing the ZrC stepwise, the diffusion coefficients were estimated to be $1.3 \times 10^{-17} \text{ m}^2/\text{s}$ for Ba-133 and $6.4 \times 10^{-18} \text{ m}^2/\text{s}$ for Ce-144 in ZrC at 1500 °C.

Minato et al. [46] have made postirradiation heating experiments on the ZrC-TRISO coated UO₂ particles at 1600 °C for 4500 h. The heated particles were irradiated to 1.5 %FIMA at 900 °C. The heating test was divided into seven time steps, and the graphite components and the carbon insulators were removed from the furnace after each time step to identify and evaluate released fission products from the particles by γ -ray spectrometry. Based on the measured fractional release, the diffusion coefficients were estimated to be $1.5 \times 10^{-18} \text{ m}^2/\text{s}$ for Cs-137 and $3 \times 10^{-16} \text{ m}^2/\text{s}$ for Ru-106 at 1600 °C. Ogawa et al. [44] previously pointed out that the diffusion coefficient for Ru in ZrC was somewhat larger than in SiC and discussed the fast diffusion of Ru by means of the atomic radius ratio of Ru/Zr. The values for fractional release of Ce-144, Eu-154, and Eu-155 were larger than that for Cs-137 though their diffusion coefficients were not obtained. This behavior was consistent with the electron probe microanalysis on the irradiated ZrC-coated particles observed by Valentine et al. [28] that Cs was retained inside the ZrC layer while Ce appeared to be both in the ZrC and outside the ZrC layer.

The diffusion coefficients for fission product species in ZrC are summarized in Table 7-7 [8, 43, 44, 45, 46] and plotted in Fig. 7-5 [46].

Hayashi et al. [47] have made postirradiation heating tests on the ZrC-TRISO coated fuel particles to compare with the results on the SiC-TRISO coated fuel particles obtained under the same experimental conditions. The heated ZrC-TRISO coated fuel particles were

Table 7-7: Diffusion coefficients for fission product species in ZrC [8, 43, 44, 45, 46]

Species	Temperature range [°C]	Diffusion coefficient [m ² /s]	Reference
Cs	1212 - 1623	$1 \times 10^{-18} - 1 \times 10^{-16}$	[43]
Cs	1260 - 1600	$2.3 \times 10^{-7} \times \exp\{-3.18 \times 10^5 / RT\}^{(1)}$	[8]
Sr	1600	1.5×10^{-15}	
Ce	1600	2.0×10^{-16}	
Sr	1400	2.0×10^{-18}	[44]
Ru	1400	1.2×10^{-16}	
Ba	1400	$2.9-4.6 \times 10^{-18}$	
Ag	1700 - 2200	$2.6 \times 10^{-10} \times \exp\{-2.25 \times 10^5 / RT\}^{(1)}$	[45]
Ba	1700 - 2200	$2.3 \times 10^{-9} \times \exp\{-3.01 \times 10^5 / RT\}^{(1)}$	
Ba	1500	1.3×10^{-17}	
Ce	1500	6.4×10^{-18}	[46]
Cs	1600	$1-5 \times 10^{-18}$	
Ru	1600	3×10^{-16}	

(1) T is temperature in [K], R is gas constant (8.314) in [J/mol K]

irradiated to 1.8 %FIMA and their maximum irradiation temperature was 1500 °C. The heating tests were performed by elevating temperature stepwise with an interval of 100 °C from 1400 to 2400 °C. The heating time was 2 h at each temperature and the released fission products were measured by γ-ray spectrometry. Fig. 7-6 [47] shows the fractional release of fission products from the ZrC-TRISO and SiC-TRISO coated particles in the postirradiation heating tests. The ZrC-TRISO coated particle has demonstrated better cesium retention than the standard SiC-TRISO coated particle by up to one order of magnitude at temperatures < 2000 °C and up to three orders of magnitude at 2400 °C. In spite of better cesium retention, the ZrC layer showed a less effective barrier to Ru-106 than the SiC layer.

The SiC-TRISO coated UO₂* particles which had a ZrC layer applied to the UO₂ kernel, have exhibited outstanding performance in the postirradiation annealing experiments [6]. Five different types of irradiated SiC-TRISO coated particles of UCO, UC₂, UO₂, UO₂*, and UO₂ with ZrC dispersed in the buffer layer were annealed at 1500 °C for 10,000 h, and the SiC-TRISO coated UO₂* particle was the only one to retain 100 % of its highly diffusive silver and europium inventories. To better appreciate how superior the retention of the SiC-TRISO coated UO₂* particle during annealing was, it should be mentioned that all 30 test particles of the other three fuel types without ZrC releases Eu-154 at levels between 15 and 100 % and 22 of 30 particles released Ag-110m at levels between 10 and 100 %, while none of ten SiC-TRISO coated UO₂* particles released either of these

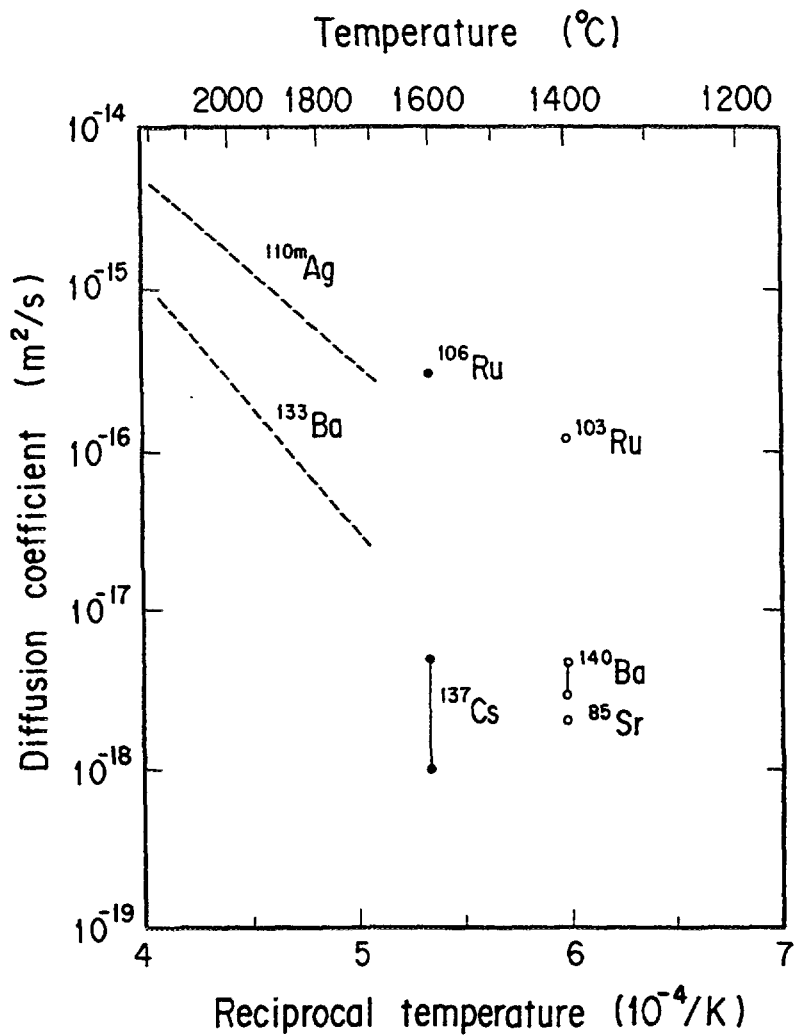


Fig. 7-5: Diffusion coefficients for fission product species in ZrC [46]. Data of solid circles are from [46], open circles from [44], and broken lines from [45].

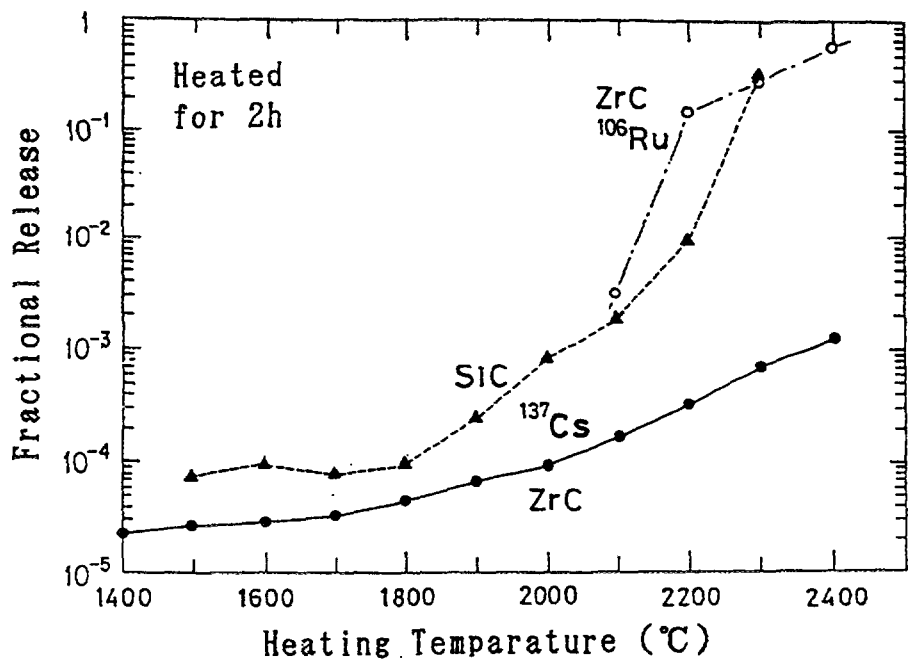


Fig. 7-6: Comparison of fractional release of fission products from the ZrC-TRISO coated fuel particles with that from the SiC-TRISO coated fuel particles [47]

isotopes [6]. Even though the numbers of particles involved in testing were very small, the results imply much improved fission product retention by the SiC-TRISO coated UO_2^* particles. Other types of coated particles could not retain silver so well [48].

7.2. FUEL ELEMENT

As far as advancement of the fuel element is concerned, the recent efforts have been focussing on a corrosion resistant spherical fuel element (protected fuel element) such as a ceramic coating on the surface of the spherical elements (protective layer) or a corrosion resistant matrix of the elements (additive matrix) by Germany, Russia, and China, and the monolithic fuel rod in Japan. This section deals with these attempts relevant to the fuel elements.

7.2.1. Corrosion Resistant Spherical Fuel Element

In order to protect the fuel element from air or steam corrosion, two measures have been attempted, one of which was the ceramic coating such as SiC or SiC+Si on the surface of the element, and the other which was an addition of SiC in the graphite matrix of the element. The former attempt was made at RWTH Aachen and KFA Jülich in Germany [49, 50], NPO "Lutch" and Kharkov of Russia [51, 52], and Tsinghua University of China [53]. The German attempt is to form the protective layer produced mainly by slip casting methods and CVD. Lutch and Kharkov institutes made the similar layer by the powder metallurgy, and furthermore they applied an intermediate layer of SiC/C (GSP) between the SiC protective layer and the fuel element [52]. The purpose of this layer is to adjust the thermal expansion coefficients between the protective layer and the graphite matrix of the element. Tsinghua University developed a different technique [53] from the German and Russian methods for production of the protective layer, where a substrate was impregnated in a melted silicon. The additive graphite matrix was tentatively examined at Tsinghua University [54]. Also, in Russia the additive matrix containing SiC, ZrC, and SiC+ZrC had been tested with a different purpose for eliminating fission product release in the past age (1959-1968).

7.2.1.1. Process for Production of Corrosion Resistant Spherical Fuel Elements

Three methods of the ceramic coating on the graphite substrates, which were a slip casting method, a coating method based on CVD, and a combination of slip/packing coating method, were reported by RWTH Aachen and KFA Jülich [49].

A flow diagram of the slip casting method is displayed in Fig. 7-7. To produce the SiC protective layer (SiCSi) on the substrates, α -SiC and graphite fine powder were primarily mixed by adding specific molding additives for preparation of the slip. The slip casting was applied to the substrates, then followed by drying them. Subsequently a heat-treatment made an infiltration into the graphite pores with liquid silicon which was converted into secondary SiC (β -SiC) in reaction with the existing carbon.

The CVD process, on the other hand, used the pyrolysis of methyltrichlorosilane (CH_3SiCl_3) and hydrogen gas at higher temperatures than 1000 °C [38]. A German company produced CVD-SiC layer of 50 - 150 μm in thickness on the spherical graphite

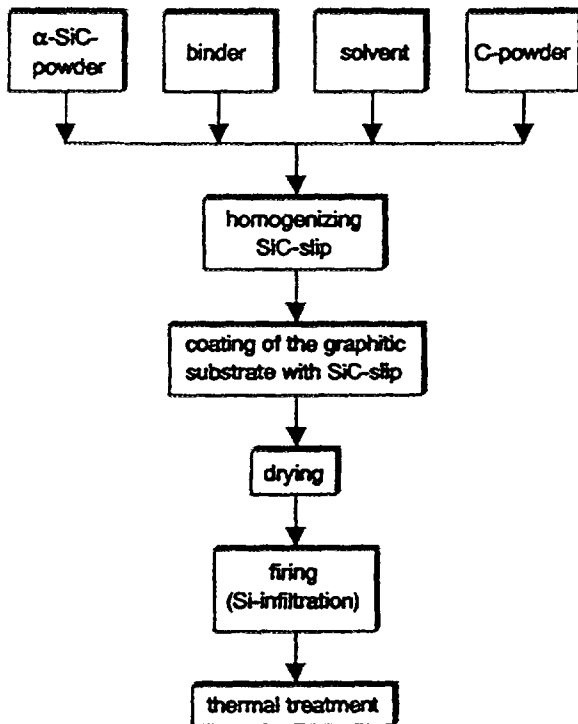


Fig. 7-7: Flow diagram of the slip casting method [49]

substrate at temperatures less than 1200 °C . Recently, a function-gradient coating of CVD-SiC/C, the composition of which changed continuously from SiC to C in layer thickness, was formed with a thickness of 200 μm .

A new method of the combination of slip and packing silication has been reported by RWTH Aachen and KFA Jülich [49]. A flow diagram of this method is exhibited in Fig. 7-8. The substrate to be coated was wetted first with a slip consisting of α -SiC powder, solvent carbon additives, and binder as well as the slip casting method. After drying the slip, a packing which consisted of 40 % of SiC powder and 60 % carbon was applied to the substrate. During a silication in a furnace at temperatures of 1600 °C to 1750 °C, a capillary diffusion of silicon took place which reacted with carbon forming SiC, and filled the existing pore volume. The resulting reaction zone between the graphite substrate and the ceramic layer consisted of α - and β -SiC which was particularly dependent on the silicon content in the packing, porosity of the substrate, and reaction temperature controlling Si partial pressure.

Another method forming the ceramic coating on the spherical substrate, so-called impregnation-reaction technique was examined at Tsinghua University [53] by use of immersion of the substrate in a silicon melt at temperatures around 1500 °C. This process consisted of the following steps:

- (a) melting of silicon in vacuum or protecting environment at a given temperature,
- (b) immersing the graphite substrate in melted silicon and keeping it in the liquid for a given time, and

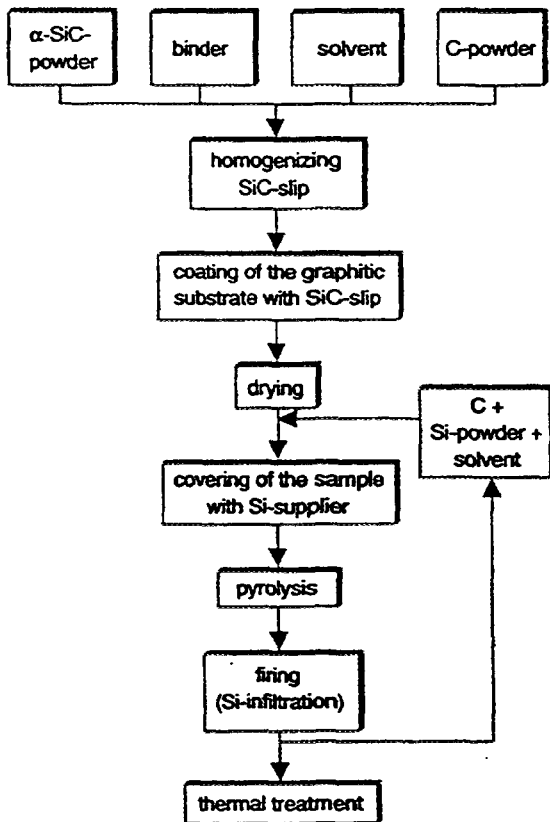


Fig. 7-8: Flow diagram of the slip/packing coating method [49]

(c) drawing out the substrate after finishing the reaction between Si and C.

Besides the ceramic coating for protection from air or steam corrosion, an improvement of the graphite matrix of the spherical fuel element was examined by adding some ceramics into the matrix at Tsinghua University [54]. On a view point of the oxidation resistance of the graphite, C-SiC-B₄C was the most effective composite. However, due to high neutron absorption cross section of boron, the composite C-SiC system was applied to the matrix. The additive matrix was prepared using a mixture of graphite powder and SiC fine powder which was formed into a cylindrical shape with 10 mm in both diameter and length, and heat-treated at 1600 °C.

7.2.1.2. Properties of Corrosion Resistant Spherical Fuel Elements

7.2.1.2.1. Composition of the Protective Layer

The composition of the SiC protective layer produced in the impregnation-reaction technique was examined by X-ray diffraction method (XRD) [53]. The results of the XRD analysis are listed with various preparation conditions and with the other properties in Table 7-8. The SiC protective layer mostly consists of β-SiC with a minor amount of Si. With increasing temperature, the fraction of β-SiC in the layer increased. An environmental effect in the composition could be seen such that the relative weight ratio of β-SiC in the layer formed in Ar was less than in vacuum. This was because the small amount of melted

Table 7-8: Characteristics of SiC protective layer prepared by the impregnation-reaction technique [53]

Sample number	Technical condition	β -SiC ratio [wt%]	$\rho_{theo}^{(1)}$ [g/cm ³]	$\rho_{meas}^{(2)}$ [g/cm ³]	Porosity [%]
1	Impregnation at 1450 °C, in vacuum for 80 min	81.4	3.05	3.01	1.3
2	Impregnation at 1550 °C, in vacuum for 60 min	83.9	3.07	3.05	0.7
3	Impregnation at 1500 °C, in vacuum for 60 min	76.3	3.00	2.98	0.77
4	Impregnation at 1500 °C, in Ar for 60 min, followed by annealing for 60 min	82.4	3.06	3.03	1.0

(1) Theoretical density of SiC/Si layer

(2) Measured density of SiC/Si layer

Si attached to the surface of the SiC layer evaporated at vacuum in the case of the vacuum treatment, resulting in an increase of SiC fraction in the composition.

7.2.1.2.2. Density and Porosity of the Protective Layer

Theoretical and measured densities of the SiC protective layer prepared by the impregnation-reaction technique are listed in Table 7-8 [53]. The measured density was obtained by the sink-float method. The theoretical one of the layer was calculated by using the results of the relative weight ratio of SiC and Si, and the theoretical densities of SiC ($\rho_{SiC}=3.21$ g/cm³) and Si ($\rho_{Si}=2.33$ g/cm³). The porosity of the layer is also given in Table 7-8, which was obtained by using ρ_{theo} and ρ_{meas} . The density of the layer was fairly high exceeding 99 % of the theoretical one.

The density and porosity of the layer prepared by the slip casting method in Germany are given together with other physical properties in Table 7-9 [50]. The results revealed that the density by this method (SiSiC) was 3.0 - 3.1 g/cm³ which was approximately 93 - 97 % of the theoretical density. The open porosity of the layer was 0 %.

The GSP layer applied in Russia had a density of 1.7 - 1.75 g/cm³ which revealed a good irradiation performance in physical and mechanical properties in the neutron fluence up to 3×10^{25} m⁻² at 1200 - 1400 °C.

Table 7-9: Physical properties of the protective layer (SiSiC) [50]

Properties	Unit	Typical values
Density	g/cm ³	3.0 - 3.1
Porosity	%	0
Bending strength	MPa	320
Weibull modulus	-	≥ 10
Compressive strength	MPa	> 1500
Tensile strength	MPa	≈ 220
Young's modulus	GPa	380
Poisson's ratio	-	0.17
Vickers hardness HV02	kN/mm ²	SiC: 27 Si: 12

7.2.1.2.3. Thickness of the Protective Layer

The thickness of the SiC protective layer grown on the graphite substrate by the impregnation-reaction technique [53] was influenced by the following facts:

1. The reaction temperature had a marked effect upon the growth rate of the SiC protective layer in such way that the higher the experiment temperature, the faster the protective layer grew.
2. The reaction proceeded rapidly in the initial time of impregnation, and it became slower after a certain reaction time. This was because the formed SiC layer hindered Si diffusion into the graphite surface.
3. The reactive environment, vacuum or Ar, did not clearly effect the growth rate of the protective layer.

IAE (Russia) preliminarily estimated an optimum thickness of the SiC protective layer in a view point of the nuclear physics [52]. By addition of 3.8 g silicon per spherical fuel element (0.033 g/cm³), the fuel burnup decreased due to a reduction of the reactivity in the plant which, however, could be compensated by an increase of U-235 enrichment from 8 to 9 %. This silicon content gave a protective layer of 150 μm in thickness.

7.2.1.2.4. Mechanical and Thermal Properties

A drop test, a thermal cycling test, and a crushing strength test on the protective layer coated on the spherical elements with three different diameters, 27, 45, and 60 mm were carried out in Kharkov [52]. In the drop test, 20 GSP elements were dropped onto a steel plate from 10 m height, resulting in no failure. In the thermal cycling test where the heat cycle was repeated 1000 times in the temperature range between 300 and 1300 °C with a heatup rate of 100 °C/min, neither peeling-off nor disturbances of the integrity of

the protective layer were observed. The static crushing strength for the elements having diameters of 27, 45, and 60 mm ranged in 8 - 23, 25 - 40, and 50 - 60 kN, respectively.

Various mechanical properties of the SiSiC protective layer tested in Germany are listed in Table 7-9 [50]. Thermal shock tests on the protective layer coated on the A3-3 graphite sphere by both the slip casting method and the slip/packing coating method were performed by a manner that the spherical sample was heated at 1500 °C and cooled in water at 20 °C. It was shown in the test that neither cracking nor peeling-off could be observed on the surface of both samples.

Thermal properties of the protective layer prepared by the slip casting method in Germany are listed in Table 7-10 [50]. It was notable that comparing the coefficient of the linear thermal expansion of the protective layer with those of A3-3 and A3-27 graphite matrices ($2.43 - 3.45 \times 10^{-6}/\text{K}$ at 20 - 500 °C), the former coefficients were a factor of 1.5 to 2 larger than those of the A3 matrices.

Table 7-10: Thermal properties of the protective layer (SiSiC) [50]

Properties	Unit	Test temperature	Typical value
Coefficient of linear thermal expansion	$10^{-6}/\text{K}$	20 - 300 °C	4.1
		20 - 600 °C	4.7
		20 - 1000 °C	6.0
Thermal conductivity	$\text{W}/(\text{m K})$	20 °C	120
		1000 °C	35
Specific heat	$\text{J}/(\text{kg K})$	20 °C	670
		1000 °C	1236
Thermal shock resistance	W/m	20 - 600 °C	9500

7.2.1.3. Corrosion

The corrosion tests of the fuel elements have been conducted in the countries relevant to the development of the protective layer.

In Germany, the tests on the protective layer (SiSiC) coated on the A3-3 graphite sphere by the slip casting method have been conducted. RWTH Aachen and KFA Jülich carried out one of the tests in natural air convection at 1400 °C for 55 h and at higher temperatures such as 1500, 1550 and 1600 °C for several hours from 0.5 to 5 h, with the result that the spheres remained totally intact. The gravimetical measurements indicated that the weight loss of the spherical sample with initial weight of 200 g ranged from 0.1 to 0.04 g [49].

Another test at GH-Duisburg University [50] which used three sources of the manufacturers, was performed in two steps of the heat-treatment, first heated in air at 1500 °C for 1 h, then followed by a heat-treatment under a regulated air circulation at 750 °C

for 24 h. The test used two samples from each manufacturing source, and it was found that the samples from one of the sources lost their weight from 200.7 g and 200.9 g to 196.3 g and 195.0 g, respectively, obviously due to degradation of the protective layer, although the samples from the other two sources remained mostly unchanged in weight. The corrosion rates of the protected A3-3 spherical graphite was measured in the temperature range between 600 and 1200 °C under regulated air circulation, and the results are presented in Fig. 7-9 [49, 50].

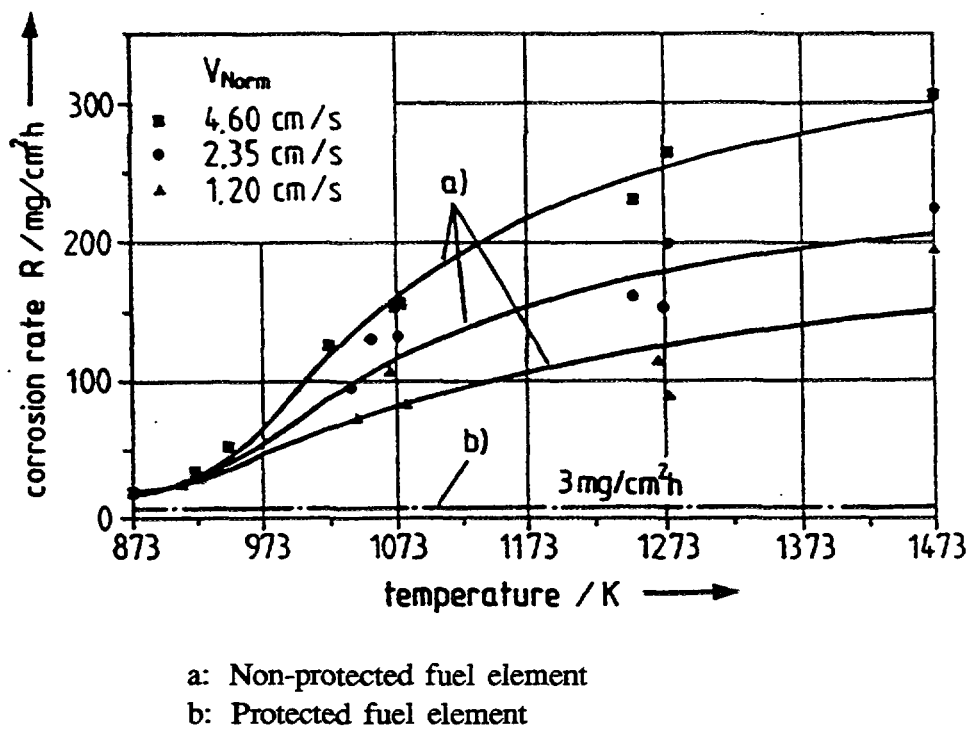


Fig. 7-9: Corrosion rates in air of non-protected and protected spherical A3-3 graphite [49,50]

The corrosion tests at Kharkov have been conducted on the protected spherical elements together with the conventional spherical fuel elements at 900-1300 °C in several environments such as air flow, nitrogen with 7 % oxygen and 5-7 % overheated steam, and water steam [52]. In the isothermal oxidation test in the air flow, it was observed that the weight change of the protected elements during the initial 2 - 3 hours was fairly larger at 1300 °C than at 1000 °C, and the weight at 1300 °C remained almost unchanged in the subsequent heating. The representative results of the corrosion resistance tested at 900 °C in the air flow are depicted in Fig. 7-10. It is obvious that the corrosion rate of the protected element having the SiC and intermediate layers of GSP graphite with a total thickness ranging from 200 - 400 μm is three orders of magnitude lower than that of the nonprotected conventional element.

Tsinghua University made corrosion tests on the protective spherical graphite samples produced by the impregnation-reaction technique [53]. The test was carried out in natural convection of air in a muffle furnace at 1000 and 1500 °C, both of which were based on

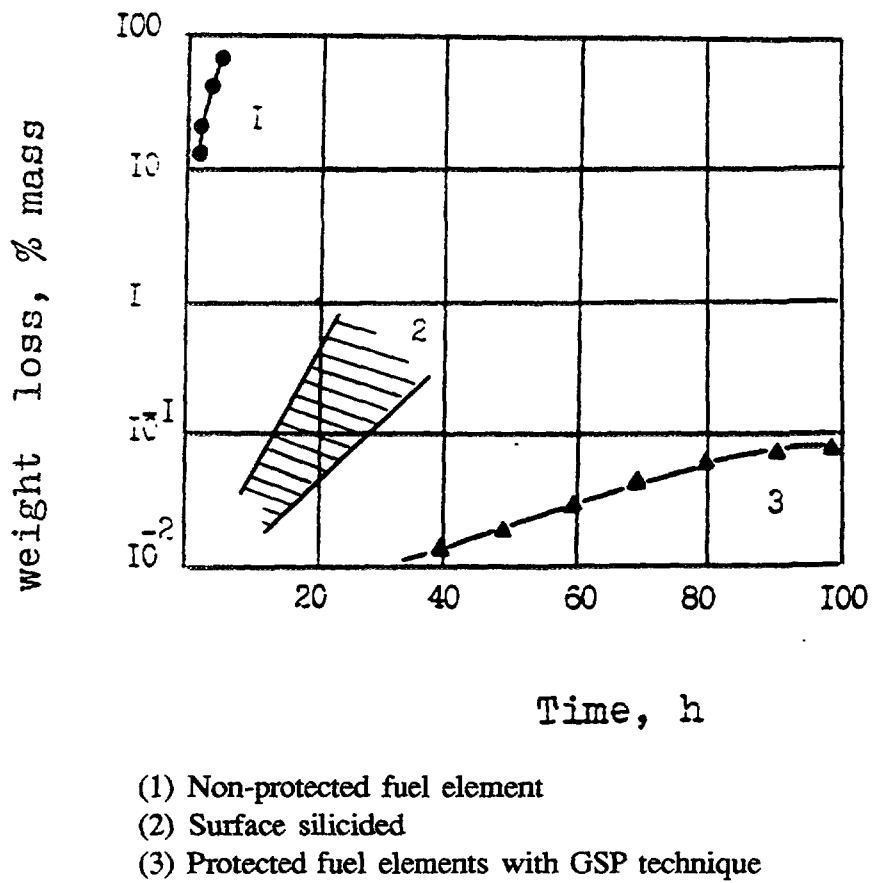


Fig. 7-10: Weight loss of non-protected and protected fuel elements in air at 900 °C [51, 52]

the reactor design for the normal operation and the accident condition, respectively. The results of the weight loss of the samples at 1000 °C are displayed in Fig. 7-11. It is shown that the weight loss velocity of both the non-protected and the protected samples decreases with time. When the samples were heated at 1000 °C for 8 h, burn-off of the non-protected sample was 68 %, while that of the protected one was only 1.7 %. The other result indicated that the weight loss of the protected sample was 1.0 % at 1500 °C for 2 h.

Also, the university analyzed the effect of the protective layer on mechanical stability and corrosion by observing the microstructure of this layer. When the graphite substrate was immersed into the melted silicon, Si permeated into open micropores on the surface, forming a SiC net there which was connected to the surface SiC layer. The formation of the SiC net was clearly observed between the surface SiC layer and the graphite substrate in the protected samples produced at 1450 °C for 3 h, and at 1550 °C for 1 h. The net played an important role in stabilization of the surface layer, preventing peeling-off of the layer by thermal and mechanical shocks, and, consequently, enhanced the corrosion resistance.

Another corrosion test was carried out on the SiC additive graphite matrix also at the Tsinghua University [54]. Isothermal heating on the non-additive standard matrix graphite and the additive graphite was conducted using a thermogravimeter in the temperature range

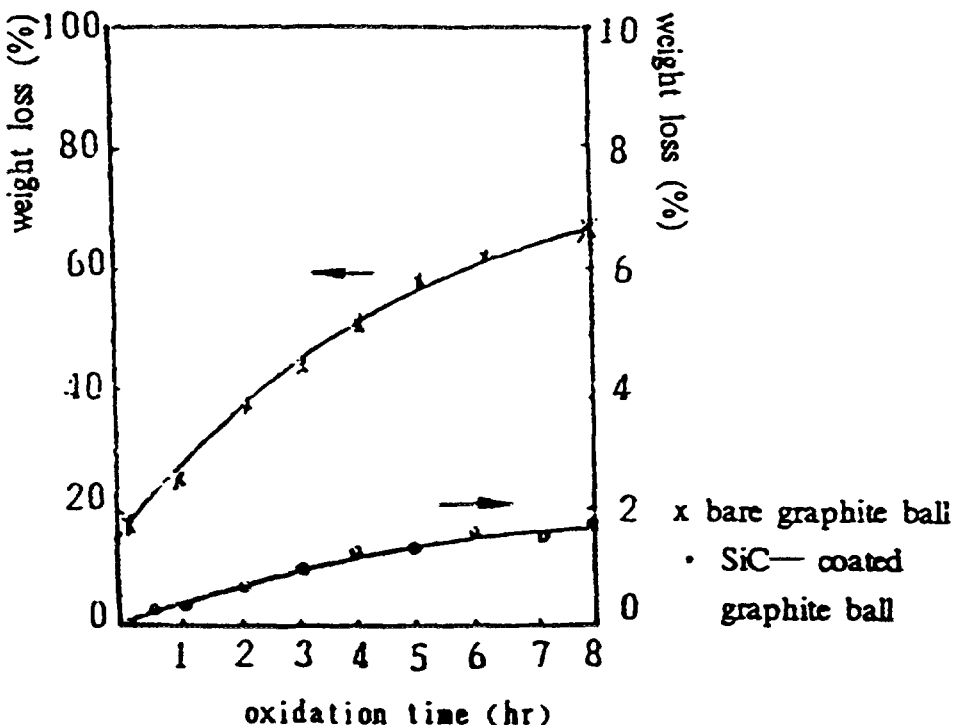


Fig. 7-11: Weight loss of SiC
at 1000 °C [53]

between 800 and 1000 °C. Oxygen partial pressure was 21.3 kPa and the gas flow rate 500 ml/min with a total pressure of 107.3 kPa. The results on the burn-off as a function of time indicated that the matrix containing SiC, produced at 1600 °C, had a lower burn-off than the standard matrix produced at 1950 °C. Typical results of the corrosion rates which were tested at 800 and 1000 °C, are exhibited as a function of the burn-off in Fig. 7-12. The corrosion rate of the additive matrix was larger than that of the standard matrix at initial time of the testing, and then it became smaller than that of the standard one in a time prior to stabilization of the rate.

Surface morphology of the additive matrix in the above mentioned experiment [54] was investigated by XRD and SEM. In the XRD analysis, a very weak diffraction peak of SiO_2 was detected in the additive matrix after the corrosion. The surface morphology by SEM disclosed that the resin-originated carbon existed among graphite grains on the surface of the additive matrix, while it disappeared in the standard matrix, indicating that SiC grains enhanced the corrosion resistance. A functional mechanism on the resistance is explained by the fact that SiO_2 was formed by a SiC-oxygen reaction which covered the surface or isolating micro-pores. A similar mechanism was also proposed in the corrosion test of the slip casting layer (SiSiC) [49].

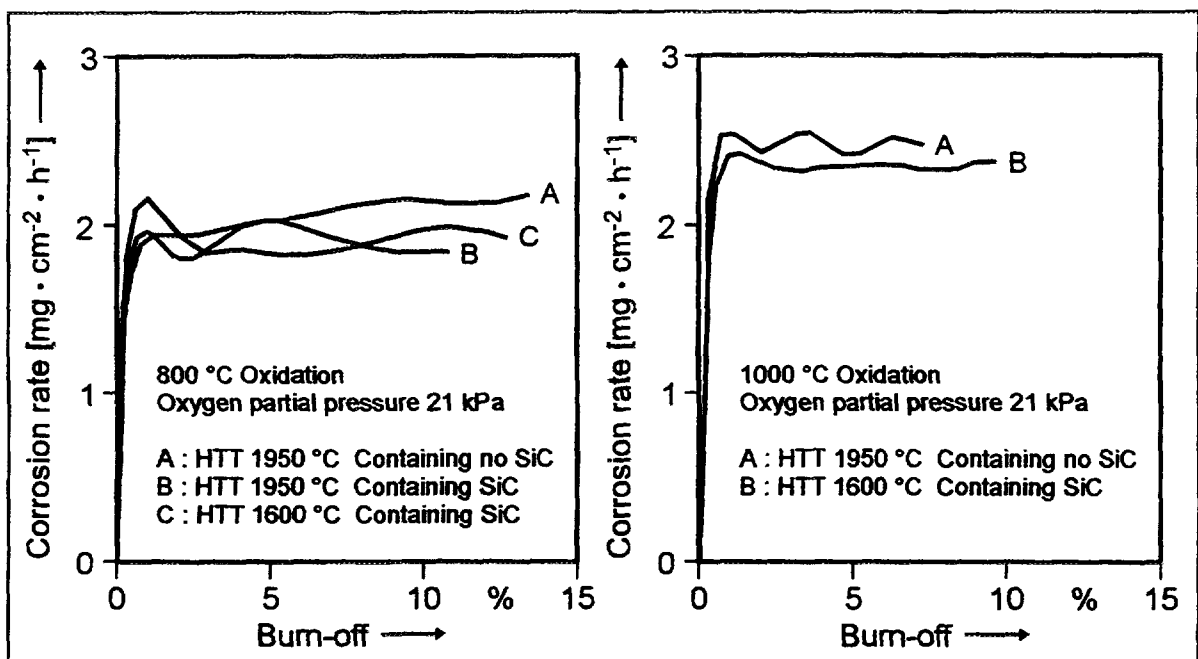


Fig. 7-12: Corrosion rates of non-additive and additive matrix at 800 and 1000 °C [54]

7.2.2. Monolithic Fuel Rod

A concept of the monolithic fuel element, which eliminated gas gaps by the use of integral cladding in the fuel rod and the block, had been conceived in the decade of 1970s in England [56] and Germany [55, 57], and several types of monolithic fuel elements, such as the rod and block were produced. A part of these elements was subjected to irradiation experiments in the Dragon Reactor in England and the Peach Bottom Reactor in USA [57, 58]. Later from 1985, Japan commenced a preliminary development of the monolithic fuel rod with the aim to reduce temperature of the conventional fuel compact (max. designed temperature 1300 - 1350 °C). According to an evaluation of the thermodynamics of the monolithic fuel rod, the fuel temperature was found to be reduced by 46 degrees from 1302 °C in the conventional fuel compact included in the standard fuel rod having the separated graphite sleeve when it was irradiated with 178 W/cm in a linear heat rate. The effect on the temperature reduction was markedly intensified with increase of the linear heat rate. Over the past 10 years, the fabrication tests and irradiation tests had been conducted on model monolithic fuel rods.

Table 7-11: Quality assurance of UKAEA monolithic fuel rods

Specified parameter	Nominal value	Range in mean values	
		Within batch	Whole production
Fuel core diameter [mm]	54.5	± 0.2	± 0.5
Fuel core length [mm]	212.	± 0.3	± 1.0
Uranium content [g]	222.	± 2.	± 7.
Uranium concentration [gU/cm ³]	0.8	± 0.01	± 0.02
Graphite matrix density [g/cm ³]	1.68	± 0.02	± 0.03
Coated particle failure fraction	≤ 10*10 ⁻⁵ (Mean value: 1.6*10 ⁻⁵)		

7.2.2.1. Development of Monolithic Fuel in the UK

7.2.2.1.1. Manufacture Process and Quality Assurance

The monolithic fuel element which is directly cooled as proposed by UKAEA [56] was of annular geometry, having the integral cladding with 1 - 2 mm in thickness on the inner and outer cylindrical surfaces, and 10 mm in thickness at the ends.

The manufacture of the rod was conducted as follows:

1. overcoating of coated particles with resinated graphite powder,
2. pre-forming of unfuelled clad components in isostatic press,
3. assembly and final pressing of the composite fuel body by isostatic press,
4. heat treatments at 850 °C in an inert atmosphere and at 1700 °C in vacuum,
5. machining to size.

A relatively large manufacturing campaign had been made using the optimized conditions to demonstrate the viability of the production route and to allow the demonstration of important properties at a statistically significant level. Seven batches of fuel rods each comprising fifteen pins were produced and detailed non-destructive and destructive analyses of product quality and properties were made. Quality assurance parameters for monolithic fuel rod are listed in Table 7-11.

7.2.2.1.2. Irradiation Experiments

The irradiation experiments had been mounted in Dragon HTGR to test the performance of the monolithic fuel rods under realistic power reactor conditions. Irradiation was made for 240 effective full power days (efpd). One of the stringer was operated at a peak outer-surface temperature of 1200 °C and reached a peak burnup of 3.0 %FIMA. The results in the post-irradiation examination indicated that the monolithic fuel rods withstood the thermal stresses of in-reactor operation satisfactorily.

7.2.2.2. Development of Monolithic Fuel in Germany

7.2.2.2.1. Fabrication Process and Physical Properties

In the development of the monolithic fuel in NUKEM/HOBEG, many efforts had been directed to fabricate moulded the prismatic fuel block together with the fuel rod and the fuel compact.

The monolithic fuel was fabricated in two steps using a combined cold-hot moulding process as shown in Fig. 7-13 [57]. In the first step, the resinated graphite matrix powder was isostatically consolidated into spheres in a rubber die at room temperature under a high forming pressure of about 1000 kg/cm², in order to obtain an isotropic structure. Subsequently, the graphite spheres were crushed to granules from which the 0.3 - 3 mm fraction was obtained by screening.

In the second step, the granulated graphite material was pre-moulded to a block in a steel die at room temperature. In order to obtain a block density of 1.4 g/cm³ suitable for assembling, a relatively low-forming pressure of about 35 kg/cm² was applied. As

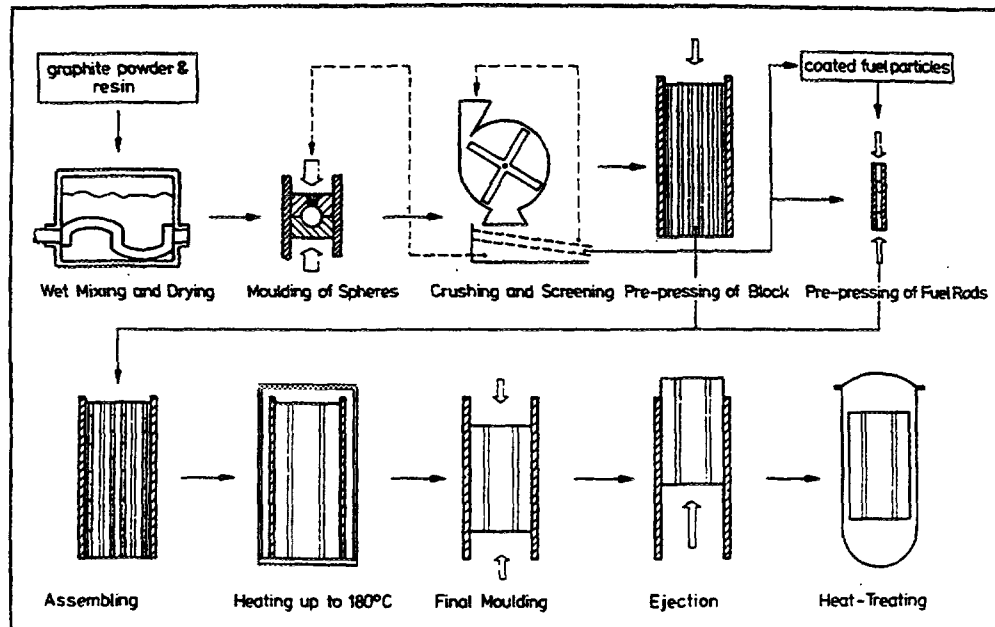


Fig. 7-13: Fabrication procedure of NUKEM/HOBEG monolithic prismatic-fuel-block

part of this procedure the cooling channels and the channels for reception of the fuel were moulded. The fuel rods were warm-moulded with coated particles and the resinated graphite powder in a steel die. After assembling the rods into the fuel channels, the entire block was heated with a tool to a temperature of 180 °C when the resin became plastic. The final moulding of the block was carried out, using a forming pressure as low as 120 kg/cm². The matrix density was obtained to be 1.95 g/cm³. After cooling to 100 °C the moulded block was ejected from the tool and heated in two stages: First heating was made up to 800 °C to carbonise the resin with argon purge and then to 1800 °C in vacuum to degas the block structure.

The NUKEM/HOBEG had experience by fabricating more than 200 moulded fuel elements, half size of the Fort St. Vrain block together with full size block elements. The physical properties of the reduced and full size moulded block are summarized in Table 7-12.

7.2.2.2. Irradiation Experiments

Irradiation experiments on monolithic segments whose geometry was different from the prismatic block were conducted in the Peach Bottom Reactor under HOBEG/GAC collaboration [58], and in the Dragon Reactor. The irradiation in Peach Bottom was conducted in FTE-18 at a maximum temperature close to 1600 °C and an average temperature of 1400 °C for 512 efpd. Fission gas release measurements for a complete fuel body at 1100 °C in the TRIGA facility revealed less than 0.1 % fuel failure. It was concluded that no irradiation damage of the BISO (Th,U)O₂ fuel occurred.

7.2.2.3. Development of Monolithic Fuel in Japan

7.2.2.3.1. Fabrication Process and Quality Assurance

A production method of the model monolithic fuel rod is to some extent similar to that of the spherical fuel elements. A flow diagram of this method is presented in Fig. 7-14 [59]. As is shown in the figure the graphite matrix powder containing the resin binder was prepared first, followed by three sub-processes using the powder, where end caps for the fuel free graphite tube, the graphite tube, and the over-coated particles were formed by a metal mold, a rubber mold under an isostatic pressure and a rotating vessel, respectively. These components were pressed all together in the rubber mold under an isostatic pressure, to form a green rod. Through a calcination process at 950 °C and sintering at 1500 - 1700 °C, the rod was inspected by X-ray radiography, then followed by machining. Typical size of the model monolithic fuel rod was either 12 or 16 mm in diameter, and ranged from 60 to 110 mm in length. Defect fractions of the coated fuel particles in the rod were measured for three fuel rods formed under a pressure of 300 - 400 kg/cm² and having a particle packing fraction of 30 vol.%. The defect fractions were less than 5*10⁻⁶ in all fuel rods, implying no particle failure.

7.2.2.3.2. Irradiation Experiments

Preliminary irradiation tests on the fuel rods [60] have been made in four capsules,

Table 7-12: Physical properties of NUKEM/HOBEG monolithic prismatic-fuel block

Block size		Reduced 1 : 2, inverse design ⁽¹⁾			Full 1 : 1, 8 row design ⁽¹⁾		
Properties	Target values	Mean value	Confidence level 95 %	Variation coefficient [%]	Mean value	Confidence level 95 %	Variation coefficient [%]
Apparent density [g/cm ³]	1.70	1.73	± 0.002	0.52	1.73	± 0.002	0.64
Compre. strength [kp/cm ²]	radial ≥ 300	323	± 12	6.1	384	± 15	7.1
	axial	324	± 15	8.4	380	± 20	9.2
Bending strength [kp/cm ²]	radial ≥ 120	157	± 8	11.8	168	± 10	14.1
	axial	137	± 5	14.1	128	± 7	16.2
Young's modulus dynamic [10 ⁻⁶ kp/cm ²]	radial ≤ 10	11.8	± 0.2	4.1	11.8	± 0.2	5.3
	axial	7.3	± 0.1	2.5	6.6	± 0.1	5.7
Heat conductivity at 20 °C [W/(cm K)]	radial ≥ 0.42	0.67	± 0.02	3.8	0.74	± 0.01	4.8
	axial	0.46	± 0.01	2.7	0.48	± 0.01	3.7
CTE (20 - 500 °C) [μm/(m K)]	radial ≤ 4	2.2	± 0.04	5.5	2.6	± 0.01	3.5
	axial	3.9	± 0.07	1.5	4.5	± 0.18	3.8

(1) In the inverse design, cooling and fuel channels are exchanged compared to the normal row design.

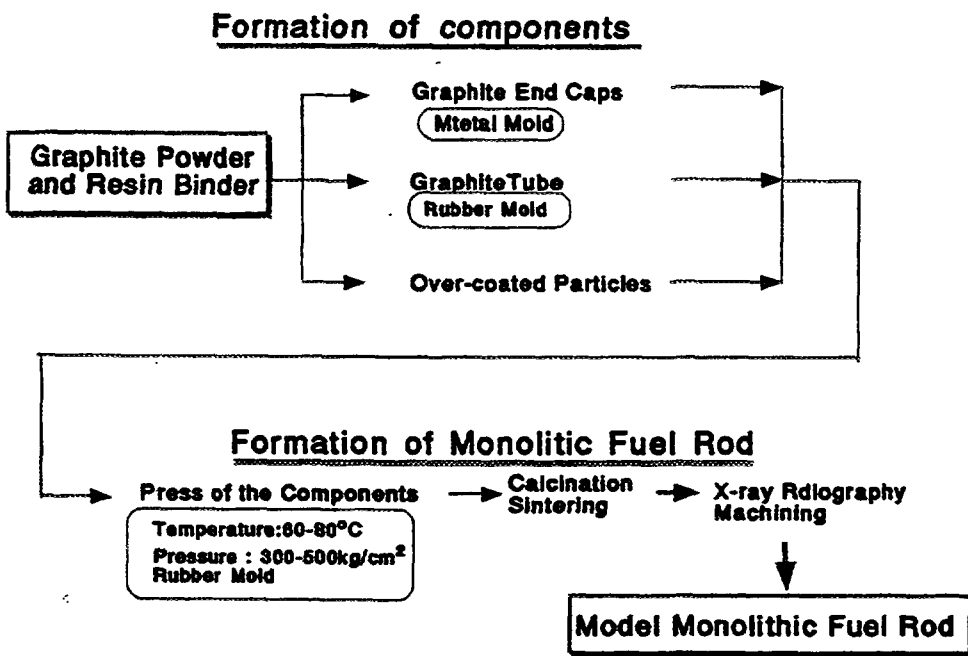


Fig. 7-14: Production method of model monolithic fuel rod in Japan [59]

two of which were irradiated at a very high temperature around 1600 °C, while the others were done at 600 - 1100 °C. Maximum burnup and maximum fast neutron fluence in these tests were around 5 %FIMA and $0.5 \times 10^{25} \text{ m}^{-2}$, respectively. The total number of the model fuel rods which were subjected to irradiation was 10. In the postirradiation examination, any peeling-off of the fuel free zone and radiation-induced cracks were not observed on the surface of the fuel rods irradiated even at approximately 1600 °C in X-ray radiography and a surface inspection. The dimensional change of the monolithic fuel rods by irradiation was compared with that of the conventional fuel compacts. Although the number of measurements for the fuel rod was limited, it might be probable that the dimensional change of the fuel rod was the same as that of the fuel compact or even smaller. The failure fraction due to irradiation in two capsules is listed in Table 7-13, showing no particle failure.

7.2.3. A Plausible Order for Developing Various Advanced Fuel Particles

On balance, it appears that development of advanced fuels be carried out on an incremental basis, with emphasis on both fuel performance and the cost to achieve the better performance. A tentative order of development that appears practical is given below:

- (1) Development and comprehensive testing of UO_2^* -based particles (i.e., UO_2 directly surrounded by a coating of ZrC, followed by the normal TRISO (SiC) coatings).
- (2) If the above coated fuel particle is successfully developed (i.e., retains key fission products much better at high temperatures and high temperature gradients than normal TRISO (SiC) coatings of UO_2 or UCO fuel), develop and comprehensively

Table 7-13: Coated fuel particle failure in the monolithic fuel rod by irradiation [60]

Capsule	Irradiation conditions			Cs-137 release fraction measured by burn-leaching	Number of failed particles (total number of tested particles)
	Maximum temperature [°C]	Estimated burnup [%FIMA]	Fast neutron fluence [m^{-2} , $E>29 fJ$]		
VOF-28H	600	≈ 2	$0.1*10^{25}$	$1.7*10^{-5}$	0 (4420)
ICF-67H	1600	≈ 5	$0.5*10^{25}$	$1.9*10^{-5}$	0 (3320)

test fuel having a UO_2^* kernel, and surrounded by TRISO (ZrC) coatings (i.e., normal TRISO (SiC) coating with the SiC coating replaced by ZrC).

- (3) If further fuel improvement is required, develop and comprehensively test fuel having a UO_2^* kernel, and surrounded by a TRISO (ZrC, SiC) coating (i.e., the UO_2^* kernel is surrounded by a buffer coating layer, a ZrC layer, a thin PyC layer, a SiC coating layer, and a pyrolytic carbon layer).
- (4) If still further improvement is needed, develop and comprehensively test coating the exterior of the fuel element with SiC.
- (5) Develop and comprehensively test monolithic-type fuel elements, with emphasis on decreasing fabrication costs of such elements.

7.3. SUMMARY OF CHAPTER 7

Efforts for the HTGR advanced fuel have been concentrating so far on the SiC-TRISO coated UO_2^* particles, the ZrC coated fuel particles, the corrosion resistant spherical fuel elements, and the monolithic fuel rod throughout the world.

Based on the limited amount of data available from irradiation and PIE heating, UO_2^* shows the promise to provide better fission product retention by:

1. SiC with lower defect fractions which is probably the most important effect,
2. the ZrC layer itself if intact, and
3. higher density kernels.

Taken together, these advantages apparently led to the improvement observed in UO_2^* particles for retention of silver and europium during 10,000 h annealing at 1500 °C [6]. No other coated particle design has ever been observed to hold silver so well [48]. These tentative conclusions are based upon limited data and very small sample populations. Nevertheless, the results are intriguing, and its ability to retain Ag-110m at high temperatures for long times (1500 °C for 10,000 h) make it an attractive candidate for further research and development.

The ZrC coating which is the most refractory material has several potential advantages compared to the conventional TRISO-coated fuel particles such as an enhanced capability for fission product retention at very high temperatures, realizing the core with a high power density, improvement in the fuel production due to enabling higher-temperature sintering of the green fuel compact. The United States, Japan, and Russia have developed the ZrC-coating layer for application in the coated particles to replace the SiC layer (ZrC-TRISO coated fuel particles), although several fuel designs with use of ZrC had been attempted besides this type of fuel in the United States.

Two major CVD-methods, the $ZrCl_4$ powder technology and the halogen-gas/Zr reaction technology which were developed in the United States and Japan, respectively, were described. In characterization of the ZrC coating, the plasma oxidation technique for removing carbon in ZrC and/or the outer PyC layer was developed, and the oxidation behavior of ZrC under the plasma was investigated in Japan.

The ZrC-TRISO coated fuel particles have been subjected to irradiation experiments under normal and accident conditions in the United States and Japan. Although the postirradiation examination in the United States resulted in a smaller capability for rare-earth fission product retention in the ZrC, it retained cesium effectively. The high retention capability for cesium in the ZrC-Carballoy layer with little free carbon was also confirmed in Japanese experiments. In the Japanese experiments, two outstanding features on the ZrC-TRISO coated fuel particles were revealed. One was that palladium attack which is a typical deterioration mechanism of the SiC layer by forming Pd_2Si in the reaction with palladium, was scarcely observed in the ZrC layer, and the other was that the layer was very resistant to the amoeba effect. Postirradiation heating tests on the irradiated ZrC-TRISO coated fuel particles were performed in Japan, and the performance of the particles was such excellent at very high temperatures that only one particle failure among 101 particles occurred at 2400 °C. Thermodynamic evaluation on oxidation of the ZrC coating layer was conducted in Japan, predicting the passive-active transient condition, and oxidation behavior under the passive and active conditions.

Metallic fission product retentiveness in the ZrC-coating layer was investigated in the United States, Russia, and Japan. The diffusion coefficients reported so far are summarized in this chapter. As far as the release behavior was concerned, the experiments confirmed that cesium retention by the ZrC coating layer was more effective than that by a SiC coating layer, but it was less effective for ruthenium.

Work on development of advanced fuels needs to continue, with increased emphasis on UO_2^* fuel kernels surrounded by TRISO (SiC) coatings.

With respect to the fuel element, the development of corrosion resistant spherical fuel elements in Germany, Russia, and China, and of the monolithic fuel rod in Japan were described.

The corrosion resistant spherical fuel elements containing a protective layer on the elements were principally aiming at protection of the elements against air or steam corrosion. Several processes for producing the SiC(Si) protective layer were reported which were the slip casting method, the CVD method, the slip/packing coating method, and

the impregnation-reaction technique. Together with the protective layer, the SiC additive graphite matrix was examined for the same purpose in China, and the intermediate layer of SiC/C (GSP) was applied between the protective layer and the fuel element for adjusting differences in the thermal expansions of these components in Russia.

Properties of the corrosion resistant fuel elements were reported, including composition, density and porosity, thickness, mechanical and thermal properties. The thermal and mechanical properties of the protective layer were summarized in a table in this document.

Corrosion tests on the protective layer were carried out under oxidative conditions. Representative results are presented in this document. All protective layers produced by the respective method were significantly effective to corrosion in air or steam environments compared to the corrosion resistance of the conventional fuel elements. The functional mechanism was explained by covering the surface or micro-pores with SiO_2 formed by a reaction of SiC and oxygen.

The monolithic fuel elements were developed in the test phase in England, Germany and Japan, aiming to reduce fuel temperature in service by eliminating the gap existing between the fuel compacts and the graphite container. England developed the monolithic fuel elements with annular geometry, and tested them in the Dragon HTGR. Germany fabricated the prismatic fuel blocks for Fort St. Vrain of the United States, and some of the monolithic segments which had a geometry different from the prismatic block, were irradiated in Peach Bottom and Dragon HTGR within the frame of a HOBEG/GA collaboration. Japan fabricated the model monolithic fuel rods and tested them in a research reactor. Good fuel performance of the monolithic fuel elements in these countries was confirmed.

REFERENCES OF CHAPTER 7

- [1] OGAWA, T., et al., Research and Development of ZrC-Coated UO_2 Particle Fuel at the Japan Atomic Energy Research Institute in Nuclear Fuel Performance, BNES London (1985) 163-169.
- [2] KASTEN, P.R., CORUM, M.R., RITTENHOUSE, P.L., Research on Very High Temperature Gas Reactors, Report EPRI ER/NP-7372, Electric Power Research Institute (1991).
- [3] WAGNER, P., HOLLABAUGH, C.M., BARD, R.J., ZrC, a Key Ingredient for High-Temperature Nuclear Fuels, Gas-Cooled Reactors with Emphasis on Advanced Systems (Proc. Symp. Jülich, 1975), IAEA-SM-200, Vol. 1, Vienna (1976) 277-287.
- [4] WAGNER, P., High-Temperature Fuel Technology for Nuclear Process Heat: ZrC-Containing Coated Particle Fuels and High Density Graphite Fuel Matrices, Report LA-6984, Los Alamos National Laboratory (1977).
- [5] BULLOCK, R.E., KAAE, J.L., Performance of Coated UO_2 Particles Gettered with ZrC, J. Nucl. Mater. **115** (1983) 69-83.
- [6] BULLOCK, R.E., Fission-Product Release during Postirradiation Annealing of Several Types of Coated Fuel Particles, J. Nucl. Mater. **125** (1984) 304-319.
- [7] WAGNER-LÖFFLER, M., Amoeba Behavior of UO_2 Coated Particle Fuel, Nucl. Techn. **35** (1977) 392-402.

- [8] FUKUDA, K., IKAWA, K., IWAMOTO, K., Fission Product Diffusion in ZrC-Coated Fuel Particles, *J. Nucl. Mater.* **87** (1979) 367-374.
- [9] HOLLABAUGH, C.M., et al., A New Method for Coating Microspheres with Zirconium Carbide and Zirconium Carbide-Carbon Graded Coats, *J. Nucl. Mater.* **57** (1975) 325-332.
- [10] WAGNER, P., et al., Factors Influencing the Chemical Vapor Deposition of ZrC, *J. Nucl. Mater.* **62** (1976) 221-228.
- [11] HOLLABAUGH, C.M., et al., Chemical Vapor Deposition of ZrC Made by Reactions of ZrCl₄ with CH₄ and with C₃H₆, *Nucl. Technol.* **35** (1977) 527-535.
- [12] IKAWA, K., Vapor Deposition of Zirconium Carbide-Carbon Composites by the Chloride Process, *J. Less-Common Metals* **29** (1972) 233-239.
- [13] IKAWA, K., IWAMOTO, K., Coating Microspheres with Zirconium Carbide-Carbon Composite by the Methylenedichloride Process, *Yogyo-Kyokai-Shi* **81** (1973) 403-406.
- [14] IKAWA, K., Vapor Deposition of Zirconium Carbide-Carbon Composites by the Iodide Process, *J. Less-Common Metals* **27** (1972) 325-332.
- [15] IKAWA, K., IWAMOTO, K., Coating Microspheres with Zirconium Carbide-Carbon Alloy by Iodide Process, *J. Nucl. Sci. Technol.* **11** (1974) 263-267.
- [16] IKAWA, K., IWAMOTO, K., Coating Microspheres with Zirconium Carbide-Carbon Alloy, *J. Nucl. Mater.* **52** (1974) 128-130.
- [17] IKAWA, K., Co-Deposition of Zirconium with Carbon by the Bromide Process, *J. Less-Common Metals* **44** (1976) 207-213.
- [18] OGAWA, T., IKAWA, K., IWAMOTO, K., Effect of Gas Composition on the Deposition of ZrC-C Mixtures: The Bromide Process, *J. Mater. Sci.* **14** (1979) 125-132.
- [19] OGAWA, T., IKAWA, K., IWAMOTO, K., Chemical Vapor Deposition of ZrC within a Spouted Bed by Bromide Process, *J. Nucl. Mater.* **97** (1981) 104-112.
- [20] ZHU, J., et al., Chemical Vapor Deposition of ZrC Coating and its Oxidation behavior, *Thermodynamics of Nuclear Materials*, (9th Int. Symp., Osaka, 1996).
- [21] OGAWA, T., FUKUDA, K., Developing ZrC Coatings for Nuclear Fuel Particles, Surface Modification Technologies (Proc. 3rd Int. Conf. Neuchatel, Switzerland (1989) 309-320.
- [22] TAMURA, K., OGAWA, T., FUKUDA, K., The Oxidation Behavior of ZrC Coating and Powder Studied by Laser Raman Spectroscopy and X-Ray Diffraction, *J. Nucl. Mater.* **175** (1990) 266-269.
- [23] OGAWA, T., FUKUDA, K., Quick Analysis of Free Carbon in Metal Carbide by Plasma Oxidation, *J. Am. Ceram. Soc.* **73** (1990) 2558-2560.
- [24] REISWIG, R.D., et al., Behavior of LASL-Made Graphite, ZrC, and ZrC-Containing Coated Particles in Irradiation Tests HT-28 and HT-29, Report LA-6211, Los Alamos National Laboratory (1976).
- [25] WAGNER, P., et al., Irradiation Test HT-31: High-Temperature Irradiation Behavior of LASL-Made Extruded Fuel Rods and LASL-Made Coated Particles, Report LA-6785-MS, Los Alamos National Laboratory (1977).
- [26] WAGNER, P., et al., Irradiation Test OF-2: High-Temperature Irradiation Behavior of LASL-Made Extruded Fuel Rods and LASL-Made Coated Particles, Report LA-6988-MS, Los Alamos National Laboratory (1977).

- [27] HOMAN, F.J., et al., Irradiation Performance of HTGR Fuel Rods in HFIR Experiments HRB-11 and -12, Report ORNL-5584, Oak Ridge National Laboratory (1980).
- [28] VALENTINE, K.H., et al., Irradiation Performance of HTGR Fuel Rods in HFIR Experiments HRB-7 and -8, Report ORNL-5228, Oak Ridge National Laboratory (1977).
- [29] KETTERER, J.W., et al., Capsule HRB-15A Postirradiation Examination Report, Report GA-A 16758, GA Technologies Inc. (1984).
- [30] HTGR FUEL TECHNOLOGY PROGRAM, Semiannual Report for the Period Ending March 31, 1983, Report GA-A 17110, GA Technologies Inc. (1983).
- [31] REYNOLDS, G.H., et al., Irradiation behavior of Experimental Fuel Particles Containing Chemically Vapor Deposited Zirconium Carbide Coatings, *J. Nucl. Mater.* **62** (1976) 9-16.
- [32] KETTERER, J.W., BULLOCK, R.E., Capsule HRB-15B Postirradiation Examination Report, Report GA-A 15940, General Atomic Company (1981).
- [33] HTGR FUEL TECHNOLOGY PROGRAM, Contract Summary Report for the Period Ending October 31, 1983, Report GA-A 17369, GA Technologies Inc. (1983).
- [34] KETTERER, J.W., MYERS, B.F., Capsule HRB-16 Postirradiation Examination Report, Document 908012/Issue N/C, GA Technologies Inc. (1985).
- [35] OGAWA, T., et al., Performance of ZrC-coated Particle Fuel in Irradiation and Postirradiation Heating Tests, *J. Am. Ceram. Soc.* **75** (1992) 2985-2990.
- [36] MINATO, K., et al., Fission Product Palladium - Silicon Carbide Interaction in HTGR Fuel Particles, *J. Nucl. Mater.* **172** (1990) 184-196.
- [37] OGAWA, T., IKAWA, K., Reactions of Pd with SiC and ZrC, *High Temp. Sci.* **22** (1986) 179-193.
- [38] BREWER, L., WENGERT, P.R., Transition Metal Alloys of Extraordinary Stability; an Example of Generalized Lewis-Acid-Base Interactions in Metallic Systems, *Metal. Trans.* **4** (1973) 83-104.
- [39] OGAWA, T., et al., A Model to Predict the Ultimate Failure of Coated Fuel Particles during Core Heatup Events, *Nucl. Technol.* **96** (1991) 314-322.
- [40] TREFILOV, V.I., MILMAN, Y.V., GRIGORIEV, O.N., Deformation and Rupture of Crystals with Covalent Interatomic Bonds in Single Crystals of Refractory Compounds (Gurin, V.N., Ed.) Pergamon Press, Oxford (1988) 225-277.
- [41] MINATO, K., FUKUDA, K., Thermodynamic Analysis of Behavior of HTGR Fuel and Fission Products under Accidental Air or Water Ingress Conditions, Response of Fuel, Fuel Elements and Gas-Cooled Reactor Cores under Accidental Air or Water Ingress Conditions (Proc. IAEA TCM, Beijing, 1993), IAEA-TECDOC-784, Vienna (1995) 86-91.
- [42] BERKOWITZ-MATTUCK, J.B., High Temperature Oxidation -IV. Zirconium and Hafnium Carbides, *J. Electrochem. Soc.* **114** (1967) 1030-1032.
- [43] STARK, JR. W.A., Cesium Solubility, Diffusion and Permeation in Zirconium Carbide, *J. Nucl. Mater.* **73** (1978) 169-179.
- [44] OGAWA, T., IKAWA, K., Diffusion of Metal Fission Products in ZrC_{1.0}, *J. Nucl. Mater.* **105** (1982) 331-334.
- [45] CHERNIKOV, A.S., et al., Fission Product Diffusion in Fuel Element Materials for HTGR, Fission Product Release and Transport in Gas-cooled Reactors (Proc. IAEA Spec. Meeting, Berkeley, 1985), IAEA IWGGCR/13, Vienna (1986) 170-181.

- [46] MINATO, K., et al., Fission Product Release from ZrC-coated Fuel Particles during Postirradiation Heating at 1600 °C, to be published in J. Nucl. Mater. (1995).
- [47] HAYASHI, K., OGAWA, T., FUKUDA, K., Release Behavior of Fission Products from Irradiated Coated Fuel Particles during Heating at Extremely High Temperature (II) - ZrC-Coated Fuel Particles, 1992 Annual Meeting of the Atomic Energy Society of Japan (1992) K33.
- [48] NABIELEK, H., BROWN, P.E., OFFERMANN, P., Silver Release from Coated Particle Fuel, Nucl. Techn. 35 (1977) 483-493.
- [49] HURTADO, A.M., SCHRÖDER, B., GOTTAUT, H., Ceramic Coatings for HTR-Graphitic Structures, Response of Fuel, Fuel Elements and Gas-Cooled Reactor Cores under Accidental Air or Water Ingress Conditions (Proc. IAEA TCM, Beijing, 1993), IAEA-TECDOC-784, Vienna (1995) 120-124.
- [50] SCHRÖDER, B., SiC Coated Spherical Fuel Elements, Fuel and Graphite for HTR (Proc. 2nd Soviet-German Sem., Jülich, 1991), Internal Report KFA-HTA-IB-3/91, Research Center Jülich (1991) 451-473.
- [51] GREBENNIK, V., Private Communication, 1994.
- [52] KONOTOP, Y.F., A Brief Review On-Going Research in Kharkov to Increase Fuel Corrosion Stability, Fuel and Graphite for HTR (Proc. 2nd Soviet-German Sem., Jülich, 1991), Internal Report KFA-HTA-IB-3/91, Research Center Jülich (1991) 475-486.
- [53] TANG, C., et al., Improvement in Oxidation Resistance of the Nuclear Graphite by Reaction-Coated SiC Coating, J. Nucl. Mater. 224 (1995) 103-108.
- [54] ZHANG, S., QIU, X., MA, C., Study of the Method to Improve the Corrosion Resistance of the Matrix Materials of Spherical Fuel, Response of Fuel, Fuel Elements and Gas-Cooled Reactor Cores under Accidental Air or Water Ingress Conditions (Proc. IAEA TCM, Beijing, 1993), IAEA-TECDOC-784, Vienna (1995) 116-120.
- [55] HROVAT, M., RACHOR, L., HUSCHKA, H., Fabrication and Properties of Molded Block Fuel Elements for HTGR's, (Proc. Eur. Nucl. Conf., 1975), Nuclear Energy Maturity 7 (1975).
- [56] ALLEN, P.L., OLDFIELD, B.W., The Development of Directly Cooled Fuels for the HTGR, TRG Report 2655(s), Reactor Fuel Element Laboratories UKAEA Reactor Group (1975).
- [57] BALTHESSEN, E., EHLERS, K., HACKSTEIN, K.G., NICKEL, H., HTGR Fuel Development and Testing, Conf-740501 (1974).
- [58] HROVAT, M., IN DER SCHMITTEN, W., Erste Bestrahlung monolithischer Block-semente im Peach-Bottom-Reaktor, Report GA-A13699, General Atomic Company (1976).
- [59] TOBITA, T., FUKUDA, K., Fabrication Tests of HTGR Fuel Rod by Rubber Molding, Annual Meeting of Atomic Energy Society of Japan, Kyoto (1986) F28.
- [60] TOBITA, T., FUKUDA, K., TSURUTA, H., Irradiation Experiment of Monolithic Fuel Rod, Annual Meeting of Atomic Energy Society of Japan, Kinki (1991) M41.

**NEXT PAGE(S)
left BLANK**

8. CONCLUSIONS

The investigation of fundamental characteristics of HTGR fuel has been in progress for 30 years. All of the HTGR reference concepts from Member States utilize fuel based on the TRISO coated fuel particle with low-enriched uranium. Two specific directions for the fuel element design have been pursued, the block type in Japan and the USA, and the spherical fuel element in Germany, Russia, and China. A key design requirement in obtaining the significant safety and radiological cleanliness of the modern HTGR is the utilization of high quality fuel. High quality was first achieved in the manufacturing of the coated fuel particle in the early 1980s. Improvements since this time have consisted of steps to reduce TRISO particle defects during fuel element fabrication and in minimizing uranium contamination in these elements. Another important aspect was the development of sensitive quality control methods such as the burn-leach technique which provides the data necessary to confirm that the fuel meets the design limit of less than 6×10^{-5} free uranium as arising from particle defects. Now, with newer data, this design limit can be further reduced to 3×10^{-5} free uranium.

The main source of fission products escaping the fuel under normal operating conditions is from uranium outside of an intact SiC layer which appears as heavy metal contamination in the fuel element matrix or as defective/failed fuel particles. There are several mechanisms which can cause a particle to fail: kernel migration, interaction of fission products with the SiC, failure of the coating as a pressure vessel, and excessive diffusion through the fuel coating layers. These failure mechanisms only exist under extreme operating conditions which result in large temperature gradients within the particle or for fuel particles manufactured outside of the specification limits. The release of fission products is primarily modeled based on diffusive transport as the key phenomena. The release of short-lived gaseous fission products from a particle kernel can be analytically determined by applying the Booth formula describing the release rate over birth rate, R/B, as a function of diffusivity and decay constant.

The performance of German high quality fuel has been tested in irradiation experiments which included a total of 19 spherical fuel elements and 276,680 TRISO particles. Gas release analysis has shown that in no single case was a particle failure caused during irradiation. The statistical derivation for the operationally related failed particle fraction in the HTR-MODUL core has been determined as 4×10^{-6} as the expected value and 2×10^{-5} as the design value.

Irradiation performance of the fuel rods contained in a cylindrical graphite block for development of the prismatic block fuel has been tested in the OGL-1 gas loop. Approximately 30 fuel rods with a total of more than 500 fuel compacts have been tested in Japan in a series of 15 experiments. The results of these tests provided comprehensive performance data on aspects such as fission gas release (R/B), metallic fission product behavior, fuel compact behavior, coated particle performance, fuel rod mechanical stability, and fission product plateout in the loop. The fuel fabrication process has steadily improved throughout the OGL-1 experiments with recent fuel quality irradiation R/B performance of less than 10^{-6} , which is significantly lower than the design limit, 5×10^{-4} .

In Russia, the feasibility of the use of “weak” irradiation (“weak” irradiation means short irradiation at room temperature) for obtaining constants necessary for the prediction of fission product release from the fuel elements during HTGR operation has been justified. In parallel, analytical methods of predicting fission product release from fuel elements have been developed. It has been shown that the reference fuel elements with nominal burnups up to $\approx 12\%$ FIMA provide fission product retention during normal operation and under accident conditions.

Fuel testing under off-normal non-oxidizing conditions has provided fuel performance information as a function of fuel temperature up to 2500 °C. Compared to other reactor systems, it is easy to examine coated particles, or even fuel elements (spheres, compacts) containing a large number of particles under extreme accident conditions. Heating experiments with half a million particles were performed in Germany up to core heatup temperatures of the HTR-MODUL (1620 °C) and a maximum burnup of about 9 %FIMA. Applications in future licensing procedures can be based on one coated particle failure in four fuel elements and no additional release of safety relevant fission products, especially iodine. Japanese heatup simulation tests with batches of 100 particles showed similarly good results. Fission product release and failure fraction during heatup can be predicted by calculations with the national models. During ramp tests (Germany, Japan, Russia, USA), silicon carbide decomposition at temperatures beyond 2000 °C leads to an increase of particle failure and subsequent fission product release.

During irradiation at very high temperatures with compacts (Japan) between 1500 and 2000 °C, particle failure was only detected at 2000 °C. Reactivity tests under pulse irradiation conditions (Japan, Russia) showed that coating failure increases with the amount of energy deposition starting from 600 J/(g UO₂).

Among the postulated accidents in gas-cooled reactors are those of water and air ingress. These accidents involving oxidation of exposed fuel kernels, carbonaceous materials, SiC and ZrC, can lead to an enhanced release of fission products and to a degradation of core components. In water ingress accidents, the interaction of exposed kernels with water vapor resulted in a significant increase in the release of fission products. No effects of the concomitant interaction of water vapor with intact fuel particles were indicated.

Three irradiation experiments, HRB-17/-18 and HFR-B1, have been conducted with the deliberate introduction of water vapor. The fuel particles contained UO₂ and a known small portion had exposed kernels. A series of discrete tests was conducted with water vapor at partial pressures in the range 0.003 to 2 kPa. The released fission gas was monitored for the isotopes Kr-85m, Kr-87, Kr-88, Xe-133, Xe-135, and Xe-138. The general sequential response of the exposed fuel kernels to water vapor consists of three stages: (1) a rapid transient release of fission gas with a concomitant increase in the steady state release, (2) a period of constant steady state release, and (3) a decline in the release to prehydrolysis values upon cessation of water vapor injection. In German experiments, a significant release of the water vapor induced Kr-85 release with higher burnup was measured for irradiation experiment HFR-K6 with low enriched UO₂ fuel and for postirradiation heating tests.

Numerous experimental and theoretical efforts have been made to examine plateau distribution of fission products in the primary circuit both under normal operating and

accident conditions. In-pile and out-of-pile deposition loops were operated in Germany (LAMINAR, VAMPYR-I and -II, SMOC), Japan (OGL-1), France (SAPHIR, COMEDIE), the UK (Dragon), and the USA (GA deposition loop, CPL-2 tests) to study systematically the ad-/desorption behavior of fission product on metallic surfaces as function of temperature and gas flow. The obtained experimental data as well as the measurements from the gas-cooled reactors AVR, THTR-300, Peach Bottom, Fort St. Vrain were taken to derive plateout parameters such as desorption energy or penetration coefficient to be used in corresponding calculation models for validation purposes.

Remobilization of fission products deposited in the primary circuit occurs during accident sequences by desorption due to flow change induced by temperature increase and/or system pressure drop by liftoff of dust-borne activities. Transient experiments in different countries showed an increase of the gas-borne dust by up to three orders of magnitude. Computer models were developed to calculate liftoff fractions. Various tube samples have been taken from deposition experiments to investigate the removal of cesium and iodine from metal surfaces by washoff and steamoff in leaching experiments at ORNL and at KFA Jülich. It was determined that accessible fission products are released in water ingress accidents through dissolution and chemical attack.

The decontamination of primary circuit components from plated-out activity is an option to mitigate radiological hazards to plant workers which is of particular interest for direct-cycle gas turbine HTGRs. It is also used for decommissioning purposes. Different forms of surface activities (in-diffusion into oxide layer, adsorption on metallic surface, deposited dust) may require different methods of decontamination encompassing mechanical, chemical, or electrochemical processes. The material composition was found to be an important parameter. Most of the decontamination work was dedicated to LWR components and circuits. However, decontamination work on HTGR circulators was performed in Germany and in the USA.

The ZrC coating which is the most refractory material has several potential advantages compared to the conventional TRISO-coated fuel particles such as an enhanced capability for fission product retention at very high temperatures, realizing the core with a high power density, improvement of fuel properties in the fuel production due to enabling higher-temperature sintering of the green fuel compact. The United States, Japan, and Russia have developed the ZrC-coating layer for application in the coated particles to replace the SiC layer (ZrC-TRISO coated fuel particles), although several fuel designs with use of ZrC had been attempted besides this type of fuel in the United States. It was proven in Japanese and US postirradiation heating tests that the ZrC coating has an effective retention capability for cesium at very high temperatures. Other features are a strong chemical resistivity against palladium corrosion and an effective elimination of the amoeba effect as well as an excellent high temperature performance. As a result, in the case of extreme air or water ingress accidents, the ZrC layer does not provide protection against destructive oxidation of the layer. Use of a SiC layer outside the ZrC layer would provide protection against oxidation.

In conclusion, in modern HTGR fuel the level of defective coated particles during manufacture is practically zero. Only during manufacture of fuel bodies does particle failure occur, but on a very low level. In-pile fuel performance is demonstrated by irradiation

testing under HTGR-typical operating conditions with no additional failure of particles. Accident behavior resulting from unrestricted core heatup is investigated by heating of irradiated fuels: at 1600 °C, all safety-relevant fission products are retained and only at 1800 °C and higher temperatures do particles start to fail excessively and to release fission products. Fission gases and iodine are only partially released from defective or failed particles. The level of release increases during water ingress. For licensing applications, a complete set of codes and data is available for predicting fission product behavior in-core and ex-core including plateout. Alternative advanced fuels are currently being evaluated for better coated particle fission product retention at extreme temperatures and for an inherent corrosive protection of fuel elements.

A.1. TRANSPORT DATA FOR DIFFUSION MODEL

The classical approach for a diffusion model is the numerical solution of the Fickian equation using **effective diffusion coefficients** for the fission product species in different kinds of reactor materials. "Effective" means that all possible transport mechanisms are summarized in a simplified single transport process. The diffusion model is generally regarded to be valid both for normal operation and for accident conditions.

The diffusion coefficients are usually given as an Arrhenius type equation as a function of temperature. Empirically found deviations from this behavior could be overcome by assuming additional dependencies, for instance on fast neutron fluence¹ or fission product concentration or burnup, or by combining diffusion processes with different activation energies in different temperature ranges:

$$D(T, \Gamma, c, \dots) = \sum_i D_{o,i}(\Gamma, c, \dots) \exp\left\{-\frac{Q_i}{R T}\right\} \quad (\text{A-1})$$

where

D_o is the pre-exponential factor [m^2/s]

Q is the activation energy [J/mol]

R is the gas constant, $R = 8.3143$ [J/(mol K)]

T is the temperature [K]

Γ is the fast neutron fluence [10^{25} m^{-2} , $E > 16 \text{ fJ}$]

c is the fission product concentration [m^{-3}]

Diffusion coefficients have been adopted from the evaluation of numerous irradiation and heating experiments with complete spherical fuel elements, fuel compacts, single fuel particles, or graphite samples.

Recommendations of transport data have been collected over many years and were continuously revised. In a joint effort of KFA and German industries within the project "Hochtemperaturreaktor-Brennstoffkreislauf" (HBK), a set of data to be used for predicting fission product transport during HTGR normal operation has been established [1]. Its purpose was to summarize the data base for HTGR design calculations for licensing procedure. A comprehensive data collection was created in the 1970s by UKAEA/AERE Harwell summarized in the so-called "Red Book" [2]. Transport data as applied to US HTGR designs have been published as part of the "Fuel Design Data Manual" [3] by General Atomics.

¹ Different units for the fast neutron fluence are found in the literature; e.g., a different cutoff limit for the neutron energy $E > 0.1$ MeV (16 fJ), $E > 0.18$ MeV (29 fJ), or EDN. The correct unit is explicitly mentioned wherever necessary.

For German fission product transport studies under accident conditions, however, additional or new recommendations have been derived from corresponding experimental data to meet the requirements of HTGR safety analyses. An extended set of transport data was given in the status report [4].

An observed high permeability for a fission product species in a material zone is simulated in a diffusion model by choosing a comparably "large" diffusion coefficient. A typical example is the buffer layer. In contrast, a complete retention can be simulated by a very "small" diffusion coefficient; e.g., for fission gases in intact particle coating layers.

A common assumption in most diffusion models is the neglect of any effects of sorption or trapping within a coating layer or of any preferential retention in a specific layer. The ratio of fission product concentrations at the surfaces of contiguous materials ("partition coefficient") is assumed to be one; consequently, the concentrations are equal at contiguous surfaces. Measurements of this ratio range from about 0.3 to 3 and may change with temperature and fast fluence [5]. For lack of adequate measurements of the ratio under a sufficiently large range of conditions, the error associated with the assumed value of 1.0 is accepted. The few experimental studies related to desorption from coating materials indicate some kind of discontinuity in concentration profiles at coating interfaces, for instance for cesium between buffer and inner pyrocarbon (PyC) layer or the significant palladium peaks at the inner surface of the SiC layer [6] in microprobe profiles. The increase of cesium concentration towards the surface of Soviet coated particles was explained by a contamination of the outer coating layer during the disintegration of the fuel sphere [7].

Experiments at KFA have been proposed in 1989 for investigation of the thermochemical partition coefficients at material boundaries to better estimate the magnitude of this effect. The development of an alternative calculation model is underway at KFA which considers the fission product transport to be dependent on the gradient of the chemical potential rather than of the concentration [8]. The modeling differences, however, are not expected to be important for small-sized HTGRs under accident conditions since the enormous retention capability of colder graphite regions in the core - described by a partition coefficient (sorption isotherms) at the graphite/coolant boundary - keeps the release of metallic fission products negligibly small.

Tables A-1 to A-5 and Figs. A-1 to A-9, respectively, summarize the actual knowledge in transport data and attempt to compare the results from different countries. Differences from the former status report [4] are explicitly mentioned.

A.1.1. Fuel Kernel

Diffusion coefficients in UO_2 fissile particle kernels which were used in recent German safety analyses have been derived from irradiation and heating experiments with designed-to-fail UO_2 particles (kernel + buffer layer). According to an evaluation of the German irradiation and heating experiment FRJ2-P28, cesium and iodine release under accident conditions is considered at KFA to be best approximated by a two-branch diffusion coefficient while those for strontium and silver were modified by a factor of 20 and 10, respectively, compared to the recommendation of the last HBK data set. A different recommendation is given for iodine at lower temperatures ($< 1000^\circ\text{C}$) which was derived

from irradiation experiments in the R2 reactor at Studsvik [9]. There is no change of KFA data compared to the status report [4].

In the US, most data were derived from ThO_2 fertile kernels. A significant dependence of the reduced diffusion coefficient on temperature and burnup but no dependence on fast fluence was found. The diffusion data for metallic fission products [10] are also used for UO_2 , with a separate set of constants used for UCO kernels which are slightly higher than those for UO_2 . UC_2 fuel is assumed to retain no metallic fission products. However, for safety analysis calculations, the use of KFA data for the metallic fission products is recommended.

Other US data recommended for cesium [11] and strontium [12] represent a fit through many data from different authors.

Japanese transport data for cesium were derived from in-pile fractional release measurements [13, 14]. The curve is below corresponding German and US data.

The diffusion data for UO_2 are summarized in Table A-1 and plotted in Fig. A-1. Data and plots for $(\text{Th},\text{U})\text{O}_2$ fuel kernels mainly used in BISO particles are not presented here; for further detail see [4].

The assumption of a **defective or failed particle** in the diffusion code FRESCO-II is equivalent to simulating an exposed particle kernel. This means that fission products released from the particle kernel by diffusive transport are immediately released to the surrounding graphite structure. The failure of a particle coating, however, is not necessarily equivalent to a non-existing coating; such an assumption is a conservative approach. There is experimental evidence for a better retention of fission products in particles with a broken coating compared to exposed kernels. The simulation of a partly existing coating as a kind of a 3rd type of particle (besides intact particles and exposed kernels) has been proposed by JAERI ([15], see also later section on silicon carbide). Another possibility of modeling a broken but still existent coating is the choice of a smaller diffusion coefficient in the kernel as an "effective" diffusion coefficient for this 3rd type of particle as has been done in the FRESCO-II code [16]. A postcalculation of the 1800 °C isothermal heating test HFR-K3/3 has shown that the reduction of the kernel diffusion coefficient by two orders of magnitude simulates a failed but still existing coating and reproduces the high-release peak of the observed IMGA bimodal distribution of single particle inventories [17].

A.1.2. Pyrocarbon

Diffusion coefficients in pyrocarbon were mostly derived from early experimental data with LTI- and HTI-PyC from BISO particles. Due to its comparably smaller retention capability, diffusion in PyC has not been investigated in that detail as it has been for the main barrier silicon carbide. At temperatures beyond 1900 °C, it is recommended to assume rapid diffusive transport (similar to the buffer layer) for metallic fission products in LTI-PyC. For HTI-PyC, this critical temperature has been assumed in German safety analysis calculations for the THTR-300 to be as low as 1200 °C, except cesium for which experimental evidence suggests much better retention than strontium or silver. The diffusion

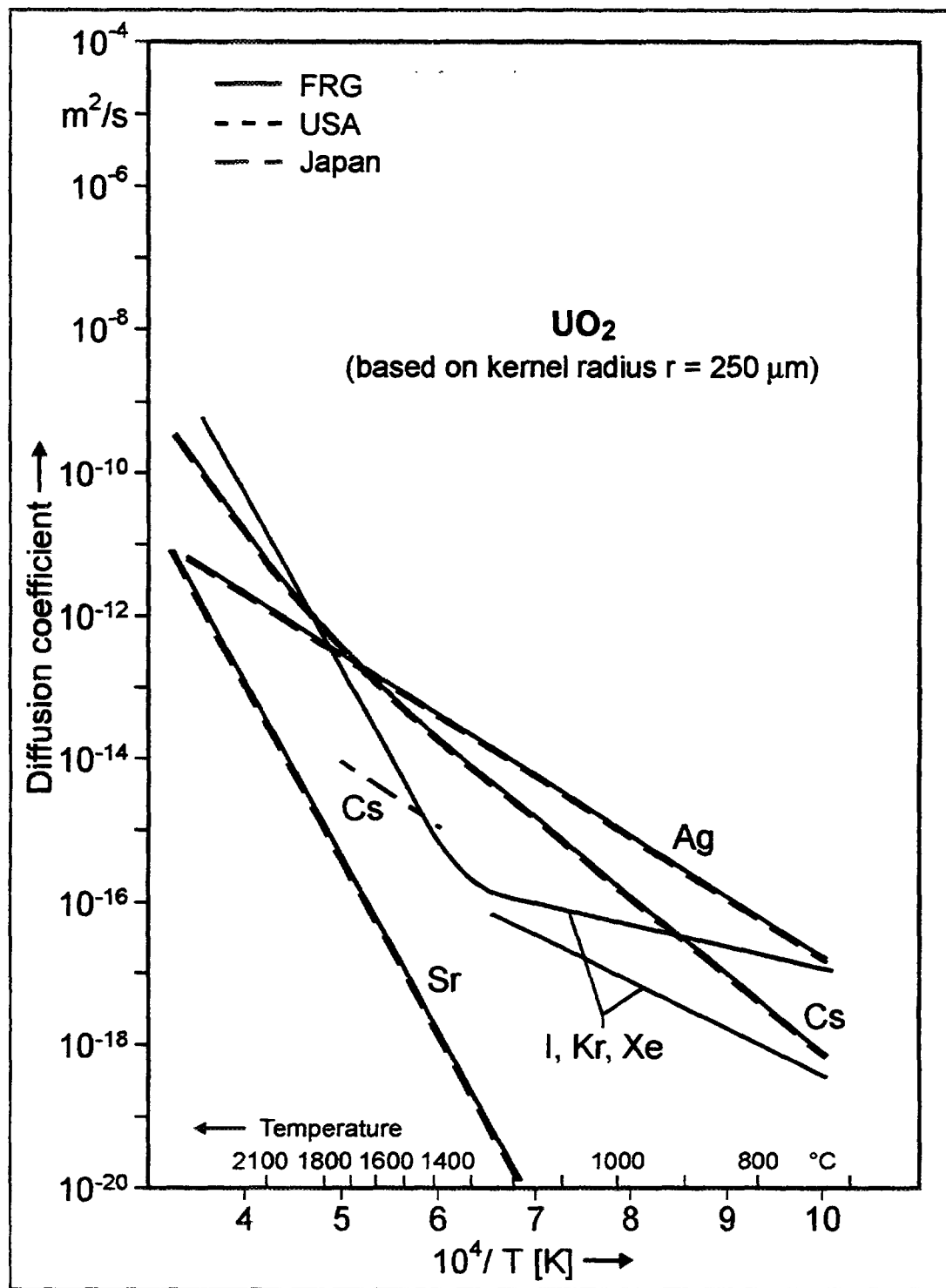


Fig. A-1: Diffusion coefficients of fission product species in UO₂ as function of temperature

Table A-1: Diffusion coefficients in UO₂ (with respect to kernel radius r = 250 μm)

	Temperature range	D _{0,1} [m ² /s]	Q ₁ [kJ/mol]	D _{0,2} [m ² /s]	Q ₁ [kJ/mol]	Reference
FRG						
Cs		5.6*10 ⁻⁸	209	5.2*10 ⁻⁴	362	[4]
Sr		2.2*10 ⁻³	488			[4]
Ag		6.7*10 ⁻⁹	165			[4]
I, Kr, Xe	NOC AC	1.3*10 ⁻¹² 8.8*10 ⁻¹⁵	126 54	6.0*10 ⁻¹	480	[4, 9] [4]
USA						
Cs		5.6*10 ⁻⁸	209	5.2*10 ⁻⁴	362	[4]
Sr		2.2*10 ⁻³	488			[4]
Ag		6.7*10 ⁻⁹	165			[4]
Japan						
Cs	1400-1720 °C	4.7*10 ⁻¹⁰	177			[13, 14]

coefficient of krypton in PyC is based on an evaluation of GA heating data at 2050 °C and ramp tests and of KFA 1600 °C tests [18]. No modification of KFA transport data is considered to take into account possible irradiation damage in PyC due to a high probability of irradiation damage annealing [18]. No change of KFA data has been made compared to the status report [4].

US recommendations for strontium and silver as well as for iodine and fission gases are identical to those at KFA. The data for cesium [11] and strontium [12] represent an average of the measurements of many authors. Early US studies [19] have also found the cesium transport data through isotropic pyrocarbon to be orders of magnitude lower than those for strontium, both being in the range of the later reported data.

In Japan, several studies have been made on cesium in different temperature ranges [14].

Diffusion data given by other authors ([7], [19], [20], [21]) are fairly close to each other despite their strong dependence on the pyrocarbon deposition conditions during manufacture and material characteristics. This dependence was reported to be the reason for the relatively large difference in JAERI and KFA activation energies for cesium [22].

The diffusion data for pyrocarbon are summarized in Table A-2 and plotted in Fig. A-2. Data and plots for HTI material mainly used in BISO particles are not presented here; for further detail see [4].

The carbonaceous **buffer layer** is assumed in the diffusion model to have no significant retention capability for fission products. In FRG calculations, a value of the diffusion coefficient of 10^{-8} m²/s with no temperature dependence (activation energy equal to zero) is used. The US recommendation for the corresponding diffusion coefficient is 10^{-10} m²/s; the difference is negligible since either one is significantly larger than the diffusion coefficient for the other coating materials.

A.1.3. Silicon Carbide

The transport properties of fission products in silicon carbide, as the most efficient barrier of the coated particle, were the subject of many detailed studies in the past years [e.g., 23]. The experimental data gave impetus to either confirm and/or refine existing models or even to develop new ones.

The original way to describe the permeability of the SiC coating for fission products was a diffusion coefficient derived from numerous heating tests at KFA with single coated fuel particles. The radionuclide cesium was investigated more than any other relevant metallic fission product species. The Arrhenius relation for cesium proposed by Allelein [24] entered the HBK data set as recommended data for use in HTGR core release predictions under normal operating conditions and was recommended in [4].

For irradiation experiments with modern HTGR fuel, the Allelein diffusion coefficient was found to overestimate in some cases the cesium release fraction from fuel particles. An evaluation of the experimental data by Christ [25] has taken the fast neutron fluence as

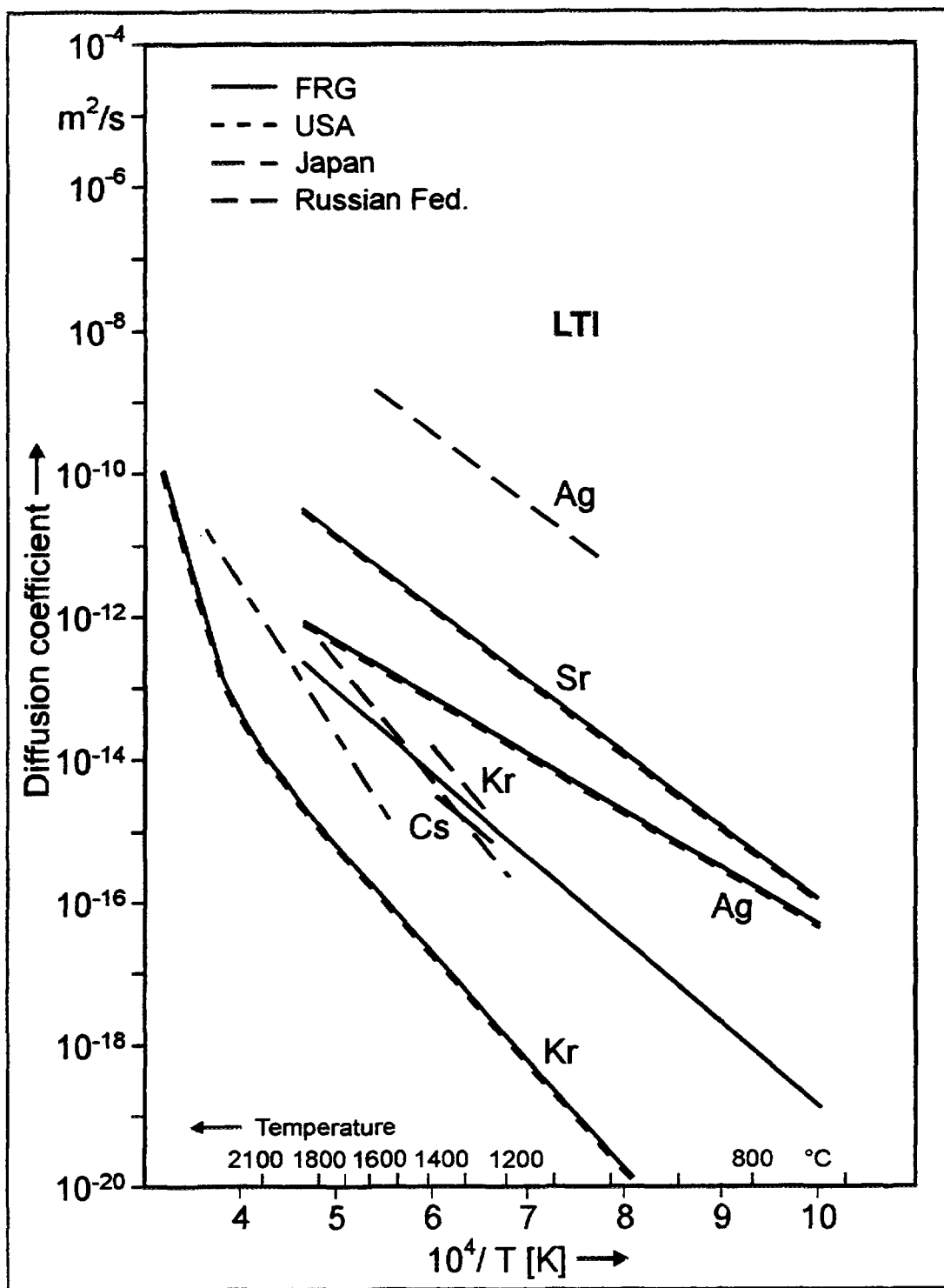


Fig. A-2: Diffusion coefficients of fission product species in LTI pyrocarbon as function of temperature

Table A-2: Diffusion coefficients in LTI pyrocarbon

	Temperature range	$D_{0,1}$ [m ² /s]	Q_1 [kJ/mol]	$D_{0,2}$ [m ² /s]	Q_1 [kJ/mol]	Reference
FRG						
Cs		$6.3 \cdot 10^{-8}$	222			[4]
Sr		$2.3 \cdot 10^{-6}$	197			[4]
Ag		$5.3 \cdot 10^{-9}$	154			[4]
Kr, Xe		$2.9 \cdot 10^{-8}$	291	$2.0 \cdot 10^5$	923	[18]
USA						
Cs	1200-1800 °C	$5.0 \cdot 10^{-5}$	318			[11]
Sr	1000-1650 °C	$2.3 \cdot 10^{-6}$	197			[12]
Ag		$5.3 \cdot 10^{-9}$	154			[21]
Kr, Xe		$2.9 \cdot 10^{-8}$	291	$2.0 \cdot 10^5$	923	[18]
Japan						
Cs	1250-1385 °C	$6.0 \cdot 10^{-9}$	198			[14]
Cs	1600-2300 °C	$1.2 \cdot 10^{-3}$	412			[14, 22]
Russian Fed.						
Ag	1400-1700 °C	$5.3 \cdot 10^{-4}$	193			[20]
Kr	1000-1630 °C	$1.1 \cdot 10^{-5}$	285			[20]

a parameter for the Arrhenius relation, thus influencing the amount of cesium penetrating the SiC layer during irradiation and the delay of the diffusive break-through at elevated temperatures. This new recommendation for the low-temperature branch of KFA data is - for zero fast fluence - lower compared to the Allelein data but will come close to it with increasing fast fluences (Fig. A-4).

A theoretical evaluation of several researchers' experimental cesium release data from coated particles was made by Myers in the early 1980s. The result was a diffusion coefficient subdivided into a low temperature branch and a high temperature branch dominant at > 1600 °C. The data at high temperatures were likewise subdivided and identified to characterize two different types of silicon carbide material [26]. The upper curve (Fig. A-4) was chosen in 1986 as the reference data for accident temperature conditions with the goal of being at least conservative in German safety analyses calculations [4].

Experimental results from heating tests in the KüFA furnace at KFA with modern HTGR spherical fuel elements beginning in 1984 [27] however, showed a discrepancy in the high temperature release behavior from single coated particles and from complete fuel balls, with the latter exhibiting much lower release fractions. Due to a considerable retentivity of the matrix graphite for metallic fission products, due to the optimized fuel manufacturing process which may have influenced the fission product transport characteristics in the particle coating, and due to the better statistics of about 10^4 particles per fuel element, experiments with single particles were no longer regarded as representative of modern high quality fuel.

This experience coincides with the fact that postcalculations of cesium release from heated fuel elements using the (upper) Myers' diffusion coefficient have led to an overestimation by up to several orders of magnitude. A recent evaluation of data from all heating experiments conducted in the KüFA furnace so far - a total of 44 tests with respect to cesium - using the diffusion code FRESCO-II has led to a new KFA recommendation for a diffusion coefficient in silicon carbide [28] which is very similar to the lower Myers curve.

An analogous evaluation has been made for strontium on the basis of 11 KüFA heating tests with modern HTGR fuel in the temperature range between 1600 and 1800 °C. The new diffusion coefficient [28] shown in Fig. A-3 has a higher activation energy resulting in a diffusion coefficient lower by a factor of about 20 at 1600 °C compared to the old recommendation. Unfortunately, the combination of this new high-temperature Arrhenius relation with the old HBK relation for normal operation temperatures into a single two-branch diffusion coefficient significantly underestimates the experimental retention quality of SiC for strontium at 1600 °C [28]. In order to benefit from this potential for reduced release, more strontium release data at lower temperatures should be made available.

KFA silver transport data have been taken from the HBK data set. No evaluation of available silver release data from KüFA heating tests has been made so far because no consistent release behavior was observed and is in many cases not reproducible by any existing model. A possible explanation as proposed by Myers could be the silver to be trapped at neutron-induced defects in the silicon carbide structure at normal operation temperatures resulting in a burst release of the trapped silver at elevated temperatures.

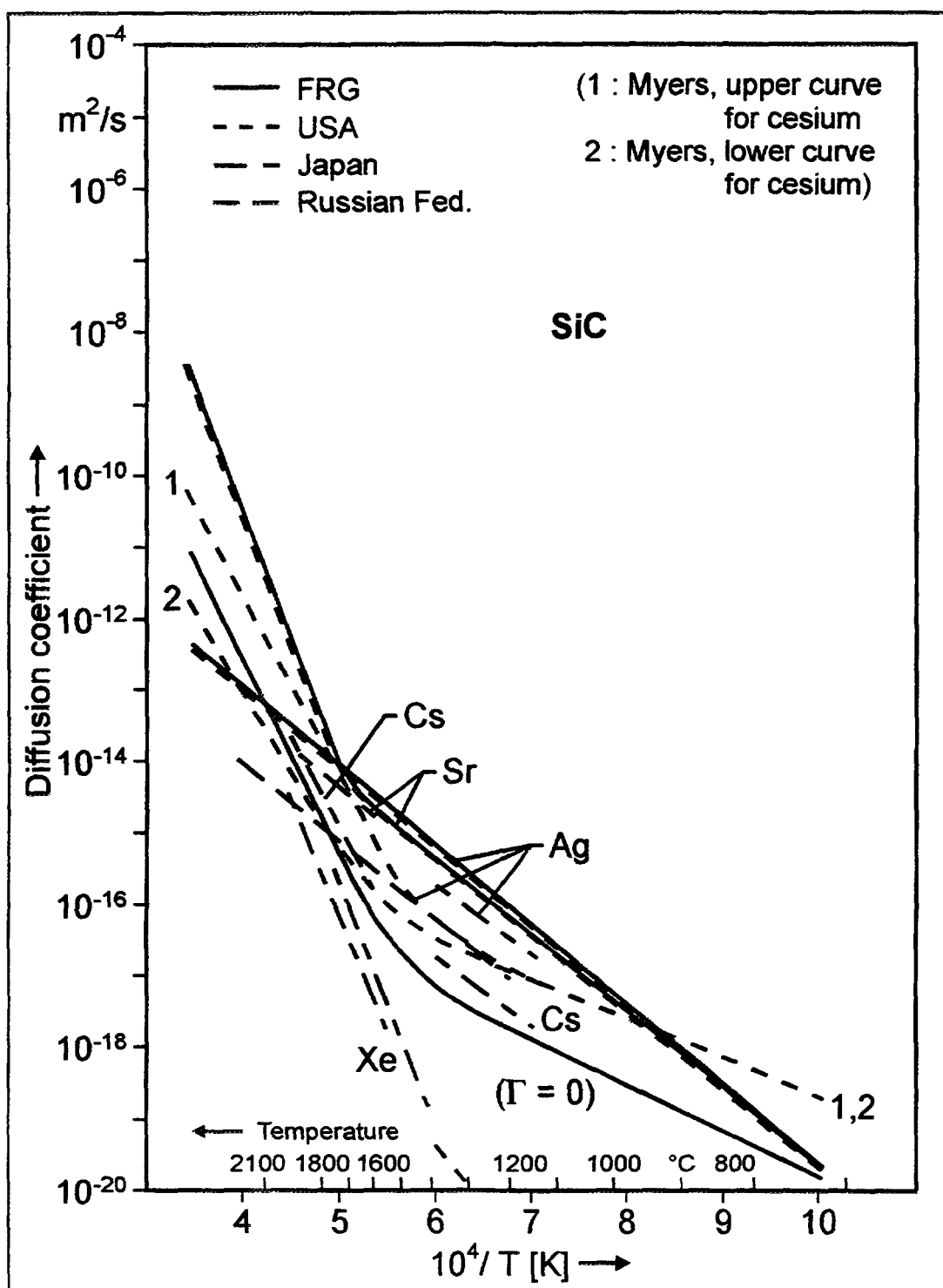


Fig. A-3: Diffusion coefficients of fission product species in silicon carbide as function of temperature

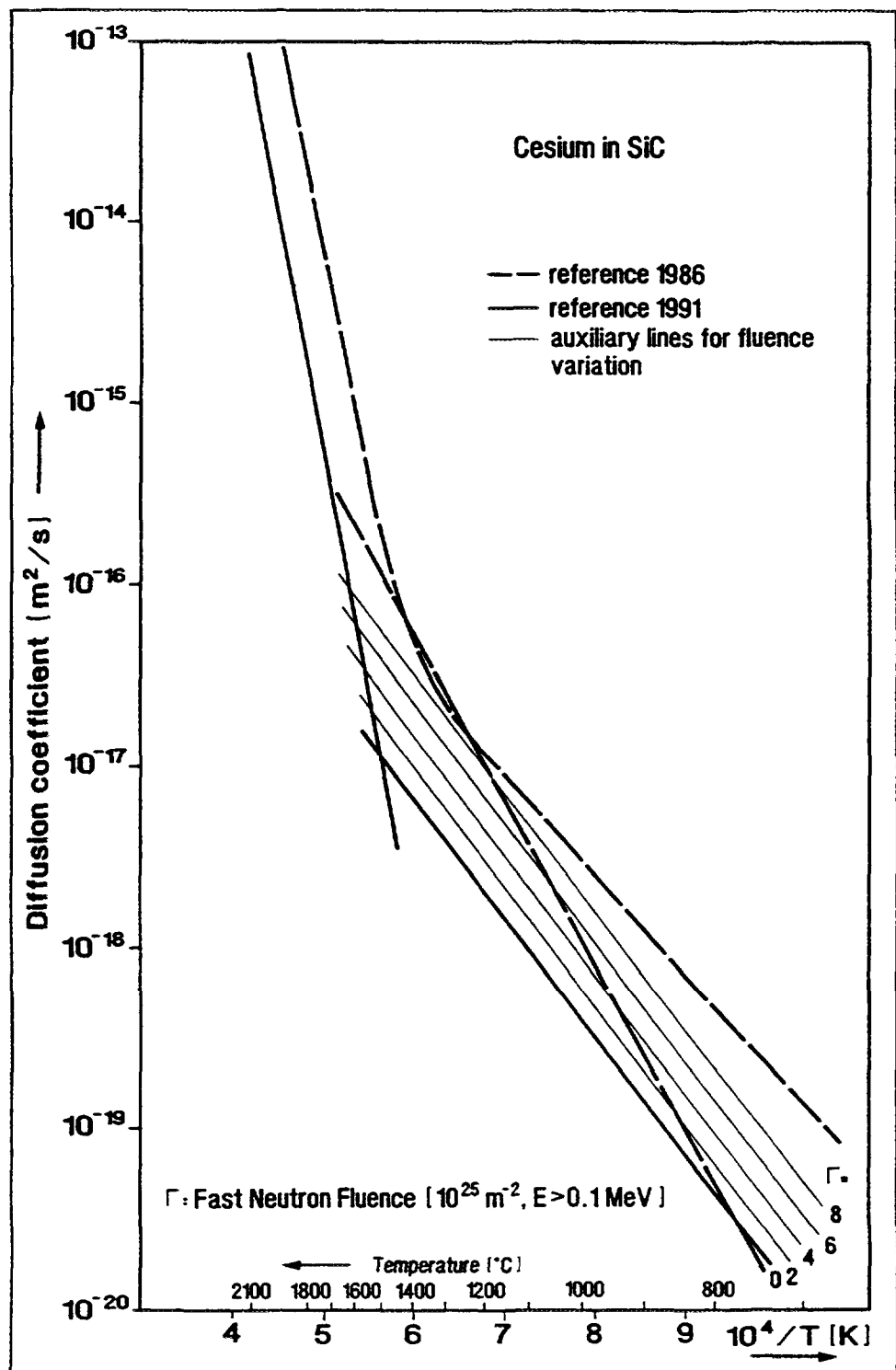


Fig. A-4: KFA diffusion coefficients of cesium in silicon carbide, comparison of 1986 and 1991 reference data and fast fluence dependence

Table A-3: Diffusion coefficients in silicon carbide

	Temperature range	$D_{0,1}$ [m ² /s]	Q_1 [kJ/mol]	$D_{0,2}$ [m ² /s]	Q_1 [kJ/mol]	Reference
FRG						
Cs		$5.5 \cdot 10^{-14} \cdot e^{\Gamma/5}$ (1)	125	$1.6 \cdot 10^{-2}$	514	[25, 28]
Sr		$1.2 \cdot 10^{-9}$	205	$1.8 \cdot 10^6$	791	[4, 16]
Ag		$3.6 \cdot 10^{-9}$	215			[4] [4]
USA						
Cs, lower		$6.7 \cdot 10^{-14}$	106	$1.1 \cdot 10^{-4}$	437	[26]
Cs, upper		$6.7 \cdot 10^{-14}$	106	$2.4 \cdot 10^{-2}$	482	[26]
Sr		$1.2 \cdot 10^{-9}$	205	$1.8 \cdot 10^6$	791	[4]
Ag		$3.6 \cdot 10^{-9}$	215			[4]
Japan						
Cs	1200-1400 °C	$\leq 6.8 \cdot 10^{-12}$	177			[13, 14]
Cs	1600-1900 °C	$2.5 \cdot 10^{-2}$	503			[34]
Sr	1600-1850 °C	$1.2 \cdot 10^{-9}$	205			[35, 14]
Ag	1200-1400 °C	$6.8 \cdot 10^{-11}$	177			[13, 14]
Xe	1400-1750 °C	$3.7 \cdot 10^1$	657			[36, 14]
	1200-1400 °C	$8.6 \cdot 10^{-10}$	326			[36, 14]
	1650-1850 °C	1.7	624			[35, 14]
Russian Fed.						
Cs	1000 °C	$2.3 \cdot 10^{-17}$				[7]
Ag	1200-2300 °C	$3.5 \cdot 10^{-10}$	213			[20]

(1) Γ : Fast neutron fluence [10^{25} m⁻², E > 16 fJ] (Γ is reactor-specific!)

According to the definition of the "Integrated Failure and Release Model for Standard Particles" which represents the US reference model [29], no diffusion of cesium (and strontium) through silicon carbide is assumed to occur. There are, however, US diffusion data available which were published before the statistical model was created [26, 30, 31, 32]. Ongoing work by Martin, based on [33], suggests that a fast-fluence-dependent diffusion coefficient similar to that of Christ [25] represents an improvement over the reference model.

No big difference between Japanese and KFA data was found for cesium and silver. For strontium, the same data as KFA for the low-temperature branch are used (Fig. A-4) [13, 14, 34, 35, 36].

The uncertainty range for transport data in silicon carbide is a result of the very low release level for high quality fuel at temperatures ≤ 1600 °C which sometimes only allows the indication of an upper limit. When considering heating tests with complete fuel elements, other parameters such as heavy metal contamination fraction in the graphite grain importance.

The approach in the JAERI code FORNAX which uses a 3rd type of particle with a degraded SiC layer simulated by larger values for the diffusion coefficient has been previously mentioned; no specific transport data have been published so far.

Röllig has recently provided an interesting analysis of the Cs-137 release data for FRG sphere R2-K13/1 heated to 1600 °C for 1000 h [37]. Nearly 2000 particles were gamma-counted, and 7 % had released over 10 % of their Cs-137 inventory, with a small number of particles releasing 50 to 90 %. Röllig applied a diffusion model to the release data, but rather than a single diffusion coefficient he assumed a log-normal distribution of values around the average diffusion coefficient. He obtained reasonable agreement with the data for particle release as a function of position within the sphere. This method of assuming a distribution of diffusion coefficients is a promising approach to account for the inherent microstructural variation in SiC and its effect on particle-to-particle release comparisons.

A.1.4. Graphite

The uncertainty for the given transport data in graphitic materials is considered to be fairly high. The metallic radionuclide transport in graphite is strongly dependent on graphite type and nature, structure, temperature, fission product concentration, state of oxidation, irradiation damage, coolant gas pressure, and interference with other fission product species. The trapping mechanism is not considered, which is known to better approximate the real transport process in graphite. The overall uncertainty range is estimated to be at least one order of magnitude, for silver as high as three orders of magnitude. For safety analysis purposes, however, transport data for the oversimplifying Fickian diffusion model in graphite can be used to obtain realistic, or at least conservative radionuclide release data.

A.1.4.1. Matrix Graphite

Effective diffusion data are relatively well known for cesium and silver [38] and strontium [39] in **German A3-3 matrix graphite** in the Henrian concentration regime as well as the influence of irradiation and corrosion on the diffusive process. The matrix graphite type A3-3 was used for the THTR-300 spherical fuel elements and was chosen to be the reference fuel element graphite for future German HTGRs. In contrast, all of the modern German fuel elements which were used in irradiation and postirradiation experiments consisted of the matrix graphite type A3-27. Comparative measurements of Hoinkis showed diffusion coefficients for cesium and silver in as-received A3-27 lower by a factor of 20 and 7, respectively, at 1000 °C compared to as-received A3-3 [38]. A more recent Hoinkis report presents the diffusion coefficients of silver in as-received A3-3, as-received A3-27, and irradiated A3-3 in the temperature range of 800 - 1300 °C [40] confirming the above single measurement (Fig. A-5). The KFA data for the metallic fission products given in Table A-4 and shown in Fig. A-5 refer to irradiated A3-3 matrix graphite, the same as in the status report [4].²

According to the experience from measurements, cesium and strontium diffusion through graphite has been assumed in German safety analyses to proceed rapidly at temperatures beyond 2000 °C, for silver already at temperatures > 1000 °C.

The evaluation of cesium inventory measurements in the matrix of heated fuel elements with the KFA code FRESCO-II have also demonstrated the diffusion coefficient in A3-27 to be at least one order of magnitude lower compared to A3-3 in the accident temperature range of 1600 to 1800 °C. But the fitted diffusion coefficients for A3-27 cannot consistently be described in a new Arrhenius relation on a lower level [28]. The choice of heavy metal contamination fraction in the matrix which is used as input data for the model calculations has a major effect on the release level from the fuel element, especially at lower heating temperatures ≤ 1600 °C (when the release from the coated particles is comparably small) and especially for strontium which is more strongly bound in graphite than is cesium.³ An adequate recommendation for cesium and strontium transport in A3-27 matrix graphite may be the reduction of the Hoinkis diffusion coefficient curves (for A3-3) by one order of magnitude which would still envelope the calculated results [28].

US diffusion data on **fuel compact matrix material**⁴ are not given due to the assumption of a rapid transport of the metallic and gaseous fission products through this porous material zone [29, 41].

Japanese data have been published for strontium in **graphite matrix** for the VHTR design [42] which is one to two orders of magnitude above German reference data. The Japanese data are, however, somewhat smaller compared to early KFA measurements conducted for strontium and cesium in irradiated A3 matrix of AVR fuel elements [43].

² The difference in KFA cesium data between Table A-4 and [4] is due to an error in the original Hoinkis paper in [38]. However, the irradiation dependence discussed in Hoinkis' paper was found to not significantly change the transport data. The difference in KFA strontium data between Table A-4 and [4] is due to a slight discrepancy between earlier reported data and the final publication [39].

³ The input data for heavy metal contamination fraction and for the diffusion coefficients in SiC and matrix graphite are usually varied until the calculated release data fit the measurements. The adjustment of fuel element release to a lower level can - if the release from the coated particles is correctly reproduced - be achieved by reducing either the diffusion coefficient in graphite or the contamination fraction. The latter is not explicitly known for every single fuel element, only average values can be estimated.

⁴ The fuel compact matrix material is not a matrix graphite but a combination of fired carbonaceous material, graphite grains, and coated fuel particles. The transport of condensable fission products will be mainly on the surfaces of the carbonaceous material. The release of condensable fission products from the compact is by desorption, homogeneous concentration within compact.

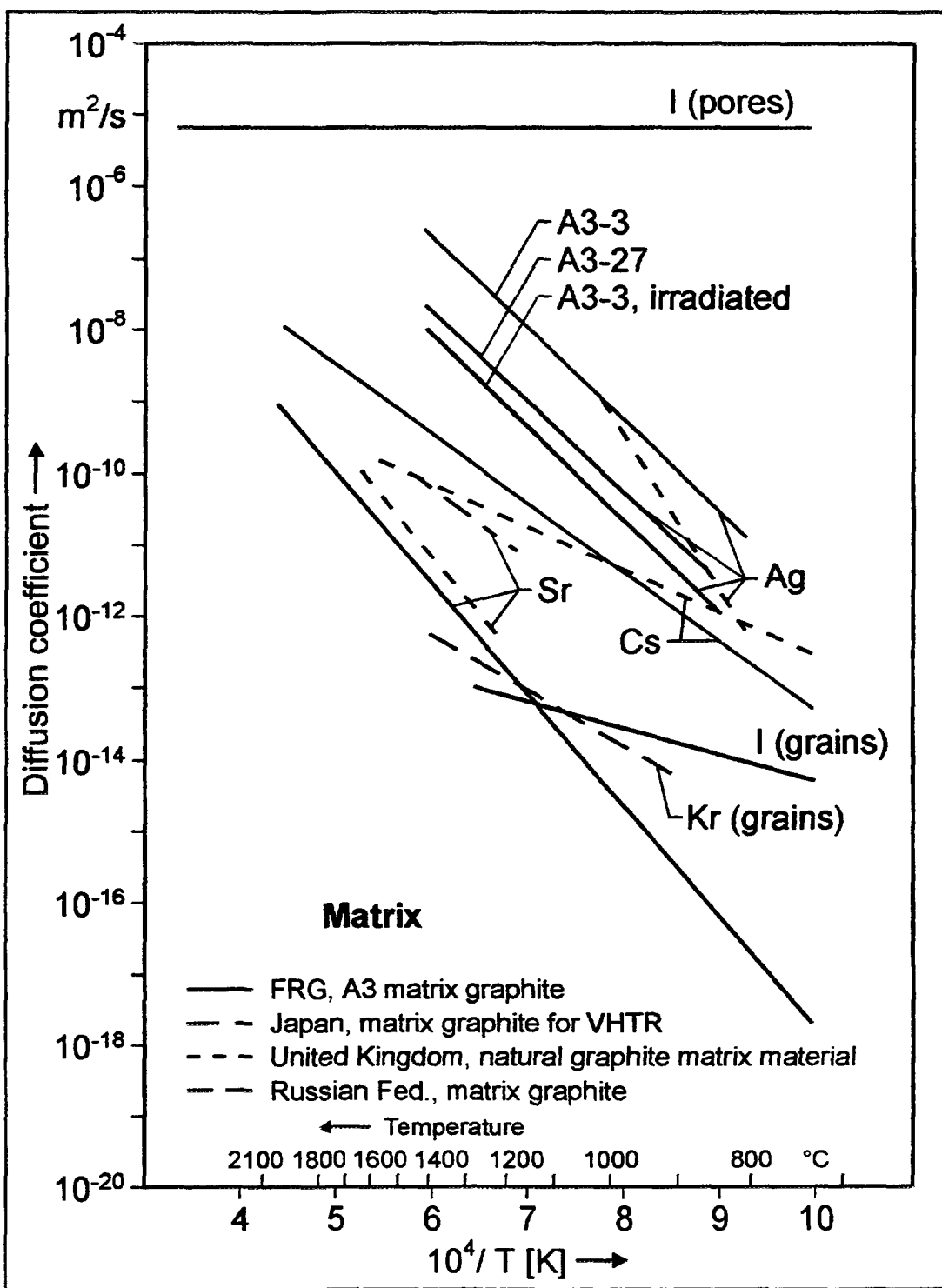


Fig. A-5: Diffusion coefficients of fission product species in matrix graphite as function of temperature

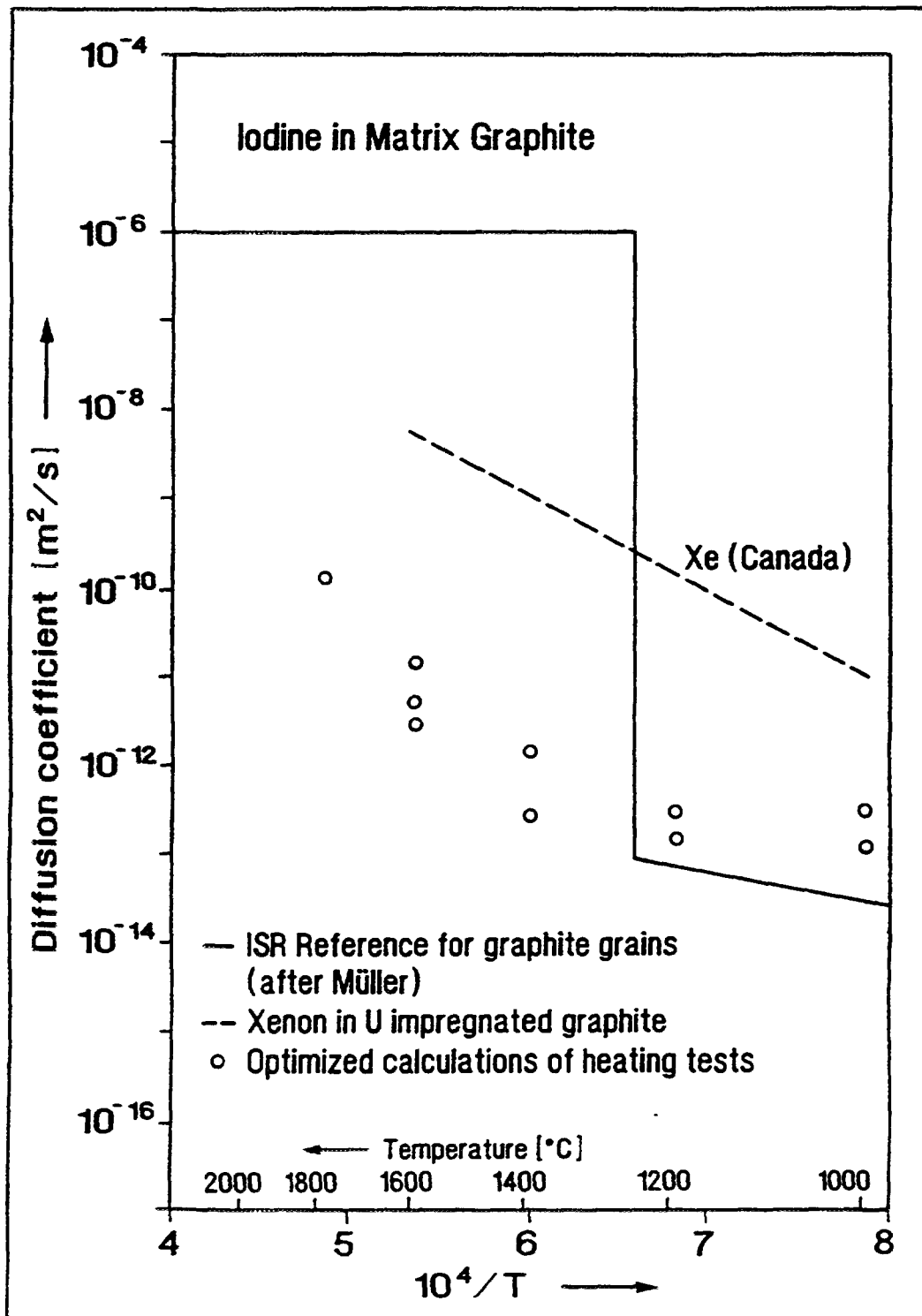


Fig. A-6: Diffusion coefficients of iodine and fission gases from uranium contamination in graphite (optimized data points related to contamination fraction of $1 \cdot 10^{-7}$)

Table A-4: Diffusion coefficients in matrix graphite materials

	Temperature range	$D_{o,1}$ [m ² /s]	Q_1 [kJ/mol]	$D_{o,2}$ [m ² /s]	Q_2 [kJ/mol]	Reference
FRG						
Cs		$3.6 \cdot 10^{-4}$	189			[38]
Sr	≤ 2000 °C	$1.0 \cdot 10^{-2}$	303			[39]
Ag	800 - 1300 °C	$6.8 \cdot 10^1$	262			[40]
Ag	800 - 1300 °C	1.3	246			[40]
Ag	800 - 1300 °C	1.6	258			[38, 40]
I in pores	≤ 2000 °C	$6.0 \cdot 10^{-6}$	0			[4]
I in grains	≤ 1250 °C	$1.0 \cdot 10^{-18}$ (1)	71			[9]
USA						
Cs, Sr, Ag		∞ (2)				[31]
Kr, Xe, I		∞ (2)				[41]
Japan						
Sr	1175-1375 °C	$2.8 \cdot 10^{-4}$	210			[42]
UK						
Cs	750-1550 °C	$3.5 \cdot 10^{-7}$	116			[44]
Sr	1200-1600 °C	$5.6 \cdot 10^{-2}$	312			[44]
Ag	800-1000 °C	$8.7 \cdot 10^7$	414			[44]
Russian Fed.						
Kr	900-1400 °C	$3.1 \cdot 10^{-8}$	151			[20]

(1) With respect to graphite grain radius $r = 6$ μm . For spherical fuel element $r = 3$ cm: $D_o = 2.5 \cdot 10^{-11}$

(2) Instantaneous release from compact

Other studies have been made with the British compacted natural graphite matrix material [44] which are fairly close to the corresponding German reference data.

Fission gases released from the coated particles are assumed in US modeling to be transported through the fuel compact matrix material without any time delay both under normal operating and accident conditions. This assumption has the same result as the German approach which uses a large diffusion coefficient for xenon in helium to simulate fission gas and iodine transport in the graphite pores (= grain boundaries). The US modeling of radionuclide transport in graphite has been recently refined by introducing the effect of graphite oxidation into the diffusion coefficient by making the pre-exponential factor a function of weight percent burnoff.

The transport behavior of iodine in graphite under accident conditions is considered in German model calculations to be similar to that of the noble gases krypton and xenon. Rather than simulating an effective, one-phase diffusion, the iodine transport is conservatively treated in the KFA reference modeling to consist of a slow diffusion phase out of the graphite grain proposed by Müller [9] at temperatures ≤ 1250 °C and of a rapid diffusion phase via the pores and the graphite grain boundaries. The iodine from the heavy metal contamination is assumed to be buried deep inside the grains. In contrast, iodine released from defective particles into the graphite is assumed to be immediately transported in the graphite pores. The quick phase transport is independent of temperature and corresponds to the diffusive behavior for xenon in helium, and does not allow for any realistic retention in the graphite.

The transport of iodine and fission gases in graphite has been recently the subject of a special series of KFA experiments [45]. Spherical fuel elements with low burnup were heated to investigate the release behavior of short-lived isotopes originating from the heavy metal contamination. Iodine release curves were found to be akin to those for xenon, with both supporting the interpretation of a release from traps in the matrix graphite. "Effective" diffusion coefficients derived from these experimental data using the FRESCO model [28] revealed (see Fig. A-6) that the reference diffusion coefficient as explained in the above paragraph was too small at lower temperatures and too large at higher temperatures > 1250 °C. But from the arrangement of the fitted data, an activation energy could be recognized which is similar to that for an effective diffusion coefficient for xenon transport in irradiated AUF graphite which was impregnated with uranium carbide [47]. This Canadian investigation had shown that relatively high fractions of xenon were retained in the graphite even at temperatures up to 2000 °C.

The above mentioned evaluation of the KFA heating experiments with the FRESCO-II code was repeated, but now using for the contamination fraction in the spheres a single value (1×10^{-7}) rather than the release value measured at the end of each series. The new calculation results shown in Fig. A-6 are up to two orders of magnitude lower than the earlier results, and the low temperature data fall close to the Müller slow phase diffusion coefficient. However, all things considered, these calculational results do not seem to represent a good basis for recommending a new diffusivity. The old one remains sufficiently conservative for safety analyses, although an approach using a trapping mechanism will be the more accurate one.

Table A-5: Diffusion coefficients in structural graphite materials

	Temperature range	$D_{o,1}$ [m ² /s]	Q_1 [kJ/mol]	$D_{o,2}$ [m ² /s]	Q_2 [kJ/mol]	Reference
FRG						
Cs	550-1450 °C	$1.7 \cdot 10^{-6}$	149			[11]
Sr	800-2200 °C	$1.7 \cdot 10^{-2}$	268			[12]
Ag	490-800 °C	1.6	258			[48]
I in pores		$6.0 \cdot 10^{-6}$	0			[4]
USA						
Cs	550-1450 °C	$1.7 \cdot 10^{-6}$	149			[11]
Sr	800-2200 °C	$1.7 \cdot 10^{-2}$	268			[12]
Japan						
Cs	750-1030 °C	$9.0 \cdot 10^{-6}$	157			[50]
Ag	750-1030 °C	$6.3 \cdot 10^{-3}$	264			[50]
Cs	600-1000 °C	$1.2 \cdot 10^{-4}$	112			[49]
Cs	600-1000 °C	$1.7 \cdot 10^{-4}$	95			[49]
UK						
Cs	450-750 °C	$5.8 \cdot 10^{-2}$	151			[44]
Sr	850-1400 °C	$8.3 \cdot 10^{-1}$	324			[44]
Ag	850-1100 °C	$1.6 \cdot 10^2$	364			[44]
Others						
Xe (Can)	900-1600 °C	$1.1 \cdot 10^{-10}$ (1)	205			[47]

(1) With respect to graphite grain radius $r = 6 \mu\text{m}$. For spherical fuel element radius $r = 3 \text{ cm}$: $D_o = 2.8 \cdot 10^{-3}$

The objectives of tests conducted in the **Russian Federation** on iodine and fission gas release from HTGR fuel element graphite were to obtain the temperature dependence of the release and to study the correlation of gaseous and aerosol fission product release [46]. The objects used for the investigations were standard spherical fuel elements, fuel element “failure” imitators, i.e., graphite spheres containing uncoated kernels instead of coated particles, uncoated kernels, coated particles with a different number of protective coatings, a mix of coated particles with kernels (in bulk), as well as “contamination” imitators, i.e., either 35 mm diameter spheres manufactured from a mix of graphite with uranium or 60 mm diameter spherical graphite models without fuel particles.

The investigations were conducted using the technique of “weak” irradiation (see section 3.4.4.). The fractional release of the iodine isotopes during isothermal heating was determined on the basis of a measurement of the activities of the daughter isotopes (Xe-135, Xe-133) built-in in the facility test section after its cooling down. The temperature dependence of the iodine release was obtained by cyclic heating of the investigated samples. The experimental results were analyzed by means of the activation model (see Appendix B).

The temperature dependence of the iodine and xenon isotopes has been obtained within the temperature range 200 - 1100 °C. It has been observed that an increase of the graphite quantity in the sample results in a relative reduction of the iodine release, an effect which is apparently connected with iodine absorption especially at low concentrations. It has also been shown that a heat treatment of the imitator samples leads to an enhanced radionuclide release and also changes the character of the temperature dependence; this influence can be explained by a probable uranium carbidization at high temperatures and, consequently, a decrease of the kernels’ retention capability. It should be noted that an estimation of the primary circuit activity using Xe-135 benchmark nuclide release data in equation (B-50) can lead to overestimated values of iodine release (for release values < 10^{-2}) [46].

A.1.4.2. Structural Graphite

No diffusion data are available for the **German** reference reflector graphite **ASR-1RS**. The US data for H-451 graphite grade have been used instead in model calculations. The transport of iodine and fission gases in structural graphite is only considered via the rapid diffusive phase since they have penetrated the graphite from the coolant side, thus being transported using the pores rather than entering the grains.

US data for cesium and strontium which approximate various authors’ measurements and are recommended to be used in HTGR core (graphite type: **H-451**) release predictions were presented in the Table A-5 to also represent KFA transport data for structural graphite. The silver transport in H-451 measured at temperatures up to 800 °C was supposed in [48] to consist of a slow phase with high concentrations near the surface and of a fast phase with low concentrations away from the surface.

JAERI studies of **IG-110** structural graphite in in-pile experiments have revealed significant differences in cesium and silver diffusion data relative to German and US data [49]. In particular, silver released from the fuel compact was found to be effectively retained in the graphite sleeve for low burnups < 2 %FIMA. Diffusion coefficients for cesium

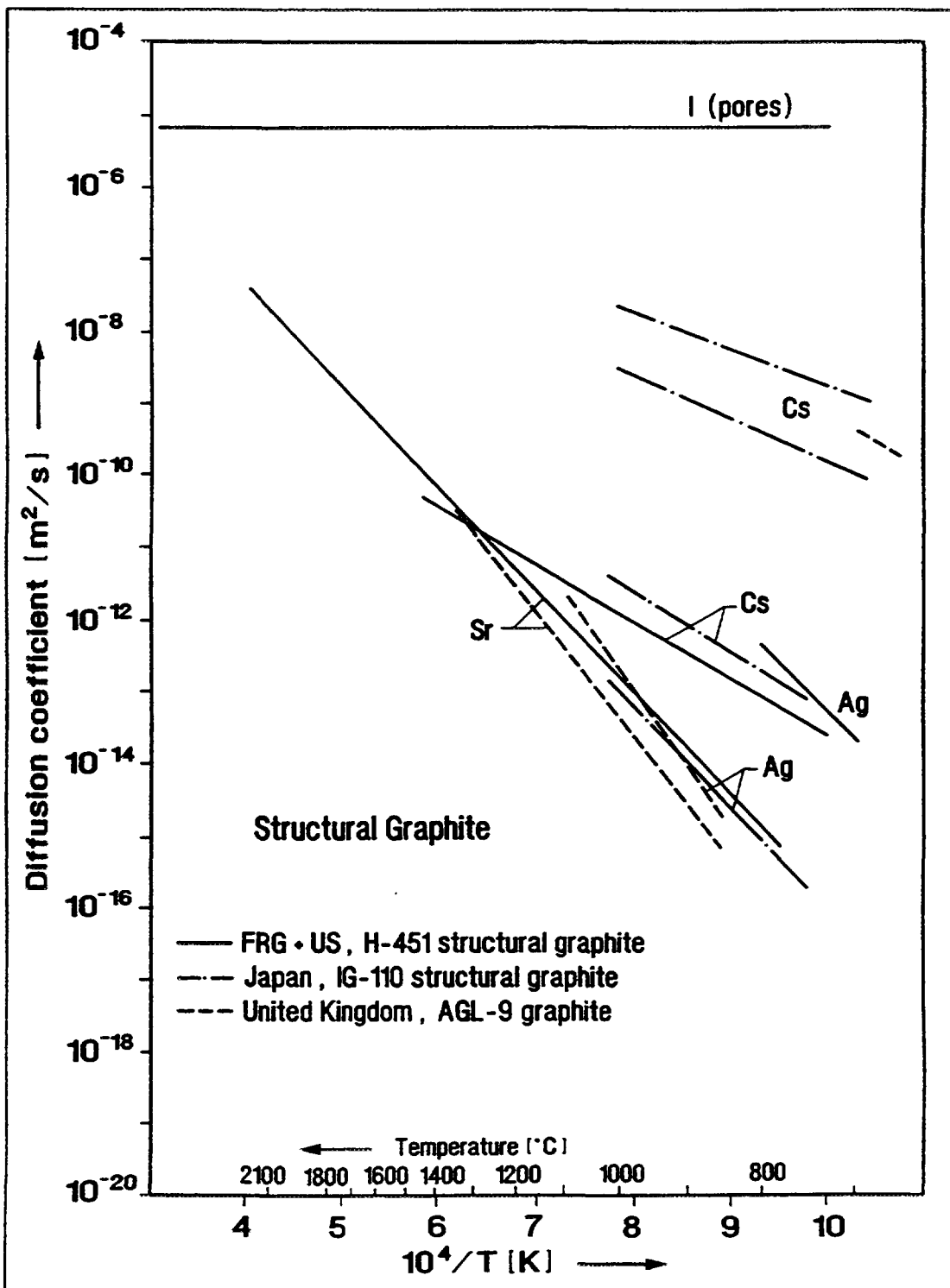


Fig. A-7: Diffusion coefficients of fission product species in structural graphite as function of temperature

obtained from experiments with Cs-impregnated IG-110 graphite specimens were found to be larger by 3-4 orders of magnitude and with a lower activation energy compared to those data obtained from the in-pile experiments. An explanation is proposed by assuming an additional trapping effect by irradiation-induced surface defects with stronger binding energies than those of existing traps [50].

British diffusion data shown in Fig. A-7 refer to fuel tube graphite AGL-9 [44].

The diffusion data for structural graphite are summarized in Table A-5 and are plotted in Fig. A-7.

A.1.4.3. Concentration Dependence of the Diffusion Coefficient

Experimental data on the **concentration dependence** of transport data have been collected by several authors (discussed in Refs. [12] and [44]). A significant effect was found for strontium where a tremendous increase of diffusivity by several orders of magnitude occurred as soon as a certain concentration was exceeded [51]. Only small effects were found for silver and cesium. The concentration dependence of strontium diffusion is expressed in the empirical equation

$$\log D(T, c_{gr}) = 4.51 - 2.58 \log c_{gr} - (29300 - 7000 \log c_{gr})/T \quad (\text{A-2})$$

where c_{gr} is the concentration in the range of 60 - 2000 [$\mu\text{g Sr/g C}$].

The following empirical strontium diffusion coefficient dependent on temperature and concentration was found to be in good agreement with experimental data and recommended for US safety studies [12]:

$$D(T, c_{gr}) = 3.47 * 10^{-13} c_{gr}^2 \exp \left\{ - \frac{64000 \chi}{R} \left(\frac{1}{T} - \frac{1}{1273} \right) \right\} \quad (\text{A-3})$$

where

$$\chi = 0.422 + \frac{0.5805}{1 + c^3/80} \quad (\text{A-4})$$

and c_{gr} is the concentration in the range of 0.7 - 50 [$\mu\text{mol Sr/g C}$]

This diffusion coefficient is plotted in Fig. A-8.

A modeling refinement for diffusive transport of cesium and strontium in graphite which simulates this effect uses the British experimental data obtained for strontium [51]. In the FRESCO model, corresponding sorption data for strontium and cesium (see following section A.2) are taken to introduce a factor consisting of the ratio of the partition coefficient based on Freundlich sorption isotherms over that based on Henry sorption isotherms [16]. The partition coefficient $\alpha = \alpha(T)$ is defined by the equation

$$c_{gas} = \alpha c_{gr} \quad (\text{A-5})$$

where

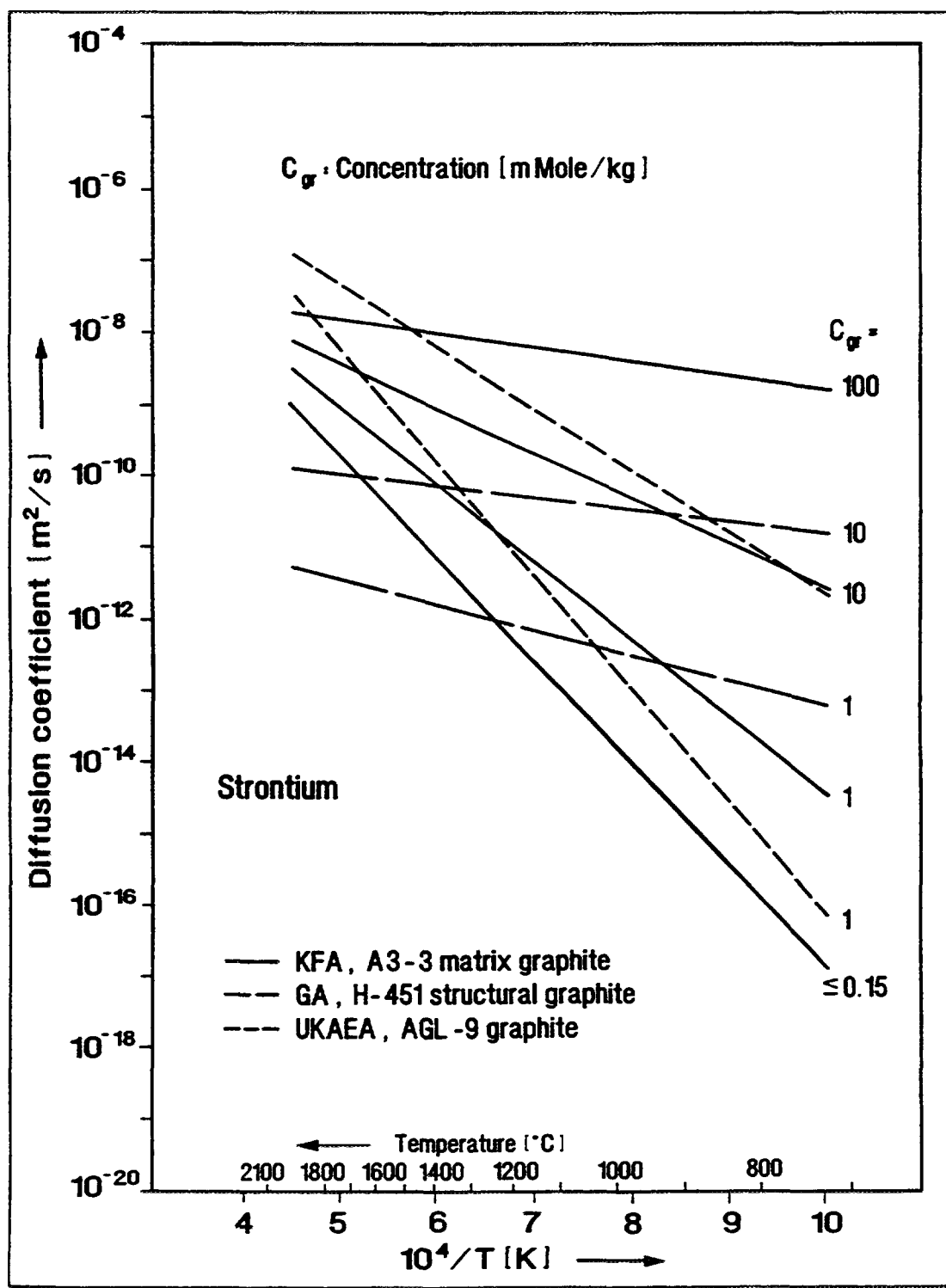


Fig. A-8: Concentration dependence of diffusion coefficient of strontium in graphite

c_{gas} is the concentration in coolant [Atoms/m³]

c_{gr} is the concentration in graphite surface layer [Atoms/m³]

The concentration dependence is given by modifying the pre-exponential term of the diffusion coefficient in graphite by a factor which is equal to 1 for the Henrian concentration regime and greater than 1 for the Freundlich concentration regime:

$$D_o^x(c_{\text{gr}}) = D_o \frac{\alpha_{\text{Freundlich}}}{\alpha_{\text{Henry}}} \quad (\text{A-6})$$

with the above definition of α .

This type of concentration dependence is presented in Fig. A-8 for strontium reproducing the results of [51], and in Fig. A-9 for cesium. This procedure is also applied to the structural graphite of the reflectors in the 'core' version of FRESCO [52].

Another approach has been proposed in [53] which is employed in the SPTRAN code. The pre-exponential factor of the diffusion coefficient is additionally dependent on temperature

$$D_o^x(T, c_{\text{gr}}) = D_o \left[1 + \left(\frac{c_{\text{gr}}}{c_t} \right)^{\tau} E_F/T \right] \quad (\text{A-7})$$

where

c_t is the transition concentration between Henry and Freundlich regime
(see following section A.2.1.)

τ is an empirical parameter

E_F is a parameter of the Freundlich sorption isotherm

E_F corresponds to E of equation (A-8) in section A.2

A value of 0.25 for the parameter τ was fitted to best approximate cesium experimental data [54]. The diffusion coefficient according to equation (A-7) is shown in Fig. A-9 (dashed curves).

A.2. SORPTION OF FISSION PRODUCTS OVER GRAPHITIC SURFACES

At the boundary between a solid and a gas, transition of diffusing atoms occur due to sorption processes. In most practical cases, these two processes are so fast that a local equilibrium between the concentration of atoms adsorbed at the solid surface and the concentration of atoms in the neighboring layer of gas ("vapor pressure") may be assumed. This means that the phenomenological data of importance are given by an isotherm which relates these two equilibrium values. Usually the equilibrium vapor pressure in the gas phase is expressed as a function of the fractional coverage of the solid surface by adsorbed atoms. In practice, adsorption is mainly of importance in the case of porous solids which have a large internal surface area per unit weight. The vapor pressure is expressed as an exponential function of temperature and sorbate concentration.

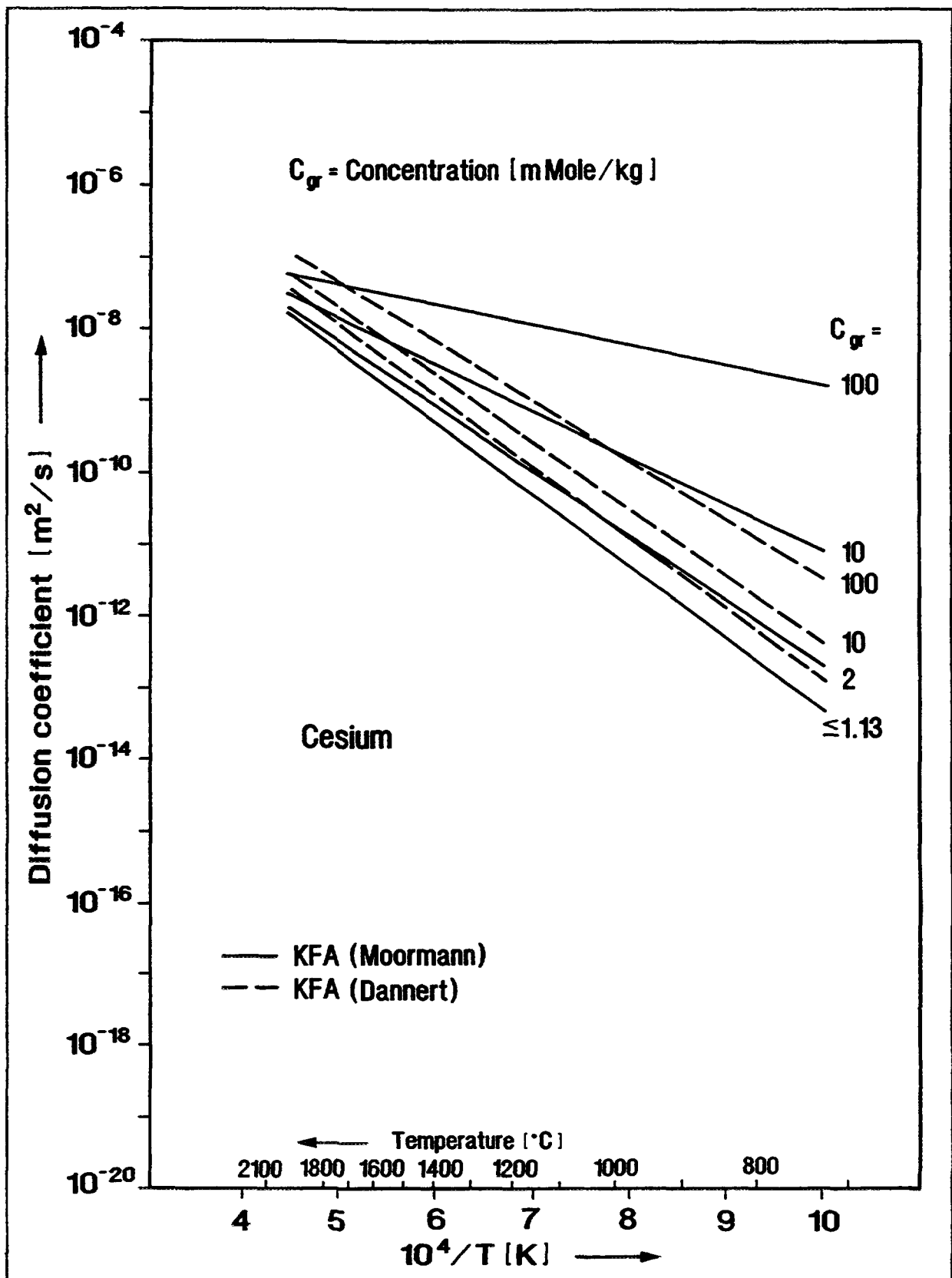


Fig. A-9: Concentration dependence of diffusion coefficient of cesium in graphite

Polymeric carbon, coked phenolic resin binder, has a particularly high sorption capacity for cesium and strontium at high temperatures. This can be attributed to its structure. Its density is low compared to that of graphite. The material has a turbustatic structure. The carbon layers are not parallel and not planar and they have many defects. This high sorption capacity of A3-3 matrix graphite containing coked ungraphitized phenolic resin binder is substantially higher than that of nuclear graphites like H-451, H-327, IG-110, BAR 675, P₃JHAN, ASR-1RS, ASR-2RS, and ATR-2E, which contain a more highly graphitized binder component.

The high values obtained for the isosteric enthalpies of sorption of cesium and strontium by the A3-3 matrix graphite show that they are strongly bound by chemisorption. Thus, the sharp reduction of the partial pressures by sorption, the high sorptive capacity, and the large quantity of the A3-3 matrix graphite present in the core of an HTGR indicate a high potential of the A3-3 matrix for the retention of cesium and strontium during normal operation and in the case of a core heatup accident. This potential increases on irradiation with fast neutrons, if the irradiation temperature is below 1135 °C, and decreases if irradiation temperatures reach 1400 °C [55].

A.2.1. Sorption Isotherms

At low concentrations, the sorption conforms to **Henry's law** (constant heat of adsorption, direct proportionality between vapor pressure and concentration of sorbed species) and at higher concentrations **Freundlich** sorption holds (characterized by decreasing heat of adsorption with increasing concentration of sorbed species).

The fission product concentration sorbed on the carbonaceous material is in equilibrium with the partial vapor pressure, p, of that fission product species. The partial vapor pressure is assumed to contain contributions from both the Freundlich (p_F) and Henrian (p_H) isotherms [12]:

$$\begin{aligned} \ln p_F &= \left(A + \frac{B}{T} \right) + \left(D + \frac{E}{T} \right) \ln c_{gr} \\ \ln p_H &= \left(A + \frac{B}{T} \right) + \left(D - 1 + \frac{E}{T} \right) \ln c_t + \ln c_{gr} \quad (\text{A-8}) \\ p &= p_F + p_H \\ \ln c_t &= d_1 - d_2 T \end{aligned}$$

where

p_F is the Freundlich isotherm vapor pressure [Pa]

p_H is the Henrian isotherm vapor pressure [Pa]

T is the temperature [K]

c_{graphite} is the concentration of sorbate species [mmol/kg C]

A, D, d_1 are constants

B, E are constants [K]

d_2 is a constant [K^{-1}]

Sorption isotherms of metallic fission products on different graphitic materials have been thoroughly measured in the past. At KFA, experiments on two different facilities have been carried out to derive sorption isotherms mostly for cesium and strontium on A3 matrix graphite [55].

In the US design, sorption effects are important both for the porous fuel compacts and for the graphite blocks. The fuel compact consists of fuel particles and graphite shim particles, bonded by a sorptive carbonaceous matrix. The same governing equations are used for the sorption isotherms for fuel compact and H-451 structural graphite [12, 32].

Design equations which incorporate the effect of fast fluence on metallic fission product sorptivity in H-451 graphite have also been derived as a modification of the above equations. These equations for cesium are reported in [32] and will not be repeated here. The sorptivity of the compact matrix material does not change with increasing fast neutron fluence [11].

The cesium concentration sorbed on compact matrix material tends to be one to two orders of magnitude higher than on unirradiated H-451 graphite; this difference narrows at higher pressures (10^{-6} Pa and higher) and lower temperatures. Cesium sorption on irradiated H-451 is closer to that of the compact matrix material. Compared to cesium, the difference in sorbate concentration between the two materials is greater for rubidium but less for strontium [56].

A modification of the sorption isotherms of cesium and strontium over matrix graphite has been proposed by Moormann [57]. These data are preferred to be used in predictive calculations to those published by the experimenters Hilpert [58, 59] and Kwasny [60]. The reason is that the latter describe the experimental results within the measured temperature and concentration ranges as given by the vertical lines in the figures. The new Moormann data set creates (almost) the same sorption isotherms in the Henry regime and overcomes the problem of "unphysical" behavior of the original equations in the Freundlich regime at higher temperatures beyond those covered by the experiments [57].

An experimental program [61] was undertaken at ORNL to extend the data on the sorption and desorption of iodine on graphite to more realistic high temperature gas-cooled reactor operating conditions. This was accomplished by heating compacts of H-451 and S-2020 graphite at 250 to 1000 °C in a continuous flow of helium and iodine over a compact. The helium was at atmospheric pressure and the partial pressures of iodine were selected from the range of 10^{-6} to 10^{-1} Pa. The desired partial pressure of iodine was governed by a refrigerator tube and checked by use of charcoal cartridges in a bypass system.

Equilibrium adsorption data for the H-451 experiments were generally well behaved and reproducible. The results obtained are shown in Fig. A-15. The lines shown for each temperature (and the band for 1000 °C) converge toward a single point and are intended to be guides for data evaluation. The consistency is good considering the large range of iodine pressures and loadings. The greatest scatter occurs at 250 and 1000 °C; poor counting statistics for the low iodine loadings at 1000 °C may have caused most of the scatter.

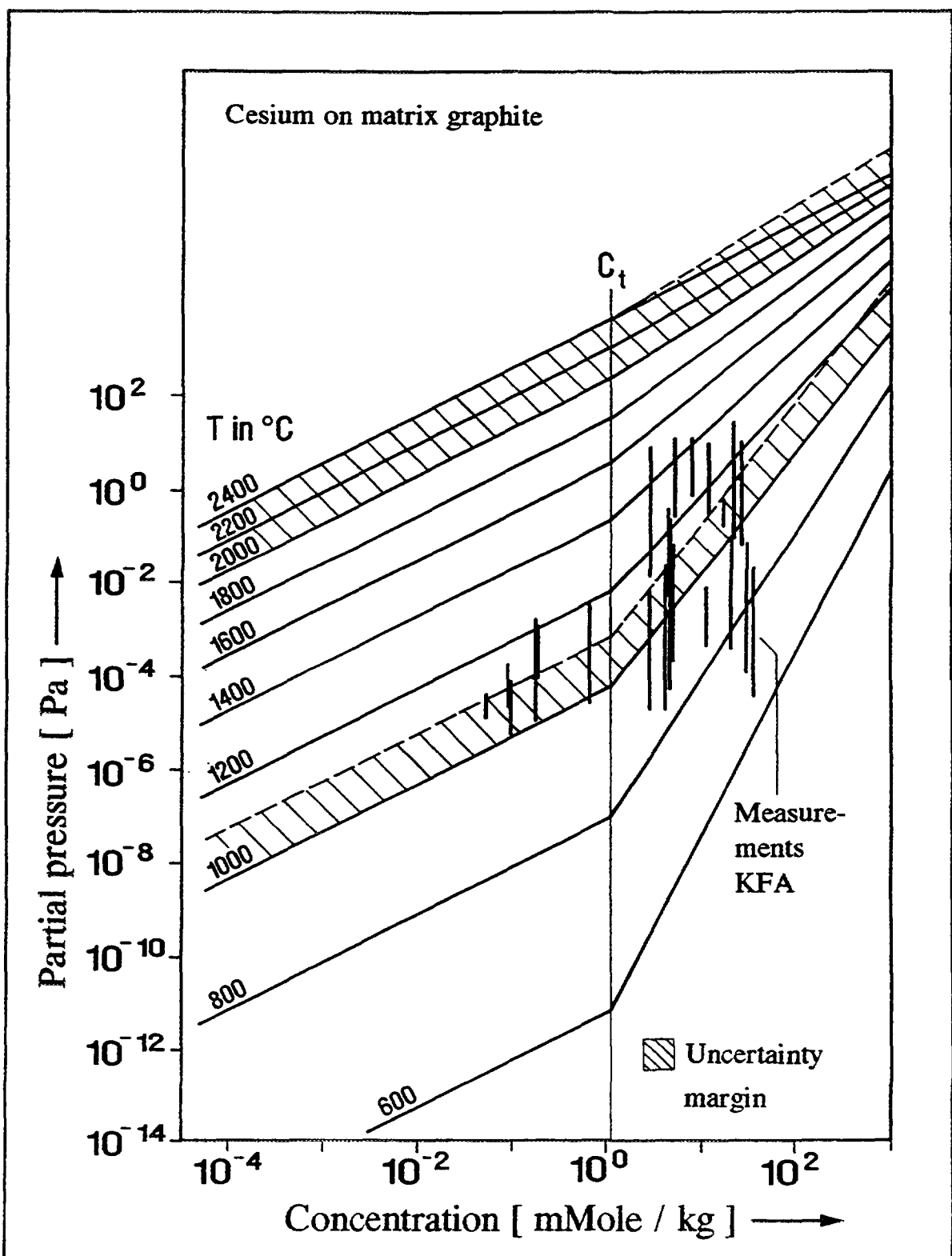


Fig. A-10: Sorption isotherms (reference data) of cesium on A3-3 matrix graphite

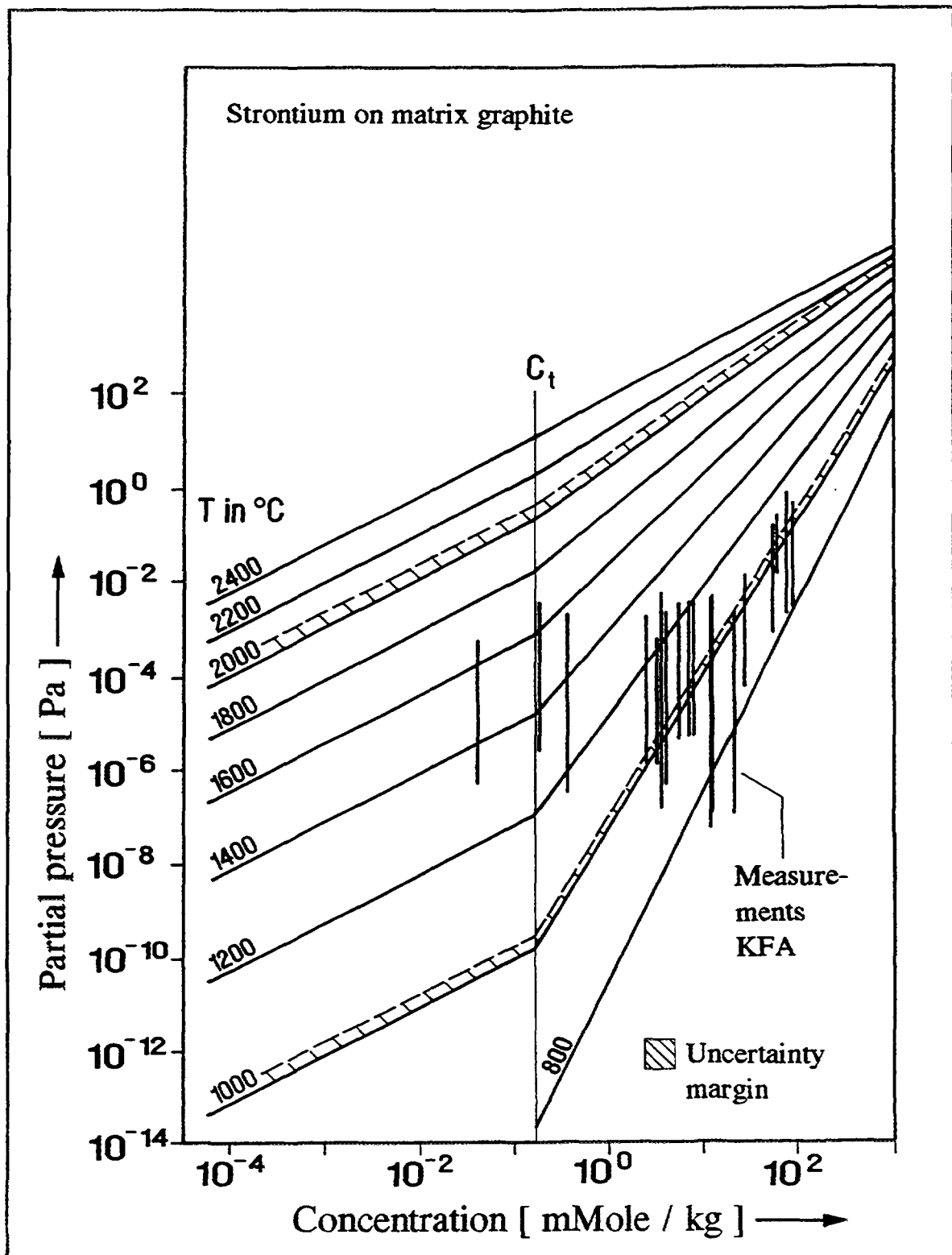


Fig. A-11: Sorption isotherms (reference data) of strontium on A3-3 matrix graphite

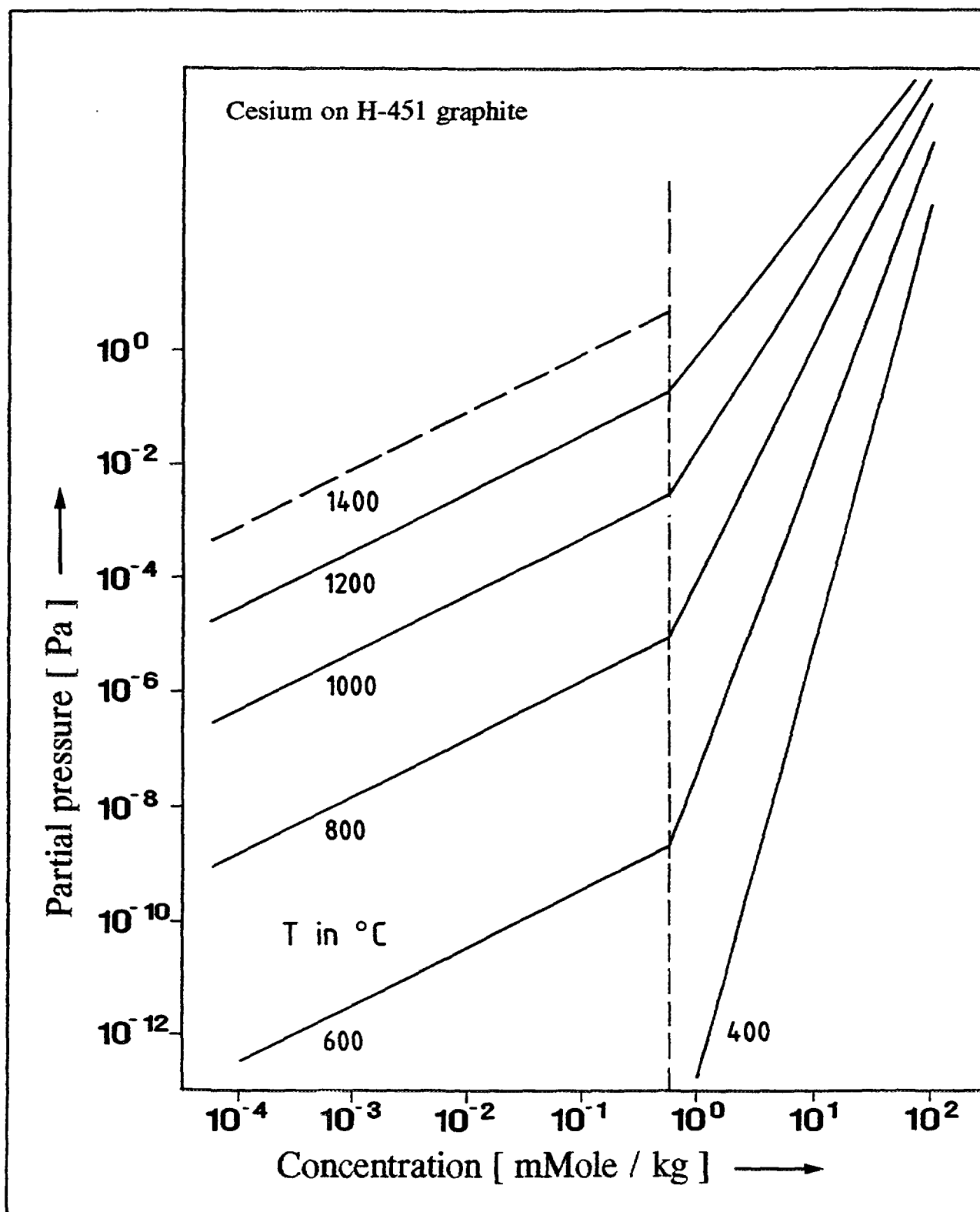


Fig. A-12: Sorption isotherms (reference data) of cesium on H-451 structural graphite

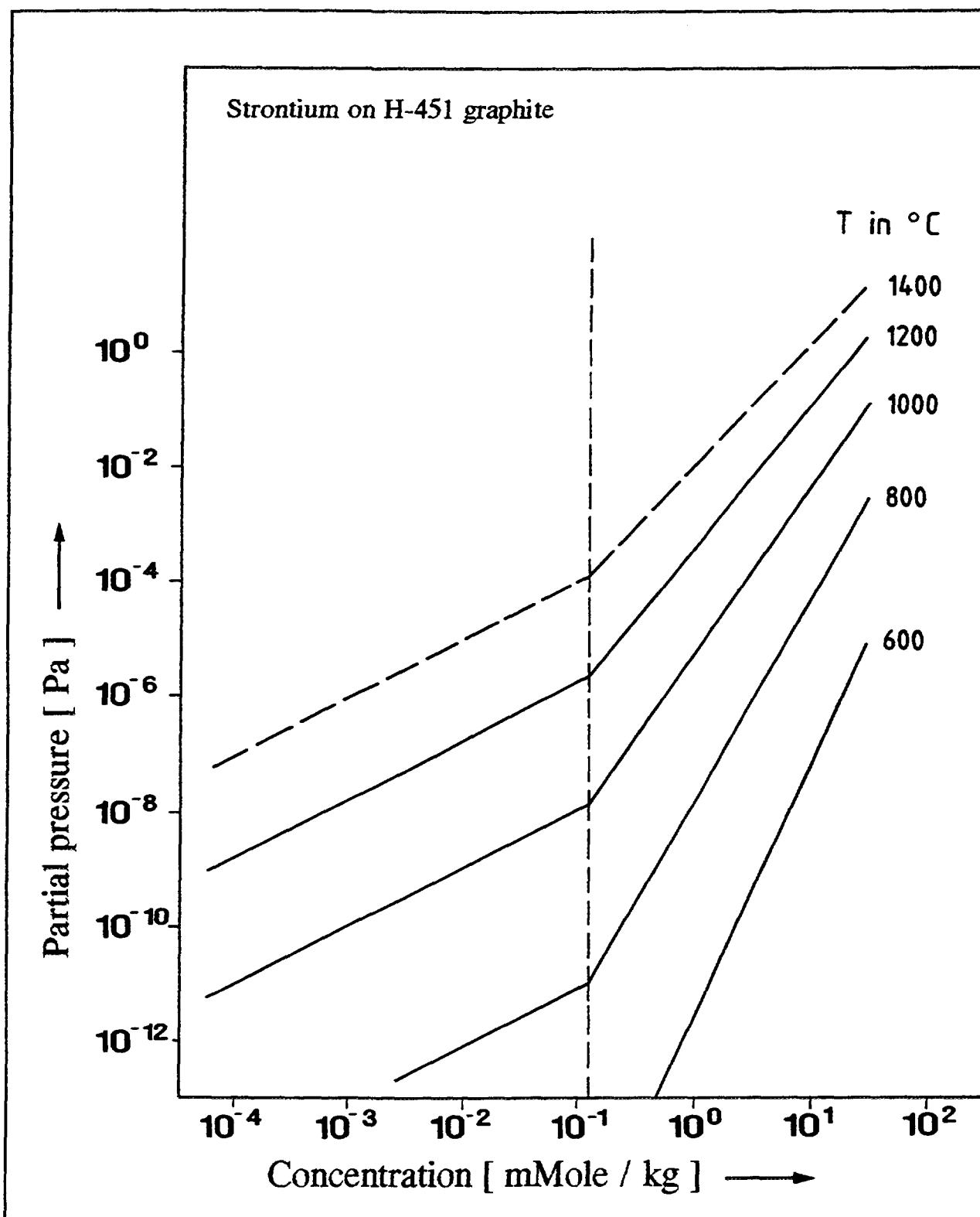


Fig. A-13: Sorption isotherms (reference data) of strontium on H-451 structural graphite

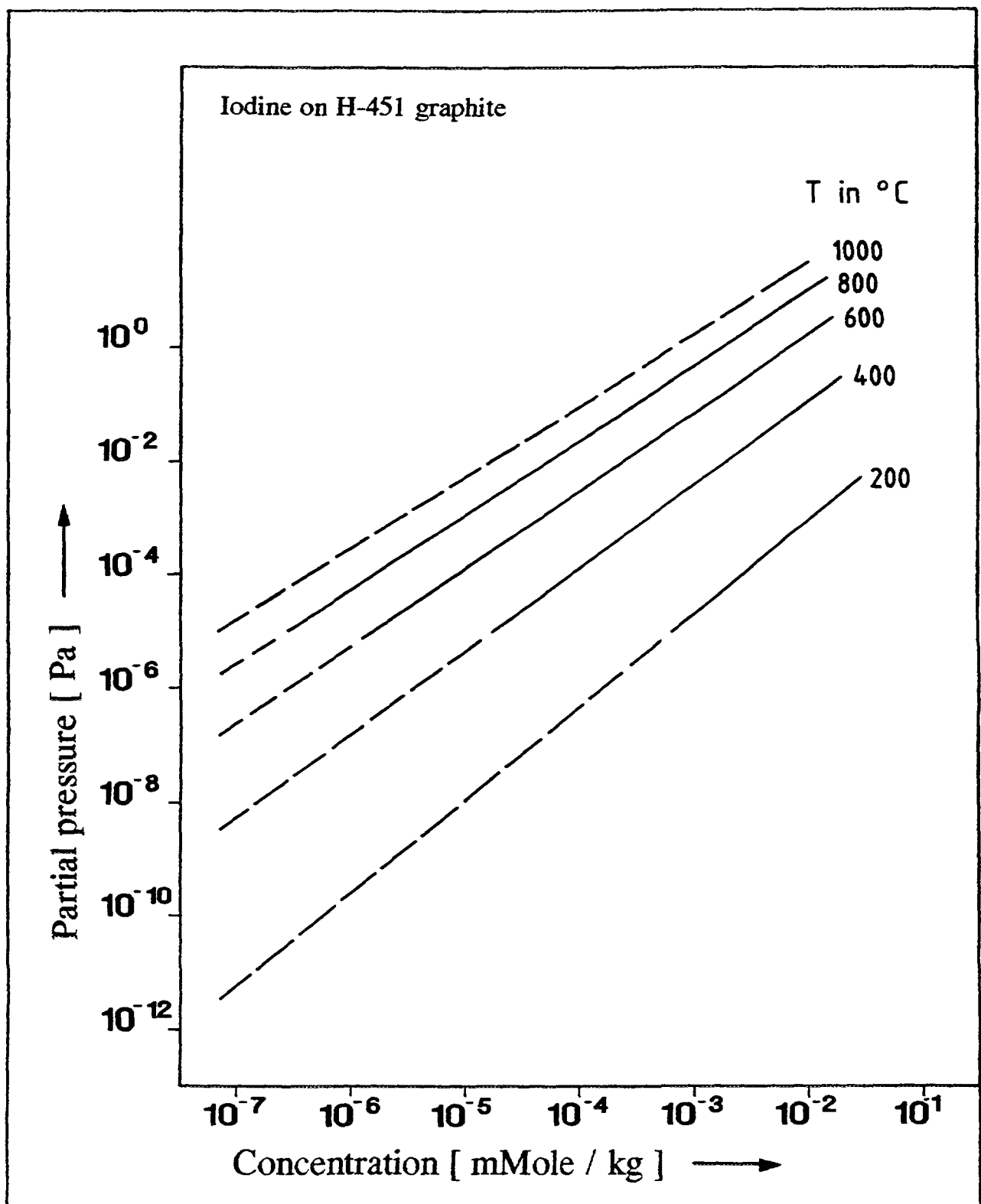


Fig. A-14: Sorption isotherms (reference data) of iodine on H-451 structural graphite

Table A-6: Sorption isotherm parameters for metallic fission products on graphitic materials used in the equations (A-8)

	Graphitic material	A	B [K]	D	E [K]	d ₁	d ₂ [K ⁻¹]	Ref.
FRG								
Cs	A3-3 Matrix	25.14	-44930	-3.118	6707	0.122	0.	[59]
Cs	A3-3 Matrix	21.95	-41853	-2.354	5013	0.122	0.	[60]
Cs	A3-3 Matrix	24.79	-44543	-0.369	3683	0.122	0.	[57]
Sr	A3-3 Matrix	10.5	-6222	-1.591	6163	-1.897	0.	[58]
Sr	A3-3 Matrix	22.80	-50617	-0.913	5214	-1.897	0.	[57]
I	H-451	14.33	-6515	1.041	284	-	-	[61]
USA								
Cs	H-451	24.00	-35730	-1.561	6123	-2.035	1.79*10 ⁻³	[11]
Sr	H-451	19.38	-40090	-0.324	4088	-2.12	0	[12]
I	H-451	14.33	-6515	1.041	284	-	-	[61]
Cs	FCMM ⁽¹⁾	19.33	-47290	1.518	4338	3.397	6.15*10 ⁻⁴	[11]
Sr	FCMM ⁽¹⁾	54.3	-149000	-8.52	28500	3.13	0.	[56]

(1) FCMM = Fuel Compact Matrix Material

Comparison of the data in Fig. A-15 with those found in an independent experimental program at GA, Fig. A-14, reveal that the loading is, for example, lower by a factor of 2 in the Fig. A-15 data at 800 °C and at iodine partial pressures of 10⁻⁶ and 10⁻⁴ Pa.

Note: This contribution is necessarily brief. The data yielded iodine isotherms differing by only a factor of 2 from previously derived isotherms. Further, the S-2020 graphite is not of general interest and the studies of adsorption rates and desorption were not particularly informative. The study was well conducted and is important in confirming the data on iodine adsorption on H-451 graphite.

Values of the constants A, B, D, E for the sorption isotherms and d₁, d₂ for the transition concentration are given in Table A-6. The sorption isotherms of cesium and strontium over matrix graphite, and of cesium, strontium, and iodine over US structural graphite H-451 are plotted in Figs. A-10 through A-14.

A.2.2. The FRESCO Approach of Sorption Modeling

The data in Table A-7 indicate the method by which sorption isotherms are represented in the **FRESCO model** both for fuel element matrix graphite and for reflector graphite [52]. Based on the ideal gas law, the partition coefficient of fission products between graphite and coolant is expressed by the ratio of concentrations in the coolant (c_{gas}) and in the graphitic surface layer (c_{graphite}) or:

$$c_{\text{gas}} = \alpha c_{\text{graphite}} \quad (\text{A-9})$$

α is dimensionless; c_{gas} and c_{graphite} have both the same dimensions for instance "Atoms/m³". For the linear and non-linear range of the sorption isotherm is:

$$\begin{aligned} \alpha_{\text{Henry}} &= \frac{1}{T} \exp \left\{ A_H + \frac{B_H}{T} \right\} \\ \alpha_{\text{Freundlich}} &= \frac{1}{T} \exp \left\{ A_F + \frac{B_F}{T} + \left(D_F + \frac{E_F}{T} \right) \ln c_{\text{graphite}} \right\} \end{aligned} \quad (\text{A-10})$$

where

- A_H, B_H are the coefficients for the linear range of sorption isotherm (Henry)
- A_F, B_F, D_F, E_F are the coefficients for the non-linear range of sorption isotherm (Freundlich)
- c_{graphite} is the concentration of sorbate species
(The transformation factor of c_{graphite}-dimension [Atoms/m³] of equation (A-9) into the c_{gr}-dimension [mmol/kg C] of equation (A-10) is hidden in the above coefficients.)

The modeling of an unresisting transition between gaseous and solid phase is given by equating the partition coefficients with 1.

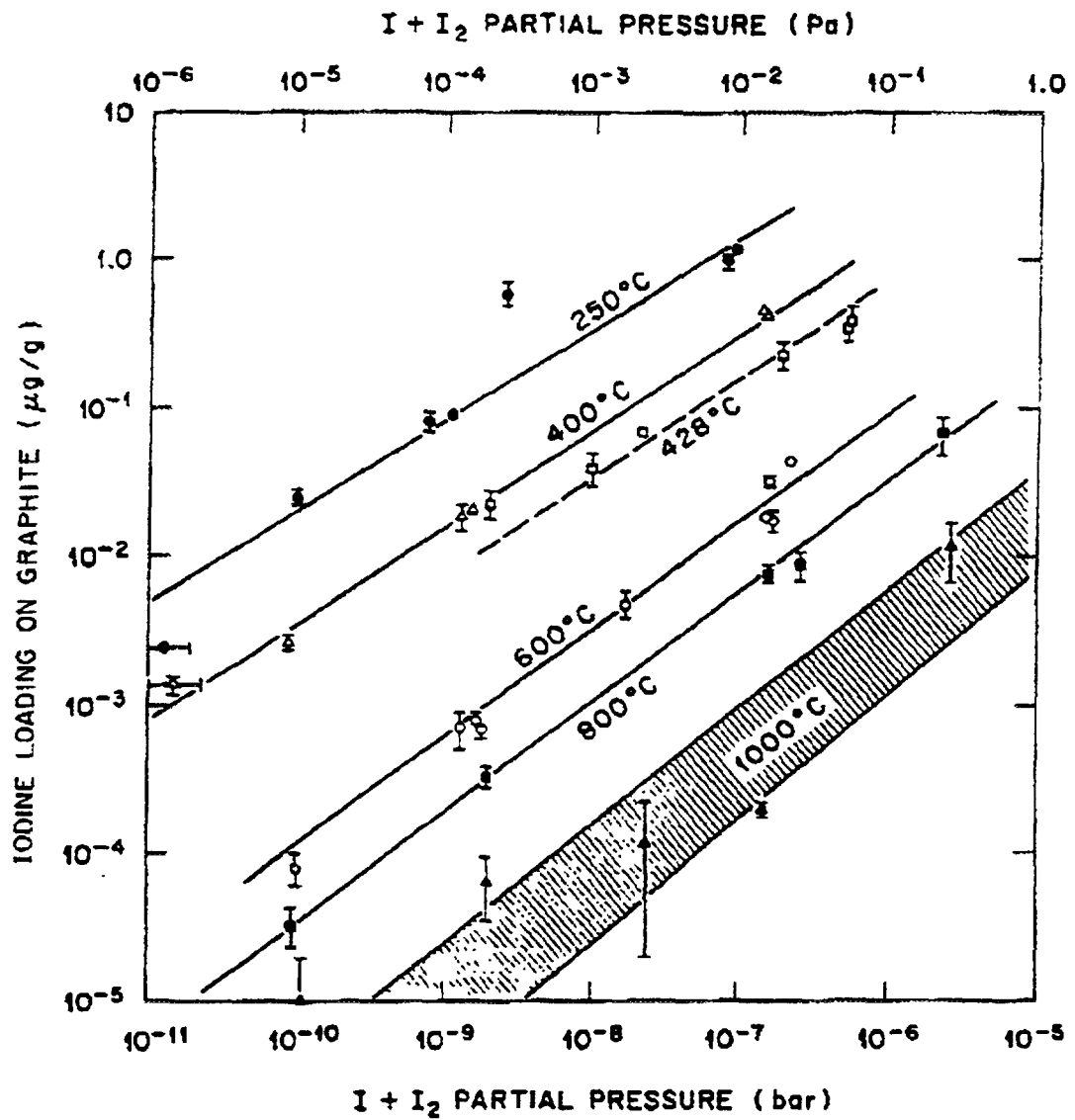


Fig. A-15: Sorption isotherms for iodine on H-451 graphite

The transformation of the constants A , B , D , E , as given in the equations (A-8) into the constants A_H , B_H , A_F , B_F , D_F , E_F , as given in the equations (A-10), is defined by the following equations:⁵

For the Henry sorption isotherms:

$$\begin{aligned} A_H &= A - \ln\left(\frac{\rho}{10^3} R\right) + (D - 1) \ln c_t \\ B_H &= B + E \ln c_t \end{aligned} \quad (\text{A-11})$$

⁵ Please note: these transformation equations are strongly dependent on the above given units for concentrations (here: mmol/kg) and pressures (here: Pa).

Table A-7: FRESCO sorption isotherm parameters for metallic fission products on graphite according to the Equations (A-10)

	A3-3 matrix graphite			H-451 structural graphite
Cesium	Reference	< 1350 °C ⁽¹⁾	≥ 1350 °C ⁽¹⁾	
A _H	21.94	24.24	25.60	22.85
B _H	-44093.	-44093.	-46297.	-39359.
A _F	22.11	24.41	25.78	21.32
B _F	-44543.	-44543.	-46769.	-35700.
D _F	-1.3689	-1.3689	-1.4824	-2.56
E _F	3683.	3683.	3867.	6120.
c _t	1.13	1.13	1.13	0.55
[mmol/kg C]				
Strontium	Reference	< 1700 °C ⁽¹⁾	≥ 1700 °C ⁽¹⁾	
A _H	23.75	24.44	25.97	19.50
B _H	-60509.	-60509.	-63537.	-48772.
A _F	20.12	20.81	22.09	16.70
B _F	-50617.	-50617.	-53150.	-40100.
D _F	-1.913	-1.913	-2.045	-1.32
E _F	5214.	52.14	5475.	4090.
c _t	0.15	0.15	0.15	0.12
[mmol/kg C]				
Iodine				
A _F	11.66			
B _F	-6516.			
D _F	0.041			
E _F	284.			

(1) Reference value + uncertainty margins to be used in safety analyses

For the Freundlich sorption isotherms:

$$\begin{aligned}
 A_F &= A - \ln\left(\frac{\rho}{10^3} R\right) \\
 B_F &= B \\
 D_F &= D - 1 \\
 E_F &= E
 \end{aligned} \tag{A-12}$$

where

ρ is the graphite density, $\rho = 1750$ [kg/m³] for A3 matrix

R is the gas constant, $R = 8.3143$ [J/(mol K)]

Table A-7 presents three data sets for cesium and strontium on A3-3 matrix graphite recommending uncertainty margins of the reference values for use in safety analysis calculations. They have been defined in [4] by factors of 2 (strontium) and 10 (cesium) on the partial pressure in the temperature range covered by the experiments and an additional 5 % on the sorption energies at higher temperatures.

A.3. INPUT DATA FOR PARTICLE FAILURE MODELS UNDER ACCIDENT CONDITIONS

A.3.1. The FRG Particle Failure Model

The **FRG particle failure model PANAMA** consists of two failure mechanisms for TRISO particles under accident conditions. The coupling of these failure mechanisms, eventually extended by the manufacture-induced defect fraction ϕ_0 , is then given by:

$$\Phi_{total} = 1 - (1 - \Phi_0) - (1 - \Phi_1) - (1 - \Phi_2) \quad (A-13)$$

In the pressure vessel model dominant in the lower temperature range, the failure of a particle occurs as soon as the stress imposed upon the SiC layer by the internal gas pressure exceeds the tensile strength. The fraction of particles that fail due to pressure vessel at time t after the initiation of an accident at a temperature T is given by [62]:

$$\Phi_1(t, T) = 1 - \exp \left\{ -\ln 2 \left(\frac{\sigma_t}{\sigma_o} \right)^m \right\} \quad (A-14)$$

where

σ_t is the stress induced in the SiC layer due to the internal gas pressure [Pa]

σ_o is the SiC tensile strength at the end of irradiation [Pa]

m is the Weibull modulus

The strength values for SiC are scattered in accordance with a Weibull distribution where m specifies the Weibull parameter.

The stress σ_t is determined based on the assumption of the SiC as a thin shell pressure vessel. Its thickness is further reduced by fission product corrosive attack on the silicon carbide. A "thinning rate" as function of temperature can be given by Montgomery employing experimental data on SiC corrosion rates [63]:

$$k_c(T) = \frac{1}{d_0} 5.87 * 10^{-7} \exp \{-Q_c / (R T)\} \quad (A-15)$$

where

- k_c is the frequency factor for SiC corrosion [s^{-1}]
- d_o is the initial SiC layer thickness [m]
- Q_c is the activation energy of SiC corrosion [J/mol]
 $Q_c = 179500$
- R is the gas constant, $R = 8.3143$ [J/(mol K)]
- T is the temperature [K]

The ideal gas law is taken to calculate the internal gas pressure depending on the geometry of kernel and void volume, the yield of stable fission gases, the gas release from the kernel (Booth formula), the heavy metal burnup, and the produced number of oxygen atoms per fission resulting in CO formation. The latter is strongly dependent on the particle type: it is highest for UO_2 [64], comparably low for $(\text{Th},\text{U})\text{O}_2$ [65] and zero for UCO [66].

The Weibull modulus as well as the layer strength are considered as silicon carbide material properties and have been measured for various unirradiated particle batches [67]. These values, however, are not available for the SiC used in the German reference particle batch EUO 2308. For safety analyses of German HTGR designs, corresponding data of the particle batch EO 1607 have been taken representing some sort of medium data (see Table A-8).

Further strength measurements of the batch EO 1607 after irradiation in the test HFR-GM1 (irradiation temperature $T_B = 1165$ °C, neutron dose $\Gamma = 3.7 * 10^{25} \text{ m}^{-2}$, $E > 16 \text{ fJ}$) have revealed a fast neutron fluence induced decrease of the medium SiC strength and a broadening of its Weibull distribution [62], i.e. a lower value for m leading to a higher failure probability of the pressure vessel. The functional dependence $m = m(\Gamma, T_B)$ and $\sigma_o = \sigma_o(\Gamma, T_B)$ deduced from this single irradiation experiment is used in the PANAMA-I code as a general rule. It thus may introduce an uncertainty into the calculation and may be a reason for the conservative results for failure fractions of particles irradiated to very high fast neutron fluences [28].

The thermal decomposition dominant at very high temperatures beyond 2000 °C is represented by a parametrization which always remains ≤ 1 :

$$\Phi_2(t, T) = 1 - \exp \left\{ -\alpha \zeta^\beta \right\} \quad (\text{A-16})$$

where

- ζ is the so-called "action integral"

$$\zeta = \int k_D(T) dt$$
- α, β are empirical constants

The action integral ζ comprises the entire temperature-time history experienced by the particles. The parameters α and β are different for loose particles or for particles in a fuel sphere and have been derived from temperature ramp tests up to 2500 °C of DR-S6

particles [68] and of AVR-GO2 spherical fuel elements [27], respectively. Values are given in Table A-8.

Thermal decomposition causes a measurable weight loss of the SiC layer which is again interpreted as a "thinning rate":

$$k_d(T) = \frac{1}{d_0} 3.75 * 10^2 \exp\{-Q_d / (R T)\} \quad (\text{A-17})$$

exhibiting a significantly higher activation energy for the thermal decomposition process.

where

k_d is the frequency factor for SiC thermal decomposition [s^{-1}]

Q_d is the activation energy of SiC thermal decomposition [J/mol]

$$Q_d = 556000$$

Predicted values for particle failure fractions under accident conditions of small modular HTGRs are expected to be very low even if an uncertainty factor as proposed in [4]⁶ is taken into account.

A.3.2. The Japanese Particle Failure Model

The Japanese particle failure model uses an approach similar to PANAMA-I also based upon a thin-shell pressure vessel model. In the model prediction, the coating is considered to fail when the stress σ due to the internal pressure exceeds the SiC strength σ_f at a given instant. The stress is related to the pressure by a thin-shell model:

$$\sigma = P \frac{r}{2d} \quad (\text{A-18})$$

where

P is the internal gas pressure [Pa]

r is the radius of the SiC shell [m]

d is the thickness of the SiC shell [m]

The SiC strength is assumed to follow Weibull statistics where the failure fraction is described by [69]:

$$\Phi = 1 - \exp\left\{-\left(\frac{\sigma}{\sigma_o}\right)^m\right\} \quad (\text{A-19})$$

where

⁶ To account for the uncertainty of PANAMA-I model calculations, the results for accident temperatures ≤ 1600 °C were recommended in [4] to be multiplied by a factor of 20. With increasing temperatures the uncertainty range should then decrease to zero (i.e. a factor of 1 on the results) when reaching 1800 °C.

- σ is the stress induced in the SiC layer due to the internal gas pressure [Pa]
- σ_0 is the characteristic SiC strength [Pa]
- m is the Weibull modulus

with the SiC strength obeying Weibull statistics. The strength σ_0 is a function of the SiC porosity P which is introduced by thermal dissociation:

$$\sigma_0 = \sigma_{\infty} e^{-n P} \quad [\text{Pa}] \quad (\text{A-20})$$

and

$$P^4 = A t \exp \{-Q / (R T)\} \quad (\text{A-21})$$

where

- σ_{∞} is a constant [Pa]
- n is a constant
- A is a constant [s^{-1}]
- t is the time [s]
- Q is the activation energy [kJ/mol]

Data are given in Table A-8.

The statistics of the fabrication parameters are also taken into account. The fabrication parameters, except the coating strength, are assumed to follow a normal distribution. The extent of the reduction of UO_2 by carbon coating should be a function of the burnup. The oxygen potential and phase boundaries of UO_{2+x} are described by the model proposed by Lindemer and Besmann [70]. The equations of state for CO and the noble gases are expressed by the Virial equations.

Good agreement has been found between model predictions and postirradiation heating test experimental results.

A.3.3. The US Particle Failure Model

In the US, the **Integrated Failure and Release Model for Standard Particles** is used as reference model [71]. Its empirical approach comprises a SiC corrosion and a SiC thermal decomposition process which are, together with the SiC layer thickness, variables with statistical Weibull distributions. The basic equation reads as follows:

$$\Phi(t, T) = 1 - \exp \{-\ln 2 \zeta^m\} \quad (\text{A-22})$$

ζ is the so-called "action" integral

$$\zeta = \int k(T) dt \quad (\text{A-23})$$

in which k presents the frequency factor for failure [s^{-1}]:

Table A-8: Input data for national particle failure models

FRG		
SiC layer strength (EO 1607, unirradiated)	834	MPa
Weibull modulus (EO 1607, unirradiated)	8.02	
Activation energies		
corrosion Q_c :	179.5	kJ/mol
thermal decomposition Q_d :	556	kJ/mol
Constants		
loose particles: α :	0.693	
loose particles: β :	0.88	
particles in fuel sphere: α :	0.0001	
particles in fuel sphere: β :	4	
USA		
SiC layer strength (after irradiation)	480	MPa
Weibull modulus (after irradiation)	5	
<i>US/FRG Statistical model, version 1985:</i>		
Activation energies		
corrosion Q_c :	252	kJ/mol
thermal decomposition Q_d :	545	kJ/mol
Constants		
A for oxidic fuel:	36.53	
A for carbidic fuel:	36.70	
Weibull modulus		
corrosion m_c :	3.3	for single experiments
	1.6	for core predictions
thermal decomposition m_d :	2.2	for single experiments
	1.5	for core predictions
<i>US/FRG Statistical model, version 1988:</i>		
Activation energy Q	545	kJ/mol
Weibull modulus m		
for individual tests:	2.0	
for core performance:	1.7	
Japan		
SiC layer strength (unirradiated)	1650	MPa
Weibull modulus (unirradiated)	5.6	
Activation energy Q	912	kJ/mol
Constants		
A:	5×10^9	s^{-1}
n:	12.5	

$$k = k_{o,i} \exp \{-Q_i/(RT)\} \quad (\text{A-24})$$

Index i = c: SiC corrosion
 = d: SiC thermal decomposition

R is the gas constant, R = 8.3143 [J/(mol K)]

T is the heating temperature [K]

Q_i is the activation energy

The exponent m in equation (A-21) is the Weibull modulus.

The pre-exponential constants k_{o,i} [s⁻¹] are given by empirical correlations:

1. SiC corrosion

$$\log k_{o,c} = -A + 3 \log T_i + \log f_{SiC} \quad (\text{A-25})$$

where

A is a constant

T_i is the irradiation temperature [K]

f_{SiC} is the fission density (fissions per unit volume inside SiC) [m³]

2. SiC thermal decomposition

$$\log k_{o,d} = -1.58 + 2.67 \log T_i + 0.61 \log \Gamma \quad (\text{A-26})$$

where Γ is the fast neutron fluence [$10^{25}/\text{m}^2$, E>29 fJ].

The two failure mechanisms are combined to a total failure fraction according to equation (A-13). Data for A, Q_i, and m_i are listed in Table A-8.

The difference in the activation energies for SiC corrosion Q_c between equations (A-15) and (A-23) is due to the fact that the 179.5 kJ/mol value is based upon all available data including the accelerated irradiation test data [63]. The 252 kJ/mol is a revised number that comes from dropping the accelerated irradiation data which were supposed to be not representative for HTGR heating conditions [72].

A revised version of this model from 1988 based on an extended set of heating test data [73] is considered to replace the original version as reference model [29]. A more recent analysis of the activation energy by Goodin has found the observed temperature dependence of FRG heating tests to be essentially equal to the activation energy of SiC thermal decomposition. This observation was interpreted such that the thermal decomposition process was the only significant failure mechanism. The fitted expression for the frequency factor to be used in equation (A-21) and (A-22), respectively, is:

$$k = 5.029 * 10^{-4} e^{-65540/T} FSIC^{2.09} FLU^{0.041} T_i^{4.14} \quad (A-27)$$

where

$$FSIC = f_{SiC} / 10^{26}$$

$$FLU = \Gamma / 10^{25}$$

Γ is the fast neutron fluence [$10^{25}/m^2$, $E > 16$ fJ]

revealing a very strong dependence on the irradiation temperature and, on the other hand, a completely negligible dependence on the neutron fluence.

A pressure vessel failure is considered insignificant compared to the above degradation processes. However, data for a mean SiC strength of US particles and its Weibull distribution have been recommended to be used in model calculations [29] (see Table A-8).

A.4. PARAMETERS IN THE MODELS FOR STEADY STATE FISSION GAS RELEASE

The following tables list values of parameters which appear in the model equations to calculate the release of fission gases from fuel particles with exposed kernels (see section 3.3.1.).

A.4.1. Parameters for HRB Fission Gas Release Model

Table A-9 contains the data to be used in the HRB model [74].

Table A-9: Values of the parameters in the HRB model for steady state fission gas release from defective TRISO particles with UO₂ kernels

Parameter	Krypton	Xenon
Recoil fraction from 500 μm UO ₂ kernel [%]	2.9	2.3
Porosity [%] kernel buffer layer	2.5 50.	
Frequency factor of reduced diffusion coefficient D _o [s ⁻¹] kernel buffer grain buffer pore	2.5*10 ⁻² 6.0*10 ⁻³ 2.0	3.6*10 ⁴ 4.9*10 ⁻⁷ 9.8*10 ⁻³
Activation energy [kJ/mol] kernel buffer grain buffer pore	314.0 106.3 54.4	460.6 33.5 33.5
Fraction of buffer pores [%] ≤ 2.9 %FIMA ≥ 3.2 %FIMA ⁽¹⁾		10 5

(1) The further reduction of the buffer fraction beyond 6 %FIMA is conservatively neglected, reduction of D_o (buffer pore) if necessary.

A.4.2. Parameters for US Fission Gas Release Model

Table A-10 contains the data to be used in the US model.

Table A-10: Values of the parameters in the US model for steady state fission gas release from fuel particles with exposed kernels

Parameters	UC _x O _y & UO ₂ kernels		ThO ₂ kernels		UC ₂ kernels	
	Krypton	Xenon	Krypton	Xenon	Krypton	Xenon
D' [s ⁻¹]	1.31*10 ⁻¹⁰	1.35*10 ⁻¹¹	8.17*10 ⁻¹²	8.44*10 ⁻¹³	1.23*10 ⁻¹⁰	1.26*10 ⁻¹¹
A	0.073	0.21	0.073	0.21	0.073	0.21
Q [kJ/mol]	53.1	45.2	53.1	45.2	53.1	45.2
exp{Q/(RT ₀)}	105.	52.4	105.	52.4	105.	52.4
σ [FIMA ⁻ⁿ]	0.739	0.739	1.43	1.43	0.	0.
m	0.33	0.33	0.9	0.9	0.	0.
α [K ⁻¹]	1.28*10 ⁻²	1.28*10 ⁻²	1.86*10 ⁻²	1.86*10 ⁻²	1.33*10 ⁻²	1.33*10 ⁻²
T _s [K]	1950.	1950.	1790.	1790.	1700.	1700.

A.4.3. Parameters for CEGB Fission Gas Release Model

Table A-11 contains the data to be used in the CEGB model [75, 76].

Table A-11: Values of the parameters in the CEGB model for steady state fission gas release from UO_2

Parameter	Value	Reference
$A [\text{m}^5]$	$2*10^{-40}$	[75]
$B [\text{m}^2(\text{m/s})^{0.5}]$	$1.41*10^{-25}$	[76]
$Q_v [\text{kJ/mol}]$	115.	[76]
$D_o [\text{m}^2/\text{s}]$	$7.6*10^{-10}$	[75]
$Q_I [\text{kJ/mol}]$	293.	[75]
$R [\text{J}/(\text{mol K})]$	8.314	

In addition, values of λ , F , T , and S/V of equations (3-9) and (3-10) appropriate for the application of equation (3-10) to a particular event, must be specified.

A.4.4. Parameters for JAERI Fission Gas Release Model

Table A-12 contains the data to be used in the JAERI model.

Table A-12: Constant K_i of noble gas and iodine

Nuclide	K_i	Nuclide	K_i
Kr-85m	1.54	Xe-133	1.31
Kr-87	1.61	Xe-135m	6.09
Kr-89	2.04	Xe-135	2.60
I-131	1.44	Xe-137	1.18
		Xe-138	1.17

A.5. MATERIAL PROPERTY DATA IN PLATEOUT CALCULATIONS

The key material property correlations used in calculating the deposition of condensable fission products in the primary circuit are convective mass transfer correlations and the sorption isotherms; these isotherms predict the equilibrium surface loading as a function of partial pressure and surface temperature. The data indicate that the structural materials in the primary circuit are essentially "perfect sinks" (zero desorption pressure) for all condensable radionuclides except for iodine, cesium, and, at the higher surface temperatures, silver and antimony. The iodine and cesium isotopes deposit preferentially in the colder locations in the primary circuit, especially the evaporator-economizer sections of the steam generator of a steam-cycle plant. For those plateout codes which model in-diffusion in the wall materials the solid-state diffusion coefficients are also important.

A.5.1. FRG Contribution

The modeling approach of the (non-activated) adsorption process does not need any material-related property data except for the molecular weight of the adsorbate and the adhesion coefficient which is here assumed to be 1. Activated adsorption would require an activation energy. Some plateout experiments reveal the tendency towards an activated adsorption, quantitative results, however, are currently not yet available.

The non-activated desorption process is mainly determined by the product of desorption constant and coverage: $\vartheta * \sigma$. The desorption constant

$$\vartheta = \vartheta_o \exp \{-Q_o/(RT)\} \exp \{-(Q_o - Q_s)\sigma/(RT)\} \quad (\text{A-28})$$

is dependent on the desorption energy Q_o , the sublimation energy Q_s , and the coverage σ . However, the dependencies on Q_s and σ are relevant only for large coverages and therefore are often neglected. The variable ϑ_o can be interpreted as an oscillation frequency of the adsorption binding. The coverage varies inversely proportional to the roughness coefficient (assumed in safety analyses to be 10 or 100 [4]).

Table A-13 contains the data necessary for the calculation of ad-/desorption processes. Cesium data were derived from the LAMINAR loop tests and iodine data were derived from the SAPHIR/PEGASE tests. All data refer to the steel Incoloy 800 unless otherwise indicated.

In the PATRAS code (see section 6.1.1.1.), the desorption coefficient is calculated by the equation

$$\vartheta = \vartheta' T \exp \{-Q_o/(RT)\} \quad (\text{A-29})$$

By comparison of the equations (A-28) (with the last expression neglected) and (A-29), it follows:

$$\vartheta'_o = \vartheta_o / T \quad (\text{A-30})$$

The temperature dependent desorption constants are depicted in Fig. A-16.

The calculation of the volume diffusion process can be made in a simple way by applying the penetration model in which a certain function of the fission product atoms that

Table A-13: Frequency factors, activation energies and penetration coefficients for the ad-/desorption processes

Element	Steel	$\langle \vartheta_{in} \rangle_0 [s^{-1}]$	$Q_0 [\text{kJ/mole}]$	$1 - \beta$
Cs, Rb	Incoloy 800	10^{11}	235	$1 \cdot 10^{-5}$
	Inconel 617	10^{11}	250	$1 \cdot 10^{-6}$
Sr, Ba	Incoloy 800	10^{11}	235	$1 \cdot 10^{-6}$
	Inconel 617	10^{11}	250	$1 \cdot 10^{-7}$
Ag	Incoloy 800	10^{11}	200	$1 \cdot 10^{-5}$
	Inconel 617	10^{11}	215	$1 \cdot 10^{-6}$
I	Incoloy 800	$10^{11} (10^{10}, 10^{12})^{(1)}$	180	0
	Inconel 617	$10^{11} (10^{10}, 10^{12})^{(1)}$	180	0

(1) Variation of ϑ_0 in the given limits due to data uncertainties

Table A-14: Frequency factors and activation energies for the transport data in oxide and metal (Incoloy 800)

Element	Oxide		Metal	
	$D_0 [\text{m}^2/\text{s}]$	$Q [\text{kJ/mole}]$	$D_0 [\text{m}^2/\text{s}]$	$Q [\text{kJ/mole}]$
Cs, Rb	$1 \cdot 10^{-13}$	42	$3 \cdot 10^{-9}$	63
Sr, Ba	$1 \cdot 10^{-14}$	42	$3 \cdot 10^{-10}$	63
Ag	$1 \cdot 10^{-13}$	42	$3 \cdot 10^{-9}$	63
I	0	0	0	0

hit the metal surface is expected to immediately penetrate the metal volume. This fraction which can also be interpreted as a penetration probability of an atom hitting the surface, is called penetration coefficient $1 - \beta$. Some data, part of them derived from experiments are listed in Table A-13. No statement can be given about the dependence of the penetration coefficient on the temperature (which one would expect).

A detailed analysis of the volume diffusion requires data on diffusivities and on the solubility of the fission products in the metallic/oxidic phase. In the PATRAS code, there is a distinction between a grain boundary diffusion and a dissolution in the grain. All other models, including PLAIN simply assume an “effective” diffusion and an “effective” solubility.

Diffusion data available from the literature scatter over a wide range. For solubilities, in principle only coarse tendencies can be given. From those of interest here, only the Ag-

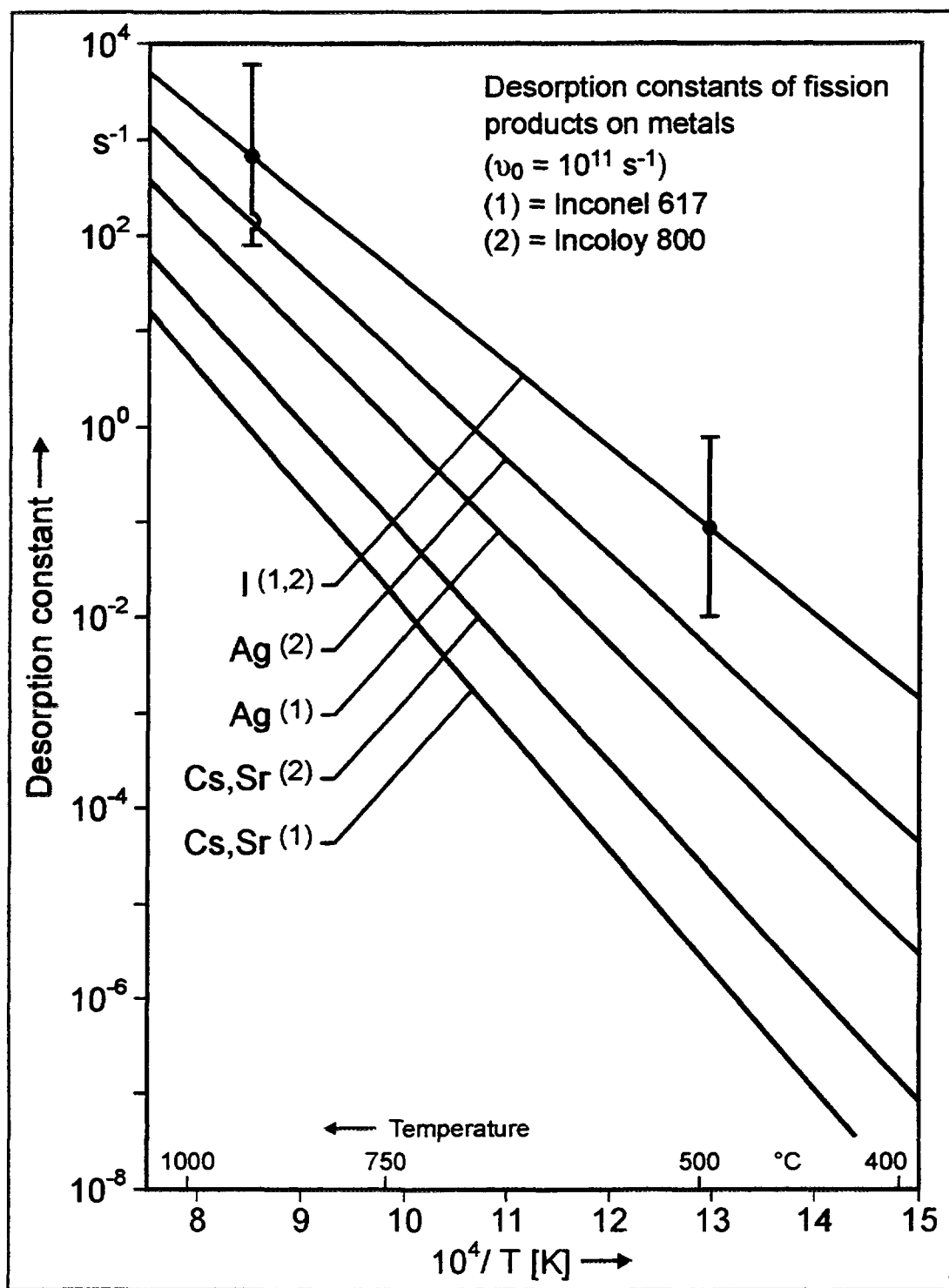


Fig. A-16: Desorption constants of important radionuclides on metals

Ni phase diagram is well known. The diffusivities in oxide and in metal recommended for use in safety analyses are listed in Table A-14.

The solubility (saturation concentration) for metallic fission products is recommended in oxide layers to have a mole ratio of $x_M = 10^{-3}$, and in the metal to have a mole ratio of $x_M = 10^{-4}$. For the transition adsorption/solution at the surface, it is assumed that in a monolayer in the oxide (geometrical surface), the fission product concentration x_L is formed according to the equation

$$x_L = x_M \sigma \quad (\text{A-31})$$

To take into account the uncertainty ranges for the transport data, for the solubilities, and for the influence of the surface roughness on the diffusion process, additional calculations should be carried out in a safety analysis by applying the x_L value varied by factors of 0.1 and 10, respectively. In such calculations, the assumption for the oxide layer thickness should be 5 μm , plus, for low alloy steels, 1 μm and 0 μm .

A.5.2. US Contribution

A.5.2.1. Mass Transfer Coefficients

The reference US correlations for predicting convective mass transfer coefficients for forced convection and free convection are cataloged in the PADLOC code [77]. In general, the Sherwood number is given as functions of the Reynolds, Schmidt, and Grashof numbers. The general forms of these relations are given below:

a. forced convection

$$h = \frac{D}{\chi} \left[\alpha_1 + \alpha_2 \left(\frac{d}{L} \right)^{\alpha_3} Re^{\alpha_4} \right] Sc^{\alpha_5} \quad (\text{A-32})$$

b. free convection

$$h = \frac{D}{\chi} \beta_1 Re^{\beta_2} Sc^{\beta_3} Gr^{\beta_4} \left(\frac{d}{L} \right)^{\beta_5} \quad (\text{A-33})$$

where

h is the mass transfer coefficient [cm/s]

D is the diffusion coefficient of fission product in helium [cm²/s]

Re is the Reynolds Number

Sc is the Schmidt Number

Gr is the Grashof Number

d is the hydraulic diameter of conduit [cm]

L is the hydrodynamic entry length [cm]

$\chi = L$ for flat plates

= d for other geometries

Table A-15: Coefficients for mass transfer correlations – forced convection

Geometry	Flow regime		α_1	α_2	α_3	α_4	α_5
Flow in tube and annular flow	Re < 2100 (laminar)	L / (d Re Sc) \geq 0.07	0	3.66	0	0	0
		L / (d Re Sc) < 0.07	0	1.86	0.33	0.33	0.33
	Re \geq 2100 (turbulent)		0	0.023	0	0.8	0.33
Aligned tube bundles in cross flow ⁽²⁾	(Re) _{max} < 1000		f(Re; 0.43, 0, 10 ³) ⁽¹⁾	f(Re; 0.52, 0.27, 10 ³) ⁽¹⁾	0	f(Re; 0.5, 0.63, 10 ³) ⁽¹⁾	0.36
	1000 \leq (Re) _{max} \leq 200,000		0	0.27	0	0.63	0.36
	(Re) _{max} > 200,000		0	0.02	0	0.84	0.36
Staggered tube bundles in cross flow ⁽²⁾	(Re) _{max} < 1000		f(Re; 0.43, 0, 10 ³) ⁽¹⁾	f(Re; 0.60, 0.40, 10 ³) ⁽¹⁾	0	f(Re; 0.5, 0.60, 10 ³) ⁽¹⁾	0.36
	1000 \leq (Re) _{max} \leq 200,000		0	0.40	0	0.60	0.36
	(Re) _{max} > 200,000		0	0.021	0	0.84	0.36
Flat plate ⁽³⁾	Re < 3.2*10 ⁵ (laminar)	0 \leq Sc \leq 0.6	0	f(Sc; 1.128, 0.664, 0.6) ⁽¹⁾	0	0.5	f(Sc; 0.5, 0.33, 0.6) ⁽¹⁾
		0.6 < Sc \leq 10	0	0.664	0	0.5	0.33
		Sc > 10	0	0.678	0	0.5	0.33
	Re \geq 3.2*10 ⁵ (turbulent)		0	0.037	0	0.8	0.33

$$(1) f(x; a, b, c) \equiv a - (a - b)(2c - x)x/c^2$$

(2) use d = outer tube diameter (3) use plate length for Re evaluation

Table A-16: Coefficients for mass transfer correlations – free convection

Geometry	Flow regime	β_1	β_2	β_3	β_4	β_5
Flow in tube and annular flow	$d \text{ Re } Sc / L \leq 30$	6	0	0	0	0
	$d \text{ Re } Sc / L > 30$	1.78	0.357	0.357	0	0.357
Vertical tube banks and vertical flat plates (KGNFP=1)	$Gr \text{ Sc} \leq 10^4$	1.295	0	0.1646	0.1646	0
	$10^4 < Gr \text{ Sc} < 10^9$	0.59	0	0.25	0.25	0
	$Gr \text{ Sc} \geq 10^9$	0.33	0	0.13	0.33	0
Horizontal tube banks and horizontal flat plates (KGNFP=1)	$Gr \text{ Sc} \leq 10^{-5}$	0.4	0	0	0	0
	$10^{-5} < Gr \text{ Sc} < 10^4$	1.962	0	0.1381	0.1381	0
	$10^4 \leq Gr \text{ Sc} < 10^9$	0.53	0	0.25	0.25	0
	$Gr \text{ Sc} \geq 10^9$	0.13	0	0.33	0.33	0

The values for α_i and β_i for different flow regimes and geometries are given in Tables A-15 and A-16.

The definitions of the dimensionless flow parameters are as follows:

1. Reynolds number

$$Re = \frac{v \rho d}{\mu} \quad (A-34)$$

where

v is the average coolant velocity [cm/s]

ρ is the density of helium [g/cm³]

μ is the dynamic viscosity of helium [g/(cm s)]

$d = 4 A/P$ is the hydraulic diameter [cm]

with A = cross section area and P = wetted perimeter

2. Schmidt number

$$Sc = \frac{\mu}{\rho D} \quad (A-35)$$

3. Grashof number

$$Gr = g L^3 [\rho_m - (\rho_m)_\infty] \rho_m / \mu_m^2 \quad (A-36)$$

Here the index m stands for mixture of fission product and helium coolant, $(\rho_m)_\infty$ is the average density in the free stream, g is the acceleration of gravity.

The formula for the diffusion coefficients is

$$D = 0.1682 \left(\frac{T_c}{1000} \right)^{1.65} \left(\frac{23.83}{p} \right) \sqrt{\left(\frac{1}{M} + 0.25 \right) / 0.257} \quad (A-37)$$

where

D is the diffusion coefficient [cm²/s]

T_c is the helium temperature [K]

p is the pressure [atm]

M is the molecular weight [g/mol]

where M is the molecular mass of the fission product species, and the dynamic viscosity is computed as [78]:

$$\mu \left[\frac{g}{cm \cdot s} \right] = 5.31 * 10^{-4} \left(\frac{T_c}{1273} \right)^{0.678} \quad (A-38)$$

Table A-17: Summary of isotherm data for sorption of Cs, Ag, and I on primary circuit alloy and tungsten [79]

Fission product	Metal or alloy	Pressure range [Pa]	Temperature range [K]	Reference	Oxidation state ⁽¹⁾
Cs	W	$10^{-12} - 1$	800 - 1200	[80]	U
Cs	Incoloy-800 Hastelloy X	$2 \times 10^{-6} - 2 \times 10^{-2}$	1073	[81] [82]	U, O
Cs	SS-304	$2 \times 10^{-5} - 5 \times 10^{-1}$	618 - 1008	[83]	U, O
Cs	Incoloy-800 INOX 347 Hastelloy B	$10^{-5} - 10^{-4}$	673 - 873	[84]	U, O
Ag	W	$5 \times 10^{-7} - 5 \times 10^{-5}$	1073 - 1273	[85]	U
I	T-22	$10^{-6} - 10^{-2}$	673 - 1073	[86]	U, O

(1) U = unoxidized, O = Oxidized

Relevant PADLOC input consists of helium mass flow rate, helium pressure, helium temperature, and wall temperature. With this input, the density is calculated from the perfect gas law

$$\rho = \frac{M p}{R T} \quad (\text{A-39})$$

where $R = 82.057$ [atm cm³/(g mol K)] is the universal gas constant. The coolant velocity follows from

$$v = \frac{\dot{m}}{\rho A} = \frac{R}{M} \dot{m} \frac{T}{A p} \quad (\text{A-40})$$

A.5.2.2. Sorption Isotherms

The reference US sorption isotherms are summarized in [79]; the experimental data used to derive these isotherms is summarized in Table A-17, and coefficients for the numerical fits of the data are given in Tables A-18 and A-19 for unoxidized and oxidized surface conditions, respectively.

The sorption of the fission products cesium, silver, and iodine on primary circuit alloys is calculated according to two equations, one of which applies to cesium and the other to silver and iodine. For cesium

$$P = \sum_{i=1}^3 b_i C^{n_i} \quad (\text{A-41})$$

Table A-18: Values of parameters and constants in the isotherms (equations A-41, A-42, A-43, and A-44) for fission products sorbed on unoxidized primary circuit alloys

El.	Alloy	Constants											
		K ₁	a ₁ ⁰	b ₁ ⁰	b ₂ ⁰	b ₃ ⁰	Q ₁	Q ₂	Q ₃	n ₁	n ₂	n ₃	δ
Cs	Carbon steel, SA-36			2.65*10 ¹⁰	1.57*10 ¹⁵	1.25*10 ²²	2.74*10 ⁵	2.62*10 ⁵	2.16*10 ⁵	1	3	8	7
	SA-387, SA-533			2.65*10 ¹⁰	1.57*10 ¹⁵	1.25*10 ²²	2.74*10 ⁵	2.62*10 ⁵	2.16*10 ⁵	1	3	8	7
	Alloy 800H			2.65*10 ¹⁰	1.57*10 ¹⁵	1.25*10 ²²	2.74*10 ⁵	2.62*10 ⁵	2.16*10 ⁵	1	3	8	7
	Hastelloy X			2.65*10 ¹⁰	1.57*10 ¹⁵	1.25*10 ²²	2.74*10 ⁵	2.62*10 ⁵	2.16*10 ⁵	1	3	8	7
	SS-304			5.30*10 ¹⁰	1.26*10 ¹⁶	3.26*10 ²⁴	2.74*10 ⁵	2.62*10 ⁵	2.16*10 ⁵	1	3	8	7
Ag	Carbon steel, SA-36	0.2	5.22*10 ⁻⁷				-2.54*10 ⁵						7
	SA-387, SA-533	0.2	5.22*10 ⁻⁷				-2.54*10 ⁵						7
	Alloy 800H	0.2	5.22*10 ⁻⁷				-2.54*10 ⁵						7
	Hastelloy X	0.2	5.22*10 ⁻⁷				-2.54*10 ⁵						7
	SS-304	0.1	5.22*10 ⁻⁷				-2.54*10 ⁵						7
I	Carbon Steel, SA-36	3.0	3.49*10 ⁻⁵				-1.11*10 ⁵						7
	SA-387, SA-533	3.0	3.49*10 ⁻⁵				-1.11*10 ⁵						7
	Alloy 800H	3.0	3.49*10 ⁻⁵				-1.11*10 ⁵						7
	Hastelloy X	3.0	3.49*10 ⁻⁵				-1.11*10 ⁵						7
	SS-304	1.5	3.49*10 ⁻⁵				-1.11*10 ⁵						7

Table A-19: Values of parameters and constants in the isotherms (equations A-41, A-42, A-43, and A-44) for fission products sorbed on oxidized primary circuit alloys

El.	Alloy	Constants											
		K ₁	a ₁ ⁰	b ₁ ⁰	b ₂ ⁰	b ₃ ⁰	Q ₁	Q ₂	Q ₃	n ₁	n ₂	n ₃	δ ⁽¹⁾
Cs	Carbon steel, SA-36			2.65*10 ⁹	1.57*10 ¹²	1.25*10 ¹⁴	2.74*10 ⁵	2.62*10 ⁵	2.16*10 ⁵	1	3	8	-
	SA-387, SA-533			2.65*10 ⁹	1.57*10 ¹²	1.25*10 ¹⁴	2.74*10 ⁵	2.62*10 ⁵	2.16*10 ⁵	1	3	8	-
	Alloy 800H			5.30*10 ⁹	1.26*10 ¹³	3.20*10 ¹⁶	2.74*10 ⁵	2.62*10 ⁵	2.16*10 ⁵	1	3	8	-
	Hastelloy X			5.30*10 ⁹	1.26*10 ¹³	3.20*10 ¹⁶	2.74*10 ⁵	2.62*10 ⁵	2.16*10 ⁵	1	3	8	-
	SS-304			5.30*10 ⁹	1.26*10 ¹³	3.20*10 ¹⁶	2.74*10 ⁵	2.62*10 ⁵	2.16*10 ⁵	1	3	8	-
Ag	Carbon steel, SA-36	2.0	5.22*10 ⁻⁷				-2.54*10 ⁵						-
	SA-387, SA-533	2.0	5.22*10 ⁻⁷				-2.15*10 ⁵						-
	Alloy 800H	1.0	5.22*10 ⁻⁷				-2.15*10 ⁵						-
	Hastelloy X	1.0	5.22*10 ⁻⁷				-2.15*10 ⁵						-
	SS-304	1.0	5.22*10 ⁻⁷				-2.15*10 ⁵						-
I	Carbon Steel, SA-36	0.4	5.11*10 ⁻⁶				-1.11*10 ⁵						-
	SA-387, SA-533	0.4	5.11*10 ⁻⁶				-1.11*10 ⁵						-
	Alloy 800H	0.4	5.11*10 ⁻⁶				-1.11*10 ⁵						-
	Hastelloy X	0.4	5.11*10 ⁻⁶				-1.11*10 ⁵						-
	SS-304	0.4	5.11*10 ⁻⁶				-1.11*10 ⁵						-

(1) No values available; assume δ' = δ in equation (6-12)

and for silver and iodine

$$P = \frac{C}{a_i(K - C)} \quad (\text{A-42})$$

with

$$\begin{aligned} a_i &= a_i^o \exp\{-Q_i/(RT)\} \\ b_i &= b_i^o \exp\{-Q_i/(RT)\} \end{aligned} \quad (\text{A-43})$$

where

P is the vapor pressure [Pa]

C is the concentration of sorbate [$\mu\text{g}/\text{cm}^2$ -geom]

n_i are constants, $i = 1, 2, 3$

K is a constant [$\mu\text{g}/\text{cm}^2$]

Q_i/R are temperature coefficients [K], $i = 1, 2, 3$

a_i in [Pa^{-1}], $i = 1, 2, 3$

b_i in [$\text{Pa}/(\mu\text{g}/\text{cm}^2)$], $i = 1, 2, 3$

a_i^o, b_i^o are constants, $i = 1, 2, 3$

For both Eqns. (A-41) and (A-42)

$$C' = \delta' C / \delta \quad (\text{A-44})$$

where

δ is the roughness of surface with sorbate concentration C

δ' is the roughness of surface with sorbate concentration C'

Thus, if the surface roughness differs from that on the reference test samples, C in Eqns. (A-41) and (A-42) is replaced by C'.

The parameters of Eqns. (A-41), (A-42), (A-43), and (A-44) are given in Table A-18 for unoxidized primary circuit alloys and in Table A-19 for oxidized primary circuit alloys.

These correlations which describe the deposition behavior of condensable radionuclides on structural metals [80, 81, 82, 83, 84, 85, 86, 87, 88] have very large uncertainties ($\gg 10x$) as discussed in [79] and [89]. A major cause of these large uncertainties is that the sorption isotherms were typically measured in the laboratory at partial pressures orders of magnitude higher than those which occur in the reactor (of the order of 10^{-15} atm); moreover, for Cs and Ag, the isotherms used for reactor design were measured on nonreference materials. The effects of surface films, dust, and particularly H_2O on plateout are also highly uncertain, as essentially no quantitative data are available.

At ORNL, a bench-scale apparatus for iodine adsorption/desorption experiments was constructed [90]. The carrier gas, helium with a reducing component or components, was fed through flow meters to the test furnace. The furnace system consisted of a clamshell heater, a quartz tube, and associated on-line γ scanning facilities. The heater had

three independent windings to maintain separate temperature zones and/or temperature gradients. Measurements of the equilibrium iodine loading at partial pressures ($> 10^{-9}$ atm) normal in laboratory experiments, were in agreement with previous measurements. However, at partial pressures of iodine expected under reactor normal operating conditions, the equilibrium loading was smaller by a factor of 10^3 than measured under partial pressures normal for laboratory experiments.

The design of the quartz furnace tube [91], as a result of the diffusion of desorbed iodine counter to the gas flow, was not suitable for measurements at low iodine partial pressures found under reactor normal operating conditions. At the pressures normal in laboratory experiments, however, the effect was negligible. The furnace quartz tube was redesigned as shown in Fig. A-17 by incorporating capillary sections in the main tube and in the insert tube used to collect volatilized iodine. Prior to start of a test, a strip of the selected primary circuit alloy was reduced by exposure to helium and reductant, for example, 4 % H₂ in He for 4 h at 500 °C. The iodine source, a palladium wire with 0.01 µg of iodine traced with I-131 adsorbed on its surface [92], was placed in the entrance region of the main tube. A portion of the iodine is volatilized from the wire into a flowing helium stream by heating the wire to 600 - 650 °C. The volatilized iodine deposits on the strip of the alloy (2.5 cm x 5.1 cm in the shape of a loose coil) located in the expanded section of the main tube; the strip is maintained at ≤ 300 °C during this operation to assure that most of the iodine is deposited on the strip. After the deposition is completed, the palladium wire is cooled to 100 - 150 °C to prevent further volatilization of iodine and the strip is heated to the desired equilibrium temperature, thus inducing volatilization of the iodine on the strip into the helium stream. The iodine in the stream enters the capillary of the insert. The insert makes a good seal against the mating surface in the main tube and is joined by a fitting to the main tube at the right-hand end, outside the furnace. Most of the iodine entering the insert is deposited in the capillary section which extends beyond the furnace; any residual in the gas is removed by charcoal traps in the expanded section of the insert. The location of the iodine during all of these steps is monitored by on-line γ scanning. During equilibrium, a known, slow flow of helium is passed over the alloy specimen which is maintained at the equilibrium temperature and from which iodine desorbs. The equilibrium concentration in the gas phase is determined by the decrease in the quantity of iodine on the strip. Good agreement was generally found between the iodine removed from the strip and that found in the downstream section of the apparatus. That the equilibrium distribution of iodine between the gas phase and the alloy surface was attained is supported by agreement of the calculated equilibria over a range of flow rates (4 to 10 cm³/min) and temperatures (500 to 700 °C).

Examples of data derived from the on-line γ counting as shown in Fig. A-18. The graphs show changes of iodine concentrations along the furnace tubes for two cases. The left hand graph displays transfer of iodine from the palladium wire to the alloy strip and the right hand graph displays transfer of iodine from the alloy strip to the capillary of the insert tube.

The deposition of condensable radionuclides in the primary circuit is presently modeled by GA as a surface phenomenon. However, there are German data, again largely on nonreference materials which imply that deposited radionuclides, especially silver, may diffuse into the interior of structural metals above about 600 °C (e.g., [88]). The current

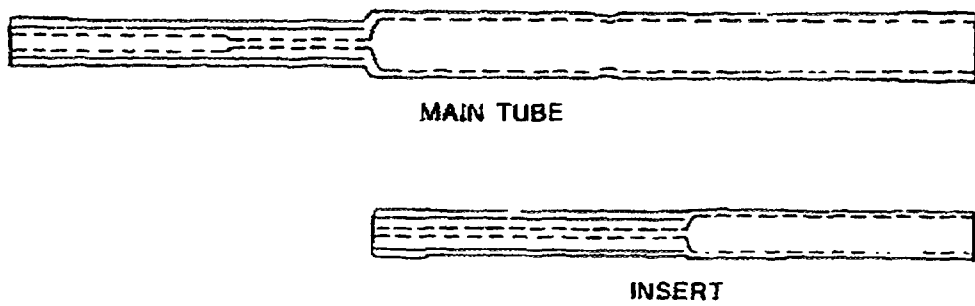


Fig. A-17: Furnace tubes for the iodine adsorption/desorption experiment

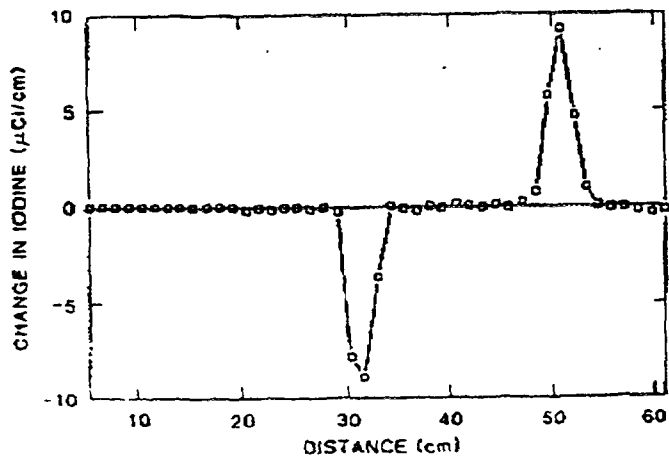
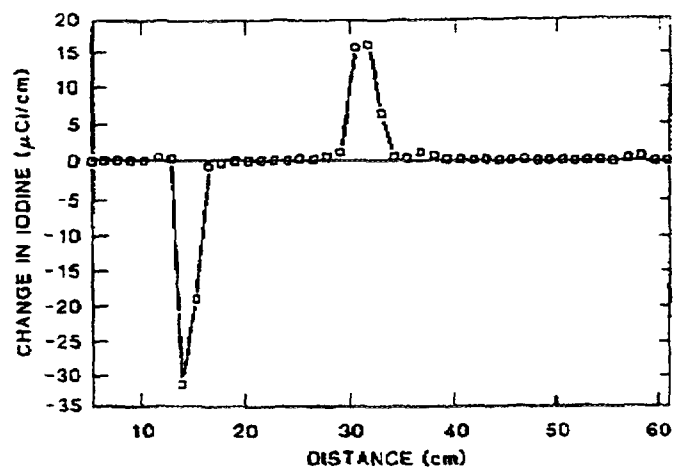


Fig. A-18: Iodine transfers during loading of the alloy strip and desorption and transfer to the insert tube

data base is inadequate to determine whether or not "in-diffusion" must be modelled under Modular HTGR operating conditions. With the exception of the hot duct, most of the plateout surface area in the primary circuit operates below 600 °C, so in-diffusion should be of limited importance for steam-cycle HTRs with core outlet temperatures of \approx 700 °C; however, possible in-diffusion effects take on increasing importance for gas turbine HTRs with core outlet temperatures of \geq 850 °C. In the latter case, significant in-diffusion of Ag and/or Cs isotopes could preclude the possibility of effective turbine decontamination prior to maintenance such as periodic reblading.

A.5.2.3. Solid-State Diffusion Coefficients

There are currently no reliable US data for the solid-state diffusion of condensable radionuclides in metal alloys or surface oxides. German data (e.g., [4]) have been utilized in the limited parametric studies of in-diffusion effects that have been performed at GA to date.

REFERENCES OF APPENDIX A

- [1] KFA-HBK, Projektbericht 1985, Internal Report KFA-HBK-IB-1/86, Research Center Jülich (1986).
- [2] UKAEA, Report TRG 1000(R), AERE Harwell, Personal Communication (1979).
- [3] GA TECHNOLOGIES, Fuel Design Data Manual, Report GA-901866, Issue F, GA Technologies Inc. (1987).
- [4] MOORMANN, R., VERFONDERN, K., Methodik umfassender probabilistischer Sicherheitsanalysen für zukünftige HTR-Anlagenkonzepte - Ein Statusbericht (Stand 1986), Band 3: Spaltproduktfreisetzung, Report Jül-Spez-388/Vol. 3, Research Center Jülich (1987).
- [5] GOODIN, D.T., Metallic Fission Product Release Models for Accident Conditions, GA Document No. 906957, GA Technologies (1983).
- [6] SCHENK, W., NABIELEK, H., Kugelbrennelemente mit TRISO-Partikeln bei Störfalltemperaturen, Report Jül-Spez-487, Research Center Jülich (1989).
- [7] GUDKOV, A.N. et al., Behavior of Solid Fission Products in Coated Fuel Particles of a High-Temperature Gas-Cooled Reactor, Atomnaya Energiya 67 (1989) 93-97.
- [8] DANNERT, V., Ein thermodynamischer Ansatz zur Spaltproduktrückhaltung - Entlastung von Barrieren, (Proc. Jahrestagung Kerntechnik '91, Bonn, 1991), Inforum GmbH, Bonn (1991) 107-110.
- [9] MÜLLER, A., Freisetzung gasförmiger Spaltprodukte (Kr, Xe, J) aus Brennelementen für gasgekühlte Hochtemperaturreaktoren, Report Jül-1295, Research Center Jülich (1976).
- [10] MYERS, B.F., Effect of Water Vapor on the Release of Fission Gases from Uranium Oxide in High-Temperature, Gas-Cooled Reactor Coated Fuel Particles, J. Am. Ceram. Soc. 75 (1992) 686-693.
- [11] MYERS, B.F., BELL, W.E., Cesium Transport Data for HTGR Systems, Report GA-A13990, General Atomic Company (1979).
- [12] MYERS, B.F., BELL, W.E., Strontium Transport Data for HTGR Systems, Report GA-A13168, General Atomic Company (1974).

- [13] FUKUDA, K., et al., Research and Development of HTGR Fuels, Report JAERI-M89-007 (1989).
- [14] MINATO, K., Diffusion Coefficients of Fission Products in UO₂, PyC, SiC, Graphite Matrix and IG-110 Graphite, Unification of Coated Particle Performance Models and Fission Product Transport Data for the HTR (IAEA Technical Workshop, Jülich), (1991).
- [15] SAWA, K. et al., Analytical Method of Fractional Release of Fission Products from Fuel Elements of HTTR, Behaviour of GCR Fuel under Accident Conditions (Proc. IAEA Specialists' Meeting, Oak Ridge, 1990), IAEA, IWGGCR/25, Vienna (1991) 55-61.
- [16] VERFONDERN, K., MÜLLER, D., FRESCO-II, Programm zur Berechnung der Spaltproduktfreisetzung aus einem HTR-Brennelement im Normalbetrieb (Bestrahlungsexperiment) und Kernaufheizstörfall (Heizexperiment) - Benutzerhandbuch, Internal Report KFA-ISR-IB-4/91, Research Center Jülich (1991).
- [17] VERFONDERN, K., Possible Explanation for HFR-K3/3 IMGA Results, Report ORNL/M-2248, Oak Ridge National Laboratory (1991).
- [18] GOODIN, D.T., NABIELEK, H., The Performance of HTR Fuel in Accidents, Technical Note KFA-HBK-TN-19/85, Research Center Jülich (1985).
- [19] GETHARD, P.E., ZUMWALT, L.R., Diffusion of Metallic Fission Products in Pyrolytic Carbon, Nucl. Appl. 3 (1967) 679-685.
- [20] CHERNIKOV, A.S. et al., Fission Product Diffusion in Fuel Element Materials for HTGR, Fission Product Release and Transport in Gas-Cooled Reactors, (Proc. IAEA Specialists Meeting, Berkeley, 1985), IAEA IWGGCR/13, Vienna (1986) 170-181.
- [21] AMIAN, W., et al., Results of Fission Product and Actinide Studies in Coated Fuel Particles and Matrix Graphite, Gas-Cooled Reactors Today (Proc. BNES Conference, Bristol, 1982), British Nuclear Energy Society, London (1982) 153-160.
- [22] HAYASHI, K., FUKUDA, K., Diffusion Coefficients of Fission Products in the UO₂ Kernel and Pyrocarbon Layer of BISO-Coated Fuel Particles at Extremely High Temperatures, J. Nucl. Mat. 174 (1990) 35-44.
- [23] WALLURA, E., et al., Siliziumcarbid-Hüllschichten von Kernbrennstoffteilchen – Eine Charakterisierungsstudie, Report Jül-1871, Research Center Jülich (1983).
- [24] ALLELEIN, H.J., Spaltproduktverhalten - speziell Cs-137 - in HTR-TRISO-Brennstoffteilchen, Report Jül-1695, Research Center Jülich (1980).
- [25] CHRIST, A., Nachrechnung von Ausheizexperimenten, Technical Note HBK-5125-BF-GHRA 001555, HRB Mannheim (1985).
- [26] MYERS, B.F., Cesium Diffusion in Silicon Carbide During Post Irradiation Anneals, Technical Note KFA-HBK-TN-01/84, Research Center Jülich (1984).
- [27] SCHENK, W., PITZER, D., NABIELEK, H., Fission Product Release Profiles from Spherical HTR Fuel Elements and Accident Temperatures, Report Jül-2234, Research Center Jülich (1988).
- [28] VERFONDERN, K., MÜLLER, D., Modeling of Fission Product Release Behavior from HTR Spherical Fuel Elements Under Accident Conditions, Behaviour of GCR Fuel under Accident Conditions (Proc. IAEA Specialists' Meeting, Oak Ridge, 1990), IAEA, IWGGCR/25, Vienna (1991) 45-54.
- [29] VERFONDERN, K., DUNN, T.D., BOLIN, J.M., Comparison of US/FRG Accident Condition Models for HTGR Fuel Failure and Radionuclide Release, Report Jül-2458, Research Center Jülich (1991).

- [30] NABIELEK, H., GONTARD, R., MYERS, B.F., 1. Version of Joint KFA/GA Fission Product Data Book, Internal Report KFA-HBK-JB-11/81, Research Center Jülich (1981).
- [31] ALBERSTEIN, D., SMITH, P.D., HAIRE, M.J., Metallic Fission Product Release from the HTGR Core, Report GA-A13258, General Atomic Company (1975).
- [32] MYERS, B.F., Selected Aspects of Fission Product Behavior in High-Temperature, Gas-Cooled Reactors, Fission Product Transport Data for the HTR (IAEA Technical Workshop, Jülich, 1992).
- [33] MARTIN, R.C., Diffusion Modeling of Fission Product Release during Depressurized Core Conduction Cooldown Conditions, Behaviour of GCR Fuel under Accident Conditions (Proc. IAEA Specialists' Meeting, Oak Ridge, 1990), IAEA, IWGGCR/25, Vienna (1991) 77-84.
- [34] MINATO, K., et al., Release Behavior of Metallic Fission Products from HTGR Fuel Particles at 1600 to 1900 °C, *J. Nucl. Mater.* **202** (1993) 47-53.
- [35] FUKUDA, K., IWAMOTO, K., Diffusion Behavior of Fission Products in Pyrolytic Silicon Carbide, *J. Nucl. Mater.* **75** (1978) 131-144.
- [36] FUKUDA, K., IWAMOTO, K., Xenon Diffusion Behavior in Pyrolytic SiC, *J. Mater. Sci.* **11** (1976) 522-528.
- [37] RÖLLIG, K., Capabilities of the Diffusion Model for Metallic Fission Products at Temperature Transients up to 1600 °C - Case: Cs-137 Release from Spherical Fuel Element R2-K13/1, Unification of Coated Particle Performance Models and Fission Product Transport Data for the HTR (IAEA Technical Workshop, Jülich, 1991) (1991).
- [38] HOINKIS, E., The Determination of Diffusion Coefficients of Cesium and Silver by the Release Method in As-Received, Oxidized and Neutron Irradiated Graphitic Matrix, Transport of Fission Products in Matrix and Graphite (Proc. Colloquium, Berlin, 1981), Report HMI-B 372, Hahn-Meitner-Institut Berlin (1983) 77-102.
- [39] HENSEL, W., HOINKIS, E., The Diffusion of Sr in the Graphitic Matrix A3-3 in Vacuum and in the Presence of Hydrogen, *J. Nucl. Mat.* **184** (1991) 88-96.
- [40] HOINKIS, E., The Diffusion of Ag in the Graphitic Matrices A3-3 and A3-27, Report HMI-B 513, Hahn-Meitner-Institut Berlin (1994).
- [41] SCHWARTZ, M.H., SEDGLEY, D.B., MENDONCA, M.M., SORS: Computer Programs for Analyzing Fission Product Release from HTGR Cores during Transient Temperature Excursions, Report GA-A12462, General Atomic Company (1974).
- [42] FUKUDA, K., SAWAI, T., IKAWA, K., Diffusion of Fission Products in Matrix Graphite for VHTR Fuel Compacts, *J. Nucl. Sci. Tech.* **21** (1984) 126-132.
- [43] ZOLLER, P., Das Transportverhalten der Spaltprodukte Cäsium und Strontium in beschichteten Brennstoffteilchen für Hochtemperatur-Reaktoren unter Bestrahlungsbedingungen, Report JüI-1324, Research Center Jülich (1976).
- [44] NABIELEK, H., Fission Product Data from the British HTR Work, Transport of Fission Products in Matrix and Graphite (Colloquium, Berlin, 1981), Paper C8 (not published in proc.).
- [45] SCHENK, W., NABIELEK, H., Iodine Retention in Spherical Fuel Elements under HTR MODUL Accident Conditions, (Proc. Jahrestagung Kerntechnik '90, Nürnberg, 1990), Inforum GmbH, Bonn (1991) 363-366.
- [46] KHROULEV, A.A., MOMOT, G.V., KUZNETSOV, A.I., High Temperature Gas-Cooled Reactor Abroad, CNIIATINF, AINF (1979) 441.

- [47] CUBICOTTI, D., The Diffusion of Xenon from Uranium Carbide Impregnated Graphite at High Temperatures, Report NAA-SR-194, North American Aviation (1952).
- [48] CAUSEY, R.A., Silver Transport in H-451 Graphite, Trans. Am. Nucl. Soc. **38** (1981) 316-317.
- [49] HAYASHI, K., FUKUDA, K., Diffusion Coefficients of Cesium in Un-Irradiated Graphite and Comparison with Those Obtained from In-Pile Experiments, J. Nucl. Mat. **168** (1989) 328-336.
- [50] HAYASHI, K. et al., In-Pile Release Behavior of Metallic Fission Products in Graphite Materials of an HTGR Fuel Assembly, J. Nucl. Mat. **149** (1987) 57-68.
- [51] SANDALLS, F.J., WALFORD, M.R., Laboratory Determinations of Strontium Diffusion Coefficients in Graphite, Report AERE-R 6911, Harwell (1972).
- [52] VERFONDERN, L., MÜLLER, D., FRESCO-I, Programm zur Berechnung der Spaltproduktfreisetzung aus dem Core eines Kugelhaufenreaktors bei Kernaufheizung - Benutzerhandbuch, Internal Report KFA-ISR-IB-2/91, Research Center Jülich (1991).
- [53] DANNERT, V., Mehrphasendiffusion von Spaltprodukten in Graphit - Ein Beitragüber die Sicherheit von Hochtemperaturreaktoren, Report JüL-2277, Research Center Jülich (1989).
- [54] KRANZ, L., Spaltprodukttransport im Hochtemperaturreaktor: Theorie, programmtechnische Umsetzung und Überprüfung an Experimenten, Report JüL-2463, Research Center Jülich (1991).
- [55] HILPERT, K., et al., Sorption of Cesium and its Vaporization from Graphitic Materials at High Temperatures, High Temp. High Press. **20** (1988) 157-164.
- [56] GENERAL ATOMIC COMPANY, HTGR Fuels and Core Development Program, Report GA-A14479, General Atomic Company (1977).
- [57] MOORMANN, R., KOSCHMIEDER, R., Versuch einer verbesserten formelmäßigen Erfassung der Cs- und Sr- / A3-3 Sorption im Freundlich-Bereich, Technical Note KFA-ISF 4/88 II, Research Center Jülich (1988).
- [58] HILPERT, K., GERADS, H., KOBERTZ, D., Sorption of Strontium by Graphitic Materials, Ber. Bunsenges. Phys. Chem. **89** (1985) 43-48.
- [59] VERFONDERN, K., HILPERT, K., MOORMANN, R., Sorption of Fission Products on Graphite and its Influence on their Release Behavior in a Pebble Bed HTR under Accident Conditions, Fission Product Release and Transport in Gas-Cooled Reactors (Proc. IAEA Specialists Meeting, Berkeley, 1985), IAEA IWGGCR/13, Vienna (1986) 371-384.
- [60] KWASNY, J., HILPERT, K., NICKELE, H., Cäsium-Sorptionsuntersuchungen an graphitischen Reaktorwerkstoffen, Report JüL-2353, Research Center Jülich (1990).
- [61] LORENZ, R.A., DYER, F.F., TOWNS, R.L., Sorption/Desorption Behavior of Iodine on Graphite, Report ORNL-TM-8284, Oak Ridge National Laboratory (1982).
- [62] VERFONDERN, K., NABIELEK, H., PANAMA - Ein Rechenprogramm zur Vorhersage des Partikelbruchanteils von TRISO-Partikeln unter Störfallbedingungen, Report JüL-Spez-298, Research Center Jülich (1985).
- [63] MONTGOMERY, F.C., Fission Product SiC Reaction in HTGR Fuel, GA Document No. 905837, General Atomic Company (1981).

- [64] PROKSCH, E., STRIGL, A., NABIELEK, H., Production of Carbon Monoxide During Burnup of UO₂ Kerneled HTR Fuel Particles, J. Nucl. Mat. **107** (1982) 280-285.
- [65] STRIGL, A., PESCHTA, G., PROKSCH, E., CO-Messungen an Mischoxidteilchen, Report CH-328/84, Austrian Research Center Seibersdorf (1984).
- [66] HOMAN, F.J., et al., Stoichiometric Effects on Performance of High-Temperature Gas-Cooled Reactor Fuels from the U-C-O System, Nucl. Techn. **35** (1977) 428-441.
- [67] WALLURA, E., et al., Siliciumcarbid-Hüllschichten von Kernbrennstoffteilchen - eine Charakterisierungsstudie, Report Jü1-1871, Research Center Jülich (1983).
- [68] GOODIN, D.T., NABIELEK, H., SCHENK, W., Accident Condition Testing of US and FRG High-Temperature Gas-Cooled Reactor Fuels, Report Jü1-Spez-286, Research Center Jülich (1985), and Report GA-A17820, GA Technologies (1985).
- [69] OGAWA, T., et al., A Model to Predict the Ultimate Failure of Coated Fuel Particles during Core Heatup Events, Nucl. Techn. **96** (1991) 314-322.
- [70] LINDEMAYER, T.B., BESSMANN, T.M., Chemical Thermodynamic Representation of <UO_{2+x}>, J. Nucl. Mater. **130** (1985) 473-488.
- [71] NABIELEK, H., VERFONDERN, K., GOODIN, D.T., HTR Fuel: Prediction of Fission Product Release in Accidents, Fission Product Release and Transport in Gas-Cooled Reactors (Proc. IAEA Specialists Meeting, Berkeley, 1985), IAEA IWGGCR/13, Vienna (1986) 155-169.
- [72] MONTGOMERY, F.C., PARTAIN, K.E., STALEY, H., Final FY 82 Report on Fission Product - SiC Reactions, GA Document No. 906641, GA Technologies Inc. (1982).
- [73] GOODIN, D.T., US/FRG Accident Condition Fuel Performance Models, GA Document No. DOE-HTGR-85107, Rev. 1, GA Technologies Inc. (1989).
- [74] RÖLLIG, K., Brennelemente unter Normal- und Störfallbedingungen, Final Report HTR-M-0210-BA-GHRA 006910, ASEA Brown Boveri, Hochtemperatur-Reaktorbau (1993).
- [75] TURNBULL, J.A., et al., The Diffusion Coefficients of Gaseous and Volatile Species During the Irradiation of Uranium Dioxide, J. Nucl. Mat. **107** (1982) 168-184.
- [76] WILLIAMSON, R., AEA Technology, UK, Facsimile message on enhanced vacancy diffusion to B. F. Myers, ORNL, June 6, 1996.
- [77] HEDRITSCH, W.W., SMITH, P.D., PADLOC, A One-Dimensional Computer Program for Calculating Coolant and Plateout Fission Product Concentrations, USDOE Report GA-A14401, General Atomic Company (1977).
- [78] WILSON, M.P.Jr., Thermodynamic and Transport Properties of Helium, Report GA-1355, General Atomic Division (1960).
- [79] MYERS, B.F., Sorption Isotherms for HTGR Alloys, GA Document 907721, Rev. 0, GA Technologies Inc. (1984).
- [80] TAYLOR, J.B., LANGMUIR, I., The Evaporation of Atoms, Ions and Electrons from Caesium Films on Tungsten, The Physical Review, September 15 (1933).
- [81] GAS TURBINE HTGR PROGRAM, Semiannual Progress Report for the Period January 1, 1976, through June 30, 1976, Report GA-A13950, General Atomic Company (1976).
- [82] GAS TURBINE HTGR PROGRAM, Quarterly Progress and Task Closeout Report for the Period Ending September 30, 1976, Report GA-A14097, General Atomic Company (1976).

- [83] MILSTEAD, C.E., ZUMWALT, L.R., Cesium Deposition on Stainless Steel, USAEC Report GA-7433, Gulf General Atomic (1966).
- [84] ABASSIN, J., et al., Etude des Isothermes d'Adsorption de Cesium sur Hastelloy B, Incoloy [sic] et Inox SS347, Compte Rendu DMG No. 40/46, Centre d'Etude Nucleaire de Grenoble (in French) (1976).
- [85] IONOV, N.J., MITTSEV, M.A., Adsorption of Silver on Tungsten, Sov. Tech. Phys. Letters 1 30 (1975).
- [86] OSBORNE, M.F., BRIGGS, R.B., WICHNER, R.P., Iodine Sorption on Low-Chromium Alloy Steel, USDOE Report ORNL/TM-7755, Oak Ridge National Laboratory (1982).
- [87] LORENZ, R.A., DYER, F.F., TOWNS, R.L., Sorption/Desorption Behavior of Iodine on Graphite, USDOE Report ORNL/TM-8284, Oak Ridge National Laboratory (1982).
- [88] RÖLLIG, K., CHRIST, A., HAASE, F.W., WIEDMANN, J., Caesium Deposition on HTR Primary Circuit Materials, (Proc. IAEA Specialists Meeting, Berkeley, 1985), IAEA IWGGCR/13, Vienna (1986) 329-350.
- [89] MYERS, B.F., Sorption Isotherms, GA Document 906034, Rev. 1, General Atomic Company (1981).
- [90] CLINTON, S.D., MAILEN, J.C., DINSMORE, T.V., Iodine Adsorption/Desorption and Liftoff from 2.25 Cr-I Mo Alloy, Report ORNL-6559, Oak Ridge National Laboratory (1989).
- [91] WILSON, J.H., MAILEN, J.C., SIMMONS, C.M., Fission Product Plateout, Liftoff and Washoff, Report of Milestone 1601.03.08, Transmittal Letter Number 0930-71-87 (1987).
- [92] CLINTON, S.D., MAILEN, J.C., DINSMORE, T.V., Initial Report on Plateout/Liftoff Testing of I₂ in Bench-Scale Facility, Report of Milestone 1601.2.8.2, ORNL/DOR-ORO/88-166 (1988).

NEXT PAGE(S)
left BLANK

Appendix B THE RUSSIAN “ACTIVATION MODEL” OF FISSION PRODUCT RELEASE FROM HTGR FUEL ELEMENTS

The technique of calculation of the fission product release from the fuel element and the core as a whole, used in the Russian Research Center Kurchatov Institute (RRC KI) at the evaluation of the tightness and activity of the HTGR reactor primary circuit is presented in this section.

B.1. INTRODUCTION

For the analysis of modes of HTGR operation, the level of radioactivity of the primary circuit coolant defining the facility radiational safety at its operation is of great importance. Its value depends on the large number of factors, the coated particles, fuel element manufacture, the stability in respect to in-pile irradiation, their operation conditions, which, in turn, are defined by such parameters as enrichment and loading of the fuel in the reactor etc.

The decision of a problem of radiation safety to a certain degree is connected with the knowledge of fission product behavior in all parts of the reactor and the nuclear power plant (NPP) as a whole, and first of all, in the nuclear fuel and the fuel element which are the first and main barriers of fission product retention.

In the RRC “Kurchatov Institute” for the analysis of fission product behavior, the phenomenological activation (two-group) model was developed and used, which has appeared to be useful and convenient in engineering practice of the analysis of fission product behavior features under various conditions.

At the same time, there are a lot of experimental data on fission product release depending on time and temperature which, as a rule, were processed with positions of traditional models using the effective diffusion coefficient or, under non-stationary conditions, the constants of the one-group model. Naturally, it is reasonable to find the opportunity of application of the gained experimental information in the activation model.

B.2. THE BASIC PRINCIPLES

The quantity of atoms of the i -th nuclide in the primary circuit of the reactor is calculated using the equation

$$\frac{dN_i}{dt} = R_i - (\lambda_i + r_i) N_i + R_{i,p.s.} \quad (B-1)$$

where

R_i is the nuclide release rate from the fuel element

$R_{i,p.s.}$ is the nuclide delivery rate (breakthrough) in the purification system

λ_i is the decay constant

r_i is the rate of nuclide removal from the coolant

The HTGR core consists of uranium-graphite spherical fuel elements in the free bulk. The fuel of the fuel elements are the coated particles – spherical UO_2 kernels with a multi-layer coating of PyC-SiC-PyC – homogeneously distributed in the graphite sphere surrounded by a uraniumless graphite shell.

The HTGR fuel element principle scheme is given in Fig. B-1.

For maintaining the coolant contamination degree at the allowable level, the fission product release from the fuel element is limited. The requirement on fuel element performance is characterized by the measured relative release of the reference radionuclides

$$F_i = \frac{\int_0^\tau R_i(t) \exp\{-\lambda_i(\tau-t)\} dt}{Q_i(\tau)} < F_{i,utm} \quad (B-2)$$

where

$F_{i,utm}$ is the utmost relative release of the reference radionuclides (which are here: Xe-133, I-131, see Table B-1)

$R_i(\tau)$ is the i-th radionuclide release rate with decay constant λ_i

$Q_i(\tau)$ is the i-th radionuclide quantity in the fuel at a certain moment

In the equilibrium case at the nominal mode, it is $R = BF$ where B is the nuclide birth rate and F is the radionuclide relative release rate.

The typical requirements on the allowable fission product release in the nominal mode at temperatures up to 1300 °C and a burnup of 8 - 15 %FIMA and other (including emergency) modes of HTGR operation (VG-400) are given in Table B-1.

The key problem of the coolant activity determination is the release value of atoms from the fuel element.

The main processes defining the fission product release and transport in various degrees accepted in the physical models are:

- the fission product kinetic release from the fuel surface layer of thickness Δ (Δ is the path of fission fragment of recoil nucleus during radioactive decay in the fuel);
- processes in the track zone of fast particles, mainly of fission fragments ("knockout"-effect);
- fission product migration under the effect of concentration gradient (diffusion) and temperature gradient;
- fission product migration with structural defects;

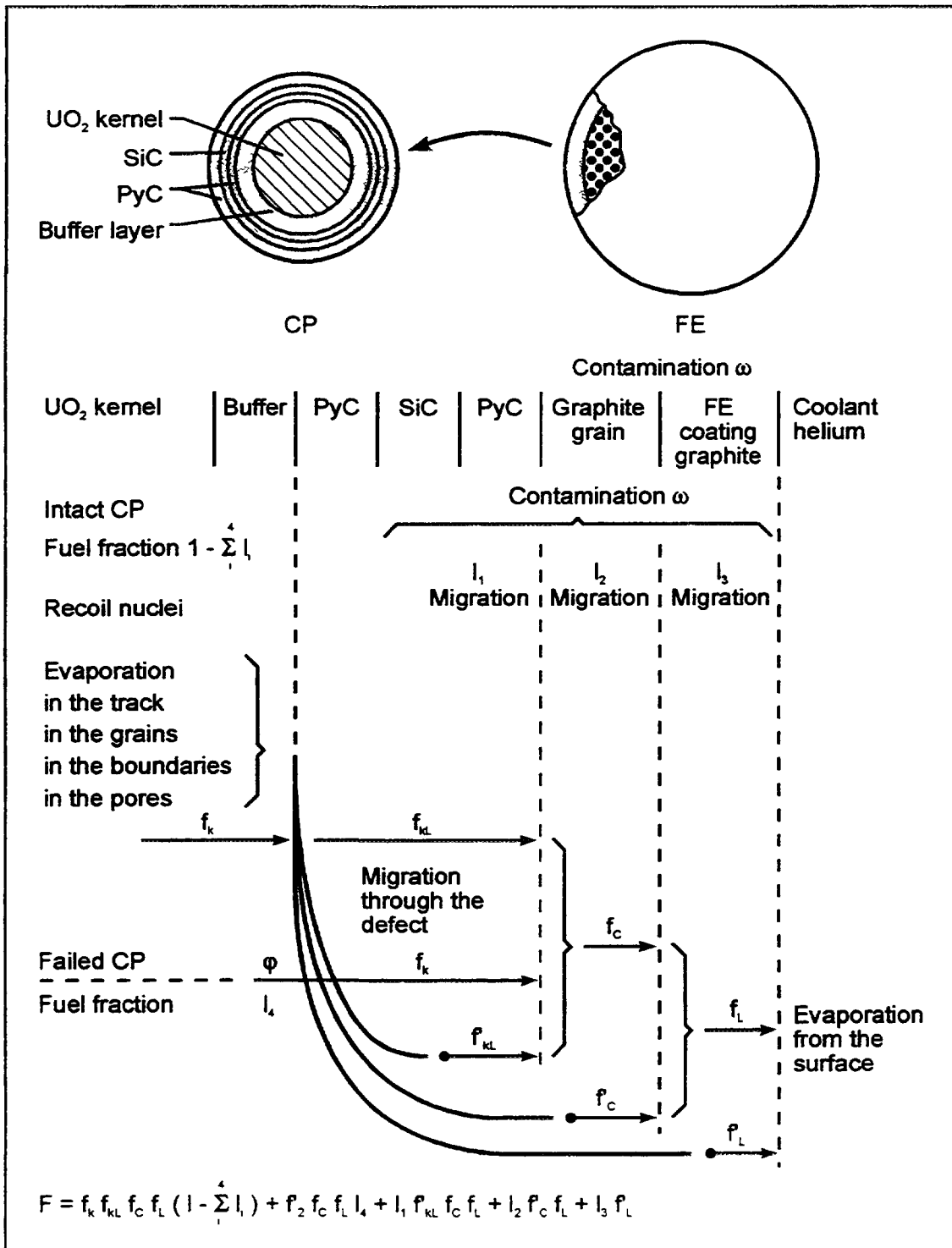


Fig. B-1: Scheme of the fission product release from HTGR fuel elements

Table B-1: Basic requirements for VG-400 fuel elements

Radionuclide	Release (R/B) $_{\infty}$	
	Design	Limiting
Xe-133	$< 10^{-5}$	$< 10^{-4}$
I-131	$< 1.3 \cdot 10^{-5}$	$< 1.3 \cdot 10^{-4}$
Cs-134, Cs-137, Sr-90 [Ci]	< 10	
Fraction of fuel elements failed during operation	$< 5 \cdot 10^{-5}$	
Fraction of fuel contaminating structural components	$< 5 \cdot 10^{-6}$	

- chemical processes in which the fuel, fission products, materials containing fission products, and others take part.

A qualitative representation of the fission product migration paths is given in Fig. B-1.

A quantitative determination of various factors influencing fission product release is an extremely difficult problem. Therefore the various phenomenological models of fission product release from the fuel element are used. These models, as a rule, are best for description of the stationary (on power, temperature conditions and conditions of the environment) modes of the fuel operation, and with low parameters effect (for example inert medium, low level of power release, low integrated burnup of the fuel, absence of phase transitions, etc.) using effective coefficients describing the fission product release from separate constructional elements of the fuel elements. For HTGR the most actual problem are the processes proceeding at high fuel temperatures.

B.3. BRIEF CHARACTERIZATION OF SOME MODELS

B.3.1. Stationary Mode, Diffusion Model

The conventional model of the fission product release from the fuel element is the diffusion model in which the fission product mass balance in the fuel element is derived from solving the diffusion equation

$$\frac{\partial c}{\partial t} = \nabla(D \nabla c) + B - \lambda c \pm \dots \quad (\text{B-3})$$

and the release rate from

$$R = -D \nabla c|_{r=a} \quad (\text{B-4})$$

where

c is the radionuclide concentration [atoms/m³]

D is the diffusion coefficient

t is the current time

In equation (B-3), the additional terms accounting for radioactive decay, chemical reactions, sorption in traps or on the surface, and others are entered.

In most cases for solving equation (B-3), the reduced diffusion coefficient D' is used

$$D' = D / a^2 \quad (\text{B-5})$$

where a is the element characteristic size (grain, coated particle kernel, fuel element, etc.)

In some cases, the effective diffusion coefficient takes into account the fission product release in the inside grain bubbles and their periodic scattering at the interaction with the fission fragment tracks and other processes.

Analytical decisions of the diffusion equation are difficult and the significant difficulties arise because of lack of necessary constants and obtaining from data on fission product release during in-pile experiments.

B.3.2. Non-Stationary Temperature Mode, One-Group Model, the CORSOR (CORSOR-M) Code

The main difficulties arise at the description of the release in non-stationary temperature conditions which are characteristic for a reactor emergency event. In this case, simplified approaches are used. In particular, in the modern mathematical programs of prediction of the fission product release, during accidents of light water reactors with loss of heat removal and the fuel heating at the expanse of radioactive decay of the radionuclides built up during reactor operation, the CORSOR code is used. The model of fission product transport by means of lattice diffusion and further volatilization from the open surface is the basis of this code.

The i-th radionuclide release has the form

$$\frac{dA_i(t)}{dt} = R_i(T) = -K_i(T) A_i(T) \quad (\text{B-6})$$

where

K_i(T) the i-th radionuclide release constant at temperature T

A_i(T) the i-th radionuclide activity

The heating process is divided in equal isothermal parts with duration δt (Fig. B-2) and the relative release for this time is determined by the correlation

$$\begin{aligned} \Delta F_j &= 1 - \exp \{-K \delta t_j\} \\ &= K \delta t_j \quad \text{for } K \delta t_j \ll 1 \end{aligned} \quad (\text{B-7})$$

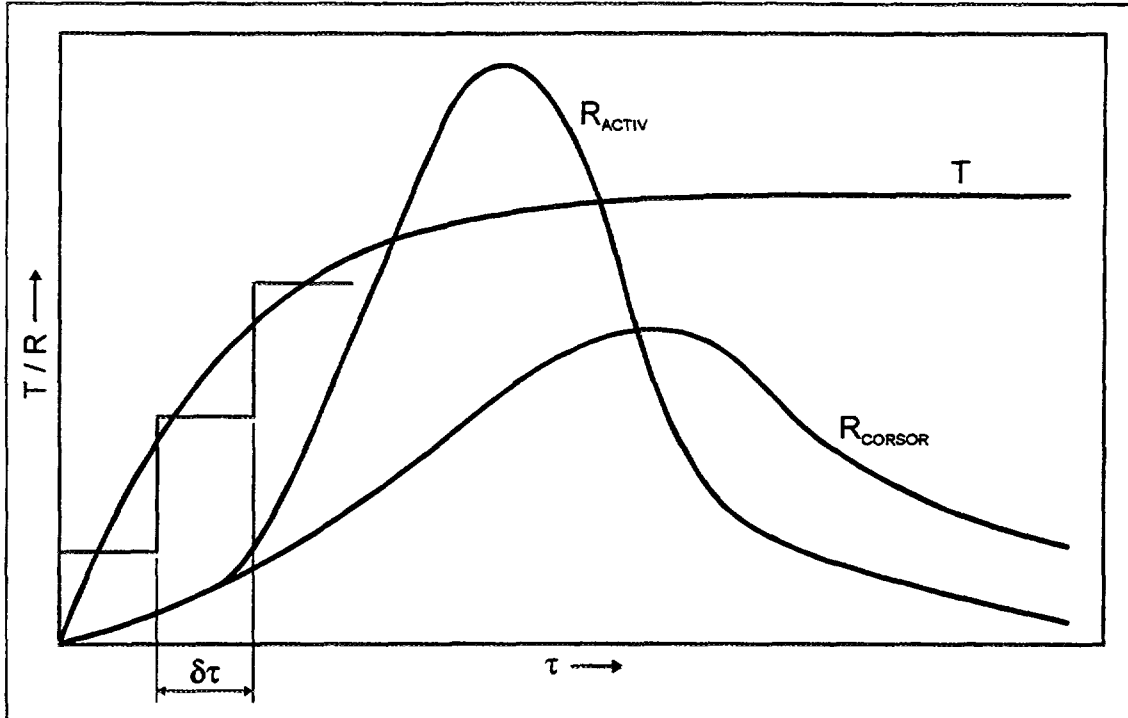


Fig. B-2: Principal diagram of change of fission product release during heating

The detailed description of this model is given in [1]. For the description of the release from the core as a whole in the CORSOR code, the core is divided in 10 radial and 24 axial zones with similar conditions the fission product concentration in each zone.

For the calculation of K in the models CORSOR and CORSOR-M, the following expressions are used:

- for CORSOR

$$K = A \exp \{ B T \} \quad (\text{B-8})$$

where

A, B are coefficients depending on the radionuclide

T is the temperature [$^{\circ}\text{C}$]

The A and B coefficients are accepted constants in the limits of one of the indicated temperature ranges: $T < 1400 \text{ } ^{\circ}\text{C}$; $1400 \text{ } ^{\circ}\text{C} < T < 2200 \text{ } ^{\circ}\text{C}$; $T > 2200 \text{ } ^{\circ}\text{C}$.

- for CORSOR-M

$$K = K_o \exp \left\{ \frac{Q}{0.001987 (T + 273)} \right\} \quad (\text{B-9})$$

where K_o and Q depend on the radionuclide and remain constant in the temperature range $900 \text{ } ^{\circ}\text{C}$ up to UO_2 melting temperature.

Thus the fission product release prediction from the fuel during accident with use of the CORSOR code requires a set of data on K release constants under various conditions of fuel heating. The K release constants are obtained from experiments simulating reactor emergencies. It is possible, that a similar approach may be used for HTGRs.

At the same time, the Chernobyl accident lessons consist in the understanding of the fact that the processes proceeding at fast temperature variation, the fission product evaporation together with fuel and chemical processes (these processes are not enough understood now) defines the fission product release in conditions characteristic for severe (beyond design) accidents.

B.4. THE ACTIVATION MODEL OF FISSION PRODUCT RELEASE

The activation model was developed at the RRC KI in the 70s on the basis of the analysis of experimental data obtained in the institute on fission product release under non-stationary conditions from GCR fuel and the published data on fission product release behavior in the fuel. The activation model is based on the following assumptions:

1. The fission products in the fuel are located in two kinds of defects:
 - defects the occurrence of which is connected with interaction of nuclear reaction (fission, radioactive decay, nuclear impact) products with the fuel (point defects, group defects)
 - structural defects (or inhomogeneity) stipulated by the fuel manufacturing technology or emerging in the fuel during the test (pores, grain boundaries, cracks, etc.)
2. The fission product (fragments, recoil nuclei) relative distribution on the defects is characterized by the spectrum on the activation energies. The qualitative representation of spectrum on the activation energies is given in Fig. B-3a.
The fission products located in point defects have the minimum activation energy; the fission products located in large structural inhomogeneities have the maximum activation energy.
3. Immediately after formation, the fission fragments with the highest probability fall in the defects of the first kind: their distribution is characterized by the initial spectrum on the activation energies (Fig. B-3b).
4. The time of fission products being in the fuel is determined by the time of their presence in the defects and the time of desorption from the opened surfaces. The time of presence in the fuel of the gaseous fission products is determined mainly by the time of their presence in the defects.

The fission products can be released from the initial defects as a result of thermal fluctuations (defect heating) and transformation (defect combination, recrystallization, cracking, etc.) – the processes mainly connected with the temperature conditions of the fuel test, chemical reactions as well as in the result of effects occurring in the zone of the recoil nuclear track (“knockout” effect) at the irradiation and the decay of the predecessor.

As an effect of these factors, a fission product redistribution to the defects (transformation of the spectrum on the activation energies) occurs, and also their release up to the

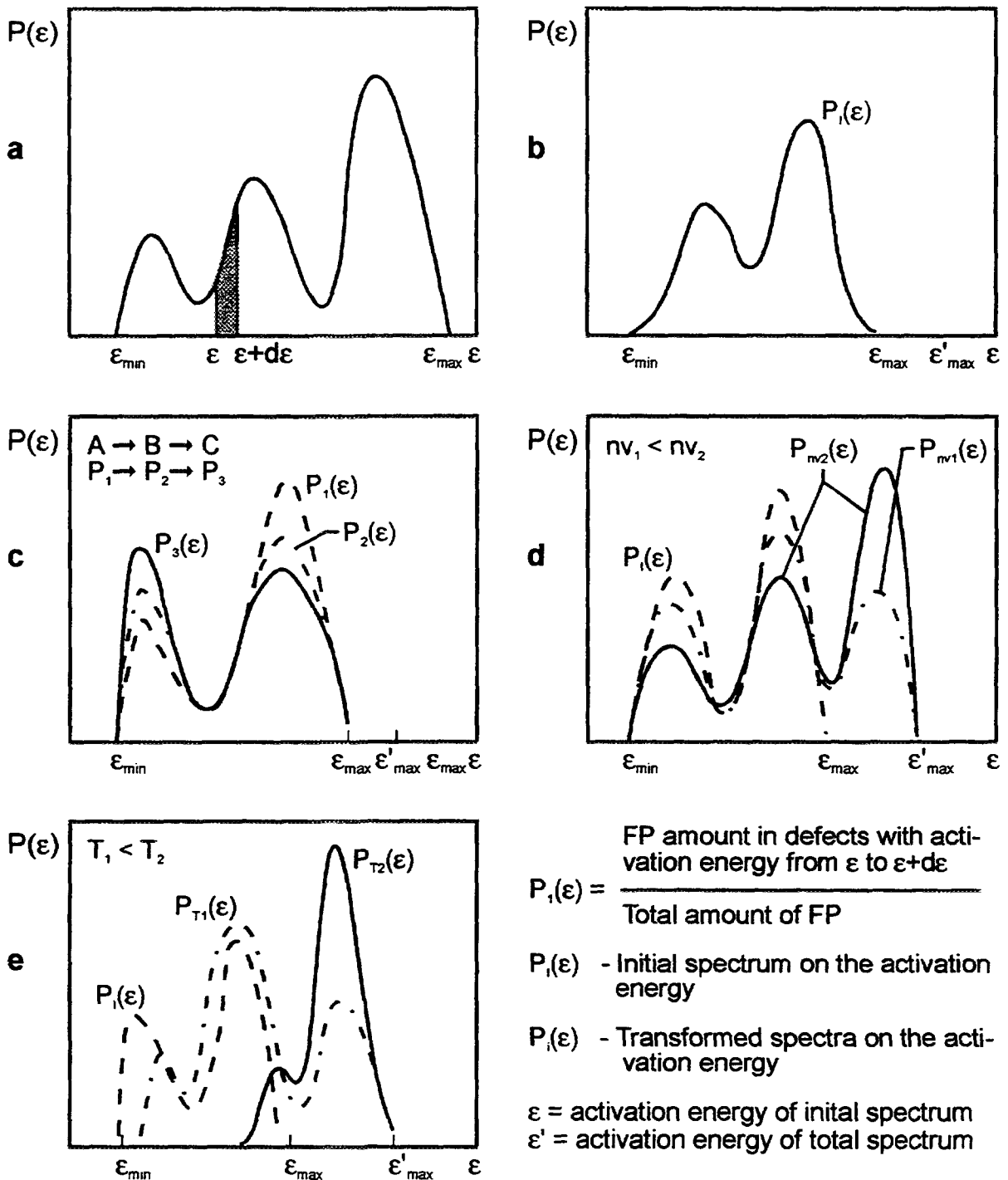


Fig. B-3: Fission product power distribution on the defects

- (a) General view
- (b) Initial spectrum on the activation energy
- (c) Radiation decay effect
- (d) Irradiation intensity effect
- (e) Irradiation temperature effect

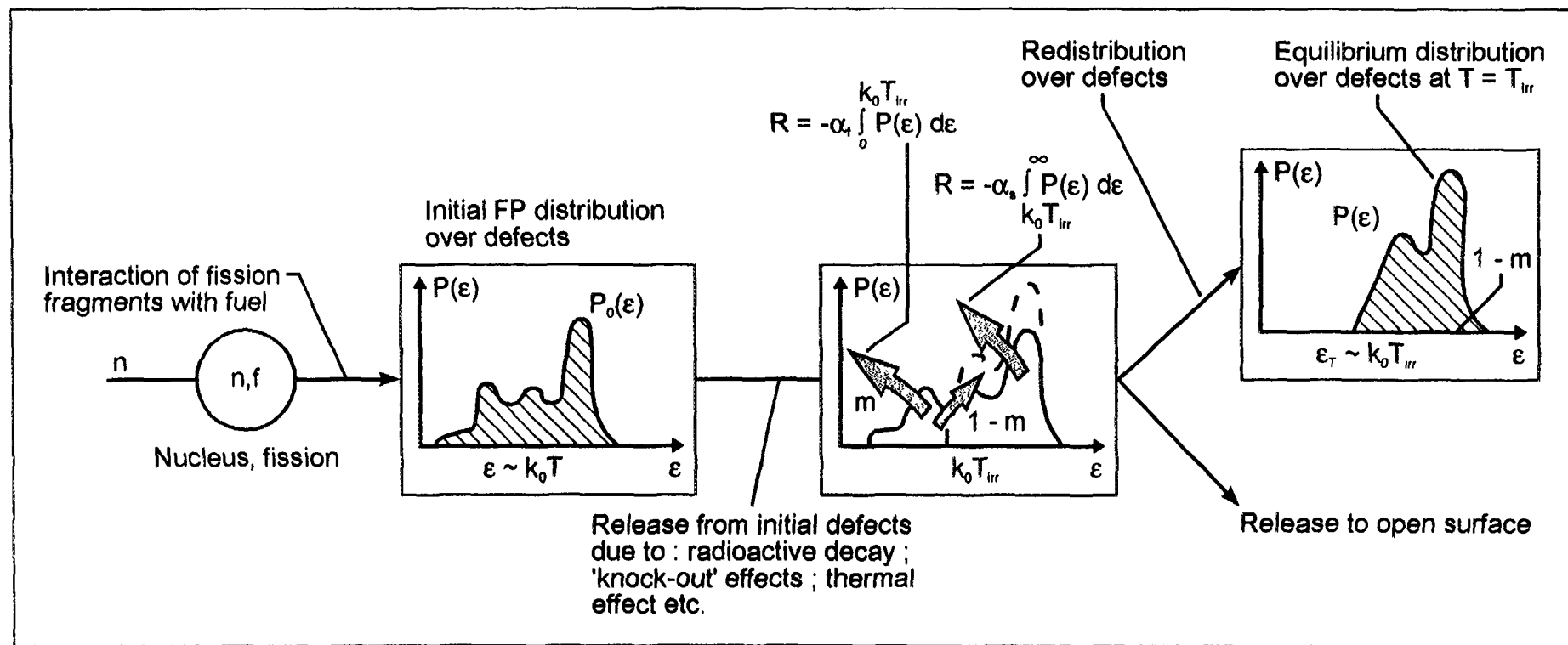


Fig. B-4: Distribution of fission products over defects during irradiation

fuel opened surface. The qualitative presentation of the effect of the indicated factors on the transformation of the spectrum on the activation energies is given in Figs. B-3c, d, e, B-4.

In accordance with the activation model, in particular for the account of the fuel element operation temperature, it is supposed that all fission products in the fuel (and other fission products containing materials) are in the substance defects which may be divided into two groups:

1. The first group of defect containing fission products is defined by the activation energy

$$\epsilon < k T \quad (\text{B-10})$$

2. the second by

$$\epsilon > k T \quad (\text{B-11})$$

where

k is the Boltzmann constant

T is the fuel operation temperature

The fission product quantity of each group at temperature T is defined by the spectral characteristic "m", the fraction of fission products released from the fuel after liberation from the defects with the activation energy $\epsilon < k T$ (Fig. B-4).

Each group of fission products is characterized by its own life time and by its own release constant, respectively:

$$\tau_f \approx 1 / \alpha_f \quad \tau_s \approx 1 / \alpha_s \quad (\text{B-12})$$

where α_f , α_s are the constants of fission product fast and slow release (Figs. B-4 and B-5), depending on the temperature

$$\alpha_f / \alpha_s = 10^2 - 10^4 \quad (\text{B-13})$$

The integrated fission product release rate dependent on the temperature only, has the form:

$$R = - \sum_{n=f,s} \alpha_n A_n \quad (\text{B-14})$$

where

A_n is the quantity of fission product of group n

α_n are the release constants

As was noted above, besides the temperature there are also other factors causing fission product release such as: fission product release at the expense of fission fragments

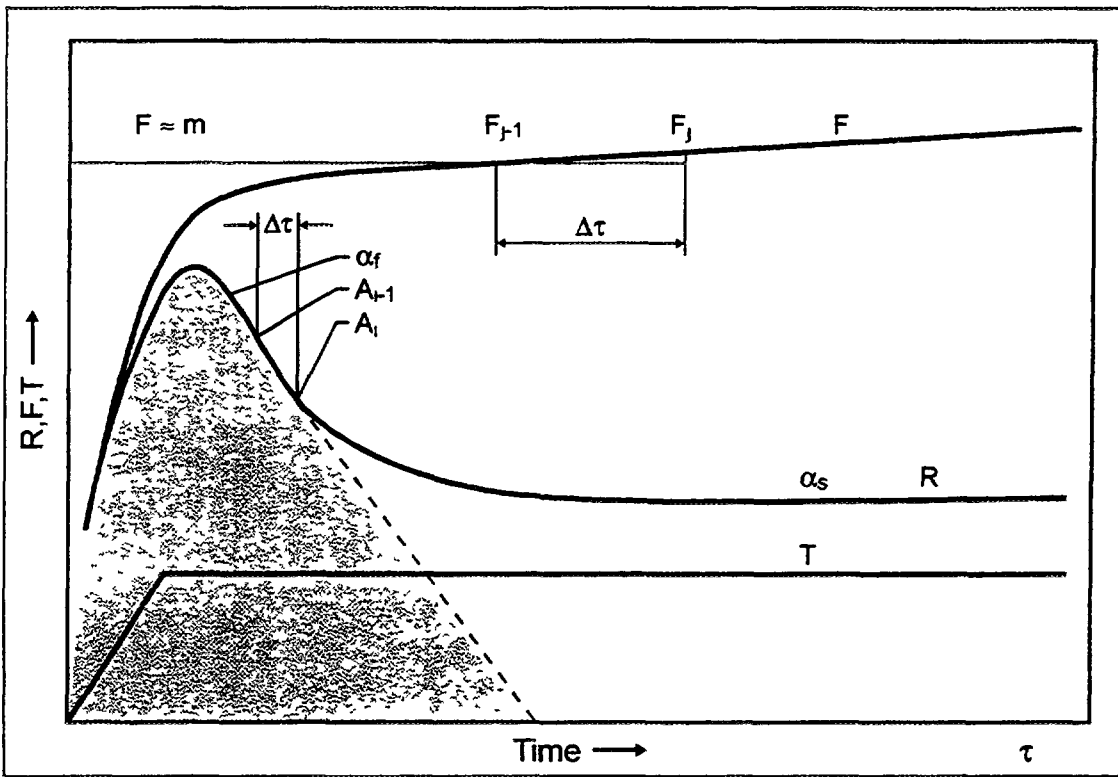


Fig. B-5: The principle diagram for determination of activation model constants

kinetic energy, the effects in the fission fragment track zone ("knockout"), and also the effects evolving in a temperature gradient field which may change the defects character and cause their movement together with the fission products (for example thermo-stresses, chemical reactions, and others). These effects may be taken into account by the introduction of additional components of the fission product release rate, i.e. in the general case, the release rate is

$$R = - \sum_n \alpha_n A_n \quad (\text{B-15})$$

where α_1 is the constant of the appropriate process.

B.5. USE OF THE ACTIVATION MODEL FOR THE ANALYSIS OF FISSION PRODUCT TRANSPORT

B.5.1. Fission Product Release at Simultaneous Irradiation and Heating

In accordance with the principles of the activation model, the balance of fission products of each part and their fractional release in simultaneous irradiation and heating under isothermal conditions are written as ($\tau \gg 1/\alpha_f$):

$$\frac{dA_{i,f}}{dt} = B_i m_i + \lambda_{i-1} A_{i-1} m_i - (\lambda_i + \alpha_{i,f} + \sigma_i \Phi) A_{i,f} \quad (\text{B-16})$$

$$\frac{dA_{i,s}}{dt} = B_i(1 - m_i) + \lambda_{i-1} A_{i-1} (1 - m_i) - (\lambda_i + \alpha_{i,s} + \sigma_i \Phi) A_{i,s} \quad (\text{B-17})$$

The basic relationships for various cases of practical importance are given as follows:

Release rate

1. precursor nuclide

$$R_1 = -(\alpha_{1,f} A_{1,f} + \alpha_{1,s} A_{1,s}) \quad (\text{B-18})$$

2. daughter nuclide

$$R_2 = -(\alpha_{2,f} A_{2,f} + \alpha_{2,s} A_{2,s} + \lambda_1 m_2 A_1) \quad (\text{B-19})$$

where

- i is the nuclide number in the decay chain
"1" = precursor nuclide, "2" = daughter nuclide
- $\alpha_{i,f}, \alpha_{i,s}$ are the release constants
- m_i are the spectral characteristics
- $A_{i,f}, A_{i,s}$ are the quantities of the fission product of each group
 $A_{i,f} + A_{i,s} = A_i$

Basic assumptions

- 1.

$$\alpha_{i,f} = \text{const}; \quad \alpha_{i,s} = f(T_j) \quad (\text{B-20})$$

2. For identical temperatures during heating up and cooling down

$$\lambda_i + \alpha_{i,n} \gg \sigma_i \Phi \quad (\text{B-21})$$

Symbols

1.

$$\lambda'_1 = \lambda_1 + \alpha_{1,s} \quad (\text{B-22})$$

2.

$$A_{i,0} = A_i(\tau = 0) \quad (\text{B-23})$$

3.

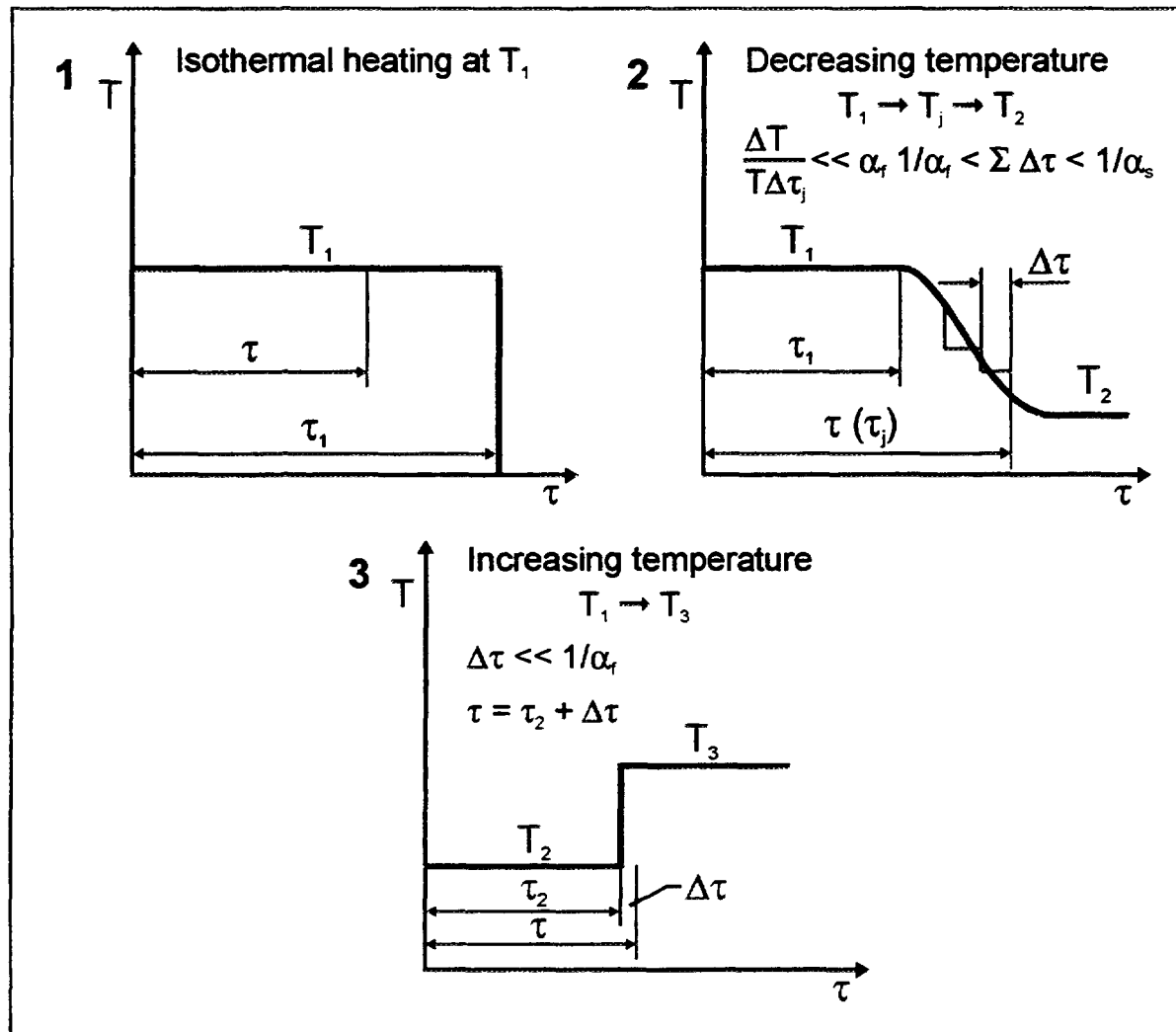
$$f(\lambda'_1, \lambda_2, \tau) = \frac{\lambda_1}{\lambda'_1 - \lambda_2} [\exp\{-\lambda_2 \tau\} - \exp\{-\lambda'_1 \tau\}] \quad (\text{B-24})$$

$$f(\lambda_1, \lambda_2, \tau) = \frac{\lambda_1}{\lambda_1 - \lambda_2} [\exp\{-\lambda_2 \tau\} - \exp\{-\lambda_1 \tau\}]$$

4.

$$\tau_j = \tau_1 + \sum_{I=1}^j \Delta\tau_I \quad (\text{B-25})$$

Calculational scheme



Release

1. For "1" nuclide:

$$\begin{aligned} F_1(T_1, \tau) &= m_1(T_1) [1 - \exp\{-\alpha_f \tau\}] \\ &\quad + [1 - m_1(T_1)] [1 - \exp\{-\alpha_{1,s}(T_1) \tau\}] \end{aligned} \quad (\text{B-26})$$

For $\tau < 1/\alpha_f$:

$$F_1(T_1, \tau) = m_1(T_1) [1 - \exp\{-\alpha_f \tau\}] \quad (\text{B-27})$$

For $1/\alpha_f \leq \tau \leq \tau_1$:

$$F_1(T_1, \tau) = m_1(T_1) + [1 - m_1(T_1)] [1 - \exp\{-\alpha_{1,s}(T_1) \tau\}] \quad (\text{B-28})$$

For "2" nuclide: For $1/\alpha_f \leq \tau \leq \tau_1$:

$$\begin{aligned} F_2(T_1, \tau) &= \{m_2(T_1) A_{2,0} \exp\{-\lambda_2 \tau\} + m_2(T_1) A_{1,0} f(\lambda'_1, \lambda_2, \tau) \\ &\quad + m_1(T_1) A_{1,0} f(\lambda_1, \lambda_2, \tau) + \alpha_{1,s}(T_1) \lambda_1 A_{1,0} [1 - m_1(T_1)] \\ &\quad \left[\frac{\exp\{-\lambda_2 \tau\}}{(\lambda_1 - \lambda_2)(\lambda'_1 - \lambda_2)} + \frac{\exp\{-\lambda_1 \tau\}}{(\lambda_2 - \lambda_1)(\lambda'_1 - \lambda_1)} + \frac{\exp\{-\lambda'_1 \tau\}}{(\lambda_2 - \lambda'_1)(\lambda_1 - \lambda'_1)} \right] \\ &\quad + \alpha_{2,M}(T_1) \lambda_1 A_{1,0} [1 - m_1(T_1)] [1 - m_2(T_1)] \\ &\quad \left[\frac{\exp\{-\lambda_2 \tau\}}{(\lambda'_2 - \lambda_2)(\lambda'_1 - \lambda_2)} + \frac{\exp\{-\lambda'_2 \tau\}}{(\lambda'_1 - \lambda'_2)(\lambda_2 - \lambda'_2)} + \frac{\exp\{-\lambda'_1 \tau\}}{(\lambda_2 - \lambda'_1)(\lambda'_2 - \lambda'_1)} \right] \\ &\quad + A_{2,0} [1 - m_2(T_1)] \exp\{-\lambda_2 \tau\} [1 - \exp\{-\alpha_{2,s}(T_1) \tau\}] \} / A_2(\tau) \end{aligned} \quad (\text{B-29})$$

For $\alpha_{1,s} = \alpha_{2,s} = \alpha_s$ and $\lambda_i \tau(\alpha_s, \tau) \ll 1$:

$$\begin{aligned} F_2(T_1, \tau) &= m_2(T_1) + [1 - m_2(T_1)] [1 - \exp\{-\alpha_s \tau\}] \\ &\quad + A_{1,0}/A_2(\tau) \{ [1 - m_1(T_1)] f(\lambda'_1, \lambda_2, \tau) m_2(T_1) + m_1(T_1) f(\lambda_1, \lambda_2, \tau) \} \end{aligned} \quad (\text{B-30})$$

For $\tau \rightarrow 0$ $\alpha_{1,s} = \alpha_{2,s} = \alpha_s$:

$$\begin{aligned} F_2(T_1, \tau) &= m_2(T_1) + [1 - m_2(T_1)] \alpha_s \tau \\ &\quad + \lambda_1 A_{1,0}/A_{2,0} \{ [1 - m_1(T_1)] m_2(T_1) + m_1(T_1) \} \end{aligned} \quad (\text{B-31})$$

2. For "1" nuclide: For $\Delta \tau_j \rightarrow 0$ and $\tau = \tau_1 + \sum_j \Delta \tau_j$:

$$F_1(T_2, \tau) = F_1(T_1, \tau) + [1 - m_1(T_1)] \sum_{j=1}^n [1 - \exp\{-\alpha_{1,s}(T_j) \Delta \tau_j\}] \quad (\text{B-32})$$

For "2" nuclide: For $\alpha_{1,s} = \alpha_{2,s} = \alpha_s$:

$$\begin{aligned}
F_2(T_2, \tau) &= F_2(T_1, \tau_1) + [1 - m_2(T_1)] \sum_{j=1}^n [1 - \exp \{-\alpha_s(T_j) \Delta \tau_j\}] \\
&+ \sum_{j=1}^n A_1(\tau_{j-1}) / A_2(\tau_j) \\
&\{[1 - m_1(T_1)] f(\lambda'_1, \lambda_2, \Delta \tau_j) m_2(T_1) + m_1(T_1) f(\lambda_1, \lambda_2, \Delta \tau_j)\}
\end{aligned} \tag{B-33}$$

3. For precursor and daughter nuclide (at $\Delta \tau \rightarrow 0$): For $\Delta \tau \ll 1/\lambda_i$:

$$F_{1(2)}(T_3, \tau) = F_{1(2)}(T_2, \tau_2) + [1 - \exp \{-\alpha_f m(T_3) \Delta \tau\}] \tag{B-34}$$

In particular, the fission product release during reactor operation at constant power (at constant temperature T_i and absence of structural changes in the fuel) without account of the precursors' influence is described by the formula [2, 3] ($\tau \gg 1/\alpha_f$):

$$\begin{aligned}
F(T_i, \tau) &= m(T_i) + \\
&[1 - m(T_i)] \frac{\alpha'(T_i)}{\alpha'(T_i) + \lambda} \left[1 - \frac{\lambda}{\alpha'(T_i)} \exp \{-\lambda \tau\} \frac{1 - \exp \{-\alpha'(T_i) \tau\}}{1 - \exp \{-\lambda \tau\}} \right]
\end{aligned} \tag{B-35}$$

where

λ is the decay constant [s^{-1}]

$\alpha'(T_i)$ is the release constant [s^{-1}] under reactor conditions for the group of atoms located in defects with energy $\epsilon > kT_{op}$

$$\alpha' = \alpha_s + \sigma \Phi$$

$\sigma \Phi$ is the release in the fission fragment track zone (at high temperature and low specific power release, $\alpha' \approx \alpha_s$)

At prolonged irradiation ($\tau \gg 1/\lambda$):

$$F(T, \tau) = m(T) + [1 - m(T)] \frac{\alpha'(T)}{\alpha'(T) + \lambda} \tag{B-36}$$

B.5.2. Release during Isothermal Heating of Previously Irradiated Fuel

The balance of fission products of each group and the fission product relative release at isothermal annealing with duration τ of previously irradiated fuel has the form:

$$\frac{dA_{i,f}}{dt} = \lambda_{i-1} A_{i-1} m_i - (\lambda_i + \alpha_{i,f}) A_{i,f} \tag{B-37}$$

$$\frac{dA_{i,s}}{dt} = \lambda_{i-1} A_{i-1} m_i - (\lambda_i + \alpha_{i,s}) A_{i,s} \tag{B-38}$$

Explanations are given in the previous section B.5.1.

In particular, for the isothermal heating (without taking account of the precursors), it is

$$F(\tau) = m(T) f(\alpha_f, \tau) + [1 - m(T)] f(\alpha_s, \tau) \quad (\text{B-39})$$

where

$$f(\alpha_{f,s}, \tau) = 1 - \exp \{-\alpha_{f,s} \tau\} \quad (\text{B-40})$$

It is necessary to note that the above expression for the relative release is true if the irradiation of the fuel specimen was conducted at low temperature. If the irradiation was carried out at the temperature (T_{op}) close to the heating temperature (or higher), it is necessary to take into account the fact that in the defects with the activation energy $\epsilon < \epsilon_{op} \approx k T_{op}$, there is practically no buildup of fission products, and then the expression

$$F(\tau) = [m(T) - m(T_{op})] f(\alpha_f, \tau) + [1 - m(T)] f(\alpha_s, \tau) \quad \text{for } T_{op} < T \quad (\text{B-41})$$

or

$$F(\tau) = [1 - m(T_{op})] f(\alpha_s, \tau) \quad \text{for } T_{op} > T \quad (\text{B-42})$$

will be more true.

In particular, in case of short isothermal annealing ($1/\alpha_f < \tau < 1/\alpha_s$) of a specimen preliminary irradiated at low temperature ($T \approx 20^\circ\text{C}$), without taking account of the precursor), the fission product relative release is

$$F \approx m \quad (\text{B-43})$$

B.5.3. Fission Product Spatial Distribution

The use of the activation model allows to predict quite well the fission product release dynamics and magnitude at the various modes of the fuel, but do not allow to obtain the fission product spatial distribution in the fuel element. However, if it is necessary to obtain the fission product spatial distribution, one could use the traditional diffusion model for describing fission product behavior in the fuel and the fuel element. In this case, the required constants of the transport could be obtained taking account of the connection of the constants of the activation and the diffusion models given in section B.8. In doing so, it is necessary to keep in mind that the fission product distribution given by the diffusion model relate to the fission products located in the defects with activation energy $\epsilon > kT$. This peculiarity must be taken into account in some practical analyses of the fuel conditions, in particular for the determination of fuel element defects by fission product release during fuel element heating after their in-pile irradiation. In this case, one could obtain improper results if the annealing temperature is lower than the fuel element operation temperature.

B.6. MAIN CORRELATIONS FOR THE CALCULATION OF COOLANT ACTIVITY

The method of fission gas and iodine (and other different nuclides) determination under normal operating conditions is characterized by a temperature dependent release rate $R(T)$, equivalent to the change of activity per unit time, of the nuclides out of a core volume element $\Delta V(T_j)$ at temperature T_j . Integration over the total core volume V provides the overall volatile fission product release into the coolant.

$$R(\tau) = \left[\sum_j R(T_j, \tau) \Delta V(T_j) \right] / V \quad (\text{B-44})$$

The main sources of fission products are identified as defective particles (ϕ) and heavy metal contamination of particle coating and matrix graphite (ω). Regarding, for completeness, also particles with an intact coating (mt), the overall release rate is as follows:

$$R(T_j, \tau) = \sum_k R_k = R_\phi + R_\omega + R_{mt} \quad (\text{B-45})$$

According to the two-group activation model, the release rate R is given by

$$R_k(T_j, \tau) = m_k f(\alpha_{k,f}, \tau) + (1 - m_k) f(\alpha_{k,s}, \tau) \quad (\text{B-46})$$

where

$$f(\alpha_{k,n}, \tau) = 1 - \frac{1 - \exp\{-\alpha_{k,n}\tau\}}{1 - \exp\{-\lambda\tau\}} \frac{\lambda \exp\{-\lambda\tau\}}{\alpha_{k,n} + \lambda} \quad (\text{B-47})$$

and

- index $k = \phi$: defective particles
- $k = \omega$: heavy metal contamination
- $k = mt$: intact particles

For most volatile nuclides, the approximation $\alpha_f \gg \lambda \gg \alpha_s$ is valid, thus:

$$R(T_j, \tau) = [m_\phi(T_j) \phi + m_\omega(T_j) \omega + m_{mt}(T_j) \{1 - \phi - \omega\}] B_j \quad (\text{B-48})$$

where

- B_j is the birth rate in volume element $\Delta V(T_j)$
- ϕ is the fraction of defective particles
- ω is the fraction of heavy metal contamination
- mt is the fraction of intact particles

Calculations have been carried out in two ways:

1. quasi-stationary assumption, reactor core does not move, temperature field and specific power are taken for the end of the reactor life.
2. for actual situation, the core moves, calculations are carried out using GAVRUSH and DINAMO computer code package for neutron-physical and thermohydraulic core analysis.

The temperature dependence of constants m and α_s is set at site by the expression:

$$m(\alpha_s) = \text{const} * \exp\left\{-\frac{\epsilon}{kT}\right\} \quad (\text{B-49})$$

The constant α_f is accepted in first approximation not to be dependent on the temperature.

The dependence of constant m on the radionuclide decay constant in the temperature range characteristic for HTGR operating conditions is accepted:

$$m_i = \text{const} * K / \sqrt{\lambda_i} \quad (\text{B-50})$$

where

$K = 1$ for Xe, I

$K = 2$ for Kr (at transition from Xe to Kr)

In the experiments, the release rates from defective particles and the fuel element graphite matrix contamination by the fuel have been measured and necessary constants were determined.

B.7. METHOD AND RESULTS OF DETERMINATION OF THE FISSION PRODUCT RELEASE CONSTANTS

The fission product release constants may be obtained at the fuel in-pile tests or during the heating of previously irradiated fuel. As a rule, the basic experiments for obtaining the fission product release constants are the modes with the temperature step change and subsequent isothermal heating. The characteristic example of the release rate change in such modes is given in Fig. B-5.

The values of the constants in first approximation may be obtained from the correlations:

$$m \approx F_j(\tau) \quad \text{for } \frac{1}{\alpha_f} < \tau \ll \frac{1}{\alpha_s} \quad (\text{B-51})$$

$$\alpha_f \approx \frac{\ln(A_{j-1}/A_j)}{\Delta \tau_j} \quad \text{for } \tau < \frac{1}{\alpha_f} \quad (\text{B-52})$$

$$\alpha_s = \frac{1}{\Delta \tau_j} \ln \left((1-m)/(1-F_j) \right) \approx \frac{F_j - F_{j-1}}{\Delta \tau_j} \quad for \quad \tau \gg \frac{1}{\alpha_f} \quad (B-53)$$

where

F_{j-1} , F_j are the relative release values measured at the moments τ_{j-1} and τ_j of the isothermal heating with $\Delta \tau_j = \tau_j - \tau_{j-1}$

A_{j-1} , A_j are the current readings of detected activities measured at τ_{j-1} and τ_j

For the determination of the constants, one must take into account the remarks noted in section B.5. about the character of the fission product buildup in low-energy defects during irradiation in the reactor. At availability of the long-lived precursors, one must also take into account buildup in the defects with low energy $\epsilon < kT$ at the expense of precursor nuclide decay.

Such approach permits to use the experimental data on fission product release obtained at the heating of the specimens initiating various coated particle damages and various nature and degree of contamination of fuel element structural components with fuel after irradiating such specimens at low temperatures (the "weak" irradiation technique), to predict the fission product release under in-pile conditions (see section 3.4.3.1.).

Feasibility of the use of the release constants obtained at "weak" irradiation of the fuel and fuel elements for the release prediction during in-pile irradiation was substantiated by the analysis of the fission product release during in-pile ampule testings of the fuel element (channel KASHTAN) (Fig. B-8).

The temperature dependence of Xe-135 spectral characteristics used for the calculations, is given in Fig. B-6. The experimental data were obtained by the "weak" irradiation technique. The release from the fuel elements is characterized by the following activation energies for homogeneous contamination of graphite:

$$E = 3.6 \cdot 10^{-20} [J] \quad at \quad T = 430 - 700 ^\circ C$$

$$E = 7.7 \cdot 10^{-20} [J] \quad at \quad T = 800 - 1200 ^\circ C$$

in the presence of coated particles with damaged coatings in the fuel element:

$$E = 2.5 \cdot 10^{-20} [J] \quad at \quad T = 250 - 900 ^\circ C$$

$$E = 1 \cdot 10^{-19} [J] \quad at \quad T = 1000 - 2500 ^\circ C$$

from uncoated kernels:

$$E = 3 \cdot 10^{-20} [J] \quad at \quad T < 900 ^\circ C$$

$$E = 3 \cdot 10^{-19} [J] \quad at \quad T > 1310 ^\circ C$$

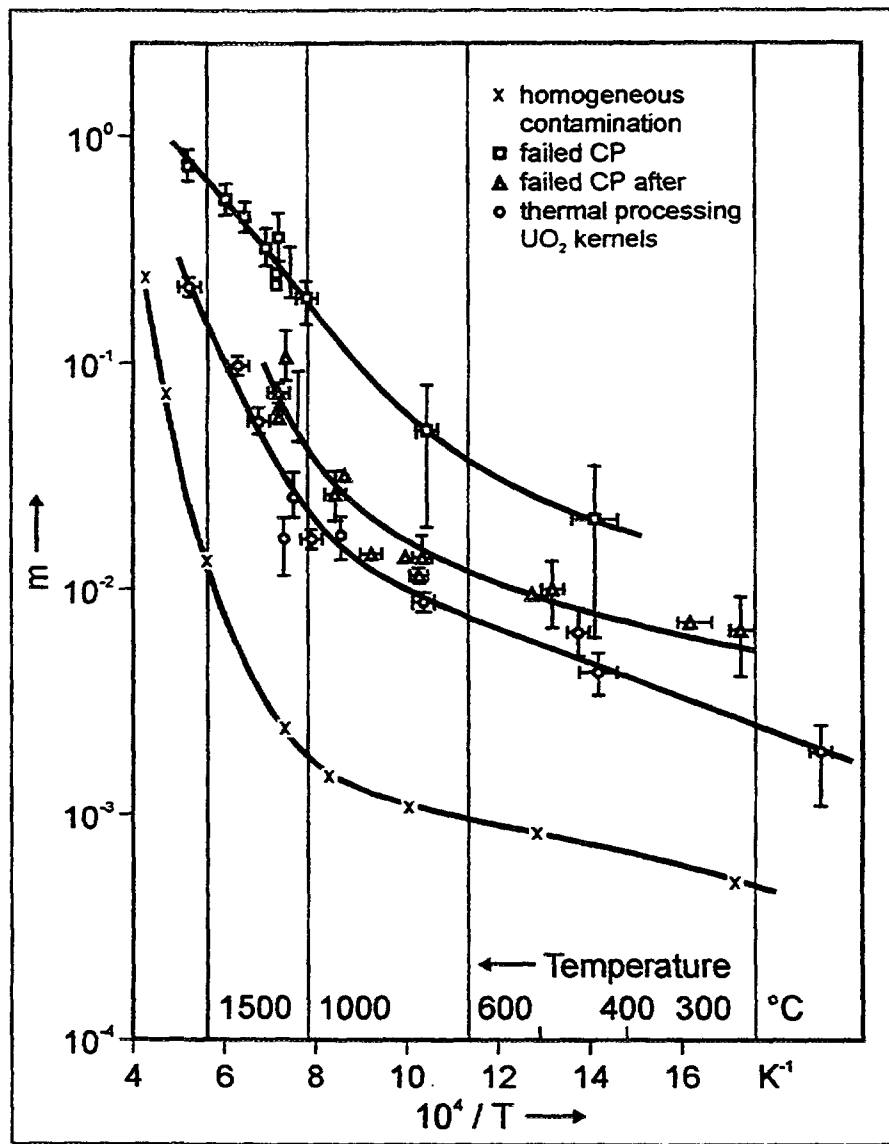


Fig. B-6: Temperature Dependence of the Xe-135 relative release

The "m" temperature dependence for cesium from graphite of various densities is given in Fig. B-7.

However, the processes changing the properties of fuel (element) – density, structure, state of the particle coatings, etc. – occur during in-pile irradiation of fuel elements at rated parameters. Therefore the prediction of fission product release under in-pile conditions using the parameters obtained by the "weak" irradiation technique can be realized, as a rule, only at the concrete stage of in-pile tests. For example, it can be made either for starting fuel loading or for the conservative evaluations of particular operation conditions (or accidents) assuming that there is a certain degree of coated particle damage and that during the considered period, there are quasi-stationary conditions of fuel element operation.

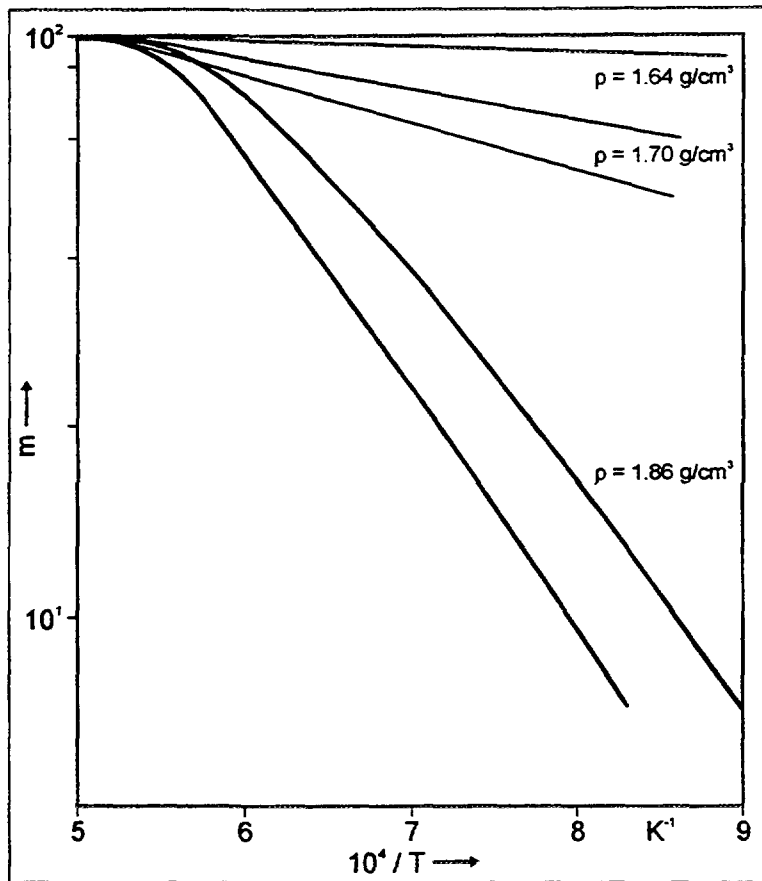


Fig. B-7: Temperature dependence of the Cs release from graphite samples with different densities

B.8. COMPARISON OF THE CONSIDERED MODEL PARAMETERS

At in-pile tests of the fuel elements, as a rule, the equilibrium relative rate of the radionuclide release is determined. On its values, using an appropriate physical model, it is possible to compare the fission product migration constants. In particular, if the diffusion model is used:

$$F \approx 3 \sqrt{D_{eff} / \lambda} \quad (B-54)$$

Taking into account that in the activation model

$$F \approx m + (1 - m) \frac{\alpha_s}{\alpha_s + \lambda} \quad (B-55)$$

or

$$\begin{aligned} F &\approx m \quad (\text{for } \lambda \gg \alpha_s) \\ m &\approx 3 \sqrt{D_{eff} / \lambda} \end{aligned} \quad (B-56)$$

leads to

$$m + (1 - m) \frac{\alpha_s}{\alpha_s + \lambda} \approx 3 \sqrt{D_{eff} / \lambda} \quad (B-57)$$

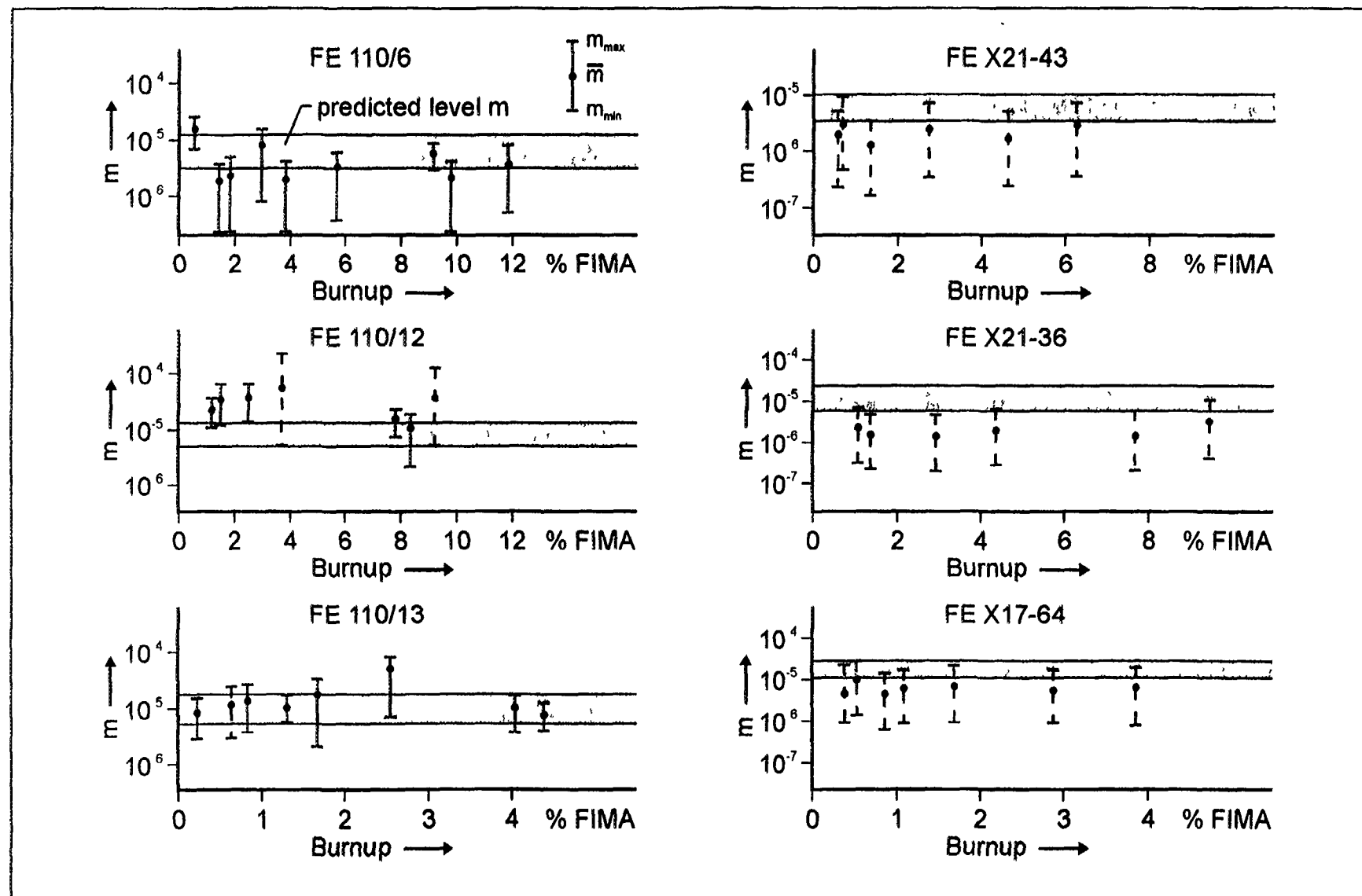


Fig. B-8: Predicted ("weak" irradiation) and experimental data of Xe-135 relative release (channel "KASHTAN-3")

This permits to use the data available in literature on diffusion coefficients and their dependencies on various parameters of fuel and fuel element for evaluation of the fission product release in terms of the activation model (and vice versa). In particular, the activation energy in the activation and diffusion models are connected by the relationship

$$2 \varepsilon_{act} \approx \varepsilon_{diff} \quad (\text{B-58})$$

Let us compare the constants obtained at the analysis of experimental results on the measurement of the release dependent on temperature in non-stationary conditions. If the two considered models are used, the fission product release from the fuel is defined by the correlations (B-6) and (B-8) (Fig. B-8).

Interconnection of the constants used in the given approaches is defined by the correlation:

$$m = \frac{\exp\{-\alpha_s \tau\} - \exp\{-K \tau\}}{\exp\{-\alpha_s \tau\} - \exp\{-\alpha_f \tau\}} \quad (\text{B-59})$$

$$m \approx \frac{K}{\alpha_f} \quad \text{for } \alpha_f > K \gg \alpha_s \quad (\text{B-60})$$

From the definition of "m" follows that $m < 1$. Hence, it is possible to assert that the release rate α_f is essentially higher, especially at relatively low temperatures, than $K(T)$.

Therefore the use of a one-group model for the analysis of experimental data and subsequent prediction of fission product release from the fuel at fast temperature processes will cause a decrease of the fission product release and so may give a wrong representation of the radionuclide release dynamics for the emergency mode.

The radionuclide release calculations will give underestimated data in this case, and the calculation of the fuel overheating temperature in the emergency mode overestimated data (for example Fig. B-9).

Accurately, it is necessary to use the correlations:

$$\begin{aligned} R_i &= -\alpha_f m A_i && \text{at heating} \\ R_i &= -\alpha_s (1 - m) A_i && \text{at cooling} \end{aligned} \quad (\text{B-61})$$

This method was used for the analysis of the Chernobyl accident.

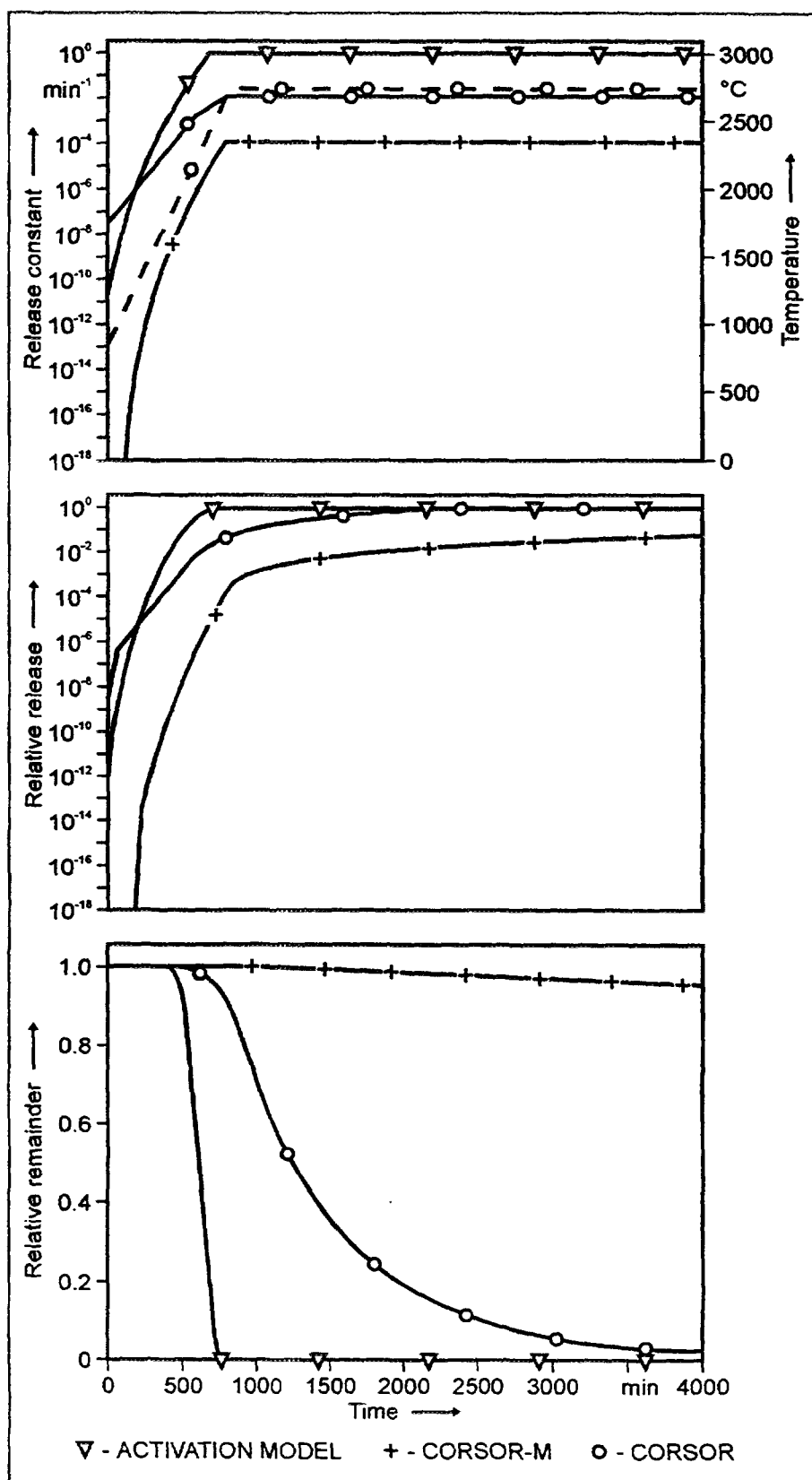


Fig. B-9: Calculation data on Ru release and content

B.9. PRELIMINARY ANALYSIS OF KR-85m RELEASE (EXPERIMENT FRJ2-P28)

As an example for the analysis of measured Kr-85 release, the experimental data for FRJ2-P28 obtained at KFA were used.

Fig. B-10 shows temperature mode and mode of change of Kr-85m samples in the FRJ2-P28 experiment. Kr-85m is the radionuclide that has no long-lived precursors. If the technique based on the activation (two-group) model for evaluation of the Kr-85m release basic constants is used, then:

1. The fuel element temperature is lower than the temperature of the previous cycle of irradiation, (T_o), therefore the release during irradiation and simultaneous heating is defined by the correlation

$$R/B = F \approx (1 - m) f(\alpha_s, \tau) \quad (\text{B-62})$$

(The expression $f(\alpha_s, \tau)$ is given in section B.6., equation (B-47), where τ is the heating time.)

The absence of information on the $m_o(T)$ value makes it impossible to determine α_s correctly. Evaluation under the assumption that $\tau < 1/\alpha_s$ gives $\alpha_s \approx 2.3 \cdot 10^{-3} \text{ h}^{-1}$.

2. The fuel element temperature is lower than the temperature of the previous cycle, therefore in the same approximation there is $\alpha_s \approx 2.0 \cdot 10^{-3} \text{ h}^{-1}$.
3. The fuel element temperature is about 10 degrees higher than the temperature at irradiation in the first cycle. In this case, the relative release (P5) defines the increase of the spectral characteristic "m" at the temperature change from $\tau_{ir}(0)$ up to $\tau_{ir}(3)$: $\Delta m \approx 1.2 \cdot 10^{-3}$. P6 value, due to lack of information, can also be characterized by the release constant $\alpha_s \approx 4.5 \cdot 10^{-3} \text{ h}^{-1}$.
4. The release in point P7 is defined by the temperature increase and makes it possible to evaluate $m(7) \approx 3.5 \cdot 10^{-2}$. The data set P8 - P12 makes an evaluation possible

Table B-2: Constants of experiment FRJ2-P28

Temperature		Constants			
		Δm	m	$\alpha_f [\text{h}^{-1}]$	$\alpha_s [\text{h}^{-1}]$
1180	1060				$2.0 \cdot 10^{-3}$
	1160				$2.3 \cdot 10^{-3}$
	1180				
	1190	$1.2 \cdot 10^{-3}$			
	1270	$3 \cdot 10^{-2}$	$3 \cdot 10^{-2}$	0.1 - 0.2	
	1285	$1.6 \cdot 10^{-2}$	$4.6 \cdot 10^{-2}$		$4.5 \cdot 10^{-3} \text{ (1)}$
	1290	$1.2 \cdot 10^{-2}$	$5.8 \cdot 10^{-2}$		$(4-5) \cdot 10^{-3}$

(1) at constant temperature decrease $\approx 3 \cdot 10^{-3} \text{ h}^{-1}$

under close isothermal conditions: $\alpha_f \approx (1-2) \cdot 10^{-1} \text{ h}^{-1}$.

The points P13 and P14 make it possible to evaluate $m(4)$, $m(4'')$, taking into account that in the first case: $\Delta T(13) \approx 15^\circ\text{C}$, in the second: $\Delta T(14) \approx 5^\circ\text{C}$. The results are: $\Delta m(13) \approx 1.6 \cdot 10^{-2}$, $\Delta m(14) \approx 1.2 \cdot 10^{-2}$.

5. Temperature decrease to $T \approx 1180^\circ\text{C}$, the release is defined by $\alpha_s \approx (4-5) \cdot 10^{-3} \text{ h}^{-1}$.
6. Further decrease of temperature with its subsequent increase up to $T \approx 1180^\circ\text{C}$, the additional warming up time plays the role. If $\tau \approx 2 \text{ h}$ is assumed, then $m(6) \approx 3 \cdot 10^{-3}$.

The results of the evaluation are listed in Table B-2 and in Fig. B-10.

From the comparison with the data on the release from the reference radionuclide specimens (“contamination” and “failed coated particles”), one could conclude that there is Kr-85 release from UO₂ coated particles with failed coatings. The fraction of the failed coated particles could make a few percent.

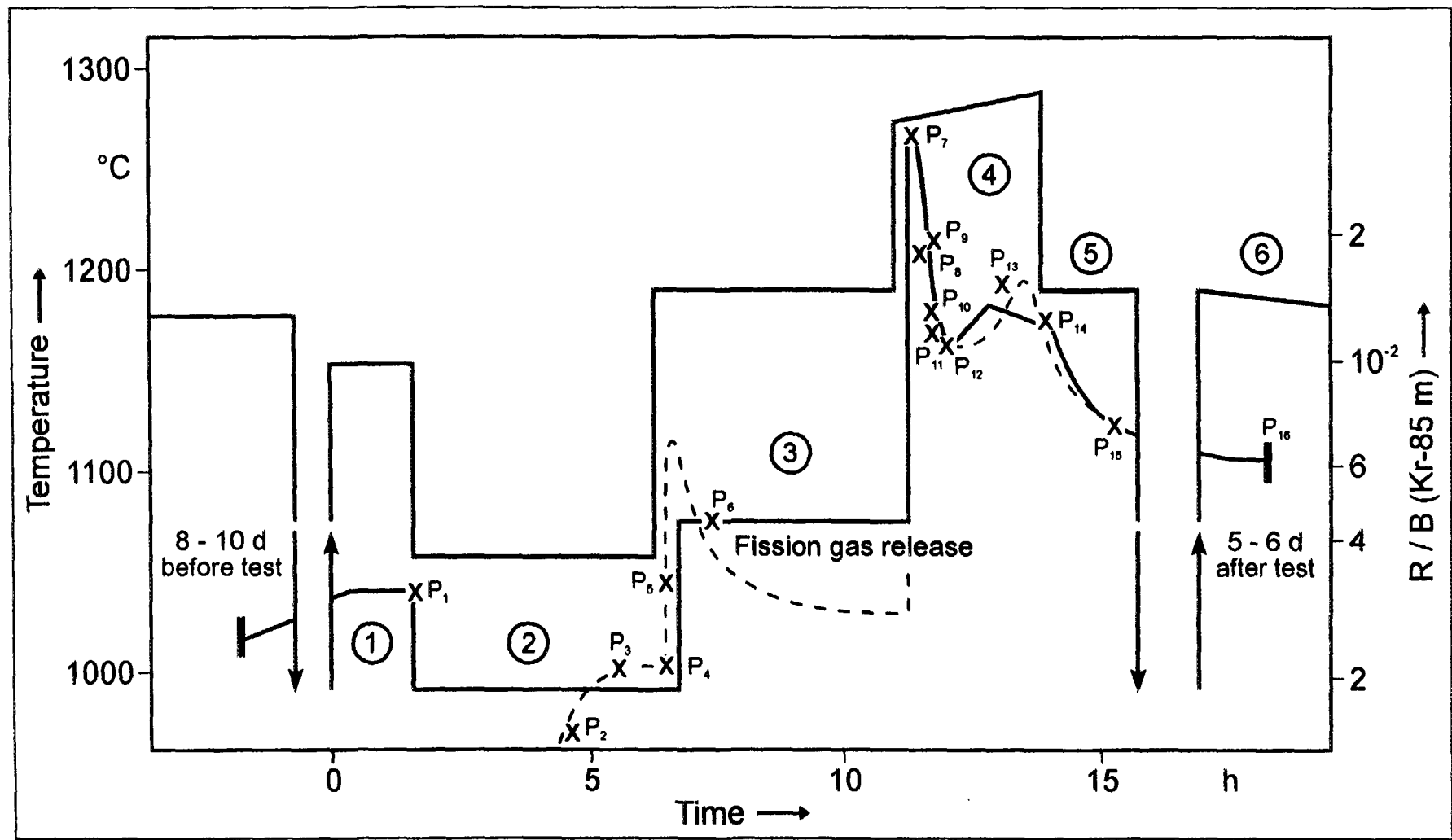


Fig. B-10: Fission gas release of Kr-85m as a function of temperature (burnup ca. 8 %FIMA) from particles with only a buffer layer (Experiment FRJ2-P28)

REFERENCES OF APPENDIX B

- [1] NRC, Technical Bases for Estimating Fission Product Behavior during LWR Accidents, Report NUREG-0772, US Nuclear Regulatory Commission (1981).
- [2] PONOMAREV-STEPNOY, N.N., KHROULEV, A.A., Release of Fission Products from High Temperature Fuel Materials, Thermo-Electric Power Generation, (3rd Int. Conf., Jülich, 1972), E-129.
- [3] KHROULEV, A.A., The Activational Model of the Fission Products Release from the HTGR Fuel Elements, Validation of Predictive Methods for Fuel and Fission Product Behavior in GCR, (Proc. 2nd RCM on CRP-2, Tokai, 1994), JAERI-Memo 07-027, Japan Atomic Energy Research Institute (1995).

Participants and Contributors to Drafting and Review

Brey, L.	IAEA, Vienna, Austria
Cleveland, J.	IAEA, Vienna, Austria
Fukuda, K.	JAERI, Tokai, Japan
Gillet, R.	CEA-CEG, Grenoble, France
Hanson, D.L.	GA, San Diego, USA
Kasten, P.R.	University of Tennessee in Knoxville, USA
Khroulev, A.	RRC-KI, Moscow, Russia
Minato, K.	JAERI, Tokai, Japan
Moormann, R.	FZJ, Jülich, Germany
Myers, B.F.	ORNL, Oak Ridge, USA
Nabielek, H.	FZJ, Jülich, Germany
Sawa, K.	JAERI, Tokai, Japan
Schenk, W.	FZJ, Jülich, Germany
Verfondern, K.	FZJ, Jülich, Germany
Williamson, R.	AEA, Harwell, UK
Xu, S.	INET, Beijing, PR China

Research Coordination Meetings

Vienna, Austria	June 23-25, 1993
Tokai, Japan	November 9-11, 1994
Vienna, Austria	December 4-8, 1995
Vienna, Austria	December 2-6, 1996